eman ta zabal zazu

Universidad del País Vasco
Euskal Herriko Unibertsitatea

Department of Theoretical Physics and History of Science

A phenomenological exploration within Theoretical Cosmology: from the Early to the Late Universe

João André Viegas Morais

Ph.D. Thesis
Leioa 2018

Department of Theoretical Physics and History of Science
University of the Basque Country (UPV/EHU)
Postal Box 644, 48080 Bilbao, Spain

Departamento de Física Teórica e Historia de la Ciencia
Universidad del País Vasco (UPV/EHU)
Apartado 644, 48080 Bilbao, España

Fisika Teorikoa eta Zientziaren Historia Saila
Euskal Herriko Unibertsitatea (UPV/EHU)
Posta Kutxatila 644, 48080 Bilbo, Espainia

The paper used in this book is FSC® and EU Ecolabel certified.

This document was generated with the 2016 LaTeX distribution.
The plots and figures of this thesis were generated with Matplotlib and Inkscape.

This work was funded by a PhD grant from the University of the Basque Country (UPV/EHU).

eman ta zabal zazu

Universidad del País Vasco
Euskal Herriko Unibertsitatea

Department of Theoretical Physics and History of Science

A phenomenological exploration within Theoretical Cosmology: from the Early to the Late Universe

Supervisor:
Dr. Mariam Bouhmadi López

Submitted by João André Viegas Morais
for the degree of Doctor of Physics

In memory of
Maria do Patrocínio
Zé Morais
Assunção
Zé Manel

Contents

List of Figures

List of Tables

Acknowledgements

First things first, I would like to thank my supervisor Mariam Bouhmadi López for the opportunity to undertake this voyage into the world of Cosmology. I am grateful for all the opportunities, guidance, support and friendship so kindly offered during the making of this PhD thesis in the last four plus years.

I am grateful to Alfredo Barbosa Henriques for all the opportunities to learn and the help provided, in particular to enter this PhD program, and I also want to thank all the other people I collaborated with over the years, namely Imanol Albarran, Salvatore Capozziello, Manuel Krämer, K. Sravan Kumar, João Marto, Salvador Robles Pérez, César M. Silva, Yaser Tavakoli and Alexander Zhuk, for allowing me the honour of having my name next to theirs in a published work about Physics.

I am grateful to the people of the Department of Theoretical Physics and History of Science of the UPV/EHU for taking the extra time and effort to organise the weekly seminars, local workshops and conferences, specialised courses and discussion groups which made the process of learning physics in the department so much richer. I am particularly grateful to Juan M. Aguirregabiria, Igor Bandos, Montserrat Barrio, José Juan Blanco Pillado, Mariam Bouhmadi López, Ivan de Martino, Iñigo L. Egusquiza, Jonathan Frazer, Alfonso García-Parrado, Ruth Lazkoz, Diego Saéz Gómez, Vincenzo Salzano, José M. Senovilla, Kepa Sousa, Jon Urrestilla, Charlotte Van Hulse, Raül Vera, Francesca Vidotto and Jeremy Watcher for the availability to supply answers when questions were thrown at them and to provide help when help was requested of them. I must also acknowledge the fascinating discussions and companionship that I had the privilege to share with the other PhD students of the department, including the first (Joanes Lizarraga, Asier López Eiguren and Pablo Jimeno–to the latter I must also thank for ending certain office traditions) and second (María Ortiz Baños, Francisco Fernandéz and Mikel Alvaréz Urquiola) generations of the F3.S2.8 office and our neighbours from F3.S2.5 (Borja Reina, Nastassja Cipriani and Iker Leanizbarrutia). In particular, to Iker, companion in arms in these last few months, I am grateful for the many times that his doubts and questions have helped me untie mental knots of my own, some of which I did not even know I had. And to Francisco, I must thank for helping to bring to life the *Tertulias Venusinas* (which I hope he and Mikel revive soon). This does not mean that I have forgotten all the others that helped, either voluntarily or on request, to keep that project alive for more than a Friday morning.

This thesis was made possible by the financial support of the UPV/EHU. In addition, I was given the possibility to attend several conferences during the last four years due to the generous support of several projects led by Mariam Bouhmadi López, Alexander Feinstein, Ruth Lazkoz and José M. Senovilla. During the making of this thesis I also had the opportunity to visit the University of Beira Interior, in Covilhã, Portugal, and the Institute of Cosmology and Gravitation in Portsmouth, United

Kingdom. To Imanol Albarran, Alexey Koshelev, K. Sravan Kumar, João Marto, Santiago Ávila, Julie Bower, Edward Macaulay, Sofia Meneses Soytia, David Wands, Hans Winther and all the others I had the pleasure to encounter, thank you for your hospitality.

***

The years that I spent in Bilbao doing this PhD were shared with a good list of friends, both old and new, who filled the good moments with bliss and made the bad ones more bearable. To the ones from Coimbra and Lisbon and now spread around the world, in particular Teresa, Henrique, Bruno, Carol, Filipe, Leonor, Luísa, Marco, Pedro, and Sónia, thank you for always keeping the distances short and for not letting me take life too seriously. To Sofia, I owe my eternal gratitude and much more for always being there when needed the most. And to the many new ones, I cannot thank you enough for all the shared moments, all the opportunities to learn and grow and all the prized conversations accompanied by a beer and a sunset in front of the baobab tree. To my hosts in the Jamel house, thank you for the patience during the last months of the writing of this thesis, and to Consuelo, my gratitude for the guidance and help in this last year.

Along the way, I have had the pleasure of meeting and starting a new project with a very special Italian hanabi maker. To Tina, thank you for all the fireworks so far–I aspire for many more in the journey to come. Finally, to my family, especially to my sister Ana and my parents Graça and Joaquim, thank you for the unconditional love, support, advice and understanding over the last 30 years.

Resumen

En esta tesis se han explorado posibles extensiones del Modelo Estándar de la Cosmología. Hemos obtenido las predicciones teóricas de los modelos considerados y sus principales características. Los resultados presentados están basados en tres proyectos principales en los que he participado conjuntamente con mi supervisora, Mariam Boudmadi López, y otros colaboradores. Estos proyectos enfocan tres áreas diferentes de investigación en la Cosmología actual: teorías métricas de gravedad modificada tipo $f(R)$ y modelos de energía oscura (EO) dinámica descrita por campos de 3-forma. Asimismo, en esta tesis hemos considerado la Cosmología Cuántica en el contexto del Universo primordial. Además, tal como sugiere el titulo, en esta tesis el foco principal se ha centrado en un tratamiento puramente teórico de los diferentes modelos considerados.

En la Parte I de esta tesis, se presentan primero, en el Capitulo 1, algunos de los principales conceptos de la Cosmología actual, como las ecuaciones de campo de la Relatividad General, la solución de Friedmann–Lemaître–Robertson–Walker para un universo homogéneo e isotrópico y el Modelo Estándar de la Cosmología, que incluye ideas tan distintas como la cosmología del *Hot Big Bang*, el modelo ΛCDM y el paradigma de la inflación primordial para describir los últimos 14 mil millones de años de la evolución de nuestro Universo. Adicionalmente, se presenta y discute la motivación para la búsqueda de nueva física más allá del modelo estándar. En particular, nos centramos en los modelos de EO dinámica, en la posibilidad de extender la acción de Einstein–Hilbert (EH) para la Relatividad General (RG) y en la búsqueda de una teoría cuántica de la gravedad. En el Capítulo 2, presentamos los principales métodos y los observables cosmológicos usados en esta tesis para caracterizar los diferentes modelos cosmológicos considerados y comparar las previsiones teóricas con los datos observacionales.

La Parte II se centra en la evolución del Universo tardío y está dividida en dos capítulos, donde cada uno corresponde a un proyecto diferente. En el Capítulo 3, se discuten los posibles efectos que una teoría de la gravedad modificada, en particular la teoría métrica de gravedad tipo $f(R)$, puede tener sobre la evolución del Universo y sobre las predicciones de los observables cosmológicos. Después de una breve introducción a este tipo de teorías y de su aplicación en la Cosmología, se presentan dos secciones donde se discute y se amplian los resultados publicados en

- **Can $f(R)$ gravity contribute to (dark) radiation?**
  J. Morais, M. Bouhmadi-López, S. Capozziello, *JCAP09 (2015) 041; e-print: arXiv:1507.02623 [gr-qc]*.

En la Sección 3.2 de este capítulo, se presenta un nuevo método de reconstrucción que permite obtener la acción $f(R)$ compatible con una expansión del fondo cosmológico previamente fijada. Este tipo de métodos es también conocido en la literatura como *designer* $f(R)$. Más específicamente,

nuestro método está basado en asociar las modificaciones de la gravedad a un fluido efectivo que, en conjunto con la materia normal, impulsa la expansión del Universo. Al imponer una ecuación de estado barotrópica al contenido total de la materia, incluyendo la materia normal y efectiva, es posible reescribir la ecuación de Friedmann modificada como una ecuación diferencial linear de segundo orden para la función $f(R)$. Utilizando este método, ha sido posible obtener por primera vez una correspondencia entre las teorías de gravedad $f(R)$ y el gas de Chaplygin generalizado y modificado (mGCG). Este fluido corresponde a una extensión del gas de Chaplygin que involucra dos nuevos parámetros del modelo. Este tipo de modelo ha sido utilizado en diferentes contextos en Cosmología, desde el Universo primordial hasta la evolución tardía del Universo.

En la Sección 3.3, se explora la posibilidad de que la radiación oscura (RO), un misterioso componente introducido para modelar un posible exceso de la materia ultra-relativista detectado en observaciones del fondo cósmico de microondas (FCM), sea una manifestación de las modificaciones de la acción de EH en las teorías métricas de gravedad tipo $f(R)$. Además de la RO, se considera que las modificaciones de la gravedad sean también responsables por la aceleración tardía del Universo. Con este fin, se asignan las modificaciones de la gravedad a un fluido efectivo descrito por un modelo mGCG que mimetiza radiación en el pasado lejano y una constante cosmológica en el presente. Es más, se obtiene la acción $f(R)$ compatible con nuestro modelo a través de una integración numérica de la ecuación de Friedman modificada y se analiza su relevancia física utilizando una perspectiva cosmográfica e imponiendo las condiciones de viabilidad física para acciones $f(R)$. Finalmente, se calculan la evolución de las perturbaciones cosmológicas lineales en el modelo desde la época inicial de radiación hasta el tiempo presente. Los efectos característicos de las modificaciones de la gravedad son identificados en la tasa de crecimiento de las perturbaciones de la materia y en el espectro de potencias de la materia.

En la segunda mitad de la Parte II de esta tesis, en el Capítulo 4, se explora un tipo diferente de extensión del Modelo Estándar de la Cosmología para la evolución del Universo tardío. En lugar de explicar los componentes oscuros a través de modificaciones de RG, se considera que la EO se describe por un campo dinámico que evoluciona con el tiempo. En particular, para describir la EO se utiliza un campo de 3-forma mínimamente acoplado a la gravedad y con un potencial positivo. Después de una primera introducción a los campos de 3-forma y sus aplicaciones cosmológicas, se presenta en la Sección 4.2 un análisis de sistemas dinámicos en modelos con materia oscura (MO) y EO descrita por un campo de 3-forma. En particular, la estabilidad global del sistema se analiza en profundidad por primera vez en este tipo de modelos. Con el fin de superar algunas dificultades encontradas en el sistema dinámico usual al estudiar puntos fijos en el infinito, introducimos una nueva representación que permite obtener sin ambigüedades la estabilidad de estos puntos. Esta representación fue publicada en nuestro artículo

- **Cosmic infinity: A dynamical system approach**
  M. Bouhmadi-López, J. Marto, J. Morais, C. M. Silva, *JCAP03 (2017) 042; e-print: arXiv: 1611.03100 [gr-qc]*.

donde las dificultades para definir la estabilidad de los puntos fijos en el infinito las resolvimos por la primera vez.

En la Sección 4.3, se discute como el *Little Sibling of the Big Rip* (LSBR) aparece de forma natural en modelos en los que la EO se describe por un campo de 3-forma. El LSBR es un evento cósmico

en el futuro que induce a la divergencia del parámetro de Hubble y a la disociación de todas las estructuras en el Universo, aunque de forma más suave que en la singularidad de tipo *Big Rip*. Después de demostrar que el LSBR aparece de forma natural en modelos cosmológicos con 3-formas para una amplia clase de potenciales independientemente de la presencia de otros tipos de materia que verifiquen la condición de energía nula, se explora la posibilidad de que una interacción entre la MO y la EO pueda prevenir este final catastrófico para el Universo. A través de un exhaustivo análisis de sistemas dinámicos se comprueba que es posible eliminar el LSBR del futuro del Universo si la interacción entre las dos componentes oscuras impide que la densidad de energía de la MO decaiga en su totalidad. Una vez identificadas las interacciones que (dentro de una clase general) son capaces de verificar esta condición, se utiliza la *statedinder hierarchy* y el método *composite null diagnosis* para caracterizar la evolución cosmológica *background* y de las perturbaciones escalares lineales en el modelo sin interacción y para dos casos con distintas interacciones que consiguen eliminar el LSBR. Se comparan los resultados obtenidos con las observaciones cosmológicas para $f\sigma_8$, donde f es la tasa de crecimiento de las perturbaciones de la materia y σ_8 es el valor cuadrático medio de la varianza de las fluctuaciones de la materia en esferas de radio $8\ h^{-1}$Mpc. Los resultados presentados en esta sección fueron publicados en el trabajo

- **Interacting 3-form dark energy models: distinguishing interactions and avoiding the Little Sibling of the Big Rip**
  J. Morais, M. Bouhmadi-López, K. Sravan Kumar, J. Marto, Y. Tavakoli, *Phys. Dark Univ. 15 (2017) 7-30*; *e-print: arXiv:1608.01679 [gr-qc]*.

En el Capítulo 5, el único capítulo de la Parte III, se estudian los efectos característicos que una época de pre-inflación imprime en el espectro de potencias primordial y en el espectro de potencias angular del FCM. Más específicamente, se estudian dos modelos inspirados en el formalismo de la Tercera Cuantización de la función de onda del Universo. En estos modelos, la época pre-inflacionaria se obtiene a través de efectos cuánticos, incluyendo interacciones cuánticas entre diferentes universos en el multiverso de la Tercera Cuantización. Este formalismo se propuso en la década de 1980 como una nueva interpretación de la Teoría Canónica de la Gravedad Cuántica que se basa en explorar los paralelismos entre la ecuación de Wheeler–deWitt y la ecuación de Klein–Gordon para un campo escalar cuántico. Algunos de los principales resultados de la Tercera Cuantización se resumen en la primera sección de este capítulo.

En la Sección 5.2, se discute la existencia de soluciones del tipo instantón Euclídeo que conectan pequeños universos bebé y universos inflacionarios en el multiverso de la Tercera Cuantización. Usando la propuesta de Vilenkin para la probabilidad de la función de onda del Universo de atravesar la región Euclídea mediante efectos cuánticos, calculamos la probabilidad de que un universo bebé, al alcanzar su tamaño máximo, dé origen a un universo inflacionario en lugar de recolapsar sobre si mismo. Los resultados presentados en esta sección fueron publicados en

- **What if? Exploring the multiverse through Euclidean wormholes**
  M. Bouhmadi-López, M. Krämer, J. Morais, S. Robles-Pérez, *Eur. Phys. J. C (2017) 77: 718*; *e-print: arXiv:1708.00025 [gr-qc]*.

En la Sección 5.3, se estudia la evolución de las perturbaciones cosmológicas escalares lineales en modelos inspirados por la Tercera Cuantización donde se obtiene una época pre-inflacionaria gracias a

considerar diferentes interacciones entre los elementos del multiverso. Nuestro análisis se centra en tres casos diferentes de comportamiento del Universo en esta época inicial: (i) el Universo evoluciona como si inicialmente estuviera dominado por materia rígida,; (ii) el Universo se comporta como si inicialmente estuviera dominado por un fluido de radiación; (iii) el Universo se comporta como si inicialmente estuviera dominado por polvo. Los efectos del modelo en el espectro de potencias primordial y el espectro de potencias angular del FCM se obtienen al asociar nuestro modelo al caso de un campo escalar mínimamente acoplado a la gravedad y utilizando la metodología habitual en modelos inflacionarios. Los parámetros del modelo son acotados mediante una comparación de las predicciones del modelo con los datos observacionales. Asimismo, se analizan las implicaciones para la interacción entre universos. Parte de los resultados presentados en esta sección fueron publicados en

- **Pre-inflation from the multiverse: Can it solve the quadrupole problem in the cosmic microwave background?**
  M. Bouhmadi-López, M. Krämer, J. Morais, S. Robles-Pérez, *Eur. Phys. J. C (2018) 78: 240; e-print: arXiv:1711.05138 [gr-qc]*.

Los demás resultados serán publicados en

- **The interacting multiverse and its effect on the cosmic microwave background**
  M. Bouhmadi-López, M. Krämer, J. Morais, S. Robles-Pérez, *; e-print: arXiv:18xx.xxxxx[gr-qc]*.

En la Sección 5.4, se discute la posibilidad de que el espectro de potencias primordial y el espectro de potencias angular del FCM contengan información no solo sobre la época pre-inflacionaria sino también sobre el período de transición hacia la inflación primordial. Se introduce una extensión de un parámetro, λ, al modelo discutido en la Sección 5.3 que permite controlar el número de e-folds necesarios para que la transición hacia la inflación se complete. Al tener en cuenta períodos de transición más largos es posible suavizar las características del potencial z''/z que controla la evolución de las perturbaciones escalares y así mejorar el ajuste del modelo con las observaciones cosmológicas. Se comprueba que las características del espectro de potencias primordial pueden ser predichas analizando la forma de z''/z en torno de la transición hacia la inflación. El espectro de potencias primordial y el espectro de potencias angular del FCM se calculan en los casos en que la época pre-inflacionaria mimetiza un Universo dominado por materia rígida o por radiación y se comparan los resultados con los datos observacionales para acotar los parámetros del modelo. Los resultados presentados en esta sección serán publicados en un futuro trabajo

- **Transition in the pre-inflationary Universe and their effects on the cosmic microwave background (working title)**
  M. Bouhmadi-López, J. Morais, .

En la Sección 5.5, se estudia el caso particular de transiciones instantáneas en el Universo primordial y las condiciones de contorno para las perturbaciones escalares en el momento de la transición, deducidas por primera vez por Deruelle y Mukhanov [136]. En el limite de valores muy altos del parámetro λ, el modelo estudiado en la Sección 5.4 presenta un salto descontinuo en el parámetro de la ecuación de estado y en el parámetro de slow-roll ϵ en el momento de la transición hacia la inflación. Además, algunos términos divergentes aparecen en el potencial z''/z que inducen una discontinuidad en la derivada de la perturbación de curvatura *comoving* y en la variable de Mukhanov–Sasaki y su derivada,

en conformidad con las condiciones de contorno de Deruelle y Mukhanov. Las mismas condiciones de contorno se obtienen utilizando la aproximación de longitud de onda grande, $k^2 \ll z'/z$, que, dado el valor tan alto de z''/z en el momento de la transición hacia la inflación, se hace válida a todas las escalas y permite obtener resultados exactos para la evolución de las perturbaciones. Se deduce la expresión analítica para el espectro de potencias primordial al fin de la inflación y se comparada con los resultados del escenario estándar de inflación con condiciones iniciales del tipo Bunch–Davies. Además, se estudia con detalle el comportamiento de la expresión encontrada en los regímenes de grandes y pequeñas escalas. Comparando el comportamiento asintótico con las ligaduras observacionales para el espectro de potencias primordial alrededor de la escala pivote de la misión Planck, se deducen ligaduras fuertes para la variación de ϵ en la transición hacia inflación que excluyen un comportamiento desacelerado en la época inicial en una situació de transición instantánea hacia la inflación. Finalmente, las predicciones analíticas del modelo son comparadas con los resultados numéricos obtenidos para valores cada vez más altos del parámetro λ. Los resultados presentados en esta sección serán publicados en un futuro trabajo citado anteriormente: *Transition in the pre-inflationary Universe and their effects on the cosmic microwave background (working title)*.

En la Parte IV se presentan las conclusiones generales y los comentarios finales de esta tesis y en la Parte V se presenta el Apéndice A, que contiene una revisión de la teoría de las perturbaciones cosmológicas lineales, y los Apéndices B, C y D, donde se incluyen cálculos y resultados auxiliares a los Capítulos 3, 4 y 5.

Otros trabajos originales publicados a lo largo de esta tesis incluyen

- **Scalar perturbations in the late Universe: viability of the Chaplygin gas models**
  M. Bouhmadi-López, M. Brilenkov, R. Brilenkov, J. Morais, A. Zhuk, *JCAP12 (2015) 037; e-print: arXiv:1509.06963 [gr-qc]*.

- **The late Universe with non-linear interaction in the dark sector: the coincidence problem**
  M. Bouhmadi-López, J. Morais, A. Zhuk, *Phys. Dark Univ. 14 (2016) 11-20; e-print: arXiv:1603.06983 [gr-qc]*.

- **K-essence model from the mechanical approach point of view: coupled scalar field and the late cosmic acceleration**
  M. Bouhmadi-López, K. Sravan Kumar, J. Marto, J. Morais, A. Zhuk, *JCAP07 (2016) 050; e-print: arXiv:1605.03212 [gr-qc]*.

- **Coupled scalar fields in the late Universe: The mechanical approach and the late cosmic acceleration**
  A. Burgazli, A. Zhuk, J. Morais, M. Bouhmadi-López, K. Sravan Kumar, *JCAP09 (2016) 045; e-print: arXiv:1512.03819 [gr-qc]*.

- **Cosmological perturbations in an effective and genuinely phantom dark energy Universe**
  I. Albarran, M. Bouhmadi-López, J. Morais, *Phys.Dark Univ. 16 (2017) 94-108*; *e-print: arXiv:1611.00392 [astro-ph.CO]*.

- **What if gravity becomes really repulsive in the future?**
  I. Albarran, M. Bouhmadi-López, J. Morais, *Eur. Phys. J. C (2018) 78: 260*; *e-print: arXiv:1706.01484 [gr-qc]*.

y también las siguientes contribuciones a *proceedings* de conferencias internacionales

- **3-Form Cosmology: Phantom Behaviour, Singularities and Interactions**
  J. Morais, M. Bouhmadi-López, J. Marto, *Universe 2017, 3(1), 21*.

- **The Third Quantization: To Tunnel or Not to Tunnel?**
  M. Bouhmadi-López, M. Krämer, J. Morais, S. Robles-Pérez, *Galaxies 2018, 6(1), 19*.

Prologue

Since ancient times, philosophers and scientist alike have discussed the idea of unifying all the processes of Nature under a single unified description. This idea of a Theory of Everything gained further attention in modern physics after the successes of Electromagnetism, in the nineteenth century, and of the Electroweak theory, in the second half of the twentieth century, in unifying two seemingly different fields of physics and remains one of the most sought after goals of theoretical physics. However, despite the great advances of the XX century that ultimately led to the Standard Model of particles and despite the hints to the existence of a Grand Unified Theory at very high energies, gravity has continuously avoided any attempt to be described at the same level of the other three forces. In fact, its very geometrical nature, as understood since the advent of General Relativity (GR) one hundred years ago, means that a separation of the gravitational interaction from the space-time is not possible in general situations. This is a critical difference between gravity and the other fundamental interactions, where a full quantum theory was first obtained by considering a *quantum* system of particles and interactions on a *classical* background. This situation is also aggravated by the non-renormalisability of GR, which prevents us from applying the full machinery of quantum field theory in a self-consistent way. A full theory of quantum gravity is still missing to this day, despite the huge theoretical advancements achieved in the last century.

On the other hand, the theory of gravitation proposed by Albert Einstein in 1915 [145], has so far passed all the experimental tests with bright colours [360]. This includes the recent discovery of gravitational waves [2] and the results 26-year long Gravity collaboration that analysed the orbit of the star S2 around the massive black hole in the centre of the Milky Way [8]. Paradoxically, this extraordinary agreement with the data makes the known limitations of GR even more enigmatic. Apart from the lack of renormalisability of the theory and the lack of a quantum description, GR, which is at the centre of modern cosmology, offers no answer to the mysteries surrounding dark matter (DM) and dark energy (DE), the two unknown fluids that comprise 95% of the content of the known Universe [287, 296]. In addition, there is no *a priori* requirement for the action that describes the gravitational interaction to be dependent only on the scalar curvature, as considered in the Einstein-Hilbert action. Over the decades, this has motivated the appearance of several proposals of extended or modified theories of gravity with equally diverse guiding principles. However, no theory has so far been able to equal the successes of GR, which continues to be the best theory of gravitation that we possess to describe the known Universe.

From an observational point of view, the low value of Newton's gravitational constant, when compared with the coupling parameters of other forces, implies that we cannot rely on laboratory-sized experiments to test the limits of the gravitational interaction. Instead, we must resort to looking to the cosmos, searching for new clues on the effects of gravity in the very large (Astronomy and Cosmology),

or the very dense (Black Hole and Neutron Star physics). It is in this context that Cosmology, which is currently undergoing a golden age in terms of precision, has moved to the forefront of theoretical physics as a favourite arena to look for imprints of modifications and extensions of GR, both in the infrared (corrections at cosmological scales) and in the ultraviolet (possible quantum effects during the primordial inflation). Furthermore, the existence of DM and DE, two of the biggest mysteries of modern day physics, was discovered and confirmed through cosmological observations and there is no reason not to believe that future observations will be essential in determining the nature of the dark sector of the Universe. In fact, several features of the Standard Model of Cosmology are sensitive to the properties of these two fluids and to even small changes in the laws of gravitation–as such, future, more precise and accurate missions might be able to detect imprints of new physics.

The work presented in this thesis explores different possible extensions to the Standard Model of Cosmology and tries to derive theoretical predictions for their characteristic imprints. The results presented are based on three main projects led by my supervisor, Mariam Bouhmadi López, and in collaboration with other authors. These projects explore three different main lines of research in modern Cosmology: effects of modified gravity, namely metric $f(R)$-gravity, in the late-time Universe; imprints of a dynamical model of DE; quantum cosmology in the context of the primordial Universe. Furthermore, as the title indicates, in this work we focus on a purely theoretical treatment of the various models presented.

In Part I of this thesis, we begin by reviewing, in Chapter 1, some of the main concepts of modern cosmology, such as the field equations of General Relativity, the Friedmann–Lemaître–Robertson–Walker solution for a homogeneous and isotropic universe and the Standard Model of Cosmology, which combines such different ideas as the Hot Big Bang cosmology, the ΛCDM model and the paradigm of primordial inflation to successfully describe the last 14 billion years of evolution of our Universe. In addition, we discuss the motivations for the search for new physics behind the standard model, in particular dynamical models of DE, the possibility of extending the Einstein–Hilbert (EH) action of GR and the search for a quantum theory of gravitation. In Chapter 2, we present the methods that were used to characterise the different cosmological models studied in this thesis. While some of these methods have a more mathematical focus, for example, a dynamical system analysis, others are based on calculating the theoretical predictions of observational quantities, such as the matter power spectrum or the angular power spectrum of the cosmic microwave background (CMB) radiation, and, therefore, allow for a direct comparison with the observational data.

On the first half of Part II, in Chapter 3, we discuss the possible effects that a modified theory of gravity, specifically metric $f(R)$-gravity, has on the evolution of the Universe and its imprints on cosmological observables. After a brief introduction to the theory of metric $f(R)$-gravity and its applications to cosmology, we present two sections where we discuss and expand on the original results first published in the work

- **Can $f(R)$ gravity contribute to (dark) radiation?**
  J. Morais, M. Bouhmadi-López, S. Capozziello, *JCAP09 (2015) 041; e-print: arXiv:1507.02623 [gr-qc]*.

In Sect. 3.2, we present a new reconstruction method which allows us to find the $f(R)$ action that is compatible with a given evolution of the FLRW cosmological background. This type of approach is commonly referred to in the literature as *designer* $f(R)$. More specifically, our method is based

on mapping the modifications of gravity onto an effective fluid that, together with normal matter, drives the expansion of the Universe. Then, by imposing a barotropic equation of state (EoS) for the total matter content, which includes normal mater and the effective $f(R)$ fluid, we are able to re-write the modified Friedmann equation as a linear second order differential equation for $f(R)$. We then show how, using this equation, we are able to successfully obtain for the first time the complete $f(R)$ mapping of the modified generalised Chaplygin gas, a 2-parameter extension of the Chaplygin gas (mGCG) model, which has several applications in cosmology, both in the late and in the early Universe.

In Sect. 3.3, we explore the possibility that dark radiation, a mysterious component that accounts for an excess of ultra-relativistic matter that was detected in observations of the CMB, is a consequence of modifications of the EH action within the context of metric $f(R)$-gravity. In addition to dark radiation, we consider that such modifications also lead to the current accelerated expansion of the Universe. In order to obtain this change between an early radiation-like behaviour and a later cosmological constant-like evolution, we map the modifications of gravity onto a mGCG with appropriate parameters and then integrate the modified Friedmann equation to obtain a numerical solution for the function $f(R)$. At the level of the FLRW background, we constraint our model using a cosmographic approach and the viability conditions for physically relevant $f(R)$ solutions. In addition, we study the evolution of the linear perturbations in our model, from the early radiation-dominated epoch till the present time. In particular, we compute the effects of the modifications of gravity on the matter power spectrum and the growth rate of the matter perturbations.

On the second half of Part II, in Chapter 4, we probe a different type of extension to the Standard Model of Cosmology. Instead of considering modifications to the theory of gravitation, we explore the possibility that DE is not a cosmological constant, but rather a dynamical field. More specifically, we describe DE by a 3-form field minimally coupled to gravity and with a positive valued potential. After an initial section where we review the 3-form field and its applications to homogeneous and isotropic cosmologies, we discuss in Sect. 4.2 the use of a dynamical system approach in models with DM and 3-form DE. In particular, we discuss for the first time how to use a compact description of the model in order to obtain a global picture of the stability of the system. Furthermore, we present a novel dynamical system representation that allows us to unequivocally study the dynamics of the system when the amplitude of the 3-form field assumes very large values. The results discussed in this section are the focus of the original work

- **Cosmic infinity: A dynamical system approach**
  M. Bouhmadi-López, J. Marto, J. Morais, C. M. Silva, *JCAP03 (2017) 042; e-print: arXiv: 1611.03100 [gr-qc]*.

and were motivated by some anomalies in the study of the stability of fixed points at very large amplitudes of the 3-form that were detected in

- **Interacting 3-form dark energy models: distinguishing interactions and avoiding the Little Sibling of the Big Rip**
  J. Morais, M. Bouhmadi-López, K. Sravan Kumar, J. Marto, Y. Tavakoli, *Phys. Dark Univ. 15 (2017) 7-30; e-print: arXiv:1608.01679 [gr-qc]*.

In Sect. 4.3, we discuss how the Little Sibling of the Big Rip (LSBR) can appear naturally in models where a 3-form field plays the role of DE. The LSBR is a cosmic abrupt event in the future that, despite being softer than the Big Rip singularity, leads to a divergence of the Hubble rate and to the dissociation of all structure in the Universe. After showing that in 3-form models within a certain class of potentials the LSBR is a general feature and that this situation is not altered by the presence of DM or other types of matter that satisfy the null energy condition, we explore the possibility that an adequate interaction between DM and DE can prevent this catastrophic end state of the Universe. We employ an extensive dynamical system analysis of the model in order to identify the types of interactions that are able to remove the LSBR and replace it by a final de Sitter-like scaling solution, where an energy transfer from DE to DM prevents the energy density of the latter from vanishing completely. For two types of interaction that fall into this category, we use the statefinder hierarchy and the composite null diagnosis to characterise the evolution of the model at the level of the homogeneous and isotropic background and at first order in cosmological perturbations. In addition, we analyse the effects of the interaction in the growth rate of the linear matter perturbations. The results presented in this section are the main focus of the aforementioned work *Interacting 3-form dark energy models: distinguishing interactions and avoiding the Little Sibling of the Big Rip*.

In Chapter 5, the only chapter of Part III, we explore the possibility of detecting imprints of a pre-inflationary epoch on the primordial power spectrum and on the angular spectrum of the CMB. More specifically, we consider different toy models, inspired by the formalism of the Third Quantisation of the wave-function of the Universe, where a pre-inflationary epoch arises due to quantum effects, including quantum interactions between different universes within the multiverse. The Third Quantisation formalism was proposed in the 1980's as a new interpretation of the Canonical Theory of Quantum Gravity, which explored the connections of the Wheeler–deWitt equation with the Klein–Gordon equation that describes the dynamics of a quantum scalar field. In the first section of Chapter 5, we present a brief introduction of the Canonical Theory of Quantum Gravity and of the Third Quantisation, where we also review some of the main results of this formalism.

In Sect. 5.2, we discuss the existence of Euclidean instanton solutions that connect small baby universes and large inflating universes in a model of the third-quantised multiverse. In addition, using the proposal of Vilenkin for the probability of the wave-function of the Universe to tunnel through the Euclidean region via quantum effects, we calculate the probability for an inflating universe to emerge, once a baby universe reaches its maximum classically allowed size. The results presented in this section were first published in the original work

- **What if? Exploring the multiverse through Euclidean wormholes**
  M. Bouhmadi-López, M. Krämer, J. Morais, S. Robles-Pérez, *Eur. Phys. J. C (2017) 77: 718; e-print: arXiv:1708.00025 [gr-qc]*.

In Sect. 5.3, we study the evolution of the linear cosmological perturbations in the scalar sector in a Third Quantisation-inspired model, where a decelerated epoch precedes a subsequent power law inflationary period. In this model, distinct pre-inflationary behaviours are obtained by changing the interaction term between different universes in the third-quantised multiverse. We focus our analysis in the cases where the Universe initially behaves as if (i) dominated by stiff matter; (ii) dominated by a radiation fluid; and (iii) dominated by pressureless dust. After mapping our model to that of a massive scalar field minimally coupled to gravity, we compute the imprints of the pre-inflationary

epoch in the primordial power spectrum at the end of inflation and in the angular power spectrum of the CMB. By comparing the results with the observational constraints from the Planck mission, we derive upper bounds on the parameters on the model and discuss its implications for the interaction strength between different universes. The results presented in this section were partially published in

- **Pre-inflation from the multiverse: Can it solve the quadrupole problem in the cosmic microwave background?**
  M. Bouhmadi-López, M. Krämer, J. Morais, S. Robles-Pérez, *Eur. Phys. J. C (2018) 78: 240; e-print: arXiv:1711.05138 [gr-qc]*.

The remainder of unpublished results will be submitted for publication as

- **The interacting multiverse and its effect on the cosmic microwave background**
  M. Bouhmadi-López, M. Krämer, J. Morais, S. Robles-Pérez, *; e-print: arXiv:18xx.xxxxx[gr-qc]*.

In Sect. 5.4, we consider the possibility that the imprints on the primordial power spectrum and on the angular power spectrum of the CMB from a pre-inflationary epoch can also contain information regarding the transition from the initial epoch to the subsequent inflation. We consider a 1-parameter extension of the Third Quantisation-inspired model introduced in Sect. 5.3, in which the new parameter λ allows us to control how many e-folds are necessary for the Universe to reach its asymptotic state during the inflationary period, and to impose whether the Universe accelerates or decelerates in the transition. When the transition takes longer to complete, i.e., for lower values of λ, the characteristic bumps of the potential z''/z around the onset of inflation are softened. This potential controls the evolution of the scalar cosmological perturbations and a softening of its features leads to a lowering of the amplitude of the peaks on the primordial power spectrum and amplifies the suppression at large scales. For the cases where the initial pre-inflationary epoch mimics a stiff matter dominated universe or a radiation dominated universe, we compute the primordial power spectrum and the angular power spectrum of the CMB and show that, for the same pre-inflationary behaviour, a shorter or longer period of transition can leave strong imprints on the theoretical predictions of the model. The characteristic scales of the model where these imprints are stronger can be predicted by the shape of the comoving Hubble wave-number and of the potential z''/z around the moment of the transition to inflation. Finally, we use the observational constraints to derive lower and upper bounds on the parameters of the model. The results presented in this section will be published in a future work

- **Transition in the pre-inflationary Universe and their effects on the cosmic microwave background (working title)**
  M. Bouhmadi-López, J. Morais, .

In Sect. 5.5, we study the case of instantaneous transitions in the early Universe and review how to impose proper matching conditions, first derived by Deruelle and Mukhanov [136], for the linear scalar perturbations at the moment of the transition. We show that in the limit of very large values of the parameter λ, the model introduced in Sect. 5.4 has a jump in the EoS parameter and in the slow-roll parameter ϵ at the onset of inflation. We calculate the limit for large λ of the potential z''/z and show that the appearance of divergent terms in z''/z at the moment of the transition leads to a jump in the derivative of the comoving curvature perturbation $\mathcal{R}_k'$ and in the Mukhanov–Sasaki variable v_k and its derivative. We show that the same boundary conditions can be obtained from

the long wavelength approximation $k^2 \ll z'/z$ which, due to the very large values of z''/z at the moment of the transition, now becomes valid at all scales. We compute the full analytic expression for the primordial power spectrum at the end of inflation in terms of general initial conditions imposed in the pre-inflationary phase and make a comparison with the standard prediction of an inflationary model with Bunch–Davies initial conditions. Using the asymptotic behaviour of the spectrum at small scales we use the observational constraints for the primordial power spectrum to impose bounds on the EoS parameter and on ϵ during the pre-inflationary epoch. In particular, we show that ϵ can only vary by up to 3% with regards to its value during the inflationary epoch, which excludes the possibility of having an initial decelerated expansion with an instantaneous transition to inflation. Finally, we corroborate our results by comparing the prediction for the primordial power spectrum from the analytical expressions with the numerical results obtained for increasingly large values of the parameter λ. The results presented in this section will be published in the aforementioned work *Transition in the pre-inflationary Universe and their effects on the cosmic microwave background (working title)*.

In Chapter 6 of Part IV we present the general conclusion of this thesis and in Part V we present a series of appendices. In the Appendix A, we review the theory of Cosmological Linear Perturbations and in the Appendices B, C and D, we present results auxiliary to the Chapters 3, 4 and 5.

Other original works published during the making of this thesis include

- **Scalar perturbations in the late Universe: viability of the Chaplygin gas models**
  M. Bouhmadi-López, M. Brilenkov, R. Brilenkov, J. Morais, A. Zhuk, *JCAP12 (2015) 037; e-print: arXiv:1509.06963 [gr-qc]*.

- **The late Universe with non-linear interaction in the dark sector: the coincidence problem**
  M. Bouhmadi-López, J. Morais, A. Zhuk, *Phys. Dark Univ. 14 (2016) 11-20; e-print: arXiv:1603.06983 [gr-qc]*.

- **K-essence model from the mechanical approach point of view: coupled scalar field and the late cosmic acceleration**
  M. Bouhmadi-López, K. Sravan Kumar, J. Marto, J. Morais, A. Zhuk, *JCAP07 (2016) 050; e-print: arXiv:1605.03212 [gr-qc]*.

- **Coupled scalar fields in the late Universe: The mechanical approach and the late cosmic acceleration**
  A. Burgazli, A. Zhuk, J. Morais, M. Bouhmadi-López, K. Sravan Kumar, *JCAP09 (2016) 045; e-print: arXiv:1512.03819 [gr-qc]*.

- **Cosmological perturbations in an effective and genuinely phantom dark energy Universe**
  I. Albarran, M. Bouhmadi-López, J. Morais, *Phys.Dark Univ. 16 (2017) 94-108*; *e-print: arXiv:1611.00392 [astro-ph.CO]*.

- **What if gravity becomes really repulsive in the future?**
  I. Albarran, M. Bouhmadi-López, J. Morais, *Eur. Phys. J. C (2018) 78: 260*; *e-print: arXiv:1706.01484 [gr-qc]*.

as well as the following contributions to conference proceedings

- **3-Form Cosmology: Phantom Behaviour, Singularities and Interactions**
  J. Morais, M. Bouhmadi-López, J. Marto, *Universe 2017, 3(1), 21*.

- **The Third Quantization: To Tunnel or Not to Tunnel?**
  M. Bouhmadi-López, M. Krämer, J. Morais, S. Robles-Pérez, *Galaxies 2018, 6(1), 19*.

Convention & Notation

In this thesis, we use the Misner Thorne and Wheeler metric signature $-+++$ [262] and the Wald definition for the Riemann tensor [347]. Roman letters, e.g. i, j, k, are used to denote the spatial indices 123, while Greek letters, e.g. α, β, γ or μ, ν, ρ, are used to denote the space-time indices 0123 .

List of symbols:

z^*	complex conjugate of z
$\hat{z}^\dagger$	Hermitian conjugate of $\hat{z}$
δ^μ_ν	Kronecker delta.
$g_{\mu\nu}$	space-time metric tensor
$\delta g_{\mu\nu}$	first order perturbation of the space-time metric tensor
∂_μ	Partial derivative with respect to the coordinate x^μ
∇_μ	Covariant derivative with respect to the space-time metric $g_{\mu\nu}$
$\Box$	d'Alembert operator with respect to the space-time metric $g_{\mu\nu}$
D_i	Covariant derivative with respect to the spatial metric γ_{ij}
∇^2	Laplacian with respect to the spatial metric γ_{ij}
$\varepsilon^{\mu_1 \cdots \mu_n}$	Levi-Civita symbol (tensor density)
$E^{\mu_1 \cdots \mu_n}$	Levi-Civita tensor
$\bar{A}$	background value of the quantity A
δA	first order perturbation of the quantity A
$R_{\mu\nu\rho}{}^\sigma$	Riemann tensor
$R_{\mu\nu}$	Ricci tensor
R	Ricci scalar curvature
${}^{(3)}R$	intrinsic spatial 3-dimensional scalar curvature
$A_{[\mu\nu]}$	anti-symmetrisation of $A_{\mu\nu}$ on the indices μ and ν
$A_{(\mu\nu)}$	symmetrisation of $A_{\mu\nu}$ on the indices μ and ν
η	conformal time

t	cosmic time

List of physical constants:

c	speed of light in vacuum
G	Newton's gravitational constant
$\hbar$	reduced Planck constant
κ^2	Einstein constant $\kappa^2 = 8\pi G/c^2$
ℓ_{P}	Planck length $\ell_{\mathrm{P}} = \sqrt{\hbar G/c^3}$
M_{P}	Planck mass $M_{\mathrm{P}} = \sqrt{\hbar c/G}$
m_{P}	reduced Planck mass $m_{\mathrm{P}} = \sqrt{\hbar c/(8\pi G)}$

List of abbreviations:

BD	Bunch–Davies
CDM	Cold Dark Matter
CMB	Cosmic Microwave Background
CND	Composite Null Diagnosis
DM	Dark Matter
DE	Dark Energy
EH	Einstein–Hilbert
Eq.	Equation
Fig.	Figure
FLRW	Friedmann–Lemaître–Robertson–Walker
GI	Gauge invariant
GR	General Relativity
KG	Klein–Gordon
LQC	Loop Quantum Cosmology
LSS	Large-Scale Structure
mGCG	Modified generalised Chaplygin gas
l.h.s.	Left-hand-side
r.h.s.	Right-hand-side
Tab.	Table
UDM	Unified Dark Matter–Energy
WDW	Wheeler–DeWitt

PART I

Introduction

1 The Standard Model of Cosmology

In this chapter we review briefly some of the key concepts of modern cosmology. We start by presenting the action and field equations of Einstein's General Relativity (GR) and go on to discuss the Cosmological Principle and the Friedmann–Lemaître–Robertson–Walker (FLRW) solution, which describes a homogeneous and isotropic universe. We discuss the Standard Model of Cosmology, which describes the last 14 billion years of the history of our Universe, from an initial primordial inflationary epoch that sets-up the initial conditions for Hot Big Bang cosmology, till the late-time evolution at low redshift, where the ΛCDM model is favoured by observations. To conclude the chapter, we discuss some of the limitations of the Standard Model, as well as its possible extensions found in literature, some of which we will explore in subsequent chapters.

1.1. Einstein field equations

The Einstein–Hilbert (EH) action of GR, first published in 1915 by David Hilbert [184], reads

$$\mathcal{S}^{\mathrm{EH}} = \frac{1}{2\kappa^2}\int \mathrm{d}^4x\sqrt{-g}R\,, \tag{1.1}$$

where $\kappa^2 = 8\pi G$ with G being Newton's gravitational constant, g is the determinant of the metric $g_{\mu\nu}$ and the scalar curvature $R := g^{\mu\nu}R_{\mu\nu}$ is the trace of the Ricci tensor, defined in terms of the connection $\Gamma^{\rho}{}_{\mu\nu}$ as [347]

$$R_{\mu\nu} := \partial_\rho\Gamma^{\rho}{}_{\mu\nu} - \partial_\nu\Gamma^{\rho}{}_{\mu\rho} + \Gamma^{\sigma}{}_{\mu\nu}\Gamma^{\rho}{}_{\sigma\rho} - \Gamma^{\sigma}{}_{\mu\rho}\Gamma^{\rho}{}_{\sigma\nu}\,, \tag{1.2}$$

where $\partial_\mu(\cdot) := \partial(\cdot)/\partial x^\mu$ indicates a partial derivative with regards to the coordinate x^μ. In this thesis, we adopt a metric approach and consider that the metric $g_{\mu\nu}$ is the only fundamental object of the gravitational sector. As such, the connection $\Gamma^{\rho}{}_{\mu\nu}$ in Eq. (1.2) is the Levi–Civita connection constructed from the metric $g_{\mu\nu}$ [347]:

$$\Gamma^{\rho}{}_{\mu\nu} := \frac{1}{2}g^{\rho\sigma}\left(\partial_\mu g_{\sigma\nu} + \partial_\nu g_{\mu\sigma} - \partial_\sigma g_{\mu\nu}\right)\,. \tag{1.3}$$

If, in addition to the EH action (1.1), we consider the existence of a cosmological constant Λ and of matter fields minimally coupled to gravity and with internal degrees of freedom $\boldsymbol{\Psi}^{(\mathrm{i})}$, then the total

action reads[1]

$$\begin{aligned}\mathcal{S}[g_{\mu\nu}, \mathbf{\Psi}^{(\mathrm{i})}] &= \mathcal{S}^{\mathrm{EH}}[g_{\mu\nu}] + \mathcal{S}^{\Lambda}[g_{\mu\nu}] + \mathcal{S}^{(\mathrm{mat})}[g_{\mu\nu}, \mathbf{\Psi}^{(\mathrm{i})}] \\ &= \frac{1}{2\kappa^2}\int \mathrm{d}^4x\sqrt{-g}\,(R - 2\Lambda) + \int \mathrm{d}^4x\sqrt{-g}\mathcal{L}^{(\mathrm{mat})}[g_{\mu\nu}, \mathbf{\Psi}^{(\mathrm{i})}]\,,\end{aligned} \tag{1.4}$$

with $\mathcal{L}^{(\mathrm{mat})}$ the Lagrangian density of the matter fields. The minimisation of Eq. (1.4) with regards to variations of the metric $g_{\mu\nu}$ leads to the Einstein field equations[2] [145]

$$G_{\mu\nu} + \Lambda g_{\mu\nu} = \kappa^2 [T^{(\mathrm{m})}]_{\mu\nu}\,, \tag{1.5}$$

where the Einstein tensor, $G_{\mu\nu}$, and the stress-energy-momentum tensor, $[T^{(\mathrm{m})}]_{\mu\nu}$, are defined as

$$G_{\mu\nu} := R_{\mu\nu} - \frac{1}{2}R\,g_{\mu\nu}\,, \qquad\qquad [T^{(\mathrm{m})}]_{\mu\nu} := -\frac{2}{\sqrt{-g}}\frac{\delta\sqrt{-g}\mathcal{L}^{(\mathrm{m})}}{\delta g^{\mu\nu}}\,. \tag{1.6}$$

The Einstein field equations (1.5), which have recently celebrated their first centenary, dictate how space-time bends and curves in the presence, or absence, of matter. In essence, they encode all the necessary information regarding the laws of gravitation in GR. On the other hand, in order to describe how matter moves in the curved space-time, we require the equations of motion for the matter degrees of freedom $\mathbf{\Psi}^{(\mathrm{i})}$, which are obtained by minimising the action (1.4) with regards to variations of $\mathbf{\Psi}^{(\mathrm{i})}$:

$$\frac{\delta\mathcal{L}^{(\mathrm{mat})}}{\delta\mathbf{\Psi}^{(\mathrm{i})}} = 0\,. \tag{1.7}$$

From the trace of Eq. (1.5), we obtain an additional relation between the scalar curvature, the cosmological constant and the trace of the stress-energy-momentum tensor, $T^{(\mathrm{m})} := [T^{(\mathrm{m})}]^{\mu}{}_{\mu}$:

$$R - 4\Lambda = -\kappa^2 T^{(\mathrm{m})}\,. \tag{1.8}$$

1.2. The matter sector

In GR, where the matter fluids are minimally coupled to gravity, the matter content can be characterised by the stress-energy-momentum tensor $[T^{(\mathrm{m})}]_{\mu\nu}$, defined in Eq. (1.6), which appears on the r.h.s. of Eq. (1.5). Using the Bianchi identities [347], it is possible to show that the Einstein tensor is divergenceless, i.e., $\nabla_\mu G^{\mu}{}_{\nu} = 0$, which, using Eq. (1.5), immediately leads to

$$\nabla_\mu [T^{(\mathrm{m})}]^{\mu}{}_{\nu} = 0\,, \tag{1.9}$$

showing that GR is compatible with the local conservation of energy and momentum. In the case where the matter Lagrangian density can be decomposed into several components $\mathcal{L}^{(\mathrm{j})}$, each representing a

[1] Notice that while in GR the metric and Palatini approaches lead to equivalent equations of motion, the same might not be true for modified theories of gravity [105, 321].

[2] Throughout this thesis, we opt to employ square brackets, when adequate, to separate labels of tensor quantities from the space-time (or spatial) indices.

separate fluid, we can define for each $\mathcal{L}_{(\mathrm{j})}$ a stress-energy-momentum tensor via Eq. (1.6):

$$[T_{(\mathrm{j})}]_{\mu\nu} := -\frac{2}{\sqrt{-g}}\frac{\delta\sqrt{-g}\mathcal{L}_{(\mathrm{j})}}{\delta g^{\mu\nu}}\,, \qquad \sum_{\mathrm{j}}[T_{(\mathrm{j})}]_{\mu\nu} = [T^{(\mathrm{m})}]_{\mu\nu}\,. \tag{1.10}$$

However, the total conservation equation (1.9) does not guarantee the conservation of each $[T_{(\mathrm{j})}]_{\mu\nu}$. Instead, we can write the individual conservation equations with an interaction vector $[Q_{(\mathrm{j})}]_\nu$ as

$$\nabla_\mu[T_{(\mathrm{j})}]^\mu{}_\nu = [Q_{(\mathrm{j})}]_\nu\,, \qquad \sum_{\mathrm{j}}[Q_{(\mathrm{j})}]_\nu = 0\,. \tag{1.11}$$

The specific form of the $[Q^{(\mathrm{j})}]_\nu$, which defines the energy and momentum transfer for the fluid j, can be obtained by using the equations of motion (1.7).

Given a time-like unit 4-vector u^μ, we can decompose a stress-energy-momentum tensor $T_{\mu\nu}$ as [144, 196, 215]

$$T_{\mu\nu} = (\rho + P)\,u_\mu u_\nu + P g_{\mu\nu} + 2u_{(\mu}q_{\nu)} + \pi_{\mu\nu}\,, \tag{1.12}$$

where ρ is the energy density, P is the pressure, q_μ is the energy flux orthogonal to u^μ ($u^\mu q_\mu = 0$) and $\pi_{\mu\nu}$ is the anisotropic stress which is traceless ($\pi^\mu_\mu = 0$) and orthogonal to u^μ ($u^\mu\pi_{\mu\nu} = 0$). These fluid variables can be defined formally as [144, 196, 215]

$$\rho := u^\mu u_\nu T^\mu{}_\nu\,, \tag{1.13}$$

$$P := \frac{1}{3}h^\mu_\nu\,T^\mu{}_\nu\,, \tag{1.14}$$

$$q^\mu := -u^\nu h^\mu_\rho T^\rho{}_\nu\,, \tag{1.15}$$

$$\pi_{\mu\nu} := \left(h_{\mu\rho}h^\sigma_\nu - \frac{1}{3}h^\sigma_\rho h_{\mu\nu}\right)T^\rho{}_\sigma\,, \tag{1.16}$$

where $h_{\mu\nu} := g_{\mu\nu} + u_\mu u_\nu$ is the 3-metric projected on the 3-dimensional space orthogonal to u^μ. In the case of a perfect fluid, both the energy-flux and the anisotropic stress vanish and so the stress-energy-momentum tensor (1.12) reduces to [144]

$$T_{\mu\nu} = (\rho + P)\,u_\mu u_\nu + P g_{\mu\nu}\,. \tag{1.17}$$

1.3. The Friedmann-Lemaître-Robertson-Walker solution

The cosmological principle states that any observer is not in a privileged position, but rather in a fairly representative region of the Universe. In other words, when viewed at large enough scales, the Universe should be roughly the same in every patch of space and in every direction we look. As such, the laws of physics that we can test in our immediate neighbourhood should remain valid throughout the Universe and be applicable in regions which are currently inaccessible to us. This is supported by modern observations, which indicate that deviations from isotropy in the cosmic microwave background radiation are of the order of 10^{-5} and that most cosmic structures have characteristic sizes of less

than a few hundred[3] megaparsec (Mpc).

The solution to Einstein field equations (1.5) that describes such a homogeneous and isotropic universe was first presented by Alexander Friedmann in the early 1920's [159, 160]. Shortly after Friedmann's death in 1925, the same solution was re-derived by Georges Lemaître [225], who immediately realised the physical implications of the model[4]. After Edward A. Milne was able to re-derive the evolution equations in Friedamnn and Lemaître's model through kinematic considerations in Newton's theory of gravity [261] (see also Refs. [207, 254]), Howard P. Robertson [297–299] and Arthur G. Walker [348, 349] analysed in detail the metric compatible with both models, showing that it represents the most general solution for a homogeneous and isotropic universe independently of the theory of gravity assumed.

The general FLRW line element can be written in coordinates $\{t,\, r,\, \theta,\, \varphi\}$ as[5]

$$\mathrm{d}s^2 = -N^2(t)\mathrm{d}t^2 + a^2(t)\left(\frac{\mathrm{d}r^2}{1-\mathcal{K}r^2} + r^2\mathrm{d}\theta^2 + r^2\sin^2(\theta)\mathrm{d}\varphi^2\right), \tag{1.18}$$

where N is the lapse function[6], a is the scale factor which we consider to have units of length and $\mathcal{K} = -1,\, 0,\, +1$. From the line element (1.18) we can write the FLRW metric and its inverse as

$$g_{\mu\nu} = \begin{pmatrix} -N^2 & 0 \\ 0 & a^2\gamma_{ij} \end{pmatrix}, \qquad g^{\mu\nu} = \begin{pmatrix} -N^{-2} & 0 \\ 0 & a^{-2}\gamma^{ij} \end{pmatrix}, \tag{1.19}$$

where the 3-metric $\gamma_{ij} = \gamma_{ij}(\vec{x})$ is given in reduced-circumference polar coordinates $\{r,\, \theta,\, \varphi\}$ as

$$\gamma_{ij} = \begin{pmatrix} \dfrac{1}{1-\mathcal{K}r^2} & 0 & 0 \\ 0 & r^2 & 0 \\ 0 & 0 & r^2\sin^2(\theta) \end{pmatrix}, \qquad \gamma^{ij} = \begin{pmatrix} 1-\mathcal{K}r^2 & 0 & 0 \\ 0 & \dfrac{1}{r^2} & 0 \\ 0 & 0 & \dfrac{1}{r^2\sin^2(\theta)} \end{pmatrix}. \tag{1.20}$$

The line element (1.18) corresponds to a foliation of space-time into space-like hypersurfaces

[3] For more than a decade, the largest structure known to humankind was the CfA2 Great Wall (~ 200Mpc) [165], supplanted in the mid 2000's by the Sloan Great Wall (~ 500 Mpc) [171]. In recent years, however, some structures were discovered that pass the 1000 Mpc mark, such as the Huge Large Quasar Group ($\lesssim 1400$ Mpc) [119] and the Hercules-Corona Borealis Great Wall (~ 2000–3000 Mpc) [188]. These structures are well above the theoretical limit for the size of structure in the ΛCDM model; the value $260\ h^{-1}$Mpc was obtained in Ref. [362] using multi-fractal analysis. However, the statistical nature of such analysis means that the discovery of a few structures above the theoretical limit do not necessarily represent an incompatibility with the cosmological principle [272].

[4] Two years before Edwin Hubble published his famous relation between the distance and the receding velocity of nearby galaxies [193], Lemaître understood that an expanding universe leads to a redshift effect of the light coming from extra-galactic sources and shortly after theorised that an extrapolation of the model implied that the Universe should have begun in an extremely hot and small *primeval atom* (the original Big Bang) at some finite time in the past [226]. These ideas eventually led to the theory of Big Bang Nucleosynthesis (BNN), initially spearheaded by Ralph A. Alpher and George Gamow [31, 161], and to the prediction [30] and discovery [286] of the cosmic microwave background (CMB) radiation.

[5] Here and throughout this work, we set the speed of light $c = 1$ unless explicitly stated otherwise.

[6] Most works on theoretical cosmology use either the cosmic time ($N = 1$) or the conformal time ($N = a$). Here, we leave the lapse function unspecified, despite the obvious extra burden in the notation, as it provides us with a fast way of obtaining the evolution equations for any choice of the time variable. This will be advantageous when numerical integrations are required, in which case we prefer to use $\log(a/a_*)$, where a_* is an arbitrary scale, as the time variable.

orthogonal to the unit 4-vector

$$n_\mu = \left(-N, \vec{0}\right) , \qquad n^\mu = \left(\frac{1}{N}, \vec{0}\right) , \tag{1.21}$$

which are endowed with a spatial 3-metric[7] $h_{\mu\nu} := g_{\mu\nu} + n_\mu n_\nu$ and have uniform spatial curvature

$${}^{(3)}R = \frac{6\mathcal{K}}{a^2} . \tag{1.22}$$

As such, in a FLRW universe, we find that the spatial sections can be closed ($\mathcal{K} = -1$), flat ($\mathcal{K} = 0$) and open ($\mathcal{K} = +1$). The local expansion scalar θ which corresponds to the expansion rate of a spatial volume a^3 is given by [246, 347]

$$\theta := \nabla_\mu n^\mu = \frac{3}{N}\frac{\dot{a}}{a} , \tag{1.23}$$

where a dot indicates a derivative with respect to t. On the other hand, the shear tensor $\sigma_{\mu\nu}$, the vorticity tensor $\omega_{\mu\nu}$ and the acceleration 4-vector a_μ are all identically zero in FLRW cosmology [246, 347]:

$$\sigma_{\mu\nu} := h^\rho_{(\mu} h^\sigma_{\nu)} \nabla_\rho n_\sigma - \frac{1}{3}\theta h_{\mu\nu} = 0 , \tag{1.24}$$

$$\omega_{\mu\nu} := h^\rho_{[\mu} h^\sigma_{\nu]} \nabla_\rho n_\sigma = 0 , \tag{1.25}$$

$$a_\mu := n^\nu \nabla_\nu n_\mu = 0 , \tag{1.26}$$

reflecting the symmetries of the geometry and the fact that an initially comoving particle remains at rest with the Hubble flow.

In a Universe described by the line element (1.18), the homogeneity and isotropy conditions imply that all 3-vectors and spatial gradients must vanish. As such, all the non-diagonal components of the Einstein field equations must vanish. Inserting Eq. (1.19) in the field equations (1.5), we find that the $(0-0)$ component reads

$$3\left(\frac{\dot{a}}{a}\right)^2 + 3\frac{N^2}{a^2}\mathcal{K} - N^2\Lambda = \kappa^2 N^2 \rho^{(\mathrm{m})} . \tag{1.27}$$

This equation relates the rate of expansion of the Universe with the total energy density, including the contributions from the matter fields, the cosmological constant and the spatial curvature. On the other hand, the $(i-i)$ component reads

$$2\frac{\ddot{a}}{a} + \left(\frac{\dot{a}}{a}\right)^2 - 2\frac{\dot{N}}{N}\frac{\dot{a}}{a} + \frac{N^2}{a^2}\mathcal{K} - N^2\Lambda = -\kappa^2 N^2 P^{(\mathrm{m})} . \tag{1.28}$$

From the expressions (1.27) and (1.28), we can obtain the acceleration of the expansion, $\ddot{a}$, in terms

[7] By comparing Eqs. (1.19), (1.21) and the definition of the induced 3-metric $h_{\mu\nu}$ constructed from the 4-vector n_μ, it can be recognised that $h_{ij} = a^2\gamma_{ij}$.

of the energy density and pressure:

$$\frac{\ddot{a}}{a} - \frac{\dot{N}}{N}\frac{\dot{a}}{a} - \frac{N^2}{3}\Lambda = -\frac{\kappa^2 N^2}{6}\left(\rho^{(\mathrm{m})} + 3P^{(\mathrm{m})}\right) . \tag{1.29}$$

In the matter sector, the isotropy and homogeneity conditions lead to the vanishing of the energy-flux 4-vector $[q^{(\mathrm{m})}]_\mu$ and the anisotropic stress tensor $[\pi^{(\mathrm{m})}]_{\mu\nu}$, and any stress-energy-momentum tensor reduces to the form of a perfect fluid, as given in Eq. (1.17). Furthermore, the conservation of the stress-energy-momentum tensor, cf. Eq. (1.9), leads to the continuity equation

$$\dot{\rho}^{(\mathrm{m})} + 3\frac{\dot{a}}{a}\left(\rho^{(\mathrm{m})} + P^{(\mathrm{m})}\right) = 0 . \tag{1.30}$$

Such an equation is equivalent to the conservation of energy in an adiabatic system as stipulated by the first law of thermodynamics. For extremely non-relativistic matter, $P_{\mathrm{m}} = 0$, this equation leads to the solution $\rho_{\mathrm{m}} \propto a^{-3}$ which guarantees that mass is conserved as the Universe expands. On the other hand, for purely relativistic matter, $P_{\mathrm{r}} = 1/3\rho_{\mathrm{r}}$, we obtain the solution $\rho_{\mathrm{r}} \propto a^{-4}$, which points to the loss of energy of ultra-relativistic particles ($E = \hbar/\lambda$) due to the redshift of the wave-length λ in an expanding universe [225]

$$\frac{\lambda(t_2)}{\lambda(t_1)} = \frac{a(t_2)}{a(t_1)} . \tag{1.31}$$

In the case of interacting fluids, the interaction 4-vector in Eq. (1.11), $[Q_{(\mathrm{j})}]_\mu$, can be decomposed as

$$[Q_{(\mathrm{j})}]_\mu = \left(-N\,Q_{(\mathrm{j})},\, \vec{0}\right) , \tag{1.32}$$

leading to a modified version of the continuity equation (1.30), which reads

$$\dot{\rho}_{(\mathrm{j})} + 3\frac{\dot{a}}{a}\left(\rho_{(\mathrm{j})} + P_{(\mathrm{j})}\right) = N\,Q_{(\mathrm{j})} . \tag{1.33}$$

Notice that the continuity equation for the total energy density requires that $\sum_{\mathrm{j}} Q_{(\mathrm{j})} = 0$.

The Hubble rate H is defined as the expansion rate of the scale factor $a(t)$ in cosmic time ($N = 1$):

$$H := \frac{1}{N}\frac{\dot{a}}{a} = \frac{\theta}{3} , \tag{1.34}$$

and allows us to re-write the Friedmann equation (1.27) in a simplified form as

$$3H^2 = \kappa^2\rho^{(\mathrm{m})} - \frac{3\mathcal{K}}{a^2} + \Lambda . \tag{1.35}$$

If we interpret the contributions of the curvature term and the cosmological constant term as energy densities, then from Eq. (1.35) we can introduce the critical energy density of the Universe

$\rho_{\rm crit} := 3H^2/\kappa^2$ and the fractional energy densities

$$\Omega^{(\rm m)} := \frac{\rho^{(\rm m)}}{\rho_{\rm crit}}\,, \qquad \Omega_{\mathcal{K}} := -\frac{3\mathcal{K}}{\kappa^2 a^2 \rho_{\rm crit}}\,, \qquad \Omega_\Lambda := \frac{\Lambda}{\kappa^2 \rho_{\rm crit}}\,. \tag{1.36}$$

In terms of these quantities, the Friedmann equation (1.35) reduces to the constraint

$$1 = \Omega^{(\rm m)} + \Omega_{\mathcal{K}} + \Omega_\Lambda\,. \tag{1.37}$$

Thus, we can consider the Universe as effectively flat as long as $\Omega^{(\rm m)} + \Omega_\Lambda \approx 1$, even if $\mathcal{K} \neq 0$.

In this section, we have discussed the highly symmetrical FLRW geometry which seems to best describe our Universe at large scales. In order to obtain a richer description of the cosmos, however, we need to also study the evolution of small inhomogeneities and anisotropies around the FLRW background. In the Appendix. A, we present a quick review of the theory of cosmological perturbations, which provides the theoretical framework to undertake such an endeavour.

1.4. The Standard Model of Cosmology

Twenty years ago, the observations of Type Ia supernovae (SNe Ia) by the Supernova Cosmology Project [287] and the High-z Supernova Search Team [296] showed that the current expansion of the Universe is incompatible with the behaviour of a dust dominated universe and instead favours a picture where the Universe started to accelerate in our recent past. These results confirmed a series of suspicions, raised in the preceding decade, that a significant contribution from a fluid similar to a cosmological constant, the so called dark energy (DE), was necessary to explain contemporary observations regarding the late time evolution of the Universe [284]. This catapulted the ΛCDM model, which describes a Universe filled by a cosmological constant Λ and cold dark matter (CDM), to the centre stage of modern cosmology.

The current Standard Model of Cosmology, or simply Concordance Model, describes a universe that at the present time is dominated by two dark components: CDM and DE, the latter in the form of a cosmological constant; but also considers the contribution of photons, in the form of the CMB radiation, of cosmic neutrinos and of non-relativistic baryons. As such, we can write the Friedmann equation as

$$H^2 = H_0^2 \left[\Omega_{\rm r,0}\left(\frac{a_0}{a}\right)^4 + \Omega_{\rm m,0}\left(\frac{a_0}{a}\right)^3 + \Omega_{\mathcal{K},0}\left(\frac{a_0}{a}\right)^2 + \Omega_{\Lambda,0}\right]\,, \tag{1.38}$$

where a 0-subscript indicates evaluation at the present time. In Eq. (1.38), $\Omega_{\rm r,0} = \Omega_{\gamma,0} + \Omega_{\nu,0}$ is the current fractional energy density of ultra-relativistic matter and includes a contribution from photons, $\Omega_{\gamma,0}$, and light neutrinos, $\Omega_{\nu,0}$. The current fractional energy density of pressureless matter is given by $\Omega_{\rm m,0} = \Omega_{\rm c,0} + \Omega_{\rm b,0}$ and includes a contribution from CDM, $\Omega_{\rm c,0}$, and from non-relativistic baryons, $\Omega_{\rm b,0}$, while the contribution of DE is given by $\Omega_{\Lambda,0}$. A contribution from spatial curvature is included in $\Omega_{\mathcal{K},0}$.

The recently released final results from the Planck mission [19], in conjunction with data from baryonic acoustic oscillations (BAO), indicate that the best fit value of the expansion rate at the

Parameter	Best-fit Value	Description
H_0	67.70	Hubble rate in km s^{-1}Mpc^{-1}
Age	13.78	Age of the Universe in billions of years (Gyr)
$\Omega_{\Lambda,0}$	0.6894	Contribution of non-relativistic matter
$\Omega_{\mathrm{m},0}$	0.3106	Contribution of non-relativistic matter
$\Omega_{\mathrm{c},0}$	0.2601	Contribution of DM
$\Omega_{\mathrm{b},0}$	0.04898	Contribution of non-relativistic baryons
$\Omega_{\mathcal{K},0}$	0.0007	Contribution of spatial curvature
$T_{\gamma,0}$	2.7255	Temperature of the photons of the CMB in K
$\Omega_{\gamma,0}$	5.395×10^{-5}	Contribution of the photons of the CMB
$\Omega_{\nu,0}$	3.732×10^{-5}	Contribution of relativistic neutrinos

Table 1.1.: Some cosmological parameters of the Concordance Model and their values obtained from the best fit values for the baseline 6-parameter ΛCDM model using the final 2018 results of the Planck mission [19] with BAO data.

present time is $H_0 = 67.70$ km s^{-1}Mpc^{-1}, and confirm that the two biggest contributions to the total energy density are from DE, $\Omega_{\Lambda,0} \simeq 0.69$, and pressureless matter, $\Omega_{\mathrm{m},0} \simeq 0.31$, with baryonic matter accounting for roughly 16% of the latter. The contribution of the curvature term is small, $|\Omega_{\mathcal{K}}| < 0.003$, indicating that at the present time the Universe is extremely flat. Assuming a (widely tested) black-body distribution for the CMB, the total energy density of photons is given as [352]

$$\rho_{\gamma,0} = \frac{\pi^2}{15\hbar^3} T_{\gamma,0}^4 \,. \tag{1.39}$$

where $T_{\gamma,0}$ is the present temperature of the photons of the CMB. Using the value $T_{\gamma,0} = 2.7255$ K (0.23 meV) obtained in Ref. [158], we find that cosmic photons account for less than 1 part in 10^4 of the current energy density of the Universe. The neutrino energy density is usually written in terms of $\rho_{\gamma,0}$ and the effective number of degrees of freedom, N_{eff}, through the parametrisation [135, 249]

$$\rho_{\nu,0} = \frac{7}{8}\left(\frac{4}{11}\right)^{4/3} N_{\mathrm{eff}}\, \rho_{\gamma,0} \,. \tag{1.40}$$

In the Standard Model of Particles, with three families of leptons, the prediction for the effective number of relativistic degrees of freedom is $N_{\mathrm{eff}} = 3.046$, where the small deviation from 3 arises from considering a non-instantaneous decoupling between neutrinos and the photon-baryon plasma before the electron-positron annihilation [249]. Historically, a small excess of $\Delta N_{\mathrm{eff}} := N_{\mathrm{eff}} - 3.046$ has been inferred from CMB observations, leaving open the possibility for the existence of an additional relativistic fluid that does not interact with light, the so called *dark* radiation [37, 181, 259]. This scenario is somewhat disfavoured by the final results of the Planck mission, which in combination with BAO data, leads to $N_{\mathrm{eff}} = 2.99^{+0.34}_{-0.33}$ [19]. Nevertheless, higher values of the effective number

Event	Time after BB	Redshift (z)	Temperature (T)
Electroweak phase transition	20 ps	10^{15}	100 GeV
QCD phase transition	20 μ	10^{12}	150 MeV
Neutrino decoupling	1 s	6×10^9	1 MeV
Big Bang Nucleosynthesis	3 min	4×10^8	0.1 MeV
Radiation-matter equality	60 kyr	3365	0.8 eV
Recombination	260 kyr	1300	0.3 eV
Decoupling	380 kyr	1090	0.26 eV
Re-ionisation	100 kyr	9	2.4 meV
Matter-DE equality	9 Gyr	0.3	0.3 meV
Present	13.8 Gyr	0	0.23 meV

Table 1.2.: Some key events in the history of the Universe based on the Concordance Model and the best-fit values from the 2018 results of Planck mission [19].

of degrees of freedom are still compatible with the data as long as H_0 is allowed to take on larger values. Restricting the analysis to the physically motivated range $\Delta N_{\rm eff} > 0$ leads to the constraint $\Delta N_{\rm eff} < 0.30$ at 95% confidence level [19].

Behind the apparently simple formula (1.38), the Concordance Model hides several key ideas of modern cosmology developed throughout the last century. Using only GR and the well known physics behind the Standard Model of Particles, it successfully describes an expanding universe that from an initial state with a temperature well above the GeV mark (the Hot Big Bang), undergoes a series of phase transitions which are triggered by the cooling down of the primordial plasma. Once the temperature reaches 0.1 MeV, at redshift $z \sim 10^8$, the process of the BBN kicks in, leading to the primordial abundances of light elements, and at 0.8 eV, $z \sim 3400$, the energy density of non-relativistic particles overcomes that of radiation; thus starts the matter-dominated epoch which promotes the growth of inhomogeneities that lead to the large scale structure (LSS) observed today. Around $T \sim 0.3$ eV, $z \sim 1300$, the first atoms start to form amid the plasma of free electrons and nuclei; shortly after, the decoupling of photons and free electrons is completed and the Universe becomes transparent to photons. This creates the last scattering surface, the remains of which form the CMB radiation. At this point, the Universe enters the so called dark ages, a period during which very little light was produced and only ends with the formation of the first stars and galaxies. Around redshift 10, $T \sim 2.4$ meV, these newly formed structures illuminate the Universe and re-ionise the neutral hydrogen in the intergalactic medium, thus creating the Lyman-α forest. Finally, at $z \sim 0.3$, when the temperature of the Universe is very close to the one observed today, the matter-dominated epoch ends once DE takes over and starts to re-accelerate the Universe.

1.5. Primordial Inflation

The Cosmological Principle, which is one of the main pillars of modern cosmology, is also intimately related to one of the biggest conceptual headaches of the Concordance Model. At the time of the last scattering surface, the celestial sphere corresponded to over 10^4 regions that had been causally disconnected for 380 thousand years. As such, the high degree of isotropy found in the CMB radiation can only be explained by fine-tuning the Universe to be extremely homogeneous at the time of the Hot Big Bang. However, no mechanism capable of setting up this degree of homogeneity is available in the Concordance model.

A solution to this so called Horizon Problem was offered by Demosthenes Kazanas [206] and Alan H. Guth [179] in the form of an initial epoch of extremely rapid growth of the scale factor. This fast primordial expansion, dubbed *inflation* by Guth, would stretch very small and homogeneous regions of space-time by several orders of magnitude in such a short period of time that inhomogeneities and anisotropies would not have time to grow, thus providing a mechanism for the fine-tuned initial conditions of the Hot Big Bang model[8]. Coincidentally, a similar inflationary period was being considered at the same time by Alexey A. Starobinsky in the context of quantum modifications of gravity [324, 325] although no mention is made to a resolution of the Horizon Problem. Shortly after, a new mechanism of inflation based on the slow-roll of a scalar field along its potential was introduced by Andrei D. Linde [235] and Andreas Albrecht and Paul J. Steinhardt [25]. Although this new inflation sought to address some problem in Guth's model related to the reheating phase, it was quickly realised that some fine-tuning of the potential and initial conditions was required in order for inflation to occur. This issue was tackled by Linde in his models of chaotic inflation [236] in which an epoch of accelerated expansion can occur for very generic initial conditions. The following years it was shown that quantum perturbations generated during inflation can also act as the seeds for the LSS observed today, with current observations preferring a near-scale-invariant primordial power-spectrum which is compatible with a wide range of single field inflation models.

The inflationary paradigm has since become widely accepted as the most *probable* mechanism to solve several shortcomings of the Hot Big Bang cosmology, and is usually considered as an integral part of the Concordance Model. Nevertheless, the idea of primordial inflation is not without its critics and several alternative paradigms to explain the Horizon Problem continue to be explored, e.g., the ekpyrotic [208] or matter bounce [156] scenarios. After the 2013 results of Planck mission [13] imposed severe constraints on the tensor-to-scalar ratio, which have been confirmed by the full mission data [18], several models that were traditionally favoured, like power-law inflation or chaotic inflation from monomial potentials, have been ruled out. Instead, models of single field inflation similar to Starobinsky's R^2 inflation [325], with concave ($\mathrm{d}^2V/\mathrm{d}\varphi^2 < 0$) nearly flat potentials during inflation are preferred by the data. This has led to a renewed interest in extended theories of gravity as a mechanism to fuel primordial inflation.

[8] In addition, to the Horizon Problem, the inflationary paradigm also solves the Flatness Problem under which the apparent flatness of the Universe could only be explained by fine-tuning $\Omega_{\mathcal{K}}$ in the distant past. A period of primordial inflation solves this problem by setting $\Omega_{\mathcal{K}}$ very close to zero at the beginning of the radiation-dominated epoch. In the context of Grant Unified Theories, a period of primordial inflation also solves the Monopole Problem, since any initial distribution of magnetic monopoles and other relics would be extremely diluted by the end of inflation [232].

1.6. Beyond the Standard Model

In the current era of precision cosmology, the Concordance Model with an initial epoch of primordial inflation allows us to describe and understand most of the last 14 billion years of our Universe using only a diminutive set of parameters. Its success stands as one of the biggest achievements of modern physics. However, several questions are still left unanswered (for a review on the future of cosmology beyond the concordance model, please see Ref. [93]), with the most immediate ones being related to the nature of the two unknown dark fluids that together comprise about 95% of the Universe. In fact, since the ΛCDM model is purely phenomenological in nature, it presents no clue on the possible origin of these fluids.

While the presence of a DM-like component is essential to obtaining correct predictions from BBN calculations [310], the growth of the LSS and gravitational lensing [186] or to explaining the rotation velocity curves of galaxies [307] and the gravitational potentials in the Bullet cluster [250], little is still known about DM beyond its gravitational effects. For a review on the current status of the search regarding the nature of DM, including a list of current DM candidates such as Weakly Interacting Massive Particles, axions and axion-like particles, primordial black holes or modified gravity, please see Refs. [40, 304].

The picture is not better when we turn our attention to DE. The historical interpretation of DE as vacuum energy fails to predict the observed value by 120 orders of magnitude, leading to the so called Cosmological Constant Problem [358]. Even if we accept the point of view that DE is nothing more than a true cosmological constant and therefore a fundamental constant of Nature, we are still left with the issue of why it became dominant only at the late time evolution, precisely only after allowing the growth of cosmological structures (Coincidence Problem). In broad terms, the various proposals of alternatives to a cosmological constant can be classified in two main categories: (i) dynamical dark energy models, where the laws of gravitation of GR are maintained and the current acceleration of the Universe is caused by a dynamical fluid, or field, that evolves in time; (ii) modified theories of gravity, where DE is in fact a manifestation of a deviation from GR in the laws of gravitation at large scales and as such no extra matter fluid is required.

Even the inflationary paradigm, despite being widely accepted as a simple and elegant solution to several shortcomings of the Hot Big Bang cosmology, does not come free of problems. While it manages to adequately set-up the initial conditions for a classical homogeneous and isotropic universe, it does not provide a clear answer as to how primordial inflation came to be or what, if anything, came before it, attracting criticism that it pushes the problem of initial conditions back in time instead of actually solving it. Furthermore, since an inflationary regime can be obtained through a multitude of models and can be embedded in several extensions of GR or quantum gravity proposals, we may lack a way of understanding which physical mechanism is responsible for the primordial acceleration of the Universe. This situation is aggravated by the lack of evidence of a cosmic background of gravitational waves, a general prediction of inflation, in the B-mode polarisation of the CMB [14, 15]. It is hoped that gravitational waves of cosmological origin will be detected in future observational missions, either through polarisation of the B-modes [173], or through direct detection [48].

From an observational point of view, there are also reasons to explore scenarios beyond ΛCDM. For example, a tension persists in the best-fit values of cosmological parameters obtained from the CMB versus those obtained from low redshift measurements, with the latter finding systematically

lower values of $\Omega_{\mathrm{m},0}$ and a larger Hubble rate [6, 245]. The existence of other inconsistencies between observations and theoretical predictions at small scales [93] are viewed by some as an indication that the dark sector of the Concordance Model needs to be modified. In addition, several anomalies in the CMB are yet to be resolved, such as the low quadrupole ($\ell = 2$) anomaly, the dip the in the angular power spectrum at $20 \lesssim \ell \lesssim 30$, or the cold spot on the southern hemisphere, first detected by the WMAP mission [56] and confirmed by Planck as true features of the CMB [19].

Dynamical Dark Energy

Since the ΛCDM model provides no explanation for the nature of DE, several alternatives have been proposed in the literature to explain the late time acceleration. In this regard, one of the main approaches is to consider that instead of a cosmological constant or vacuum energy with $w = -1$, DE is some unknown dynamical field or matter fluid capable of fuelling an accelerated expansion. Such an approach seeks to preserve GR as the theory of gravitation, as well as the assumption of homogeneity and isotropy in the late Universe, at the expense of introducing exotic matter in our Universe that can violate the Null Energy Condition. Perhaps the most widespread class of dynamical DE are the so called Quintessence models [101, 293], where the late time acceleration is obtained through a scalar field slow-rolling down a potential, much like in single field inflation. Alternatives to this scenario include models based on the Chaplygin gas [57, 60, 205] and 3-form fields [216, 217]. In some cases, a dynamical DE is incorporated in a unified description of the dark sector including DM. These are the so called *unified dark matter-energy* models (UDM), of which the Chaplygin Gas is one of the first examples. From a phenomenological point of view, several parametrisations of the EoS parameter w have been considered in the literature, such as the wCDM model or the CPL parametrisation [116, 237] (for additional strategies employed in the parametrisation of DE please see Ref. [194]). However, despite these efforts in trying to explain the current acceleration of the Universe, no significant deviations from a cosmological constant have been observed so far–the 1-year results of the Dark Energy Survey point to $w = -1$ [6] even when the wCDM parametrisation is considered–foiling hopes that characteristic imprints from a dynamical DE would be detected [367].

Dark Interactions

The idea that the unknown components of the Universe, namely DM and DE, have some kind of interaction either between them or with other forms of mater can be seen as natural: *If we know so little about their nature and given that they overwhelmingly dominate the energy content of the Universe then why should interactions not be considered?* and as potentially necessary: *Given that neither DM or DE seems to interact with light, some other way of detecting them is necessary in order for us to understand what comprises them*.

From a more fundamental point of view, the idea of interactions involving DM also finds motivation in the idea that DM is in fact a very massive particle yet to be discovered. If so, future observational missions may be ale to detect imprints from DM decaying into lighter particles, or being scattered in galaxy or cluster collisions. Several attempts have been made to derive constrains on the interacting properties of DM using cluster collisions [250], interactions with solar neutrinos [230], gamma-ray emissions in DM-rich dwarf galaxies [10, 273, 317], X-ray emissions from galaxy clusters [92, 201], or measuring couplings to the electromagnetic fields [172]. A review of current and future searches for

evidence of interactions in different DM models can be found in Refs. [128, 304].

Due to the lack of an obvious candidate for DE based on fundamental physics, interactions involving DE tend to be more phenomenological in nature and usually take into account only pressureless matter as the other interacting component, so that $Q_{\rm DE} = -Q_{\rm m} = Q$. A usual interaction term considered in the case of Quintessence models with a scalar field φ is $Q \propto 3\dot{\varphi}\rho_{\rm m}$ [32], which can be readily interpreted as coming from a ϕ-dependence of the mass of the matter particles. Other interaction terms considered in the literature include $Q \propto 3\Gamma\rho_{\rm m}$ and $Q \propto 3(\dot{a}/a)\rho_{\rm m}$ which can be interpreted for example as a decay or production of massive particles with a production/annihilation rate proportional to Γ or $\dot{a}/a$ [64, 98, 99, 345]. Variations found in the literature include replacing $\rho_{\rm m}$ by a linear combination of $\rho_{\rm m}$ and $\rho_{\rm DE}$ [68, 98, 99, 117] or by the *quadratic* term $\rho_{\rm m}\rho_{\rm DE}/(\rho_{\rm m}+\rho_{\rm DE})$ [38, 68, 78, 99], or even considering a dependence on the derivatives $\dot{\rho}_{\rm m}$ and $\dot{\rho}_{\rm DE}$ [68]. It has been shown that UDM models can also be stated in the context of interacting DE by choosing an appropriate interaction term [351]. More recently, several works have explored the possibility of using the action functionals developed by[9] J. David Brown [89] to find Lagrangian based formulations of interactions between DE and DM [58, 66, 67, 153, 220, 291], in an attempt to eliminate ambiguities in the definition of the interaction 4-vector Q_μ.

Current analysis based on data from CMB, low redshift space distortions and cosmic chronometers on the interaction between DM and DE suggest that in wCDM models an energy transfer occurs from DM to DE when $-1 < w_{\rm DE}$ and from DE to DM when a (mild) phantom behaviour ($w_{\rm DE} < -1$) is considered [125, 154, 155, 277, 345]. An interaction between matter and a running vacuum energy has also been found to alleviate some of the discrepancies between CMB and LSS measurements [309, 318] and it has been argued that it could explain the Coincidence Problem [125, 155, 318]. Despite showing a preference for an interacting model, these results do not exclude the ΛCDM model and the derived constraints on the coupling constants indicates that the interaction must be mild until the present time.

Modified Gravity

The road to modified (or extended) theories of gravity is a long and rich one. Since the birth of Einstein's theory of gravitation in 1915 [145], many different proposals of theories of gravity have been put forward, from Brans-Dicke models [85] and Hordenski's generalisation of scalar-tensor theories [187] to the studies on renormalisability of quadratic gravity by Stelle [328, 329] and Starobinsky's famous R^2 model [325]. For a review on this topic please see for example Ref. [104, 152].

So far, GR has passed with bright colours all the tests designed to check its limits [360] and it is in perfect agreement with the recent detection of gravitational waves [2] and with the results of the 26-year long Gravity collaboration that analysed the orbit of the star S2 around the massive black hole in the centre of the Milky Way [8]. In fact, the multi-messenger detection of gravitational waves from the black hole-neutron star binary [3] has led to severe constraints on potential modifications of GR, in practice excluding from cosmological applications at late-time all theories that predict a deviation between the speed of light and the speed of the gravitational waves. Nevertheless, there are many

[9] Earlier efforts on the topic of hydrodynamical fluids in curved space-times include works by Abraham H. Taub [331], Bernard F. Schutz [314, 315] and by Schutz and Rafael Sorkin [316]. A review on this topic that includes physical applications can be found in Ref. [33].

extensions of GR that satisfy the constraints imposed by gravitational wave astronomy and many indications still subsist that a modified theory of gravity may need to be considered, from the known problems to explain the nature of DE, the capability of MOND to tackle several shortcomings of the ΛCDM model at small scales [93], to the preference of the R^2 model to explain the low tensor-to-scalar ratio implied by the results of Planck [18]. In addition, many models of modified gravity can be obtained as the low energy limit of more fundamental theories, such as string theory, that try to unify gravity with the other fundamental forces.

Effects of Quantum of Gravity

Finding a theory of Quantum Gravity has been one of the more elusive pursuits of modern physics in the XX and XXI centuries. After the introduction of GR in 1915, it was soon realised [88] that the geometrical nature of gravity and its intricate connection to the space-time created serious difficulties in repeating the successes of obtaining a quantum description for the other fundamental forces. In 1967, Bryce DeWitt published his Canonical Theory of Quantum Gravity [137] which built on the efforts from Paul Dirac [138, 139] and from Richard Arnowitt, Stanley Deser and Charles Misner [39], among others, to provided the first full theory that attempted to quantise gravity. In that seminal work, DeWitt also presented for the first time the Wheeler–DeWitt (WDW) equation, which serves as an analogous to the Schrödinger equation for GR. However, the fact that the inner-product associated to this equation is not positive definite has created ambiguities in interpretation of the solutions of the theory [202, 221], even in the simplest of models, which to date have not yet been completely resolved. Nevertheless, the WDW equation has served as one of the pillars of subsequent attempts to quantise gravity, such as loop quantum gravity and string theory. For reviews of the history and of the current status of the different approaches to Quantum Gravity, please see [211, 260, 305].

Due to the weak coupling of gravity to matter, it is expected that the effects of quantum gravity will only become important at very high energy densities or in regions of the space-time where the curvature is close to the Planck scale. Within the context of cosmology, it is generally expected that quantum effects of gravity play a crucial role in the earlier stages of the Universe. In addition to the fact that quantum fluctuations during the primordial inflation can act as the seeds for the LSS and the anisotropies of the CMB, there have been various attempts to use Quantum Gravity to explain the very beginning of our Universe and to provide a mechanism that sets the proper conditions for inflation to occur. In addition, it has been shown that quantum effects can be crucial in avoiding certain future cosmological singularities [23, 29].

If any imprints of these early times are left on the primordial power spectrum at the end of inflation, then they should lead to the appearance of special features in the CMB. Coincidentally, the existence of several anomalies in the angular power spectrum of the CMB at the largest scales [18, 19], precisely the ones that are expected to be more sensitive to pre-inflationary effects, provide a window to search for new physics and hints of Quantum Gravity. Furthermore, the recent detection of gravitational waves and the possibility of measuring the cosmological background of gravitational waves in the next decades, either directly or through the B-mode polarisation of the CMB, might provide us with a new important way of probing Quantum Cosmology in the early Universe.

2 Tools to characterise cosmological models

As the list of proposed extensions and modifications to the Concordance Model grows, so does the need for more advanced methods and techniques that can successfully select viable candidates to describe our Universe. In order to be considered as viable, a given cosmological model should not only be able to accommodate the current observational data, but also verify a certain degree of *naturalness*, i.e., it should be compatible with the cosmological observations without the need for fine-tuning the parameters of the model. The fact that extensions to the Standard Model of Cosmology usually introduce new degrees of freedom and parameters to the theory can also be seen as a double-edged sword. While the increased flexibility in the dynamics can in principle reduce the deviation between theoretical predictions and observations, the higher number of parameters has the undesired consequence of lowering the goodness of the fit. In fact, one of the main strengths of the ΛCDM model is that it is able to adjust the current observations to an astounding level of precision with a minimal set of parameters. In addition, the great level of freedom in how to extend the Standard Model of Cosmology[1] can lead to the existence of several viable cosmological models with very different underlying physical motivations but which are difficult to distinguish, at least at the level of the FLRW background geometry. It is, therefore, desirable to have a toolbox of methods that is capable to characterise a given cosmological model, identify its characteristic imprints and to provide a measure of the generality of the dynamics and the capacity to reproduce the observational data without a need for fine-tuning.

In this chapter, we present the main techniques that will be used in this thesis to characterise the models presented in the ensuing chapters. The methods presented here give emphasis to a phenomenological and theoretical approach to cosmology and therefore do not employ a detailed analysis of the observational data. Instead, we focus on providing a characterisation of the dynamics of a given model and on computing the theoretical predictions for cosmological observables, at the level of the FLRW background and of the linear scalar cosmological perturbations.

2.1. Dynamical system analysis

An explicit solution of the continuity equation (1.30) is usually only available for the simplest models, as in the case of a fluid with constant EoS parameter w. In contrast, for models with additional

[1] This can be viewed as a consequence of the lack of a unequivocal guiding principle, either from fundamental physics or from cosmological observations, on how to extend the theory.

degrees of freedom, a numerical integration of the equations of motion may be required to determine the evolution of the model. While these solutions are of interest on their own, in particular if special regimes of the model can be identified, the fact that they depend on the initial conditions specified for the integration means that they do not necessarily capture all of the interesting features of the model. In this sense, a dynamical system approach has long proven to be a useful tool in cosmology, allowing us to obtain a qualitative description of the system, to identify possible initial and final states, or even, in some cases, to estimate the probability of the occurrence of certain kinds of behaviour. Within the context of late-time cosmology and primordial inflation, dynamical system analysis has recurrently been used in models with different types of matter fields, such as scalar fields, K-essence and 3-forms, and in models of modified theories of gravity or quantum cosmology in a semi-classical regime. A compendium on the application of dynamical systems in cosmology can be found in Refs. [121, 346], while a recent review can be found in [44].

Perhaps the most common application of a dynamical system analysis found in literature is the case of a universe filled by a scalar field φ with a potential $V(\varphi)$. For completeness, here we also consider the presence of a pressureless fluid (e.g., DM).Following the strategy defined in Ref. [124**?**]

$$y := \sqrt{\frac{\kappa^2}{6}}\frac{\dot{\varphi}}{H}\,, \qquad z := \sqrt{\frac{\kappa^2}{3}}\frac{\sqrt{V}}{H}\,, \qquad s := \sqrt{\frac{\kappa^2}{3}}\frac{\sqrt{\rho_{\rm m}}}{H}\,, \tag{2.1}$$

which have the advantage of possessing a clear physical interpretation: y^2 and z^2 correspond, respectively, to the fractional kinetic and potential energy densities of the scalar field, while s^2 corresponds to the fractional energy density of the pressureless matter. As such, they respect the Friedmann constraint (1.37) which can now be written as

$$1 = y^2 + z^2 + s^2\,. \tag{2.2}$$

In order to obtain a closed system of evolution equations, we can define an additional variable based on the scalar field[2], e.g, $X := \sqrt{3\kappa^2/2}\varphi$. Then, using the constraint (2.2) to eliminate the variable s, we obtain a 3-dimensional set of equations[3] that completely describes the evolution of the system:

$$\tilde{X}_x = 3y\,, \tag{2.3}$$

$$y_x = -\frac{3}{2}\left[\left(1 - y^2 + z^2\right)y - \frac{\lambda(X)}{3}z^2\right]\,, \tag{2.4}$$

$$z_x = \frac{3}{2}\left[1 + y^2 - z^2 - \frac{\lambda(X)}{3}y\right]z\,. \tag{2.5}$$

Here, an x subscript corresponds to a derivative with respect to $x := \log(a/a_*)$, a_* being an arbitrary constant, and the factor $\lambda(\varphi)$ is defined as

$$\lambda(X) := -\frac{3}{V}\frac{\mathrm{d}\,V}{\mathrm{d}\,X}\,. \tag{2.6}$$

[2]Other common choices for an additional dynamical variable that provide a closed set of evolution equations include a compact function of φ, which allows us to obtain a compact phase space, or the quotient $\lambda(\varphi)$, defined in Eq. (2.6), which can be used as long as $(\mathrm{d}^2V/\mathrm{d}\varphi^2)/(\mathrm{d}V/\mathrm{d}\varphi)$ is an invertible function of φ.

[3]In the particular case of the exponential potentials, the variable φ decouples from the rest of the system, allowing for a further reduction of the dimensions of the system [124].

Notice that, due to the presence of a factor V^{-1} in the r.h.s. of Eq. (2.6), the strategy described above is not applicable to the cases where the potential of the scalar field has zeroes at finite values of φ, e.g., monomial potentials $V \propto \varphi^n$. In such cases, a different, usually model dependent, approach need to be employed, as in the case of Refs. [26, 27].

The main focus of a dynamical system analysis is to study the trajectories of a set of differential equations in order to better understand the dynamics of the model and possibly to identify approximate behaviours in certain regions of the phase space. One of the most important steps in order to achieve this goal is to study the position and stability of the fixed points of the system, i.e., the static solutions of the evolution equations. While the position of a given fixed point can provide us with information regarding the value of physical quantities, determining its stability allows us to determine whether the static solution corresponds to a possible initial (repulsive) or final (attractive) state of the system, or even if it represents an approximate solution that some trajectories follow before being repelled away from the fixed point.

In the case of the system defined above, the fixed points $\{X_{\rm fp},\, y_{\rm fp},\, z_{\rm fp}\}$ can be found simply by solving the set of Eqs. (2.3)–(2.5) for $X_x = y_x = z_x = 0$. On the other hand, determining the local or global stability of the system around $\{X_{\rm fp},\, y_{\rm fp},\, z_{\rm fp}\}$ usually reveals itself a more laborious task. While various methods can be found in the literature to determine the stability of a fixed point, in this work, we will focus mainly on three:

- Linear Stability Theory

  If all the eigenvalues γ_i of the Jacobian of the system (2.3)–(2.5) at a fixed point $\{X_{\rm fp},\, y_{\rm fp},\, z_{\rm fp}\}$ have non-zero real part, then the fixed point is called hyperbolic and its stability can be determined using linear stability theory. Eigenvalues with negative real part represent directions[4] along which the trajectories evolve towards the fixed point, while eigenvalues with positive real part correspond to directions along which the trajectories move away from $\{X_{\rm fp},\, y_{\rm fp},\, z_{\rm fp}\}$. As such, we can classify a hyperbolic fixed point as attractive (stable) if all its eigenvalues have negative real part, as repulsive (unstable) if all its eigenvalues have positive real part and as a saddle if some eigenvalues have negative real part and others have positive real part.

- Centre Manifold Theory.

  If for an isolated fixed point, the Jacobian of the system (2.3)–(2.5) has at least one eigenvalue with vanishing real part, then the use of linear stability theory is no longer valid. Instead, we can employ methods based on centre manifold theory [65, 111, 295]. In general, such methods consist in separating the system into its stable, unstable and centre manifolds, each of which is associated, respectively, to the eigenvalues with negative, positive and zero real part. Then, an appropriate mapping of the stable and unstable manifolds onto the centre manifold allows us to determine the stability of the fixed point.

[4] The directions along which the system is stable or unstable correspond to the ones given by the eigenvector $\vec{v}_i$ associated to the eigenvalue γ_i.

- Linear Stability for Non-Isolated Fixed Points

  In the case that the system (2.3)–(2.5) admits as static solutions the elements of a continuous set $\mathcal{N}_\alpha$ characterised by a parameter α, any $\{X_{\rm fp}, y_{\rm fp}, z_{\rm fp}\} \in \mathcal{N}_\alpha$ is called a non-isolated fixed point. Here, linear stability theory breaks down since at least one of the eigenvalues, whose eigenvector corresponds to a direction tangent to $\mathcal{N}_\alpha$, is zero. Nevertheless, if all other eigenvalues have non-zero real part, then the fixed point is called normally hyperbolic [41, 121] and the stability of the system along the directions orthogonal to $\mathcal{N}_\alpha$ can be decided by applying Linear Stability Theory to the reduced set of non-zero eigenvalues.

2.2. Cosmography and Statefinder parameters

Once a given cosmological model is considered and the matter content fixed, Eqs. (1.27), (1.28) and (1.30) allow us to fully describe the evolution of a FLRW universe. However, the solutions obtained in this way have the obvious drawback of being model dependent, not only with regards to the matter fluids considered but also, in a more general setting, to the theory of gravity employed. As an alternative, Steven Weinberg proposed the use of cosmography [357], which aims to provide a kinematic-based characterisation of the Universe. Since the FLRW line-element (1.18) represents the most general description for a homogeneous and isotropic universe, a cosmographic approach can in principle be used to derive "model-independent" constraints on the matter content of the Universe, or even on the laws of gravitation [43, 69, 73, 107, 108, 343, 344].

The starting point in cosmography is a Taylor expansion of the scale factor around the present time. Considering the cosmic time ($N = 1$) as the independent variable, we obtain [343, 344]

$$\frac{a}{a(t_0)} = 1 + H_0\,(t-t_0) - \frac{q_0}{2}H_0^2\,(t-t_0)^2 + \frac{j_0}{3!}H_0^3\,(t-t_0)^3 + \frac{s_0}{4!}H_0^4\,(t-t_0)^4 + \frac{l_0}{5!}H_0^5\,(t-t_0)^5 + \mathcal{O}\,(t-t_0)^6\,, \tag{2.7}$$

where a 0-subscript indicates evaluation at $t = t_0$. The cosmographic parameters q, j, s and l are called *deceleration parameter*, *jerk*, *snap* and *lerk*, respectively, and are defined as [343, 344]

$$q := -\frac{1}{a}\frac{\mathrm{d}^2 a}{\mathrm{d}t^2}H^{-2}\,, \qquad j := \frac{1}{a}\frac{\mathrm{d}^3 a}{\mathrm{d}t^3}H^{-3}\,, \qquad s := \frac{1}{a}\frac{\mathrm{d}^4 a}{\mathrm{d}t^4}H^{-4}\,, \qquad l := \frac{1}{a}\frac{\mathrm{d}^5 a}{\mathrm{d}t^5}H^{-5}\,. \tag{2.8}$$

Notice that knowing the cosmographic parameters is equivalent to knowing the expansion of the Universe, since inverting the relations in (2.8) allows us to write down the time derivatives of the Hubble rate in terms of the cosmographic parameters [107]:

$$\dot{H} = -H^2\,(q+1)\,, \tag{2.9}$$

$$\ddot{H} = H^3\,[(j-1)+3\,(q+1)]\,, \tag{2.10}$$

$$\dddot{H} = H^4\left[(s-1)-4\,(j-1)-3\,(q+1)^2-6\,(q+1)\right]\,, \tag{2.11}$$

$$\ddddot{H} = H^5\left\{(l-1)-5\,(s-1)+10\,(j-1)\,[10+(q+1)]+30\,(q+1)^2+10\,(q+1)\right\}\,. \tag{2.12}$$

Higher order derivatives can be obtained in a similar fashion by extending the cosmographic expansion (2.7) and, as a general rule, each new time derivative of the Hubble rate depends linearly on the cosmographic parameter of corresponding order.

In an expanding universe, a photon emitted at a time t_* with a wave-length λ_*, is redshifted at the present time according to the relation [225]

$$1+z=\frac{\lambda(t_0)}{\lambda(t_*)}=\frac{a_0}{a(t_*)}\,. \tag{2.13}$$

This redshift effect is essential to determine how long ago a given photon was emitted and how far did it travel before being detected on Earth. However, the various cosmological distances used in the literature, such as the physical distance[5] [108, 344]

$$D=c\int_{t_*}^{t_0}\mathrm{d}t=c\,(t_0-t_*)\,, \tag{2.14}$$

or the luminosity distance [108, 344]

$$D_L=c\frac{a(t_0)}{a(t_*)}\int_{t_*}^{t_0}\mathrm{d}t\frac{a(t_0)}{a(t)}\,, \tag{2.15}$$

require the knowledge of the evolution of the Universe since the instant t_* till the present time. This limitation can be circumvented by using cosmography to derive approximate relations between the various cosmological distances and the redshift z that depend solely on quantities evaluated at the present time.

For example, in the case of the physical distance D, we can apply a cosmographic expansion to the r.h.s. of Eq. (2.13) which, after using the definition (2.14) to eliminated t_*-t_0 in favour of D/c, allows us to relate the redshift z with the cosmographic parameters through [344]

$$z=\frac{H_0}{c}D+A_2\frac{H_0^2}{c^2}D^2+A_3\frac{H_0^3}{c^3}D^3+A_4\frac{H_0^4}{c^4}D^4+A_5\frac{H_0^5}{c^5}D^5+\mathcal{O}\left(H_0D/c\right)^6\,. \tag{2.16}$$

Here, the coefficients A_i are defined by

$$A_2=\frac{1+(q_0+1)}{2}\,, \tag{2.17}$$

$$A_3=\frac{1+(j_0-1)+6\,(1+q_0)}{3!}\,, \tag{2.18}$$

$$A_4=\frac{1-(s_0-1)+8\,(j_0-1)+6\,(q_0+1)^2+24\,(q_0+1)}{4!}\,, \tag{2.19}$$

$$A_5=\frac{1+(l_0-1)-10\,(s_0-1)+20\,(j_0-1)\,(3+q_0)+90\,(q_0+1)^2+80\,(q_0+1)}{5!}\,. \tag{2.20}$$

Notice that to first order in D, Eq. (2.16) reduces to the original Hubble's law $v=H_0D$ with $v=cz$ [193]. An inversion of the series in (2.16) allows us to obtain $D(z)$ to arbitrary order in z, providing us

[5] In the definitions (2.14) and (2.15), we leave explicit the dependence on the speed of light c, which in the rest of this thesis is set to 1.

with non-linear corrections to the relation between the physical distance travelled by a photon emitted by source at a given redshift and detected on Earth at the present. Such a relation depends only on the present day values $\{q_0,\, j_0,\, s_0,\, l_0\}$ and not on the precise history of the expansion of the universe since the photon was emitted. In a similar fashion, other cosmological distances can be described in terms of the cosmographic parameters, as presented in Refs. [108, 344].

If the theory of gravitation is specified, cosmography can also be employed to set constraints on the EoS of the matter content of the Universe. In Ref. [343], this possibility is explored by considering a Taylor expansion:

$$\frac{P(\rho)}{\rho_0} = w_0 + c_{a,0}^2 \left(\frac{\rho}{\rho_0} - 1\right) + \frac{P_0^{(2)}\rho_0}{2}\left(\frac{\rho}{\rho_0} - 1\right)^2 + \frac{P_0^{(3)}\rho_0^2}{3!}\left(\frac{\rho}{\rho_0} - 1\right)^3 + \mathcal{O}\left(\frac{\rho}{\rho_0} - 1\right)^4 , \tag{2.21}$$

where the coefficients in the expansion are defined as[6]

$$w := \frac{P}{\rho}\,, \qquad c_a^2 := \frac{\mathrm{d}P}{\mathrm{d}\,\rho} = \frac{\dot{P}}{\dot{\rho}}\,, \qquad P^{(2)} = \frac{\mathrm{d}^2 P}{\mathrm{d}\,\rho^2}\,, \qquad P^{(3)} = \frac{\mathrm{d}^3 P}{\mathrm{d}\rho^3}\,. \tag{2.22}$$

The first term in the expansion (2.21) corresponds to the EoS parameter w while the coefficient in the second term is usually called the adiabatic squared speed of sound c_a^2. Using the cosmographic expressions (2.9)–(2.12) in conjunction with the Friedmann equation, the continuity equation and the EoS expansion (2.21), we can obtain expressions for w, c_a^2, $P^{(2)}$ and $P^{(3)}$ which allow us to characterise the matter content in terms of the cosmographic parameters and the spatial curvature term $\mathcal{K}/(aH)^2$ [343]. As in the case of Eqs. (2.9)–(2.12), each additional order considered in the EoS expansion (2.21) requires the knowledge of an additional cosmographic parameter.

Despite the interesting premise of cosmography of finding model independent constraints on the evolution of the Universe, the great difficulties in obtaining precise measurements for the jerk and the snap (and of course the lerk) mean that any practical application of the cosmographic approach beyond the deceleration parameter is, at the moment, severely limited. An additional limitation comes from the fact that the one-to-one mapping found for the simple case of $P(\rho)$ is not maintained in models with more degrees of freedom, e.g., if DE is modelled by a scalar field with an unknown potential $V(\varphi)$ or by metric $f(R)$-gravity [95]. This lack of correspondence, as well as the existence of an apparent bias of the results on the variable used to perform the cosmographic expansion, led the authors[7] of Ref. [95] to strongly criticise the use of cosmography, stating that "this method seems unable to provide reliable or useful results for cosmological applications".

The Statefinder Hierarchy

An alternative point of view for the application of cosmography is to use the coefficients of the cosmographic expansion as discriminators between different cosmological models. This is the strategy

[6] In the case of non-barotropic fluids, the total derivatives with respect to the energy density in (2.22) can be expanded in terms of time derivatives.

[7] The lack of a one-to-one correspondence between the cosmographic parameters and the cosmological parameters had been previously pointed out to us by Ruth Lazkoz and Vincenzo Salzano in a private conversation.

employed in Refs. [21, 308] in which a pair of statefinder parameters $\{r^{\rm SF},\, s^{\rm SF}\}$ constructed from the deceleration parameter and the jerk were introduced as a diagnostic for DE models[8]. These were later generalised to higher orders in the cosmographic expansion by the introduction of the statefinder hierarchies [34]

$$S_3^{(1)} := j = r^{\rm SF}\,, \qquad S_3^{(2)} := \frac{1}{3}\frac{S_3^{(1)}-1}{q-1/2} = s^{\rm SF}\,, \tag{2.23}$$

$$S_4^{(1)} := s + 3\,(q+1)\,, \qquad S_4^{(2)} := \frac{1}{\alpha}\frac{S_4^{(1)}-1}{q-1/2}\,, \tag{2.24}$$

$$S_5^{(1)} := l - 2\,(3q+4)\,(q+1)\,, \qquad S_5^{(2)} := \frac{1}{\alpha}\frac{S_5^{(1)}-1}{q-1/2}\,, \tag{2.25}$$

where α is an arbitrary constant. It was argued by the authors of Ref. [34] that the second hierarchy of statefinders, $S_i^{(2)}$ helps to break the degeneracies with regards to the DE energy density and recent studies based on BAO data support the statefinder hierarchy as a suitable tool to distinguish DE models [355]. One of the main points in the definitions of $S_i^{(1)}$ and $S_i^{(2)}$ is that the statefinder parameters are normalised with regards to the standard cosmological model; it can be checked that for ΛCDM, we have $\{S_i^{(1)},\, S_i^{(2)}\} = \{1,\, 0\}$ at all orders. As such, the statefinder hierarchy is said to define a null diagnostic for the ΛCDM model.

2.3. Growth of Structure and the Composite Null Diagnosis

After the moment of radiation-matter equality, when the Universe starts to be dominated by non-relativistic baryonic matter, the pressure of radiation is no longer capable of preventing the collapse of matter. As a consequence, initially small perturbations in the energy density of the background FLRW start to grow in amplitude once their characteristic size becomes smaller than the Hubble horizon, eventually leading to the appearance of the LSS observed today. The growth of these structures is usually described in terms of the perturbation density contrast of matter:

$$\delta_{\rm m}(t,\,\vec{x}) := \frac{\rho_{\rm m}(t,\,\vec{x}) - \bar{\rho}_{\rm m}(t)}{\bar{\rho}_{\rm m}(t)}\,. \tag{2.26}$$

The evolution of $\delta_{\rm m}$ can be obtained in a self-consistent way by using the cosmological perturbation theory [215, 270] up to arbitrary order. In particular, for small perturbations satisfying $|\delta_{\rm m}| < 1$, we can restrict the analysis to linear order[9], which has the advantage of allowing a Fourier decomposition of the cosmological perturbations into independent Fourier modes[10]

$$\delta_{{\rm m},\vec{k}}(t) = \int \frac{{\rm d}^3\vec{k}}{(2\pi)^{3/2}}\delta_{\rm m}(t,\,\vec{x})\,{\rm e}^{{\rm i}\vec{k}\cdot\vec{x}}\,. \tag{2.27}$$

[8] Here, we introduce the superscript SF when referring to the statefinder pair $\{r^{\rm SF},\, s^{\rm SF}\}$ defined in [21, 308] so as to avoid confusion with previous notation.

[9] Please see the Appendix A for a quick review of the Theory of Linear Cosmological Perturbations

[10] Due to the high level of isotropy, it is usually assumed that the Fourier modes depend only on the amplitude of the wavelength $k := |\vec{k}|$ and not on the direction of $\vec{k}$. As such, from this point onwards we drop the vectorial notation in the subscript of the Fourier modes.

For a ΛCDM universe, or in models where the perturbations of DE can be disregarded, the evolution of $\delta_{\mathrm{m},k}(t)$ in the Newtonian gauge[11] is given by the closed equation [134]:

$$\ddot{\delta}^{(N)}_{\mathrm{m},k} + 2H\left[1+\Delta_1(k)\right]\dot{\delta}^{(N)}_{\mathrm{m},k} - \frac{\kappa^2\bar{\rho}_{\mathrm{m}}}{2}\left[1+\Delta_0(k)\right]\delta^{(N)}_{\mathrm{m},k} = 0\,, \tag{2.28}$$

where the mode-dependent factors Δ_i are defined as

$$\begin{aligned}\Delta_1(k) :=& -\frac{9}{2}\frac{\Omega_{\mathrm{m}}\left(\frac{aH}{k}\right)^2 - 3\Omega_{\mathrm{m}}\left(1+2\frac{\dot{H}}{H^2}\right)\left(\frac{aH}{k}\right)^4}{2-9\Omega_{\mathrm{m}}\left(\frac{aH}{k}\right)^2 - 27\Omega_{\mathrm{m}}\left(\frac{aH}{k}\right)^4} \\ \approx& -\frac{9}{4}\Omega_{\mathrm{m}}\left(\frac{aH}{k}\right)^2 + \mathcal{O}\left[\left(\frac{aH}{k}\right)^4\right], \end{aligned} \tag{2.29}$$

$$\begin{aligned}\Delta_0(k) :=& 6\frac{\left(1+2\frac{\dot{H}}{H^2}\right)\left(\frac{aH}{k}\right)^2 - 9\Omega_{\mathrm{m}}\left(1+\frac{\dot{H}}{H^2}\right)\left(\frac{aH}{k}\right)^4}{2-9\Omega_{\mathrm{m}}\left(\frac{aH}{k}\right)^2 - 27\Omega_{\mathrm{m}}\left(\frac{aH}{k}\right)^4} \\ \approx& 3\left(1+2\frac{\dot{H}}{H^2}\right)\left(\frac{aH}{k}\right)^2 + \mathcal{O}\left[\left(\frac{aH}{k}\right)^4\right]. \end{aligned} \tag{2.30}$$

For modes well inside the Hubble horizon, i.e., for $k^2 \gg a^2H^2$, we find that the factors Δ_i vanish at leading order in aH/k and Eq. (2.28) reduces to

$$\ddot{\delta}^{(N)}_{\mathrm{m},k} + 2H\dot{\delta}^{(N)}_{\mathrm{m},k} - \frac{\kappa^2}{2}\bar{\rho}_{\mathrm{m}}\delta^{(N)}_{\mathrm{m},k} = 0\,. \tag{2.31}$$

The same equation can be deduced from Newtonian perturbation theory and for the comoving density contrast $\delta^{(C)}_{\mathrm{m},k}$, showing that at small scales all these different quantities coincide. In the rest of this section, and unless stated otherwise, we consider that the regime $k^2 \gg a^2H^2$ holds and drop the superscript (N).

During the matter dominated era, the general solution of Eq. (2.31) is

$$\delta_{\mathrm{m},k} = C_1 a^{-3/2} + C_2 a\,. \tag{2.32}$$

where C_1 and C_2 are integration constants. This linear growth of matter perturbations in a matter dominated universe is a well known prediction of GR and is expected to be affected in modified theories of gravity where an effective gravitational coupling G_{eff} is introduced, e.g., metric $f(R)$-gravity [322]. Once DE starts to dominate and accelerates the background, the growth of the matter density perturbations is slowed down and can be characterised through the linear growth function $D(a)$

$$D(a) := \frac{\delta_{\mathrm{m},k}(a)}{\delta_{\mathrm{m},k}(a_0)}\,. \tag{2.33}$$

[11] The issue of gauge dependence of the perturbation variables was a major source of confusion in the field of cosmological perturbations until the seminal work of James M. Bardeen [46], where the theory was re-stated in terms of gauge-invariant (GI) quantities. In this thesis, a perturbation δX with a superscript (N) indicates a GI invariant quantity that reduces to δX in the Newtonian gauge, cf. Eq. (A.54), while a perturbation δX with a superscript (C) indicates a GI invariant quantity that reduces to δX in the comoving gauge, cf. Eq. (A.56). A further discussion on this issue can be found in the Appendix A and references therein.

In the CDM and ΛCDM models, D is independent of the scale considered, however, in more rich DE models or in modified theories of gravity a mode dependence can appear. Thus, $D(a)$ can provide a powerful tool to discriminate between different late-time models.

An alternative way of characterising the growth of structure is to define the growth rate

$$f(a) := \frac{\mathrm{d}\log D(a)}{\mathrm{d}\log a}\,. \tag{2.34}$$

Notice that $f(a) = 1$ during the matter dominated era when the matter density perturbations grow linearly with the scale factor. For DM–DE models that closely mimic ΛCDM, i.e., with a slowly varying EoS parameter $w_{DE} \approx -1$, it was found that the growth rate at late-time can be approximated reasonably well by the mode-independent parametrisation [238, 239, 354]

$$f(a) \simeq \Omega_{\mathrm{m}}^{\gamma}(a)\,. \tag{2.35}$$

Here, $\gamma = \gamma(a)$ is the growth index, which for ΛCDM reads $\simeq 0.55$ to leading order in $1/a$ [239]. By integrating Eq. (2.34) we can write $D(a)$ in terms of the growth index as

$$D(a) = \exp\left(\int_{a_0}^{a} \frac{\Omega_{\mathrm{m}}^{\gamma}}{a}\mathrm{d}\,a\right)\,. \tag{2.36}$$

In Ref. [34], the statefinder hierarchy (2.23)–(2.25) was complemented with information about the growth of structure by using the fractional growth rate

$$\epsilon(a) := \frac{f(a)}{f_{\Lambda\mathrm{CDM}}(a)}\,, \tag{2.37}$$

By construction, $\epsilon = 1$ in the case of ΛCDM, meaning that statefinder hierarchy together with the fractional growth parameter $\epsilon(a)$ forms a composite null diagnosis (CND) for ΛCDM.

2.4. The Matter Power Spectrum

The distribution of a given linear perturbation $\delta_{\vec{k}}(t)$ in the momentum space can be characterised by the power spectrum $P_\delta(\vec{k}) := \langle|\delta_{\vec{k}}|^2\rangle$ through the relation [338]:

$$\langle\delta_{\vec{k}}(t)\,\delta_{\vec{k}'}(t)\rangle = (2\pi)^{3/2}\delta^{(3)}(\vec{k}+\vec{k}')\,P_\delta(t,\,\vec{k})\,. \tag{2.38}$$

Here, $\langle\cdot\rangle$ denotes an average over realisations and $\delta^{(3)}(\vec{k}+\vec{k}')$ is the 3-dimensional delta function in momentum space. Under the assumption of homogeneity and isotropy, the power spectrum depends only on the amplitude $k = |\vec{k}|$ and we can write simply $P_\delta(t,\,k)$.

Of particular interest in late-time cosmology is the power spectrum of the matter density contrast $P_{\delta_{\mathrm{m}}}(t,\,k)$, or simply matter power spectrum, which provides a measure of the collapse of matter into structures of size $\lambda = 1/k$. Its shape and amplitude are sensitive not only to the characteristics of DM, but also to non-clustering components, such as DE and massive neutrinos, non-linear effects such as BAO, and to the theory of gravitation considered. In Fig. 19 of Ref. [19], it can be seen that the

linear matter power spectrum predicted by the Concordance Model, with initial conditions compatible with single field inflation, provides an extremely good fit to the observations from different sources; in particular, the shape of $P_\delta(k)$ is heavily constrained in the range $\times 10^{-2}\ h\ \text{Mpc}^{-1} \lesssim k \lesssim 2 \times 10^{-1}\ h\ \text{Mpc}^{-1}$. Therefore, $P_{\delta_\text{m}}(t,\, k)$ can be used as a powerful tool to discriminate viable models for the late-time evolution of the Universe.

Observationally, the matter power spectrum is related to the number density of galaxies, δ_g, which, in the absence of non-Gaussianities, can be related to the density contrast of DM through the k-independent bias parameter b [350]:

$$\delta_g = b\,\delta_\text{c}\,. \tag{2.39}$$

In Refs. [90, 350], it was argued that, under the assumption that galaxies are comoving with the surrounding DM halos, the bias parameter should be defined in the rest frame of DM. As such, the theoretical predictions for P_{δ_m} should be computed using a GI quantity[12] that reduces to δ_m in the frame comoving with pressureless matter. Such a quantity can be constructed as[13]

$$\delta^{(C)}_{\text{m},k} := \delta_{\text{m},k} + \frac{a}{N}\frac{\dot{\bar{\rho}}_\text{m}}{\bar{\rho}_\text{m}}\,(v_{\text{m},k} + B) = \delta^{(N)}_{\text{m},k} - 3aHv^{(N)}_{\text{m},k}\,, \tag{2.40}$$

where v_m is the peculiar velocity potential of pressureless matter, B is the potential that defines the perturbation of the shift vector for scalar cosmological linear perturbations and $v^{(N)}_{\text{m},k}$ is the GI quantity that reduces to v_m in the Newtonian gauge[14]. After these considerations, we can write the theoretical prediction of the matter power spectrum as

$$P_{\delta_\text{m}} = \langle|\delta^{(C)}_{\text{m},k}|^2\rangle = \langle|\delta^{(N)}_{\text{m},k} - 3aHv^{(N)}_{\text{m},k}|^2\rangle\,. \tag{2.41}$$

While P_δ characterises the distribution of the perturbations in the momentum space, the distribution in real-space coordinates is described by the two-point correlation function [338]

$$\xi_\delta(t,\,\vec{r}) = \langle\delta(t,\,\vec{x})\,\delta(t,\,\vec{x}+\vec{r})\rangle\,, \tag{2.42}$$

which corresponds to the Fourier transform of the power spectrum[15] $P_\delta(t,\,k)$:

$$\xi_\delta(t,\,\vec{r}) = \int \frac{\mathrm{d}^3\vec{k}}{(2\pi)^{3/2}} P_\delta(t,\,k)\,\mathrm{e}^{\mathrm{i}\vec{k}\cdot\vec{r}} = (2\pi)^{3/2}\int \frac{\mathrm{d}k}{k}\,\frac{k^3}{2\pi^2}P_\delta(t,\,k)\frac{\sin(kr)}{kr}\,. \tag{2.43}$$

Under the assumption of isotropy, the two-point correlation function depends only on the distance $r = |\vec{r}|$ between two points and not on the direction $\vec{r}$. It gives a measure of the probability that, for a random galaxy at a point $\vec{x}$, another galaxy is found at a distance r.

From the two-point correlation function, we can calculate the variance of the distribution of the

[12] Following Bardeen [46], any physical observable should be represented by a GI quantity.

[13] In the last equality of Eq. (2.40), we have assumed the absence of interaction for pressureless matter so that the continuity equation reads $\dot{\bar{\rho}}_\text{m} = -3(\dot{a}/a)\bar{\rho}_\text{m}$.

[14] For a more complete discussion and definition of these quantities, please see the Appendix A.

[15] The dimensionless quantity $k^3/(2\pi^2)P_\delta(t,\,k)$ found in the integrand of the r.h.s. of Eq. (2.43), is commonly preferred in the context of primordial inflation in detriment of $P_\delta(t,\,k)$. As such, it is usually referred to as the primordial power spectrum and will be denoted in this thesis by $\mathcal{P}_\delta(t,\,k)$ [352].

perturbations as [338]

$$\sigma^2 := \langle \delta(t,\, x)\, \delta(t,\, x) \rangle = \xi_\delta(t,\, 0)\,. \tag{2.44}$$

Then, we can relate σ with the power spectrum P_δ by using Eq. (2.43). In practice, the variance is computed using a window function W_R that selects galaxy counts inside a volume with a characteristic radius R:

$$\sigma_R^2 = (2\pi)^{3/2} \int \frac{\mathrm{d}k}{k} \frac{k^3}{2\pi^2} P_\delta(t,\, k) W_R^2(k)\,. \tag{2.45}$$

Typical choices for the window functions include the Gaussian and top-hat functions [338]. One particularly important parameter in cosmology is the root mean square of the variance of mass perturbations on a sphere of radius $R = 8\ h^{-1}$Mpc, computed with a top-hat window function. This parameter, denominated σ_8, is employed in the normalisation of the amplitude of the matter power spectrum and can help to mitigate the effect of some degeneracies in the data through the use of certain specific parameter combinations, such as $f\sigma_8$ in redshift space distortions measurements [319] and $S_8 := \sigma_8(\Omega_\mathrm{m})^{0.5}$, which was found to minimise the correlation with Ω_m in cosmic shear experiments [335].

2.5. The Primordial Power Spectrum

According to the paradigm of primordial inflation, small quantum fluctuations in the primordial Universe are amplified during inflation and act as the seeds for the classical perturbations in the Hot Big Bang cosmology, which eventually lead to the anisotropies of the CMB in the last scattering surface and to the LSS observed today. One quantity that is of special interest in order to connect the primordial quantum perturbations with the distribution of the classical perturbations during the radiation dominated epoch is the GI comoving curvature perturbation [49, 53]

$$\mathcal{R} := \psi - \frac{a}{N}\frac{\dot{a}}{a}(v + B) = \Psi - \frac{a}{N}\frac{\dot{a}}{a} v^{(N)}\,, \tag{2.46}$$

where B and ψ are one of the four metric potentials that characterise the scalar sector of the cosmological perturbations, cf. Eq. (A.9) for the complete perturbed FLRW line element, and Ψ is the Bardeen potential that reduces to ψ in the Newtonian gauge [46]. From the perturbed Einstein field equations it is possible to derive the equation for the time derivative of $\mathcal{R}$ for a given Fourier mode [53]:

$$\dot{\mathcal{R}}_k = \frac{1}{1+\bar{w}}\frac{\dot{a}}{a}\left[-\frac{\delta P_k^{(\mathrm{nad})}}{\bar{\rho}} + \frac{1}{3\Omega^{(\mathrm{m})}} \left(\frac{k}{aH}\right)^2 \left(\frac{\kappa^2}{3}\Pi_k + 2c_a^2 \Psi_k \right) \right]\,, \tag{2.47}$$

where $\delta P^{(\mathrm{nad})}$ is the non-adiabatic component of the isotropic pressure (cf. Eq. (A.48)) and Π is the anisotropic stress potential (cf. Eq. (A.42)). From this equation we find that, under adiabatic conditions, the comoving curvature perturbation remains constant during super-horizon evolution ($k \ll aH$). Thus, for most of the physically relevant modes, we can use the value of $\mathcal{R}$ at the end of inflation to set-up the initial conditions for perturbations during the radiation dominated epoch,

without having to specify the mechanism of reheating.

The value of the comoving curvature perturbation $\mathcal{R}$ at the end of inflation is usually given in terms of the primordial power spectrum [49]

$$\mathcal{P}_{\mathcal{R}}(k) = \frac{k^3}{2\pi^2}|\mathcal{R}_k|^2\,, \tag{2.48}$$

where we recall that the lack of dependence on the direction of $\vec{k}$ reflects the isotropic evolution of the Universe. This is commonly parameterised as

$$\mathcal{P}^{\rm fit}_{\mathcal{R}}(k) = A_S\left(\frac{k}{k_*}\right)^{n_s-1}\,, \tag{2.49}$$

where k_* is a pivot scale, A_s is the normalisation of the primordial power spectrum at the pivot scale and n_s is the scalar spectral index. In the Planck mission, the pivot scale was chosen to be 0.05 Mpc^{-1} and the final best-fit values for the parameters of the primordial power spectrum, when BAO measurements are included, are $A_s = 2.107\times10^{-9}$ and $n_s = 0.9682$ [19], confirming a preference for a near scale-invariant but red-tilted power spectrum that excludes a pure de Sitter inflation at more than 8σ [18]. A deviation from (2.49) is nevertheless possible as long as the corresponding scales are sufficiently far away from[16] k_*. In fact, any imprints of a pre-inflationary evolution are expected to appear at very large scales, $k \ll k_*$, while the reheating dynamics could affect scales much smaller than the pivot scale, $k \gg k_*$. Modifications of the primordial power spectrum at small scales have also been proposed as a mechanism to create primordial black holes [163].

In the case of single field inflation, where we can write the peculiar velocity of the scalar field as $v_\varphi + B = (N/a)\delta\varphi/\dot{\varphi}$, the evolution of the scalar perturbations during inflation is usually computed in terms of the Mukhanov-Sasaki variable[17] [215, 269, 270, 311]

$$v := a\left(\delta\varphi + \frac{\dot{\varphi}}{\dot{a}/a}\psi\right) = z\mathcal{R}\,, \qquad\qquad z := a\frac{\dot{\varphi}}{\dot{a}/a}\,, \tag{2.50}$$

as the second order variation of the action reduces, in the conformal time η ($N = a$), to that of a simple harmonic oscillator with variable mass [53, 267]:

$$\delta^{(2)}\mathcal{S} = \frac{1}{2}\int \mathrm{d}\eta\,\mathrm{d}^3\vec{x}\left[(v')^2 - \mathrm{D}_i v\,\mathrm{D}^i v + \frac{z''}{z}v^2\right]\,. \tag{2.51}$$

In the previous equation, a prime indicates a derivative with respect to the conformal time η and D_i is the covariant derivative with respect to the 3-metric γ_{ij} defined in Eq. (1.20). Using a Legendre transformation, we are able to write down the corresponding Hamiltonian and apply a canonical quantisation procedure that promotes v to a quantum operator $\hat{v}$ evolving on a classical FLRW background. This operator can then be decomposed into mode functions v_k which satisfy the

[16] Through reconstruction methods, the pure power-law behaviour of the primordial power spectrum was confirmed by the Planck mission in the range 0.005 Mpc$^{-1} \lesssim k \lesssim 0.2$ Mpc^{-1} [18].

[17] Here, we remind the reader that despite the use of the letter v for the Mukhanov-Sasaki variable, it does not represent a velocity potential. We choose to follow the notation found in the literature hoping that it does not lead to any confusion. In addition, the variable z defined in Eq. (2.50) has no connection with the cosmological redshift.

Mukhanov-Sasaki equation [53, 268]

$$v_k'' + \left(k^2 - \frac{z''}{z}\right) v_k = 0\,, \tag{2.52}$$

and verify the normalisation condition [53, 268]

$$v_k v_k^{*\prime} - v_k' v_k^* = \mathrm{i}\hbar\,. \tag{2.53}$$

After computing the evolution of v_k until the moment of horizon crossing, we can use the definition (2.50) to write $\mathcal{P}_{\mathcal{R}}(k)$ given in Eq. (2.48) in terms of v_k:

$$\mathcal{P}_{\mathcal{R}}(k) = \frac{k^3}{2\pi^2}\frac{|v_k|^2}{z^2}\,. \tag{2.54}$$

2.6. The CMB angular power spectrum

The anisotropies in the CMB can be described in terms of the temperature fluctuations in the black body distribution of the cosmic photons [140, 352]:

$$T_\gamma(t,\,\vec{x},\,\vec{p}) = \bar{T}_\gamma(t) + \delta T_\gamma(t,\,\vec{x},\,\vec{p}) = \bar{T}_\gamma(t)\left[1 + \Theta(t,\,\vec{x},\,\vec{p})\right]\,. \tag{2.55}$$

Here, $\vec{x}$ and $\vec{p}$ are the position and direction of propagation of the photon and $\bar{T}_\gamma(t)$ is the temperature of the background radiation fluid. In order to analyse the profile of temperature perturbations in the celestial sphere, it is advantageous to decompose $\Theta(t,\,\vec{x},\,\vec{p})$ in spherical harmonics $Y_{\ell m}$:

$$\Theta(t,\,\vec{x},\,\vec{p}) = \sum_{\ell=0}^{+\infty}\sum_{m=-\ell}^{+\ell} a_{\ell m}(t,\vec{x}) Y_{\ell m}(\vec{p})\,, \tag{2.56}$$

where the coefficients $a_{\ell m}(t,\vec{x})$ encode the information regarding the temperature fluctuations at a multipole ℓ. In a background that is isotropic on average, the mean value of all the $a_{\ell m}(t,\vec{x})$'s vanishes while its variance can be expressed in terms of the angular power spectrum $C_\ell := \langle |a_{\ell m}|^2\rangle$ as [140, 352]

$$\langle a_{\ell m}^* a_{\ell' m'}\rangle = \delta_{\ell\ell'}\,\delta_{mm'} C_\ell(t)\,, \tag{2.57}$$

Due to the homogeneity and isotropy assumptions, the angular power spectrum cannot depend either on the position $\vec{x}$ or the multipole moments m. The coefficients $a_{\ell m}(t,\vec{x})$ can also be related to the Fourier mode $\Theta_{\vec{k}}(t,\vec{p})$ by multiplying (2.56) by $Y_{\ell' m'}(\vec{p})$, integrating over the angular section of $\vec{p}$ and using the orthonormality of the spherical harmonics to write [140]

$$a_{\ell m} = \int \mathrm{d}\,\Omega_p\,\Theta(t,\,\vec{x},\,\vec{p}) Y_{\ell m}^*(\vec{p}) = \int \frac{\mathrm{d}^3\vec{k}}{(2\pi)^{3/2}}\mathrm{d}\,\Omega_p\,\Theta_{\vec{k}}(t,\,\vec{p}) Y_{\ell m}^*(\vec{p})\,\mathrm{e}^{\mathrm{i}\vec{k}\cdot\vec{x}}\,. \tag{2.58}$$

Assuming that the photons of the CMB are free streaming since the time of the last scattering, we can write $\vec{x} = -D_*\vec{p}$, where $D_* = \eta_0 - \eta_*$ is the comoving distance to the surface of last scattering. This

allows us to write down the angular power spectrum in terms of the dimensionless power spectrum of the temperature fluctuations as [140, 352]

$$C_\ell(t_*) = 4\pi \int_0^{+\infty} \frac{\mathrm{d}k}{k} \mathcal{P}_\Theta(t_*,\, k)\, j_\ell^2(kD_*)\,. \tag{2.59}$$

where $j_\ell(z)$ is the spherical Bessel function [7, 283]. Since the function $j_\ell^2(kD_*)$ peaks at $k = \ell/D_*$, the previous equation is well approximated by [352]

$$C_\ell(t_*) \approx \frac{\pi}{2\ell(\ell+1)} \mathcal{P}_\Theta(\ell/D_*)\,, \tag{2.60}$$

leading to the definition of the normalised angular power spectrum $D_\ell := \ell(\ell+1)/(2\pi)C_\ell$. After three generations of observational missions – CoBE, WMAP and Planck – the features of the CMB over the whole sky have been mapped to an astounding precision and have provided us with one of the pictures of the evolution of the Universe over 14 billion years, since the Hot Big Bang till the present time, and over a wide range of scales. From the amplitude and position of the peaks on the angular power spectrum, the near scale invariant shape at low multipoles or the exponential damping at high ℓ, we are able to probe such different aspects of the Concordance Model, such as the physics of inflation, the spatial geometry of the Universe, the density of DM and of non-relativistic baryons, the signature of DE through the integrated Sachs–Wolfe and the Rees–Sciama effects or the photon diffusion that affects the smallest scales.

For each multipole ℓ, the number of independent estimates of the angular power spectrum is reduced to $2\ell+1$ due to the fact that we have access to only one Universe. As such, the observed value of C_ℓ^{obs} averaged over multipole moments is given by

$$C_\ell^{\mathrm{obs}} = \frac{1}{2\ell+1} \sum_{m=-\ell}^{+\ell} (a_{\ell m}^{\mathrm{obs}})^* a_{\ell m}^{\mathrm{obs}}\,, \tag{2.61}$$

and has a minimum theoretical uncertainty of

$$\frac{\Delta C_\ell}{C_\ell} = \sqrt{\left\langle \left(\frac{C_\ell - C_\ell^{\mathrm{obs}}}{C_\ell} \right)^2 \right\rangle} = \sqrt{\frac{2}{2\ell+1}}\,. \tag{2.62}$$

This is the formula of the well known Cosmic Variance that limits our knowledge of the Universe for low multipoles, i.e., at the largest scales observed today.

PART II

Late Universe

3 Modified Gravity: $f(R)$-gravity

In this chapter we consider the effects of a modified theory of gravity, in particular of metric $f(R)$-gravity [104, 130, 152, 322], which generalises the EH gravitational action to include a non-linear dependence on the scalar curvature. This idea was first proposed by H. A. Buchdahl [91] and has gained redoubled attention in the last decade as a possible candidate to explain the dark sector of the Universe and the recent success of the R^2 model [325] in explaining the current observation from the primordial Universe [18]. We begin this chapter by presenting a brief review of the main properties of $f(R)$-gravity and its applications to Cosmology. We then move on to present a novel reconstruction method in which an appropriate $f(R)$ action is deduced by imposing a barotropic EoS $P(\rho)$ for the total matter content of the Universe. Finally, in the last section, we discuss the possibility that dark radiation, an excess of relativistic content not accounted for by the CMB photons or the three families of neutrinos in the Standard Model of particles, is a manifestation of modified gravity. The main results in this chapter were published in Ref. [264].

3.1. Metric $f(R)$-gravity: A brief review

3.1.1. The $f(R)$ action

If we take in mind the interpretation of modified gravity as an extension of GR, then we can write the $f(R)$ action as an EH term, cf. Eq. (1.1), plus a *modification* term which depends on a generic function $f(R)$ of the scalar curvature R [130, 152, 322]:

$$\mathcal{S}^{(f)} = \frac{1}{2\kappa^2}\int \mathrm{d}^4x\sqrt{-g}\,[R + f(R)]\ . \tag{3.1}$$

It can be easily verified that the EH action with a cosmological constant can be accommodated by setting $f(R) = -2\Lambda$. If in addition to the action (3.1) we consider the presence of matter fields, $\mathbf{\Psi}^i$, minimally coupled to gravity, the total action is given by

$$\mathcal{S} = \frac{1}{2\kappa^2}\int \mathrm{d}^4x\sqrt{-g}\,[R + f(R)] + \mathcal{S}^{(\mathrm{m})}[g_{\mu\nu}, \mathbf{\Psi}^{(\mathrm{i})}]\,. \tag{3.2}$$

After minimising the total action (3.2) with regards to variations of the metric $g_{\mu\nu}$ and lowering one index, we obtain the generalised Einstein equations of metric $f(R)$-gravity [130, 152, 322]:

$$(1+f_R)G^{\mu}{}_{\nu} + \frac{1}{2}\left(Rf_R - f\right)\delta^{\mu}_{\nu} - \left(\nabla^{\mu}\nabla_{\nu} - \delta^{\mu}_{\nu}\Box\right) f_R = \kappa^2 [T^{(\mathrm{m})}]^{\mu}{}_{\nu}\,, \tag{3.3}$$

where $\Box := \nabla^{\mu}\nabla_{\mu}$ is the d'Alembert operator and $f_R := (\mathrm{d}f/\mathrm{d}R)$.

Since we are considering that matter is minimally coupled to gravity, the stress-energy-momentum tensor $[T^{(\mathrm{m})}]^{\mu}{}_{\nu}$ is divergenceless and the usual continuity relations for the matter content are recovered. This can be checked by taking the divergence of Eq. (3.3) and using the Bianchi identities and the definition of the Einstein tensor to obtain

$$R^{\mu}{}_{\nu}\nabla_{\mu} f_R - \left(\Box\,\nabla_{\nu} - \nabla_{\nu}\Box\right) f_R = \kappa^2 \nabla_{\mu}[T^{(\mathrm{m})}]^{\mu}{}_{\nu}\,. \tag{3.4}$$

From the definition of the Riemann tensor and its symmetry properties we find that the terms on the l.h.s. of the previous equation cancel each other, leading automatically to

$$\nabla_{\mu}[T^{(\mathrm{m})}]^{\mu}{}_{\nu} = 0\,. \tag{3.5}$$

3.1.2. An extra degree of freedom

The modified Einstein field equations (3.3) are, in general, of fourth order in derivatives of the metric. This contrasts with GR, where the equations of motion are of second order, and points to the existence of an extra degree of freedom in metric $f(R)$-gravity. This can be seen more easily by looking at the trace of Eq. (3.3) [130, 152, 322]:

$$3\Box f_R + (f_R - 1)\,R - 2f = \kappa^2 T^{(\mathrm{m})}\,. \tag{3.6}$$

Contrary to GR, this equation is no longer an algebraic relation between the scalar curvature and the trace of the stress-energy-momentum tensor. In fact, for a generic $f(R)$ function, Eq. (3.6) describes the propagation of a new massive scalar degree of freedom, f_R, which is sometimes called *scalaron*.

Following similar results for quadratic gravity (see, e.g., [332] and other references in [322]), it was quickly realised that the action (3.1) of metric $f(R)$-gravity is dynamically equivalent to[1]

$$\mathcal{S}^{(\mathrm{BD})}\frac{1}{2\kappa^2}\int \mathrm{d}^4x\sqrt{-g}\,[\phi R - V(\phi)] + \mathcal{S}^{(\mathrm{m})}[g_{\mu\nu}, \boldsymbol{\Psi}^{(\mathrm{i})}]\,, \tag{3.7}$$

with the identification

$$\phi := 1 + f_R\,, \qquad \text{and} \qquad V(\phi) := R(\phi)(1+f_R) - [R(\phi) + f(R(\phi))]\,. \tag{3.8}$$

The action (3.7) falls in the category of models of massive gravity proposed by O'Hanlon [278] which correspond to a subcategory of Brans-Dicke gravity [85] with Brans-Dicke parameter $\omega_0 = 0$. When viewed as such, metric $f(R)$-gravity can be considered as a scalar-tensor theory, which in turn is a

[1] It is common to find in the literature the statement that the equivalence between metric $f(R)$-gravity and its Brans-Dicke representation depends on the inequality $f_{RR} \neq 0$. More precisely, one requires that the mapping $1+f_R = \phi$ be invertible, of which $f_{RR} \neq 0$ is a sufficient, although not necessary, condition [282].

particular case of the more general framework of Hordenski theories [187]. After the recent constraints on the velocity of gravitational waves derived from the observation of the neutron stars merger event GW170817 [3–5], $f(R)$-gravity is one of the few sub-categories of Hordenski theories that remain a viable candidate for DE [126, 147, 223].

Minimising (3.7) with regards to the metric $g_{\mu\nu}$ and the scalar field ϕ leads to the equations of motion [282, 322]

$$G_{\mu\nu} = \frac{\kappa^2}{\phi} T^{(\mathrm{m})}{}_{\mu\nu} - \frac{1}{2} V(\phi) g_{\mu\nu} + \frac{1}{\phi} \left[\nabla_\mu \nabla_\nu \phi - g_{\mu\nu} \Box \phi \right] , \tag{3.9}$$

$$3\Box\phi + 2V(\phi) - \phi \frac{\mathrm{d}V}{\mathrm{d}\phi} = \kappa^2 T^{(\mathrm{m})} . \tag{3.10}$$

It can be checked that the substitution of (3.8) in the previous two equations leads immediately to the modified Einstein equations (3.3) and the trace equation (3.6). This shows that the actions (3.2) and (3.7) are dynamically equivalent.

The existence of this extra degree of freedom has led to several constraints being introduced to ensure that $f(R)$ is physically viable and free of dynamical instabilities [192, 327]:

1. Imposing that gravity is attractive since BBN implies that the effective gravitational coupling $G_f = G/(1 + f_R)$ must be positive and consequently

$$1 + f_R > 0 , \tag{3.11}$$

   for all R since early times.

2. If the effective gravitational constant at the present time is to match Newton's gravitational constant G, then the extra degree of freedom f_R must verify

$$f_R(a_0) \approx 0 . \tag{3.12}$$

3. The scalaron is not a tachyon [327]

$$f_{RR} > 0 . \tag{3.13}$$

   This condition is intrinsically related to the Dolgov-Kawasaki instability which was first discovered for the model $f(R) = -\mu^4/R$ [141] and later generalised for any $f(R)$ function [151].

4. The existence of stable de Sitter solutions [149, 150] imposes that:

$$m_{\mathrm{eff}}^2 = \frac{(1 + f_R)^2 - 2(R + f) f_{RR}}{(1 + f_R) f_{RR}} > 0. \tag{3.14}$$

   This condition is much weaker than the previous ones since: (i) the early "de Sitter-like" inflationary phase of the universe must be unstable in order for the transition to a radiation-dominated epoch to occur; and (ii) while current observations suggest that our universe is evolving towards a de Sitter-like phase, we cannot guarantee that it will remain so forever.

3.1.3. FLRW cosmology in $f(R)$-gravity

Let us now consider a homogeneous and isotropic universe described by the FLRW line element (1.18). After a substitution in the modified Einstein equations (3.3), the $(0-0)$ and $(i-i)$ components can be written, respectively, as [130, 152, 322]

$$(1+f_R)\left[\left(\frac{\dot{a}}{a}\right)^2+\frac{N^2}{a^2}\mathcal{K}\right]-N^2\frac{Rf_R-f}{6}+\frac{\dot{a}}{a}(\dot{f_R})=\frac{\kappa^2N^2}{3}\rho^{(\mathrm{m})}\,, \tag{3.15}$$

$$(1+f_R)\left[2\frac{\ddot{a}}{a}+\left(\frac{\dot{a}}{a}\right)^2-2\frac{\dot{N}}{N}\frac{\dot{a}}{a}+\frac{N^2}{a^2}\mathcal{K}\right]-N^2\frac{Rf_R-f}{2}+\left(2\frac{\dot{a}}{a}-\frac{\dot{N}}{N}\right)(\dot{f_R})+(\ddot{f_R})$$
$$=\;-\kappa^2N^2P^{(\mathrm{m})}\,. \tag{3.16}$$

Here, we recall that a dot indicates a derivative with respect to the time variable t. These equations, which reduce to Eqs. (1.27) and (1.28) when we set $f(R)\equiv 0$, show that in metric $f(R)$-gravity the gravitational constant $G=\kappa^2/(8\pi)$ is replaced by an effective gravitational coupling $G_f:=G/(1+f_R)$ that depends implicitly on the curvature of space-time through the derivative f_R. Such an effective coupling is characteristic of scalar-tensor theories [148, 152]. In addition to Eqs. (3.15) and (3.16), we can obtain from the trace equation (3.6) the evolution equation for the extra degree of freedom f_R:

$$\ddot{f_R}+\left(3\frac{\dot{a}}{a}-\frac{\dot{N}}{N}\right)\dot{f_R}-\frac{N^2}{3}\left[(f_R-1)\,R-2f\right]=\kappa^2N^2\left(\frac{\rho^{(m)}}{3}-P^{(m)}\right)\,. \tag{3.17}$$

However, out of the three equations (3.15), (3.16) and (3.17) only two are linearly independent.

In the presence of matter, the Einstein field equations and the equation of motion of f_R are complemented by the continuity equation

$$\dot{\rho}^{(\mathrm{m})}+3\frac{\dot{a}}{a}\left(\rho^{(\mathrm{m})}+P^{(\mathrm{m})}\right)=0\,. \tag{3.18}$$

Since (3.18) assumes the same form as in GR, any solution $\rho(a)$ found for a particular EoS remains valid in metric $f(R)$-gravity. However, the dependence of such solution on the cosmic time will be changed as the relation $a(t)$ is dictated by the modified Friedmann equation (3.15).

3.1.4. $f(R)$-gravity as an anisotropic fluid

Contrary to GR, the two Eqs. (3.15) and (3.16) represent a system of fourth order in derivatives of the scale factor. This means that, given a function $f(R)$, finding general solutions for the evolution of the FLRW background is an extremely difficult task, even in the absence of matter. Therefore, when approaching modified theories of gravity from a phenomenological point of view, it is often advantageous to rewrite the modified Einstein equations in such a way that all the new terms coming from the modifications of GR appear on the r.h.s., thus forming a new effective stress-energy-momentum tensor. In the case of metric $f(R)$-gravity, a reorganisation of Eq. (3.3) leads to [51, 130]:

$$G_{\mu\nu}=\kappa^2\left(T^{(\mathrm{m})}_{\mu\nu}+T^{(f)}_{\mu\nu}\right)\,, \tag{3.19}$$

where [51, 130]

$$T^{(f)}_{\mu\nu} = -\frac{1}{\kappa^2}\left[\frac{Rf_R - f}{2}g_{\mu\nu} + (G_{\mu\nu} + g_{\mu\nu}\Box - \nabla_\mu\nabla_\nu)\, f_R\right] . \tag{3.20}$$

Notice that in this representation we no longer consider an effective gravitational coupling for matter, as all the effects of the modification of gravity are now incorporated in $T^{(f)}_{\mu\nu}$. The Bianchi identities and the conservation of the stress-energy-momentum tensor of matter lead automatically to the condition $\nabla_\mu[T^{(f)}]^\mu{}_\nu = 0$.

From the definitions (1.13)–(1.16) and the effective stress-energy-momentum tensor (3.20) we can define the effective fluid quantities for metric $f(R)$-gravity:

$$\rho^{(f)} = \frac{1}{\kappa^2}\left[\frac{Rf_R - f}{2} - u^\mu u^\nu G_{\mu\nu} f_R - h^{\mu\nu}\nabla_\mu\nabla_\nu f_R\right] , \tag{3.21}$$

$$P^{(f)} = -\frac{1}{\kappa^2}\left[\frac{Rf_R - f}{2} + \frac{h^{\mu\nu}}{3}G_{\mu\nu} f_R + \left(\frac{2}{3}h^{\mu\nu} - u^\mu u^\nu\right)\nabla_\mu\nabla_\nu f_R\right] , \tag{3.22}$$

$$[q^{(f)}]_\mu = \frac{1}{\kappa^2}u^\nu h^\rho_\mu\,(G_{\nu\rho} - \nabla_\nu\nabla_\rho)\, f_R\,, \tag{3.23}$$

$$[\pi^{(f)}]_{\mu\nu} = -\frac{1}{\kappa^2}\left(h^\rho_\mu h^\sigma_\nu - \frac{1}{3}h_{\mu\nu}h^{\rho\sigma}\right)(G_{\rho\sigma} - \nabla_\rho\nabla_\sigma)\, f_R\,. \tag{3.24}$$

We thus find that in general the modifications introduced by metric $f(R)$-gravity cannot be mapped onto a perfect fluid [51] unless the symmetries of the space-time impose that Eqs. (3.23) and (3.24) vanish[2]. Following the interpretation of metric $f(R)$-gravity as a scalar-tensor theory, we can define a 4-velocity for the effective fluid as [289, 334]

$$[u^{(f)}]_\mu := \frac{\nabla_\mu f_R}{\sqrt{X}}\,, \qquad\qquad X := -\nabla^\mu f_R \nabla_\mu f_R\,. \tag{3.25}$$

Inserting $[u^{(f)}]_\mu$ in Eqs. (3.21)–(3.24) leads to

$$\rho^{(f)} = \frac{1}{\kappa^2}\left[\frac{Rf_R - f}{2} - [u^{(f)}]^\mu[u^{(f)}]^\nu G_{\mu\nu} f_R - \theta^{(f)}\sqrt{X}\right] , \tag{3.26}$$

$$P^{(f)} = -\frac{1}{\kappa^2}\left[\frac{Rf_R - f}{2} + \frac{1}{3}[h^{(f)}]^{\mu\nu}G_{\mu\nu} f_R + \frac{2}{3}\theta^{(f)}\sqrt{X} - [u^{(f)}]^\mu\nabla_\mu\sqrt{X}\right] , \tag{3.27}$$

$$[q^{(f)}]_\mu = -\frac{\sqrt{X}}{\kappa^2}[a^{(f)}]_\mu + \frac{f_R}{\kappa^2}[u^{(f)}]^\nu[h^{(f)}]^\rho_\mu G_{\nu\rho}\,, \tag{3.28}$$

$$[\pi^{(f)}]_{\mu\nu} = \frac{\sqrt{X}}{\kappa^2}[\sigma^{(f)}]_{\mu\nu} - \frac{f_R}{\kappa^2}\left([h^{(f)}]^\rho_\mu[h^{(f)}]^\sigma_\nu - \frac{1}{3}[h^{(f)}]_{\mu\nu}[h^{(f)}]^{\rho\sigma}\right)G_{\rho\sigma}\,, \tag{3.29}$$

where $\theta^{(f)}$, $[\sigma^{(f)}]_{\mu\nu}$ and $[a^{(f)}]_\mu$ are the expansion rate, shear tensor and acceleration vector of the effective fluid with regards to the 4-velocity defined in Eq. (3.25) and which can be obtained by replacing n_μ by $[u^{(f)}]_\mu$ in Eqs. (1.23) and (1.24).

[2] This is precisely the case in a FLRW universe, where $G_{0i}f_R = \nabla_0\nabla_i f_R = 0$ and $(G_{ij} - \nabla_i\nabla_j)f_R \propto g_{ij}$ imply that both the energy flux $q^{(f)}_\mu$ and the anisotropic stress $\pi^{(f)}_{\mu\nu}$ vanish.

In a FLRW universe, where the r.h.s. of Eq. (3.23) and (3.24) vanish, the energy density and pressure of the effective fluid become [130]

$$\rho^{(f)} = \frac{1}{\kappa^2}\left[\frac{Rf_R - f}{2} - \frac{3}{N^2}\left(\left(\frac{\dot{a}}{a}\right)^2 + \frac{N^2}{a^2}\mathcal{K}\right)f_R - \frac{1}{N^2}\frac{\dot{a}}{a}(\dot{f_R})\right], \tag{3.30}$$

$$\begin{aligned} P^{(f)} = & -\frac{1}{\kappa^2}\left[\frac{Rf_R - f}{2} - \frac{1}{N^2}\left(2\frac{\ddot{a}}{a} + \left(\frac{\dot{a}}{a}\right)^2 - 2\frac{\dot{N}}{N}\frac{\dot{a}}{a} + \frac{N^2}{a^2}\mathcal{K}\right)f_R \right. \\ & \left. - \frac{1}{N^2}\left(2\frac{\dot{a}}{a} - \frac{\dot{N}}{N}\right)(\dot{f_R}) - \frac{1}{N^2}(\ddot{f_R})\right]. \end{aligned} \tag{3.31}$$

With these definitions, we can write Eqs. (3.15) and (3.16) in a GR-like formulation as

$$\left(\frac{\dot{a}}{a}\right)^2 + \frac{N^2}{a^2}\mathcal{K} = \frac{\kappa^2 N^2}{3}\left(\rho^{(\mathrm{m})} + \rho^{(f)}\right), \tag{3.32}$$

$$2\frac{\ddot{a}}{a} + \left(\frac{\dot{a}}{a}\right)^2 - 2\frac{\dot{N}}{N}\frac{\dot{a}}{a} + \frac{N^2}{a^2}\mathcal{K} = -\kappa^2 N^2\left(P^{(\mathrm{m})} + P^{(f)}\right). \tag{3.33}$$

3.1.5. Linear Perturbations in metric $f(R)$

Let us now consider the case of linear perturbations in metric $f(R)$-gravity. In Ref. [270] the evolution of linear scalar perturbations in vacuum, both in the classical and semi-classical regime, was discussed using a conformal transformation $g_{\mu\nu} \to f_R g_{\mu\nu}$ that brings $f(R)$-gravity in the Jordan frame to a scalar field theory in the Einstein frame. Around the same period, a series of papers [196–198] presented the full equations for the linear perturbations in the Jordan frame as a particular case of $f(\phi, R)$ theories. More recently, the renewed interest in modified theories of gravity has led to a further exploration of the dynamics of linear perturbations in $f(R)$-gravity, see for example the extensive list of references in [130]. In fact, metric $f(R)$-gravity has become one of the few examples of modified gravity fully implemented in mainstream cosmological codes [52, 191].

At first order in perturbations, the modified Einstein field equations (3.3) read [134]:

$$(1+f_{\bar{R}})\delta G^{\mu}{}_{\nu} + \left(\bar{R}^{\mu}{}_{\nu} + \delta^{\mu}_{\nu}\bar{\Box} - \bar{\nabla}^{\mu}\bar{\nabla}_{\nu}\right)\delta f_R + \delta^{(1)}\left(\delta^{\mu}_{\nu}\Box - \nabla^{\mu}\nabla_{\nu}\right)f_{\bar{R}} = \kappa^2[\delta T^{(\mathrm{m})}]^{\mu}{}_{\nu}, \tag{3.34}$$

where the third term on the l.h.s. should be read as

$$\begin{aligned} \delta^{(1)}\left(\delta^{\mu}_{\nu}\Box - \nabla^{\mu}\nabla_{\nu}\right)f_{\bar{R}} = & \left(\bar{\nabla}_{\rho}\bar{\nabla}_{\nu}f_{\bar{R}}\right)\delta g^{\mu\rho} - \delta^{\mu}_{\nu}\left(\bar{\nabla}_{\sigma}\bar{\nabla}_{\rho}f_{\bar{R}}\right)\delta g^{\rho\sigma} \\ & -\frac{1}{2}\bar{\nabla}_{\rho}f_{\bar{R}}\left[2\delta^{\mu}_{\nu}\bar{\nabla}^{\lambda}\delta g^{\rho}_{\lambda} + \bar{\nabla}^{\rho}\left(\delta g^{\mu}_{\nu} - \delta^{\mu}_{\nu}\delta g^{\sigma}_{\sigma}\right) - \bar{\nabla}^{\mu}\delta g^{\rho}_{\nu} - \bar{\nabla}_{\nu}\delta g^{\rho\mu}\right]. \end{aligned} \tag{3.35}$$

Although the perturbation δf_R can be related with the metric perturbations through

$$\delta f_R = f_{\bar{R}\bar{R}}\delta R = -f_{\bar{R}\bar{R}}\left(\bar{R}_{\rho\sigma} + \bar{g}_{\rho\sigma}\bar{\Box} - \bar{\nabla}_{\rho}\bar{\nabla}_{\sigma}\right)\delta g^{\rho\sigma}, \tag{3.36}$$

it is advantageous when treating linear perturbations in $f(R)$ gravity to maintain the variable $\delta F := \delta f_R$. In fact, this quantity represents a true extra degree of freedom in the scalar sector which is introduced

by the modifications to gravity in accordance with the discussion in Sect. 3.1.2. Its evolution equation is obtained from the first order perturbation of the trace equation (3.6):

$$\bar{\Box}\delta F + \delta^{(1)}\Box f_{\bar{R}} + \frac{1}{3}\left(\bar{R} - \frac{1+f_{\bar{R}}}{f_{\bar{R}\bar{R}}}\right)\delta F = -\frac{\kappa^2}{3}\left(\delta\rho - 3\delta P\right) , \tag{3.37}$$

where we have used (3.36) to replace δR by $\delta F/f_{\bar{R}\bar{R}}$ and where

$$\delta^{(1)}\Box f_{\bar{R}} = -\left(\bar{\nabla}_\sigma\bar{\nabla}_\rho f_{\bar{R}}\right)\delta g^{\rho\sigma} - \frac{1}{2}\bar{\nabla}_\rho f_{\bar{R}}\left(2\bar{\nabla}^\lambda\delta g^\rho_\lambda - \bar{\nabla}^\rho\delta g^\sigma_\sigma\right) . \tag{3.38}$$

When treating the modifications of gravity in terms of an effective fluid, we find that the first order perturbation of the effective energy density, pressure, energy-flux and anisotropic stress, cf. Eqs. (3.21)–(3.24), with respect to a generic 4-velocity u^μ read

$$\begin{aligned}
\delta\rho^{(f)} = & -\left[\bar{u}^\mu\bar{u}^\nu\delta G_{\mu\nu} + 2\bar{G}_{\mu\nu}\bar{u}^\mu\delta u^\nu + \bar{h}^{\mu\rho}\delta\Gamma^\nu_{\mu\rho}\bar{\nabla}_\nu + 2\bar{u}^\mu\delta u^\nu\bar{\nabla}_\mu\bar{\nabla}_\nu\right]\frac{f_{\bar{R}}}{\kappa^2} \\
& + \left[\frac{\bar{R}}{2} - \bar{u}^\mu\bar{u}^\nu\bar{G}_{\mu\nu} - \bar{h}^{\mu\nu}\bar{\nabla}_\mu\bar{\nabla}_\nu\right]\frac{\delta F}{\kappa^2} , \qquad (3.39) \\
\delta P^{(f)} = & -\frac{1}{3}\left[\bar{u}^\mu\bar{u}^\nu\delta G_{\mu\nu} + 2\bar{u}^\mu\bar{G}_{\mu\nu}\delta u^\nu + \left(2\bar{h}^{\mu\nu} - 3\bar{u}^\mu\bar{u}^\nu\right)\delta\Gamma^\rho_{\mu\nu}\bar{\nabla}_\rho - 2\bar{u}^\mu\delta u^\nu\bar{\nabla}_\mu\bar{\nabla}_\nu\right]\frac{f_{\bar{R}}}{\kappa^2} \\
& - \left[\frac{\bar{R}}{2} + \frac{1}{3}\bar{h}^{\mu\nu}\bar{G}_{\mu\nu} + \left(\frac{2}{3}\bar{h}^{\mu\nu} - \bar{u}^\mu\bar{u}^\nu\right)\bar{\nabla}_\mu\bar{\nabla}_\nu\right]\frac{\delta F}{\kappa^2} , \qquad (3.40) \\
[\delta q^{(f)}]_\mu = & \left[\bar{u}^\nu\bar{u}^\rho\delta u_\mu + \bar{h}^\nu_\mu\delta u^\rho\right]\left(\bar{G}_{\nu\rho} - \bar{\nabla}_\nu\bar{\nabla}_\rho\right)\frac{f_{\bar{R}}}{\kappa^2} + \bar{u}^\nu\bar{h}^\rho_\mu\left(\delta G_{\nu\rho} - \delta\Gamma^\sigma_{\nu\rho}\bar{\nabla}_\sigma\right)\frac{f_{\bar{R}}}{\kappa^2} \\
& + \bar{u}^\nu\bar{h}^\rho_\mu\left(\bar{G}_{\nu\rho} - \bar{\nabla}_\nu\bar{\nabla}_\rho\right)\frac{\delta F}{\kappa^2} , \qquad (3.41) \\
[\delta\pi^{(f)}]_{\mu\nu} = & -2\left(\bar{u}^\sigma\bar{h}^\rho_{(\mu}\delta u_{\nu)} - \frac{1}{3}\bar{h}_{\mu\nu}\bar{u}^\sigma\delta u^\rho\right)\left(\bar{R}_{\rho\sigma} - \bar{\nabla}_\rho\bar{\nabla}_\sigma\right)\frac{f_{\bar{R}}}{\kappa^2} \\
& - \left(\bar{h}^\rho_\mu\bar{h}^\sigma_\nu - \frac{1}{3}\bar{h}_{\mu\nu}\bar{h}^{\rho\sigma}\right)\left(\delta G_{\rho\sigma} - \delta\Gamma^\lambda_{\rho\sigma}\bar{\nabla}_\lambda\right)\frac{f_{\bar{R}}}{\kappa^2} \\
& - \left(\bar{h}^\rho_\mu\bar{h}^\sigma_\nu - \frac{1}{3}\bar{h}_{\mu\nu}\bar{h}^{\rho\sigma}\right)\left(\bar{G}_{\rho\sigma} - \bar{\nabla}_\rho\bar{\nabla}_\sigma\right)\frac{\delta F}{\kappa^2} . \qquad (3.42)
\end{aligned}$$

In the last two equations we have used the results $h^\nu_\mu[q^{(f)}]_\nu = [q^{(f)}]_\mu$ and $h^\rho_\mu[\pi^{(f)}]_{\rho\nu} = [\pi^{(f)}]_{\mu\nu}$ to simplify the expressions obtained. If we take into account the 4-vector defined in Eq. (3.25) as the 4-velocity of the effective fluid, then the first order perturbations $[u^{(f)}]^\mu$and $[u^{(f)}]_\mu$ are given by

$$[\delta u^{(f)}]^\mu = \frac{1}{2}[\bar{u}^{(f)}]^\mu[\bar{u}^{(f)}]_\nu[\bar{u}^{(f)}]_\rho\delta g^{\nu\rho} + [\bar{h}^{(f)}]^{\mu\nu}\left(\frac{\bar{\nabla}_\nu\delta F}{\sqrt{\bar{X}}} - [\bar{u}^{(f)}]_\rho\delta g^\rho_\nu\right) , \tag{3.43}$$

$$[\delta u^{(f)}]_\mu = -\frac{1}{2}[\bar{u}^{(f)}]_\mu[\bar{u}^{(f)}]_\nu[\bar{u}^{(f)}]_\rho\delta g^{\nu\rho} + [\bar{h}^{(f)}]^\nu_\mu\frac{\bar{\nabla}_\nu\delta F}{\sqrt{\bar{X}}} . \tag{3.44}$$

Inserting Eqs. (3.25), (3.43) and (3.44) in Eqs. (3.39)–(3.42) we are able to obtain the fluid quantities with respect to the 4-vector $[u^{(f)}]^\mu = \nabla^\mu f_R/\sqrt{X}$.

Cosmological perturbations

While the results so far presented are valid for linear perturbations around a generic background, in this work we are interested in the specific case of perturbations in a FLRW universe. As such, from this point onward we consider the perturbed FLRW line element in the Newtonian gauge:

$$\mathrm{d}s^2 = -N^2\,(1+2\Phi)\,\mathrm{d}t^2 + a^2(1-2\Psi)\delta_{ij}\mathrm{d}x^i\mathrm{d}x^j\,, \tag{3.45}$$

where we recall that Φ and Ψ are the GI Bardeen potentials [46]. The new degree of freedom δF transforms as a 4-scalar under gauge transformations and so we can define the GI quantity

$$\delta F^{(N)} = \delta F - \dot{f}_{\bar{R}}\frac{\sigma}{N}\,, \tag{3.46}$$

where σ is the comoving shear potential defined in Eq. (A.16). We recall that the superscript (N) indicates that $\delta F^{(N)}$ reduces to the perturbation δF in the Newtonian gauge, where $\sigma = 0$. Using Eq. (3.36) we can relate $\delta F^{(N)}$ to the Bardeen potentials and their derivatives in Fourier space as

$$\begin{aligned}\frac{\delta F_k^{(N)}}{6} = &-\frac{f_{\bar{R}\bar{R}}}{N^2}\left[\ddot{\Psi}_k + \left(4\frac{\dot{a}}{a} - \frac{\dot{N}}{N}\right)\dot{\Psi}_k + \frac{\dot{a}}{a}\dot{\Phi}_k + \left(\frac{\ddot{a}}{a} - \left(\frac{\dot{a}}{a}\right)^2 - \frac{\dot{N}}{N}\frac{\dot{a}}{a}\right)\Phi_k\right]\\ &- \frac{k^2}{3a^2}f_{\bar{R}\bar{R}}\left(2\Psi_k - \Phi_k\right)\,,\end{aligned} \tag{3.47}$$

This equation has no analogue in GR, where both $\delta F^{(N)}$ on the l.h.s. and $f_{\bar{R}\bar{R}}$ on the r.h.s. vanish identically. The evolution equation for $\delta F_k^{(N)}$ can be obtained from Eq. (3.37) and reads [198]

$$\begin{aligned}&\delta\ddot{F}_k^{(N)} + \left(3\frac{\dot{a}}{a} - \frac{\dot{N}}{N}\right)\delta\dot{F}_k^{(N)} - \frac{N^2}{3}\left(\bar{R} - \frac{1+f_{\bar{R}}}{f_{\bar{R}\bar{R}}}\right)\delta F_k^{(N)} + \frac{N^2}{a^2}k^2\delta F_k^{(N)}\\ &\quad - \dot{f}_{\bar{R}}\left(3\dot{\Psi}_k + \dot{\Phi}_k\right) + 2\left[\ddot{f}_{\bar{R}} + \left(3\frac{\dot{a}}{a} - \frac{\dot{N}}{N}\right)\dot{f}_{\bar{R}}\right]\Phi_k = \frac{\kappa^2N^2}{3}\left(\delta\rho_k^{(N)} - 3\delta P_k^{(N)}\right)\,.\end{aligned} \tag{3.48}$$

The equations of motion for the metric perturbations are obtained from the first order perturbation of the modified Einstein field equations (3.34). In Fourier space, the individual $(0-0)$, $(0-i)$, $(i-i)$

and $(i-j)$, with $i \neq j$, components of the modified Einstein equations read [198]

$$(1+f_R)\ \left[\frac{\dot{a}}{a}\dot{\Psi}_k + \left(\frac{\dot{a}}{a}\right)^2\Phi_k + \frac{N^2}{3a^2}k^2\Psi_k\right] - \frac{1}{2}\dot{f}_{\bar{R}}\left[\dot{\Psi}_k + 2\frac{\dot{a}}{a}\Phi_k\right]$$
$$- \frac{1}{2}\left[\frac{\dot{a}}{a}\delta\dot{F}^{(N)} - \left(\frac{\ddot{a}}{a} - \frac{\dot{N}}{N}\frac{\dot{a}}{a}\right)\delta F_k^{(N)}\right] - \frac{1}{6}\frac{N^2}{a^2}k^2\delta F_k^{(N)} = -\frac{\kappa^2N^2}{6}\delta\rho_k^{(N)}\,, \tag{3.49}$$

$$(1+f_R)\ \left(\dot{\Psi}_k + \frac{\dot{a}}{a}\Phi_k\right) - \frac{1}{2}\dot{f}_{\bar{R}}\Phi_k - \frac{1}{2}\delta\dot{F}_k^{(N)} + \frac{1}{2}\frac{\dot{a}}{a}\delta F_k^{(N)} = -\frac{\kappa^2Na}{2}\left(\bar{\rho}+\bar{P}\right)v_k^{(N)}\,, \tag{3.50}$$

$$(1+f_R)\ \left[\ddot{\Psi}_k + \left(3\frac{\dot{a}}{a} - \frac{\dot{N}}{N}\right)\dot{\Psi}_k + \frac{\dot{a}}{a}\Phi_k + \left(\frac{\ddot{a}}{a} - \left(\frac{\dot{a}}{a}\right)^2 - \frac{\dot{N}}{N}\frac{\dot{a}}{a}\right)\Phi_k\right] + (1+f_R)\,\frac{N^2}{3a^2}k^2\left(\Psi_k - \Phi_k\right)$$
$$+ \frac{1}{2}\left[\dot{f}_{\bar{R}}\left(\dot{\Phi}_k + 2\dot{\Psi}_k\right) + 2\left(\ddot{f}_{\bar{R}} - \frac{\dot{N}}{N}\dot{f}_{\bar{R}}\right)\Phi_k\right] - \frac{1}{2}\left[\delta\ddot{F}_k^{(N)} + \left(2\frac{\dot{a}}{a} + \frac{\dot{N}}{N}\right)\delta\dot{F}_k^{(N)}\right]$$
$$+ \frac{1}{2}\left[\frac{\ddot{a}}{a} + 2\left(\frac{\dot{a}}{a}\right)^2 - \frac{\dot{N}}{N}\frac{\dot{a}}{a}\right]\delta F_k^{(N)} - \frac{N^2}{3a^2}k^2\delta F_k^{(N)} = \frac{\kappa^2N^2}{2}\delta P_k^{(N)}\,, \tag{3.51}$$

$$(1+f_R)\ \left(\Psi_k - \Phi_k\right) - \delta F_k^{(N)} = \kappa^2\Pi_k\,. \tag{3.52}$$

The presence of the term $\delta F_k^{(N)}$ in Eq. (3.52) shows explicitly that the modification of gravity contributes to the anisotropy of the perturbations, in accordance with the picture of $f(R)$-gravity as an anisotropic fluid, as discussed in the previous section. In fact, we can use Eqs. (3.39), (3.40) and (3.42) to define the GI energy density and pressure perturbations, $\delta\rho^{(f,N)}$ and $\delta P^{(f,N)}$, and the GI anisotropic stress potential of the effective fluid as

$$\delta\rho_k^{(f,N)} = \frac{6}{\kappa^2N^2}f_R\left[\frac{\dot{a}}{a}\dot{\Psi}_k + \left(\frac{\dot{a}}{a}\right)^2\Phi_k + \frac{N^2}{3a^2}k^2\Psi_k\right] - \frac{3}{\kappa^2N^2}\dot{f}_{\bar{R}}\left[\dot{\Psi}_k + 2\frac{\dot{a}}{a}\Phi_k\right]$$
$$+ \frac{3}{\kappa^2N^2}\left[\frac{\dot{a}}{a}\delta\dot{F}^{(N)} - \left(\frac{\ddot{a}}{a} - \frac{\dot{N}}{N}\frac{\dot{a}}{a}\right)\delta F_k^{(N)}\right] + \frac{k^2}{\kappa^2a^2}\delta F_k^{(N)}\,, \tag{3.53}$$

$$\delta P_k^{(f,N)} = -\frac{2}{\kappa^2N^2}f_R\left[\ddot{\Psi}_k + \left(3\frac{\dot{a}}{a} - \frac{\dot{N}}{N}\right)\dot{\Psi}_k + \frac{\dot{a}}{a}\Phi_k + \left(\frac{\ddot{a}}{a} - \left(\frac{\dot{a}}{a}\right)^2 - \frac{\dot{N}}{N}\frac{\dot{a}}{a}\right)\Phi_k\right]$$
$$- \frac{2}{3\kappa^2}\frac{k^2}{a^2}\left[f_R\left(\Psi_k - \Phi_k\right) - \delta F_k^{(N)}\right] - \frac{1}{\kappa^2N^2}\left[\dot{f}_{\bar{R}}\left(\dot{\Phi}_k + 2\dot{\Psi}_k\right) + 2\left(\ddot{f}_{\bar{R}} - \frac{\dot{N}}{N}\dot{f}_{\bar{R}}\right)\Phi_k\right]$$
$$+ \frac{1}{\kappa^2N^2}\left[\delta\ddot{F}_k^{(N)} + \left(2\frac{\dot{a}}{a} + \frac{\dot{N}}{N}\right)\delta\dot{F}_k^{(N)}\right] - \frac{1}{\kappa^2N^2}\left[\frac{\ddot{a}}{a} + 2\left(\frac{\dot{a}}{a}\right)^2 - \frac{\dot{N}}{N}\frac{\dot{a}}{a}\right]\delta F_k^{(N)}\,, \tag{3.54}$$

$$\Pi_k^{(f)} = \frac{1}{\kappa^2}\left[\delta F_k^{(N)} - f_R\left(\Psi_k - \Phi_k\right)\right]\,. \tag{3.55}$$

By defining the 4-velocity of the effective fluid as in Eq. (3.25), we find that the perturbation $[\delta u^{(v)}]^\mu$ and $[\delta u^{(v)}]^\mu$ take the form of Eqs. (A.39) and (A.40) with the peculiar velocity potential in the Newtonian gauge, $v^{(f.N)}$, given by:

$$v^{(f,N)} = \frac{N}{a}\left(\frac{\delta F}{\dot{f}_{\bar{R}}} - \frac{\sigma}{N}\right) = \frac{N}{a}\frac{\delta F^{(N)}}{\dot{f}_{\bar{R}}}\,. \tag{3.56}$$

In addition, an energy-flux potential $q^{(f)}$ needs to be taken into account:

$$q^{(f)} = \frac{1}{a\,N}\left[2\left(\dot{\Psi}+\frac{\dot{a}}{a}\Phi\right)\frac{f_R}{\kappa^2} - \frac{\dot{\delta F}^{(N)}}{\kappa^2} - \left(\frac{(\dot{f}_R)}{(f_R)} - 2\frac{\dot{a}}{a} - \frac{\dot{N}}{N}\right)\frac{\delta F^{(N)}}{\kappa^2} \right.$$
$$\left. -2\left(\frac{\ddot{a}}{a} - \left(\frac{\dot{a}}{a}\right)^2 - \frac{\dot{N}}{N}\frac{\dot{a}}{a}\right)\frac{f_R}{(\dot{f}_R)}\frac{\delta F^{(N)}}{\kappa^2}\right], \tag{3.57}$$

since the choice of the 4-velocity (3.25) does not set the energy-flux to zero[3]. In fact, the form of the expression (3.23) suggest that in metric $f(R)$-gravity it is not possible to choose a $[u^{(f)}]^\mu$ such that $[q^{(f)}]_\mu$ is identically zero, independently of the geometry. These definitions differ slightly from the ones in [198] due to the different way of defining the effective stress-energy-momentum tensor in Eq. (3.20).

In the absence of anisotropies coming from the matter sector, Eq. (3.52) can be used to eliminate one of the Bardeen potentials in favour of $\delta F_k^{(N)}$. In addition, from a combination of Eqs. (3.49) and (3.50), we can obtain the equivalent to the Poisson equation (A.77) in metric $f(R)$-gravity [198]

$$-\frac{1}{2}\dot{f}_{\bar{R}}\left(\dot{\Psi}_k+\frac{\dot{a}}{a}\Phi_k\right) - \frac{1}{2}\left[\frac{\dot{a}}{a}\dot{\delta F}_k^{(N)} - \left(\frac{\ddot{a}}{a} - \left(\frac{\dot{a}}{a}\right)^2 - \frac{\dot{N}}{N}\frac{\dot{a}}{a}\right)\delta F_k^{(N)}\right]$$
$$+\frac{1}{3}\frac{N^2}{a^2}k^2\left[(1+f_R)\,\Psi_k - \frac{1}{2}\delta F_k^{(N)}\right] = -\frac{\kappa^2 N^2}{6}\delta\rho_k^{(C)}\,, \tag{3.58}$$

In contrast with GR, Eq. (3.58) no longer represents an algebraic relation between the gravitational potential Ψ and the comoving energy density $\delta\rho^{(C)} = \delta\rho^{(N)} + \dot{\bar{\rho}}(a/N)v^{(N)}$. This difference is a reflection of the extra degree of freedom in the scalar sector. Nevertheless, using Eqs. (3.50), (3.52) and (3.58), we can eliminate the Bardeen potentials and their derivatives in favour of $\delta F^{(N)}$ and the matter perturbation variables, which in vacuum leads to a closed differential equation for $\delta F^{(N)}$.

Evolution of matter perturbations

As discussed above, the matter sector is not modified in metric $f(R)$-gravity, therefore the first order perturbation of the conservation equations remains unaltered [49, 246]:

$$\dot{\delta}_k^{(N)} + 3\frac{\dot{a}}{a}\left(c_s^2-\bar{w}\right)\delta_k^{(N)} - (1+\bar{w})\left[9\left(\frac{\dot{a}}{a}\right)^2\left(c_s^2-c_a^2\right) + \frac{N^2}{a^2}k^2\right]\frac{a}{N}v_k^{(N)} = 3\,(1+\bar{w})\,\dot{\Psi}_k\,, \tag{3.59}$$

$$\dot{v}_k^{(N)} + \frac{\dot{a}}{a}\left(1-3c_s^2\right)v_k^{(N)} + \frac{N}{a}\frac{c_s^2\delta_k^{(N)}}{1+\bar{w}} - \frac{N}{3a}\frac{k^2}{a^2}\frac{\Pi_k}{\bar{\rho}+\bar{P}} = -\frac{N}{a}\Phi_k\,. \tag{3.60}$$

Nevertheless, the existence of the extra degree of freedom does affect the evolution of the matter perturbations. For example, in the commonly employed quasi-static approximation, the evolution of the matter density contrast in a universe filled only by pressureless matter is given by a modified

[3] We recall that in general, the first order perturbation of the stress-energy-momentum tensor has a contribution from the perturbation of the energy-flux, cf. Eq. (A.44), with $[\delta T^{(N)}]^0_i = (a/N)\partial_i\left[(\bar{\rho}+\bar{P})v^{(N)}+q\right]$.

version of Eq. (2.31) [336, 365]:

$$\ddot{\delta}^{(N)}_{\mathrm{m},k} + 2H\dot{\delta}^{(N)}_{\mathrm{m},k} - 4\pi\tilde{G}_f\bar{\rho}_{\mathrm{m}}\delta^{(N)}_{\mathrm{m},k} = 0\,, \tag{3.61}$$

where the effective gravitational coupling $\tilde{G}_{\mathrm{eff}}$ reads

$$\tilde{G}_f := \frac{G}{1+f_R}\frac{1+4\frac{f_{RR}}{1+f_R}\frac{k^2}{a^2}}{1+3\frac{f_{RR}}{1+f_R}\frac{k^2}{a^2}}\,. \tag{3.62}$$

Notice that $\tilde{G}_f$ deviates from the effective coupling $G_f = G/(1+f_R)$ introduced in Sect. 3.1.3 and in the limit of $k \gg a^2(1+f_R)/(f_{RR})$ we have $\tilde{G}_f = (4/3)G_f$. This means that the effects of $f(R)$-gravity are felt at sufficiently small scales (large k), even when the background evolution follows that of GR, i.e., when $|f_R| \ll 1$. However, the quasi-static approximation that leads to Eq. (3.61) has been criticised in the literature for imposing too strong conditions on the gravitational potentials Φ and Ψ [55, 134]. In Ref. [134], a fourth order equation for $\delta^{(N)}_{\mathrm{m}}$ in metric $f(R)$-gravity was derived for a universe filled only by dust. It was shown that, in the sub-horizon limit, a second order differential equation is once more obtained [134]:

$$\ddot{\delta}^{(N)}_{\mathrm{m},k} + 2H\dot{\delta}^{(N)}_{\mathrm{m},k} - H^2\frac{\left(\frac{\ddot{H}}{H^3}+2\frac{\dot{H}}{H}\right)\dot{H} + 16\left(\frac{f_{RR}}{1+f_R}\frac{k^2}{a^2}\right)^4\left(\frac{\ddot{H}}{H^3}+4\frac{\dot{H}}{H}\right)\frac{\kappa^2\bar{\rho}_{\mathrm{m}}}{1+f_R}}{\dot{H} + 24\left(\frac{f_{RR}}{1+f_R}\frac{k^2}{a^2}\right)^4\left(\frac{\ddot{H}}{H^3}+4\frac{\dot{H}}{H}\right)H^2}\delta^{(N)}_{\mathrm{m},k} = 0\,. \tag{3.63}$$

Despite the fact that the zeroth order coefficient In Eq. (3.63) has a different k-dependence when compared with Eq. (3.61), both equations possess the same large k limit. Therefore, even if the assumption of constancy of the gravitational potentials is not respected, Eq. (3.61) predicts the correct behaviour of the matter density contrast when $k \gg a^2(1+f_R)/(f_{RR})$. In this regime, if matter completely dominates the energy budget of the Universe ($\Omega_{\mathrm{m}} \approx 1$) and the deviations from GR are small ($|f_R| \ll 1$), the general solution to Eqs. (3.61) and (3.63) is

$$\delta_{\mathrm{m},k} = C_1 a^{-\frac{\sqrt{33}+1}{4}} + C_2 a^{\frac{\sqrt{33}-1}{4}}\,. \tag{3.64}$$

By comparing Eq. (3.64) with the result in Eq. (2.32), it becomes apparent that metric $f(R)$-gravity predicts a stronger collapse of matter, with regards to GR, during the matter dominated epoch at very small scales (large k). This is reflected in the higher prediction for the growth rate (cf. Eq. (2.34)) during the matter era:

$$f^{(f)} = \frac{\sqrt{33}-1}{4} \approx 1.19\,, \tag{3.65}$$

when compared with the standard result $f = 1$ in GR.

3.1.6. Cosmography in $f(R)$-gravity

Since the objective of cosmography is to derive model independent constraints on the evolution of the late Universe, it is in principle an ideal tool to differentiate between theories of gravity. In the context

of $f(R)$-gravity, the cosmographic approach has been applied to since the end of the last decade in an attempt to obtain constraints on the function $f(R)$ and its derivatives (see e.g. Refs. [43, 73, 107] for works of cosmography in $f(R)$-gravity and Refs. [42] for works of cosmography applied in other modified theories of gravity).

In order to extend the cosmographic approach to $f(R)$-gravity, we need to write the scalar curvature and its time derivatives in terms of the cosmographic parameters [43, 73, 107]:

$$R = 6H^2\left[2-(q+1)+\frac{\mathcal{K}}{a^2H^2}\right], \tag{3.66}$$

$$\dot{R} = 6H^3\left[(j-1)-(q+1)-2\frac{\mathcal{K}}{a^2H^2}\right], \tag{3.67}$$

$$\ddot{R} = 6H^4\left\{(s-1)+(q+1)^2+6\,(q+1)+2\frac{\mathcal{K}}{a^2H^2}\left[2+(q+1)\right]\right\}, \tag{3.68}$$

$$\dddot{R} = 6H^5\left\{(l-1)-(s-1)-(j-1)\left[6+2\,(q+1)\right]-18\,(q+1)^2-14\,(q+1)\right.$$
$$\left.-2\frac{\mathcal{K}}{a^2H^2}\left[4+(j-1)+9\,(q+1)\right]\right\}. \tag{3.69}$$

Here, we recall that within the context of cosmography we work with the cosmic time ($N=1$). By replacing these derivatives in the Friedmann and Raychaudhuri equations, i.e., Eqs (3.15) and (3.16), we are able to obtain the expressions for $(\dot{f}_R)$ and $(\ddot{f}_R)$:

$$\frac{(\dot{f}_R)}{H} = 1+\Omega_{\mathcal{K}}-\Omega^{(\mathrm{m})}+\frac{f}{6H^2}+q\,f_R\,, \tag{3.70}$$

$$\frac{(\ddot{f}_R)}{H^2} = -\left[1+3\Omega_{\mathcal{K}}-(4+3w)\,\Omega^{(\mathrm{m})}+\frac{f}{6H^2}+2\,(q+1)\left(\Omega_{\mathcal{K}}-\Omega^{(\mathrm{m})}+\frac{f}{6H^2}\right)\right]$$
$$+\left[1-2\Omega_{\mathcal{K}}+2\,(q+1)^2-5\,(q+1)\right]f_R\,. \tag{3.71}$$

Higher order derivatives $\mathrm{d}^i(f_R)/\mathrm{d}t^i$ can also be written in terms of the cosmographic parameters, the values of f and f_R and the parameters that characterise the matter fluid. Notice that each new derivative $\mathrm{d}^i(f_R)/\mathrm{d}t^i$ requires the knowledge of an extra cosmographic parameter and a new time derivative of the pressure $P^{(m)}$. From Eqs. (3.70) and (3.71), we find that even in the simple case where the matter content of the universe behaves as dust, $P^{(m)}=0$, we require the values of f/H^2 and f_R, apart from $\Omega_{\mathcal{K}}$ and $\Omega^{(\mathrm{m})}$, in order to constrain the derivatives of the new degree of freedom. As pointed out in[4] [95], this lack of one-to-one correspondence means that in order to set constraints on the derivatives $\mathrm{d}^i(f_R)/\mathrm{d}t^i$ we need either to define sensible priors on f and f_R, or fix their values through complementary tests or physical considerations.

In [43, 73, 107] this limitation was overcome by arguing that if around the present time the $f(R)$ function is to be sufficiently close to the EH action with a cosmological constant then the higher order

[4] A similar argument had previously been presented to us by Ruth Lazkoz and Vincenzo Salzano in a private conversation.

terms in the Taylor expansion of $f(R)$ around R_0

$$f(R) = f_0 + f_{R,0}\,(R-R_0) + \frac{f_{RR,0}}{2!}\,(R-R_0)^2 + \frac{f_{RRR,0}}{3!}\,(R-R_0)^3 + \mathcal{O}\left[R-R_0\right]^4 , \tag{3.72}$$

should have a residual contribution. Thus, truncating the series at a sufficiently higher order should not incur in a large error in the calculations. If we disregard terms of order $\mathcal{O}[R-R_0]^4$ in Eq. (3.72), we can then write the t-derivatives of f_R as

$$(\dot{f_R}) = \left[f_{RR,0} + (R-R_0)\,f_{RRR,0}\right]\dot{R}\,, \tag{3.73}$$

$$(\ddot{f_R}) = \left[f_{RR,0} + (R-R_0)\,f_{RRR,0}\right]\ddot{R} + \dot{R}^2 f_{RRR,0}\,, \tag{3.74}$$

$$(\dddot{f_R}) = \left[f_{RR,0} + (R-R_0)\,f_{RRR,0}\right]\dddot{R} + 3\ddot{R}\dot{R}f_{RRR,0}\,. \tag{3.75}$$

If, in addition, we consider that around the present time $f_R \approx 0$, so that the effective gravitational coupling G_f coincides with the gravitational constant G, a substitution of Eqs. (3.73)–(3.75) in Eqs. (3.70), (3.71) and the first time derivative of (3.71) leads to [43, 73, 107]

$$\frac{R_0+f_0}{6H_0^2} = -\frac{\mathcal{A}_0\Omega_0^{(\mathrm{m})}+\mathcal{B}_0}{\mathcal{D}}\,, \tag{3.76}$$

$$1 + f_{R,0} = 1\,, \tag{3.77}$$

$$\frac{f_{RR,0}}{(6H_0^2)^{-1}} = -\frac{\mathcal{A}_2\Omega_0^{(\mathrm{m})}+\mathcal{B}_2}{\mathcal{D}}\,, \tag{3.78}$$

$$\frac{f_{RRR,0}}{(6H_0^2)^{-2}} = -\frac{\mathcal{A}_3\Omega_0^{(\mathrm{m})}+\mathcal{B}_3}{(j_0-q_0-2-2\Omega_{\mathcal{K}})\,\mathcal{D}}\,, \tag{3.79}$$

where the explicit formulas of the coefficients $\mathcal{A}_i$, $\mathcal{B}_i$ and $\mathcal{D}$ are presented in the Appendix. B.1. In the case of a spatially flat Universe filled by dust, the coefficients $\mathcal{A}_i$ reduce to the ones found in Refs. [73, 107, 264]. Finally, if J matter fluids are considered, each with fractional energy density $\Omega_{(\mathrm{j})}$, $\mathrm{j}=1,\ldots,\mathrm{J}$, the terms $\mathcal{A}_i\Omega^{(\mathrm{m})}$ in Eqs. (3.76)–(3.78) can be expanded as

$$\mathcal{A}_i\,\Omega^{(\mathrm{m})} = \sum_{\mathrm{j}=1}^{\mathrm{J}} \mathcal{A}_{i,(\mathrm{j})}\Omega_{(\mathrm{j}),0}\,, \tag{3.80}$$

where $\mathcal{A}_{i,(\mathrm{j})}$ is given by the same formula as $\mathcal{A}_i$ with all the fluid quantities replaced by the respective values for the fluid j. This is the case of Ref. [264], where the quantities $\mathcal{A}_i$ and $\mathcal{C}_i$ correspond to $\mathcal{A}_{i,\mathrm{m}}$ and $\mathcal{A}_{i,\mathrm{r}}$, respectively, with $\Omega_{\mathcal{K}}=0$.

3.2. The modified generalised Chaplygin Gas as $f(R)$ gravity

Since the modified Einstein equations in metric $f(R)$-gravity (3.3) are of fourth order in derivatives of the metric, the task of finding exact solutions for a given function f can become extremely difficult, even in the case of a highly symmetrical FLRW universe. As discussed in Sect. 3.1.4, an alternative approach is to define an effective stress-energy-momentum tensor and treat the

modifications to the Einstein equations as an effective fluid. Once the FLRW background is fixed we can look for the functions $f(R)$ that are compatible with such an evolution. This approach, also dubbed *designer-$f(R)$*, has been successful in finding various solutions of cosmological interest [76, 103, 106, 109, 133, 143, 182, 275, 276] including mapping the ΛCDM model in $f(R)$-gravity [133, 143, 182].

In this section, we consider an extension of these methods to the case where the total energy density and pressure of the universe, including the contribution from matter and the effective $f(R)$-fluid (cf. Eqs. (3.30) and (3.31)):

$$\rho := \rho^{(\mathrm{m})} + \rho^{(f)}\,, \qquad\qquad P := P^{(\mathrm{m})} + P^{(f)}\,, \tag{3.81}$$

follow a barotropic EoS, i.e., $P = P(\rho) = w(\rho)\,\rho$. Choosing $N = 1$ so that t is the cosmic time and disregarding the spatial curvature ($\mathcal{K} = 0$), we can re-write the Friedmann and Raychaudhuri equations (3.32) and (3.33) as

$$H^2 = \frac{\kappa^2}{3}\rho\,, \qquad\qquad \dot{H} = -\frac{\kappa^2}{2}\,(1+w)\,\rho\,. \tag{3.82}$$

In turn, the scalar curvature becomes

$$R = \kappa^2\,(\rho - 3P)\,, \tag{3.83}$$

which allows us to write the derivatives $\dot{R}$, f_R and f_{RR} as

$$\dot{R} = -3\kappa^2 H\left(1-3c_a^2\right)(1+w)\,\rho\,, \tag{3.84}$$

$$f_R = \frac{\left(1-3c_a^2\right)^{-1}}{\kappa^2}\frac{\mathrm{d}f}{\mathrm{d}\rho}\,, \tag{3.85}$$

$$f_{RR} = \frac{\left(1-3c_a^2\right)^{-2}}{\kappa^2}\left(\frac{\mathrm{d}^2 f}{\mathrm{d}\rho^2} + \frac{3P^{(2)}}{\left(1-3c_a^2\right)}\frac{\mathrm{d}f}{\mathrm{d}\rho}\right)\,, \tag{3.86}$$

where c_a^2 is the total adiabatic squared speed of sound and $P^{(2)} := \mathrm{d}^2P/\mathrm{d}\rho^2$. Replacing these derivatives in the modified Friedmann equation (3.15) allows us to write

$$(1+w)\left(1-3c_a^2\right)\rho^2\frac{\mathrm{d}^2}{\mathrm{d}\rho^2}(R+f) + \left[3\,(1+w)\,P^{(2)}\rho - \frac{1+3w}{6}\left(1-3c_a^2\right)\right]\rho\frac{\mathrm{d}}{\mathrm{d}\rho}(R+f) - \frac{\left(1-3c_a^2\right)^2}{6}(R+f) = -\left(1-3c_a^2\right)^2\frac{\kappa^2}{3}\rho^{(\mathrm{m})}\,. \tag{3.87}$$

Any homogeneous and isotropic relativistic model with total energy density ρ and total pressure $P(\rho)$ can be described by an $f(R)$ model as long as f satisfies Eq. (3.87). The presence of a non-homogeneous term dependent on the matter energy density on the r.h.s. of (3.87) means that a general solution to this equation might not always be found. Nevertheless, we can look for solutions of the homogeneous equation which correspond to vacuum solutions.

As an example of the applications of Eq. (3.87) we consider the case of constant w, which implies $c_a^2 = w$ and $P^{(2)} = 0$. In this case we obtain the following differential equation after dividing all the

terms in Eq. (3.87) by $1-3w$:

$$(1+w)\,\rho^2\frac{\mathrm{d}^2}{\mathrm{d}\rho^2}\,(R+f)-\frac{1+3w}{6}\rho\frac{\mathrm{d}}{\mathrm{d}\rho}\,(R+f)-\frac{1-3w}{6}\,(R+f)=\,-\,(1-3w)\,\frac{\kappa^2}{3}\rho^{(\mathrm{m})}\,. \quad (3.88)$$

The general solution to this equation in the absence of matter is [103, 143, 264]

$$R+f=C_+\rho^{\beta_+}+C_-\rho^{\beta_-}\,, \quad (3.89)$$

where the exponents $\beta_\pm$ are given by [103, 143, 264]

$$\beta_\pm=\frac{1}{2}\left\{1+\frac{1+3w}{6(1+w)}\pm\sqrt{\frac{2(1-3w)}{3(1+w)}+\left[1+\frac{1+3w}{6(1+w)}\right]^2}\right\}\,. \quad (3.90)$$

Since the scalar curvature is proportional to the energy density ρ, the solution (3.89) can be rewritten in terms of R as

$$R+f=D_+R^{\beta_+}+D_-R^{\beta_-}\,. \quad (3.91)$$

The argument on the square root in Eq. (3.90) vanishes when $w=-(13\pm4\sqrt{6})/3$, being negative inside the interval defined by those points and positive otherwise. Thus, for $w>-1$, the exponents $\beta_\pm$, and consequently the solution $R+f$ in Eq. (3.91), are always real valued. We note that real valued solutions for $f(R)$ can also be obtained when the coefficients $\beta_\pm$ acquire a complex phase, as was recently shown in Ref. [29]. In the limit of $w\to-1$ we find that only the solution β_+ in Eq. (3.90) as a finite limit and leads to the solution

$$R+f=D_+R^2\,, \quad (3.92)$$

which is precisely the function that in vacuum leads to a static solution of the trace equation, $\Box R=0$, for all values of the scalar curvature R.

3.2.1. Solution for the mGCG

Let us now consider the case of the modified generalised Chaplygin gas (mGCG) [57, 60, 205] (see also [70, 83] and references therein) whose equation of state reads

$$P=\beta\rho-(1+\beta)\,\frac{A}{\rho^\alpha}\,. \quad (3.93)$$

Here, α and β are parameters of the mGCG subject to the conditions $\alpha\neq-1$ and $-1<\beta\leq1$. For earlier attempts of describing the GCG in $f(R)$ gravity see Ref. [106]. The conservation of the energy momentum tensor implies that the energy density of the mGCG scales as

$$\rho(a)=\rho_0\left[A_s+(1-A_s)\left(\frac{a_0}{a}\right)^{3\xi}\right]^{\frac{1}{1+\alpha}}\,, \quad (3.94)$$

where the factor ξ is defined as $\xi \equiv (1+\beta)(1+\alpha)$, and A_s is a dimensionless constant such that $A_s \equiv A/\rho_0^{1+\alpha}$. Here, we will restrict our analysis to the case $0 < A_s < 1$, which guarantees that the mGCG does not induce any singular behaviour for finite values of a. By defining the characteristic scale factor a_*

$$a_* = \left(\frac{1-A_s}{A_s}\right)^{\frac{1}{3\xi}} a_0\,, \tag{3.95}$$

we can re-write Eq. (3.94) as

$$\rho(a) = \rho_{\rm dS}\left[1+\left(\frac{a_*}{a}\right)^{3\xi}\right]^{\frac{1}{1+\alpha}}\,, \tag{3.96}$$

where $\rho_{\rm dS} \equiv \rho_0 A_s^{1/(1+\alpha)} = A^{1/(1+\alpha)}$. Eq. (3.96) allows us to identify two regimes with distinct behaviour of the mGCG, one for $a < a_*$ and another for $a > a_*$. Whether each of these regimes corresponds to a dominance of the first or second term inside the squared brackets in (3.96) depends on the sign of the parameter ξ. For $\xi > 0$, we have that

$$\rho(a) \approx \begin{cases} \rho_{\rm dS}\left(\dfrac{a_*}{a}\right)^{3(1+\beta)}\,, & \text{if } a \ll a_*\,, \\ \rho_{\rm dS}\,, & \text{if } a \gg a_*\,, \end{cases} \tag{3.97}$$

while for $\xi < 0$ we obtain the same behaviour but in an inverted chronological order

$$\rho(a) \approx \begin{cases} \rho_{\rm dS}\,, & \text{if } a \ll a_*\,, \\ \rho_{\rm dS}\left(\dfrac{a_*}{a}\right)^{3(1+\beta)}\,, & \text{if } a \gg a_*\,. \end{cases} \tag{3.98}$$

For a complete review of the behaviour of the mGCG, inclusively in the case of $\beta = -1$ which can lead, for example, to the appearance of a Little Sibling of the Big Rip type of singularity [77], see e.g. Ref. [72].

Using Eq. (3.93), we find that the EoS parameter w, the adiabatic squared speed of sound c_a^2 and the second derivative $P^{(2)}$ for the mGCG model are

$$w(\rho) = \beta - (1+\beta)\left(\frac{\rho_{\rm dS}}{\rho}\right)^{1+\alpha}\,, \tag{3.99}$$

$$c_a^2(\rho) = \beta + \alpha\,(1+\beta)\left(\frac{\rho_{\rm dS}}{\rho}\right)^{1+\alpha}\,, \tag{3.100}$$

$$P^{(2)}(\rho) = -\frac{\alpha\xi}{\rho}\left(\frac{\rho_{\rm dS}}{\rho}\right)^{1+\alpha}\,. \tag{3.101}$$

Inserting this in the differential equation (3.87), we obtain

$$A_2(\rho)\,\rho^2\frac{{\rm d}^2}{{\rm d}\rho^2}(R+f) + A_1(\rho)\,\rho\frac{\rm d}{{\rm d}\rho}(R+f) + A_0(\rho)\,(R+f) = 0\,, \tag{3.102}$$

where the ρ-dependent coefficients are defined as

$$A_2(\rho) = (1+\beta)\left[1-\left(\frac{\rho_{\rm dS}}{\rho}\right)^{1+\alpha}\right]\left[4-3(1+\beta)\left(1+\alpha\left(\frac{\rho_{\rm dS}}{\rho}\right)^{1+\alpha}\right)\right], \tag{3.103}$$

$$A_1(\rho) = -\frac{1-9\beta^2}{6}+\frac{1}{2}\left[1-3\beta+\alpha(1+3\beta)-6\alpha\xi\right](1+\beta)\left(\frac{\rho_{\rm dS}}{\rho}\right)^{1+\alpha} + \frac{3}{2}\alpha(1+2\alpha)(1+\beta)^2\left(\frac{\rho_{\rm dS}}{\rho}\right)^{2(1+\alpha)}, \tag{3.104}$$

$$A_0(\rho) = -\frac{1}{6}\left[4-3(1+\beta)\left(1+\alpha\left(\frac{\rho_{\rm dS}}{\rho}\right)^{1+\alpha}\right)\right]^2. \tag{3.105}$$

In order to solve this differential equation, we now introduce the variable y, defined as[5] [264]

$$y := \left(\frac{\rho_{dS}}{\rho}\right)^{1+\alpha}. \tag{3.106}$$

The variable y is finite and restricted to the interval $(0,1)$, approaching unity when the mGCG is near the de Sitter regime, and vanishing asymptotically when the energy density of the mGCG scales as $a^{-3(1+\beta)}$. By construction, y is also normalised so that its present day value is $y_0 = A_s$. Using y as the independent time variable, we can re-write the differential equation (3.102) as

$$\frac{{\rm d}^2}{{\rm d}y^2}(R+f)+\left(\frac{6\xi+9\beta+7}{6\xi}\frac{1}{y}+\frac{1}{3\xi}\frac{1}{y-1}-\frac{1}{y-y_1}\right)\frac{\rm d}{{\rm d}y}(R+f) - \frac{\alpha}{2(1+\alpha)^2}\frac{y-y_1}{y^2(y-1)}(R+f)=0, \tag{3.107}$$

where $y_1 := (1-3\beta)/[3\alpha(1+\beta)]$. Eq. (3.107) is a second order linear differential equation with four regular singular points [185] at $y=0$, $y=1$, $y=y_1$ and $y=+\infty$. Its general solution was obtained in [264] and reads

$$(R+f)(y) = C_+ g_+(y) + C_- g_-(y), \tag{3.108}$$

where $C_\pm$ are arbitrary constants and the two linearly independent solutions $f_\pm$ of Eq. (3.107) are

$$g_\pm(y) = y^{\frac{\pm\lambda_\beta-(9\beta+7)}{12\xi}}\left\{\left(b_3^\pm-1\right)\left[\left(2b_1^\pm-b_2^\pm+1\right)y-\left(b_3^\pm+b_1^\pm-2b_2^\pm\right)\right]F\left[b_1^\pm,b_2^\pm;b_3^\pm-1;y\right] + \left[b_1^\pm-\left(b_3^\pm-b_2^\pm-b_1^\pm-1\right)\left(2+3b_1^\pm-2b_2^\pm\right)\right](y-1)\,y\,F\left[1+b_1^\pm,1+b_2^\pm;b_3^\pm;y\right]\right\}. \tag{3.109}$$

Here, $F[b,c;d;y]$ is the hypergeometric function [7, 283] and we have introduced the $\{\beta,\,\xi\}$-dependent

[5] In Ref. [264], the variable defined in Eq. (3.106) is denoted by x. Here, we adopt the new notation y since x is reserved for the logarithm of the scale factor.

constants

$$\lambda_\beta := \sqrt{9\beta^2 + 78\beta + 73}\,, \tag{3.110}$$

and

$$b_1^\pm := \frac{3\beta + 5 \pm \lambda_\beta}{12\xi}\,, \qquad b_2^\pm := 1 + \frac{-(3\beta+1) \pm \lambda_\beta}{12\xi}\,, \qquad b_3^\pm = 2 \pm \frac{\lambda_\beta}{6\xi}\,. \tag{3.111}$$

The differential equation (3.107) has four regular singularities in the expanded complex plane and therefore falls outside the category of Riemann's differential equation [283]. Nevertheless, for some choices of the parameters $\{\alpha, \beta\}$, or equivalently $\{\beta, \xi\}$, the singular point y_1 reduces to one of the other singularities: $y = 0$ (if $\beta = 1/3$), $y = 1$ (if $\xi = 4/3$) or $y = +\infty$ (if $\alpha = 0$). In such cases, Eq. (3.107) not only possesses three regular singularities but falls in the category of the hypergeometric differential equation[6] [7, 283].

3.2.2. Special Case: From radiation to de Sitter ($\beta = 1/3$)

We now look at the case of $\beta = 1/3$ (with $\alpha \neq 0$) which leads to $y_1 = 0$. In such a case, the mGCG mimics a radiation fluid when the first term in the EoS (3.93) dominates. Therefore, this particular case of the mGCG has applications in the early Universe in models with pre-inflationary evolution and in the transition from inflation to radiation during the reheating phase. In addition, it can be employed in order to obtain a smooth transition between an initial (dark) radiation behaviour and a later effective cosmological constant. A substitution in the differential equation (3.107) allows us to obtain a hypergeometric differential equation [7, 283] for $f(x)$:

$$y\,(1-y)\,\frac{\mathrm{d}^2}{\mathrm{d}y^2}\,(R+f) - \frac{6y-5}{4\,(1+\alpha)}\,\frac{\mathrm{d}}{\mathrm{d}y}\,(R+f) + \frac{\alpha}{2\,(1+\alpha)^2}\,(R+f) = 0\,. \tag{3.112}$$

As long as α does not satisfy any of the equalities $1+\alpha = 5/(4n)$ and $1+\alpha = 1/(2n)$, where n is an integer, this equation admits as solutions the two pairs of linearly independent functions

$$g_1(y) = F\left[\frac{1}{2\,(1+\alpha)}\,, -1 + \frac{1}{1+\alpha}\,; \frac{5}{4\,(1+\alpha)}\,; y\right]\,, \tag{3.113}$$

$$g_2(y) = y^{1-\frac{5}{4(1+\alpha)}}\,F\left[-\frac{1}{4\,(1+\alpha)}\,, 1 - \frac{3}{4\,(1+\alpha)}\,; 2 - \frac{5}{4\,(1+\alpha)}\,; y\right]\,, \tag{3.114}$$

and

$$g_3(y) = F\left[\frac{1}{2\,(1+\alpha)}\,, -1 + \frac{1}{1+\alpha}\,; \frac{1}{4\,(1+\alpha)}\,; 1-y\right]\,, \tag{3.115}$$

$$g_4(y) = (1-y)^{1-\frac{1}{4(1+\alpha)}}\,F\left[\frac{3}{4\,(1+\alpha)}\,, 1 + \frac{1}{4\,(1+\alpha)}\,; 2 - \frac{1}{4\,(1+\alpha)}\,; 1-y\right]\,, \tag{3.116}$$

[6] Notice that special care has to be taken in the overlapping case of $\beta = 1/3$ and $\alpha = 0$ which implies $\xi = 4/3$, as there is no appropriate limit for y_1.

such that $R+f = C_1\, g_1(y) + C_2\, g_2(y) = C_3\, g_3(y) + C_4\, g_4(y)$, where the C_i's are arbitrary constants. We recall that the pairs $\{g_1,\, g_2\}$ and $\{g_3,\, g_4\}$ are related through a linear transformation [7, 283], with $\{g_1,\, g_2\}$ being more appropriate for the description of the behaviour around $y=0$, i.e., when the mGCG behaves as radiation, and $\{g_3,\, g_4\}$ more appropriate for the behaviour around $y=1$ where the mGCG mimics a cosmological constant. Alternatively, these solutions can be recovered from Eq. (3.109) by using the contiguous relations of the hypergeometric functions (cf. the Appendix B.4).

In the particular case $\beta = 1/3$, the first term on the EoS (3.93) does not contribute to the scalar curvature, which can be written in terms of y as

$$R = R_{\rm dS} y^{\frac{\alpha}{1+\alpha}}\,, \qquad\qquad R_{\rm dS} := 4\rho_{\rm dS}\,, \tag{3.117}$$

where we have introduced the asymptotic value of the scalar curvature $R_{\rm dS}$. Thus, for $\alpha/(1+\alpha) < 0$, i.e., for $-1 < \alpha < 0$, the scalar curvature is defined in the range $]R_{\rm dS},\, +\infty[$ while for $\alpha/(1+\alpha) > 0$, i.e., for $\alpha \in \mathbb{R}/[-1,\, 0]$, R is defined in the range $]0,\, R_{\rm dS}[$. Introducing (3.117) in the solutions (3.113)–(3.116) we find that [264]

$$g_1(R) = F\left[\frac{1}{2\,(1+\alpha)}\,, -1+\frac{1}{1+\alpha}\,; \frac{5}{4\,(1+\alpha)}\,; \left(\frac{R}{R_{\rm dS}}\right)^{1+\frac{1}{\alpha}}\right]\,, \tag{3.118}$$

$$g_2(R) = \left(\frac{R}{R_{\rm dS}}\right)^{1-\frac{1}{4\alpha}} F\left[-\frac{1}{4\,(1+\alpha)}\,, 1-\frac{3}{4\,(1+\alpha)}\,; 2-\frac{5}{4\,(1+\alpha)}\,; \left(\frac{R}{R_{\rm dS}}\right)^{1+\frac{1}{\alpha}}\right]\,, \tag{3.119}$$

$$g_3(R) = F\left[\frac{1}{2\,(1+\alpha)}\,, -1+\frac{1}{1+\alpha}\,; \frac{1}{4\,(1+\alpha)}\,; 1-\left(\frac{R}{R_{\rm dS}}\right)^{1+\frac{1}{\alpha}}\right]\,, \tag{3.120}$$

$$\begin{aligned} g_4(x) = {} & \left[1-\left(\frac{R}{R_{\rm dS}}\right)^{1+\frac{1}{\alpha}}\right]^{1-\frac{1}{4(1+\alpha)}} \\ & \times F\left[\frac{3}{4\,(1+\alpha)}\,, 1+\frac{1}{4\,(1+\alpha)}\,; 2-\frac{1}{4\,(1+\alpha)}\,; 1-\left(\frac{R}{R_{\rm dS}}\right)^{1+\frac{1}{\alpha}}\right]\,. \end{aligned} \tag{3.121}$$

Notice that when written in terms of R, the functions f_i, $i=1,2,3,4$ can in principle be extended beyond the value $R_{\rm dS}$ by analytical continuation. The extended function, if real, would allows us to obtain an $f(R)$ function that, while capable to mimic a mGCG behaviour, is not restricted in the values of R imposed by that model.

In order to fix the linear coefficients C_i for the solutions f_i, we look at the stability conditions for metric $f(R)$-gravity presented in Sect. 3.1.2. In particular we require that $1+f_R = g_r > 0$ and that $f_{RR} = g_{RR} > 0$ during the history of evolution of the model and that at the present time $f_R \approx 0$. In order to decide which values of the parameter α can give the desired behaviour, we begin by looking at how the solutions found evolve near the asymptotic values $y=0$ and $y=1$. In Tab. 3.1 we present the asymptotic values of f_1, f_2 and their R-derivatives for different values of the parameter α. Notice that apart from $\alpha=-1$ and $\alpha=0$, the value $\alpha=1/4$ is excluded as it leads to a special case of the hypergeometric differential equation (3.112), where solutions of the type in (3.113) and (3.114) are no longer valid. In addition, the values $\alpha=-1/4$ and $\alpha=1$ are listed as they represent values where the behaviour of the second derivatives $f_{1,RR}$ and $f_{2,RR}$ change. From analysing this table we find that:

α	-1	$-\frac{1}{4}$	0	$\frac{1}{4}$	1	
g_1	1	1	1	1	1	1
$g_{1,R}$	$-\infty$	0^-	0^-	0^-	0^-	0^-
$g_{1,RR}$	$+\infty$	0^+	0^+	0^-	0^-	$-\frac{2}{5}R_{\rm dS}^{-2}$ $-\infty$
g_2	0^+	$+\infty$	$+\infty$	$+\infty$	0^+	0^+
$g_{2,R}$	0^+	$+\infty$	$+\infty$	$-\infty$	$+\infty$	$+\infty$
$g_{2,RR}$	$+\infty$	0^+	$2R_{\rm dS}^{-2}$ $+\infty$	$+\infty$	$-\infty$	$-\infty$
R	0^+	$+\infty$	$+\infty$	0^+	0^+	0^+

Table 3.1.: Limiting value of the functions f_1, f_2 and its R-derivatives as $x \to 0$ for different values of the parameter α. For comparison, we include the asymptotic value of the scalar curvature. Values of α for which the solutions are not defined are indicated by a double vertical line.

a) If $\alpha < -1$, there is a de Sitter epoch before the mGCG mimics a radiation fluid. In this case, there is no solution where both the first and second derivative of g converge to a finite value as the model evolves towards the radiation dominated epoch at $R = 0$. At best, we can choose $g(R) = C_2\, g_2(R)$, with $C_2 > 0$, so that both $g(R)$ and its first derivative are finite as the scalar curvature vanishes. In this case, g_R vanishes at $R = 0$ implying a divergence of the effective coupling G_f that would exponentiate the strength of gravity beyond that of the other interactions.

b) For $-1 < \alpha < 0$, the mGCG mimics a radiation fluid with infinite scalar curvature in the past. Although this asymptotic behaviour is different from the one of a pure radiation fluid in GR, where $R = 0$, we point out that a divergent scalar curvature in a radiation-dominated epoch is not in itself problematic. In fact, any small deviation from $w = 1/3$ in Eq. (3.83), even if subdominant with respect to ρ, can drive R away form zero. In this case, we find that g_2 gives once again the desired behaviour as g_2, $g_{2,R}$ and $g_{2,RR}$ remain positive during the radiation epoch[7]. For $-1 < \alpha < 0$, the behaviour at high curvature in the expression (3.119) is dominated by the term $R^{1-\frac{1}{4\alpha}}$. The change in qualitative behaviour of the second derivative changes at $\alpha = -1/4$ thus corresponds to the case where this leading term is R^2.

c) In the case of $0 < \alpha$, initially the mGCG mimics a radiation fluid and, contrary to the previous case, the scalar curvature vanishes in the past, much like a pure radiation fluid in GR. In this case, we find that we can obtain finite values of g, g_R and g_{RR} in the past if we set $g(R) = C_1 g_1(R)$ and $0 < \alpha \leq 1$. In addition, imposing $C_1 < 0$ guarantees that g_R and g_{RR} approach zero from positive values and therefore verify the stability conditions. The fact that g_R approaches zero implies that G_f would diverge in the past and that gravity would be much stronger than any other interaction in the Universe. At low curvature, the leading term, beyond the constant term, in Eq. (3.118) is $R^{1+1/\alpha}$. The change in the qualitative behaviour of the second derivative $g_{1,RR}$ observed in Tab. 3.1 for $\alpha = 1$, reflects that in that case the leading term becomes R^2.

[7] Here, we point out that since R diverges for $x = 0$, there exists no problem in the divergence of g_2, $g_{2,R}$ and $g_{2,RR}$ in Tab. 3.1.

α	$-\frac{5}{4}$	-1	$-\frac{3}{4}$	0	
g_3	1	1	1	1	1
$g_{3,R}$	$2R_{\rm dS}^{-1}$	$2R_{\rm dS}^{-1}$	$2R_{\rm dS}^{-1}$	$2R_{\rm dS}^{-1}$	$2R_{\rm dS}^{-1}$
$g_{3,RR}$	$-\frac{2R_{\rm dS}^{-2}}{\alpha(5+4\alpha)}$	$-\frac{2R_{\rm dS}^{-2}}{\alpha(5+4\alpha)}$	$-\frac{2R_{\rm dS}^{-2}}{\alpha(5+4\alpha)}$	$-\frac{2R_{\rm dS}^{-2}}{\alpha(5+4\alpha)}$	$-\frac{2R_{\rm dS}^{-2}}{\alpha(5+4\alpha)}$
g_4	0^+	0^+	$+\infty$	0^+	0^+
$g_{4,R}$	0^-	0^-	$-\infty$	$+\infty$	$-\infty$
$g_{4,RR}$	$+\infty$	0^+	$+\infty$	$-\infty$	$-\infty$

Table 3.2.: Limiting value of the functions f_3, f_4 and its R-derivatives as $x \to 1$ for different values of the parameter α. Values of α for which the solutions are not defined are indicated by a double vertical line.

In Tab. 3.2, we present the asymptotic value of g_3, g_4 and their R-derivatives as y approaches unity, i.e., when the mGCG mimics a cosmological constant, and for different values of the parameter α. Notice that apart from $\alpha = -1$ and $\alpha = 0$, the values $\alpha = -5/4$ and $\alpha = -3/4$ are excluded as they lead to a special case of the hypergeometric differential equation where the solutions (3.115) and (3.116) may no longer be valid. From this table we conclude that:

a) For $\alpha < -1$, i.e., when the radiation epoch is preceded by a de Sitter-like stage, we can obtain a solution with finite and positive values of g, g_R and g_{RR} at $R = R_{\rm dS}$ by restricting α to the interval $]-5/4, -1[$ and setting $g = C_3 g_R + C_4 g_4$ with $C_3 > 0$. For smaller values of α. it is possible to obtain solutions for which g and g_R are finite and positive by setting $C_3 > 0$ but the second derivative will either become negative ($C_4 = 0$) or diverge with positive values ($C_4 > 0$).

b) In the case of $-1 < \alpha < 0$, we find that solutions with appropriate behaviour of g, g_R and g_{RR} at $R = R_{\rm dS}$ can be obtained by setting $g = C_3 g_3$ with $C_3 > 0$. Using the relation between g_3 and the solutions g_1 and g_2, we find that $C_3 > 0$ leads to a positive coefficient for g_2 which implies that such a solution is also well behaved for large scalar curvature, cf. Tab. 3.1, with g, g_R and g_{RR} growing with positive values as R tends to infinity.

c) Finally, in the range $0 < \alpha$, we find that it is not possible to obtain a solution for which both g_R and g_{RR} are finite and positive around $R_{\rm dS}$. However, we can always set $g = C_3 g_3 + C_4 g_4$, with $C_4 < 0$, so that g_R and g_{RR} remain positive as R converges to $R_{\rm dS}$. The solution $g = C_1 g_1$, with $C_1 < 0$, which is well behaved for $R \approx 0$ falls into this category.

In Ref. [264], we focused on the case of $0 < \alpha < 1$ with $R + f(R) = g(R) = C_1 g_1(R)$ and $C_1 < 0$ which allowed us to obtain a well behaved solution with no divergences in the past evolution of the system. As mentioned above, in this case the conditions $1 + f_R > 0$ and $f_{RR} > 0$ are satisfied as R goes to zero, at $y = 0$. In order to fix the value of C_1 we imposed the additional condition that $f_R = 0$ at the present time. Recalling that $y_0 = A_s$, we obtain

$$C_1(\alpha,\, A_s) = -\frac{2}{5}\frac{A_s^{\frac{1}{1+\alpha}}}{R_{\rm dS}} F\left[\frac{1}{1+\alpha},\, 1+\frac{1}{2\,(1+\alpha)};\, 1+\frac{5}{4\,(1+\alpha)};\, A_s\right]. \tag{3.122}$$

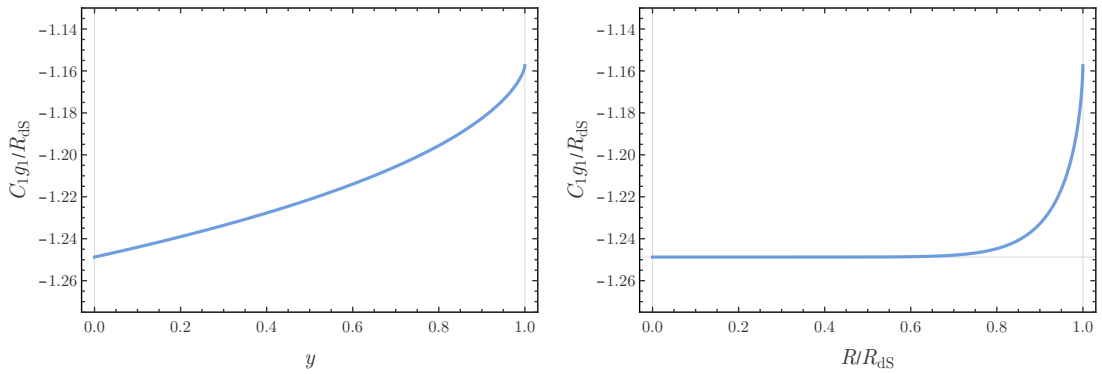

Figure 3.1.: Evolution of $R + f = C_1 g_1$ as a function of (left panel) the dimensionless variable y and (right panel) the scalar curvature R, with the linear coefficient C_1 defined by Eq. (3.122). The plots are obtained using the values $\alpha = 0.1$ and $A_s = 0.8$.

The solution $R + f = C_1\, g_1$ with C_1 defined by Eq. (3.122) is plotted in Fig. 3.1. We find that the positiveness of $1 + f_R$ and f_{RR} is extended to all $R \in]0,\, R_{\rm dS}[$, thus ensuring that the effective gravitational coupling is positive and that the solution found avoids the Dolgov-Kawasaki instability[8]. This, coupled with the fact that the function $R + f$ itself is negative throughout the whole range $R \in]0,\, R_{\rm dS}[$ implies that the effective mass (3.14) is positive, in particular during the late asymptotic de Sitter phase.

3.2.3. Discussion

In this Section, we have described a new method within the reconstruction approach known as *designer* $f(R)$ to obtain solutions in metric $f(R)$-gravity that are compatible with a given evolution of a FLRW Universe. Specifically, we have worked out the differential equation that defines the function $f(R)$ when the total energy budget of the Universe, including the contribution from matter and the effective fluid arising from the modifications of gravity, satisfies a barotropic EoS $P(\rho)$. The homogeneous solutions to such an equation represent vacuum solutions and can be used to search for solutions in the general case when matter is included. This method could in principle be generalised to include a non-barotropic EoS, such as $P(\rho,\, \dot{\rho})$, or to include the effects of viscosity. However, due to the difficulty of finding exact solutions even in the most simple cases, it is unclear whether such an extension would be fruitful.

Using this reconstruction method, we have fully mapped the modified generalised Chaplygin gas (mGCG), a 2-parameter extension of the Chaplygin gas which was originally proposed as an alternative to DM and DE [57, 60, 205], onto $f(R)$-gravity in the absence of matter fluids. Unfortunately, the analytical expressions of the solutions obtained are quite cumbersome. This reflects one of the main disadvantages of employing the strategy of *designer* $f(R)$–while it can provide us with exact solutions for $f(R)$, often-times these are extremely complicated to handle analytically and as a consequence the physical interpretation of the solution becomes quite a difficult task. Nevertheless, for specific values of the parameters of the model the complexity of the solutions found is substantially reduced,

[8] As observed on the r.h.s. panel of Fig. 3.1, $R + f(R)$ in an increasing function of R with positive curvature.

allowing for a more detailed study of the physical implications of the model.

One of such cases is obtained when we fix the parameter $\beta = 1/3$, in which case the mGCG interpolates between radiation and an effective cosmological constant. Such a behaviour of the mGCG can be considered both in the context of reheating [74, 76] or at late-time to obtain a unified description for dark radiation and DE [264]. In this case, the differential equation for $f(R)$ reduces to that of a hypergeometric function, greatly simplifying the solution with respect to the general case. Using the conditions for the physical viability of $f(R)$ actions and the asymptotic behaviour of the hypergeometric functions, we were then able to classify the solution found, defining intervals of interest for the mGCG parameter α. In particular, when the mGCG mimics radiation in the past and a cosmological constant in the future, we find that adequate solutions can be found for $0 < \alpha < 1$ which are well behaved at all points except in the extremely distant future.

3.3. Dark radiation as $f(R)$-gravity

The concept of a dark radiation (DR), an unknown relativistic component that much like DM and DE only interacts gravitationally with normal matter, was introduced after an excess in the radiation content of the Universe was detected in CMB observations [37] that could not be explained by the photons from the last scattering surface or the three families of leptons in the Standard Model. The radiation content is usually parameterised in terms of an effective number of relativistic degrees of freedom $N_{\rm eff}$, cf. Eq. (1.40) and the Standard Model of particles with three families of leptons predicts $N_{\rm eff} = 3.046$, where the deviation from 3 is due to thermodynamic considerations [249]. Some of the first models proposed to explain this excess theorised the existence of additional sterile neutrinos [1, 37], an idea that seemed supported by initial best-fit values of $N_{\rm eff}$ close to 4. However, subsequent missions lowered this number considerably, making it incompatible with a new species of (sterile) neutrinos. Other proposals that have been explored include dark photons that interacts only with DM particles [9], thermal axions from Quantum Chromodynamics [37], or an extra contribution from the decay of dark matter particles into very light particles [181, 259]. The final results of Planck mission, in conjunction with BAO measurements, fix the value $N_{\rm eff} = 2.99^{+0.34}_{-0.33}$ [19], which supports the Concordance Model with no DR component. However, higher values of the effective number of degrees of freedom are still compatible with the data as long as H_0 is allowed to take on larger values. In fact, restricting the analysis to the physically motivated range $\Delta N_{\rm eff} > 0$ leads to the constraint $\Delta N_{\rm eff} < 0.30$ at 95% confidence level.

In this section we explore the possibility that DR is the manifestation of a modification of gravity, namely within the context of metric $f(R)$-gravity. The main results presented in this section[9] were published in Ref. [264]. We note that at the time of the publication, the partial results of Planck mission indicated a higher value of the number of effective degrees of freedom, $N_{\rm eff} = 3.15$ [16], which represented a 3.4% excess with regards to the theoretical prediction from the Standard Model. This value is within the 95% confidence level interval presented in the final Planck data release [19].

[9] With regards to the results present in Ref. [264], in this section we add a further study of the dependence of the cosmographic parameters on the mGCG that accounts for DR and DE, an analytical solution for $f(R)$ in a universe filled by radiation and pressureless dust and where the modifications to gravity account for a DR component and a study of the growth rate of the matter perturbations.

3.3.1. Background model

Let us consider a model of a universe filled by dust (DM and baryonic matter), radiation (photons and neutrinos) and by a mGCG fluid which behaves as (dark) radiation in the past and as an effective cosmological constant in the future. After solving the continuity equation for each individual fluid, the Friedmann equation for such universe reads

$$3H^2 = \rho_{\mathrm{r},0}\left(\frac{a_0}{a}\right)^4 + \rho_{\mathrm{m},0}\left(\frac{a_0}{a}\right)^3 + \rho_{\mathrm{Ch},0}\left[A_s + (1-A_s)\left(\frac{a_0}{a}\right)^{4(1+\alpha)}\right]^{\frac{1}{1+\alpha}}, \tag{3.123}$$

where the mGCG parameters verify $0 < A_s < 1$ and $0 < 1+\alpha$. For $a \ll a_* = [(1-A_s)/A_s]^{\frac{1}{4(1+\alpha)}}$ the mGCG energy density behaves as

$$\rho_{\mathrm{Ch}}(a) \approx \Omega_{\mathrm{dr},0}\left(\frac{a_0}{a}\right)^4, \qquad \Omega_{\mathrm{dr},0} := (1-A_s)^{\frac{1}{1+\alpha}}\Omega_{\mathrm{Ch},0}\,, \tag{3.124}$$

thus contributing to the total amount of the relativistic content of the Universe in the past:

$$\Omega_{\mathrm{rel}}(a) = (\Omega_{\mathrm{r},0} + \Omega_{\mathrm{dr},0})\left(\frac{a_0}{a}\right)^4. \tag{3.125}$$

At late-time, for $a \gg a_*$, the mGCG behaves instead as an effective cosmological constant with

$$\rho_{\mathrm{Ch}}(a) \approx \rho_{\mathrm{dS}}\,, \qquad \rho_{\mathrm{dS}} := A_s^{\frac{1}{1+\alpha}}\rho_{\mathrm{Ch},0}\,. \tag{3.126}$$

Phenomenologically, the total relativistic content of the Universe is parameterised as

$$\Omega_{\mathrm{rel},0} = \left[1 + \frac{7}{8}\left(\frac{4}{11}\right)^{4/3} N_{\mathrm{eff}}\right]\Omega_{\gamma,0} = \left[1 + \frac{7}{8}\left(\frac{4}{11}\right)^{4/3}\left(N_{\mathrm{eff}}^{(\nu)} + N_{\mathrm{eff}}^{(\mathrm{dr})}\right)\right]\Omega_{\gamma,0}\,. \tag{3.127}$$

By comparing Eq. (3.124) with the parametrisation (3.127) we can write $\Omega_{\mathrm{r},0}$ and $\Omega_{\mathrm{dr},0}$ as

$$\Omega_{\mathrm{r},0} = \left[1 + \frac{7}{8}\left(\frac{4}{11}\right)^{4/3} N_{\mathrm{eff}}^{(\nu)}\right]\Omega_{\gamma,0} = (1-D)\,\Omega_{\mathrm{rel},0}\,, \tag{3.128}$$

$$\Omega_{\mathrm{dr},0} = \frac{7}{8}\left(\frac{4}{11}\right)^{4/3} N_{\mathrm{eff}}^{(\mathrm{dr})}\Omega_{\gamma,0} = D\Omega_{\mathrm{rel},0}\,, \tag{3.129}$$

where $D = D(N_{\mathrm{eff}}^{(\mathrm{dr})}) \in [0,\,1]$ is the percentage of relativistic matter that corresponds to DR:

$$D(N_{\mathrm{eff}}^{(\mathrm{dr})}) := \frac{\frac{7}{8}\left(\frac{4}{11}\right)^{4/3} N_{\mathrm{eff}}^{(\mathrm{dr})}}{1 + \frac{7}{8}\left(\frac{4}{11}\right)^{4/3}\left(N_{\mathrm{eff}}^{(\nu)} + N_{\mathrm{eff}}^{(\mathrm{dr})}\right)}\,. \tag{3.130}$$

In addition, using the equalities (3.128) and (3.129) in conjunction with the Friedmann constraint

$$1 = \Omega_{\mathrm{r},0} + \Omega_{\mathrm{m},0} + \Omega_{\mathrm{Ch},0}\,, \tag{3.131}$$

Free parameters	$\{\alpha,\, D\}$	α
$\Omega_{\mathrm{m},0}$	0.3065	0.3065
z_{eq}	3361	3361
D	—	1.377×10^{-2}
$\Omega_{\mathrm{rel},0}$	9.117×10^{-5}	9.117×10^{-5}
$\Omega_{\mathrm{r},0}$	$9.117\times10^{-5}(1-D)$	8.991×10^{-5}
$\Omega_{\mathrm{dr},0}$	$9.117\times10^{-5}D$	1.255×10^{-6}
$\Omega_{\mathrm{Ch},0}$	$0.6934+9.117\times10^{-5}D$	0.6934
A_s	$1-\left(\frac{D}{7682.93+D}\right)^{1+\alpha}$	$1-\left(1.792\times10^{-6}\right)^{1+\alpha}$

Table 3.3.: Values of relevant physical quantities for the model (3.123) in terms of the choice of the parameters $\{\alpha,\, D\}$ and $\{\alpha\}$. For the value of $\Omega_{\mathrm{m},0}$ and z_{eq} we use the TT+lowP+lensing+ext best-fit values of Planck mission [16]. On the rightmost column we fix D using the formula (3.130) and the best-fit value for N_{eff}.

and the definition of the redshift at dust-radiation equality $1+z_{\mathrm{eq}} := \Omega_{\mathrm{m},0}/\Omega_{\mathrm{rel},0}$, we are able to write the mGCG parameter A_s as

$$A_s = 1-\left[\frac{\frac{D}{1+z_{\mathrm{eq}}}\Omega_{\mathrm{m},0}}{1-\left(1+\frac{1-D}{1+z_{\mathrm{eq}}}\right)\Omega_{\mathrm{m},0}}\right]^{1+\alpha}. \tag{3.132}$$

Thus, we can fully characterise the model in terms of the four parameters $\{\Omega_{\mathrm{m},0},\, z_{\mathrm{eq}},\, \alpha,\, D\}$. Notice that, if we take $D=0$, we recover the ΛCDM model with a radiation component, independently of the value of α.

In order to fix the parameters of the model, we use the best-fit values for $\Omega_{\mathrm{m},0}$ and z_{eq} from Planck mission [16]. This allows us to write all the relevant quantities of the model in terms of the parameters $\{\alpha,\, D\}$, or, equivalently, $\{\alpha,\, N_{\mathrm{eff}}^{(\mathrm{dr})}\}$. Alternatively, we can take the observational value $N_{\mathrm{eff}}=3.15$ [16] to fix the parameter D at 1.377%. In this case only α remains as a free parameter. In Tab. 3.3, we present the values of the relevant physical quantities of the model in terms of the free parameters $\{\alpha,\, D\}$ and in terms of α when D is fixed using the formula (3.130) and the best-fit value of N_{eff} from Planck mission [16]. In Fig. 3.2, we show on the l.h.s. panel the evolution of the squared Hubble rate and on the r.h.s. panel the evolution of the individual fractional energy densities of pressureless matter Ω_{m} (blue solid curve), of radiation, Ω_{r} (red dashed curve), and of the mGCG, Ω_{Ch} (green dot-dashed curve), for the choice of the parameters $D=1.377\%$ and $\alpha=0.1$. Initially, during the radiation dominated epoch, the contribution of photons and neutrinos is dominant but there is a small but constant contribution from the mGCG in the form of DR. After the radiation-matter equality (leftmost thin vertical line), as pressureless matter starts to dominate the energy budget of the Universe, the contribution of radiation and the contribution of the mGCG become residual. Close

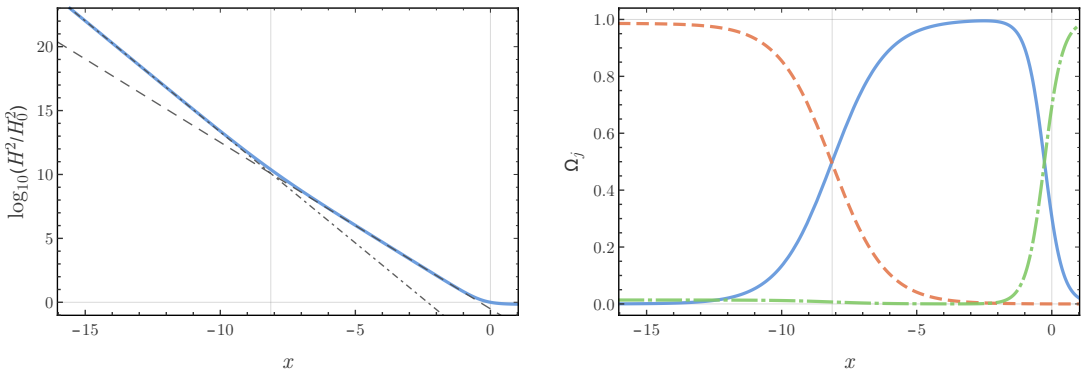

Figure 3.2.: (Left panel) Evolution of H^2/H_0^2 (solid blue curve) as a function of $x = \log(a/a_0)$. For comparison, the approximate behaviours during the radiation dominated and matter dominated epochs are shown as dot-dashed and dashed black curves, respectively. (Right panel) The fractional energy density of pressureless matter (blue solid curve), of radiation (red dashed curve) and of the mGCG (green dot-dashed curve) as functions of x. The vertical lines represent, from left to right, the moment of radiation-matter equality and the present time. The plots shown were obtained using the values of Tab. 3.3 with $D = 1.377\%$ and $\alpha = 0.1$.

to the present time, however, the mGCG starts to mimic a cosmological constant and overcomes matter as the main component of the Universe.

3.3.2. Cosmography

In order to test the validity of our model, we now apply a cosmographic approach. We begin by presenting the theoretical predictions of the model (3.123) for the cosmographic parameters $\{q_0,\, j_0,\, s_0,\, l_0\}$ in terms of the cosmological parameters $\{\Omega_{\mathrm{m},0},\, \Omega_{\mathrm{r},0},\, \alpha,\, A_s\}$ [264] :

$$q_0 = -1 + \frac{3}{2}\Omega_{\mathrm{m},0} + 2\Omega_{\mathrm{r},0} + 2\,(1 - A_s)\,[1 - \Omega_{\mathrm{m},0} - \Omega_{\mathrm{r},0}]\ , \tag{3.133}$$

$$j_0 = 1 + 2\Omega_{\mathrm{r},0} + 2\,(1 - A_s)\,(1 + 4\alpha A_s)\,[1 - \Omega_{\mathrm{m},0} - \Omega_{\mathrm{r},0}]\ , \tag{3.134}$$

$$\begin{aligned} s_0 = {} & 1 - \frac{9}{2}\Omega_{\mathrm{m},0} - [12 + 3\Omega_{\mathrm{m},0} + 4\Omega_{\mathrm{r},0}]\,\Omega_{\mathrm{r},0} \\ & - (1 - A_s)\left\{4\left[3 - 8\alpha^2 A_s + 8\alpha(1+\alpha)A_s^2\right] + 3(1 + 4\alpha A_s)\Omega_{\mathrm{m},0} + 8(1 + 2\alpha A_s)\Omega_{\mathrm{r},0}\right\} \\ & \times [1 - \Omega_{\mathrm{m},0} - \Omega_{\mathrm{r},0}] - 4\,(1 - A_s)^2\,(1 + 4\alpha A_s)\,[1 - \Omega_{\mathrm{m},0} - \Omega_{\mathrm{r},0}]^2\ , \end{aligned} \tag{3.135}$$

$$\begin{aligned} l_0 = {} & 1 + 3\Omega_{\mathrm{m},0} + \frac{27}{2}\Omega_{\mathrm{m},0}^2 + [28 + 72\Omega_{\mathrm{m},0} + 76\Omega_{\mathrm{r},0}]\,\Omega_{\mathrm{r},0} \\ & + 4\,(1 - A_s)\left\{7 + 4\alpha\left(3 + 2\alpha + 8\alpha^2\right)A_s - 8\alpha\left(5 + 22\alpha + 24\alpha^2\right)A_s^2\right. \\ & \quad + 32\alpha\left(2 + 7\alpha + 6\alpha^2\right)A_s^3 + 9\left[2 + \alpha(1 - 4\alpha)A_s + 4\alpha(1 + 2\alpha)A_s^2\right]\Omega_{\mathrm{m},0} \\ & \quad \left. + 2\left[19 + 2\alpha(5 - 12\alpha)A_s + 24\alpha(1 + 2\alpha)A_s^2\right]\Omega_{\mathrm{r},0}\right\}[1 - \Omega_{\mathrm{m},0} - \Omega_{\mathrm{r},0}] \\ & + 4\,(1 - A_s)^2\left[19 + 4\alpha(5 - 12\alpha)A_s + 16\alpha(3 + 7\alpha)A_s^2\right][1 - \Omega_{\mathrm{m},0} - \Omega_{\mathrm{r},0}]^2\,. \end{aligned} \tag{3.136}$$

As expected, for $A_s = 1$ ($D = 0$), the previous expressions reduce to the ones of ΛCDM with a radiation component. Using the values and formulas of Tab. 3.3 we can write the cosmographic parameters in terms of the free parameters α and D as

$$q_0 = -0.54007 + \Delta q_0(\alpha, D)\,, \tag{3.137}$$
$$j_0 = 1.0002 + \Delta j_0(\alpha, D)\,, \tag{3.138}$$
$$s_0 = -0.38042 + \Delta s_0(\alpha, D)\,, \tag{3.139}$$
$$l_0 = 3.1922 + \Delta l_0(\alpha, D)\,, \tag{3.140}$$

where the first term corresponds to the base value obtained in ΛCDM with a radiation component ($D = 0$) and the second term corresponds to a correction derived from the contribution of the mGCG. In Fig. 3.3 we present the contours on the $\{\alpha, D\}$ plane of $|\Delta q_0/q_0^{\rm base}|$, $|\Delta j_0/j_0^{\rm base}|$, $|\Delta s_0/s_0^{\rm base}|$ and $|\Delta l_0/l_0^{\rm base}|$. The number of dots in each contour line indicates the (negative) order of magnitude of the deviation, e.g., a dot-dot-dashed line in the panel of the cosmographic parameter X indicates the contour where $|\Delta X/X_0^{\rm base}| = 10^{-2}$. Therefore, darker regions correspond to higher deviations from the base value. As long as we choose α close to 0, we find that the deviations introduced by the mGCG do not contribute significantly for the cosmographic parameters and we can use the values obtained for ΛCDM with a radiation component. This is to be expected as $\alpha = 0$ corresponds to the case where the mGCG behaves exactly as a cosmological constant plus a radiation term, which has a very small contribution to the cosmographic parameters at the present time. For the choice of parameters $\{\alpha, D\} = \{0.1, 1.377\}$, which will be used in the numerical results of the following sections, we find that the deviation of the cosmographic parameters with regards to the base value is less than 10^{-4}, as indicated by the red point in Fig. 3.3.

3.3.3. $f(R)$ solution for the background

Having defined the evolution of the FLRW background, we wish to find a compatible $f(R)$ function that can accommodate the mGCG contribution in Eq. (3.123). Unfortunately, the presence of dust-like matter and radiation means that we can no longer use the solutions (3.113)–(3.116) found in the previous section. Instead, we opt to integrate numerically the modified Friedmann equation (3.15), which, working with $x := \log(a/a_0)$ as the time variable[10], can be re-written as

$$(R+f)_{xx} + \left[1 - \frac{R}{6H^2} - \frac{R_{xx}}{R_x}\right](R+f)_x + \frac{R_x}{6H^2}(R+f) = R_x \frac{\rho_{\rm r} + \rho_{\rm m}}{3H^2/\kappa^2}\,. \tag{3.141}$$

Here, an x-subscript indicates a derivative with respect to x and $\rho_{\rm r}$ and $\rho_{\rm m}$ are the radiation and matter energy density, corresponding to the first two terms of Eq. (3.123). In order to impose boundary conditions in this equation, we assume that the deviation from GR with a cosmological constant is small at the present time and therefore we can write

$$(R+f)_0 = R_0 - 6H_0^2\left[1 - \Omega_{{\rm r},0} - \Omega_{{\rm m},0}\right]\,, \qquad (R+f)_x(x = x_0) = R_x(x = x_0)\,. \tag{3.142}$$

[10] With this choice for the time variable, the lapse function becomes $N = 1/H$.

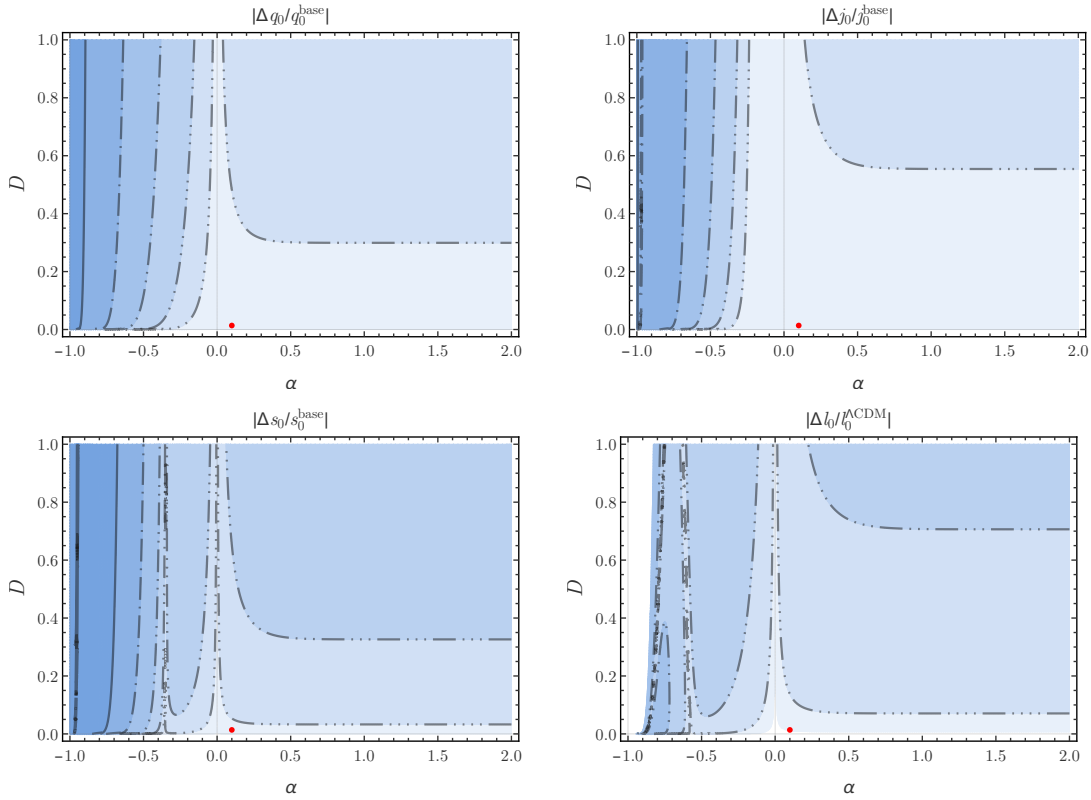

Figure 3.3.: Contour lines of the fractional deviations $|\Delta q_0/q_0^{\rm base}|$ (Top-Left Panel), $|\Delta j_0/j_0^{\rm base}|$ (Top-Right Panel), $|\Delta s_0/s_0^{\rm base}|$ (Bottom-Left Panel) and $|\Delta l_0/l_0^{\rm base}|$ (Bottom-Right Panel) on the $\{\alpha,\, D\}$ plane. The number of dots in each contour line indicates the (negative) order of magnitude of the deviation, e.g., a dot-dot-dashed line indicates a deviation of 10^{-2}. Darker regions indicate regions of higher deviation from the base value. The choice $\{\alpha,\, D\} = \{0.1,\, 1.377\}$ used for the numerical results in the rest of the section is indicated by a red point.

Using the cosmographic formulas (3.76)–(3.79) for $f(R)$-gravity, we can calculate the values of the function f and its derivatives that are compatible with the cosmographic parameters obtained for the background model as

$$\frac{(R+f)_0}{6H_0^2} = 0.57451, \qquad \frac{f_{RR,0}}{(6H_0^2)^{-1}} = 1.4962\times 10^{-16}, \qquad \frac{f_{RRR,0}}{(6H_0^2)^{-2}} = 1.3017\times 10^{-4}. \quad (3.143)$$

Of course, the values here obtained via the cosmographic approach are consistent with the assumption that $f(R)$ is close to GR with a cosmological constant at the present and with the boundary conditions imposed above.

In Figs. 3.4 and 3.5, we present the numerical solutions and their R-derivatives (continuous blue curve) obtained when $D = 1.377\%$. For comparison, we also show the behaviour of the Einstein-Hilbert action $R - 2\Lambda$ (red dashed curve) and of the expansion obtained from the cosmographic approach (green dot-dashed line). As expected, during the late-time evolution the solution $R + f(R)$ obtained mimics very closely the Einstein-Hilbert action and the expansion derived from the values of the

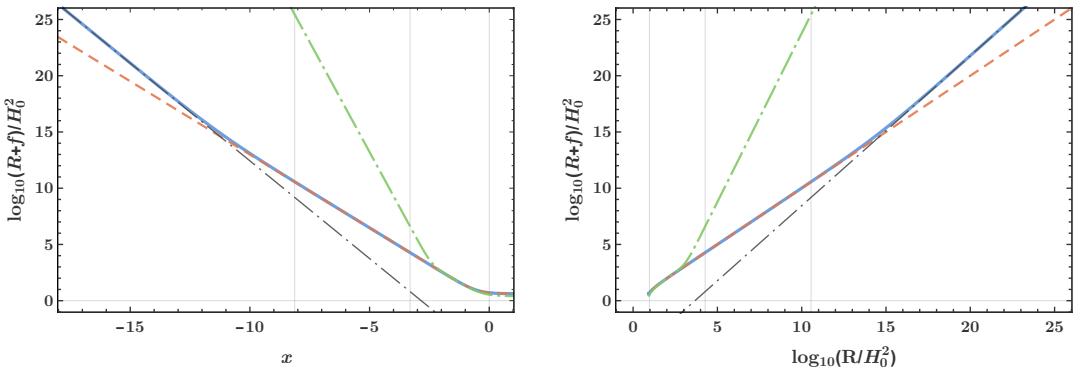

Figure 3.4.: The numerical solution of the function $f(R)$ as a function of $x = \log(a/a_0)$ (left panel) and of R (right panel) is shown as a continuous blue curve. The corresponding behaviour in the case of GR is shown as a red dashed curve, while the Taylor expansion obtained from the cosmographic approach, cf. Eq (3.143), is shown as a green dot-dashed curve. The asymptotic behaviour at high energy density is shown as a thin black dot-dashed curve. The integration of Eq. (3.141) was performed using the boundary conditions (3.142) and with the choice for the free parameters: $D = 1.377\%$ and $\alpha = 0.1$.

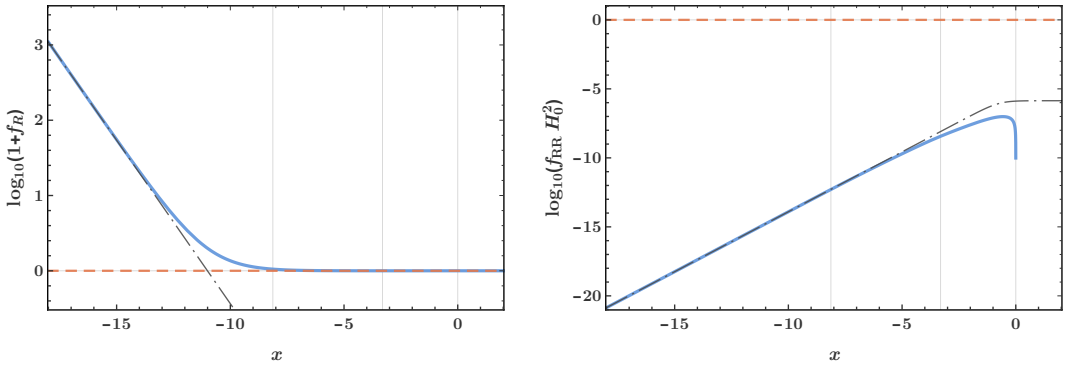

Figure 3.5.: The numerical solution for $1 + f_R$ (left Panel) and f_{RR} (right Panel) of the solution plotted in Fig. 3.5 as functions of $x = \log(a/a_0)$ is shown as a continuous blue curve. The corresponding behaviour in the case of GR is shown as a red dashed curve. The asymptotic behaviour at high energy density is shown as a thin black dot-dashed curve. The integration of Eq. (3.141) was performed using the boundary conditions (3.142) and with the choice for the free parameters: $D = 1.377\%$ and $\alpha = 0.1$.

cosmographic parameters. In addition, we note that the numerical solution obtained satisfies the stability criteria of Sect. 3.1.2, since $1 + f_R$ and f_{RR} remain positive and finite throughout the evolution till the present time. However, in the future f_{RR} becomes negative, as can be seen by the downward vertical evolution of the blue curve on the rhs panel of Fig. 3.5. As a consequence, the effective mass m^2_{eff} also becomes negative, which suggests that the de Sitter evolution of this $f(R)$ solution might suffer from a Dolgov-Kawasaki-like instability [141, 151]. We stress, however, that this would happen only in the future and we have no guarantee that indeed a de Sitter-like stage would be the asymptotic behaviour of our Universe.

During the radiation dominated epoch, we find that $R + f(R) \propto R^{4/3}$ with the fitted values

$$R + f(R) \approx 1.28067 \times 10^{-5} R^{4/3}\,, \qquad (\text{for } D = 1.377\%)\,. \tag{3.144}$$

Such a behaviour is indicated by the thin black dot-dashed curve in Fig. 3.5. In order to make sense of this behaviour for $f(R)$, we write the matter energy density, the Hubble rate and the scalar curvature at beyond leading order during the radiation dominated epoch as

$$\rho^{(\mathrm{m})} \approx \frac{3H_0^2}{\kappa^2}\left[\Omega_{\mathrm{r},0}\left(\frac{a_0}{a}\right)^4 + \Omega_{\mathrm{m},0}\left(\frac{a_0}{a}\right)^3\right], \tag{3.145}$$

$$H^2 \approx H_0^2\left[(\Omega_{\mathrm{r},0} + \Omega_{\mathrm{dr},0})\left(\frac{a_0}{a}\right)^4 + \Omega_{\mathrm{m},0}\left(\frac{a_0}{a}\right)^3\right], \tag{3.146}$$

$$R \approx 3H_0^2\Omega_{\mathrm{m},0}\left(\frac{a_0}{a}\right)^3. \tag{3.147}$$

By replacing these variable in the modified Friedmann equation (3.15), we obtain a differential equation for $R + f$ in terms of the rescaled scalar curvature $r := R/(\Omega_{\mathrm{m},0}H_0^2)$:

$$\left[1 + \frac{1}{1+z_{\mathrm{eq}}}\left(\frac{r}{3}\right)^{1/3}\right] r^2 (R+f)_{rr} - \left[\frac{1}{6} + \frac{1}{1+z_{\mathrm{eq}}}\left(\frac{r}{3}\right)^{1/3}\right] r (R+f)_r - \frac{(R+f)}{6} = \frac{\Omega_{\mathrm{m},0}H_0^2}{3}\left[1 + \frac{1-D}{1+z_{\mathrm{eq}}}\left(\frac{r}{3}\right)^{1/3}\right] r\,. \tag{3.148}$$

Here, an r-subscript indicates a derivative with respect to r. The general solution of this equation is

$$R + f = \Omega_{\mathrm{m},0}H_0^2\left[1 + \frac{6D}{1+z_{\mathrm{eq}}}\left(\frac{r}{3}\right)^{1/3}\right] r + C_- g_-(r) + C_+ g_+(r)\,. \tag{3.149}$$

where the solutions $g_\pm$ to the homogeneous equation are defined as

$$g_\pm(r) = r^{\frac{7\pm\sqrt{73}}{12}} F\left[\frac{-9\pm\sqrt{73}}{4}, \frac{7\pm\sqrt{73}}{4}; 1 \pm \frac{\sqrt{73}}{2}, -\frac{1}{1+z_{\mathrm{eq}}}\left(\frac{r}{3}\right)^{\frac{1}{3}}\right]. \tag{3.150}$$

At large curvature, the two homogeneous solutions $g_\pm$ behave as $R^{4/3}$, much like the leading term of the non-homogeneous solution in Eq. (3.149), justifying the asymptotic behaviour shown in Fig. 3.4. In fact, the non-homogeneous term in Eq. (3.149) accounts for only about 50% of the $R^{4/3}$-coefficient in the fitted values (3.144), with the rest being determined by the homogeneous part of the solution.

3.3.4. Growth of Linear Perturbations

We next analyze the evolution of the scalar perturbations in our model, since the radiation epoch till the present time, and compare it with the evolution of perturbations in the concordance ΛCDM model with a radiation component. In particular, we will look for the effects of the $f(R)$ modifications in the matter power spectrum as measured today.

In a metric $f(R)$ theory, in the absence of an anisotropic stress from the matter sector, the off-diagonal $(i-j)$ component of the perturbed Einstein equations (3.52) in Fourier space relates the

Bardeen potentials Φ and Ψ with the perturbation $\delta F := \delta f_R$ as [112, 134, 290, 320]

$$(1+f_R)\,(\Psi_k - \Phi_k)\,f_R = \delta F_k\,. \tag{3.151}$$

This equation shows how $f(R)$-gravity breaks the equality between the Bardeen potentials that characterise GR in the absence of anisotropies from the matter sector, contributing to the total anisotropy of the Universe. We now introduce the new set of variables Ψ^+ and Ξ to replace the Bardeen potentials

$$\Psi^+ \equiv \frac{\Phi+\Psi}{2}\,, \qquad\qquad \Xi \equiv \frac{\delta F}{1+f_R} = \Psi - \Phi\,. \tag{3.152}$$

Here, and in the rest of this section, we drop the k subscript so as to simplify the notation. Notice that Ψ^+ corresponds to the variable Φ^+ in Ref. [290], while Ξ corresponds to the variable χ of the same reference divided by $1+f_R$. We choose to work with the variable Ξ instead of χ, because this choice directly reflects the difference between the two potentials and allow us a better control of the numerical integrations, even when the theory deviates considerably from GR ($|f_R| \gg 0$). In order to obtain the evolution equations for these variables, we can combine the $(0-0)$ and $(i-0)$ components of the Einstein equations as

$$\Psi^+_x = -\Psi^+ - \frac{1}{4}\frac{(f_R)_x}{1+f_R}\left(2\Psi^+ - 3\Xi\right) - \frac{\kappa^2(\bar\rho+\bar P)}{2(1+f_R)H^2}aH\,v^{(N)}\,, \tag{3.153}$$

$$\begin{aligned}\Xi_x = \Xi &+ \frac{\kappa^2(\bar\rho+\bar P)}{(1+f_R)H^2}aH\,v^{(N)} + \frac{1}{2}\frac{(f_R)_x}{1+f_R}\left(2\Psi^+ - 3\Xi\right) - 2\frac{1+f_R}{(f_R)_x}\frac{H_x}{H}\Xi \\ &- \frac{2}{3}\frac{1+f_R}{(f_R)_x}\left[2\frac{k^2}{(aH)^2}\Psi^+ + \frac{\kappa^2\bar\rho}{(1+f_R)H^2}\left(\delta^{(N)} - 3H(1+w)a\,v^{(N)}\right)\right]\,,\end{aligned} \tag{3.154}$$

where we recall that $\delta^{(N)}$ and $v^{(N)}$ are GI quantities that reduce to the total fractional energy density perturbation δ and peculiar velocity v in the Newtonian gauge. Eqs. (3.153) and (3.154) are equivalent to the ones obtained in Ref. [290]. Here, however, we have used the evolution equation for Ψ^+ (3.153) to eliminate the dependence of Ξ_x on Ψ^+_x in Eq. (3.154). Equations (3.153) and (3.154) are complemented by the evolution equations, two for each fluid, for the perturbations of the matter fluids. In the present case, where we consider the presence of dust and radiation fluids, the evolution equations read

$$(\delta^{(N)}_{\rm r})_x - \frac{4}{3}\frac{k^2}{(aH)^2}v^{(N)}_{\rm r} = 4\Psi^+_x + 2\Xi_x\,, \tag{3.155}$$

$$(v^{(N)}_{\rm r})_x + \frac{1}{4aH}\delta^{(N)}_{\rm r} = -\frac{1}{2aH}\left(2\Psi^+ - \Xi\right)\,, \tag{3.156}$$

$$(\delta^{(N)}_{\rm m})_x - \frac{k^2}{(aH)^2}aH\,v^{(N)}_{\rm m} = 3\Psi^+_x + \frac{3}{2}\Xi_x\,, \tag{3.157}$$

$$(v^{(N)}_{\rm m})_x + v^{(N)}_{\rm m} = -\frac{1}{2aH}\left(2\Psi^+ - \Xi\right)\,. \tag{3.158}$$

Here, the perturbations $\delta^{(N)}_{\rm i}$ and $v^{(N)}_{\rm i}$, with ${\rm i} = {\rm r}, {\rm m}$, are the GI quantities that reduce, respectively, to the fractional energy density perturbation and to the peculiar velocity potential in the Newtonian

gauge[11] .

In order to set initial conditions for the matter perturbation variables well inside the radiation-dominated epoch, we assume the usual adiabatic conditions that apply for modes well outside the Hubble horizon ($k^2 \ll (aH)^2$) [244]

$$\delta_{\rm m}^{(N)} = \frac{3}{4}\delta_{\rm r}^{(N)} = \frac{3}{4}\delta^{(N)}\,, \qquad\qquad v_{\rm m}^{(N)} = v_{\rm r}^{(N)} = v^{(N)}\,. \tag{3.159}$$

Having fixed the initial relations between the individual fluid variable and the total matter perturbations, we can use Eqs. (3.153) and (3.154) to obtain $\delta^{(N)}$ and $v^{(N)}$ in terms of the initial values of Ψ^+, Ξ and their derivatives. In GR, where $\Xi = \Xi_x = 0$ and $\Psi^+ = \Psi = \Phi$, an explicit solution for the evolution of the gravitational potential for modes outside the Hubble horizon can be obtained and, to leading order in $k^2/(aH)^2$, we find that the $(0-0)$ and $(0-i)$ components of the perturbed Einstein equations allow us to relate the initial values of δ and v with the gravitational potential Φ as

$$\Phi_{\rm ini} = -\frac{1}{2}\delta_{\rm ini}^{(N)}\,, \qquad\qquad \Phi_{\rm ini} = -2a_{\rm ini}H_{\rm ini}\,v_{\rm ini}^{(N)}\,. \tag{3.160}$$

These can then be related to the comoving curvature perturbation $\mathcal{R}$ through the relation, valid for constant EoS parameter w and for modes outside the Hubble horizon [53]

$$\mathcal{R} = \frac{5+3w}{3+3w}\Phi\,. \tag{3.161}$$

Using this relation[12], and the fact the comoving curvature perturbation remains constant for super-horizon evolution in adiabatic conditions, we can relate the value of the gravitational potential during the radiation dominated epoch with the value of $\mathcal{R}$ at the end of inflation, as given by the primordial power spectrum

$$\mathcal{P}_{\mathcal{R}} = \frac{k^3}{2\pi^2}|\mathcal{R}|^2 = A_S\left(\frac{k}{k_*}\right)^{n_s-1}\,. \tag{3.162}$$

The best-fit of the 2015 Planck mission[13] [16] for the primordial power spectrum $P_{\mathcal{R}}$ set $n_s = 0.9681$ for the scalar index and $A_S = 2.143\times10^{-9}$ for the amplitude of the scalar primordial power spectrum at the pivot scale k_* that corresponds to 0.05 Mpc^{-1}.

In metric $f(R)$-gravity, however, the existence on an additional degree of freedom in the scalar sector spoils this relationship between the gravitational potential and the matter variable in the initial radiation-dominated epoch. In fact, it is no longer guaranteed that a static solution for Ψ^+ is obtained for the modes outside the Hubble horizon. In order to set initial conditions for the numerical integrations, we then have to take into account the possible contribution of the four variables

$$\Psi^+(x_{\rm ini})\,, \qquad \Psi_x^+(x_{\rm ini})\,, \qquad \Xi(x_{\rm ini})\,, \qquad \Xi_x(x_{\rm ini})\,. \tag{3.163}$$

Here, we are helped by the linearity of the Eqs. (3.153)–(3.158), which allows to write the general

[11] For the definition of these GI quantities, please see Eq. (A.54) of the Appendix A.

[12] We stress that the relation (3.161), which is derived in GR, is not necessarily valid in metric $f(R)$ theories, where a new scalar degree of freedom, δF, needs to be taken into account.

[13] Here, we employ the best-fit values that we used in our published work of 2015 [264].

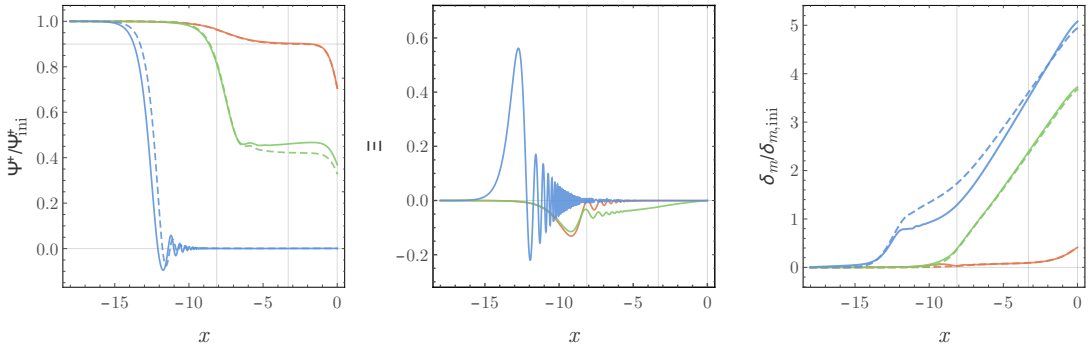

Figure 3.6.: Evolution of Ψ^+ (Left panel), Ξ (Middle Panel) and $\delta_{\rm m}$ (Right panel) for three different wave-numbers: $k = k_0$ (red); $k = 10^2 k_0$ (green) and $k = 10^4 k_0$ (blue). The results in our $f(R)$ model are shown in solid curves while the evolution in GR for the ΛCDM model with a radiation component is shown as a dashed curved for comparison. The effects of the modification of gravity are felt more strongly at smaller scales.

solution for $\Theta(x) = \{\Psi^+(x),\, \Xi(x),\, \delta_{\rm r}(x),\, v_{\rm r}(x),\, \delta_{\rm m}(x),\, v_{\rm m}(x)\}$ as

$$\Theta(x) = c_1\Theta_{1000}(x) + c_2\Theta_{0100}(x) + c_3\Theta_{0010}(x) + c_4\Theta_{0001}(x) \tag{3.164}$$

where the subscript on the four individual solutions on the r.h.s. indicates that those particular solutions were obtained by integrating the set of equations (3.153)–(3.158) with all but one of parameters in (3.163) set to zero, e.g., $\Theta_{1000}(x)$ is the numerical solution for $\Theta(x)$ obtained by setting $\Psi^+(x_{\rm ini}) = 1$ and $\Psi^+_x(x_{\rm ini}) = \Xi(x_{\rm ini}) = \Xi_x(x_{\rm ini}) = 0$. In order to restrict the freedom in setting the initial conditions, we assume that the power-law dependence with k in Eq. (3.162) is maintained, so that the linear coefficients c_i are independent of the wave-number. For example, in the case of Θ_{1000}, which corresponds arguably to the situation with the least deviations from GR in the initial conditions, the perturbed Einstein field equations (3.49) and (3.50) imply the initial conditions

$$\begin{aligned}
\delta_{\rm ini} &= -2\frac{3\,(1+f_R)\,H^2}{\kappa^2\bar\rho}\left[1 - \frac{(f_R)_x}{1+f_R} + \frac{k^2}{3a^2H^2}\right]\Psi^+_{\rm ini} \\
&\approx -2(1+D)\,[1+f_R-(f_R)_x]\,\Psi^+_{\rm ini}\,, \qquad (3.165)\\
v^{(N)}_{\rm ini} &= -\frac{1}{2aH}\frac{3H^2(1+f_R)}{\kappa^2\bar\rho}\left(1 - \frac{1}{2}\frac{(f_R)_x}{1+f_R}\right)\Psi^+_{\rm ini} \\
&\approx -\frac{1}{2aH}\,(1+D)\left[1+f_R - \frac{1}{2}(f_R)_x\right]\Psi^+_{\rm ini}\,. \qquad (3.166)
\end{aligned}$$

Even for a small percentage of DR, the corrections to the initial conditions (3.160) can become significant if $f_R \gg 1$ during the radiation dominated epoch.

In Fig. 3.6, we present the evolution of Ψ^+ (Left panel), Ξ (middle panel) and $\delta^{(N)}_{\rm m}$ (Right panel) obtained in the case of Θ_{1000} with the initial value of Ψ^+ given by the relations (3.161) and (3.162). In all panels, we present the evolution of three different modes with wave-numbers: $k = k_0 \approx 2.2\times10^{-4}$ hMpc^{-1} (red); $k = 10^2 k_0 \approx 2.2\times10^{-2}$ hMpc^{-1} (green) and $k = 10^4 k_0 \approx 2.2$ hMpc^{-1} (blue). For each mode, we present as well the evolution in GR with the usual initial conditions (dashed curves).

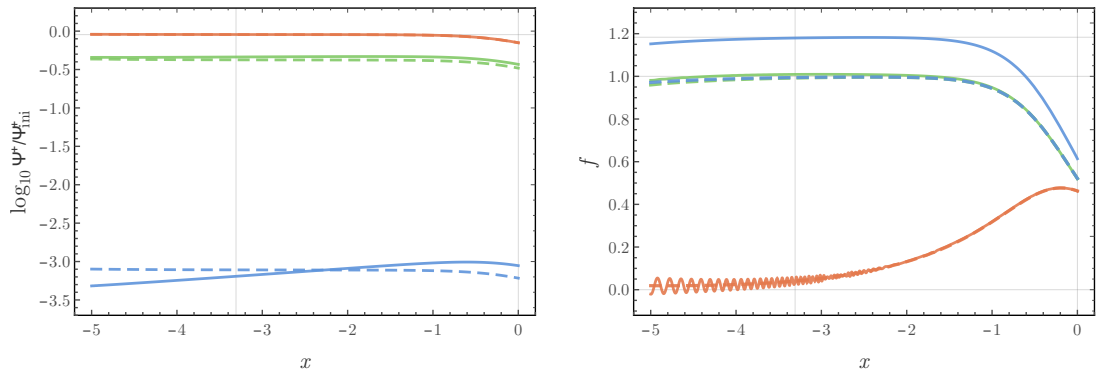

Figure 3.7.: Comparison of the evolution of $\log_{10}\Psi^{+}$ (left panel) and the growth rate f (right panel) in the case of our $f(R)$ model (solid curves) and in ΛCDM with a radiation component in GR (dashed curves). Each colour corresponds to a different wave-number: $k = k_0$ (red); $k = 10^2 k_0$ (green) and $k = 10^4 k_0$ (blue). The deviations from GR become obvious at small scales and indicate a stronger collapse matter.

We find that for low k (red curves), the difference between the evolution in GR and in our $f(R)$ model is negligible, with the potential Ψ^{+} becoming constant during the matter era, with $9/10$ of its initial value. This behaviour, observed as well in GR, is predicted from Eq. (3.161) and the conservation of the comoving curvature perturbation at large scales in the transition from the radiation dominated era to the matter dominated era. For intermediate scales (green curves) we find that some deviations from GR start to be observed, in particular Ψ^{+} no longer remains constant during the matter dominated era, in contrast with the assumptions of the quasi-static approximation [336, 365]. For low scales, we find that the evolution of the modes start to deviate greatly from the behaviour in GR after the modes re-enter the horizon. In particular, we observe that the matter density contrast has a slower growth before the end of the radiation dominated epoch, which seems to be associated to a faster decay of the gravitational potential and a higher deviation from isotropy due to the scalar Ξ. Once the matter dominated epoch begins, however, the growth of the matter perturbations is accelerated, with $\delta_{\rm m}^{(N)}$ eventually surpassing the predictions of GR at late-time.

In order to better visualise the effects of $f(R)$ gravity in the evolution of the perturbations during the matter dominated epoch, we plot in Fig. 3.7 the logarithm of the potential Ψ^{+} (left panel) and the growth rate f (right panel) for $x \in (-5, 0)$. We find that the approximation of static Ψ^{+} becomes increasingly worse for larger wave-numbers, i.e., for small scales, which are precisely the scales that are more affected by the modification of gravity. These results is in accordance with the criticism of the quasi-static approximation in Refs. [55, 134]. From the analysis of the growth rate we confirm that the evolution in our $f(R)$ model follows closely the case in GR for modes with small and intermediate values of k. Notice that the latter are inside the comoving Hubble horizon during most of the matter dominated epoch, however, their wave-number is not large enough for the effects of $f(R)$-gravity to kick in. For the modes with the largest wave-numbers, however, we find that $f \approx (\sqrt{33} - 1)/4$ during most of the matter dominated epoch, which is the value predicted for the smallest scales in an $f(R)$ model where the evolution of the Universe is dominated by pressureless matter and $|f_R| \approx 0$, cf. Eq. (3.65).

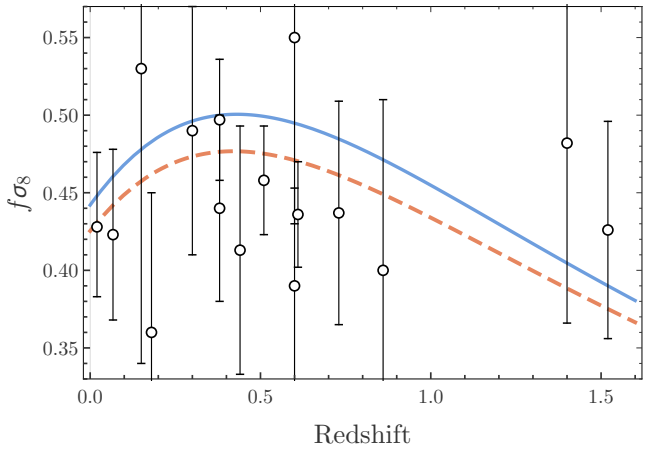

Figure 3.8.: Evolution of $f\sigma_8$ in the of our $f(R)$ model (solid blue curve) and for ΛCDM (dashed red curve). The various data points plotted, and respective error bars, are presented in Tab. 3.4.

Finally, we present in Fig. 3.8 the evolution of $f\sigma_8$ in our model (blue solid curve) and in ΛCDM (red dashed curve), where σ_8 is the root mean square of mass fluctuations on spheres of radius 8 h^{-1}Mpc. The temporal evolution of σ_8 was obtained through the formula [356]

$$\sigma_8(x) = \sigma_8(0)\frac{\delta_{\rm m}(x)}{\delta_{\rm m}(0)}\,, \tag{3.167}$$

assuming the best-fit value of the 2015 Planck results for the present day value $\sigma_8(0) = 0.8154$ [16] and using the evolution of $\delta_{\rm m}$ for the mode with wavenumber $k_8 = 0.125\ h{\rm Mpc}^{-1}$. For comparison, we also plot several available observational data points and their respective error bars, which we enumerate in Tab. 3.4. From Fig. 3.8, it is evident that the modification of gravity in our model leads to a higher value of $f\sigma_8$, when compared with the results for ΛCDM. This result is in agreement with the results obtained above for the growth rate f, cf. Fig. 3.7, which was found to be substantially higher than in GR for modes with wavenumber above $k_{\rm eq}$. In particular, we find that this increase spoils slightly the agreement of the predictions of our model with some data points at redshift $0.2 \sim 0.9$.

The matter power spectrum

In order to decide on the viability of the model at the perturbative level, we analyse how the $f(R)$ corrections affect the matter power spectrum $P_{\delta_{\rm m}}$ [233]. As discussed in Sect. 2.4, the theoretical predictions for the matter power spectrum is obtained from the GI comoving fractional energy density perturbation[14] $\delta_{\rm m}^{(C)}$:

$$P_{\delta_{\rm m}} \equiv \langle|\delta_{\rm m}^{(C)}|^2\rangle = \langle|\delta_{\rm m} - 3aH\,v_{\rm m}|^2\rangle. \tag{3.168}$$

The numerical results can be seen in Fig. 3.9, where we show on the panel of the l.h.s. the matter power spectrum obtained from Θ_{1000} (blue solid curve) with the initial value of Φ given by Eqs. (3.161)

[14] For a complete definition of $\delta_{\rm m}^{(C)}$, please see Eq. (A.56) of the Appendix A.

z	$f\sigma_8$	Survey	Ref.
0.02	$0.428^{+0.048}_{-0.045}$	6dF Galaxy Survey + SNe Ia	[195]
0.067	$0.423^{+0.055}_{-0.055}$	6dF Galaxy Survey	[59]
0.15	$0.53^{+0.19}_{-0.19}$	SDSS MGS	[190]
0.18	$0.36^{+0.09}_{-0.09}$	GAMA	[62]
0.3	$0.49^{+0.08}_{-0.08}$	SDSS LRG	[280]
0.38	$0.44^{+0.06}_{-0.06}$	GAMA	[62]
0.38	$0.497^{+0.039}_{-0.039}$	BOSS DR12	[20]
0.44	$0.413^{+0.080}_{-0.080}$	WiggleZ	[61]
0.51	$0.458^{+0.035}_{-0.035}$	BOSS DR12	[20]
0.60	$0.390^{+0.063}_{-0.063}$	WiggleZ	[61]
0.60	$0.55^{+0.12}_{-0.12}$	VIPERS	[288]
0.61	$0.436^{+0.034}_{-0.034}$	BOSS DR12	[20]
0.73	$0.437^{+0.072}_{-0.072}$	WiggleZ	[61]
0.86	$0.40^{+0.11}_{-0.11}$	VIPERS	[288]
1.4	$0.482^{+0.116}_{-0.116}$	FastSound	[281]
1.52	$0.426^{+0.070}_{-0.070}$	BOSS DR14 quasars	[364]

Table 3.4.: Available observational data points for $f\sigma_8$ at different at redshift in the interval $(0,\, 1.52)$, which are plotted in Fig. 3.8. For each data point we present, in order, the value of the effective redshift, the value of $f\sigma_8$ and its respective error, the corresponding survey, and the reference from which the values were taken.

and (3.162). For comparison, we also present the prediction of the ΛCDM model in GR (red dashed curve). The changes on the shape of the spectrum appear on the high k regime of the spectrum ($k \geq k_{eq} \approx 0.01$ Mpc^{-1}), which is consist with the scale-dependent effects of $f(R)$ which mostly affect the growth of the matter perturbations at higher k [134, 290]. On the panel on the r.h.s. of Fig. 3.9, we show the matter power spectrum obtained by fine-tuning the initial conditions in order to minimise the deviations from the spectrum of the ΛCDM model. By comparing the two panels in Fig. 3.9, we find that, although this procedure minimises the difference between the matter power spectrum obtained in our model and the prediction of GR, it does not improve the results in the sense that it cannot resolve the difference in tilt between the two power spectra for $k > k_{eq} \approx 0.01$ Mpc^{-1}. In addition, attempting to alter $P_{\delta_{\rm m}}$ at small scales (large k) seems to spoil the agreement with the predictions of GR at large scales (low k).

3.3.5. Discussion

About 95% of our Universe is composed by *dark* fluids of which we know very little about apart from their gravitational effects in the cosmological expansion. This lack of knowledge has fuelled the idea that these exotic types of matter are instead the manifestation of modifications to Einstein's General Relativity felt only at cosmological scales. In this section, we have investigated the possibility

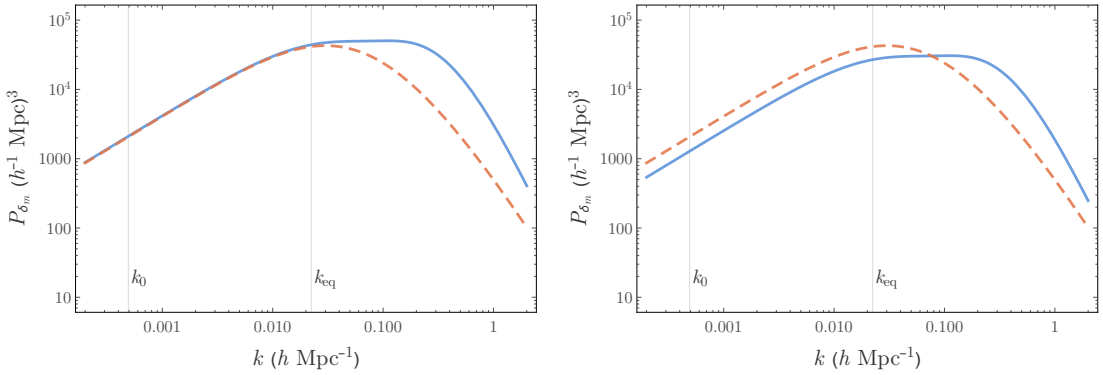

Figure 3.9.: Matter power spectrum obtained from the $f(R)$ model with $D = 1.377\%$ (blue solid curve) compared with the GR prediction (red dashed curve). (Left panel) The matter power spectrum obtained from Θ_{1000} with the gravitational potential Ψ^+ given by the relations (3.161) and (3.162). (Right panel) The matter power spectrum obtained by fitting the coefficients c_1, c_2, c_3 and c_4 in Eq. (3.164) in order to minimise the deviations from the predictions of ΛCDM in GR.

that such a modification of gravity could account for dark radiation, a potential excess of relativistic content in our Universe that cannot be accounted for by the CMB radiation or neutrinos, and for dark energy. In particular, we have assumed that the effective energy density of $f(R)$ follows that of a modified generalised Chaplygin gas (mGCG) that mimics (dark) radiation in the past and a cosmological constant in the recent late-time evolution. In addition to the mGCG, we have considered the presence of radiation (photons and ultra-relativistic neutrinos) and pressureless matter (baryons and DM). Using a *designer* $f(R)$-approach and the cosmographic parameters derived from the best-fit values the 2015 Planck mission, we were able to find a numerical solution for $f(R)$ that is compatible with the specified background evolution and that satisfies the viability conditions [141, 151] till at least the present time. Not surprisingly, we have found that during the matter and DE dominated eras, the solution tracks the Einstein-Hilbert action with a cosmological constant. However, in the asymptotic past, when the mGCG behaves as radiation, we found that the numerical solution for $R + f$ behaves instead as $\propto R^{4/3}$. In order to understand this behaviour, we then determined the general solution for $f(R)$ in a matter and radiation filled universe, where the modifications of gravity account for an excess in the radiation content. We found that at high scalar curvature, the general solution behaves precisely as $R^{4/3}$, independently of the initial conditions, or the linear coefficients, chosen.

In order to decide on the viability of the model, we then computed the evolution of the linear perturbations since the past radiation dominated epoch till the present time. Using linear perturbation theory in $f(R)$ gravity, we integrated numerically the evolution equations for the perturbations of radiation, pressureless matter, the gravitational potentials and the new scalar degree of freedom of δf_R gravity since the radiation-dominated epoch, when the relevant modes were well outside the Hubble horizon, and until the present time. For simplicity, we have disregarded the effects of anisotropies coming from the relativistic components, i.e., photons and neutrinos, as well as the drag of baryons by the radiation fluid that affect the smaller scales before the photon-baryon decoupling. The viability of the model was asserted by contrasting the prediction for $f\sigma_8$ with the available data points and

by comparing the matter power spectrum obtained, at the present time, in our model and in ΛCDM with a radiation component. We found that the imprints from the modifications to gravity appear prominently on smaller scales, a characteristic feature of $f(R)$-gravity. In particular, we found that the shape of the matter power spectrum in our $f(R)$ model is able to perfectly mimic the prediction of GR for modes with wave-number up to ~ 0.01 Mpc^{-1}, i.e., for large and intermediate scales. However, modes with higher wave-number, which are the modes that enter the comoving Hubble horizon during the radiation dominated epoch when $f(R) \propto R^{4/3}$, we find that the predictions of our model deviate significantly from the results of GR due to the higher growth rate of the matter perturbations predicted by $f(R)$ gravity, which is also reflected in a higher prediction for $f\sigma_8$ in comparison with ΛCDM. Unfortunately, this is precisely the region where observational data strongly constraints the shape of the matter power spectrum.

In the derivation of the numerical results for the linear perturbations, we have assumed that initial conditions analogous to the ones of GR could be used. As such, we have assumed the initial adiabaticity of radiation and matter and used the predictions of single-field inflation to set up the k-dependence for the initial values of the gravitational potential and the new degree of freedom, as well as for their derivatives. It remains to be checked that such initial conditions are compatible with the $R^{4/3}$ behaviour of $f(R)$ during the radiation epoch and it is quite possible that a change of the initial conditions could strongly alter the predictions of the model at the present time.

4 Dark Energy: 3-form field

In this chapter we focus on the possibility of explaining DE without modifying the laws of gravity by introducing a new dynamical field, a 3-form, to describe DE. The 3-form field, a totally anti-symmetric tensor of rank $(0,3)$, was initially employed as a mechanism to obtain an effective cosmological constant [142] and has more recently been proposed, in the late 2000's, as an alternative to the scalar field and K-essence models to describe primordial inflation and also DE [166, 216, 217, 219]. While in some works 3-forms appear as the exterior derivative of 2-form like objects such as axions, e.g., in the context of string cosmology [123, 243] and pre-big-bang scenarios [164], here, we treat the 3-form as a true dynamical field with a kinetic term of its own. When viewed as such, the 3-form field minimally coupled to gravity can be mapped onto a perfect fluid as it is a perfect candidate for applications in FLRW cosmology. Within the context of primordial inflation, the issue of ghosts and Laplacian instabilities was addressed in Ref. [131], while the predictions of model, including non-Gaussianities, were studied in models with one [271] or multiple [222, 323] 3-form fields. The implications of this kind of fields the reheating phase were also considered in Ref. [132] while a model of Brane-world inflation driven by a confined 3-form field on a brane hypersurface was studied in [47]. More recently, the Hamiltonian formulation of the 3-form was studied in Ref. [81].

We begin the chapter by presenting a brief review of the main characteristics of the 3-form field and its applications to cosmology. In Sect. 4.2, we discuss the application of a dynamical system approach to cosmological models with 3-form fields and the importance of determining the global stability of the model, including the fixed points at infinite values of the amplitude of the field, and how a new dynamical system representation allows us to unequivocally determine the stability at infinity. In the final Sect. 4.3, we address the issue of the appearance of certain types of cosmic events in 3-form cosmology and how they can be avoided by considering an appropriate interaction between DM and the 3-form field playing the role of DE. The main results of this chapter were published in Refs. [80, 265].

4.1. The 3-form field: A brief review

4.1.1. The 3-form action

The action of a 3-form field $A_{\mu\nu\rho}$ minimally coupled to gravity, with a canonical kinetic term and with a potential V, is [166, 217]

$$S = \int \mathrm{d}^4\mathbf{x}\sqrt{-g}\mathcal{L} = \int \mathrm{d}^4\mathbf{x}\sqrt{-g}\left[-\frac{1}{48}F^{\mu\nu\rho\sigma}F_{\mu\nu\rho\sigma} - V\left(A^{\mu\nu\rho}A_{\mu\nu\rho}\right)\right] . \tag{4.1}$$

where $F_{\mu\nu\rho\sigma}$ is the strength tensor of the 3-form, defined as [166]

$$F_{\mu\nu\rho\sigma} := 4\partial_{[\mu}A_{\nu\rho\sigma]} = \partial_\mu A_{\nu\rho\sigma} - \partial_\sigma A_{\mu\nu\rho} + \partial_\rho A_{\sigma\mu\nu} - \partial_\nu A_{\rho\sigma\mu} . \tag{4.2}$$

Here, the square brackets in the indices denote anti-symmetrisation [347]. By minimising the action (4.1) with respect to variations of the 3-form field, we obtain the equations of motion of the 3-form [219]

$$\nabla_\sigma F^\sigma{}_{\mu\nu\rho} - 12\frac{\mathrm{d}V}{\mathrm{d}\left(A^2\right)}A_{\mu\nu\rho} = 0 , \tag{4.3}$$

where we use the notation $A^2 = A^{\mu\nu\rho}A_{\mu\nu\rho}$ introduced in Refs. [216, 217, 219]. Using the anti-symmetrisation proprieties of the strength tensor, we can obtain an additional constraint on the 3-form by taking the divergence of Eq. (4.3) which leads to [219]

$$\frac{\mathrm{d}V}{\mathrm{d}\left(A^2\right)}\nabla^\mu A_{\mu\nu\rho} + \frac{\mathrm{d}^2V}{\mathrm{d}\left(A^2\right)^2}A_{\mu\nu\rho}\nabla^\mu A^2 = 0 . \tag{4.4}$$

In general, any p-form field in $d-$dimensions has a Hodge dual $(d-p)-$form [166, 271, 361]. In the case of the 3-form field $A_{\mu\nu\rho}$ and its field tensor $F_{\mu\nu\rho\sigma}$, which is a 4-form, the respective Hodge duals are a vector field $B^\mu := (A_{\nu\rho\sigma})^*$ and a scalar field $\phi := (F_{\mu\nu\rho\sigma})^*$ that verify the following relations

$$B^\mu = \frac{1}{3!}E^{\mu\nu\rho\sigma}A_{\nu\rho\sigma} , \qquad A_{\mu\nu\rho} = E_{\mu\nu\rho\sigma}B^\sigma , \qquad A^2 = -6B^2 , \tag{4.5}$$

$$\phi = \frac{1}{4!}E^{\mu\nu\rho\sigma}F_{\mu\nu\rho\sigma} , \qquad F_{\mu\nu\rho\sigma} = -E_{\mu\nu\rho\sigma}\phi , \qquad F^2 = -24\phi^2 . \tag{4.6}$$

Here, $E_{\mu\nu\rho\sigma}$ is the four dimensional Levi-Civita tensor. Using these definitions, the equation of motion (4.3) and the constraint (4.21), the 3-form action (4.1) can then be recast either as a scalar field theory for ϕ or, alternatively, as a vector field theory for B^μ. Notice, however, that in these alternative representations, the kinetic terms for ϕ or B^μ are not the canonical ones. For a complete review of these alternative descriptions, please see Ref. [271].

4.1.2. The 3-form field as a perfect fluid

The stress-energy-momentum tensor of the 3-form obtained from the action (4.1) reads [166, 219]

$$[T_A]_{\mu\nu} = \frac{1}{6}F_{\mu}{}^{\alpha\beta\gamma}F_{\nu\alpha\beta\gamma} + 6\frac{\partial V}{\partial (A^2)}A_{\mu}{}^{\alpha\beta}A_{\nu\alpha\beta} - \left[\frac{1}{48}F^2 + V\left(A^2\right)\right]g_{\mu\nu}\,. \tag{4.7}$$

A preferential 4-velocity vector for the 3-form can be defined using the Hodge dual B^{μ} [361]:

$$[u_A]^{\mu} := \frac{B^{\mu}}{\sqrt{-B^2}} = \frac{E^{\mu\nu\rho\sigma}A_{\nu\rho\sigma}}{\sqrt{6A^2}}\,. \tag{4.8}$$

An immediate consequence of this definition is that the 4-velocity is orthogonal to the 3-form, i.e.:

$$[u_A]^{\mu}A_{\mu\nu\rho} = 0\,. \tag{4.9}$$

Using the definition (4.8), we can recast the stress-energy-momentum tensor (4.7) as

$$[T_A]_{\mu\nu} = 2\frac{\mathrm{d}V}{\mathrm{d}(A^2)}A^2[u_A]_{\mu}[u_A]_{\nu} + \left[\frac{1}{48}F^2 - V(A^2) + 2\frac{\mathrm{d}V}{\mathrm{d}(A^2)}A^2\right]\,. \tag{4.10}$$

With $[T_A]_{\mu\nu}$ written in this form, it is an easy exercise to define the fluid quantities (1.13)–(1.16), with the energy density and pressure of the 3-form field reading:

$$\rho_A = -\frac{1}{48N^2}F^2 + V(A^2)\,, \qquad P_A = \frac{1}{48N^2}F^2 - V(A^2) + 2\frac{\mathrm{d}V}{\mathrm{d}(A^2)}A^2\,, \tag{4.11}$$

while the energy flux, $[q_A]^{\mu}$, and the anisotropic stress, $[\pi_A]_{\mu\nu}$, vanish. Thus, much like the minimally coupled scalar field, a 3-form field can be mapped onto a perfect fluid, making it a good candidate for applications in FLRW cosmology.

4.1.3. FLRW cosmology with 3-form fields

Let us now consider a homogeneous and isotropic universe described by the FLRW line element (1.18). In such a Universe, the condition (4.9) for the 4-velocity $[u_A]^{\mu}$ implies that the 3-form field is orthogonal to the unit normal that defines the spatial hypersurfaces, hence, the only non-zero components of $A_{\mu\nu\rho}$ are purely spatial and can be parameterised in terms of a scalar quantity $\chi(t)$ as [166, 216, 217, 219]

$$A_{ijk} = \chi\, E_{ijk}\,, \qquad A^2 = 6\chi^2\,. \tag{4.12}$$

In addition, from the definition of the strength tensor, cf. Eq. (4.2), we find [166, 216, 217, 219]

$$F_{0ijk} = \left(\dot{\chi} + 3\frac{\dot{a}}{a}\chi\right)E_{ijk}\,, \qquad F^2 = -\frac{24}{N^2}\left(\dot{\chi} + 3\frac{\dot{a}}{a}\chi\right)^2\,. \tag{4.13}$$

In Eqs. (4.12) and (4.13), E_{ijk} is the 3-dimensional Levi-Civita tensor induced on the spatial hypersurfaces[1]. The equation of motion of the field $\chi(t)$ is obtained from Eq. (4.3) and reads [166, 216, 217, 219]:

$$\ddot{\chi} + \left(3\frac{\dot{a}}{a} - \frac{\dot{N}}{N}\right)\dot{\chi} + 3\left[\frac{\ddot{a}}{a} - \left(\frac{\dot{a}}{a}\right)^2 - \frac{\dot{a}}{a}\frac{\dot{N}}{N}\right]\chi + 2N^2\frac{\mathrm{d}\,V}{\mathrm{d}\,(\chi^2)}\chi = 0\,. \tag{4.14}$$

Substituting Eq. (4.12) in (4.11) we find that the energy density and pressure of the 3-form field can be written in terms of the field χ and its derivatives as [216, 217, 219]

$$\rho_A = \frac{1}{2N^2}\left(\dot{\chi} + 3\frac{\dot{a}}{a}\chi\right)^2 + V(\chi^2)\,, \tag{4.15}$$

$$P_A = -\frac{1}{2N^2}\left(\dot{\chi} + 3\frac{\dot{a}}{a}\chi\right)^2 - V(\chi^2) + 2\frac{\mathrm{d}V}{\mathrm{d}(\chi^2)}\chi^2\,. \tag{4.16}$$

As such, the Friedmann equation (1.27) and the Raychaudhuri equation (1.28) in a universe filled by a 3-form field and other matter fluids with energy density $\rho^{(\mathrm{m})}$ and $P^{(\mathrm{m})}$ become

$$\left(\frac{\dot{a}}{a}\right)^2 + \frac{N^2}{a^2}\mathcal{K} = \frac{\kappa^2 N^2}{3}\rho^{(\mathrm{m})} + \frac{\kappa^2}{6}\left(\dot{\chi} + 3\frac{\dot{a}}{a}\chi\right)^2 + \frac{\kappa^2 N^2}{3}V(\chi^2)\,, \tag{4.17}$$

$$\begin{aligned} 2\frac{\ddot{a}}{a} + \left(\frac{\dot{a}}{a}\right)^2 - 2\frac{\dot{N}}{N}\frac{\dot{a}}{a} + \frac{N^2}{a^2}\mathcal{K} - N^2\Lambda = & -\kappa^2 N^2 P^{(\mathrm{m})} + \frac{\kappa^2}{6}\left(\dot{\chi} + 3\frac{\dot{a}}{a}\chi\right)^2 + \frac{\kappa^2 N^2}{3}V(\chi^2) \\ & - \kappa^2 N^2\frac{\mathrm{d}V}{\mathrm{d}(\chi^2)}\chi^2\,. \end{aligned} \tag{4.18}$$

Notice that whenever the derivative of the potential vanishes, the 3-form mimics a cosmological constant behaviour with $P_A = -\rho_A$. On the other hand, if $V_{,\chi^2} < 0$, i.e., for potentials decreasing in χ^2, the 3-form field acquires a phantom-like behaviour as $w = P_A/\rho_A < -1$. Thus, contrary to the case of a scalar field, a 3-form field minimally coupled to gravity and with a canonical kinetic term can violate the null energy condition $\rho + P \geq 0$ even if the potential is positive valued.

4.1.4. The critical points χ_{c}

We now focus on the case of a spatially flat Universe filled only by a 3-form. Inserting the Raychaudhuri equation (4.18) in the evolution equation (4.14) and choosing to work with the cosmic time ($N = 1$), we obtain a scalar-field-like equation of motion

$$\ddot{\chi} + 3H\dot{\chi} + V_{\chi}^{(\mathrm{eff})} = 0\,, \tag{4.19}$$

[1] The Levi-Civita tensor is defined as $E_{ijk} := \sqrt{h}\,\varepsilon_{ijk}$, where h is the determinant of the 3-metric induced on the spatial hypersurfaces and ε_{ijk} is the Levi-Civita symbol that satisfies $\varepsilon_{ijk} = +1$ if ijk is an even permutation of 123, $\varepsilon_{ijk} = -1$ if ijk is an odd permutation of 123 and $\varepsilon_{ijk} = 0$ otherwise. The Levi-Civita tensor and symbol satisfy $E_{ijk}E^{ijk} = \varepsilon_{ijk}\varepsilon^{ijk} = 6$.

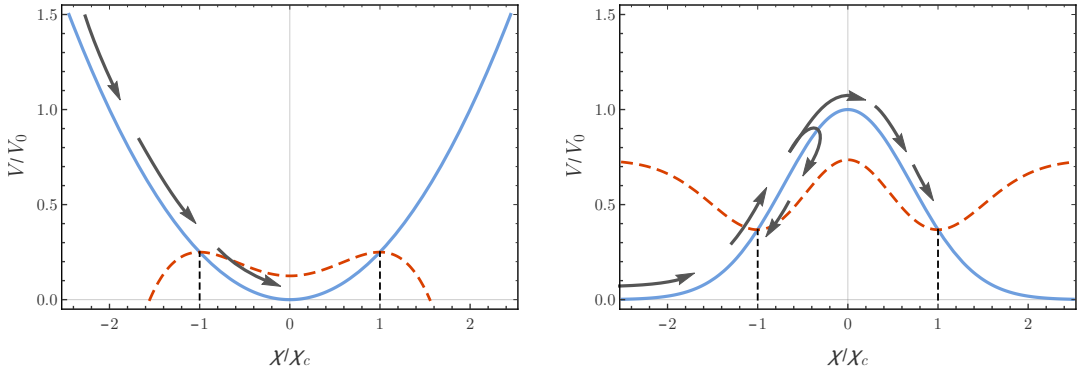

Figure 4.1.: Possible evolution of the χ field for (left panel) a quadratic potential $V = V_0(\chi/\chi_c)^2$ and (right panel) a Gaussian potential $V = V_0 \exp(-\chi^2/\chi_c^2)$. While the 3-form potential V is plotted as a solid blue curve, the effective potential $V^{(\mathrm{eff})}$ defined implicitly by (4.20) is shown as a dashed red curve. The critical points $\pm\chi_c$ are stationary points of the effective potential and indicate static solutions of $\chi(t)$.

with an effective potential V^{eff} defined by the equality [216, 217]

$$V_\chi^{(\mathrm{eff})} = -\frac{3\kappa^2}{2}\left(\chi^2 - \frac{2}{3\kappa^2}\right) V_\chi \,. \tag{4.20}$$

Here, we have introduced the notation $V_\chi = \mathrm{d}\,V/\mathrm{d}\,\chi$ which we will use throughout the rest of this chapter, along with $V_{\chi\chi} = \mathrm{d}^2\,V/\mathrm{d}\,\chi^2$ and $V_{\chi^2} = \mathrm{d}\,V/\mathrm{d}\,(\chi^2)$.

Equation (4.19) admits as static solutions any point χ for which the derivative of the effective potential vanishes. This includes not only stationary points of the 3-form potential $V(\chi)$, but also the two points $\chi = \pm\chi_c$ with $\chi_c := \sqrt{2/(3\kappa^2)}$. These play a critical role in 3-form cosmology since, as noted in Refs. [216, 217], for non-negative-valued potentials the Friedmann equation (4.17) imposes the constraint

$$(\dot\chi + 3H\chi)^2 \leq 9H^2\chi_c^2 \,. \tag{4.21}$$

For expanding Universes, this inequality implies that for large values of the field χ, more precisely for $|\chi| > \chi_c$, the field decays monotonically towards the interval $[-\chi_c, \chi_c]$, independently of the shape of the potential, and once it is inside that interval it never escapes. Since this is a compact interval, the critical points can act as local maxima or minima of the potential and therefore can correspond to unstable or stable equilibrium points, respectively, as seen in Fig. 4.1. Notice that the constraint (4.21) automatically implies that any static solution of Eq. (4.19) for $|\chi| > \chi_c$ is not physically viable.

The stability of the two equilibrium points $\pm\chi_c$ can also be understood by analysing the sign of the second derivative of the effective potential:

$$V^{\mathrm{eff}}_{,\chi\chi}(\pm\chi_c) = -2\frac{V_{,\chi}(\pm\chi_c)}{\pm\chi_c} = -4V_{,\chi^2}(\pm\chi_c) \,. \tag{4.22}$$

If $V_{,\chi^2}(\pm\chi_c)$ is positive, the points $\pm\chi_c$ represent two maxima of the effective potential which represent unstable equilibrium states. On the other hand, if $V_{,\chi^2}(\pm\chi_c) < 0$ the same points represent

two minima of the effective potential that represent stable static solutions (see Fig. 4.1).

4.2. Dynamical system analysis with 3-forms

A dynamical system approach was first employed in the context of 3-form cosmology with a DM component in Ref. [216]. Following a usual strategy employed in cosmology, three compact variables related to the fractional energy density of pressureless matter, eg., CDM, and to the fractional kinetic and potential energy densities of the 3-form were introduced[2]

$$s := \sqrt{\frac{\kappa^2 \rho_{\rm m}}{3H^2}}\,, \quad y := \frac{\dot{\chi} + 3H\chi}{3H\chi_{\rm c}}\,, \quad z := \sqrt{\frac{\kappa^2 V}{3H^2}}\,, \tag{4.23}$$

with $0 \leq s \leq 1$, $-1 \leq y \leq 1$, and $0 \leq z \leq 1$. These variables satisfy the Friedmann constraint

$$1 = s^2 + y^2 + z^2\,, \tag{4.24}$$

which allows the elimination of one variable from the system. An autonomous dynamical system can be obtained by defining a fourth variable X:

$$X := \frac{\chi}{\chi_{\rm c}}\,, \tag{4.25}$$

where the rescaling is chosen so that the critical values $\chi = \pm\chi_{\rm c}$ correspond to $X = \pm 1$. Using the variables (4.23) and (4.25) we can write the evolution equations for a cosmological model with CDM and a 3-form field as

$$X_x = 3(y - X)\,, \tag{4.26}$$

$$y_x = \frac{1}{2}\left[3\left(1 - y^2 - z^2\right) y + (1 - Xy)\,\lambda(X) z^2\right]\,, \tag{4.27}$$

$$z_x = \frac{1}{2} z\left[3\left(1 - y^2 - z^2\right) - \left(y - X + Xz^2\right)\lambda(X)\right]\,, \tag{4.28}$$

$$s = \sqrt{1 - y^2 - z^2}\,. \tag{4.29}$$

Notice that, contrary to the case of quintessence, here we cannot separate the variable X from the system by choosing an exponential potential. In Eqs. (4.26)–(4.28) we use a subscript x to indicate a derivative with respect to $x = \log(a/a_0)$, a notation that will be employed throughout the rest of this chapter, and the factor $\lambda(X)$ is defined as

$$\lambda(X) := -\sqrt{\frac{6}{\kappa^2}}\frac{V_\chi}{V} = -3\frac{V_X}{V}\,. \tag{4.30}$$

The set of Eqs. (4.26)-(4.30) defines the evolution of the system in a 3-dimensional phase-space $\mathcal{M}$ that corresponds to a half-cylinder of radius unity and infinite height: $-1 \leq y \leq 1$, $0 \leq z \leq \sqrt{1 - y^2}$,

[2] Here, we prefer the letter s for the variable related to the CDM energy density, in detriment of the letter w used in [216].

and $-\infty < X < +\infty$. The borders of the half-cylinder

$$\begin{aligned}\mathcal{M}_0 &= \left\{(X,\, y,\, z) \in \mathbb{R}^3 \,:\, z = 0 \,\wedge\, -1 \leq y \leq 1\right\}\,,\\ \mathcal{M}_1 &= \left\{(X,\, y,\, z) \in \mathbb{R}^3 \,:\, y^2 + z^2 = 1 \,\wedge\, z \geq 0\right\}\,,\end{aligned} \tag{4.31}$$

represent two invariant subsets of the system: the plane $\mathcal{M}_0$ corresponds to a model with CDM and a massless 3-form, which has been found to be equivalent to ΛCDM [216]; the surface $\mathcal{M}_1$ represents a universe filled solely by a 3-form field [131]. In refs. [65, 265] the variable X was replaced by the compact variable[3]

$$u := \frac{2}{\pi}\arctan\left(X\right)\,, \tag{4.32}$$

with $-1 \leq u \leq 1$. This substitution allowed for the identification of the fixed points at infinite values of the field χ [265], i.e. for $u = \pm 1$. Some of the new fixed points at infinite χ were found to correspond to the asymptotic past of the system. These points are characterised by their extremely repulsive nature [265]. With this new variable, the model is described by the set of equations

$$u_x = \frac{6}{\pi}\cos^2\left(\frac{\pi u}{2}\right)\left[y - \tan\left(\frac{\pi u}{2}\right)\right]\,, \tag{4.33}$$

$$y_x = \frac{1}{2}\left\{3\left[1 - y^2 - z^2\right]y + \lambda\left(u\right)z^2\left[1 - \tan\left(\frac{\pi}{2}u\right)y\right]\right\}\,, \tag{4.34}$$

$$z_x = \frac{1}{2}z\left\{3\left[1 - y^2 - z^2\right] - \lambda\left(u\right)\left[y - \tan\left(\frac{\pi}{2}u\right)\left(1 - z^2\right)\right]\right\} \tag{4.35}$$

defined on the half-cylinder $\tilde{\mathcal{M}}$ of unity radius and height: $-1 \leq y \leq 1$, $0 \leq z \leq \sqrt{1 - y^2}$, and $-1 < u < +1$. The fractional energy density of DM, $\Omega_{\rm m} = s^2$, is given by Eq. (4.29) and the total EoS parameter can be written in terms of the dynamical variables as

$$w_{\rm tot} = \frac{P_\chi}{\rho_{\rm m} + \rho_\chi} = -\left(y^2 + z^2\right) - \frac{1}{3}\lambda(u)\tan\left(\frac{\pi}{2}u\right)z^2\,. \tag{4.36}$$

In addition to the subsets $\tilde{\mathcal{M}}_0$ and $\tilde{\mathcal{M}}_1$ that map $\mathcal{M}_0$ and $\mathcal{M}_1$ in the new representation, we find that the top and bottom borders of the cylinder also represent invariant subsets of the system:

$$\tilde{\mathcal{M}}_\pm = \left\{(u,\, y,\, z) \in \mathbb{R}^3 \,:\, u = \pm 1\right\}\,. \tag{4.37}$$

Since trajectories in these subsets represent dynamics where the value of the field stays at infinity, there is no general physical interpretation to $\tilde{\mathcal{M}}_\pm$.

4.2.1. Fixed points: a new classification

The fixed points of the system (4.26)-(4.30) were classified in Ref. [216] into three different categories: a saddle point A with $(X,\, y,\, z) = (0, 0, 0)$ that corresponds to an unstable matter era; two points B with $(X,\, y,\, z) = (\pm 1, \pm 1, 0)$ that for some choices of the potential represent late-time attractors with

[3] This compact variable was first proposed in Ref. [65] where it was identified by the letter x. To avoid a potential confusion with the nomenclature, we adopt the letter u for the compact variable, as used in Ref. [265]

kinetic dominance of the 3-form; a set of points C corresponding to local extrema of the potential within the interval $[-\chi_c, \chi_c]$ and which can be either attractors or saddle points. In Ref. [265], we proposed an alternative classification that takes into account the possibility of having fixed points at $u = \pm 1$, i.e., at $\chi = \pm\infty$:

- **Type I:** these fixed points verify $z = 0$ for finite values of the 3-form field χ, i.e., $u_{\rm fp} \neq \pm 1$. This category therefore includes the points A and B of Ref. [216]. Solving Eqs. (4.33) and (4.34) for u and y we find that, for choices of potentials such that $\lambda(u)$ is well defined for all values of u, any fixed point $(u_{\rm fp}, y_{\rm fp}, z_{\rm fp})$ of this category must verify

$$(u_{\rm fp},\, y_{\rm fp},\, z_{\rm fp}) : \begin{cases} u_{\rm fp} & = \dfrac{2}{\pi} \arctan\left(y_{\rm fp}\right) , \\ y_{\rm fp}\left(1 - y_{\rm fp}^2\right) & = 0 , \\ z_{\rm fp} & = 0 . \end{cases} \tag{4.38}$$

  Since the factor $\lambda(u)$ is absent from (4.38) we conclude that the existence of fixed points of Type I does not depend on the shape of the potential of the 3-form field. As will be seen below, the same is not true for their stability.

  From the condition (4.38) we can identity the fixed points $(u_{\rm fp},\, y_{\rm fp},\, z_{\rm fp})$ of Type I as

$$\textbf{Type I fixed points:} \qquad \begin{cases} p_0 := (0,\, 0,\, 0) , \\ p_1^{\pm} := \left(\pm\frac{1}{2},\, \pm 1,\, 0\right) . \end{cases} \tag{4.39}$$

  The respective sets of eigenvalues $\{\lambda\}$ for the fixed points of Type I are

$$\{\lambda\}_{p_0} = \left\{-3,\, \frac{3}{2},\, \frac{3}{2}\right\} , \qquad\qquad \{\lambda\}_{p_1^{\pm}} = \{-3,\, -3,\, 0\} . \tag{4.40}$$

  Thus, we find that p_0 is a saddle point (unstable) while the stability of $p_1^{\pm}$ cannot be decided by the linear stability theory due to the presence of an eigenvalue with zero real part. Instead, we resort to the method described in [80] (see also Refs. [65, 295]) based on centre manifold theory [111] and find that p_1^{+} (p_1^{-}) is an attractor if $\lambda_{fp} := \lambda(u_{\rm fp}) > 0$ ($\lambda_{fp} < 0$) and a saddle-node if $\lambda_{fp} < 0$ ($\lambda_{fp} > 0$). For solutions with $\lambda_{fp} = 0$, which are cases where the values $\pm\chi_c$ represent stationary points of the potential $V(\chi)$ the stability will depend on the derivatives of the factor $\lambda(u)$, i.e., on higher order derivatives of V.

  Since for fixed points of Type I we have $z_{\rm fp} = 0$, we find from Eq. (4.36) that the total parameter of EoS at the fixed points of Type I is given by $w_{\rm tot} = -y_{\rm fp}^2$. Therefore, p_0 corresponds to a DM-domination evolution while at $p_1^{\pm}$, which correspond to asymptotic scenarios where the field χ evolves towards the static solution at the critical points $\pm\chi_c$, we have $w_{\rm tot} = -1$. It will be shown later that despite the value of the total EoS suggesting a de Sitter behaviour, these points actually correspond to a divergence of the Hubble rate with constant $\dot{H}$, i.e., to a Little Sibling of the Big Rip (LSBR) cosmic event [77].

- **Type II:** in this category we consider all the fixed points that, for finite values of χ, have

non-zero values of the variable z. Solving the system of Eqs. (4.33), (4.34), and (4.35) for $u' = y' = z' = 0$, we find that any solution $(u_{\rm fp}, y_{\rm fp}, z_{\rm fp})$ in this category must verify

$$(u_{\rm fp},\, y_{\rm fp},\, z_{\rm fp}) : \begin{cases} u_{\rm fp} & = \dfrac{2}{\pi} \arctan\left(y_{\rm fp}\right) , \\ \lambda_{fp} z_{\rm fp}^2 & = 0 \,, \\ 1 - y_{\rm fp}^2 - z_{\rm fp}^2 & = \dfrac{1}{3} \lambda_{fp} y_{\rm fp} z_{\rm fp}^2 \,, \\ z_{\rm fp}^2 & \neq 0 \,, \end{cases} \tag{4.41}$$

which imply that $s_{fp} = 0$ and $\lambda_{fp} = 0$, i.e., this category includes all the Type C fixed points in Ref. [216]. Solving (4.41) we find that there exists one fixed point $p_2 = (u_{\rm fp},\, y_{\rm fp},\, z_{\rm fp})$ per each u_λ that is a solution of $\lambda(u_\lambda) = 0$:

$$\textbf{Type II fixed points:} \qquad p_2 = \left(u_\lambda,\, \tan\left(\frac{\pi}{2} u_\lambda\right) ,\, \sqrt{1 - \tan^2\left(\frac{\pi}{2} u_\lambda\right)}\right) . \tag{4.42}$$

From Eq. (4.36), we obtain that for fixed points of Type II, the total EoS parameter is $w_{\rm tot} = -1$. As such, and since $V_\chi = 0$ at p_2, i.e., $\dot{H} = 0$, for well behaved potentials these points correspond to de Sitter solutions.

The eigenvalues of the fixed point p_2 are given by

$$\{\gamma\}_{p_2} = \left\{-3,\, -\frac{3}{2}\left[1 + F(u_\lambda)\right] ,\, -\frac{3}{2}\left[1 - F(u_\lambda)\right]\right\} , \tag{4.43}$$

where

$$F(u_\lambda) := \sqrt{1 + \frac{8}{3\pi} \frac{\cos^2\left(\frac{\pi}{2} u_\lambda\right)}{1 + \cos\left(\frac{\pi}{2} u_\lambda\right)} \frac{\mathrm{d}\,\lambda}{\mathrm{d}\,u}(u_\lambda)} \,. \tag{4.44}$$

We thus find that p_2 represents a saddle point (unstable) whenever $\mathrm{d}\,\lambda/\mathrm{d}\,u(u_\lambda) > 0$, i.e., when u_λ represents a maximum of the potential with $V_{\chi\chi}(u_\lambda) < 0$) and an attractor when $\mathrm{d}\,\lambda/\mathrm{d}\,u(u_\lambda) < 0$ i.e., when u_λ represents a minimum of the potential with $V_{\chi\chi}(u_\lambda) > 0$). For solutions with $\mathrm{d}\,\lambda/\mathrm{d}\,u(u_\lambda) = 0$, which is equivalent to the first and second derivative of the potential vanishing at the fixed point, a zero eigenvalue appears and an analysis based on linear stability theory breaks down. While methods based on centre manifold theory [111] could be used to decide the stability of the fixed point, the results would be strongly dependent on the shape of the potential considered and a case by case analysis might be necessary. As such, we do not explore the issue any further for now.

- **Type III:** here we include all the points lying on the planes $u = \pm 1$, which correspond to infinite values of the 3-form field χ. Since the inequality (4.21) forces the 3-form field to decay to the interval $[-\chi_{\rm c}, \chi_{\rm c}]$, any Type III fixed point present in the system will necessarily be unstable[4].

[4]The existence of Type III fixed points, i.e. fixed points at infinite χ, was discussed for the first time in [265], even though the compact variable employed in Eq. (4.32) was first introduced in Ref. [65]

Due to the appearance of divergent terms in the y' and z' equations ($\tan(\pi u/2) \to \pm\infty$ as $u \to \pm 1$), extra care is needed when identifying the position of fixed points of Type III and a general analysis for any type of potential is not possible. For example, in the case of power law potentials we find that $\lambda(u) \propto 1/\tan(\pi u/2)$ and all divergences in the equations are automatically cancelled, while in the case of a Gaussian potential with positive ξ the variable z must vanish sufficiently fast as $u \to \pm 1$ in order to cancel the divergences of $\lambda(u) \propto \tan(\pi u/2)$ and $\tan(\pi u/2)$ and even so divergences will appear when calculating the eigenvalues of the Jacobian of the system at the fixed points[265].

In Ref. [265], the proper identification and characterisation of the fixed points at χ-infinity encountered three main difficulties. First, the fact that a trigonometric, instead of a polynomial, relation was employed in Eq. (4.32) made it more difficult to identify the divergence rate of the equations. Secondly, the fact that z depends on u through the potential, means that one has to take special care and understand what is the behaviour of z as $u \to \pm 1$. For potentials that vanish at infinite χ the variable z may tend to zero sufficiently fast and cancel the divergent terms in u, e.g. the case of the Gaussian potential which was extensively discussed in Ref. [265]. Finally, even after the correct fixed points with $u = \pm 1$ were identified, their stability needed to be clarified. In order to try and solve some of the issues regarding the dynamics at infinity, we proposed in Ref. [80] a new dynamical system description of models with 3-forms which allowed us to properly analyse the stability of the fixed points at infinite values of χ. We present such a description in the next section.

4.2.2. Dynamics at infinity

When a compactification scheme is employed, like the one in (4.32), some terms may appear in the new evolution equations that diverge as the old variables approach infinity. When this happens, the dynamical system obtained after the compactification can be written as [146, 169, 170, 204, 366]

$$\begin{bmatrix} u' \\ y' \\ z' \end{bmatrix} = \frac{1}{g(u)} \begin{bmatrix} f_1(u,\, y,\, z) \\ f_2(u,\, y,\, z) \\ f_3(u,\, y,\, z) \end{bmatrix} , \tag{4.45}$$

where $g(u)$ vanishes as $u \to \pm 1$, the functions f_i are all well defined at $u = \pm 1$ and at least one of f_i's does not vanish at $u = \pm 1$. The divergence carried by $g(u)$ can then be washed away by defining a new time variable τ, $d\tau = g^{-1}(u)\, dx$ [146, 169, 170], such that the previous system can be written as

$$\frac{\partial}{\partial \tau} \begin{bmatrix} u \\ y \\ z \end{bmatrix} = \begin{bmatrix} f_1(u,\, y,\, z) \\ f_2(u,\, y,\, z) \\ f_3(u,\, y,\, z) \end{bmatrix} . \tag{4.46}$$

The fixed points at χ-infinity can now be identified as the points $(\pm 1,\, y,\, z)$ such that $f_1 = f_2 = f_3 = 0$ [146, 169, 170]. A correct identification of these fixed points depends on whether or not the function $g(u)$ carries the divergent leading order of the equations, so that all the divergent terms are cancelled through a proper redefinition of the time variable. If this is not the case, we run the risk of "overshooting" in the divergence cancellation and introduce artificial fixed points in the system.

We now present an alternative dynamical system description which tries to avoid the issues mentioned above. We begin by employing a new compactification scheme for χ

$$\frac{\chi}{\chi_c} = \frac{v}{1-v^2}\,, \tag{4.47}$$

with $v \in [-1,\,1]$. Note that the values $v = \pm 1$ correspond to $\chi \to \pm\infty$. By employing the relation (4.47), we ensure that all the divergent terms appear as powers of $(v \pm 1)$ with negative exponents, facilitating the identification of the leading order of the divergence.

In a second step, we decompose the variable z and isolate its explicit dependence on v. To do this, we first rescale the potential V as

$$V(v) = \frac{3H_0^2}{\kappa^2} V_*(v)\,, \tag{4.48}$$

where H_0 is the current value of the Hubble parameter and V_* is a dimensionless function of v. Next, we introduce the compact Hubble rate[5]

$$h := \frac{(H/H_0)^2}{1+(H/H_0)^2}\,, \tag{4.49}$$

defined in the interval $[0,\,1]$, with $h = 0$ corresponding to a Minkowski space-time, $H = 0$, and $h = 1$ to the limit[6] $H \to +\infty$. Using Eqs. (4.48) and (4.49), we can write the variable z as

$$z^2 = \frac{1-h}{h} V_*(v)\,. \tag{4.50}$$

We are now in a position to write the set of evolution equations for the dynamical variables $(v,\,y,\,h)$. From the Friedmann equation and the evolution equations (4.26), (4.27), (4.47) and (4.50), we obtain

$$v' = 3\frac{1-v^2}{1+v^2}\left[y\left(1-v^2\right) - v\right]\,, \tag{4.51}$$

$$y' = \frac{3}{2}\left\{y\left(1-y^2\right) - \frac{1-h}{h}\left[V_*(v)y + \frac{1-v^2}{1+v^2}\frac{\partial V_*}{\partial v}\left(1-v^2-vy\right)\right]\right\}\,, \tag{4.52}$$

$$h' = -3\,(1-h)\left[h\left(1-y^2\right) + (1-h)\left(\frac{1-v^2}{1+v^2}v\frac{\partial V_*}{\partial v} - V_*(v)\right)\right]\,. \tag{4.53}$$

For each type of potential, we can replace $V_*(v)$ in Eqs. (4.52) and (4.53), identify the leading divergent term in order to proceed with the appropriate time redefinition and divergence cancellation, and finally calculate the fixed points at infinity and study their stability. In addition, from Eqs. (4.24) and (4.50), we can write s as

$$s^2 = 1 - y^2 - \frac{1-h}{h} V_*(v)\,. \tag{4.54}$$

[5] A similar compact variable related to the Hubble rate was introduced in [27].
[6] We are assuming expanding cosmologies, i.e. $H \geq 0$.

Let us now look at the invariant sets $\mathcal{M}_0$ and $\mathcal{M}_1$, cf. Eq. (4.31), in this new description. First, we note that the set $\mathcal{M}_0$ is no longer present in the system for a general potential. Instead, the behaviour of the system in $\mathcal{M}_0$ is given by the set of equations (4.51), (4.52) and (4.53) with the null potential $V_* \equiv 0$. In the case of $\mathcal{M}_1$, i.e. in the absence of CDM, the combination of Eq. (4.50) with the condition $z^2 + y^2 = 1$ allows us to express h as

$$h = \frac{V_*(v)}{1 - y^2 + V_*(v)} \,. \tag{4.55}$$

As such, we can drop Eq. (4.53) and rewrite Eqs. (4.51) and (4.52) as

$$v' = \, 3\frac{1-v^2}{1+v^2}\left[y\left(1-v^2\right) - v\right] \,, \quad y' = \, -\frac{3}{2}\left(1-y^2\right)\frac{1-v^2}{1+v^2}\frac{1}{V_*}\frac{\partial V_*}{\partial v}\left(1 - v^2 - vy\right) \,. \tag{4.56}$$

These equations are equivalent to the ones obtained in Ref. [131] in the context of 3-form inflation.

4.2.3. Example: the Gaussian potential

In the previous sections we have discussed the use of a dynamical system description to cosmological models with a 3-form field. In particular, we introduced a new classification of the fixed points of the system and a new compactification strategy that take into account the dynamics of the system at infinite values of the field χ and allow us to define a global picture of the stability of the model. As an example of the applicability of the methods defined above, we now consider the case where the 3-form has a Gaussian potential

$$V = V_0 \, \mathrm{e}^{-\frac{\xi}{9}\frac{\chi^2}{\chi_c}} \,, \tag{4.57}$$

and calculate the position of the fixed points as well as their respective stability. This case was first analysed in Ref. [265] where infinite eigenvalues were found for the fixed points of Type III and in fact served as the motivation for the new dynamical system description presented in the last Section and published in [80].

We begin by working out the fixed points of Type I:

$$\textbf{Type I fixed points:} \quad \text{(Gaussian potential)} \qquad \begin{cases} p_0 = (0,\, 0,\, 0) \,, \\ p_1^{\pm} = \left(\pm\frac{1}{2},\, \pm 1,\, 0\right) \,. \end{cases} \tag{4.58}$$

As can be seen from Eq. (4.40), the fixed point p_0 corresponds to a saddle point (unstable) representing an epoch of DM domination. Using an analysis based on centre manifold theory, we find that the points $p_1^{\pm}$ represent attractors that lead the Universe into a LSBR event in the future if $\xi > 0$ and become unstable saddle points if $\xi < 0$.

Since the Gaussian potential has only one stationary point at $\chi = 0$, i.e., at $u = 0$, there is only

one fixed point of Type II:

$$\textbf{Type II fixed points:} \quad p_2 = (0,\, 0,\, 1)\ , \qquad \text{(Gaussian potential)} \tag{4.59}$$

This corresponds to a scenario where the content of the Universe is completely dominated by the 3-form potential. The eigenvalues of the Jacobian in this case are

$$\{\gamma\}_{p_2} = \left\{-3, -\frac{3}{2}\left(1+\sqrt{1+\frac{4\xi}{9}}\right), -\frac{3}{2}\left(1-\sqrt{1+\frac{4\xi}{9}}\right)\right\}\ , \tag{4.60}$$

which leads to the conclusion that p_2 is a saddle point node for $\xi > 0$ [216].

Finally, there exist three pairs of Type III fixed points for the Gaussian potential:

$$\textbf{Type III fixed points:} \quad \text{(Gaussian potential)} \qquad \begin{cases} \pi_0^{\pm} = (\pm 1,\, 0,\, 0)\ , \\ \pi_{+1}^{\pm} = (\pm 1,\, 1,\, 0)\ , \\ \pi_{-1}^{\pm} = (\pm 1,\, -1,\, 0)\ , \end{cases} \tag{4.61}$$

whose eigenvalues are[7]

$$\{\gamma\}_{\pi_0^{\pm}} = \left\{3,\, \frac{3}{2},\, +\infty\right\}\ , \qquad \{\gamma\}_{\pi_{-1}^{\pm}} = \{3,\, -3,\, +\infty\}\ , \qquad \{\gamma\}_{\pi_{+1}^{\pm}} = \{3,\, -3,\, +\infty\}\ . \tag{4.62}$$

while the total parameter of EoS is $w_{\rm tot} = -y_{\rm fp}^2$. Therefore, $\pi_0^{\pm}$ correspond to a DM-dominated epoch, while in $\pi_{\pm 1}^{\pm}$ the energy budget is entirely dominated by the kinetic term of the 3-form.

The existence of infinite eigenvalues reflects the existence of divergences that arise from the compactification strategy employed in the definition of the variable u. In the alternative dynamical system representation introduced in Sect. 4.2.2, the fixed points $\pi_0^{\pm}$ are mapped onto a new pair of isolated fixed points $\Pi_0^{\pm}$ in the space $(v,\, y,\, h)$:

$$\Pi_0^{\pm} = (\pm 1,\, 0,\, 1)\ , \tag{4.63}$$

with eigenvalues

$$\{\gamma\}_{\Pi_0^{\pm}} = \left\{3,\, 3,\, \frac{3}{2}\right\}\ . \tag{4.64}$$

The repulsive nature of these fixed point tells us that these can correspond to the asymptotic initial state of the system, i.e., to an initial epoch entirely dominated by DM.

In the new representation, the other four points $\pi_{+1}^{\pm}$ and $\pi_{-1}^{\pm}$ are now mapped onto a continuous

[7] The infinite value of the eigenvalue was obtained by computing the characteristic polynomial of the Jacobian near the fixed point and then taking an appropriate limit of the formulas obtained. In particular, we first took the limit of $z \to 0$ and only afterwards the limit $u \to \pm 1$. This is in accordance with the previous statement that the variable z vanishes faster than $\tan(\pi u/2)$ divergence as $u \to \pm 1$.

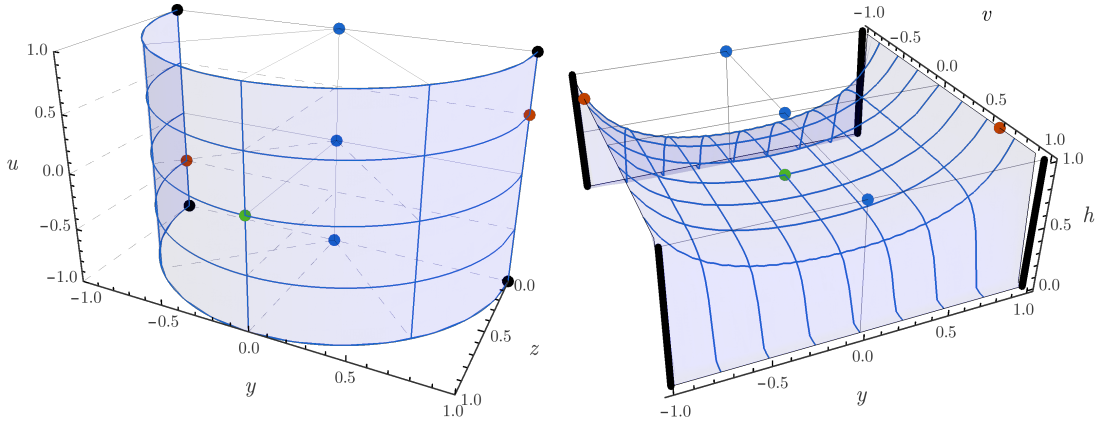

Figure 4.2.: The position of the fixed points in (left panel) the dynamical system $\{u,\, y,\, z\}$ and in (right panel) the new representation $\{v,\, y,\, h\}$. Matching fixed points in the two representations are marked with the same colour. The invariant subsets $\mathcal{M}_1$ which correspond to the case of no DM are highlighted in blue.

set of fixed points (cf. Fig. 4.2)

$$\Pi^{\pm}_{+1} = (\pm 1,\, +1,\, h_{fp})\,, \qquad \Pi^{\pm}_{-1} = (\pm 1,\, -1,\, h_{fp})\,, \tag{4.65}$$

where the value of the reduced Hubble rate h_{fp} varies in the range $\in (0,\, 1]$. The eigenvalues for each solution in $\Pi^{\pm}_{+1}$ and $\Pi^{\pm}_{-1}$ are

$$\{\gamma\}_{\Pi^{\pm}_{+1}} = \{3,\, -3,\, 0\}\,, \qquad \{\gamma\}_{\Pi^{\pm}_{-1}} = \{3,\, -3,\, 0\}\,, \tag{4.66}$$

and the existence of a null eigenvalue simply reflects the fact that $\Pi^{\pm}_{+1}$ and $\Pi^{\pm}_{-1}$ do not represent isolated fixed points. In fact, the eigenvectors associated with $\gamma = 0$ correspond to the direction $\vec{e}_h$ tangent to the set. Since the other two eigenvalues have non-zero real part, every point in the sets $\Pi^{\pm}_{+1}$ and $\Pi^{\pm}_{-1}$ is normally hyperbolic [41, 121] and the stability of the trajectories along the remaining directions can be determined by applying the usual linear stability theory, leading to the conclusion that $\pi^{\pm}_{+1}$ and $\pi^{\pm}_{-1}$ are saddle points. Here we point out that using the sign of the infinite eigenvalues in (4.62) to determine the stability of the solutions according to the rules of linear stability theory leads to the same results, an assumption used in Ref. [265].

4.2.4. Discussion

A dynamical system approach is a common technique to study the dynamics of a given cosmological model. By studying the local stability of the fixed points of the system using methods based on using linear stability theory and centre manifold theory [65, 111, 295], as well as the notion of normal stability for non-isolated fixed points [41, 121], we are able to qualitatively characterise the system and understand its possible initial and end state solutions. Within the context of late-time cosmologies with CDM and 3-form DE, the dynamical system employed usually corresponds to mapping the model to a semi-cylinder of unit radius and whose height corresponds either to the field χ [216] or a compact

variable of χ [65, 265]. Such a compactification is necessary if we are to find fixed points at infinity and therefore provide a global picture of the dynamics of the model. We stress that it is imperative that the compactification scheme be chosen with care, since it can lead to divergences in the equations.

In this section, we have reviewed the dynamical system description of a model with CDM and a 3-form and presented the new classification of fixed points we defined in [265], which for the first time included fixed points at infinite values of the χ field used to parameterise the 3-form. To overcome some problems related to the stability analysis of these fixed points at infinity, a new dynamical system description was introduced by us in [80], which was based on a different compactification scheme [146, 169, 170, 204, 366]. In this new representation, the variable z related to the fractional potential energy density of the 3-form is replaced by a reduced Hubble rate variable h. As a consequence, the information regarding the individual energy density contribution of the 3-form and DM is no longer readily available in this new representation and the graphical representation of the system becomes less intuitive (cf. Fig. 4.2). However, these are minor setbacks as the new dynamical system allows for a proper study of the stability of the fixed points at infinite values of the field χ, as was shown for the case where the 3-form has a Gaussian potential.

As a final comment, we point out that in general the usefulness and applicability of a specific dynamical system representation depends on the model at hand. The two strategies discussed in this section are no exception–the representation $\{u, y, z\}$ is perfectly capable of describing the dynamics of the model at late-time, i.e., for finite values of χ, and provides a more intuitive interpretation of the dynamical variables used. On the other hand, the representation $\{v, y, h\}$ may be preferable to describe the dynamics at infinity. Furthermore, both these representations fail in the case of potentials with zeros at finite values of χ, as this can lead to the appearance of divergent terms in the evolution equations. Such limitations appear as well in quintessence models where DE is modelled by a scalar field and specific strategies were developed to obtain a coherent description for monomial [27] and Starobinsky-like [26] potentials. It remains to be checked if a similar strategy could prove fruitful in the case of a 3-form field.

4.3. The Little Sibling of the Big Rip in 3-form Cosmology

The LSBR, as first analysed in Ref. [77], is a late-time cosmological event which happens at an infinite cosmic time and where the Hubble parameter diverges but the first time derivative of the Hubble parameter remains finite. In the same paper, it was shown that the presence of a LSBR event in the future of the Universe leads in a finite interval of time from the present to a dissociation of the local structure of the Universe, which starts by destroying the large scale structures and then gradually affects structures of smaller size. This type of behaviour can be induced by a fluid with the simple EoS [77]

$$P = -\rho - A\,, \tag{4.67}$$

where A is a positive constant, although it can appear as well in models of modified generalised Chaplygin gas [84]. The constant A in Eq. (4.67), however small, is the leading term contributing to $\dot{H}$ and leads the Hubble rate to diverge linearly with the cosmic time and logarithmically with the scale factor. Here, and in the rest of this section, a dot represents a derivative with respect to the

cosmic time ($N = 1$). We now show how a LSBR event appears naturally in some 3-form cosmological models with positive-valued potentials.

As discussed in Sect. 4.1.4, the equation of motion of the χ field admits as static solutions the critical points $\pm\chi_c$. These two points have the particularity of saturating the Friedmann equation in a spatially flat Universe, leading to the constraint (4.21). If $V(\pm\chi_c) > 0$, the only way for the static solutions to represent physically accessible states is for the Hubble rate to diverge as $\chi \to \pm\chi_c$ and $\dot{\chi} \to 0$. However, this divergence does not propagate to the first derivative of H, as we find from Eqs. (4.17) and (4.18) that in the absence of other matter fluids

$$\dot{H}_{(\chi\to\pm\chi_c)} = \mp\frac{\kappa^2}{2}\chi_c V_{,\chi}(\pm\chi_c) = -\frac{2}{3}V_{,\chi^2}(\pm\chi_c)\,. \tag{4.68}$$

This means that $\dot{H}$ converges to a constant whose sign depends on the value of $V_{,\chi^2}(\pm\chi_c)$. In the case that $V_{,\chi^2}(\pm\chi_c) < 0$, near the critical points the Hubble rate grows linearly with time

$$H(t) \approx H(t_i) - \frac{2}{3}V_{,\chi^2}(\pm\chi_c)\,(t - t_i)\ , \tag{4.69}$$

where t_i is an arbitrary constant. It can as well be shown that the Hubble rate grows logarithmically with the scale factor

$$H^2(t) \approx H^2(t_i) - \frac{4}{3}V_{,\chi^2}(\pm\chi_c)\log\left(\frac{a(t)}{a(t_i)}\right)\ . \tag{4.70}$$

This behaviour is precisely the one observed in a fluid with EoS (4.67) which leads the Universe to hit a LSBR event in the future[8]. Since in this case these points represent local minima of the potential, recall that the field χ cannot escape the interval $[-\chi_c,\, \chi_c]$, we find that the solution leading to LSBR final state is a local attractor.

We have just seen that in spatially flat FLRW model with just a 3-form field, if $V(\pm\chi_c) > 0$ and $V_{\chi^2}(\pm\chi_c) < 0$ the universe can be led to a LSBR in the asymptotic future. We can now consider whether the addition of other (non-interacting) matter fluids can change the end state of the Universe. In this case, the equality (4.20) that defines the effective potential must be replaced by [216, 217]

$$V_\chi^{(\mathrm{eff})} = -\frac{3\kappa^2}{2}\left(1 + w^{(\mathrm{m})}\right)\rho^{(\mathrm{m})} - \frac{3\kappa^2}{2}\left(\chi^2 - \frac{2}{3\kappa^2}\right)V_\chi\,, \tag{4.71}$$

where quantities with the superscript (m) refer to the matter content apart form the 3-form field. If these matter fluids respect the null energy condition $\rho^{(\mathrm{m})} + P^{(\mathrm{m})} \geq 0$ then the previous equation indicates that in the asymptotic future, when $\rho^{(\mathrm{m})}$ has completely decayed due to the expansion of the Universe, the static solutions $\chi(t) = \pm\chi_c$ are recovered. Even in the case where $\rho^{(\mathrm{m})}$ evolves towards an effective cosmological constant, the presence of the factor $1 + w^{(\mathrm{m})}$ in Eq. (4.71) shows that these solutions are not affected. We thus conclude that the LSBR remains a possible final state of the Universe even in the presence of other matter fields that satisfy the null energy condition.

As discussed above, a LSBR cosmic event can occur in models where DE is modelled by a 3-form

[8] The conclusion that the Hubble parameter diverges as the system evolves towards the static solution depends strongly on the assumption that the potential is positive valued at the critical points. In addition, whether the divergence is of the type of a LSBR event requires the asymptotic value of $\dot{H}$ to be finite and positive.

field (minimally coupled to gravity and with a canonical kinetic term) playing the role of DE, even when the potential of the 3-form is always non-negative. In this scenario, the Universe would end up in a final state of super-accelerated expansion, $\dot{H} > 0$, that would eventually destroy all the structures in it. Furthermore, such a catastrophic fate is not altered by the presence of other types of matter, such as DM, that satisfy the null energy condition, at least as long as there is no interaction with the 3-form. There is, however, the possibility that this scenario can be avoided by an appropriate interaction between DM and DE. If this interaction is able to maintain the field χ away from the critical points χ_c in the asymptotic future, then the LSBR might be removed as the end state of the Universe. This possibility was considered in Ref. [265] and the main results of that work are presented in the remainder of this section.

4.3.1. The model

Let us now consider a model of a spatially flat universe filled by a 3-form field $A_{\mu\nu\rho}$ with a potential $V(A^2)$ playing the role of DE and by pressure-less matter, e.g., CDM. The evolution of the 3-form is encoded in the scalar variable $\chi(t)$, cf. Eq. (4.12), and we consider the existence of an interaction Q between DM and DE such that

$$\dot{\rho}_{\rm DM} = -3H\rho_{\rm m} - Q\,, \qquad \dot{\rho}_{\chi} = -3H\left(\rho_{\chi} + P_{\chi}\right) + Q\,. \tag{4.72}$$

Independently of the specific form of the interaction term Q in the previous equations, its sign indicates the direction of the energy transfer between DM and the 3-form field: if $Q > 0$ there is an energy transfer from DM to the 3-form field and if $Q < 0$ there is an energy transfer from the 3-form field to DM. We recall that despite this interaction between the individual fluids, the total energy density $\rho_{\rm tot} = \rho_{\rm m} + \rho_{\chi}$ is always conserved, in agreement with the Bianchi identities.

The Friedmann and Raychaudhuri equations (4.17) and (4.18) in this model can be written

$$H^2 = \frac{\kappa^2}{3}\rho_{\rm m} + \frac{\kappa^2}{6}\left(\dot{\chi} + 3H\chi\right)^2 + \frac{\kappa^2}{3}V(\chi^2)\,, \tag{4.73}$$

$$\dot{H} = -\frac{\kappa^2}{2}\left(\rho_{\rm m} + V_{,\chi}\chi\right)\,. \tag{4.74}$$

Due to the interaction with DM, the evolution equation for χ, cf. Eq. (4.14), compatible Eq. (4.72) becomes

$$\ddot{\chi} + 3H\dot{\chi} + 3\dot{H}\chi + V_{,\chi} = \frac{Q}{\dot{\chi} + 3H\chi}\,. \tag{4.75}$$

From the conservation equations (4.72), we can define the effective parameters of EoS of CDM and the 3-form as

$$w_{\rm DM}^{\rm eff} = \frac{Q}{3H\rho_{\rm DM}}\,, \qquad\qquad w_{\chi}^{\rm eff} = -1 + \frac{V_{\chi}\chi - Q/(3H)}{\frac{1}{2}(\dot{\chi} + 3H\chi)^2 + V}\,, \tag{4.76}$$

while the total EoS parameter reads

$$w_{\rm tot} = -1 + \frac{\rho_{\rm m} + V_\chi \chi}{\rho_{\rm m} + \frac{1}{2}\left(\dot{\chi} + 3H\chi\right)^2 + V(\chi^2)} \,. \tag{4.77}$$

Choice of potential

Having defined the main components of our model, we are now left with the task of specifying the potential of the 3-form and the functional form of the interaction term Q. We begin by fixing the potential of the 3-form, whose shape is essential in guaranteeing that a LSBR event occurs in the non-interacting model, i.e., when $Q = 0$. With this in mind, we consider the Gaussian potential

$$V(\chi) = V_0 \, \mathrm{e}^{-\frac{\xi}{9}\frac{\chi^2}{\chi_{\rm c}^2}} \,, \tag{4.78}$$

where V_0 and ξ are positive constants. This potential has the particularity of satisfying $\chi V_\chi < 0$ for $\forall \chi \neq 0$, therefore leading to a phantom-like behaviour of the 3-form everywhere except at the origin. Such a behaviour leads to a LSBR whenever the field χ tends to the static solutions at the critical points $\chi(t) = \pm\chi_{\rm c}$.

Another desirable characteristic of the Gaussian potential is that, despite the phantom-like behaviour, we can have a positive squared speed of sound of the 3-form, $c_{s\chi}^2$, for an arbitrarily large interval around the origin by controlling the parameter ξ. In fact, since for a 3-form $c_{s\chi}^2$ is given by [216]

$$c_{s\chi}^2 := \frac{\chi V_{\chi\chi}}{V_\chi} = 1 - \frac{2\xi}{9}\frac{\chi^2}{\chi_{\rm c}^2} \,, \tag{4.79}$$

we find that $0 \leq c_s^2 \leq 1$ in the interval $\chi \in [-\sqrt{9/(2\xi)}\chi_{\rm c}, \sqrt{9/(2\xi)}\chi_{\rm c}]$, which includes the critical points $\pm\chi_{\rm c}$ if $0 < \xi < 9/2$. Thus, at late-time the model is free of instabilities caused by a superluminal or imaginary speed of sound of the 3-form [131, 216]. For large values of χ^2, however, $c_{s\chi}^2$ becomes increasingly negative, as such the model may not be physically viable in that regime. Nevertheless, the model remains valid and physically relevant at late-time when $\chi \in [-\chi_{\rm c}, \chi_{\rm c}]$ and can be used as a candidate for DE. In addition, for large values of χ the 3-form field behaves asymptotically as a cosmological constant, therefore, it is possible that any instabilities arising from a negative value of c_s^2 are suppressed. For an extended discussion on different type of potentials, please see the Sect. 4.2 of Ref. [265].

Choice of interaction

Finally, we look at the form of the interaction term Q. In the context of cosmological models with 3-form fields, an interacting 3-form as been considered in Refs. [65, 218, 265, 274] in the context of models in which the 3-form field plays the role of DE, while in Ref. [132] a coupling between a 3-form and a scalar field is considered as a mean to describe the reheating period that ends the 3-form fuelled inflation.

Starting from a phenomenological approach, we consider the general class of interactions

$$Q = 3H\left(\rho_{\rm m}+\rho_\chi\right)\sum_{i,j=0}\lambda_{ij}\left(\frac{\rho_{\rm m}}{\rho_{\rm m}+\rho_\chi}\right)^i\left(\frac{\rho_\chi}{\rho_{\rm m}+\rho_\chi}\right)^j, \tag{4.80}$$

where i, j are non-negative integers and λ_{ij} are dimensionless couplings that determine the strength of each interaction term. The expression (4.80) represents a natural higher order generalisation of the frequently considered linear interaction $Q = 3H\left(\lambda_{\rm m}\rho_{\rm m}+\lambda_{\rm DE}\rho_{\rm DE}\right)$ [68] and includes as well the case of $Q = 3H\lambda\,\rho_{\rm m}\rho_{\rm DE}/(\rho_{\rm m}+\rho_{\rm DE})$, inspired from two-body chemical reactions [38, 78]. While it is not derived from fundamental physics, its simple mathematical structure does bring some advantages as it facilitates a dynamical systems analysis of the model at hand and in some cases even allows for an explicit solution to be obtained. If the sum in Eq. (4.80) is truncated up to an order n such that $i+j\leq n$, we can take advantage of the degeneracy in the λ_{ij}'s to re-write the interaction as

$$Q = 3H\left(\rho_{\rm m}+\rho_\chi\right)\sum_{i=0}^{n}\alpha_i\left(\frac{\rho_\chi}{\rho_{\rm m}+\rho_\chi}\right)^i, \tag{4.81}$$

thus reducing the number of coupling coefficients from $(n+2)(n+1)/2$ to just $n+1$. In the following analysis we will consider only interaction that are up to quadratic order in the expansion (4.81). By truncating the expansion (4.81) to quadratic order, we are able to cover most of the cases of interactions considered in the literature as well as verify if important features appear in the evolution of the model due to the inclusion of a non-linear term.

4.3.2. Dynamical system analysis

In order to study the dynamics of our model, we now employ a dynamical system analysis. We choose to employ the same set of variables discussed in Sect. 4.2:

$$u = \frac{2}{\pi}\arctan\left(\frac{\chi}{\chi_{\rm c}}\right), \qquad y := \frac{\dot\chi+3H\chi}{3H\chi_{\rm c}}, \qquad z := \sqrt{\frac{\kappa^2V}{3H^2}}, \qquad s := \sqrt{\frac{\kappa^2\rho_{\rm m}}{3H^2}}, \tag{4.82}$$

which where first introduced in Ref. [65] and represent a compactification of the variables used in Refs. [131, 216, 218, 222, 274]. We recall that $\{u,\,y,\,z,\,s\}$ verify

$$-1\leq u\leq 1, \qquad 0\leq s\leq 1, \qquad 0\leq z\leq 1, \qquad -1\leq y\leq 1, \tag{4.83}$$

and satisfy the Friedmann constraint $y^2 + z^2 + s^2 = 1$. With an interaction Q between DM and the 3-form turned on, the dynamical system (4.33)–(4.35) that describes the model becomes

$$u_x = \frac{6}{\pi}\cos^2\left(\frac{\pi u}{2}\right)\left[y - \tan\left(\frac{\pi u}{2}\right)\right], \tag{4.84}$$

$$y_x = \frac{1}{2}\left\{3\left[1 - y^2 - z^2\right]y + \lambda(u)\, z^2\left[1 - \tan\left(\frac{\pi}{2}u\right)y\right]\right\} + \frac{\kappa^2}{6yH^3}Q\,, \tag{4.85}$$

$$z_x = \frac{1}{2}z\left\{3\left[1 - y^2 - z^2\right] - \lambda(u)\left[y - \tan\left(\frac{\pi}{2}u\right)(1 - z^2)\right]\right\}, \tag{4.86}$$

$$s = \sqrt{1 - y^2 - z^2}\,. \tag{4.87}$$

We recall that we are using $x = \log(a/a_0)$ as our time variable and a subscript x indicates a derivative with respect to x. In addition, for the case of a Gaussian potential (4.78) we can write the factor $\lambda(u)$, which is defined in Eq. (4.30), as

$$\lambda(u) = \frac{2\xi}{3}\tan\left(\frac{\pi}{2}u\right), \tag{4.88}$$

and the quadratic interaction (4.81) can be written in terms of the dynamical variables as

$$Q = \frac{9H^3}{\kappa^2}\sum_{i=0}^{2}\alpha_i\left(y^2 + z^2\right)^i. \tag{4.89}$$

The total EoS parameter (4.77) can now be written in terms of the dynamical system variables as

$$w_{\rm tot} = -\left(y^2 + z^2\right) - \frac{2\xi}{9}\tan^2\left(\frac{\pi}{2}u\right)z^2\,, \tag{4.90}$$

while the individual effective EoS parameters, cf. Eq. (4.76), read

$$w_{\rm DM}^{\rm eff} = \frac{1}{1 - y^2 - z^2}\sum_{i=0}^{2}\alpha_i\left(y^2 + z^2\right)^i, \tag{4.91}$$

$$w_{\chi}^{\rm eff} = -1 - \frac{2\xi}{9}\tan^2\left(\frac{\pi}{2}u\right)\frac{z^2}{y^2 + z^2} - \frac{1}{y^2 + z^2}\sum_{i=0}^{2}\alpha_i\left(y^2 + z^2\right)^i. \tag{4.92}$$

The set of Eqs. (4.84), (4.85), and (4.86), complemented with Eqs. (4.88), constitutes a three-dimensional autonomous system that defines the evolution of the dimensionless variables $(u,\, y,\, z)$ which encode the evolution of our model of interacting DM and 3-form. In the following sections, we will identify the position of the fixed points of the model according to the classification defined in Sect. (4.2) as well as study their stability. Notice, however, that the inclusion of an interaction term leads to a modification of the conditions (4.38) and (4.41) that define the position of the fixed points of Types I and II. Taking into account Eqs. (4.88) and (4.89), those conditions are now replaced,

respectively, by

$$(u_{\rm fp},\, y_{\rm fp},\, z_{\rm fp}) : \begin{cases} u_{\rm fp} & = \dfrac{2}{\pi}\arctan\left(y_{\rm fp}\right)\,, \\ y_{\rm fp}\left(1-y_{\rm fp}^2\right) & = -\dfrac{1}{y_{\rm fp}}\sum_{i=0}^{2}\alpha_i\left(y_{\rm fp}^2+z_{\rm fp}^2\right)^i\,, \\ z_{\rm fp} & = 0\,, \end{cases} \tag{4.93}$$

and

$$(u_{\rm fp},\, y_{\rm fp},\, z_{\rm fp}) : \begin{cases} u_{\rm fp} & = \dfrac{2}{\pi}\arctan\left(y_{\rm fp}\right)\,, \\ \xi y_{\rm fp} z_{\rm fp}^2 & = -\dfrac{3}{2\xi y_{\rm fp}}\sum_{i=0}^{2}\alpha_i\left(y_{\rm fp}^2+z_{\rm fp}^2\right)^i\,, \\ 1-y_{\rm fp}^2-z_{\rm fp}^2 & = \dfrac{2}{9}\xi y_{\rm fp}^2 z_{\rm fp}^2\,. \end{cases} \tag{4.94}$$

Replacing the equalities (4.93) and (4.94) in Eq. (4.90), we find that the value of the total EoS parameter at the fixed points of Type I and II is not affected by the interaction and $w_{\rm tot} = -y_{\rm fp}^2$ for the fixed points of Type I and $w_{\rm tot} = -1$ for the fixed points of Type II.

From (4.93) we find that the quadratic interaction (4.81) removes completely the fixed points associated to the LSBR if

$$\alpha_0 + \alpha_1 + \alpha_2 \neq 0\,. \tag{4.95}$$

If we impose this condition back on Eq. (4.88) we obtain the general form of the interactions belonging to the class (4.81) that do remove LSBR event:

$$Q \neq \frac{9H^3}{\kappa^2}\left[\left(y^2+z^2\right)-1\right]\left[\alpha_1+\alpha_2+\alpha_2\left(y^2+z^2\right)\right]\,, \tag{4.96}$$

which, can be recast in terms of the CDM related variable s as

$$Q \neq -\frac{9H^3}{\kappa^2}s^2\left[\alpha_1+\alpha_2+\alpha_2\left(y^2+z^2\right)\right]\,. \tag{4.97}$$

This condition tells us that the LSBR event is completely removed as a possible final state of the model as long as the interaction is not proportional to a power of the DM energy density $\rho_{\rm m}^n$ with $n \geq 1$. This result can be understood by looking at the conservation equation for DM (4.72) which for $Q = 3H\rho_{\rm m}^n g(y,\, z)$ becomes

$$\dot{\rho}_{\rm m} + 3H\left[1+g(y,\, z)\rho_{\rm m}^{n-1}\right]\rho_{\rm m} = 0\,. \tag{4.98}$$

For well behaved $g(y,\, z)$ this equation admits as solution $\rho_{\rm m} = 0$ and therefore does not exclude *a priori* the possibility that the end state of the Universe is characterised by a vanishing contribution of DM to the matter content and therefore at very late-time the 3-form field is not affected by the presence of DM and drives the universe towards a LSBR event. Notice that this condition is completely independent of the shape of the potential, therefore, it is not limited to the case of a 3-form with a Gaussian potential, as long as the potential used leads to a LSBR in the future.

General Stability

By solving the set of equalities (4.93), we can calculate the position of fixed points of Type I in terms of the interaction couplings $\{\alpha_0, \alpha_1, \alpha_2\}$ as

$$\textbf{Type I fixed points:}\ (\text{Quadratic interaction}) \qquad \begin{cases} \hat{p}_0^{\pm}: & (u_{\rm fp}, y_{\rm fp}, z_{\rm fp}) = \left(\pm\frac{2}{\pi}\arctan\left(\hat{y}_-\right), \pm\hat{y}_-, 0\right), \\ \hat{p}_1^{\pm}: & (u_{\rm fp}, y_{\rm fp}, z_{\rm fp}) = \left(\pm\frac{2}{\pi}\arctan\left(\hat{y}_+\right), \pm\hat{y}_+, 0\right), \end{cases} \tag{4.99}$$

where $\hat{y}_\pm$ is defined as

$$\hat{y}_\pm^2 = \frac{1+\alpha_1}{2\left(1-\alpha_2\right)}\left[1 \pm \sqrt{1+4\alpha_0\frac{1-\alpha_2}{\left(1+\alpha_1\right)^2}}\right]. \tag{4.100}$$

As in the non-interacting case, we find that the existence of fixed points of Type I does not depend on the shape of the potential and $w_{\rm tot} = -y_{\rm fp}^2$. By comparing Eq. (4.99) with the position of the fixed points of Type I in the non-interacting case, cf. Eq. (4.58), we conclude that as we switch off the interaction the pairs of fixed points $\hat{p}_0^{\pm}$ and $\hat{p}_1^{\pm}$ obtained above converge, respectively, to the points p_0 and $p_1^{\pm}$ of the non-interacting case.

In the regime of weak interactions, i.e., for small coefficients $|\alpha_i| \ll 1$, expanding (4.100) at first order in the α_i's leads to

$$\hat{y}_-^2 \simeq -\alpha_0\,, \qquad\qquad \hat{y}_+^2 \simeq 1 + (\alpha_0+\alpha_1+\alpha_2)\,. \tag{4.101}$$

Thus, the fixed points $\hat{p}_0^{\pm}$ correspond to a scaling behaviour between CDM and DE, with a near complete CDM dominance, if $\alpha_0 < 0$ and to a matter dominated epoch if $\alpha_0 = 0$, in which case $\hat{y}_- = 0$ and $\hat{p}_0^{\pm} = p_0^{\pm}$. In addition, we find that the existence of the fixed points $\hat{p}_0^{\pm}$ is dependent on the condition $\alpha_0 \leq 0$. On the other hand, the fixed points $\hat{p}_1^{\pm}$ only exist in the system if $\alpha_0+\alpha_1+\alpha_2 \leq 0$ and corresponds either to a scaling behaviour with 3-form dominance if $\alpha_0+\alpha_1+\alpha_2 < 0$ or to possible LSBR events if $\alpha_0+\alpha_1+\alpha_2 = 0$. We recall that previously, cf. Eq. (4.95), we found that the condition for the removal of fixed points associated to the LSBR was precisely $\alpha_0+\alpha_1+\alpha_2 \neq 0$.

The eigenvalues of the Jacobian at $\hat{p}_0^{\pm}$ and $\hat{p}_1^{\pm}$ can be written in terms of $\hat{y}_\pm^2$, α_1, and α_2 as

$$\{\gamma\}_{\hat{p}_0^{\pm},\hat{p}_1^{\pm}} = \left\{-3, \frac{3}{2}(1-\hat{y}_\pm^2), -3\left[2\left(1-\alpha_2\right)\hat{y}_\pm^2 - \left(1+\alpha_1\right)\right]\right\}, \tag{4.102}$$

where $\hat{y}_-$ ($\hat{y}_+$) on the above formula corresponds to the case $\hat{p}_0^{\pm}$ ($\hat{p}_1^{\pm}$). We find that the Jacobian has two negative and one positive eigenvalues if $\hat{y}_\pm^2 \neq 1$ and two negative and one null eigenvalues when $\hat{y}_\pm^2 = 1$. This implies that $\hat{p}_0^{\pm}$ always correspond to two saddle points, while the pair $\hat{p}_1^{\pm}$ represent two saddles points if $\hat{y}_+^2 \neq 1$, i.e., when LSBR event is removed. In the case of $\hat{y}_+^2 = 1$, we find through methods based on centre manifold theory that the stability condition is analogous to the one found in the case of no interaction: $\hat{p}_1^{+}$ ($\hat{p}_1^{-}$) is an attractor if $\xi > 0$ and a saddle node if $\xi < 0$. Therefore, we find that quadratic interactions (4.88) that do not satisfy the inequality (4.95) not only fail to remove the fixed points associated to the LSBR event, they also do not change their stability.

In order to find the position of the fixed points of Type II, we recast the condition (4.94) as

$$\alpha_2\beta^2 + (\alpha_1 - 1)\,\beta + (1 + \alpha_0) = 0\,, \tag{4.103}$$

$$\left(\beta - y_{\rm fp}^2\right) y_{\rm fp}^2 - \frac{9}{2\xi}\,(1 - \beta) = 0\,, \tag{4.104}$$

with $u_{\rm fp} = (2/\pi)\arctan(y_{\rm fp})$ and

$$\beta := y_{\rm fp}^2 + z_{\rm fp}^2\,. \tag{4.105}$$

The quantity β represents the fractional energy density of DE at the fixed point and satisfies $0 < \beta \leq 1$. An immediate conclusion from Eq. (4.103) is that, for the class of interactions considered, the value of β is determined solely by the interaction coefficients α_i and does not depend on the choice of the potential. In addition, as discussed above the total parameter of EoS is $w_{\rm tot} = -1$ independently of the potential considered and the coupling coefficients.

The solutions to Eq. (4.103) are

$$\beta_\pm = \frac{1 - \alpha_1}{2\alpha_2}\left[1 \pm \sqrt{1 - 4\alpha_2\frac{1 + \alpha_0}{(1 - \alpha_1)^2}}\right]\,, \tag{4.106}$$

which, at first order in the coefficients α_i can be written as

$$\beta_+ \simeq \frac{1 - \alpha_1}{\alpha_2} - 1 - (\alpha_0 + \alpha_1 + \alpha_2)\,, \qquad \beta_- \simeq 1 + (\alpha_0 + \alpha_1 + \alpha_2)\,. \tag{4.107}$$

In the regime of small coefficients, $|\alpha_i| \ll 1$, the solution β_+ is outside the interval $(0, 1]$ and can be disregarded, while the solution β_- lies within the interval $(0, 1]$ and is close to unity ($\beta_- \lesssim 1$) for $\alpha_0 + \alpha_1 + \alpha_2 \lesssim 0$, indicating a 3-form dominance near the fixed points. The same condition was found for the existence of the Type I fixed points $\hat{p}_1^\pm$.

By setting $\beta = \beta_-$ in Eq. (4.104) and solving for $y_{\rm fp}$, we find that the dynamical system has at most two pairs of fixed points of Type II:

Type II fixed points:
(Quadratic interaction
+ Gaussian potential)

$$\begin{cases} \tilde{p}_1^\pm = & \left(\pm\dfrac{2}{\pi}\arctan\left(\tilde{y}_+\right),\, \pm\tilde{y}_+,\, \sqrt{\beta_- - \tilde{y}_+^2}\right)\,, \\ \tilde{p}_2^\pm = & \left(\pm\dfrac{2}{\pi}\arctan\left(\tilde{y}_-\right),\, \pm\tilde{y}_-,\, \sqrt{\beta_- - \tilde{y}_-^2}\right)\,, \end{cases} \tag{4.108}$$

where

$$\tilde{y}_\pm^2 = \frac{\beta_-}{2}\left(1 \pm \Delta\right)\,, \qquad \Delta\left(\beta, \xi\right) := \sqrt{1 - \frac{18}{\xi}\frac{1 - \beta_-}{\beta_-^2}}\,. \tag{4.109}$$

For $\xi > 0$, we find that $0 \leq \Delta < 1$, which ensures the existence of Type II fixed points, as long as

$$\frac{9}{\xi}\left(\sqrt{1 + \frac{2\xi}{9}} - 1\right) \leq \beta_- \leq 1\,, \qquad 0 < \xi < \frac{9}{2}\,. \tag{4.110}$$

For general values of the parameters of the model $(\xi, \alpha_0, \alpha_1, \alpha_2)$, the expressions for the eigenvalues of the Jacobian for the Type II fixed points are too cumbersome to be used to draw conclusions on the stability of the system by analytical methods. An alternative strategy devised by us in Ref. [265] is to employ the Hurwitz criterion (cf. Ref. [283] for the definition and Appendix C.1 for its application to the cubic case) to determine whether all three eigenvalues have negative real part, in which case the fixed point is stable, or if at least one of the eigenvalues has a positive real part, in which case the fixed point is unstable. Let us write the characteristic polynomial of the Jacobian, J, of the dynamical system at the fixed point as

$$\det\left(J - \gamma\,\mathbb{I}_3\right) = a_0 + a_1\gamma + a_2\gamma^2 - \gamma^3\,, \tag{4.111}$$

where $\mathbb{I}_3$ is the 3×3 identity matrix and a_i, $i = 0, 1, 2$, are constant coefficients and the roots γ of $\det(J - \gamma\mathbb{I}_3)$ are the eigenvalues of the Jacobian. Then, using Hurwitz criterion we can state that all three γ's have negative real part if and only if

$$a_0 < 0\,, \qquad \operatorname{sign} a_1 = \operatorname{sign} a_0\,, \qquad a_1 a_2 + a_0 > 0\,. \tag{4.112}$$

As a corollary, when $a_0 > 0$ there is at least one positive eigenvalue and the fixed point is unstable. Although we were not able to obtain a general result for the stability of fixed points of Type II using this method, from analogy with the non-interaction case it might be expected that late-time attractors are provided by the pair $\tilde{p}_1^{\pm}$, while the pair $\tilde{p}_2^{\pm}$ gives unstable points. This was confirmed for specific subclasses of interactions presented below.

If we consider the upper limit $\beta_- = 1$ in Eq. (4.110), we find from Eq. (4.109) that $\Delta = 1$. In this case, the pairs $\tilde{p}_1^{\pm}$ and $\tilde{p}_2^{\pm}$ converge, respectively, to the points $p_1^{\pm}$ and p_2 obtained when $Q = 0$. In fact, solving Eq. (4.106) for $\beta_- = 1$ leads to the equality[9] $\alpha_0 + \alpha_1 + \alpha_2 = 0$, of which the non-interacting case $\alpha_i = 0$ is a trivial solution. Since the points $p_1^{\pm}$ belong to the Type I category ($z_{\rm fp} = 0$), when $\beta_- = 1$ the only fixed point of Type II is $\tilde{p}_2 = p_2$. The analysis of the system around this point presents serious challenges as the interaction term in Eq. (4.85) is proportional to $1/y$. This limitation of the dynamical system representation seems to arise from the choice of the phenomenological interaction (4.89) which does not cancel this divergent factor. Nevertheless, as stated above $\beta_- = 1$ occurs only for those interactions for which the LSBR event is not removed. For those cases, we expect that all the trajectories of interest converge to one of the fixed points corresponding to the LSBR and not to $\tilde{p}_2$. As such, we will not look into the stability of this point with further detail.

The opposite limiting case occurs when β_- approaches the lower bound in Eq. (4.110), i.e., when $\xi = 18(1-\beta_-)/\beta_-^2$. In this case, the parameter Δ vanishes, $\tilde{y}_-^2 = \tilde{y}_+^2$ and the two pairs of fixed points $\tilde{p}_1^{\pm}$ and $\tilde{p}_2^{\pm}$ merge into one single pair of fixed points of Type II:

Type II fixed points for $\Delta = 0$:
(Quadratic interaction
+ Gaussian potential)

$$\tilde{p}_\Delta^{\pm} = \left(\frac{2}{\pi}\arctan\left(\sqrt{\frac{\beta_-}{2}}\right), \pm\sqrt{\frac{\beta_-}{2}}, \sqrt{\frac{\beta_-}{2}}\right)\,. \tag{4.113}$$

[9] Notice that this implies that the interaction does not remove the LSBR event, cf. Eq. (4.95).

Notice that since for small interaction couplings we have $\beta_- \lesssim 1$, this case implies potentials that are extremely flat around $\chi = 0$. In addition, we find that one of the eigenvalues of the Jacobian is always zero at $\tilde{p}^{\pm}_{\Delta}$:

$$\{\gamma\}_{\tilde{p}^{\pm}_{\Delta}} = \left\{0\,,\, \frac{3F}{2}\left(1+\sqrt{1-4G}\right)\,,\, \frac{3F}{2}\left(1-\sqrt{1-4G}\right)\right\}\,. \tag{4.114}$$

Here, the factors $F = F(\alpha_1,\, \alpha_2,\, \beta_-)$ and $G = G(\alpha_1,\, \alpha_2,\, \beta_-)$ are defined as

$$F(\alpha_1,\, \alpha_2,\, \beta_-) := \frac{1+(\alpha_1-3)\,\beta_- + 2\alpha_2\beta_-^2}{\beta_-}\,, \tag{4.115}$$

$$G(\alpha_1,\, \alpha_2,\, \beta_-) := \frac{2+(\alpha_1-8)\,\beta + (2\alpha_2-3\alpha_1+10)\,\beta^2 - (6\alpha_2-\alpha_1+3)\,\beta^3 + 2\alpha_2\beta^4}{\left[1+(\alpha_1-3)\,\beta+2\alpha_2\beta^2\right]^2}\,, \tag{4.116}$$

and for convenience we have used Eq. (4.103) to eliminate α_0 in favour of β_-.

Since one of the eigenvalues vanishes, the analysis of the linearised system is not valid to fully characterise the stability of the system near the fixed points and centre manifold theory needs to be employed. Nevertheless, if $G < 0$ one of the eigenvalues of the system has a positive real part and the fixed point is necessarily unstable. When $\Delta = 0$, the limit $\beta_- = 1$ implies $\xi = 0$, which corresponds to the special case of a 3-form with a constant potential[10]. In this case, the 3-form behaves as a cosmological constant with $P_\chi = -\rho_\chi$ and the dynamical system employed in this section becomes degenerate as the two variables y and z can be replaced by the single variable $\sqrt{\beta} = \sqrt{y^2+z^2}$ and the variable u decouples from the rest of the dynamical system ($\lambda(u) \equiv 0$). As such, we will not explore this case any further.

In order to identify the fixed points Type III in our model with a Gaussian potential with $\xi > 0$, we assume that, as $u \to \pm 1$, the variable $z_{\rm fp}$ vanishes sufficiently fast so as to cancel the divergence of $\tan(\pi u/2)$, i.e., we assume that $z\tan(\pi u/2) = 0$ in the limit of very large χ. This assumption is supported by the fact that we have

$$z \propto \frac{\exp\left[-\dfrac{\xi}{18}\tan^2\left(\dfrac{\pi}{2}u\right)\right]}{H}\,, \tag{4.117}$$

which for $u \to \pm 1$ goes to zero faster than $\tan(\pi u/2)$ as long as the asymptotic value of H remains positive. The fact that $z_{\rm fp} = 0$ suggests an analogy with the results found for the fixed points of Type I. In fact, we find that as we turn on the interaction four pairs of fixed points appear

Type III fixed points:
(Quadratic Interaction)

$$\begin{cases} \hat{\pi}^{\pm}_{-0}: & (u_{\rm fp},\, y_{\rm fp},\, z_{\rm fp}) = (\pm 1,\, -\hat{y}_-,\, 0)\,, \\ \hat{\pi}^{\pm}_{+0}: & (u_{\rm fp},\, y_{\rm fp},\, z_{\rm fp}) = (\pm 1,\, +\hat{y}_-,\, 0)\,, \\ \hat{\pi}^{\pm}_{-1}: & (u_{\rm fp},\, y_{\rm fp},\, z_{\rm fp}) = (\pm 1,\, -\hat{y}_+,\, 0)\,, \\ \hat{\pi}^{\pm}_{+1}: & (u_{\rm fp},\, y_{\rm fp},\, z_{\rm fp}) = (\pm 1,\, +\hat{y}_+,\, 0)\,, \end{cases} \tag{4.118}$$

where $y^2_{\rm fp}$ is given by Eq. (4.100). Notice that $\hat{\pi}^{\pm}_{-0}$ and $\hat{\pi}^{\pm}_{+0}$ correspond to a decomposition of π^+_0

[10] Notice that a different limit is obtained in Eq. (4.108) if we set $\beta_- = 1$ without imposing $\Delta = 0$ first. In fact, from Eq. (4.109) we find that unless $\xi = 18(1-\beta_-)/\beta_-^2$, the equality $\beta_- = 1$ implies $\Delta = 1$.

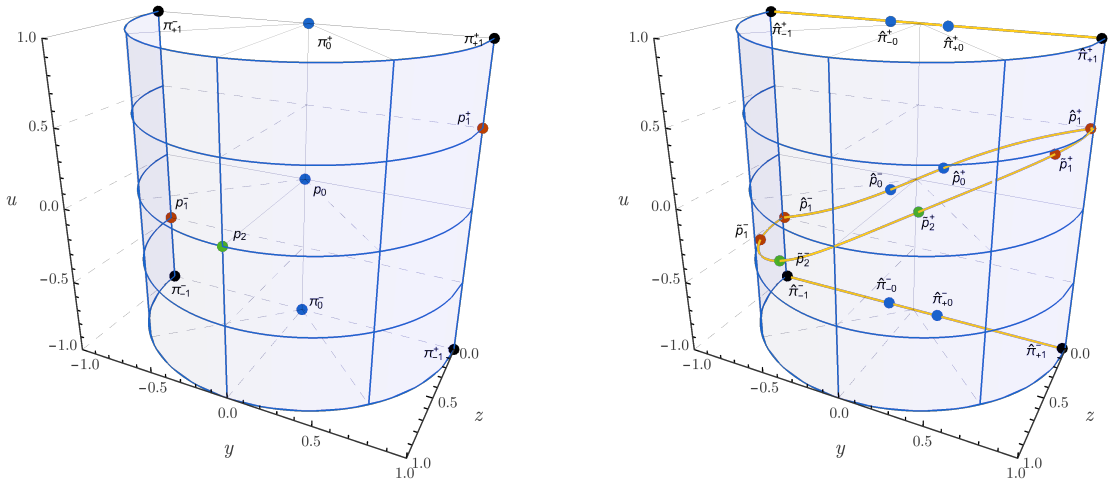

Figure 4.3.: (Left panel) The position of the fixed points of the dynamical system (u, y, z) in the case of a Gaussian potential when the interaction between DM and DE is switched off. (Right panel) The position of the fixed points changes when, for the same potential, we turn on a quadratic interaction of the kind described in Eq. (4.81) with small coefficients α_i. It is possible to observe how each fixed point in the non-interacting case, except for $\hat{\pi}^{\pm}_{\pm 1}$, splits in two points once the interaction is turned on. As the strength of the interaction coefficients changes, the new fixed points move along the yellow curves. For sufficiently flat potentials, the pairs $\tilde{p}^{\pm}_1$ and $\tilde{p}^{\pm}_2$ may coalesce and give rise to the fixed points $\tilde{p}^{\pm}_{\Delta}$, cf. Eq. (4.113). To obtain this figure we used the values $\xi = 1$, $\alpha_0 = \alpha_2 = -0.03$, and $\alpha_1 = +0.03$.

and π^{-}_0, obtained in the non-interaction scenario, into a new pair of fixed points each. In addition, $\hat{\pi}^{\pm}_{-1}$ and $\hat{\pi}^{\pm}_{+1}$ correspond to the two pairs $\pi^{\pm}_{-1}$ and $\pi^{\pm}_{+1}$ found when $Q = 0$. The eigenvalues of the Jacobian for these fixed points are

$$\{\gamma\}_{\hat{\pi}^{\pm}} = \left\{3,\, 3\,(1+\alpha_1) - 6\,(1-\alpha_2)\, y^2_{\rm fp},\, +\infty\right\}\,. \tag{4.119}$$

Under the previous assumption that an infinite but positive eigenvalue corresponds to a direction in which the system is extremely repulsive, we find that $\pi^{\pm}_{\pm 0}$, with $y^2_{\rm fp} = y^2_{-} \sim 0$ correspond to repulsive points representing the asymptotic past, while the two pairs $\pi^{\pm}_{\pm 1}$, with $y^2_{\rm fp} = y^2_{+} \sim 1$ correspond to saddle points.

Examples

So far, in this section we have determined the position and stability of all the fixed points of the system when considering a quadratic interaction (4.81) between DM and the 3-form DE with generic values for the coupling coefficients $\{\alpha_0,\, \alpha_1,\, \alpha_2\}$ and under the assumption of weak interactions, i.e., $|\alpha_i| \ll 1$. In Fig. 4.3, we compare the position of the fixed points when $Q = 0$ (left panel) and when the quadratic interaction is turned on (right panel). In general, when one of the fixed points obtained in the non-interacting case (left panel) is affected, it decomposes into two new fixed points whose position moves along the yellow lines, depending on the value of the interaction couplings $\{\alpha_0,\, \alpha_1,\, \alpha_2\}$. The only exception are the points in the corners of the subset $\tilde{\mathcal{M}}_0 = \{(u,\, y,\, z) : z = 0\}$ which are displaced along the y direction without giving rise to a new solution.

Inter.	F.P.	Constraints	$(u_{\rm fp},\, y_{\rm fp},\, z_{\rm fp})$	Stability	Descr.
0	p_0		$(0,\, 0,\, 0)$	Saddle	DM
	$p_1^{\pm}$		$(\pm 1/2,\, \pm 1,\, 0)$	Attractive	LSBR
	p_2		$(0,\, 0,\, 1)$	Saddle	dS
	$\pi_0^{\pm}$		$(\pm 1,\, 0,\, 0)$	Repulsive	DM
	$\pi_{+1}^{\pm}$		$(\pm 1,\, 1,\, 0)$	Saddle	K
	$\pi_{-1}^{\pm}$		$(\pm 1,\, -1,\, 0)$	Saddle	K
I	$\hat{p}_0^{\pm}$	$-1 < \alpha_{\rm m} < 0$	$\left(\pm\frac{2}{\pi}\arctan\lvert\alpha_{\rm m}\rvert^{\frac{1}{2}},\, \pm\lvert\alpha_{\rm m}\rvert^{\frac{1}{2}},\, 0\right)$	Saddle	S-DM
	$\hat{p}_1^{\pm}$		$(\pm 1/2,\, \pm 1,\, 0)$	Attractive	LSBR
	$\tilde{p}_2$		$(0,\, 0,\, 1)$	N/A	dS
	$\hat{\pi}_{+0}^{\pm}$	$-1 < \alpha_{\rm m} < 0$	$\left(\pm 1,\, \lvert\alpha_{\rm m}\rvert^{\frac{1}{2}},\, 0\right)$	Repulsive	S-DM
	$\hat{\pi}_{-0}^{\pm}$	$-1 < \alpha_{\rm m} < 0$	$\left(\pm 1,\, -\lvert\alpha_{\rm m}\rvert^{\frac{1}{2}},\, 0\right)$	Repulsive	S-DM
	$\hat{\pi}_{+1}^{\pm}$		$(\pm 1,\, 1,\, 0)$	Saddle	K
	$\hat{\pi}_{-1}^{\pm}$		$(\pm 1,\, -1,\, 0)$	Saddle	K
II	$\hat{p}_0^{\pm}$	$\alpha_{\rm mm} < 0$	$\left(\pm\frac{2}{\pi}\arctan\left\lvert\frac{\alpha_{\rm mm}}{1-\alpha_{\rm mm}}\right\rvert^{\frac{1}{2}},\, \pm\left\lvert\frac{\alpha_{\rm mm}}{1-\alpha_{\rm mm}}\right\rvert^{\frac{1}{2}},\, 0\right)$	Saddle	S-DM
	$\hat{p}_1^{\pm}$		$(\pm 1/2,\, \pm 1,\, 0)$	Focus Node	LSBR
	$\tilde{p}_2$		$(0,\, 0,\, 1)$	N/A	dS
	$\hat{\pi}_{+0}^{\pm}$	$\alpha_{\rm mm} < 0$	$\left(\pm 1,\, \left\lvert\frac{\alpha_{\rm mm}}{1-\alpha_{\rm mm}}\right\rvert^{\frac{1}{2}},\, 0\right)$	Repulsive	S-DM
	$\hat{\pi}_{-0}^{\pm}$	$\alpha_{\rm mm} < 0$	$\left(\pm 1,\, -\left\lvert\frac{\alpha_{\rm mm}}{1-\alpha_{\rm mm}}\right\rvert^{\frac{1}{2}},\, 0\right)$	Repulsive	S-DM
	$\hat{\pi}_{+1}^{\pm}$		$(\pm 1,\, 1,\, 0)$	Saddle	K
	$\hat{\pi}_{-1}^{\pm}$		$(\pm 1,\, -1,\, 0)$	Saddle	K
III	$\hat{p}_0$		$(0,\, 0,\, 0)$	Saddle	DM
	$\hat{p}_1^{\pm}$		$(\pm 1/2,\, \pm 1,\, 0)$	Focus Node	LSBR
	$\tilde{p}_2$		$(0,\, 0,\, 1)$	N/A	dS
	$\hat{\pi}_0^{\pm}$		$(\pm 1,\, 0,\, 0)$	Repulsive	DM
	$\hat{\pi}_{+1}^{\pm}$		$(\pm 1,\, 1,\, 0)$	Saddle	K
	$\hat{\pi}_{-1}^{\pm}$		$(\pm 1,\, -1,\, 0)$	Saddle	K

Table 4.1.: The fixed points found for a universe filled by DM and by DE modelled by a 3-form DE with a Gaussian potential. We present the results in the case of no interaction between DM and DE and for the interactions I, II, and III presented in Sect. 4.3.2. For each point, we present the constraints associated for their existence, their coordinates in $\{u,\, y,\, z\}$ space, their stability and the type of evolution they represent: DM – DM dominance; LSBR – a LSBR event; dS – de Sitter expansion; K – 3-form kinetic dominance; S-DM – scaling solution with DM dominance. The stability of the points $\tilde{p}_2$ in the cases of interactions I, II and III, which is indicated as not available (N/A), was not determined since in those cases the interaction term has divergent factors at the fixed point.

Inter.	F.P.	Constraints	$(u_{\rm fp},\, y_{\rm fp},\, z_{\rm fp})$	Stability	Descr.
0	p_0		$(0,\, 0,\, 0)$	Saddle	DM
	$p_1^{\pm}$		$(\pm 1/2,\, \pm 1,\, 0)$	Attractive	LSBR
	p_2		$(0,\, 0,\, 1)$	Saddle	dS
	$\pi_0^{\pm}$		$(\pm 1,\, 0,\, 0)$	Repulsive	DM
	$\pi_{+1}^{\pm}$		$(\pm 1,\, 1,\, 0)$	Saddle	K
	$\pi_{-1}^{\pm}$		$(\pm 1,\, -1,\, 0)$	Saddle	K
IV	$\hat{p}_0$		$(0,\, 0,\, 0)$	Saddle	DM
	$\hat{p}_1^{\pm}$	$-1 < \alpha_\chi < 0$	$\left(\pm\frac{2}{\pi}\arctan\lvert 1+\alpha_\chi\rvert^{\frac{1}{2}},\, \pm\lvert 1+\alpha_\chi\rvert^{\frac{1}{2}},\, 0\right)$	Saddle	dS-K
	$\tilde{p}_1^{\pm}$	$\frac{1}{2} - \frac{\sqrt{9+2\xi}}{6} < \alpha_\chi < 0$	$\left(\pm\frac{2}{\pi}\arctan\left\lvert\frac{1+\Delta}{2}\beta_-\right\rvert^{\frac{1}{2}},\, \pm\left\lvert\frac{1+\Delta}{2}\beta_-\right\rvert^{\frac{1}{2}},\, \left\lvert\frac{1-\Delta}{2}\beta_-\right\rvert^{\frac{1}{2}}\right)$	Attractive	dS-K
	$\tilde{p}_2^{\pm}$	$\frac{1}{2} - \frac{\sqrt{9+2\xi}}{6} < \alpha_\chi < 0$	$\left(\pm\frac{2}{\pi}\arctan\left\lvert\frac{1-\Delta}{2}\beta_-\right\rvert^{\frac{1}{2}},\, \pm\left\lvert\frac{1-\Delta}{2}\beta_-\right\rvert^{\frac{1}{2}},\, \left\lvert\frac{1+\Delta}{2}\beta_-\right\rvert^{\frac{1}{2}}\right)$	Unstable	dS-P
	$\tilde{p}_\Delta^{\pm}$	$\alpha_\chi = \frac{1}{2} - \frac{\sqrt{9+2\xi}}{6}$	$\left(\pm\frac{2}{\pi}\arctan\left\lvert\frac{\beta_-}{2}\right\rvert^{\frac{1}{2}},\, \pm\left\lvert\frac{\beta_-}{2}\right\rvert^{\frac{1}{2}},\, \left\lvert\frac{\beta_-}{2}\right\rvert^{\frac{1}{2}}\right)$	Saddle	dS-3F
	$\pi_0^{\pm}$		$(\pm 1,\, 0,\, 0)$	Repulsive	DM
	$\pi_{+1}^{\pm}$		$\left(\pm 1,\, +\lvert 1+\alpha_\chi\rvert^{\frac{1}{2}},\, 0\right)$	Saddle	K
	$\pi_{-1}^{\pm}$		$\left(\pm 1,\, -\lvert 1+\alpha_\chi\rvert^{\frac{1}{2}},\, 0\right)$	Saddle	K
V	$\hat{p}_0$		$(0,\, 0,\, 0)$	Saddle	DM
	$\hat{p}_1^{\pm}$	$\alpha_{\chi\chi} < 0$	$\left(\pm\frac{2}{\pi}\arctan\lvert 1-\alpha_{\chi\chi}\rvert^{-\frac{1}{2}},\, \pm\lvert 1-\alpha_{\chi\chi}\rvert^{-\frac{1}{2}},\, 0\right)$	Saddle	dS-K
	$\tilde{p}_1^{\pm}$	$-\frac{\xi}{18} < \alpha_{\chi\chi} < 0$	$\left(\pm\frac{2}{\pi}\arctan\left\lvert\frac{1+\Delta}{2}\beta_-\right\rvert^{\frac{1}{2}},\, \pm\left\lvert\frac{1+\Delta}{2}\beta_-\right\rvert^{\frac{1}{2}},\, \left\lvert\frac{1-\Delta}{2}\beta_-\right\rvert^{\frac{1}{2}}\right)$	Attractive	dS-K
	$\tilde{p}_2^{\pm}$	$-\frac{\xi}{18} < \alpha_{\chi\chi} < 0$	$\left(\pm\frac{2}{\pi}\arctan\left\lvert\frac{1-\Delta}{2}\beta_-\right\rvert^{\frac{1}{2}},\, \pm\left\lvert\frac{1-\Delta}{2}\beta_-\right\rvert^{\frac{1}{2}},\, \left\lvert\frac{1+\Delta}{2}\beta_-\right\rvert^{\frac{1}{2}}\right)$	Unstable	dS-P
	$\tilde{p}_\Delta^{\pm}$	$\alpha_{\chi\chi} = -\frac{\xi}{18}$	$\left(\pm\frac{2}{\pi}\arctan\left\lvert\frac{\beta_-}{2}\right\rvert^{\frac{1}{2}},\, \pm\left\lvert\frac{\beta_-}{2}\right\rvert^{\frac{1}{2}},\, \left\lvert\frac{\beta_-}{2}\right\rvert^{\frac{1}{2}}\right)$	Saddle	dS-3F
	$\pi_0^{\pm}$		$(\pm 1,\, 0,\, 0)$	Repulsive	DM
	$\pi_{+1}^{\pm}$		$\left(\pm 1,\, +\lvert 1-\alpha_{\chi\chi}\rvert^{-\frac{1}{2}},\, 0\right)$	Saddle	K
	$\pi_{-1}^{\pm}$		$\left(\pm 1,\, -\lvert 1-\alpha_{\chi\chi}\rvert^{-\frac{1}{2}},\, 0\right)$	Saddle	K

Table 4.2.: The fixed points found for a universe filled by DM and by DE modelled by a 3-form DE with a Gaussian potential in the case of no interaction and for the interactions IV and V in Sect 4.3.2. For each point, we present the constraints associated for their existence, their coordinates in $\{u,\, y,\, z\}$ space, their stability and the type of evolution they represent: DM – DM dominance; LSBR – a LSBR event; dS – de Sitter expansion; K – 3-form kinetic dominance; dS-P – de Sitter scaling solution dominated by the potential energy of the 3-form; dS-K – de Sitter scaling solution dominated by the kinetic energy of the 3-form; dS-3F – de Sitter scaling solution dominated by the 3-form. The values of β_- and Δ in the case of the interactions IV and V are given by the formulas (4.106) and (4.109). We include once more the case of no interaction so as to facilitate the comparison of the position of the fixed points when the interactions are turned on.

Next, we present the results for five specific sub-classes of the quadratic interaction (4.81) that were studied in Ref. [265]:

I) $Q = 3H\alpha_{\rm m}\rho_{\rm m}$ – In the context of 3-forms this interaction has been studied before in Refs. [65, 274]. Comparison with Eq. (4.88) immediately shows that this type of interaction corresponds to setting $\alpha_0 = \alpha_{\rm m}$, $\alpha_1 = -\alpha_{\rm m}$, and $\alpha_2 = 0$. Since in this case Q is proportional to the energy density of DM the fixed points corresponding to LSBR are not removed. In fact, this interaction affects only the fixed points $\hat{p}_0^{\pm}$, $\hat{\pi}_{-0}^{\pm}$ and $\hat{\pi}_{+0}^{\pm}$ which now correspond to scaling solutions with DM dominance.

II) $Q = 3H\alpha_{\rm mm}\rho_{\rm m}^2/(\rho_{\rm m}+\rho_\chi)$ – This interaction, which is quadratic in the dynamical variables y and z can be obtained by setting $\alpha_0 = \alpha_{\rm mm}$, $\alpha_1 = -2\alpha_{\rm mm}$, and $\alpha_2 = \alpha_{\rm mm}$. As in the case of the previous linear interaction, the only affected fixed points are $\hat{p}_0^{\pm}$, $\hat{\pi}_{-0}^{\pm}$ and $\hat{\pi}_{+0}^{\pm}$ which correspond to scaling solutions with DM dominance.

III) $Q = 3H\alpha_{{\rm m}\chi}\rho_{\rm m}\rho_\chi/(\rho_{\rm m}+\rho_\chi)$ – In the context of wCDM, this type of *mixed* interaction has been studied as a possible solution to the coincidence problem [38, 78]. We can map it to the formulation in (4.88) by setting $\alpha_0 = 0$, $\alpha_1 = \alpha_{m\chi}$, and $\alpha_2 = -\alpha_{m\chi}$. As in the previous two cases, the interaction coefficients do not satisfy the condition (4.95) and, therefore, the fixed points corresponding to LSBR are not removed. In addition, in this case the fixed points associated to matter dominance are not affected due to the presence of the interaction.

IV) $Q = 3H\alpha_\chi\rho_\chi$ – This linear interaction proportional to the energy density of DE is also commonly considered in the literature in the context of wCDm models [64, 99]. A comparison with Eq. (4.88) immediately leads to the equalities $\alpha_0 = 0$, $\alpha_1 = \alpha_\chi$, and $\alpha_2 = 0$. Contrary to the three previous interactions, in this case the inequality (4.95) is satisfied, meaning that the fixed points $p_1^{\pm}$ are shifted in the phase space and the final stage of the evolution of the Universe is no longer a LSBR. On the other hand, the position the fixed points associated to DM dominance are not affected.

V) $Q = 3H\alpha_{\chi\chi}\rho_\chi^2/(\rho_{\rm m}+\rho_\chi)$ – This interaction, quadratic in the dynamical variables, can be mapped to the formulation (4.88) by setting $\alpha_0 = 0$, $\alpha_1 = 0$, and $\alpha_2 = \alpha_{\chi\chi}$. Similarly to the case IV, the fixed points associated to DE dominance are shifted from their original position, thus removing the LSBR, while the fixed points associated to DM are left unaffected.

In Tabs. 4.1 and 4.2 we present the general characteristics of the fixed points for each interaction and compare them with the non-interacting case. For each fixed point we present the constraints found for its existence, the position on the $\{u,\, y,\, z,\}$ space, the result of the stability analysis using the methods delineated above[11] and an identifier to which kind of behaviour it represents. For the interactions I, II and III we did not analyse the stability of the fixed point p_2 due to the presence of divergent terms in the interaction term in Eq. (4.85). Of all the cases studied, only the interactions IV and V are able to remove the LSBR event in the future, replacing it by attractive de Sitter points $\tilde{p}_1^{\pm}$ representing a scaling solution with almost complete DE dominance:

$$\Omega_{\rm DE}(x\to+\infty) \approx 1 - |\alpha_0+\alpha_1+\alpha_2|\,, \qquad \Omega_{\rm m}(x\to+\infty) \approx |\alpha_0+\alpha_1+\alpha_2|\,. \tag{4.120}$$

[11] A detailed calculation of the stability of each fixed point can be found in Ref. [265].

4.3.3. Composite Null Diagnosis

In the previous section we have applied a dynamical systems analysis to determine which subclasses of the general quadratic interaction could remove the LSBR event from the future history of the Universe in a model of interacting DM and 3-form DE. Out of five specific examples commonly found in the literature, we found that two of them, $Q_{\rm IV} = 3H\alpha_\chi\rho_\chi$ and $Q_{\rm V} = 3H\alpha_{\chi\chi}\rho_\chi^2/(\rho_{\rm m}+\rho_\chi)$, are able to replace the LSBR by a de Sitter solution corresponding to a scaling solution with near total DE dominance. We now explore the possibility of distinguishing these two cases between themselves and from the non-interacting case using a cosmographic approach based on the statefinder hierarchy and the fractional growth rate, which together form a composite null diagnosis for ΛCDM [34].

From the EoS (4.67) we can obtain the cosmographic parameters q, j, s and l, cf. Eq. (2.8), as the Universe heads towards a LSBR event:

$$q \approx -1 - \frac{1}{3\log(a)} + \mathcal{O}\left[\frac{1}{\log(a)}\right]^2, \tag{4.121}$$

$$j \approx 1 + \frac{1}{\log(a)} + \mathcal{O}\left[\frac{1}{\log(a)}\right]^2, \tag{4.122}$$

$$s \approx 1 + \frac{2}{\log(a)} + \mathcal{O}\left[\frac{1}{\log(a)}\right]^2, \tag{4.123}$$

$$l \approx 1 + \frac{10}{3\log(a)} + \mathcal{O}\left[\frac{1}{\log(a)}\right]^2. \tag{4.124}$$

Replacing these expressions in the Statefinder hierarchy (2.23)–(2.25) we obtain[12]

$$S_3^{(1)} \approx 1 + \frac{1}{\log(a)} + \mathcal{O}\left[\frac{1}{\log(a)}\right]^2, \qquad S_3^{(2)} \approx -\frac{2}{9\log(a)} + \mathcal{O}\left[\frac{1}{\log(a)}\right]^2, \tag{4.125}$$

$$S_4^{(1)} \approx 1 + \frac{1}{\log(a)} + \mathcal{O}\left[\frac{1}{\log(a)}\right]^2, \qquad S_4^{(2)} \approx -\frac{2}{9\log(a)} + \mathcal{O}\left[\frac{1}{\log(a)}\right]^2, \tag{4.126}$$

$$S_5^{(1)} \approx 1 + \frac{4}{\log(a)} + \mathcal{O}\left[\frac{1}{\log(a)}\right]^2, \qquad S_5^{(2)} \approx -\frac{8}{9\log(a)} + \mathcal{O}\left[\frac{1}{\log(a)}\right]^2, \tag{4.127}$$

We thus find that although the limiting values of the Statefinders are the same as for[13] ΛCDM, before the Universe reaches its end state there is a deviation from the point $\{S_1^{(n)}, S_2^{(n)}\} = \{1, 0\}$ that characterises that model. Interestingly, this deviation does not depend on the parameter A in the EoS (4.67).

In the rest of this section, we will apply the statefinder hierarchy to our model of interacting DM and 3-form DE. In order to obtain the expressions for the statefinders $S_1^{(n)}$, $n = 3, 4, 5$, in terms of

[12] In Ref. [34], the definition of the statefinders $S_2^{(4)}$ and $S_2^{(5)}$ depends on an arbitrary constant α. Here we have chosen $\alpha = 3$.

[13] In this, the LSBR differs from other cosmic events like the Big Rip, whose end-point in the Statefinder diagrams deviates slightly from ΛCDM [24].

the dynamical system variables we write the deceleration parameter as

$$q(u,\,y,\,z)=\frac{1+3w_{\rm tot}}{2}=-1+\frac{3}{2}\left(1-y^2-z^2\right)-\frac{\xi}{3}\tan^2\left(\frac{\pi}{2}u\right)z^2\,, \tag{4.128}$$

where $w_{\rm tot}$ was obtained in Eq. (4.90). The higher order cosmographic parameters and the corresponding statefinders $S_n^{(1)}$, $n=3,4,5$ can be obtained by using the relation

$$\frac{\mathrm{d}}{\mathrm{d}\,x}\left(\frac{1}{a}\frac{\mathrm{d}^n}{\mathrm{d}\,t^n}H^{-n}\right)=\left(\frac{1}{a}\frac{\mathrm{d}^{n+1}}{\mathrm{d}\,t^{n+1}}H^{-n+1}\right)-\left(\frac{1}{a}\frac{\mathrm{d}^n}{\mathrm{d}\,t^n}H^{-n}\right)\left[1-n\,(1+q)\right]\,. \tag{4.129}$$

The first of the statefinder parameters reads [265]

$$\begin{aligned}S_3^{(1)}=1+\xi z^2\left\{\tan\left(\frac{\pi}{2}u\right)y\left[2-\frac{2\xi}{9}\tan^2\left(\frac{\pi}{2}u\right)\right]-\tan^2\left(\frac{\pi}{2}u\right)\left[1-\frac{2\xi}{9}\tan^2\left(\frac{\pi}{2}u\right)\right]\right\}\\+\frac{9}{2}\left[\alpha_0+\alpha_1\left(y^2+z^2\right)+\alpha_2\left(y^2+z^2\right)^2\right]\,,\end{aligned} \tag{4.130}$$

while the expressions for $S_4^{(1)}$ and $S_5^{(1)}$ are too cumbersome to be presented here.

The non-interacting case

We begin our analysis by finding the solution for the non-interacting model with DM and 3-form DE with a Gaussian potential that best mimics the behaviour of ΛCDM model until the present time. If we take as reference values for the present day values of the relative energy density of DM, $\Omega_{\rm DM,0}$, and of the parameter of EoS of the 3-form field, $w_{\chi,0}$, the following two best-fit values of the Planck 2015 mission [11, 16] for a DE model with constant parameter of EoS, w:

$$\Omega_{\rm m}=0.3065\,,\qquad\qquad w_{\rm d}=-1.006\,, \tag{4.131}$$

then we can write the following present day conditions

$$\Omega_{\rm m,0}=1-y_0^2-z_0^2=0.3065\,,\qquad w_{\chi,0}=-1-\frac{2}{9}\xi\frac{z_0^2}{y_0^2+z_0^2}\tan^2\left(\frac{\pi}{2}u_0\right)=-1.006\,. \tag{4.132}$$

In addition, we can fix the current value of the deceleration parameter as

$$q_0=-0.5340\,. \tag{4.133}$$

Notice that this value deviates by only 1.2% from the value of q_0 found for ΛCDM model. We stress that the values in Eq. (4.131) were obtained by fitting the wCDM model to the observational data and therefore do not correspond to the best-fit values of the model analysed here, there DE is modelled by a 3-form. Nevertheless, we take them as a guiding line to analyse our model.

If we fix the value of the potential parameter[14] ξ, Eqs. (4.132) provide us with two out of three

[14] In the rest of this section we will present the results obtained for $\xi=1$. This value respects the condition $0<\xi<9/2$ that ensures that the squared speed of sound of the 3-form is positive in the interval $[-\chi_{\rm c},\,\chi_{\rm c}]$, cf. Eq. (4.79), and at the same time it is large enough so as to not make the potential too flat around the origin. Recall that for a constant potential the 3-form behaves exactly as a cosmological constant.

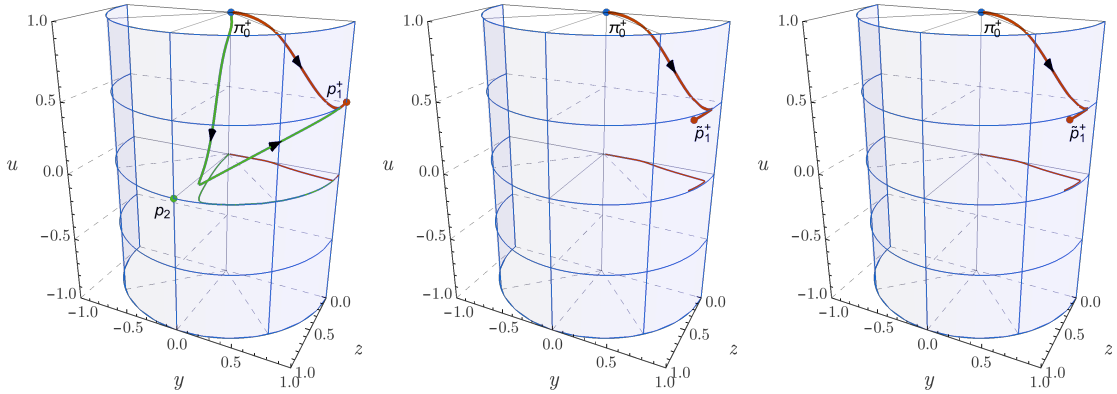

Figure 4.4.: (Left panel) Trajectories, in the 3-dimensional space $(u,\, y,\, z)$, of the two solutions $\mathcal{P}_z^I$ (red thick line) and $\mathcal{P}_z^{II}$ (green thick line) that were found to minimise the deviation from ΛCDM in the case of no interaction. (Middle panel) Trajectory obtained when interaction IV is considered with $\alpha_\chi = -0.03$. (Right panel) Trajectory obtained when interaction V is considered with $\alpha_{\chi\chi} = -0.03$. On both the middle and right panels, the initial conditions are set in the past, at redshift 6, using the values of the dynamical variables for the trajectory $\mathcal{P}_z^I$. The thin lines indicate the projection, on the plane yOz, of the trajectory of the same colour. The labelled points indicate the fixed points, see Table 4.2 for the classification, near which the trajectories pass.

necessary initial conditions for the dynamical variables $\{u,\, y,\, z\}$. In order to obtain a third condition, in Ref. [265] we opted to minimise the quantity

$$\mathrm{d}S_n^{(1)} := \left[\sum_{n=3}^{5}\left(S_n^{(1)} - 1\right)^2\right]^{1/2}, \tag{4.134}$$

with respect to the fraction of the energy density of the 3-form that, at the present time, corresponds to the potential energy:

$$\mathcal{P}_z := \frac{z_0^2}{y_0^2 + z_0^2}\,. \tag{4.135}$$

By construction, $\mathrm{d}S_n^{(1)}$ vanishes in the case of the ΛCDM model. As an indication of the sensitivity of the statefinder parameters with respect to small perturbations of the initial conditions, we also expand each parameter f around the solution $(u_0,\, y_0,\, z_0)$ as

$$\begin{aligned} f(u_0 + \delta u,\, y_0 + \delta y,\, z_0 + \delta_z) &\approx f(u_0,\, y_0,\, z_0) + \sum_{X=u,y,z} \left(\partial_X f\right)_{(u_0,\, y_0,\, z_0)}\, \delta X \\ &= f(u_0,\, y_0,\, z_0)\left[1 + \sum_{X=u,y,z}\left(\frac{\delta \log f}{\delta \log X}\right)_{(u_0,\, y_0,\, z_0)} \frac{\delta X}{X_0}\right]. \end{aligned} \tag{4.136}$$

The higher the absolute value of $(\delta \log f/\delta \log X)_{(u_0,\, y_0,\, z_0)}$ the more susceptible the parameter is to variations of the initial conditions. Thus, a trajectory with somewhat robust values of the statefinder parameters should present small values of these coefficients.

#	$\mathcal{P}_z^{\#}$	X	$S_3^{(1)}$	$\frac{\delta \log S_3^{(1)}}{\delta \log X}$	$S_4^{(1)}$	$\frac{\delta \log S_4^{(1)}}{\delta \log X}$	$S_5^{(1)}$	$\frac{\delta \log S_5^{(1)}}{\delta \log X}$
I	0.02051	$u_0 = 0.5436$	1.009	-7.554×10^{-4}	1.019	2.522×10^{-2}	1.014	1.182×10^{-1}
		$y_0 = 0.8242$		2.275×10^{-2}		-1.786×10^{-2}		1.972×10^{-1}
		$z_0 = 0.1193$		1.926×10^{-2}		3.621×10^{-2}		3.095×10^{-2}
II	0.9721	$u_0 = 0.1052$	1.013	-6.063×10^{-3}	1.032	6.291×10^{-2}	0.9991	-4.478×10^{-1}
		$y_0 = 0.1394$		3.076×10^{-2}		-4.786×10^{-4}		4.454×10^{-1}
		$z_0 = 0.8158$		2.477×10^{-2}		4.235×10^{-2}		1.737×10^{-1}

Table 4.3.: For the two solutions $\mathcal{P}_z^I$ and $\mathcal{P}_z^{II}$, we present the current values of the dynamical variables and the statefinder parameters using as reference the best-fit values of the Planck mission presented in Eq. (4.131) [11, 16]. For each statefinder parameter, we present the deviation of the present day values for small perturbations of the values of the dynamical variables. This values were obtained for $\xi = 1$.

In Tab. 4.3 we present the two sets of initial conditions which minimise $\mathrm{d}S_n^{(1)}$ with respect to $\mathcal{P}_z$:

$$\mathcal{P}_z^I \simeq 0.02051\,, \qquad \mathrm{d}S_n^{(1)} = 0.02526\,, \tag{4.137}$$

$$\mathcal{P}_z^{II} \simeq 0.9721\,, \qquad \mathrm{d}S_n^{(1)} = 0.03455\,, \tag{4.138}$$

the corresponding values of the statefinders parameters and the sensitivity coefficients $\delta S_n^{(1)}/\delta X$. On the left panel of Fig. 4.4 we also present the trajectories in the 3-dimensional space $\{u,\, y,\, z\}$ obtained from these initial conditions. Notice that situation I corresponds to a kinetic dominance of the energy density of the 3-form at the present time and therefore the trajectory in red starts near the fixed point π_0^+ and evolves towards the final LSBR state p_1^+ without approaching any other fixed point, while II corresponds to a dominance of the potential energy at the present time and so, even though the trajectory starts at π_0^+, if first passes near p_2 before finally heading towards p_1^+.

The values of $\delta \log S_n^{(1)}/\delta \log X$ presented in Tab. 4.3 indicate that the statefinder parameters are only slightly sensitive to changes of the initial conditions, from which we deduce that nearby trajectories are also compatible with the current observations, i.e., the trajectories chosen in this way are not special solutions of the system. Notice that due to the symmetry of the system with regards to $\{u,\, y,\, z\} \to \{-u,\, -y,\, z\}$, we only present the solutions with positive u_0. Despite obtaining small values in both cases I and II, the results for $\mathrm{d}S_n^{(1)}$ suggest that we should pick the trajectory I if we want a behaviour that is as close as possible to ΛCDM at the present time. This is corroborated if we look at the temporal evolution of the fractional energy densities and EoS parameters, represented in Figs. 4.5 and 4.6. This preference for the kinetic dominated solution from the cosmological evolution is in concordance with the fact that a massless 3-form behaves exactly like a cosmological constant [216].

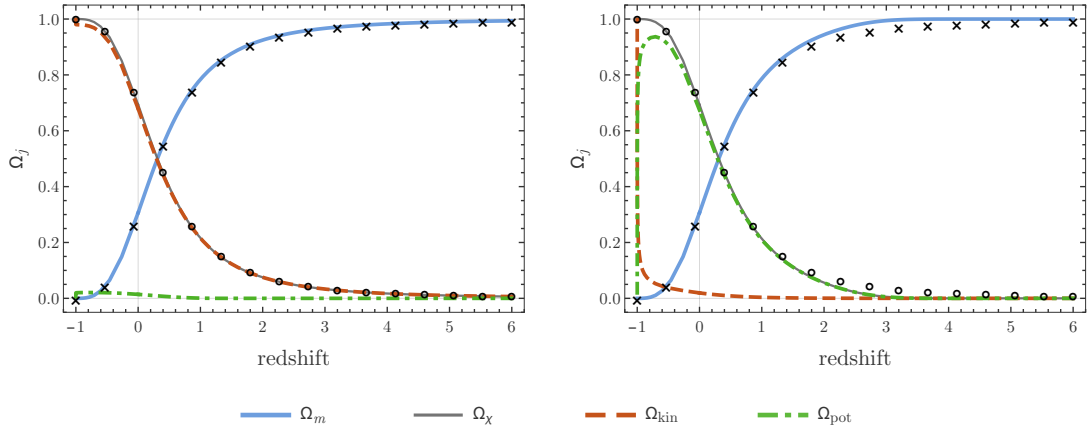

Figure 4.5.: The evolution of the relative energy densities of DM (blue thick curve) and DE (black thin curve), and of the individual components that contribute to the energy density of DE: kinetic energy (red dashed curve) and potential energy (green dot-dashed curve), in terms of the redshift. The circles and crosses indicate, respectively, the values of Ω_Λ and $\Omega_{\rm m}$ for the ΛCDM model. The left panel show the evolution in the case $\mathcal{P}_z^I$ and the right panel shows the evolution for the case $\mathcal{P}_z^{II}$.

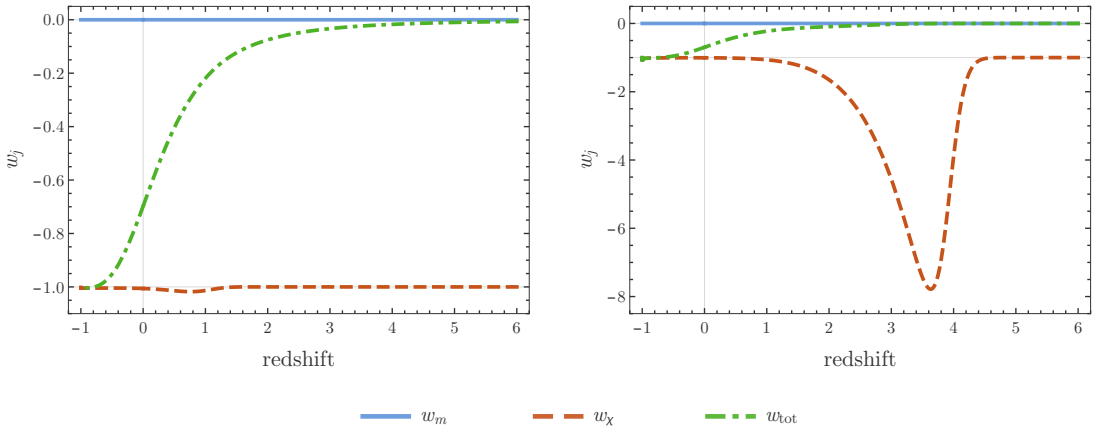

Figure 4.6.: The evolution of the parameter of EoS of DM (blue thick curve), of DE (red dashed curve), and of the total fluid (green dot-dashed curve) in terms of the redshift. The left panel show the evolution in the case $\mathcal{P}_z^I$ and the right panel shows the evolution for the case $\mathcal{P}_z^{II}$.

The cases of interactions IV and V

Having defined the background evolution in the case of no interaction between DM and the 3-form, we now look at what happens when we turn on the interaction. In particular, we will focus our analysis in the two cases studied in the previous section that remove the LSBR event: interactions IV and V. According to Table 4.2, both interactions IV and V introduce two late-time attractors, $\tilde{p}_1^{\pm}$, into the

Inter.	X	$S_3^{(1)}$	$S_4^{(1)}$	$S_5^{(1)}$	$\Omega_{\rm m}$	w_χ	$w_\chi^{\rm eff}$	$w_{\rm DM}^{\rm eff}$
IV	$u_0 = 0.5155$ $y_0 = 0.8223$ $z_0 = 0.1319$	0.9183	0.9752	0.6560	0.3065	-1.006	-0.9761	-0.06788
V	$u_0 = 0.5362$ $y_0 = 0.8238$ $z_0 = 0.1218$	0.9452	0.9297	0.8061	0.3065	-1.006	-0.9858	-0.04325

Table 4.4.: Present day values of the dynamical variables, the statefinder parameters, and the cosmological parameters $\Omega_{\rm m}$, w_χ, $w_\chi^{\rm eff}$, and $w_{\rm DM}^{\rm eff}$, obtained for the interactions IV and V. In each case, the present time is defined as the moment when the energy density of DM reaches the value 0.3065 [11, 16]. These results were obtained for $\alpha_\chi = \alpha_{\chi\chi} = -0.03$ and setting the initial conditions at redshift 6 using the values of the trajectory $\mathcal{P}_z^I$.

system as long as the interaction parameters of each interaction satisfy the inequalities

$$\frac{1-\sqrt{1+2\xi/9}}{2} < \alpha_\chi < 0\,, \qquad\qquad -\frac{\xi}{18} < \alpha_{\chi\chi} < 0\,. \tag{4.139}$$

For the reference value $\xi = 1$ that we have considered for the non-interacting model, these inequalities imply $-5.277\times10^{-2} < \alpha_\chi < 0$ and $-5.556\times10^{-2} < \alpha_\chi < 0$, values which respect our initial assumption of weak interactions, i.e., $|\alpha_i| \ll 1$. In addition, these late-time attractors correspond to scaling solutions with DE dominance where the Universe enters a de Sitter epoch at late-time. The fraction of the total energy density that corresponds to DE, β_-, is given for each case by

$$\beta_- = \frac{1}{1-\alpha_\chi} \approx 1+\alpha_\chi\,, \qquad\qquad \beta_- = \frac{1-\sqrt{1-4\alpha_{\chi\chi}}}{2\alpha_{\chi\chi}} \approx 1+\alpha_{\chi\chi}\,. \tag{4.140}$$

Since we wish to study the imprints of the interactions on the evolution of the system, we opt to select trajectories that follow the evolution of the non-interacting case in the past, where the 3-form is subdominant with regards to DM and therefore the effects of the selected interactions are weak. We impose initial conditions for $\{u,\, y,\, z\}$ using the values of the trajectory $\mathcal{P}_z^I$ taken at redshift 6 ($x_{\rm ini} = -\log 7 \simeq -1.946$), which was found to be the one with smallest deviation from ΛCDM at the present time. In order to facilitate the comparison of the results for the two interactions, we choose the same value for both couplings: $\alpha_\chi = \alpha_{\chi\chi} = -0.03$. This value is sufficiently large, in modulus, for the interactions to leave noticeable imprints on the cosmological evolution while at the same time not saturating the constraints (4.139). We also note that this value is compatible with the observational results obtained in Refs. [125, 154]. From Eq. (4.140) we find that this leads to the 3-form representing $\sim 97\%$ of the energy content of the Universe in the final de Sitter state:

$$(\text{Inter. IV}) \quad \beta_- = 0.9709\,, \qquad\qquad (\text{Inter. V}) \quad \beta_- = 0.9717\,. \tag{4.141}$$

The trajectories obtained are represented in the 3-dimensional space $\{u,\, y,\, z\}$ on the middle (interaction

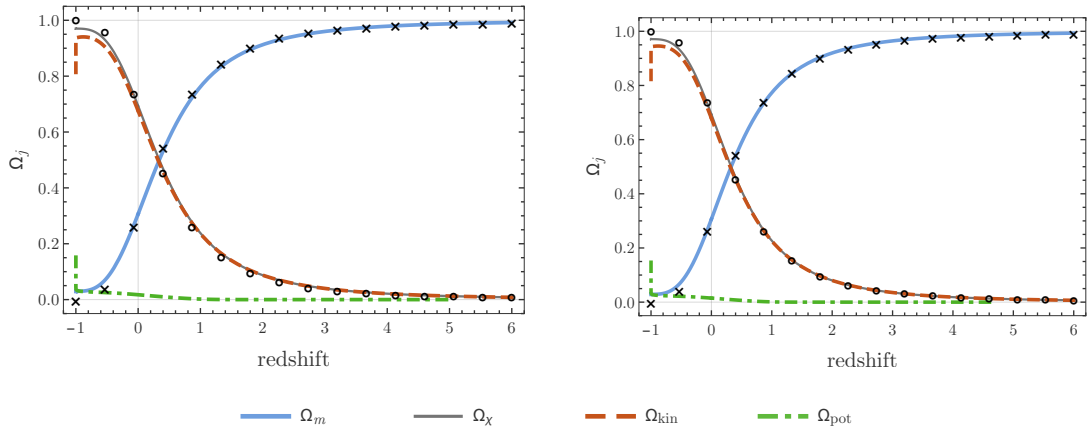

Figure 4.7.: The evolution of the relative energy densities of DM (blue solid curve) and DE (thin solid curve), and of the individual components that contribute to the energy density of DE: kinetic energy (red dashed curve) and potential energy (green dot-dashed curve), in terms of the redshift. (Left panel) Evolution of the system in the case of the interaction IV for $\alpha_\chi = -0.03$ and $\xi = 1$. (Right panel) Evolution for the case of the interaction V with $\alpha_{\chi\chi} = -0.03$ and $\xi = 1$. For each case the moment of redshift 0 is defined as the moment when $\Omega_{\rm m} = 0.3065$ [11, 16]. The circles and crosses indicate, respectively, the values of Ω_Λ and $\Omega_{\rm m}$ for the ΛCDM model.

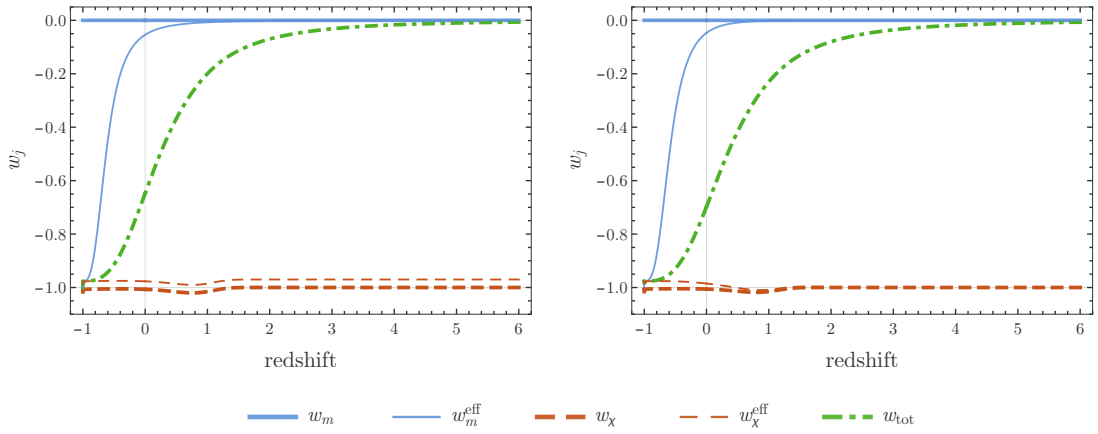

Figure 4.8.: The evolution of the parameter of EoS of DM (solid blue thick curve), of DE (dashed red thick curve), and of the total fluid in terms of the redshift (dot-dashed green thick curve). The effective EoS parameter of DM and DE are represented as a solid blue thin curve and a dashed red thin curve, respectively. (Left panel) Evolution in the case of the interaction IV for $\alpha_\chi = -0.03$ and $\xi = 1$. (Right panel) Evolution in the case of the interaction V with $\alpha_{\chi\chi} = -0.03$ and $\xi = 1$. In each case, the moment of redshift 0 is defined as the moment when $\Omega_{\rm m} = 0.3065$ [11, 16].

IV) and right (interaction V) panels of Fig. 4.4. Notice that each case follows closely the non-interacting curve of the trajectory $\mathcal{P}_z^I$ (left panel) till reaching the vicinity of the fixed point $\hat{p}_1^+$ which, due to the interaction between DM and DE, has been shifted away from the position $\{1/2,\, 1,\, 0\}$ that characterises the LSBR.

In Tab. 4.4, we present the values of the dynamical system variables, the statefinder parameters and several cosmological quantities evaluated at the present time, $x = 0$, defined in each case as the moment when $\Omega_{\rm m} = 0.3065$ [11, 16]. [15] Using the values of the statefinder parameters in Tab. 4.4 we can calculate the measure of deviation from ΛCDM, $\mathrm{d}S_n^{(1)}$, at the present time:

$$(\text{Inter. IV}) \quad \mathrm{d}S_n^{(1)} = 0.3544\,, \qquad\qquad (\text{Inter. V}) \quad \mathrm{d}S_n^{(1)} = 0.2134\,. \tag{4.142}$$

The smaller value for the interaction V can be explained by the fact that, for equal values of α_χ and $\alpha_{\chi\chi}$, the quadratic interaction takes a longer time to have strong effects on the evolution of the Universe. This can also be observed in Figs. 4.7 and 4.8, where we find that the quadratic interaction (right panels) follows ΛCDM more closely than the linear one.

The statefinder diagnosis

Up to this point, we have discussed how to select the trajectories in the 3-dimensional space $\{u,\, y,\, z\}$, see Fig. 4.4, in the non-interacting model and when interactions of type IV and V are considered. We now show how all these cases, despite their similar evolution, can be differentiated using the statefinder hierarchy diagnosis [34], even though the end point in the planes $\{S_3^{(1)},\, S_4^{(1)}\}$ and $\{S_3^{(1)},\, S_5^{(1)}\}$ are the same[16] for a LSBR event (no interaction) and for a de Sitter phase (interactions IV and V).

In Figs. 4.9, 4.10 and 4.11 we present the evolution, from redshift 6 and till the distant future, of the statefinder parameters $S_3^{(i)}$, $S_4^{(i)}$ and $S_5^{(i)}$, with $i = 1, 2$, for the three cases in study: no interaction (solid blue curve); interaction IV (dashed red curve); interaction V (dot-dashed green curve). We find that differences in the three cases start to become more noticeable in the recent past, for redshift $\lesssim 1$, in particular for the statefinders $S_3^{(1)}$, $S_4^{(1)}$ and $S_5^{(1)}$ (left panels). This is precisely the epoch when the interactions, whose strength depends on the relative energy density of DE, start to become important.

In general, we find that the case where the interaction IV is turned on presents the larger deviations from ΛCDM and from the non interacting case. This can be understood by the fact that, during the transition from the matter dominated epoch to the latter accelerated expansion fuelled by DE, the interaction term $Q_{\rm V}$ is suppressed by a factor $\Omega_\chi < 1$ with regards to $Q_{\rm IV}$.

One particular difference between the interacting and non-interacting models is that the statefinder parameters seem to approach the asymptotic value from opposite directions. For example, in the case of the statefinder $S_3^{(1)}$, the three models have the same asymptotic value $S_3^{(1)} = 1$. However, as can observed in Fig. 4.9, after some small oscillations around redshift 1 the solid blue curve (no interaction)

[15] Notice that since the transfer of energy from DE to DM (the coupling coefficients are negative) delays the decay of the energy density of DM, by fixing $x = 0$ in this way we are affecting the value of the redshift corresponding to the moment in the past where the initial conditions for the integration are set. In other words, in the cases where the interactions IV and V are turned on $x_{\rm ini} < -\log(7)$.

[16] In a LSBR cosmic event, where the Hubble rate diverges while its time derivatives remain constant, any contribution to the cosmographic parameters from terms $H^{-(n+1)}(\mathrm{d}^n H/\mathrm{d}t^n)$ vanishes asymptotically. As such, all the cosmographic parameters, and consequently all the statefinder parameters, converge to their respective values in the ΛCDM model, where $\mathrm{d}^n H/\mathrm{d}t^n$ is asymptotically zero in the future.

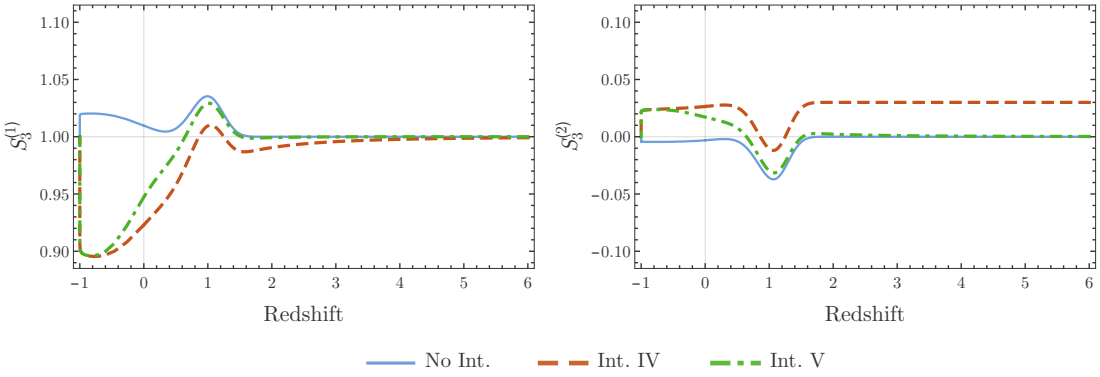

Figure 4.9.: The evolution of the statefinder parameters $S_3^{(1)}$ and $S_3^{(2)}$, in terms of the redshift for the cases of no interaction (solid blue curve), of the interaction IV (dashed red curve) and of the interaction V (green dot-dashed curve).

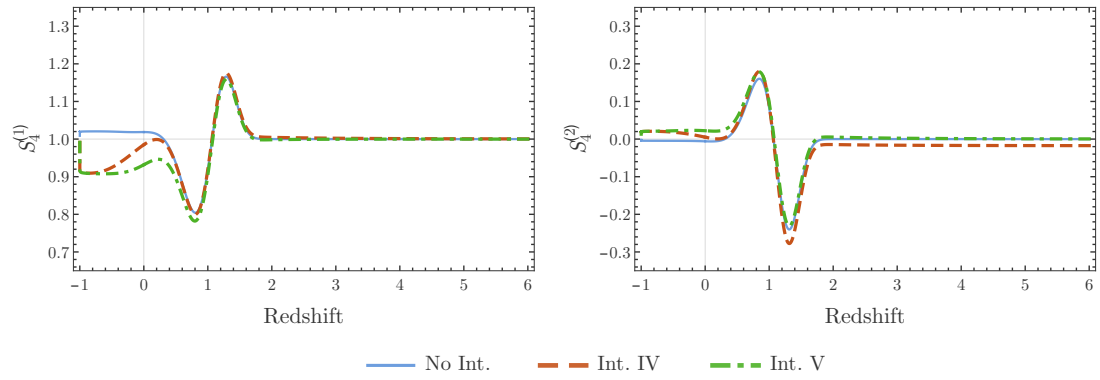

Figure 4.10.: The evolution of the statefinder parameters $S_4^{(1)}$ and $S_4^{(2)}$, in terms of the redshift for the cases of no interaction (solid blue curve), of the interaction IV (dashed red curve) and of the interaction V (green dot-dashed curve).

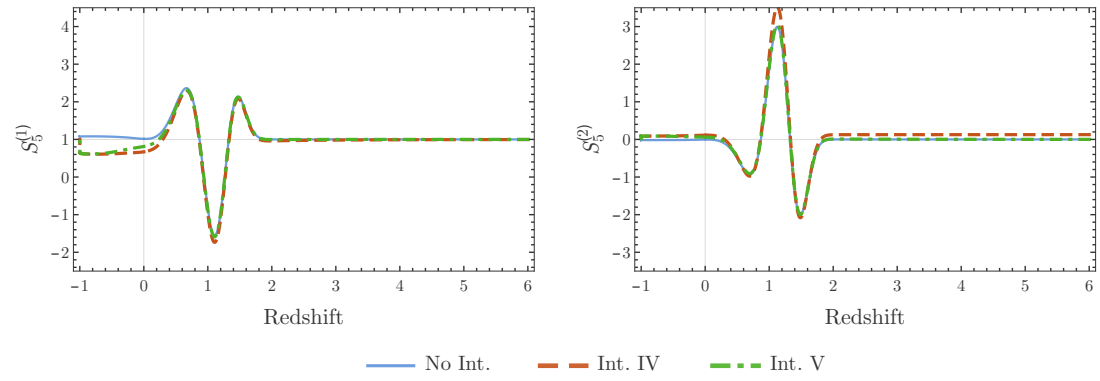

Figure 4.11.: The evolution of the statefinder parameters $S_5^{(1)}$ and $S_5^{(2)}$, in terms of the redshift for the cases of no interaction (solid blue curve), of the interaction IV (dashed red curve) and of the interaction V (green dot-dashed curve).

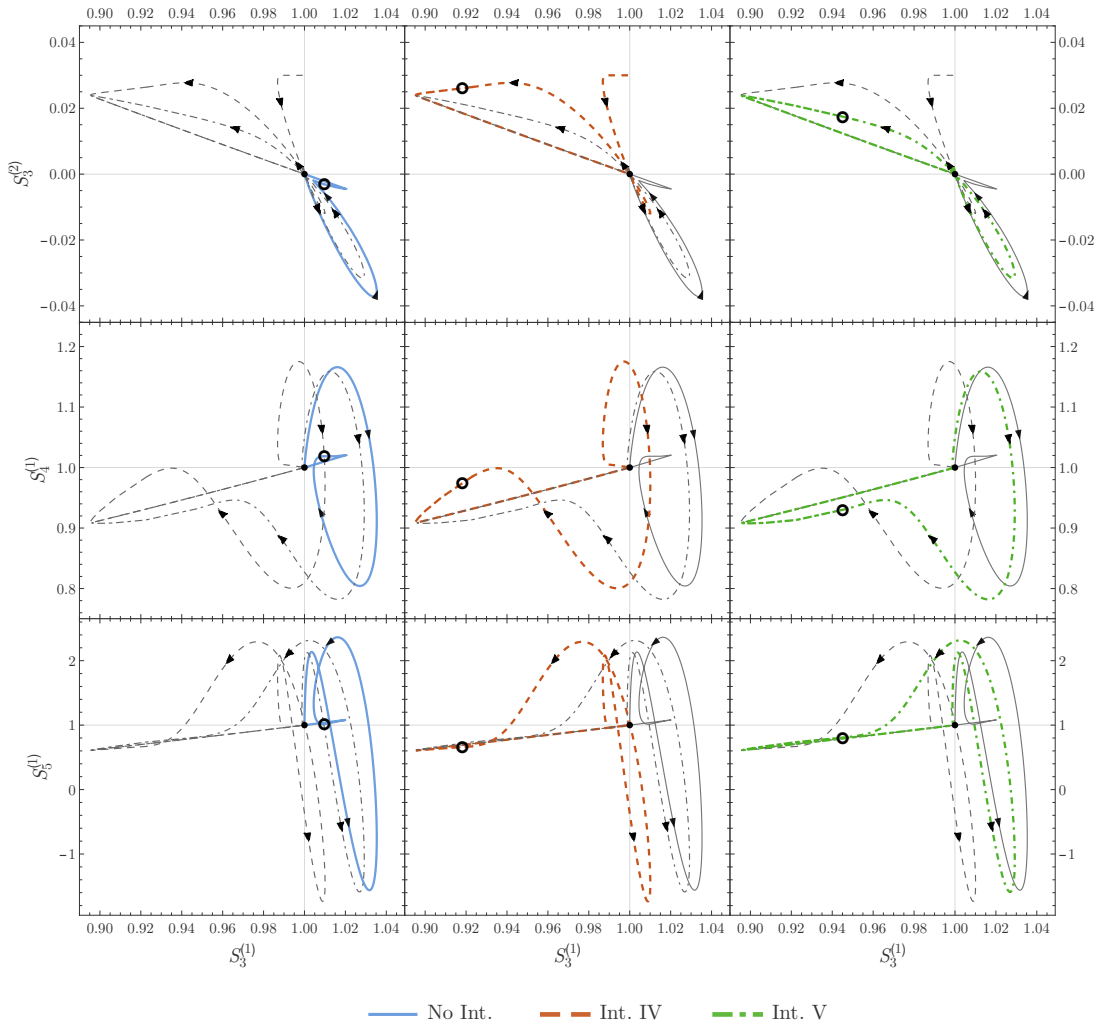

Figure 4.12.: The statefinder diagnosis $\{S_3^{(1)}, S_3^{(2)}\}$ (top panels), $\{S_3^{(1)}, S_4^{(1)}\}$ (middle panels) and $\{S_3^{(1)}, S_5^{(1)}\}$ (bottom panels) for the non-interacting 3-form DE model (solid blue curve), and when the interactions IV (dashed red curve) and V (dot-dashed green green) are turned on. The black points indicate the predictions for ΛCDM. Present day values are indicated by a circle and direction of temporal evolution is indicated by black arrows.

seems to stabilise at $S_3^{(1)} \sim 1.02$ without ever crossing the asymptotic value 1. In the two interacting models, a similar oscillatory behaviour can be found around redshift 1. Afterwards the value of $S_3^{(1)}$ starts to decay monotonically till it reaches a minimum value $S_3^{(1)} \sim 0.9$. At this point, and before the Universe approaches the final de Sitter phase, the energy budget is almost entirely dominated by DE, $\Omega_\chi \lesssim 1$, which means that $Q_{\rm IV} \approx Q_{\rm V}$. After this point, the two curves corresponding to the interacting models (red dashed and green dot-dashed) become indistinguishable. A similar pattern of behaviour is observed for all the statefinder parameters plotted in Figs. 4.9, 4.10 and 4.11.

Before the end of the DM dominated epoch, i.e., for redshift $\gtrsim 2$, the statefinders $S_3^{(2)}$, $S_4^{(2)}$ and

$S_5^{(2)}$ (right panels) single out the case of the linear interaction IV. This can be explained by the fact that, contrary to the interaction V which is quadratic in ρ_χ, the interaction IV has a non-negligible contribution to the effective EoS parameter of DE when the Universe is dominated by DM. Thus, in this case the 3-form does not mimic exactly a cosmological constant with $w_\chi^{\rm eff} \simeq -1$ in the past. This sensitivity of the statefinders $S_n^{(2)}$ to a change in the EoS parameter of DE had already been pointed out in Ref. [34] as one of the main advantages of introducing a second family of statefinder parameters which can break some of the degeneracies in the statefinders $S_n^{(1)}$.

The effects mentioned above can be observed in Fig. 4.12, where we present the statefinder diagnosis $\{S_3^{(1)}, S_3^{(2)}\}$ (top panels), $\{S_3^{(1)}, S_4^{(1)}\}$ (middle panels) and $\{S_3^{(1)}, S_5^{(1)}\}$ (bottom panels) of the non-interacting model (solid blue curves) and of the two models with the interaction IV (dashed red curves) and interaction V (dot-dashed green curves) turned on. In each map, a black point indicates the final asymptotic state, a circle indicates present day values and the arrows indicate the direction of temporal evolution. The imprints of the interaction IV during the DM dominated era are particularly visible on the planes $\{S_3^{(1)}, S_3^{(2)}\}$ and $\{S_3^{(1)}, S_4^{(1)}\}$, where the initial behaviour of the red dashed curve diverges from that of the other two curves.

The similar future asymptotic behaviour of the curves of the two interacting models is also captured in the statefinder diagnosis. On all panels, the red dashed and green dot-dashed curves overlap after the minimum value $S_3^{(1)} \sim 0.9$ is reached. Furthermore, the difference in behaviour between the non-interacting models and the two models where the interaction between DM and DE is turned on is clearly visible in the maps $\{S_3^{(1)}, S_4^{(1)}\}$ and $\{S_3^{(1)}, S_5^{(1)}\}$. In the non-interacting case, the curves approaches the final points $\{1, 1\}$ from the first quadrant, while in the two interacting cases the curves approach $\{1, 1\}$ from the third quadrant. This seems to reflect the fact that in the non-interacting case we have a late-time phantom like behaviour, while in the two cases where the interaction is turned on, the total EoS parameter never crosses the threshold $w_{\rm tot} = -1$ (see for example Fig. 1 of Ref. [24] for a comparison of the statefinder diagnosis in the cases of quintessence and phantom-like behaviours).

Finally, we note that while the statefinder diagnosis can positively distinguish the three models at hand, the pairs $\{S_3^{(1)}, S_4^{(1)}\}$ and $\{S_3^{(1)}, S_5^{(1)}\}$ seem to be particularly good identifiers of each individual model. As noted in Ref. [34], the fact that $S_4^{(1)}$ and $S_5^{(1)}$ include higher order derivatives of the Hubble rate makes these parameters more sensitive to small differences in the cosmological expansion. However, the increased difficulty in calculating with precision higher order derivatives of H from the current observational data presents a serious drawback in the use of these statefinder parameters, in particular $S_5^{(1)}$ [34].

The growth of perturbations

In order to complement the statefinder hierarchy with information from the growth of structure in our model and complete the composite null diagnosis (CND) [127], we need to compute the evolution of linear perturbations in the late Universe. Since we do not have a covariant formulation of the interactions between DM and the 3-form, we compute the evolution of DM perturbations assuming that perturbations of the 3-form remain small and can be ignored. This is somewhat justified by the fact that at late-time the 3-form with a Gaussian potential has an EoS parameter very close to -1 and positive c_s^2, which prevents the collapse of the DE perturbations.

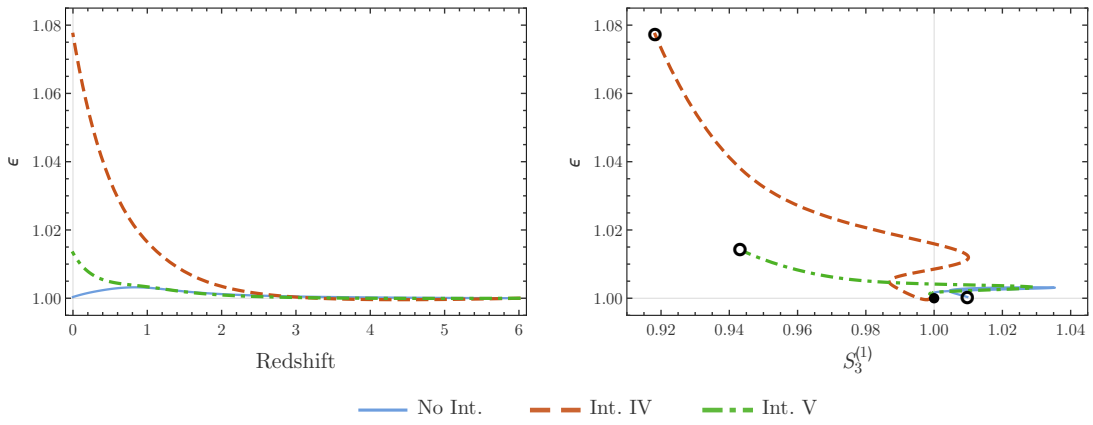

Figure 4.13.: (Left panel) Evolution of the fractional growth rate ϵ in the case of no interaction (solid blue curve) and when the interactions IV (dashed red curve) and V (dot-dashed green curve) are considered. (Right panel) The CND map $\{S_3^{(1)}, \epsilon\}$ for the same models. The point $\{1, 1\}$ indicates the prediction for the ΛCDM model and a circle indicates present day values.

During the late-time evolution of the Universe, under the assumption that we can disregard the DE perturbations, the evolution of the modes well inside the Hubble horizon ($k^2 \gg a^2H^2$) and within the linear regime is given by [127, 240] (cf. Eq. (2.31))

$$\ddot{\delta}_{\rm m} + 2H\dot{\delta}_{\rm m} - \frac{\kappa^2}{2}\rho_{\rm m}\delta_{\rm m} = 0\,. \tag{4.143}$$

This equation can be written in terms of the dynamical system variables $\{u,\, y,\, z\}$ as

$$(\delta_{\rm m})_{xx} + \frac{1}{2}\left[1 + 3\left(y^2 + z^2\right) + \frac{2}{3}\xi\, z^2 \tan^2\left(\frac{\pi}{2}u\right)\right](\delta_{\rm m})_x - \frac{3}{2}\left[1 - \left(y^2 + z^2\right)\right]\delta_{\rm m} = 0\,, \tag{4.144}$$

where we have also changed the time variable from the cosmic time t to $x = \log(a/a_0)$. For each of the trajectories defined in this section, we obtained the temporal evolution of the linear perturbation $\delta_{\rm m}$ by integrating Eq. (4.144) numerically since the matter-dominated era till the present time. The initial conditions were set at redshift 6, when all relevant modes are inside the Hubble horizon. Using the prediction of GR that $\delta_{\rm m} \propto a$ in a matter dominated universe, we fixed $(\delta_{\rm m})_x(x_{\rm ini}) = \delta_{\rm m}(x_{\rm ini}) = 1$, where $x_{\rm ini} = -\log(7) \simeq -1.946$. Notice that since the CND requires a comparison with the growth of structure in the ΛCDM model, we repeated the integration of Eq. (4.143) for that case as well.

Once the evolution of $\delta_{\rm m}$ was obtained, we computed the growth rate (cf. Eq. (2.34))

$$f(x) = \frac{\partial \log(\delta_{\rm m})}{\partial x}\,, \tag{4.145}$$

and subsequently the fractional growth rate [34]

$$\epsilon(x) := \frac{f(x)}{f_{\Lambda{\rm CDM}}(x)}\,. \tag{4.146}$$

The results obtained for the cosmological evolution of the fractional growth rate ϵ in the three models studied in this section are presented on the l.h.s. panel of Fig. (4.13). While the deviations of the growth rate from ΛCDM are less than 1% in the non-interacting case, when the interactions IV and V are turned on the growth rate becomes increasingly larger as the Universe evolves. This difference reflects the increasing strength of the interactions IV and V as DE becomes the dominant component in the Universe. Notice that the Interaction IV, being the one that is more intense for a given value of ρ_χ, presents a more distinct profile.

The CND mapping $\{S_3^{(1)}, \epsilon\}$ is presented on the r.h.s. panel of Fig. 4.13, where we recall that the ΛCDM model corresponds to the black point $\{1, 1\}$ and the present day values of each curve are indicated by a circle. The distinct curves obtained for each model show that the CND is a good tool to complement the statefinder hierarchy to differentiate between DE models. We note that, as found in Fig. 4.12, the curve corresponding to the model with the interaction IV has a distinct initial behaviour, reflecting the fact that in that case the 3-form does not behave like a cosmological constant in the past.

In order check if the results obtained are in accordance with current cosmological observations, we also compare the predicted values of the growth rate with the measurements of SDSS III BOSS DR12 [312]:

$$f(z_{\rm eff} = 0.38) = 0.638 \pm 0.080\,, \tag{4.147}$$

$$f(z_{\rm eff} = 0.51) = 0.715 \pm 0.090\,, \tag{4.148}$$

$$f(z_{\rm eff} = 0.61) = 0.753 \pm 0.088\,. \tag{4.149}$$

As can be seen from Fig. 4.13, for all the values of redshift considered, the deviation of ϵ from unity is below 5% for all the cases considered, which falls well inside the 1σ interval for all the observational points. This agreement suggests that our choice for the value of the interaction parameters α_χ and $\alpha_{\chi\chi}$, which was motivated from constraints derived for the wCDM model, is viable from an observational point of view. In addition, we present in Fig. 4.14 the evolution of $f\sigma_8$ for the three models considered, where σ_8 is the root mean square of mass fluctuations on spheres of radius 8 h^{-1}Mpc. The temporal evolution of σ_8 was obtained through the formula [356]

$$\sigma_8(x) = \sigma_8(0)\frac{\delta_{\rm m}(x)}{\delta_{\rm m}(0)}\,, \tag{4.150}$$

assuming the best-fit value of the Planck mission for the present day value $\sigma_8(0) = 0.8110$ [19]. For comparison, we also plot several available observational data points and their respective error bars, which we enumerate in Tab. 4.5. From Fig. 4.14 we find that all models are compatible with the data, even if the model with the linear interaction IV (red dashed curve) presents higher values at redshift $z \lesssim 0.5$, which seems to spoils the agreement with the measurements at $z \lesssim 0.1$. We point out that the results obtained for the ΛCDM model are indistinguishable from the blue curve of the non-interacting model in Fig. 4.14.

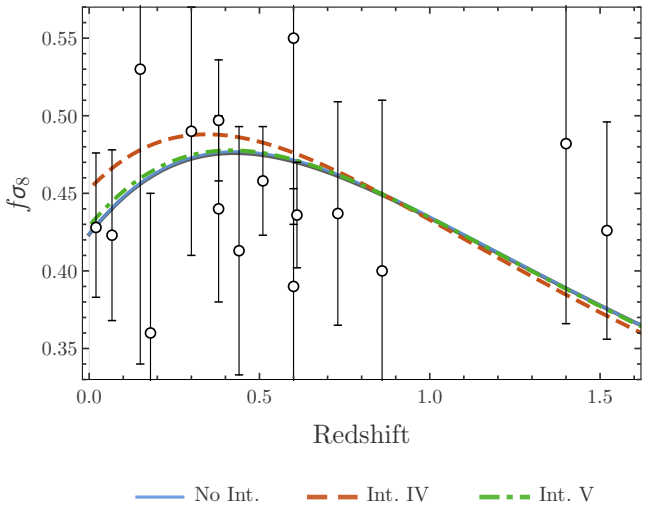

Figure 4.14.: Evolution of $f\sigma_8$ in the case of no interaction (solid blue curve) and when the interactions IV (dashed red curve) and V (dot-dashed green curve) are considered. The curve obtained for the ΛCDM is indistinguishable from the blue curve obtained for the non-interacting case. The various data points plotted, and respective error bars, are presented in Tab. 4.5.

z	$f\sigma_8$	Survey	Ref.
0.02	$0.428^{+0.048}_{-0.045}$	6dF Galaxy Survey + SNe Ia	[195]
0.067	$0.423^{+0.055}_{-0.055}$	6dF Galaxy Survey	[59]
0.15	$0.53^{+0.19}_{-0.19}$	SDSS MGS	[190]
0.18	$0.36^{+0.09}_{-0.09}$	GAMA	[62]
0.3	$0.49^{+0.08}_{-0.08}$	SDSS LRG	[280]
0.38	$0.44^{+0.06}_{-0.06}$	GAMA	[62]
0.38	$0.497^{+0.039}_{-0.039}$	BOSS DR12	[20]
0.44	$0.413^{+0.080}_{-0.080}$	WiggleZ	[61]
0.51	$0.458^{+0.035}_{-0.035}$	BOSS DR12	[20]
0.60	$0.390^{+0.063}_{-0.063}$	WiggleZ	[61]
0.60	$0.55^{+0.12}_{-0.12}$	VIPERS	[288]
0.61	$0.436^{+0.034}_{-0.034}$	BOSS DR12	[20]
0.73	$0.437^{+0.072}_{-0.072}$	WiggleZ	[61]
0.86	$0.40^{+0.11}_{-0.11}$	VIPERS	[288]
1.4	$0.482^{+0.116}_{-0.116}$	FastSound	[281]
1.52	$0.426^{+0.070}_{-0.070}$	BOSS DR14 quasars	[364]

Table 4.5.: Available observational data points for $f\sigma_8$ at different at redshift in the interval $(0, 1.52)$, which are plotted in Fig. 4.14. For each data point we present, in order, the value of the effective redshift, the value of $f\sigma_8$ and its respective error, the corresponding survey, and the reference from which the values were taken.

4.3.4. Discussion

In this Section, we have shown how a Little Sibling of the Big Rip (LSBR) cosmic event can appear in 3-form cosmology. While in this type of event the Universe can mimic a ΛCDM behaviour until the present time, which means that it is not ruled out by current cosmological observations, its future behaviour is radically different from the exponential expansion fuelled by a cosmological constant and can lead to the destruction of all structure we observe in the Universe [77]. While in models with scalar fields a LSBR event appears only when a kinetic term with reversed sign is considered [22], in 3-form cosmology such an event can appear in models where both the kinetic and potential energy are positive. Furthermore, the presence of other types of matter, e.g., dark matter, that respect the null energy condition does not change the end state of the Universe. As a practical case, we have selected the Gaussian potential for the 3-form field, which was found to be capable of driving the Universe towards a LSBR without leading to superluminal propagation or collapse of DE perturbations during the late-time evolution.

Once the desired potential of the 3-form field, compatible with a LSBR event, was fixed, we addressed the possibility that an interaction between DM and DE could remove this divergence of the Hubble rate from the future evolution of the Universe. Following a phenomenological approach, we considered a type of quadratic interaction, cf. Eq. (4.81), that generalises some of the cases found in the literature. Through an extensive dynamical analysis we were able to find which subclasses of interactions can remove the LSBR. We conclude that as long as the interaction term Q is not proportional to $\rho_{\rm m}$ or $\rho_{\rm m}^2$, an energy transfer from DE to DM can lead to an alternative final stage of the Universe represented by a de Sitter expansion. However, instead of a ΛCDM type of behaviour, a scaling behaviour between the two dark components of the Universe is obtained, where the energy density of the Universe is almost totally dominated by DE but where DM maintains a constant residual contribution.

After selecting two interactions of interest that remove the LSBR, one linear and one quadratic in the 3-form energy density ρ_χ, we employed the Statefinder hierarchy and the Composite Null Diagnostic (CND) to find distinguishable imprints of the model. In order to best compare the evolution in the non-interacting and interacting cases, we first selected the trajectory of the non-interacting mode that, at the present time, minimises the deviations from ΛCDM. Using this trajectory to set initial conditions in the past, we then obtained the trajectories for the other two models where the interaction is turned on. Then, by mapping the trajectories of the three models in the space of statefinders $\{S_3^{(1)}, S_3^{(2)}\}$, $\{S_3^{(1)}, S_4^{(1)}\}$, $\{S_3^{(1)}, S_5^{(1)}\}$ and $\{S_3^{(1)}, \epsilon\}$ we showed that both the Statefinder hierarchy and the CND can pinpoint relevant differences between the cases under scope. More importantly, we found sufficient evidences to discriminate, at present, between the linear and quadratic DE interaction. For all the models considered, the results for the growth rate of the matter perturbations are within the observational constraints of the SDSS III data [312] for the growth rate f and are compatible with available observational points for $f\sigma_8$, as shown in Fig. 4.14.

A limitation in the analysis is related to the fact that the evolution of matter fluctuations was computed assuming that perturbations of DE could be disregarded, i.e., the DM perturbations are only affected by the 3-form through background terms. While this assumption is somewhat justifiable by the shape of the 3-form potential and the fact that DE behaves almost as a cosmological constant until the present time, a full analysis would require taking into account the evolution of DE perturbations as well. However, in order to apply the full theory of linear perturbations, a covariant description of the

interaction would also be necessary, preferably deduced from a total action describing the 3-form and DM. Such an approach was undertaken in [218] for a specific type of coupling and could be generalised by using a Lagrangian description of perfect fluids [89] and considering the presence of coupling terms like, for example, $E^{\mu\nu\rho\sigma}A_{\mu\nu\rho}u_{\sigma}$. This type of approach has been explored recently in the literature in the context of quintessence [58, 66, 67, 153, 291] and has the advantage of eliminating any ambiguity in defining the interaction 4-vector Q_{μ} both at the background level and at first order in perturbations.

PART III

The Early Universe

5 Pre-inflation in the Third Quantisation: possible observational imprints

5.1. Third Quantisation - A Brief Review

5.1.1. Quantum Cosmology

The field of Quantum Cosmology began in 1967 with DeWitt's seminal paper [137] introducing his Canonical Theory of Quantum Gravity. In it, DeWitt took the quantisation procedure for constrained Hamiltonian systems developed by Dirac in the previous decade [138, 139] and applied it to the ADM action of General Relativity [39], obtaining in this way a master wave equation for gravitational systems – the Wheeler-DeWitt (WDW) equation [137, 359]. After discussing some of the general properties of this equation, including its similarities with the Klein-Gordon (KG) equation for a scalar field, DeWitt applied his newly introduced theory to the case of a closed FLRW universe. The Canonical Theory of Quantum Gravity, and in particular WDW equation, served as a pivotal point of several approaches to Quantum Gravity and Quantum Cosmology developed over the ensuing decades. In this section, we follow [211] and briefly review the derivation of the WDW equation for a FLRW universe filled by a minimally coupled scalar field φ with a potential $V(\varphi)$.

Let us consider the classical line element for a FLRW universe (cf. Eq. (1.18)):

$$\mathrm{d}s^2 = -N^2(t)\mathrm{d}t^2 + a^2(t)\left(\frac{\mathrm{d}r^2}{1-\mathcal{K}r^2} + r^2\mathrm{d}\Omega^2\right) . \tag{5.1}$$

We recall that N is the lapse function, the scale factor $a(t)$ has dimensions of length and $\mathcal{K}$ is $+1$ for a closed universe, 0 for a spatially flat universe and -1 for an open hyperbolic universe. Since the shift vector vanishes in a FLRW geometry, the second fundamental form and its trace reduce to [211]

$$K_{ij} = \frac{1}{N}\frac{\dot{a}}{a}h_{ij} , \qquad K = \frac{3}{N}\frac{\dot{a}}{a} , \tag{5.2}$$

while the spatial extrinsic curvature reads ${}^{(3)}R = 6\mathcal{K}/a^2$. Here and throughout this chapter, a dot indicates a derivative with respect to the time variable t. The total action of the model can be written as

$$\mathcal{S} = \mathcal{S}^{\mathrm{ADM}} + \mathcal{S}_\varphi , \tag{5.3}$$

where $\mathcal{S}^{\mathrm{ADM}}$ is the ADM action for GR with a cosmological constant Λ [39, 137]:

$$\mathcal{S}^{\mathrm{ADM}} = \frac{1}{2\kappa^2}\int \mathrm{d}t\,\mathrm{d}^3x N\sqrt{h}\left(K_{ij}K^{ij} - K^2 + {}^{(3)}R - 2\Lambda\right), \tag{5.4}$$

and $\mathcal{S}_\varphi$ is the action of a minimally coupled scalar field φ with a potential $V(\varphi)$:

$$\mathcal{S}^{\varphi} = -\int \mathrm{d}t\,\mathrm{d}^3x N\sqrt{h}\left(\frac{1}{2}g^{\mu\nu}\partial_\mu\varphi\,\partial_\nu\varphi + V\right). \tag{5.5}$$

Substitution of Eqs. (5.1) and (5.2) in Eqs. (5.4) and (5.5) then leads to [211]

$$\mathcal{S} = \int \mathrm{d}t\,\mathrm{d}^3x N\sqrt{h}\left\{-\frac{3}{\kappa^2}\left(\frac{1}{N}\frac{\dot{a}}{a}\right)^2 + \frac{3\mathcal{K}}{\kappa^2 a^2} - \frac{\Lambda}{\kappa^2} + \frac{1}{2}\left(\frac{\dot{\varphi}}{N}\right)^2 - V(\varphi)\right\}. \tag{5.6}$$

In order to obtain the Hamiltonian formulation of this model, we introduce the canonical variables of the minisuperspace $\{q^1, q^2\} = \{a, \varphi\}$, so that the action (5.6) can be written as

$$\mathcal{S} = \mathrm{Vol}\int \mathrm{d}t\, N\left(\frac{1}{2}G_{AB}\frac{\dot{q}^A\dot{q}^B}{N^2} - \mathcal{V}\left(q^A\right)\right). \tag{5.7}$$

Here, we have introduced the minisuperspace metric G_{AB}:

$$G_{AB} := \begin{pmatrix} -\frac{6}{\kappa^2}a & 0 \\ 0 & a^3 \end{pmatrix}, \tag{5.8}$$

the generalised potential $\mathcal{V}$:

$$\mathcal{V}\left(q^A\right) := \frac{3a^3}{\kappa^2}\left[\frac{\Lambda}{3} + \frac{\kappa^2 V(\varphi)}{3} - \frac{\mathcal{K}}{a^2}\right], \tag{5.9}$$

and the volume factor Vol:

$$\mathrm{Vol} := \int \mathrm{d}r\,\mathrm{d}\Omega\frac{\sqrt{h}}{a^3} = 4\pi\int \mathrm{d}r\frac{r^2}{\sqrt{1-\mathcal{K}r^2}}, \tag{5.10}$$

In the case of a closed spatial geometry ($\mathcal{K} = +1$), Vol corresponds to the volume of a 3-sphere of unit radius: $2\pi^2$, where a factor 2 needs to be included so as to account for the two halves of the 3-sphere. In the cases of a flat or open spatial geometries ($\mathcal{K} = 0$ and $\mathcal{K} = -1$, respectively), where the spatial hypersurfaces have infinite volume, the integral (5.10) has to be considered over a finite region of space.

Writing the action (5.7) as $\mathcal{S} = \int \mathrm{d}t L$, where L is the total Lagrangian, we can define the canonical momenta π_a and π_φ as [211]

$$\pi_a := \frac{\partial L}{\partial \dot{a}} = -\frac{6\mathrm{Vol}}{\kappa^2}\frac{a\dot{a}}{N}, \qquad \pi_\varphi := \frac{\partial L}{\partial \dot{\varphi}} = \mathrm{Vol}\,a^3\frac{\dot{\varphi}}{N}. \tag{5.11}$$

Likewise, we can define the canonical momentum of the lapse function, π_N, as

$$\pi_N := \frac{\partial L}{\partial \dot{N}} = 0\,. \tag{5.12}$$

The independence of the action on the derivative of N is reflected on last equality of Eq. (5.12), which is known as one of the primary constraints[1]. From the definitions (5.11) and (5.12) we can construct the canonical Hamiltonian as [211]

$$\begin{aligned} H &= \pi_N \dot{N} + \pi_A \dot{q}^A - L \\ &= N\left(\frac{1}{2}\frac{1}{\mathrm{Vol}} G^{AB}\pi_A\pi_B + \mathrm{Vol}\,\mathcal{V}(\alpha,\,\varphi)\right) \\ &= N\mathrm{H}\,. \end{aligned} \tag{5.13}$$

From the preservation of the primary constraint, we obtain the secondary (Hamiltonian) constraint which can be written in terms of the Poisson bracket of π_N and H as

$$\{\pi_N,\,H\} = -\mathrm{H} = 0\,. \tag{5.14}$$

At the classical level, this equation leads to the Friedmann equation (with $N = 1$)

$$3\left(\frac{\dot{a}}{a}\right)^2 = \kappa^2\left(\frac{1}{2}\dot{\varphi}^2 - \frac{3\mathcal{K}}{\kappa^2 a^2} + \frac{\Lambda}{\kappa^2} + V(\varphi)\right)\,. \tag{5.15}$$

The quantisation procedure that leads to the Wheeler-DeWitt equation follows from introducing a wave function $\Psi[a,\,\varphi]$ that describes the state of the universe and from imposing that the Hamiltonian constraint (5.14) becomes a condition on Ψ, i.e., $\hat{\mathrm{H}}\Psi = 0$ [137, 211]. The variables a and φ are promoted to quantum field operators $\hat{a}$ and $\hat{\varphi}$ that act on Ψ and their canonical momenta π_a and π_φ now become

$$\pi_a \to \hat{\pi}_a := -\mathrm{i}\hbar\frac{\partial}{\partial a}\,, \qquad\qquad \pi_\varphi \to \hat{\pi}_\varphi := -\mathrm{i}\hbar\frac{\partial}{\partial \varphi}\,. \tag{5.16}$$

If we choose the Laplace-Beltrami operator [211]

$$\nabla^2_{\mathrm{LB}} := \frac{1}{\sqrt{-G}}\partial_A\left(\sqrt{-G}G^{AB}\partial_B\right) = -\frac{\kappa^2}{6}\frac{1}{a^2}\partial_a\left(a\,\partial_a\right) + \frac{1}{a^3}\left(\partial_\varphi\right)^2\,, \tag{5.17}$$

to fix the factor ordering in the Hamiltonian via the substitution $G^{AB}\pi_A\pi_B \to -\hbar^2\nabla^2_{\mathrm{LB}}$, we arrive to the Hamiltonian operator

$$\hat{\mathrm{H}} = -\frac{\hbar^2}{2\mathrm{Vol}}\nabla^2_{\mathrm{LB}} + \mathrm{Vol}\,\mathcal{V}(\alpha,\,\varphi)\,. \tag{5.18}$$

Finally, by applying this operator to the wave-function and taking into account the Hamiltonian

[1] A second primary constraint is obtained in the general theory from to the independence of the Lagrangian with regards to the shift vector N^i. In FLRW cosmology, where the shift vector vanishes, such a constraint does not contain any additional information about the system.

constraint $\hat{\mathrm{H}}\Psi = 0$, we obtain the WDW equation [211]

$$\left[\frac{\hbar^2\kappa^2}{12\mathrm{Vol}}\frac{1}{a^2}\partial_a\left(a\,\partial_a\right) - \frac{\hbar^2}{2\mathrm{Vol}}\frac{1}{a^3}\left(\partial_\varphi\right)^2 + \mathrm{Vol}\,\mathcal{V}\left(q^A\right)\right]\Psi = 0\,. \tag{5.19}$$

This equation has the form of a KG equation, where the scale factor plays the role of the time variable and φ that of a spatial coordinate. This led DeWitt to identify a natural KG-like inner product between two states Ψ_1 and Ψ_2 [137], which in the case of the minisuperspace $\{a,\,\varphi\}$ reduces to [213, 214, 255]

$$\langle\Psi_1(a,\,\varphi),\Psi_2(a,\,\varphi)\rangle = \mathrm{i}\int \mathrm{d}\varphi\, a\left(\Psi_1^*\partial_a\Psi_2 - \Psi_2\partial_a\Psi_1^*\right)\,. \tag{5.20}$$

Unfortunately, just as in the case of the KG equation, the inner product (5.20) is plagued by the fact that it is not positive-definite. This leads to the existence of solutions with zero or negative probability $\langle\Psi,\Psi\rangle$ [137] and therefore (5.20) cannot be used in general as a probability amplitude [221].

5.1.2. Third Quantisation

For the ordinary scalar field, the problem of negative probability states was settled by reinterpreting the KG equation within quantum field theory, which lead to the identification of the scalar field as the quantum field of a spin 0 particle. In the Third Quantisation formalism [45, 255, 300, 306, 330], the same approach is applied to the wave-function of the WDW equation, with a second quantisation being applied to the WDW wave-function (thus the name *Third Quantisation*). In a cosmological context, it seems only natural to identify the quanta of the second quantised WDW wave-function field with individual universes[2] within multi-universe states. This natural appearance of the concept of the *multiverse* within the Third Quantisation picture has remained as the main force driving the development of the formalism since the first tentative studies regarding a possible solution to the cosmological constant problem [45, 168, 189, 255, 256, 306, 330] three decades ago, with very few works published outside the field of cosmology, e.g., [257, 279]. For a review of key aspects of the Third Quantisation formalism, we refer the reader to [202, 221].

The process of third quantising the wave-function of the WDW equation begins with introducing the minisuperspace action [189, 300, 306]

$$S^\Psi = \int \mathrm{d}q^A\,\sqrt{-\tilde{G}}\,\Psi^*\hat{\mathrm{H}}\Psi\,, \tag{5.21}$$

for the wave-function field Ψ. Notice that here we introduce a new re-scaled minisuperspace metric $\tilde{G}_{AB} := (1/\hbar)G_{AB}$ so that (5.21) has the proper units of an action functional. The minimisation of Eq. (5.21) with regards to $\delta\Psi^*$ leads immediately to the WDW equation (5.19), showing that the action $\mathcal{S}^\Psi$ is dynamically equivalent the canonical quantum theory obtained from the action (5.6). If we now employ a field redefinition $\Psi \to \sqrt{\hbar/(2\mathrm{Vol})}\Psi$ and integrate the r.h.s. of (5.21) by parts we

[2] For a further illustration of the analogy between the Third Quantisation of the WDW equation and the second quantisation of the KG equation, cf. the table in Fig 1 of [300] which first appeared in [330].

can, after disregarding total derivative terms, rewrite $\mathcal{S}^{\Psi}$ as

$$S^{\Psi} = \int \mathrm{d}q^A \sqrt{-\tilde{G}} \left(\tilde{G}^{AB} \partial_A \Psi^* \partial_B \Psi + \frac{2\mathrm{Vol}^2}{\hbar} \mathcal{V}(q^A) \Psi^* \Psi \right) , \tag{5.22}$$

which is the KG action (with a reversed sign) for a complex scalar field [268, 333] with a coordinate dependent mass. As in the case of the complex scalar field, the action (5.22) has a $U(1)$ symmetry associated to the gauge transformation $\Psi \to \mathrm{e}^{-\mathrm{i}\theta}\Psi$. Based on this symmetry we can define a conserved current density [255]

$$j^A = \mathrm{i}\sqrt{-\tilde{G}} \left(\Psi^* \partial^A \Psi - \Psi \partial^A \Psi^* \right) , \tag{5.23}$$

and its respective conserved charge [255]

$$Q = \int \mathrm{d}\varphi \, j^{\alpha} = - \langle \Psi, \Psi \rangle . \tag{5.24}$$

This completes the correspondence of the wave-function Ψ of a canonically quantised FLRW universe with a complex scalar field living in (1+1) minisuperspace.

The quantisation of the wave-function field follows along the lines of the second quantisation of the complex scalar field. We first identify Ψ and its complex conjugate as canonical variables and define their canonical momentum densities as

$$\pi_{\Psi} := \frac{\partial \mathcal{L}^{\Psi}}{\partial(\partial_a \Psi)} = -\sqrt{\frac{\kappa^2}{6}} a \, \partial_a \Psi^* , \qquad \pi_{\Psi^*} := \frac{\partial \mathcal{L}^{\Psi}}{\partial(\partial_a \Psi^*)} = -\sqrt{\frac{\kappa^2}{6}} a \, \partial_a \Psi , \tag{5.25}$$

where $\mathcal{L}^{\Psi}$ is the Lagrangian density deduced from (5.22). The corresponding Hamiltonian H^{Ψ} is

$$\begin{aligned} H^{\Psi} &:= \int \mathrm{d}\psi \left(\pi_{\Psi} \partial_a \Psi + \pi_{\Psi^*} \partial_a \Psi^* - \mathcal{L}^{\Psi} \right) \\ &= - \int \mathrm{d}\psi \sqrt{\frac{6}{\kappa^2}} \frac{1}{a} \left(\pi_{\Psi} \pi_{\Psi^*} - \partial_{\varphi} \Psi \partial_{\varphi} \Psi^* + \frac{2\mathrm{Vol}^2 a^3}{\hbar^2} \mathcal{V}(a, \varphi) \Psi^* \Psi \right) . \end{aligned} \tag{5.26}$$

Then, we promote Ψ, Ψ^*, π_{Ψ} and π_{Ψ^*}, together with the Hamiltonian H^{Ψ}, to quantum operators that act on a new multiverse wave-function $\Phi[q^A, \Psi]$ which contains all the information regarding the multi-universe state and whose evolution is given by the Schrödinger-like equation

$$\mathrm{i}\hbar \frac{\partial}{\partial a} |\Phi\rangle = \hat{H}^{\Psi} |\Phi\rangle . \tag{5.27}$$

In order to complete the quantisation of the wave-function field, we need to define a Hilbert space of the solutions of (5.19) re-normalisable with regards to (5.20). Here, some difficulties are encountered since the φ-dependence of the generalised potential $\mathcal{V}$ makes a mode expansion of Ψ a non-trivial endeavour. Different approaches to tackle this issue can be found in the literature, e.g. the Born-Oppenheimer approximation [209, 210], the superadiabatic expansion [212, 214] or an analogy with quantum optics [300]. This situation is nevertheless simplified in the case of a constant potential where the squared mass term depends exclusively on the time-like variable a which we explore next.

5.1.3. Example: Constant potential

As an example of the Third Quantisation of the wave-function of a FLRW universe, we now consider a model with a minimally coupled scalar field with a constant potential $V(\varphi) = 3H_{\rm dS}^2/\kappa^2$ and a vanishing cosmological constant[3] [79, 189, 203, 213, 266, 300]. In such a case, a mode expansion of Ψ is readily available and, using the same methods of quantum field theory, we can define annihilation and creation operators that act on a vacuum state – the void – thus leading to an explicit description of the system in terms of multi-universe states.

Before continuing with the quantisation procedure, we note that the Third Quantisation action $\mathcal{S}^{\Psi}$ can be simplified by changing the minisuperspace coordinates from the scale factor a to $\alpha := \log(a/\ell_{\rm P})$ and making the scalar field dimensionless through the redefinition $\varphi \to (\kappa^2/6)^{1/2}\varphi$. This leads to (5.22) being rewritten as

$$\mathcal{S}^{\Psi} = \int \mathrm{d}\alpha\, \mathrm{d}\varphi \left[-\partial_\alpha \Psi^* \partial_\alpha \Psi + \partial_\varphi \Psi^* \partial_\varphi \Psi + \frac{\Omega^2(\alpha)}{\hbar^2} \Psi^* \Psi \right] , \tag{5.28}$$

where[4]

$$\Omega^2(\alpha) := \frac{12 \mathrm{Vol}^2 a^3}{\kappa^2} \mathcal{V}(\alpha) = \sigma^2 \ell_{\rm P}^6 \, \mathrm{e}^{6\alpha} \left[H_{\rm dS}^2 - \frac{\mathcal{K}}{\ell_{\rm P}^2 \, \mathrm{e}^{2\alpha}} \right] , \qquad \sigma := \frac{6\mathrm{Vol}}{\kappa^2} . \tag{5.29}$$

Minimising (5.29) with regards to variations of Ψ^* leads to the equation of motion

$$\left[\hbar^2 \partial_\alpha^2 - \hbar^2 \partial_\varphi^2 + \Omega^2(\alpha, \varphi) \right] \Psi = 0 , \tag{5.30}$$

which is equivalent to the WDW equation (5.19).

As in the case of cosmological perturbations around a FLRW background, we can use the fact that Ω^2 in (5.29) is independent of the scalar field to expand Ψ in terms of K-modes via the Fourier expansion [213, 300]

$$\Psi(\alpha, \varphi) = \int \frac{\mathrm{d}K}{\sqrt{2\pi}} \Psi_K(\alpha) \, \mathrm{e}^{\mathrm{i}K\varphi} . \tag{5.31}$$

Each of the mode functions Ψ_K satisfies the mode evolution equation

$$\left[\hbar^2 \partial_\alpha^2 + \Omega_K^2(\alpha) \right] \Psi_K = 0 , \qquad \Omega_K^2(\alpha) := \hbar^2 K^2 + \Omega^2(\alpha) , \tag{5.32}$$

which is obtained from replacing (5.31) into (5.30). Given the inner product (5.20) we can choose

[3] Formally, this is equivalent to a model with a massless scalar field φ and a cosmological constant $\Lambda = 3H_{\rm dS}^2$. While this model is interesting on its own, it is well known that a flat potential is not compatible with the cosmological observational constraints for the primordial power spectrum [15]. Nevertheless, R^2 Starobinsky-like models, with a near flat plateau on which an observationally viable inflation occurs, were given a centre-stage position since the results of Planck mission came out [16]. Therefore, and given the lack of a complete mode expansion when the full potential is considered, we use the constant potential model as a first approximation of these models. We expect this approximation to be valid as long as the scalar field is far away from the minimum of the potential at $\varphi = 0$.

[4] Notice that in the case of a FLRW universe with a closed spatial section, Vol corresponds to the volume of a 3-sphere with unit radius, $2\pi^2$, and so σ reduces to the definition found in [79, 162, 266].

the following normalisation condition for the mode functions [268, 333]

$$\Psi_K^* \partial_\alpha \Psi_K - \Psi_K \partial_\alpha \Psi_K^* = -\mathrm{i}\hbar \,. \tag{5.33}$$

In the case of a flat spatial geometry with $\mathcal{K} = 0$, the general solution of Eq. (5.32) that satisfies the normalisation (5.33) can be obtained explicitly [189]:

$$\Psi_K = \sqrt{\frac{\hbar\pi}{6\sinh\left(\pi K/3\right)}} \left(C_{1,K}\, J_{-\mathrm{i}\frac{K}{3}} \left[B\, \mathrm{e}^{3\alpha} \right] + C_{2,K}\, J_{\mathrm{i}\frac{K}{3}} \left[B\, \mathrm{e}^{3\alpha} \right] \right) . \tag{5.34}$$

Here, the dimensionless constant B is defined as

$$B = \frac{\sigma H_{\mathrm{dS}} \ell_{\mathrm{P}}^3}{3\hbar} \,, \tag{5.35}$$

and the linear coefficients $C_{1,K}$ and $C_{2,K}$ satisfy the relation $|C_{1,K}|^2 - |C_{2,K}|^2 = 1$.

By applying the same mode expansion (5.31) to the canonical conjugate momenta[5], $\pi_\Psi := -\partial_\alpha \Psi^*$ and $\pi_{\Psi^*} := -\partial_\alpha \Psi = \pi_\Psi^*$, we can write the Hamiltonian of the wave-function field as [203]

$$\begin{aligned} H^\Psi &= \int \mathrm{d}\varphi \, \left(\pi \, \partial_\alpha \Psi + \pi^* \partial_\alpha \Psi^* - \mathcal{L}^\Psi \right) \\ &= -\int \mathrm{d}\varphi \left(\pi^* \pi + \partial_\varphi \Psi^* \partial_\varphi \Psi + \frac{\Omega^2(\alpha)}{\hbar^2} \Psi^* \Psi \right) \\ &= -\int \mathrm{d}K \left(\pi_K^* \pi_K + \frac{\Omega_K^2(\alpha)}{\hbar^2} \Psi_K^* \Psi_K \right) . \end{aligned} \tag{5.36}$$

Thus, in K-space the Hamiltonian H^Ψ takes the form of an infinite sum of decoupled harmonic oscillators with a time variable frequency $\Omega_K(\alpha)/\hbar$ [228, 229]. We are therefore in a position to apply the full machinery of canonical quantisation for the harmonic oscillator and promote Ψ, Ψ^*, π and π^* to quantum field operators satisfying the usual equal-time commutation relations [268, 333]

$$\left[\hat{\Psi}(\alpha,\, \varphi),\, \hat{\pi}(\alpha,\, \varphi') \right] = \left[\hat{\Psi}^\dagger(\alpha,\, \varphi),\, \hat{\pi}^\dagger(\alpha,\, \varphi') \right] = \mathrm{i}\hbar\, \delta\left(\varphi - \varphi'\right) , \tag{5.37}$$

$$\left[\hat{\Psi}(\alpha,\, \varphi),\, \hat{\pi}^\dagger(\alpha,\, \varphi') \right] = \left[\hat{\Psi}^\dagger(\alpha,\, \varphi),\, \hat{\pi}(\alpha,\, \varphi') \right] = 0 \,. \tag{5.38}$$

These can be expanded in terms of K-modes as [268]

$$\hat{\Psi}(\alpha,\, \varphi) = \int \frac{\mathrm{d}K}{\sqrt{2\pi}} \left(\Psi_K(\alpha)\, \mathrm{e}^{\mathrm{i}K\varphi} \hat{b}_K + \Psi_K^*(\alpha)\, \mathrm{e}^{-\mathrm{i}K\varphi} \hat{c}_K^\dagger \right) , \tag{5.39}$$

$$\hat{\Psi}^\dagger(\alpha,\, \varphi) = \int \frac{\mathrm{d}K}{\sqrt{2\pi}} \left(\Psi_K(\alpha)\, \mathrm{e}^{\mathrm{i}K\varphi} \hat{c}_K + \Psi_K^*(\alpha)\, \mathrm{e}^{-\mathrm{i}K\varphi} \hat{b}_K^\dagger \right) , \tag{5.40}$$

$$\hat{\pi}(\alpha,\, \varphi) = \int \frac{\mathrm{d}K}{\sqrt{2\pi}} \left(\pi_K(\alpha)\, \mathrm{e}^{-\mathrm{i}K\varphi} \hat{b}_K^\dagger + \pi_K^*(\alpha)\, \mathrm{e}^{\mathrm{i}K\varphi} \hat{c}_K \right) , \tag{5.41}$$

[5] In order to minimise indices and simplify the notation, in the following treatment we drop the subscript Ψ when writing the momenta of the wave-function field.

$$\hat{\pi}^{\dagger}(\alpha,\,\varphi) = \int \frac{\mathrm{d}K}{\sqrt{2\pi}} \left(\pi_K(\alpha)\, \mathrm{e}^{-\mathrm{i}K\varphi} \hat{c}_K^{\dagger} + \pi_K^{*}(\alpha)\, \mathrm{e}^{\mathrm{i}K\varphi} \hat{b}_K \right) , \tag{5.42}$$

where the pairs $\{\hat{b}_K,\, \hat{b}_K^{\dagger}\}$ and $\{\hat{c}_K,\, \hat{c}_K^{\dagger}\}$ act as time-independent annihilation and creation operators of two types of universes[6] characterised by the mode K. From the canonical commutation relations (5.37) and (5.38) we find that the two types of annihilation and creation operators satisfy the usual relations [268]

$$\left[\hat{b}_K,\, \hat{b}_{K'}^{\dagger}\right] = \left[\hat{c}_K,\, \hat{c}_{K'}^{\dagger}\right] = \delta(K - K') \,, \tag{5.43}$$

$$\left[\hat{b}_K,\, \hat{b}_{K'}\right] = \left[\hat{c}_K,\, \hat{c}_{K'}\right] = \left[\hat{b}_K,\, \hat{c}_{K'}^{\dagger}\right] = 0 \,. \tag{5.44}$$

The rest of the commutation relations can be derived by Hermitian conjugation of Eqs. (5.43) and (5.44). Using the annihilation and creation operators $\{\hat{b}_K,\, \hat{b}_K^{\dagger}\}$ and $\{\hat{c}_K,\, \hat{c}_K^{\dagger}\}$, we can define a void state, interpreted as the absence (nothingness) of universes, by the eigenvalue equations

$$\hat{b}_K |0_K,\, \alpha\rangle = 0 \,, \qquad\qquad \hat{c}_K |0_K,\, \alpha\rangle = 0 \,, \tag{5.45}$$

with the absolute WDW void given by $|0,\, \alpha\rangle = \prod_K |0_K,\, \alpha\rangle$. A Fock space of states with occupation numbers $n_K^{(b)}$, for universes of type b, and $n_K^{(c)}$, for universes of type c, can be constructed by successive application of the creation operators $\hat{b}_K^{\dagger}$ and $\hat{c}_K^{\dagger}$ [268]

$$|n_K^{(b)},\, n_K^{(c)},\, \alpha\rangle := \frac{\left(\hat{b}_K^{\dagger}\right)^{n_K} \left(\hat{c}_K^{\dagger}\right)^{m_K}}{\sqrt{n_K!\, m!}} |0_K,\, \alpha\rangle \,. \tag{5.46}$$

These number states satisfy the relations

$$\hat{b}_K |n_K^{(b)},\, n_K^{(c)},\, \alpha\rangle = \sqrt{n_K^{(b)}}\, |n_K^{(b)} - 1,\, n_K^{(c)},\, \alpha\rangle \,, \tag{5.47}$$

$$\hat{b}_K^{\dagger} |n_K^{(b)},\, n_K^{(c)},\, \alpha\rangle = \sqrt{n_K^{(b)} + 1}\, |n_K^{(b)} + 1,\, n_K^{(c)},\, \alpha\rangle \,, \tag{5.48}$$

$$\hat{c}_K |n_K^{(b)},\, n_K^{(c)},\, \alpha\rangle = \sqrt{n_K^{(c)}}\, |n_K^{(b)},\, n_K^{(c)} - 1,\, \alpha\rangle \,, \tag{5.49}$$

$$\hat{c}_K^{\dagger} |n_K^{(b)},\, n_K^{(c)},\, \alpha\rangle = \sqrt{n_K^{(c)} + 1}\, |n_K^{(b)},\, n_K^{(c)} + 1,\, \alpha\rangle \,. \tag{5.50}$$

leading to the definition of the number operators for universes of types b and c as $\hat{n}_K^{(b)} := \hat{b}_K^{\dagger} \hat{b}_K$ and $\hat{n}_K^{(c)} := \hat{c}_K^{\dagger} \hat{c}_K$. Via substitution in (5.24), we find that the operator corresponding to the conserved WDW charge

$$\hat{Q} = \int \mathrm{d}K \, \left(\hat{n}_K^{(b)} - \hat{n}_K^{(c)} \right) , \tag{5.51}$$

counts the difference of numbers between the two different types of universes for each mode.

[6] In particle physics, the existence of two types of particles leads to the notion of the pair *particle* and *anti-particle*. In this work, we will refrain from using this terminology for the quanta of the wave-function field so as to avoid the idea of *anti-universe*.

Substituting (5.39), (5.40), (5.41) and (5.42) in (5.36) and making use of the relations (5.43) and (5.44) we can express the Hamiltonian of the third quantised wave-function field as [333]

$$\hat{H}^{\Psi} = \int \mathrm{d}K \left(\frac{\hat{b}_{-K}\hat{c}_{K} + \hat{b}_{K}\hat{c}_{-K}}{2} F_{K}^{*}(\alpha) + \frac{\hat{b}_{-K}^{\dagger}\hat{c}_{K}^{\dagger} + \hat{b}_{K}^{\dagger}\hat{c}_{-K}^{\dagger}}{2} F_{K}(\alpha) + \left[\hat{b}_{K}^{\dagger}\hat{b}_{K} + \hat{c}_{K}^{\dagger}\hat{c}_{K} + \delta(K) \right] E_{K}(\alpha) \right), \tag{5.52}$$

where

$$F_{K}(\alpha) := \left(\partial_{\alpha}\Psi_{K}\right)^{2} + \Omega_{K}^{2}\Psi_{K}^{2}\,, \qquad E_{K}(\alpha) := \left|\partial_{\alpha}\Psi_{K}\right|^{2} + \Omega_{K}^{2}\left|\Psi_{K}\right|^{2}. \tag{5.53}$$

Since the Hamiltonian $\hat{H}^{\Psi}$ is a sum of decoupled individual Hamiltonians for each mode, we can write the wave-function Φ as the product of every K-mode wave-function Φ_{K}:

$$|\Phi\rangle = \prod_{K} |\Phi_{K}\rangle\,, \tag{5.54}$$

all of which satisfy an independent Schrödinger-like equation

$$\mathrm{i}\hbar \frac{\partial}{\partial\alpha} |\Phi_{K}\rangle = \hat{H}^{\Psi} |\Phi_{K}\rangle\,, \tag{5.55}$$

obtained from inserting (5.54) in Eq. (5.27).

In the limit of very small values of the scale factor ($\alpha \to -\infty$) the squared frequency Ω_{K}^{2}, defined in Eq. (5.29), is dominated by the K^{2} term. This allows to define a BD-like void state [189] with the lowest expectation value for the Hamiltonian (5.52):

$$\Psi_{K} = \sqrt{\frac{\hbar}{2K}}\, \mathrm{e}^{\mathrm{i}K\alpha}\,. \tag{5.56}$$

Notice that this corresponds to the asymptotic behaviour of (5.34) with $C_{2,K} = 0$. Due to the explicit time dependence of $\Omega^{2}(\alpha)$, this initial state will no longer correspond to the void as $\alpha \to +\infty$ ($a \to +\infty$). In the picture of b- and c-universes this means that new universes are created as the system evolves and the *in-out* formalism can be used to compute the distribution of universes created Refs. [189, 203, 306]. Using semi-classical considerations, the authors of Refs. [189, 203, 306] argue that each of these individual universes follow the evolution of the semi-classical solution to the WDW equation which satisfies the effective Friedmann equation:

$$\left(\frac{1}{a}\frac{\mathrm{d}a}{\mathrm{d}t}\right)^{2} = \frac{\hbar^{2}K^{2}}{\sigma^{2}a^{6}} - \frac{\mathcal{K}}{a^{2}} + H_{\mathrm{dS}}^{2}\,. \tag{5.57}$$

5.1.4. Introducing interactions

One of the attractive features of the Third Quantisation formalism in treating the multiverse is the possibility of introducing interactions between universes in a simple and straightforward way. In

[45, 168, 189, 306, 330] this idea was explored by considering 3-point interactions between a *parent* (large) universe in a sea of *baby* universes. This saw the introduction of cubic terms in the Third Quantisation action, which in turn led to the appearance of non-linear modifications of the WDW equation.

An alternative approach to the possibility of interactions in the multiverse, which finds motivation in quantum entanglement, is considered in [28, 301–303]. There, N different universes are identified by labelled wave-function fields Ψ_J, $J = 1, 2, \ldots, N_{\rm uni}$, and mixed (quadratic) terms are introduced in the total action, in analogy with a system of quantum entangled particles [301]. A simple phenomenological model based on a system of coupled oscillators with time-dependent frequency was explored in [28, 302], where the following total Hamiltonian was considered:

$$H^{(\rm tot)} = \sum_{n=1}^{N_{\rm uni}} H^{\Psi_n} + H^{(\rm int)} \,, \tag{5.58}$$

where each H^{Ψ_n} is of the form of the non-interacting Hamiltonian (5.36) and the interaction term $H^{(\rm int)}$ was taken to be of the form

$$H^{(\rm int)} = \int \mathrm{d}\varphi \sum_{n=1}^{N_{\rm uni}} C(\alpha) \left|\Psi_n - \Psi_{n+1}\right|^2 \,. \tag{5.59}$$

The coupling $C(\alpha)$, which is phenomenological in nature, was assumed to be the same for all pairs $\Psi_n \Psi_{n+1}$ and cyclic conditions were assumed, i.e., $\Psi_{N_{\rm uni}+1} = \Psi_1$ in Eq. (5.59).

The total Hamiltonian (5.58) with an interaction of the form in Eq. (5.59) can be simplified by means of a discrete Fourier transformation [302]

$$\Psi_l = \frac{1}{\sqrt{N_{\rm uni}}} \sum_{n=1}^{N_{\rm uni}} \mathrm{e}^{-2\pi \mathrm{i}\, ln/N_{\rm uni}} \Psi_n \,, \qquad \Psi_l^* = \frac{1}{\sqrt{N_{\rm uni}}} \sum_{n=1}^{N_{\rm uni}} \mathrm{e}^{2\pi \mathrm{i}\, ln/N_{\rm uni}} \Psi_n^* \,, \tag{5.60}$$

$$\pi_l = \frac{1}{\sqrt{N_{\rm uni}}} \sum_{n=1}^{N_{\rm uni}} \mathrm{e}^{-2\pi \mathrm{i}\, ln/N_{\rm uni}} \pi_n \,, \qquad \pi_l^* = \frac{1}{\sqrt{N_{\rm uni}}} \sum_{n=1}^{N_{\rm uni}} \mathrm{e}^{2\pi \mathrm{i}\, ln/N_{\rm uni}} \pi_n^* \,, \tag{5.61}$$

which, when inserted in (5.58) leads to

$$H^{(\rm tot)} = \int \mathrm{d}\varphi \sum_{l=1}^{N_{\rm uni}} \left[\pi_K^* \pi_K + \partial_\varphi \Psi_K^* \, \partial_\varphi \Psi_K + \frac{\Omega_l(\alpha, \varphi)}{\hbar^2} \Psi_K^* \, \Psi_K \right] \,. \tag{5.62}$$

Here, the new squared frequency $\Omega_l(\alpha, \varphi)$ reads

$$\Omega_l(\alpha, \varphi) := \sigma^2 \ell_{\rm P}^6 \, \mathrm{e}^{6\alpha} \left[\frac{\Lambda}{3} + \frac{\kappa^2 V(\varphi)}{3} - \frac{\mathcal{K}}{\ell_{\rm P}^2 \, \mathrm{e}^{2\alpha}} + \frac{4\hbar^2}{\sigma^2 \ell_{\rm P}^6} \frac{C(\alpha)}{\mathrm{e}^{6\alpha}} \sin^2\left(\frac{\pi l}{N_{\rm uni}}\right) \right] \,. \tag{5.63}$$

The shape of Eq. (5.62) shows that in passing from the n-representation to the new l-representation we obtain a system of N uncoupled Hamiltonians, each representing a series of harmonic oscillators whose frequency, in the approximation of $\partial_\varphi \Psi \approx 0$, is given by Ω_l. Notice that the effect of the interaction in the old representation is now translated in the presence of an additional term in Ω_l^2.

The expression for the frequency Ω_l can be simplified by following [302] and writing $C(\alpha)$ as

$$C(\alpha) = \frac{\sigma^2}{4\hbar^2}\frac{N_{\rm uni}^2}{\pi^2}a^2\lambda^2(a) = \frac{\sigma^2}{4\hbar^2}\frac{N_{\rm uni}^2}{\pi^2}\ell_{\rm P}^2\,{\rm e}^{2\alpha}\lambda^2(\alpha)\,, \tag{5.64}$$

where the new coupling $\lambda(\alpha)$ has dimensions of length. Replacing this expression in (5.63) leads to

$$\Omega_l(\alpha,\varphi) := \sigma^2\ell_{\rm P}^6\,{\rm e}^{6\alpha}\left[\frac{\Lambda}{3} + \frac{\kappa^2 V(\varphi)}{3} - \frac{\mathcal{K}}{\ell_{\rm P}^2\,{\rm e}^{2\alpha}} + \frac{N_{\rm uni}^2}{\pi^2}\sin^2\left(\frac{\pi l}{N_{\rm uni}}\right)\frac{\lambda^2(\alpha)}{\ell_{\rm P}^4\,{\rm e}^{4\alpha}}\right]. \tag{5.65}$$

In Ref. [302], it was argued that, through a mechanism of vacuum decay, the most probable configuration in the l-representation is that of small l. If we assume this to be the case and consider the limit of a very high number of universes, $l \ll N_{\rm uni}$, then we can replace the $\sin$ function in (5.65) by its limiting expression for small arguments, obtaining

$$\Omega_l(\alpha,\varphi) \simeq \sigma^2\ell_{\rm P}^6\,{\rm e}^{6\alpha}\left[\frac{\Lambda}{3} + \frac{\kappa^2 V(\varphi)}{3} - \frac{\mathcal{K}}{\ell_{\rm P}^2\,{\rm e}^{2\alpha}} + \frac{l^2\lambda^2(\alpha)}{\ell_{\rm P}^4\,{\rm e}^{4\alpha}}\right]. \tag{5.66}$$

We can now make use of the phenomenological nature of the universe-universe coupling to consider the situation when λ is a power of the scale factor – $\lambda = \lambda_*(a/a_*)^s$, where λ_* and a_* are arbitrary constants with units of length and s is a real number. Of particular interest are the cases of [75, 82, 83, 302]: $s = 2$ which introduces an effective cosmological constant; $s = 1$ which introduces an effective curvature term; $s = 1/2$ which introduces an effective dust term; $s = 0$ which introduces an effective radiation term; $s = -1$ which introduces an effective stiff-matter term.

As in the case of a constant potential treated in the previous section, the authors of [302] use semi-classical considerations, as well as the approximation $\partial_\varphi\Psi \approx 0$ which amounts to disregard the momentum of the scalar field, to argue that each individual universe in the l-representation follows the evolution dictated by the effective Friedmann equation

$$\left(\frac{1}{a}\frac{{\rm d}a}{{\rm d}t}\right)^2 = \frac{\Lambda}{3} + \frac{\kappa^2 V(\varphi)}{3} - \frac{\mathcal{K}}{a^2} + \frac{l^2\lambda^2(a)}{a^4}\,. \tag{5.67}$$

If we consider that the potential of the scalar field is almost constant during the evolution of the system, $V(\varphi) = 3H_{\rm dS}^2/\kappa^2$, while absorbing the cosmological constant in $V(\varphi)$, and consider the case of a power-law dependence of $\lambda(a)$, the previous equation reduces to

$$\left(\frac{1}{a}\frac{{\rm d}a}{{\rm d}t}\right)^2 = H_{\rm dS}^2 - \frac{\mathcal{K}}{\ell_{\rm P}^2\,{\rm e}^{2\alpha}} + \frac{l^2\lambda_*^2}{a_*^4}\left(\frac{a_*}{a}\right)^{4-2s}. \tag{5.68}$$

As a last note, we point out that while the Third Quantisation formalism was invoked to justify the multi-universe system, no actual quantisation of the N wave-function fields was performed up to this point. As discussed above, this would require specifying the shape of the potential of the scalar field in order to find a mode decomposition of the fields, so as to write the quantum analogues of Ψ and π in terms of creation and annihilation operators. In the case of a constant potential, this would add a new $\sim a^{-6}$ term to the effective Friedmann equation coming from the momentum of the scalar field. However, except for the case of $\lambda \sim a^{-1}$, this new term is subdominant with regards to the l^2 term

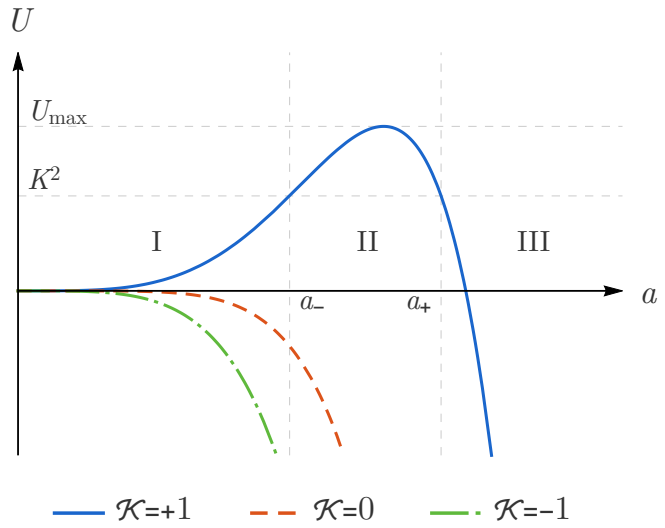

Figure 5.1.: The potential U in the cases of a closed, flat and open spatial geometry. For $\mathcal{K} = +1$ there is a classically forbidden region between a_- and a_+.

that arises from the universe-universe coupling and, therefore, we choose to disregard it.

5.2. Tunnelling in a closed universe

We now return to the case of a non-interacting universe filled by a massless scalar field with a constant potential, which was introduced previously in Sect. 5.1.3. In such a case, the wave-function mode function Ψ_K satisfies the WDW mode equation (5.32)

$$\frac{\partial^2 \Psi_K}{\partial \alpha^2} + \left[K^2 + \frac{\Omega_K^2(\alpha)}{\hbar^2} \right] \Psi_K = 0 \,, \tag{5.69}$$

where the mode-dependent Ω_K is defined in Eq. (5.32). The evolution of this mode in the minisuperspace can be compared to that of a particle travelling along the semi-axis $0 < a$ (recall that $\alpha := \log(a/\ell_{\rm P})$) in a potential $U = -\Omega_K^2(a)/\hbar^2$, where the term K^2 plays the role of the total energy of the particle (cf. Fig. 5.1). For flat or open spatial geometries, the potential U is always non-positive and decreasing with a, therefore Ψ_K represents an unbounded state which classically corresponds to a universe that expands from $a = 0$ to infinite radius.

In the case of a closed FLRW universe, however, the situation becomes more interesting – due to the opposite signs of the curvature and cosmological constant terms, the potential U becomes positive for small values of the scale factor[7] with a maximum value $U_{\rm max}$ at $a = (2/3)^{1/2} H_{\rm dS}^{-1}$. This entraps the modes with lowest mode-numbers ($K^2 < U_{\rm max}$) in a finite region $\mathrm{I} : a \in (0, a_-)$ from which, classically, they cannot escape. Thus, the classical interpretation of solutions in this region is that of a *baby* universe that expands to a maximum size and then collapse. This picture is similar to

[7] More precisely, we find that $0 < U$ for $0 < a < H_{\rm dS}^{-1}$.

the situation presented[8] in [306] and [71]. Another classically allowed region is III : $a \in (a_+, +\infty)$, where semi-classical solutions would correspond to universes that can contract from infinite radius until reaching $a = a_+$, at which point they bounce and start to expand in an accelerated fashion *ad infinitum*. Separating these two regions, is the potential barrier which defines a classically forbidden region II : $a \in (a_-, a_+)$.

The border points a_- and a_+ that delimit the regions I, II, and III can be obtained by calculating the positive solutions of the following cubic equation in a[9].

$$K^2 = \frac{27}{4} K^2_{\rm max} \left[(H_{\rm dS} a)^4 - (H_{\rm dS} a)^6 \right] , \tag{5.70}$$

where

$$K_{\rm max} := \frac{2\sigma}{3\sqrt{3}\hbar H^2_{\rm dS}} = \frac{\pi}{\sqrt{3}} \frac{1}{\gamma} . \tag{5.71}$$

Here, the dimensionless parameter $\gamma := \hbar^2 H^2_{\rm dS}/M^2_{\rm P}$ indicates how close the energy density during inflation is to the Planck scale. The equation (5.70) can be rewritten as a cubic equation in the dimensionless variable $x := (H_{\rm dS} a)^2$ and for $K < K_{\rm max}$ possesses three real roots: x_+, x_- and $-x_0$, defined for each mode K as [79, 162]

$$x_+(K) = \frac{1 + 2\cos\left(\frac{\theta_K}{3}\right)}{3} , \qquad (0 < x_+) \tag{5.72}$$

$$x_-(K) = \frac{1 - 2\cos\left(\frac{\theta_K + \pi}{3}\right)}{3} , \qquad (0 \leq x_- \leq x_+) \tag{5.73}$$

$$x_0(K) = \frac{-1 + 2\cos\left(\frac{\theta_K - \pi}{3}\right)}{3} \qquad (x_0 \leq 0) , \tag{5.74}$$

where the mode dependent phase θ_K is given by [79, 162]

$$\theta_K := \arccos\left[1 - 2\left(\frac{K}{K_{\rm max}}\right)^2\right] = 2\arcsin\left(\frac{K}{K_{\rm max}}\right) \in [0, \pi] . \tag{5.75}$$

In Fig. 5.2 we show how the value of x_+, x_- and x_0 depends on the ratio $K/K_{\rm max}$. For $0 < K < K_{\rm max}$, we find two positive roots, x_+ and x_-, with $x_- \leq x_+$, which we can associate with the two physical scales $a_- := H^{-1}_{\rm dS}(x_-)^{1/2}$ and $a_+ := H^{-1}_{\rm dS}(x_+)^{1/2}$. These two roots merge for $K = K_{\rm max}$, with $x_+(K_{\rm max}) = x_-(K_{\rm max}) = 2/3$, and become complex for larger values. This is in accordance with the fact that for K larger than the $K_{\rm max}$ barrier the modes Ψ_K can evolve freely in the semi-axis $0 < a$. The third root $-x_0$, which as can be seen in Fig. 5.2 can be continued for $K_{\rm max} < K$, is always negative and therefore has no correspondence with a physical scale.

Using a semi-classical WKB approximation in the classically allowed regions I and III, we obtain the

[8] We stress that in those works the role of the total energy is played by the constants ε [306] or $\tilde{K}^2$ [71], which come from considering a massless conformal scalar field whose kinetic term, classically, goes as a^{-4}. Note how this difference is reflected in the powers of the terms of the potential barrier.

[9] In the present case of a closed FLRW universe, the σ factor that appears in the definition of $K_{\rm max}$, cf. (5.70), and which is defined in (5.29) assumes the value $\sigma = 12\pi^2/\kappa^2 = 3\pi/(2G)$, thus agreeing with the notation in [79, 162, 266]. In this case we can write $K_{\rm max} = (\pi M^2_{\rm P})/(\sqrt{3}\hbar^2 H^2_{\rm dS})$, where we recall that $M_{\rm P}$ is the Planck mass.

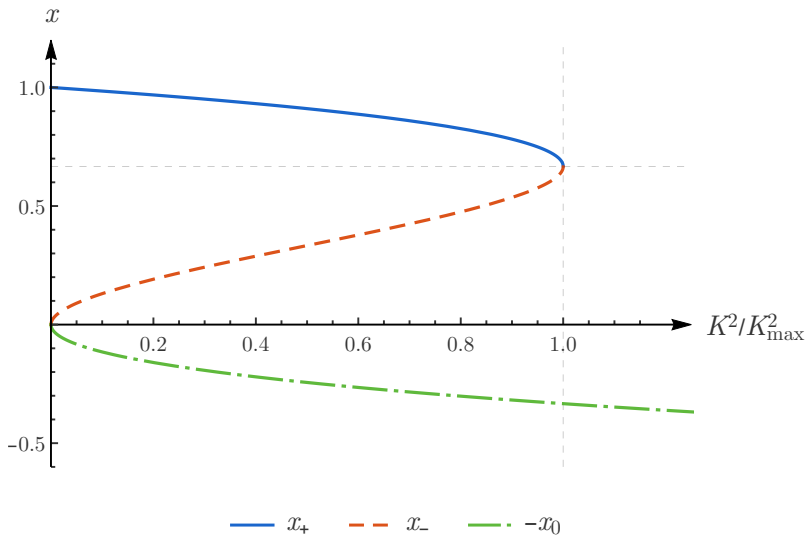

Figure 5.2.: Dependence of the solutions (5.72), (5.73) and (5.74) on the mode number K. The solutions x_+ and x_- are real valued for $0 \leq K^2 \leq K^2_{\rm max}$, merging for $K = K_{\rm max}$ with $x_+(K_{\rm max}) = x_-(K_{\rm max}) = 2/3$. For $K_{\rm max} < K$ the negative root x_0 can be continued even though the phase θ_K assumes complex values, cf. Eq. (5.75).

pair of solutions [211, 253]

$$\Psi^{\rm I\pm}_K = \sqrt{\frac{\hbar}{2}}\frac{\mathrm{e}^{\pm\frac{\mathrm{i}}{\hbar}S^{\rm I}_0(K)}}{(K^2-U)^{1/4}}\,, \qquad \Psi^{\rm III\pm}_K = \sqrt{\frac{\hbar}{2}}\frac{\mathrm{e}^{\pm\frac{\mathrm{i}}{\hbar}S^{\rm III}_0(K)}}{(K^2-U)^{1/4}}\,, \tag{5.76}$$

where $S^{\rm I}_0 := \hbar\int_{-\infty}^{\alpha}\mathrm{d}\alpha'\sqrt{K^2-U(\alpha')}$ and $S^{\rm III}_0 := \hbar\int_{\log(a_+/\ell_{\rm P})}^{\alpha}\mathrm{d}\alpha'\sqrt{K^2-U(\alpha')}$. The pre-factor $\sqrt{\hbar/2}$ is included so that $\Psi^{\pm}_K$ is normalised with regards to (5.33). The classical momentum is then given by [211]

$$\pi_\alpha = -\mathrm{i}\hbar\frac{\partial S^K_0}{\partial\alpha} = \pm\hbar\sqrt{K^2-U}\,. \tag{5.77}$$

Equating π_α in the previous equation with the canonical momentum derived from (5.6), fixing $N = 1$ so as to select the classical cosmic time and changing variables from α to the scale factor a leads to the following Friedmann equation, valid both in the regions I and III depicted in Fig. 5.1:

$$\left(\frac{1}{a}\frac{\mathrm{d}a}{\mathrm{d}t}\right)^2 = \frac{\hbar^2}{\sigma^2a^6}\left(K^2-U\right) = \frac{\hbar^2K^2}{\sigma^2a^6} - \frac{1}{a^2} + H^2_{\rm dS}\,. \tag{5.78}$$

Notice that for the limiting points $a = a_-$ and $a = a_+$ the r.h.s. of this equation vanishes, i.e., they correspond to bouncing points where the Hubble rate vanishes. Therefore, classical solutions of expanding universes in region I bounce back once they reach a_- and start to contract, while solutions of asymptotically de Sitter universes in region III, which initially are contracting, will reach a minimum size at a_+ before entering a final inflating epoch. This is in accordance with the interpretation

presented above for the wave-function with mode K as describing a particle moving in a potential U.

5.2.1. Background solutions

In order to obtain explicit solutions of Eq. (5.78), we introduce the conformal time $\mathrm{d}\eta := a^{-1}\mathrm{d}t$ and change variables from the scale factor to $x = (H_{\rm dS}a)^2$. The Friedmann equation (5.78) can then be rewritten as

$$\mathrm{d}\eta = \pm\frac{\mathrm{d}x}{\sqrt{(x-x_+)(x-x_-)(x+x_0)}}\,, \tag{5.79}$$

where x_+, x_- and $-x_0$ are the real roots of Eq. (5.70). In the particular case of $K = 0$, which corresponds to the model of *creation from nothing* analysed in [340, 341], the integral of Eq. (5.79) in the region[10] $x_+ < x$ can be expressed in terms of elementary functions. For a general value of the mode K in the interval $0 < K < K_{\rm max}$, however, an explicit integration of Eq. (5.79) requires specific variable substitutions for each separate region. The strategy followed in [79], where the solutions were derived in terms of elliptic integrals and Jacobi elliptic functions goes as follows.

In region $\mathrm{I} : x \in (0,\, x_-)$, we employ the change of variable [79]

$$x \to \xi^{\rm I} := \arccos\left(\sqrt{\frac{x_+ - x_-}{x_+ - x}\,\frac{x+x_0}{x_- + x_0}}\right)\,. \tag{5.80}$$

Applying the substitution (5.80) in Eq. (5.79) and integrating from $\xi^{\rm I}$ to $\xi^{\rm I}(x_-) = 0$, we obtain for the expanding branch

$$\mathcal{H}_{\rm dS}\,(\eta_- - \eta) = F\left(\xi^{\rm I}|k^2\right)\,, \tag{5.81}$$

where $\eta_- := \eta(x_-)$, $F\,(z|m)$ is the elliptical integral of the first kind [7, 283] and we have introduced as well the constants

$$\mathcal{H}_{\rm dS} := \sqrt{x_0 + x_+}\,, \qquad\qquad k^2 := \frac{x_- + x_0}{x_+ + x_0} \leq 1\,. \tag{5.82}$$

The solution $a(\eta)$ can then be obtained by using the relation of the elliptic integrals with the Jacobi elliptic function $\mathrm{sn}(u|m)$ [7, 283] to invert the solution (5.81). After some algebra we arrive to the solution [79]

$$a^2(\eta) = a_-^2 - \left(a_0^2 + a_-^2\right)\frac{(1-\tilde{k}^2)\mathrm{sn}^2\left[\mathcal{H}_{\rm dS}\,(\eta_- - \eta)\big|k^2\right]}{1 - k^2\,\mathrm{sn}^2\left[\mathcal{H}_{\rm dS}\,(\eta_- - \eta)|k^2\right]}\,. \tag{5.83}$$

A similar change of variable [79]

$$x \to \xi^{\rm III} :=\ \arcsin\left(\sqrt{\frac{x-x_+}{x-x_-}}\right)\,, \qquad\qquad \xi^{\rm III} \in \left[0,\,\frac{\pi}{2}\right]\,, \tag{5.84}$$

valid for $x \in (x_-,\, x_+)$, can be applied to (5.79) in the region III, after which an integration from

[10] Notice that in this case we have $x_- = 0$ and so the region I disappears.

$\xi^{\rm III}(x_+) = 0$ to $\xi^{\rm III}$ leads to

$$\mathcal{H}_{\rm dS}\left(\eta - \eta_+\right) = F\left(\xi^{\rm III}\middle|k^2\right) . \tag{5.85}$$

Inverting (5.85), we then obtain the scale factor as a function of the conformal time in the asymptotically de Sitter region [79]

$$a^2(\eta) = a_+^2 + \left(a_+^2 - a_-^2\right)\frac{\mathrm{sn}^2\left[\mathcal{H}_{\rm dS}\left(\eta - \eta_+\right)\middle|k^2\right]}{\mathrm{cn}^2\left[\mathcal{H}_{\rm dS}\left(\eta - \eta_+\right)\middle|k^2\right]} . \tag{5.86}$$

Applying a semi-classical WKB approximation to the classically forbidden region II, where the potential barrier U is higher than K^2, leads to the pair of tunnelling solutions

$$\Psi_K^{\rm II\pm} = \sqrt{\frac{\hbar}{2}}\frac{\mathrm{e}^{\pm\frac{1}{\hbar}S_0^{\rm II}(K)}}{\left(U - K^2\right)^{1/4}} , \tag{5.87}$$

where $S_0^{\rm II} := \hbar\int_{\log(a_-/\ell_{\rm P})}^{\alpha}\mathrm{d}\alpha'\sqrt{U(\alpha') - K^2}$. As noted by Coleman [120], these solutions correspond to Euclidean instanton solutions and so, in order to obtain an evolution equation we need to perform a Wick rotation and define a Euclidean time $\tilde{t} := -it$. We can now define the Euclidean momentum as

$$\tilde{\pi}_\alpha = \pm\hbar\frac{\partial S_0^{\rm II}(K)}{\partial\alpha} , \tag{5.88}$$

which leads to the Euclidean equivalent of the Friedmann equation (5.78)

$$\left(\frac{1}{a}\frac{\mathrm{d}a}{\mathrm{d}\tilde{t}}\right)^2 = -\frac{\hbar^2K^2}{\sigma^2a^6} + \frac{1}{a^2} - H_{\rm dS}^2 . \tag{5.89}$$

For $K = 0$ the solution of this equation in the region $0 < x < x_+$ gives the S^4 instanton discussed in [340, 341]. In order to find a solution for a general K within the interval $0 < K < K_{\rm max}$, we can rewrite Eq. (5.89) in terms of the conformal Euclidean time $\mathrm{d}\tilde{\eta} := a^{-1}\mathrm{d}\tilde{t}$ as

$$\mathrm{d}\tilde{\eta} = \pm\frac{\mathrm{d}x}{\sqrt{(x_+ - x)(x - x_-)(x + x_0)}} . \tag{5.90}$$

After introducing the change of variable [79]

$$x \to \xi^{\rm II} := \arccos\left(\sqrt{\frac{x - x_-}{x_+ - x_-}}\right) , \qquad \xi^{\rm II} \in \left[0, \frac{\pi}{2}\right] , \tag{5.91}$$

we can integrate Eq. (5.90) from $\xi^{\rm II}$ to $\xi^{\rm II}(x_+) = 0$ and obtain

$$\mathcal{H}_{\rm dS}\left(\tilde{\eta}_+ - \tilde{\eta}\right) = F\left(\xi^{\rm II}\middle|k^2\right) . \tag{5.92}$$

Inverting this equation we finally obtain the solution for the scale factor as a function of the conformal Euclidean time [79]

$$a^2\left(\tilde{\eta}\right) = a_+^2 - \left(a_+^2 - a_-^2\right)\mathrm{sn}^2\left[\mathcal{H}_{\rm dS}\left(\tilde{\eta}_+ - \tilde{\eta}\right)\right] . \tag{5.93}$$

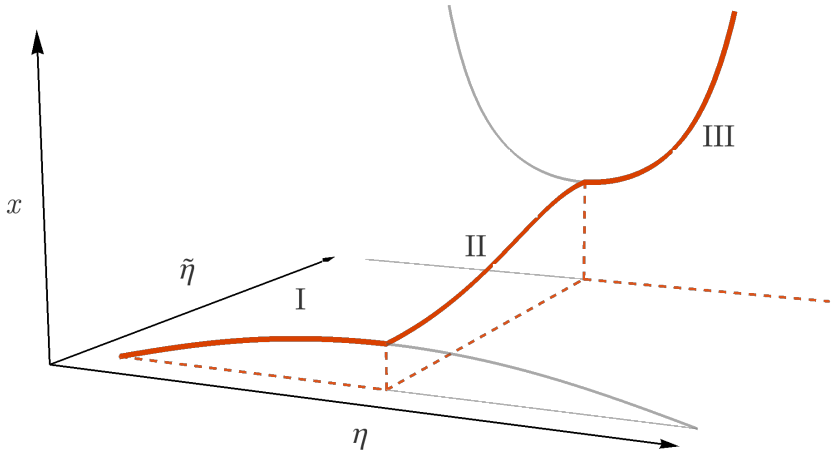

Figure 5.3.: Representation of the solutions (5.83), (5.86) and (5.93) for the squared scale factor $x := a^2 H_{\rm dS}^2$ as a function of the conformal Lorentzian time η and the conformal Euclidean time $\tilde{\eta}$. The thick red line represents the evolution of the squared scale factor for a baby universe (I) that once it reaches its maximum size traverses the Euclidean wormhole (II) and emerges as an expanding universe (III) that starts to inflate. The classical continuation of the evolution in the baby and inflating universes, i.e., the bouncing solutions, is shown as a thin grey line.

A combined representation of the solutions (5.83), (5.86) and (5.93) is plotted in Fig. 5.3 as a thick red line, showing how the two expanding branches in regions I and III, with the normalisation $\eta_- = 0$, can be connected by the instanton solution in the region II. Thus a *baby* universe with $a < a_-$ can quantum tunnel through the instanton solution and emerge as an asymptotically de Sitter universe with $a_+ < a$, thus escaping the classical collapse. The continuation of the classical solutions in the regions I and II, i.e., the bouncing classical solutions, are plotted in a thin grey line.

5.2.2. Quantum tunnelling

In the previous section, we have discussed how a classically forbidden region appears in a model of a closed FLRW universe filled with a scalar field with a (near) constant potential $V(\varphi)$. At the semi-classical level this region corresponds to a Euclidean instanton similar to the ones found in [340, 341] and [167]. This instanton connects the two classically allowed regions I and III (cf. Fig. 5.1) corresponding to a *baby* universe and an asymptotically inflating one, thus allowing for the former to avoid its classical collapse by tunnelling quantum mechanically through the Euclidean region II. Following Vilenkin's proposal for tunnelling transition [341, 342], we now calculate the probability that this process can occur.

As discussed in [341, 342], the tunnelling probability of an outgoing wave solution traversing the

potential barrier U can be approximated by[11]:

$$\mathcal{P}_K^{(a_-\to a_+)} \approx \exp\left[-\frac{2}{\hbar}\int_{a_-}^{a_+}\frac{\mathrm{d}a}{a}\,S_0^{\mathrm{II}}(K)\right] = \exp\left[-\frac{3\pi}{2\gamma}I_{(K/K_{\mathrm{max}})}\right], \tag{5.94}$$

where $I_{(K/K_{\mathrm{max}})}$ represents the following integral[12]

$$I_{(K/K_{\mathrm{max}})} := \int_{x_-}^{x_+}\frac{\mathrm{d}x}{x}\sqrt{(x_+-x)(x-x_-)(x+x_0)}\,. \tag{5.95}$$

The subscript (K/K_{max}) is introduced here to indicate that the integral in (5.95) is a function of the ratio K/K_{max}, exclusively, as x_+, x_- and x_0 depend on K only through the phase θ_K defined in (5.75).

The integral on the r.h.s. of (5.95) can be solved directly in the extremal cases of $K=0$ and $K=K_{\mathrm{max}}$. For $K=0$, we have $x_+=1$ and $x_-=x_0=0$ and the integral in Eq. (5.95) becomes trivial, leading to $I_{(0)}=2/3$. On the other hand, for $K=K_{\mathrm{max}}$ the limits of integration are equal and the integral vanishes: $I_{(1)}=0$. For a general value of K satisfying $0<K<K_{\mathrm{max}}$, an explicit solution for $I_{(K/K_{\mathrm{max}})}$ was obtained by us in [79] by means of the variable substitution

$$x\to\xi := \arccos\left(\sqrt{\frac{x-x_-}{x_+-x_-}}\right), \qquad\qquad \xi\in\left[0,\,\frac{\pi}{2}\right]. \tag{5.96}$$

This leads to $I_{(K/K_{\mathrm{max}})}$ being written as a linear combination of complete elliptic integrals of the first, $K(m)$, second, $E(m)$, and third, $\Pi(n|m)$, kinds [7, 283]:

$$I_{(K/K_{\mathrm{max}})} = \begin{cases} \dfrac{2}{3}\,, & K=0\,, \\ \dfrac{2}{3}\left[C_K K\left(\tilde{k}^2\right)+C_E E\left(\tilde{k}^2\right)+C_\Pi\Pi\left(q^2\,\middle|\,\tilde{k}^2\right)\right], & 0<K<K_{\mathrm{max}}\,, \\ 0\,, & K=K_{\mathrm{max}}\,. \end{cases} \tag{5.97}$$

The auxiliary parameters $\tilde{k}$ and q are defined as[13]

$$\tilde{k} := \sqrt{\frac{x_+-x_-}{x_++x_0}} \qquad \text{and} \qquad q := \sqrt{\frac{x_+-x_-}{x_+}}\,, \tag{5.98}$$

while the linear coefficients C_K, C_E and C_Π can be written in terms of $\tilde{k}$, q and $\mathcal{H}_{\mathrm{dS}}$, where the

[11] The quantity $S_0^{\mathrm{II}}(K)$ corresponds to the $p(a)$ defined in [341, 342]. This correspondence is the origin of the factor 2 in the expression for the tunnelling probability (5.94) which does not appear in the expression $\mathcal{P}\approx\exp(-|S_E|)$ found in [341].

[12] Please notice that the factor $1/2$ in the definition (3.2) of [79] is absorbed by the pre-factor in Eq. (5.94).

[13] Notice that the parameter q is unrelated to the deceleration parameter defined in Sect. 2.2.

latter was defined in Eq. (5.82), as

$$C_K := \mathcal{H}_{\rm dS}^3 \left(1 - \tilde{k}^2 - 3\frac{\tilde{k}^4}{q^4}\left(1 - q^2\right)\right) , \tag{5.99}$$

$$C_E := -\mathcal{H}_{\rm dS}^3 \left(1 + \tilde{k}^2 - 3\frac{\tilde{k}^2}{q^2}\right) , \tag{5.100}$$

$$C_\Pi := 3\mathcal{H}_{\rm dS}^3 \left(1 - \frac{\tilde{k}^2}{q^2}\right)\left(\tilde{k}^2 - \frac{\tilde{k}^2}{q^2}\right) . \tag{5.101}$$

A detailed derivation of Eq. (5.97) can be found in the Appendix A of Ref. [79].

Inserting the solution (5.97) in the expression (5.94), we can write the tunnelling probability as [79]

$$\mathcal{P}_K \approx \begin{cases} \exp\left[-\dfrac{\pi}{\gamma}\right] , & K = 0 , \\ \exp\left[-\dfrac{\pi}{\gamma}\left[C_K\, K\left(\tilde{k}^2\right) + C_E\, E\left(\tilde{k}^2\right) + C_\Pi\, \Pi\left(\kappa^2 \,|\, \tilde{k}^2\right)\right]\right] , & 0 < K < K_{\rm max} , \\ 1 , & K = K_{\rm max} . \end{cases} \tag{5.102}$$

In this expression, the linear coefficients C_K, C_E and C_Π and the auxiliary parameters $\mathcal{H}_{\rm dS}$, $\tilde{k}$ and q are functions only of the ratio $K/K_{\rm max}$ (through the angle α_K). Therefore, the tunnelling probability $\mathcal{P}_K$ is a bivariate function of the parameter γ, which controls how close the energy scale during inflation is to the Planck scale, and of the ratio $K/K_{\rm max}$, which relates the momentum of the scalar field with the maximum of the potential barrier U. In the top panel of Fig. 5.4, we plot the tunnelling probability as a function of γ and $K/K_{\rm max}$, while in the bottom panels we present the projection of $\mathcal{P}_K$ for different fixed values of $K/K_{\rm max}$ (bottom-left) and for different fixed values of γ (bottom-right).

Due to the factor $-(1/\gamma)$ in the argument of the exponential in Eq. (5.102), we find that the probability that a *baby* universe tunnels through the potential barrier is extremely suppressed for universes with low energy scales of inflation, as can be seen in Fig. 5.4. Then, if we consider an initial collection of *baby* universes with a flat distribution of values of γ and could count the universes that are able to surpass the potential barrier and start to inflate, we should find a final distribution of inflating universes highly peaked around the maximum allowed values of energy scale during inflation. This is analogous to the situation discussed in [341], where an identical suppression led to the interpretation that universes with the highest values of the vacuum energy were the ones more probable to nucleate and therefore "*(. . .) an observer who can do a statistical survey of all nucleating universes (. . .) will find that the most of the universes nucleate with* $\phi = \phi_{\rm max}$" [341].

This suppression of the tunnelling probability can nevertheless be avoided if K is high enough, as we find from Fig. 5.4 that $\mathcal{P}_K$ grows monotonically with K, reaching unity when $K = K_{\rm max}$. This should be expected since the Euclidean region ceases to be present in that limit, which means that even for very small values of γ there is a small range of values of K around $K_{\rm max}$, for which the *baby* universe is likely to tunnel through the Euclidean region and start to inflate. For universes with sub-Planckian inflationary energy scales, like ours, this provides a mechanism to counter the exponential suppression due to $\gamma \ll 1$ in the expression (5.102). Notice that current observational data set an upper limit of 8.8×10^{13} GeV for the energy scale during inflation [48], which corresponds to γ of the order of

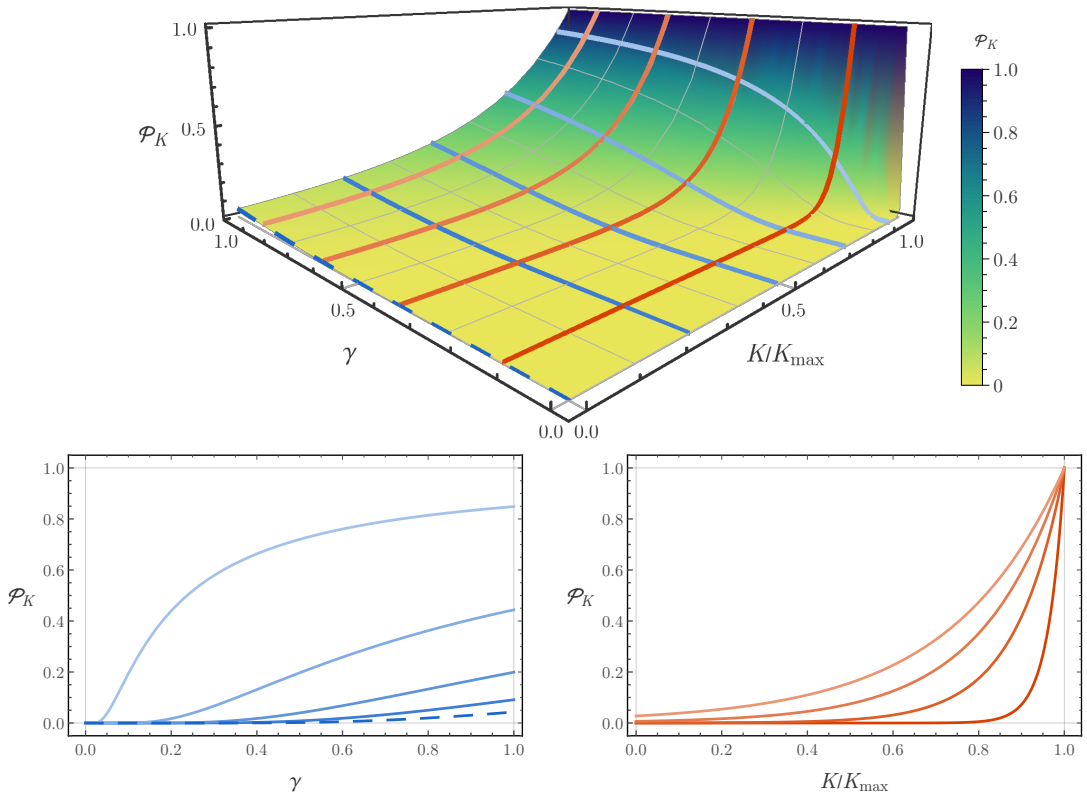

Figure 5.4.: The tunnelling probability $\mathcal{P}_K$ as a function of the ratio $K/K_{\rm max}$ and of the inflationary scale parameter $\gamma := \hbar^2 H_{\rm dS}^2/M_{\rm P}^2$. In the two bottom panels we plot the tunnelling probability when (left panel, from bottom/darker to top/lighter) fixing $K/K_{\rm max} = 0, 1/4, 1/2, 3/4, 95/100$; and when (right panel, from bottom/darker to top/lighter) fixing $\gamma = 1/8, 3/8, 5/8, 7/8$. The tunnelling probability for the case of the creation of an expanding universe from nothing (K = 0) is indicated by a dashed blue line.

$10^{-11} \sim 10^{-12}$ [79]. For such a small value of γ the tunnelling probability distribution is extremely peaked around $K = K_{\rm max}$, meaning that unless $K \approx K_{\rm max}$ our universe would be extremely unlikely to occur. Notice that the conclusion could be different if the *no boundary condition* of Hartle and Hawking were to be assumed [180].

5.2.3. Discussion

In this section, we have addressed the semi-classical solution of a spatially closed universe where, in addition to the kinetic and potential energy density of the scalar field, we account for a contribution from the spatial curvature. In the context of the Third Quantisation of the multiverse filled by a minimally coupled scalar field, such a scenario corresponds to the semi-classical evolution of each individual universe created as the multiverse evolves. By considering the contribution of the (negative) curvature term, we observed how, when the kinetic energy of the scalar field is low enough, the effective Friedmann equation describes three separate regions of space-time: (I) a baby universe that

grows to a maximum size and then collapses on itself and (III) a large asymptotically de Sitter universe that shrinks to a minimum size and then starts to inflate eternally, separated by (II) a Euclidean region which we identified as a wormhole solution. The existence of this wormhole suggests that, while regions I and III are classically disconnected, they are linked by quantum effects. Therefore, we can consider the scenario where a baby universe reaches its maximum size but, instead of starting to collapse, quantum tunnels through the Euclidean region and emerges as a de Sitter-like inflating universe. Using appropriate variable substitutions, we have obtained analytical expressions for the background solutions for the evolution of the scale factor in each of the three regions. Such solutions can be seen as a generalisation of the ones found for Giddings–Strominger's instanton [167] and for Vilenkin's proposal of *creation from nothing* [341].

In addition to the background solutions, we have computed the probability for a baby universe to tunnel through the Euclidean region using the transition amplitude proposed in [341, 342]. These results, represented in Fig. 5.4 show that the probability for transition increases with higher values of the kinetic energy of the scalar field, parameterised by K, and higher values of the energy density during the inflationary regime at large a, which is parameterised by $\gamma := \hbar^2 H_{\rm dS}^2/M_{\rm P}^2$. This effect can be understood by the fact that the potential barrier created by the curvature term (cf. Fig. 5.1) decreases in width and amplitude when one of these parameters increases. Since current bounds set the scale of inflation at 8.8×10^{13} GeV [48] we find that $\gamma \lesssim 5.2 \times 10^{-11}$. For such a small value, the probability of quantum tunnelling for a baby universe is extremely suppressed[14] unless $K \sim K_{\rm max}$. Assuming that this was how our Universe came to existence, this extremely low value suggests that either ours is a case with high values of K, or that the rate of production of low-K universes is high enough that the probability of at least one baby universe to overcome the quantum barrier is close to one.

5.3. Cosmological Perturbations in a toy model I

In the previous sections, we have reviewed several models, cf. Eqs. (5.57) and (5.68), for a semi-classical universe where the Friedmann equation has the functional form

$$\left(\frac{a'}{a}\right)^2 = a^2 H_{\rm dS}^2 \left[1 - \frac{\mathcal{K}}{(aH_{\rm dS})^2} + \frac{Q^2}{(aH_{\rm dS})^\beta}\right] . \tag{5.103}$$

Here, we remind that a prime indicates a derivative with respect to the conformal time η. The first term inside the brackets on the r.h.s. of Eq. (5.103) leads to an asymptotic de Sitter phase with energy density $\rho_{\rm dS} = 3H_{\rm dS}^2/\kappa^2$ at large values of the scale factor. The second term comes from the curvature of the spatial hypersurfaces and in the third term Q is a dimensionless positive parameter that determines the strength of a pre-inflationary epoch during which the effective EoS parameter is given by $w = -1 + \beta/3$. For $\beta = 6$, $\beta = 4$ and $\beta = 3$, the pre-inflationary epoch in Eq. (5.103) mimics the behaviour of a stiff-matter, radiation and dust dominated universe, respectively.

We are now interested in considering the evolution of the cosmological perturbations in these models. As a first approach, we will treat the problem in the framework of quantum linear cosmological perturbations around a (semi) classical background and, for simplicity, we will disregard the curvature

[14] Notice that in Eq. (5.102) a factor $-\gamma^{-1}$ appears on the exponent of the tunnelling probability.

term. To treat the evolution of the quantum perturbations, we employ the quantum operator[15] constructed from the Mukhanov-Sasaki variable $v := a[\delta\varphi + (\varphi'/\mathcal{H})\psi]$, which in single field inflation models encodes all the information of the scalar sector (up to first order in the perturbations). Following the usual procedure of quantum field theory, the operator $\hat{v}$ can be expanded in k-modes as

$$\hat{v}(\eta, \vec{x}) = \int \frac{\mathrm{d}^3\vec{k}}{(2\pi)^{3/2}} \left[v_{\vec{k}}(\eta)\, \mathrm{e}^{\mathrm{i}\vec{k}\cdot\vec{x}} \hat{a}^-_{\vec{k}} + v^*_{\vec{k}}(\eta)\, \mathrm{e}^{-\mathrm{i}\vec{k}\cdot\vec{x}} \hat{a}^+_{\vec{k}} \right] , \tag{5.104}$$

where $a^-_{\vec{k}}$ and $a^+_{\vec{k}}$ are time-independent annihilation and creation operators for quanta of $\hat{v}$ and the mode functions $v_{\vec{k}}$ satisfy the evolution equation [53, 267]

$$v''_{\vec{k}} + \left(k^2 - \frac{z''}{z} \right) v_{\vec{k}} = 0 , \tag{5.105}$$

and the normalisation condition [53, 267]

$$v_{\vec{k}} v^{*\prime}_{\vec{k}} - v_{\vec{k}}{}' v^*_{\vec{k}} = \mathrm{i}\hbar . \tag{5.106}$$

Since the mode equation (5.105) and the normalisation condition (5.106) depend only on the magnitude of $\vec{k}$ and not on its direction, in the rest of the chapter we will use the subscript k instead of $\vec{k}$.

In inflationary models with no pre-inflationary effects, it is customary to fix the initial conditions for the mode functions by imposing that in the asymptotic past the Bunch-Davies vacuum solution [94, 115, 313]

$$v_k \simeq \sqrt{\frac{\hbar}{2k}}\, \mathrm{e}^{-\mathrm{i}k(\eta-\eta_0)} , \tag{5.107}$$

is recovered. However, if one introduces a pre-inflationary epoch, imposing these initial conditions may be no longer valid and, in addition, the amplitude of the modes at the moment of horizon crossing during inflation could differ widely from the initial prediction. Such variations can have consequences for the late-time evolution of the Universe, since these quantum fluctuations are the seeds that lead to the Large Scale Structure observed today. In the following sections, we present the results obtained regarding the study of the effects of a pre-inflationary epoch in the models described by Eq. (5.103) on the primordial power spectrum [49]

$$\mathcal{P}_{\mathcal{R}}(k) = \frac{k^3}{2\pi^2} |\mathcal{R}_k|^2 = \frac{k^3}{2\pi^2} \frac{|v_k|^2}{z^2} , \tag{5.108}$$

and on the normalised angular power spectrum of the temperature-temperature polarisation of the CMB [15, 352]

$$D^{TT}_\ell = \int_0^{+\infty} \frac{\mathrm{d}k}{k} [\Delta^s_{l,T}(k)]^2 \mathcal{P}_{\mathcal{R}}(k) . \tag{5.109}$$

Here, ℓ is the multipole number and the transfer function $\Delta^s_{l,T}$ contains all the information regarding the evolution of the classical perturbations after the end of inflation and till the moment of the last

[15] In the Appendix D.3, we review the canonical quantisation procedure of the Mukhanov-Sasaki variable.

scattering surface. The results we present next were first published in Refs. [82, 266].

5.3.1. The Model

Cosmological observations of the CMB show that at the end of inflation the primordial power spectrum, $\mathcal{P}_{\mathcal{R}}$, had a near scale-invariant shape with a red tilt, $n_s < 1$, inferred at more than 5σ confidence level [15]. Such a value excludes a pure de Sitter inflationary scenario which lead us to relax the asymptotic de Sitter behaviour in Eq. (5.103) and replace the constant term $H_{\rm dS}^2$ by a power of the scale factor $H_{\rm dS}^2(a_*/a)^\alpha$, where a_* is a reference scale. For positive but small values of α, this power-law inflation behaviour leads to a slightly red-tilted $P_{\mathcal{R}}$ compatible with observations[16]. With these considerations in mind and after dropping the curvature term, we rewrite Eq. (5.103) as

$$H^2 = H_{\rm dS}^2 \left[\left(\frac{a_*}{a} \right)^\alpha + \frac{Q^2}{(aH_{\rm dS})^\beta} \right] , \tag{5.110}$$

where $H := \dot{a}/a$ is the Hubble rate. The second term on the r.h.s. of the new Friedmann equation (5.110) leads to a decelerated initial epoch if $\beta > 2$. In such a case, the comoving wavenumber of the Hubble horizon, $k_H := aH$, reaches the minimum value [82]

$$k_{\rm min} := a_* H_{\rm dS} \left[\frac{\beta - \alpha}{2 - \alpha} \left(\frac{2 - \alpha}{\beta - 2} \right)^{\frac{\beta-2}{\beta-\alpha}} \right]^{\frac{1}{2}} \left[\frac{Q^2}{(a_* H_{\rm dS})^\beta} \right]^{\frac{1}{2}\frac{2-\alpha}{\beta-\alpha}} , \tag{5.111}$$

when the scale factor reaches the value [82]

$$a_{\rm trans} := a_* \left[\frac{\beta - 2}{2 - \alpha} \frac{Q^2}{(a_* H_{\rm dS})^\beta} \right]^{\frac{1}{\beta-\alpha}} , \tag{5.112}$$

during the transition from the initial decelerated epoch to inflation. Here, we recall that we are considering values $0 \lesssim \alpha < 1$ and $\beta > 2$, therefore the parameters $k_{\rm min}$ and $a_{\rm trans}$ are always real valued and positive.

For small values of the scale factor, $a \ll a_{\rm trans}$, the first term on the r.h.s. of (5.110) is negligible and we obtain the scaling behaviour $H^2 \propto a^{-\beta}$. In this case, the potential z''/z tracks the squared comoving Hubble wavenumber k_H^2 as

$$\frac{z''}{z} \simeq \left(2 - \frac{\beta}{2} \right) k_H^2 . \tag{5.113}$$

As discussed in the Appendix D.3, the general solution for the mode functions v_k in this case can be

[16] Despite having attractive features like a simple shape for $P_{\mathcal{R}}$ and the availability of analytical solutions for the perturbations in single-field models, power-law inflation [241, 242] is ruled out by observations due to the high values of tensor-to-scalar ratio that they predict [15]. Nevertheless, while we wait for the detection of cosmological gravitational waves, power-law inflation models continue to be a good toy models to analyse pre-inflationary effects in the scalar sector.

written in terms of Hankel functions [7, 283] as

$$v_k = \frac{\sqrt{\pi\hbar(\eta-\eta_c)}}{2}\left(B_{1,k}\,H_\nu^{(1)}\left[k(\eta-\eta_c)\right] + B_{2,k}\,H_\nu^{(2)}\left[k(\eta-\eta_c)\right]\right). \tag{5.114}$$

Here, the minimum conformal time η_c and the order of the Hankel functions are defined as

$$\eta_c = \eta_1 - \frac{2}{\beta-2}\frac{1}{a(\eta_1)H(\eta_1)}, \qquad \lambda := \frac{1}{2}\frac{6-\beta}{\beta-2}, \tag{5.115}$$

where η_1 is an arbitrary integration constant and the linear coefficients satisfy the relation

$$|B_{1,k}|^2 - |B_{2,k}|^2 = -1, \tag{5.116}$$

which is derived from the normalisation condition (5.106). The Bunch-Davies vacuum solution (5.107), minus an arbitrary phase with no physical implication, is recovered in the asymptotic future, $1 \ll k(\eta-\eta_c)$, for the choice of coefficients $|B_{2,k}| = 1$ and $B_{1,k} = 0$. In the numerical calculations that we present in the following sections, this will be the choice of the linear coefficients used for setting the initial conditions of the perturbations during the pre-inflationary epoch.

In the opposite asymptotic regime, $a_* \ll a$, the first term on the r.h.s. of (5.110) becomes dominant and we recover a period of power-law inflation $H^2 \propto a^{-\alpha}$. As in the previous case, the potential z''/z tracks the comoving Hubble horizon

$$\frac{z''}{z} \simeq \left(2-\frac{\alpha}{2}\right)k_H^2, \tag{5.117}$$

and the general solution for the mode functions is

$$v_k = \frac{\sqrt{\pi\hbar(\eta_c-\eta)}}{2}\left[C_{1,k}\,H_\nu^{(1)}\left[k(\eta_c-\eta)\right] + C_{2,k}\,H_\nu^{(2)}\left[k(\eta_c-\eta)\right]\right], \tag{5.118}$$

with

$$\eta_c = \eta_1 + \frac{2}{2-\alpha}\frac{1}{a(\eta_1)H(\eta_1)}, \qquad \lambda := \frac{1}{2}\frac{6-\alpha}{2-\alpha}. \tag{5.119}$$

Notice that in this case the conformal time is defined only for $\eta < \eta_c$ and η_c corresponds to the asymptotic future. The linear coefficients $C_{i,k}$, with $i = 1, 2$, satisfy the constraint

$$|C_{1,k}|^2 - |C_{2,k}|^2 = 1. \tag{5.120}$$

The Bunch-Davies solution can be recovered in the asymptotic past, when $1 \ll k(\eta_c-\eta)$, if we choose $|C_{1,k}| = 1$ and $C_{2,k} = 0$.

5.3.2. Parameters of the model

As stated above, we fix the initial conditions for the modes v_k during the pre-inflationary era by requiring that the BD vacuum is recovered in the limit of $1 \ll k\eta$ (cf. Eq. (5.107) and the asymptotic behaviour of (5.114)). For modes with wavenumber below $k_{\rm min}$, this regime is never achieved and

we expect to find strong modifications in the primordial power spectrum. However, for modes with $k_{\rm min} \ll k$ there should be enough time between the first Horizon crossing during the pre-inflationary era and the onset of inflation for the mode to reach the BD solution before exiting the Hubble horizon. In this regime, we expect to recover the theoretical predictions for the primordial power spectrum $\mathcal{P}_{\mathcal{R}}$. We can then use this result to fix some of the parameters of our model $\{H_{\rm dS},\, a_*,\, \alpha,\, Q\}$ presented in Eq. (5.110). As we will show below, under certain considerations this strategy allows us to use the cosmological observations to fix all but one of the initial parameters.

As long as $Q \ll (a_* H_{\rm dS})^\beta$, the second term on the r.h.s. of (5.110) becomes negligible for $a \gtrsim a_*$ and the wavenumber of the mode that crosses the horizon at a_* verifies $k \approx a_* H_{\rm dS} \gg k_{\rm min}$. As such, and as long as $z''/z \ll (a_* H_{\rm dS})^2$ during the transition from decelerated expansion to inflation, we can assume that power-law inflation predictions for the primordial power spectrum are recovered for $k \gtrsim a_* H_{\rm dS}$, i.e.:

$$\mathcal{P}_{\mathcal{R}}(k \gtrsim a_* H_{\rm dS}) \approx \mathcal{P}^*_{\mathcal{R}} \left(\frac{k}{a_* H_{\rm dS}}\right)^{-\frac{2\alpha}{2-\alpha}} , \tag{5.121}$$

where

$$\mathcal{P}^*_{\mathcal{R}} = \frac{(2-\alpha)^{\frac{4}{2-\alpha}}}{2\pi\alpha} \left(\frac{\Gamma\left(\frac{1}{2}\frac{6-\alpha}{2-\alpha}\right)}{\Gamma\left(\frac{3}{2}\right)}\right)^2 \frac{\hbar^2 H^2_{\rm dS}}{M^2_{\rm P}} . \tag{5.122}$$

If we compare (5.121) with the observational fit of the Planck mission [16] and use the freedom in choosing the value of a_* to fix $k_* = a_* H_{\rm dS}$, we can write the parameters $\{H_{\rm dS},\, a_*,\, \alpha\}$ in terms of the cosmological parameters $\{n_s,\, A_s,\, k_*\}$ as

$$\alpha = 2\frac{1-n_s}{3-n_s} , \tag{5.123}$$

$$H_{\rm dS} = \frac{\pi}{2}\frac{\sqrt{(1-n_s)\, A_s}}{\Gamma\left(2-n_s/2\right)} \left(\frac{3-n_s}{4}\right)^{1-\frac{n_s}{2}} \frac{M_{\rm P}}{\hbar} , \tag{5.124}$$

$$a_* = \frac{2k_*}{\pi}\frac{\Gamma\left(2-n_s/2\right)}{\sqrt{(1-n_s)\, A_s}} \left(\frac{3-n_s}{4}\right)^{\frac{n_s}{2}-1} \frac{\hbar}{M_{\rm P}} . \tag{5.125}$$

Notice that these relations are independent of the value of β and are valid as long as the condition $Q \ll (a_* H_{\rm dS})^\beta$ holds. Using the 2015 constraints from the Planck mission in combination with lensing effects and external data (BAO+JLA+H0) [16], we then find

$$\alpha \simeq 0.03275 , \qquad H_{\rm dS} \simeq 1.055 \times 10^{-5}\, (M_{\rm P}/\hbar) , \qquad a_* \simeq 2.099 \times 10^{7}\, (\hbar/M_{\rm P}) . \tag{5.126}$$

As reference, we note that the present day values for the Hubble rate and scale factor are $H_0 \approx 1.184 \times 10^{-61}\, (M_{\rm P}/\hbar)$ and $a_0 = H_0^{-1} \approx 8.449 \times 10^{60}\, (\hbar/M_{\rm P})$. With these values, the corresponding wavenumbers are $k_0 = 1$ and $k_* \approx 221.3$. Notice that k_0 and k_* are dimensionless due to the fact that the scale factor has dimensions of length and we are considering $c = 1$.

At this point we have fixed three of the four initial parameters of the model, leaving only Q as a free parameter. This parameter must satisfy the initial assumption $Q \ll (a_* H_{\rm dS})^\beta$ in order to validate

the analysis presented in this subsection. Nevertheless, by looking at the shape of the potential z''/z during the transition between the two asymptotic epochs, we can derive more strict bounds on Q, such that imprints of the pre-inflationary epoch appearing in the primordial power spectrum satisfy the observational constraints. We now show how this can be achieved for the three particular cases of interest: $\beta = 6$; $\beta = 4$ and $\beta = 3$.

Case 1: $\beta = 6$ (stiff matter)

The first case we analyse is that of $\beta = 6$, in which the Q-term in Eq. (5.110) leads to a pre-inflationary epoch that mimics a stiff-matter-dominated universe. The appearance of this extra term in the Friedmann equation was obtained in [266] via the momentum of the scalar field[17]. Classically, this new term corresponds to the kinetic energy density of the scalar field, which means that the initial epoch would be one of kinetic domination. An alternative way of obtaining a similar initial epoch is by considering a model of interacting universes with a specific type of interaction coupling [82, 302]. In that case, we can obtain a pre-inflationary era where $H^2 \propto a^{-6}$, while maintaining an extreme slow-roll regime for the scalar field in which the potential energy density remains approximately constant during the interval of evolution even if $V(\varphi)$ is not asymptotically flat.

In order to set lower and upper bounds on Q we analyse the shape of the comoving wavenumber of the Hubble horizon, k_H^2, and the potential z''/z. In Fig. 5.5, we plot k_H^2 and z''/z (left upper panel) as well as their ratio (left lower panel) around the transition from decelerated expansion to inflation. In the asymptotic regions, the potential z''/z tracks k_H^2 according to Eqs. (5.113) and (5.117). However, near the transition we observe the presence of two prominent bumps; a first smaller bump appears close to the moment of no acceleration and a second larger one is visible when inflation is already under way. As the value of the free parameter Q increases, the minimum of k_H^2 and the bumps in the potential z''/z are shifted upwards up, affecting higher wavenumbers, as can be seen on the r.h.s. panel of Fig. 5.5.

We expect that the shape of the potential z''/z can be related to potential imprints on the primordial power spectrum. In order to check this assumption, we define three extra wavenumbers, apart from $k_{\rm min}$, that characterise the model (cf. left lower panel of Fig. 5.5):

a) We define $k_{\rm a}$ as the mode that crosses the potential z''/z when the ratio $(z''/z)/k_H^2$ reaches the local minimum before the transition to inflation. Through numerical investigation we find $k_{\rm a} \simeq 2.149 k_{\rm min}$ independently of the value of Q.

b) We define $k_{\rm b}$ as the mode that crosses the potential z''/z when the ratio $(z''/z)/k_H^2$ reaches the local maximum after the beginning of inflation. Through numerical investigation we find $k_{\rm b} \simeq 3.548 k_{\rm min}$ also independently of the parameter Q.

c) Additionally, we consider $k_{\rm c} := 10 k_{\rm min}$ since when this mode crosses the potential z''/z, the ratio $(z''/z)/k_H^2$ has already reached (approximately) its asymptotic value during inflation.

When computing the primordial power spectrum at the end of inflation, we will look for imprints around $k_{\rm min}$, $k_{\rm a}$, $k_{\rm b}$ and $k_{\rm c}$. In particular, since the potential z''/z has already reached its asymptotic shape when the mode $k_{\rm c}$ crosses the horizon, we expect that any deviation from the prediction of power-law inflation for the primordial power spectrum should appear only in the range $k \lesssim k_{\rm c}$. Thus,

[17] Notice that $Q = \tilde{K}$ in the notation of [266].

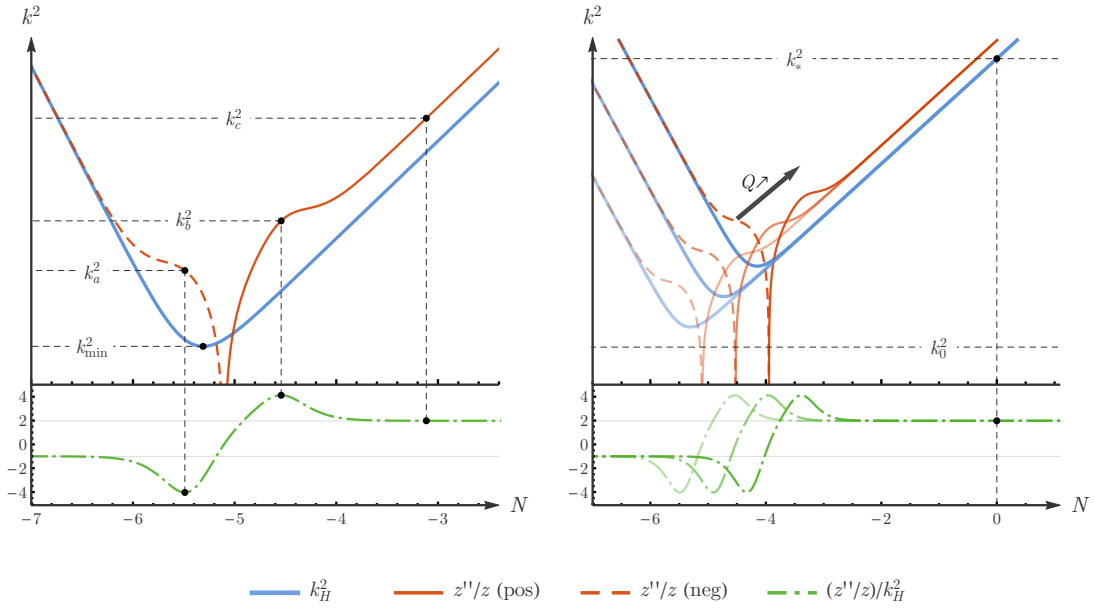

Figure 5.5.: Evolution of the squared comoving Hubble horizon, k_H^2, the potential z''/z and of the ratio $(z''/z)/k_H^2$ for the model (5.110) with $\beta = 6$ around the period of transition from the decelerated pre-inflationary epoch to the later power-law inflation. (Left panel) The four wavenumbers that characterise the model: $k_{\rm min}$, $k_{\rm a}$, $k_{\rm b}$ and $k_{\rm c}$; are defined based on the shape of k_H^2, z''/z and $(z''/z)/k_H^2$. (Right panel) As the value of the free parameter Q increases, the characteristic shape of k_H^2 and z''/z during the transition to inflation starts to affect increasingly higher wavenumbers. In order for imprints of the model to appear on the observable range of wavenumbers while at the same time satisfying observational constraints, $k_{\rm c}$ should be above k_0 but well below k_*.

if we are to leave $\mathcal{P}_\mathcal{R}$ unaffected for $k \gtrsim k_*$, $k_{\rm c}$ should be well below the pivot scale. On the other hand, in order for any imprints to appear on the observable range of wavenumbers, $k_{\rm c}$ should be above the wavenumber corresponding to the Hubble horizon at the present time, k_0. By imposing that $k_0 \lesssim k_{\rm c} \ll k_*$, we arrive at the following lower and upper bounds for the free parameter Q:

$$2.730 \times 10^{-11} k_*^3 \lesssim Q \ll 3.541 \times 10^{-4} k_*^3 \,, \tag{5.127}$$

or, equivalently,

$$2.958 \times 10^{-4} k_0^3 \lesssim Q \ll 3.837 \times 10^{3} k_0^3 \,. \tag{5.128}$$

If we insert these values in Eq. (5.112) we are able to calculate the number of e-folds of inflation before $a = a_*$ as:

$$2.544 < \log\left(\frac{a_*}{a_{\rm trans}}\right) \lesssim 8.034 \,. \tag{5.129}$$

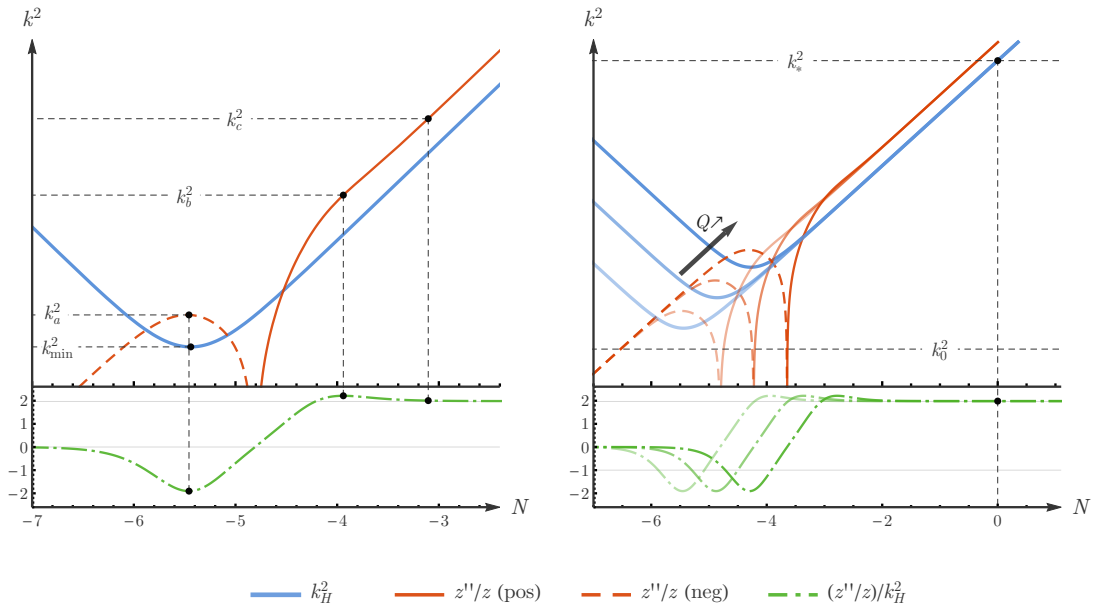

Figure 5.6.: Evolution of the squared comoving Hubble horizon, k_H^2, the potential z''/z and of the ratio $(z''/z)/k_H^2$ for the model (5.110) with $\beta = 4$ around the period of transition from the decelerated pre-inflationary epoch to the later power-law inflation. (Left panel) The four wavenumbers that characterise the model: $k_{\rm min}$, $k_{\rm a}$, $k_{\rm b}$ and $k_{\rm c}$; are defined based on the shape of k_H^2, z''/z and $(z''/z)/k_H^2$. (Right Panel) As the value of the free parameter Q increases, the characteristic shape of k_H^2 and z''/z during the transition to inflation starts to affect increasingly higher wavenumbers. In order for imprints of the model to appear on the observable range of wavenumbers while at the same time respecting the constraints for $\mathcal{P}_{\mathcal{R}}$, the characteristic scale $k_{\rm c}$ should be above k_0 but well below k_*.

Case 2: $\beta = 4$ (radiation)

The second case we consider is that of $\beta = 4$, where the Q-term[18] in the Friedmann equation (5.110) leads to a pre-inflationary epoch that mimics a radiation-dominated universe. In Ref. [82], this kind of behaviour is obtained by introducing an interaction between universes where the universe-universe couplings (cf. Eq. (5.68)) have specific dependence on the scale factor.

As in the previous case, we look at the shape of the potential z''/z around the transition to the inflationary era for clues on which range of wavenumbers the primordial power spectrum may have imprints of the pre-inflationary era. We find a first bump in z''/z near the point of no acceleration, followed by a second bump after inflation begins (cf. the left upper of Fig. 5.6) which now appears much less pronounced and can be better identified by analysing the ratio $(z''/z)/k_H^2$ (left lower panel of Fig. 5.6). As in the previous case, the minimum of the comoving Hubble horizon and the bumps of the potential are shifted to higher wavenumbers when the free parameter Q is increased.

As before, we introduce three extra wavenumbers, apart from $k_{\rm min}$, that characterise the model:

a) We define $k_{\rm a}$ as the wavenumber of the mode that crosses the potential z''/z when the ratio

[18] In Ref. [82], we employed the notation Q_K for the parameter Q.

$(z''/z)/k_H^2$ reaches the local minimum before the transition to inflation. Using a numerical analysis, we find $k_{\rm a} \simeq 1.381 k_{\rm min}$ independently of the value of Q.

b) We define $k_{\rm b}$ as the wavenumber of the mode that crosses the potential z''/z when the ratio $(z''/z)/k_H^2$ reaches the local maximum after the beginning of inflation. Using a numerical analysis, we find $k_{\rm b} \simeq 4.626 k_{\rm min}$ independently of the value of the parameter Q.

c) We consider $k_{\rm c} := 10 k_{\rm min}$ since when the respective mode crosses the potential z''/z, the ratio $(z''/z)/k_H^2$ has already reached (approximately) its asymptotic value during inflation.

If we consider values of the characteristic wavenumber within the range $k_0 \lesssim k_{\rm c} \ll k_*$, so that imprints on the power spectrum appear in the observable range without violating observational constraints, we obtain the following lower and upper bounds for the free parameter Q:

$$8.931 \times 10^{-8} k_*^2 \lesssim Q \ll 4.784 \times 10^{-3} k_*^2 \,, \tag{5.130}$$

or

$$4.373 \times 10^{-3} k_0^2 \lesssim Q \ll 2.343 \times 10^{2} k_0^2 \,. \tag{5.131}$$

Inserting the constraint (5.131) in Eq. (5.112) allows us to limit the number of e-folds of inflation before $a = a_*$ as:

$$2.689 < \log\left(\frac{a_*}{a_{\rm trans}}\right) \lesssim 8.178 \,. \tag{5.132}$$

Case 3: $\beta = 3$ (dust)

The third and last case we analyse is $\beta = 3$, in which a pre-inflationary epoch mimics a dust-dominated universe. This type of behaviour was studied in [82], where the Q-term in (5.110) appears due to the introduction of a phenomenological two-universe interaction with a specific a-dependence of the coupling (cf. Eq. (5.68)). When analysing the shape of z''/z to try to impose bounds on Q, we now find that while the potential still has a bump near the moment of no acceleration, no second bump in z''/z and $(z''/z)/k_H^2$ appears after the beginning of inflation, as can be seen in Fig. 5.7. As expected, higher values of the free-parameter Q shift the features of the k_H^2 and z''/z upwards, thus the effects of the pre-inflationary epoch should be seen at higher wavenumbers.

As in the previous cases, we define extra characteristic wavenumbers based on the shape of the potential z''/z around the transition (cf. left lower panel of Fig. 5.7):

a) We define $k_{\rm a}$ as the wavenumber of the mode that crosses the potential z''/z when the ratio $(z''/z)/k_H^2$ reaches the local minimum before the transition to inflation. Through a numerical study, we find $k_{\rm a} \simeq 1.001 k_{\rm min}$ independently of the value of Q. Notice that since $k_{\rm a}$ coincides with $k_{\rm min}$ it does not introduce a new characteristic scale of the model.

b) In this case no local maximum appears in $(z''/z)/k_H^2$ after the transition to inflation. As such, we do not define $k_{\rm b}$ for $\beta = 3$.

c) We consider $k_{\rm c} := 10 k_{\rm min}$ since when the respective mode crosses the potential z''/z, the ratio $(z''/z)/k_H^2$ has already reached (approximately) its asymptotic value during inflation.

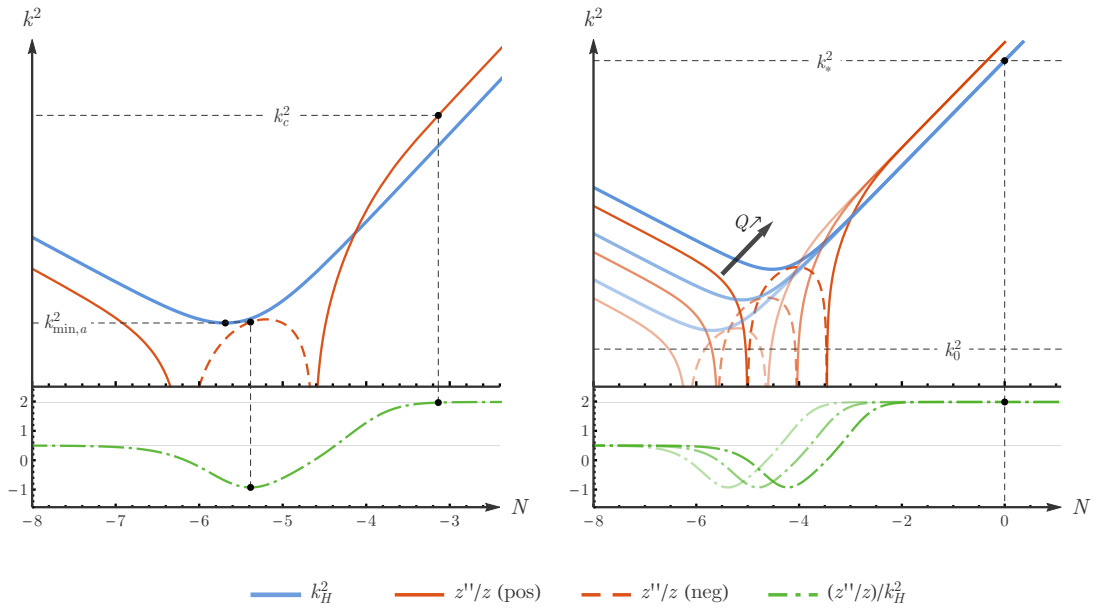

Figure 5.7.: Evolution of the squared comoving Hubble horizon, k_H^2, the potential z''/z and of the ratio $(z''/z)/k_H^2$ for the model (5.110) with $\beta = 3$ around the period of transition from the decelerated pre-inflationary epoch to the later power-law inflation. (Left panel) Based on the shape of k_H^2, z''/z and $(z''/z)/k_H^2$, two characteristic wavenumbers can be defined: k_{min} and k_{c} ($k_{\mathrm{a}} \approx k_{\mathrm{min}}$). Contrary to the previous cases, no bump in the shape of z''/z appears after the onset of inflation. (Right panel) As the value of the free parameter Q increases, the characteristic shape of k_H^2 and z''/z during the transition to inflation starts to affect increasingly higher wavenumbers. In order for imprints of the model to appear on the observable range of wavenumbers while at the same time fulfilling the constraints for $\mathcal{P}_{\mathcal{R}}$, the characteristic scale k_{c} should be above k_0 but well below k_*.

Using k_{c} as a reference value for the maximum wavenumber with imprints of the model, we are able to define the following lower and upper bounds for the free parameter Q so that effects from the pre-inflationary epoch appear on the primordial power spectrum in the range of observable modes, while at the same time respecting the constraints around the pivot scale:

$$5.564 \times 10^{-6} k_*^{3/2} \lesssim Q \ll 1.916 \times 10^{-2} k_*^{3/2}\,, \tag{5.133}$$

or

$$1.832 \times 10^{-2} k_0^{3/2} \lesssim Q \ll 6.307 \times 10^{1} k_0^{3/2}\,. \tag{5.134}$$

Finally, through substitution in Eq. (5.112) we obtain the number of e-folds of inflation before $a = a_*$:

$$2.894 < \log\left(\frac{a_*}{a_{\mathrm{trans}}}\right) \lesssim 8.383\,. \tag{5.135}$$

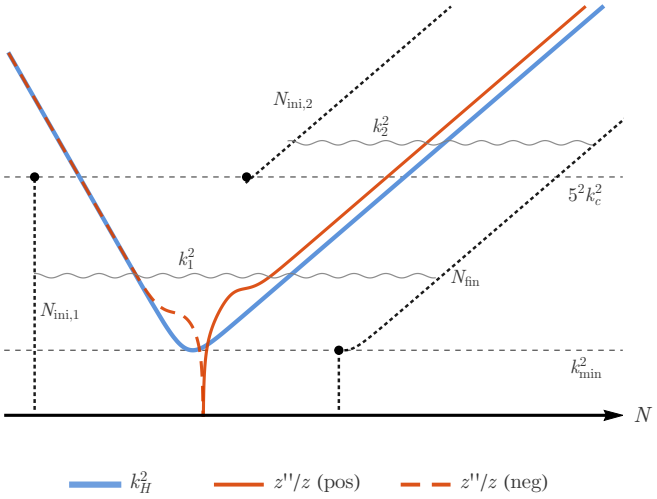

Figure 5.8.: The initial conditions for the numerical integration are set for each mode depending on whether the wavenumber k is above or below the threshold $5k_{\rm c}$. For modes with wavenumber $k_1 < 5k_{\rm c}$, the initial conditions are set at $N_{\rm ini,1}$ well during the pre-inflationary epoch. For modes with higher wavenumber $5k_{\rm c} < k_2$, the initial conditions are set at some $N_{\rm ini,2}$ e-folds before the mode exits the Hubble horizon during inflation. After the mode exits the horizon, at $N_{\rm fin}$, the numerical integration is stopped. For the modes with lowest wavenumbers $k < k_{\rm min}$ the stopping point is the same as for $k_{\rm min}$.

5.3.3. Numerical Results

The mode equation (5.105) is a second order linear differential equation for a one-dimensional complex variable. In order to solve this equation numerically, we follow the same decomposition strategy employed in Refs. [74–76, 83, 183, 258, 263] and therefore we introduce the variables

$$X_k := \frac{1}{\hbar^{1/2}} v_k \,, \qquad\qquad Y_k := -\frac{1}{\mathrm{i}k} X_k' \,. \tag{5.136}$$

This allows us to re-write the mode equation as a set of two first order linear differential equations:

$$X_k' = -\mathrm{i}kY_k \,, \qquad\qquad Y_k' = -\frac{\mathrm{i}}{k}\left(k^2 - \frac{z''}{z}\right) X_k \,. \tag{5.137}$$

In addition, the normalisation condition (5.106) becomes

$$X_k Y_k^* + X_k^* Y_k = \frac{1}{k} \,. \tag{5.138}$$

If we further decompose X_k and Y_k into their real and imaginary components: $X_k^{\rm re}$, $X_k^{\rm im}$, $Y_k^{\rm re}$ and $Y_k^{\rm im}$; and change the time variable from the conformal time η to the number of e-folds $N := \log(a/a_*)$,

$\mathbf{i}$	$\mathbf{Q_i}$ $(\beta = 6)$	$\mathbf{Q_i}$ $(\beta = 4)$	$\mathbf{Q_i}$ $(\beta = 3)$
1	$1.78 \times 10^{-4} k_0^3$	$3.16 \times 10^{-3} k_0^2$	$1.33 \times 10^{-2} k_0^{3/2}$
2	$1.00 \times 10^{-3} k_0^3$	$1.00 \times 10^{-2} k_0^2$	$3.16 \times 10^{-2} k_0^{3/2}$
3	$5.62 \times 10^{-3} k_0^3$	$3.16 \times 10^{-2} k_0^2$	$7.50 \times 10^{-2} k_0^{3/2}$
4	$3.16 \times 10^{-2} k_0^3$	$1.00 \times 10^{-1} k_0^2$	$1.78 \times 10^{-1} k_0^{3/2}$
5	$1.78 \times 10^{-1} k_0^3$	$3.16 \times 10^{-1} k_0^2$	$4.22 \times 10^{-1} k_0^{3/2}$
6	$1.00 \times 10^{0} k_0^3$	$1.00 \times 10^{0} k_0^2$	$1.00 \times 10^{0} k_0^{3/2}$
7	$5.63 \times 10^{0} k_0^3$	$3.16 \times 10^{0} k_0^2$	$2.37 \times 10^{0} k_0^{3/2}$
8	$3.16 \times 10^{1} k_0^3$	$1.00 \times 10^{1} k_0^2$	$5.62 \times 10^{0} k_0^{3/2}$
$\mathbf{Q_{min}}$	$2.96 \times 10^{-4} k_0^3$	$4.37 \times 10^{-3} k_0^2$	$1.83 \times 10^{-2} k_0^{3/2}$
$\mathbf{Q_{max}}$	$3.84 \times 10^{3} k_0^3$	$2.34 \times 10^{2} k_0^2$	$6.31 \times 10^{1} k_0^{3/2}$

Table 5.1.: The values of the free parameter, Q_i, for each of the eight numerical runs, as defined in Eq. (5.141). For completeness, the values $Q_{\rm min}$ and $Q_{\rm max}$, which correspond to the upper and lower bounds in (5.128), (5.131) and (5.134) are also shown.

we obtain the following four-dimensional system of first-order linear differential equations

$$\frac{\mathrm{d}}{\mathrm{d}N}\begin{pmatrix} X_k^{\rm re} \\ X_k^{\rm im} \\ Y_k^{\rm re} \\ Y_k^{\rm im} \end{pmatrix} = \frac{k}{k_H}\begin{pmatrix} 0 & 0 & 0 & 1 \\ 0 & 0 & -1 & 0 \\ 0 & \left(1 - \frac{1}{k^2}\frac{z''}{z}\right) & 0 & 0 \\ -\left(1 - \frac{1}{k^2}\frac{z''}{z}\right) & 0 & 0 & 0 \end{pmatrix} \cdot \begin{pmatrix} X_k^{\rm re} \\ X_k^{\rm im} \\ Y_k^{\rm re} \\ Y_k^{\rm im} \end{pmatrix} , \tag{5.139}$$

subjected to the constraint

$$2k\left(X_k^{\rm re}Y_k^{\rm re} + X_k^{\rm im}Y_k^{\rm im}\right) = 1\,. \tag{5.140}$$

To set the initial conditions for the numerical integrations, we use the characteristic wavenumber $k_{\rm c}$, whose value for each β was introduced in the previous section, to define two ranges of modes:

I) For $k < 5k_{\rm c}$, we set the initial conditions for the perturbations deep inside the pre-inflationary era, at $N = N_{\rm ini,1}$ (cf. the mode k_1 in Fig. 5.8). The initial values of the integration variables are fixed using the solutions (5.114) for $\beta = 6, 4, 3$ and setting $B_{1,k} = 0$ and $B_{2,k} = 1$. This choice for the linear coefficients ensures that the BD vacuum solution is recovered for modes well inside the Hubble horizon.

II) For $5k_{\rm c} < k$, we assume that the modes have time to reach a BD vacuum state before the onset of inflation. Therefore, we use the solutions (5.118) for $\beta = 6, 4, 3$, with $C_{1,k} = 1$ and $C_{2,k} = 0$ to specify the initial values of the integration variables some $N_{\rm ini,2}$ e-folds before the moment of horizon crossing (cf. the mode k_2 in Fig. 5.8).

The convergence of the numerical solutions is ensured by stopping the numerical integration not at horizon crossing but some $N_{\rm fin}$ e-folds after the mode has exited the comoving Hubble horizon, as

shown in Fig. 5.8. For modes that verify $k < k_{\rm min}$, which never cross the comoving Hubble horizon, we stop the integration at the same moment as for $k_{\rm min}$.

Using the method aforementioned, we have performed eight numerical runs for each $\beta = 6, 4, 3$ and fixing the value of the free parameter Q as

$$Q_i = 10^{\frac{\beta}{4}\left(\frac{i}{2}-3\right)} k_0^{\frac{\beta}{2}} \,, \tag{5.141}$$

with $i = 1, 2, \ldots, 8$. In Tab. 5.1 we present the numerical value of each Q_i for each run. We note that all values are well below the upper limits defined for each respective β. From the results of the numerical integrations, we have computed the primordial power spectrum $\mathcal{P}_{\mathcal{R}}$ at the end of inflation and, using the CLASS code [63, 227], we obtained the normalised angular power spectrum D_ℓ^{TT} [15] for each numerical run. The baseline 6-parameter ΛCDM model was assumed for the late-time cosmology and the values of its parameters are the ones found from the best-fit to the 2015 data release of the Planck mission in combination with lensing effects and external data (BAO+JLA+H0) [16].

Case 1: $\beta = 6$ (stiff matter)

In Fig. 5.9, we present the theoretical predictions for the primordial power spectra obtained from the different numerical runs for $\beta = 6$ and compare them with the observational fit. On the l.h.s. panel, where we present the spectrum obtained for a single run, Q_6, we can see how the shape of $\mathcal{P}_{\mathcal{R}}$ can be related to the characteristic scales $k_{\rm min}$, $k_{\rm a}$, $k_{\rm b}$ and $k_{\rm c}$ defined in the previous section:

- For $k < k_{\rm min}$, the primordial power spectrum is highly suppressed. The suppression ends around $k_{\rm min}$ where $\mathcal{P}_{\mathcal{R}}(k_{\rm min}) \approx \mathcal{P}_{\mathcal{R}}^{(\rm fit)}(k_{\rm min})$;
- For $k \approx k_{\rm a}$, we observe a peak with a very large amplitude $\mathcal{P}_{\mathcal{R}}(k_{\rm a}) \approx 3.6\mathcal{P}_{\mathcal{R}}^{(\rm fit)}(k_{\rm a})$;
- For $k \approx k_{\rm b}$, there is a visible knee in the spectrum after the main peak, with amplitude $\mathcal{P}_{\mathcal{R}}(k_{\rm b}) \approx 2.1\mathcal{P}_{\mathcal{R}}^{(\rm fit)}(k_{\rm b})$;
- For $k \lesssim k_{\rm c}$, the primordial power spectrum still presents some imprints of the pre-inflationary epoch but the deviation from the observational fit starts to become small;
- For $k_{\rm c} < k$, no distinction exists between the predictions of the model and the observational fit.

We note that no special features appear around the threshold $k = 5k_{\rm c}$ between the two regions with different rules for defining the initial conditions for the numerical integrations. This confirms that the strategy employed does not affect the final results. On the r.h.s. panel, we present the results for all eight runs, with lighter coloured curves corresponding to smaller value of Q. All the spectra obtained follow the observational fit well before the pivot scale is reached.

In Fig. 5.10, we present the normalised angular power spectra D_ℓ^{TT} obtained from the numerical results for $\mathcal{P}_{\mathcal{R}}$ (blue) and compare it with the theoretical prediction from the best-fit (red dashed) and with the observational (binned) data points from the Planck mission and their respective error bars. In both panels, lighter blue curves correspond to smaller values of the free parameter Q. The imprints of the model on D_ℓ^{TT} follow the same tendency observed for the primordial power spectrum: on the lowest multipoles the blue curves observe a suppression, followed by a strong peak on intermediate

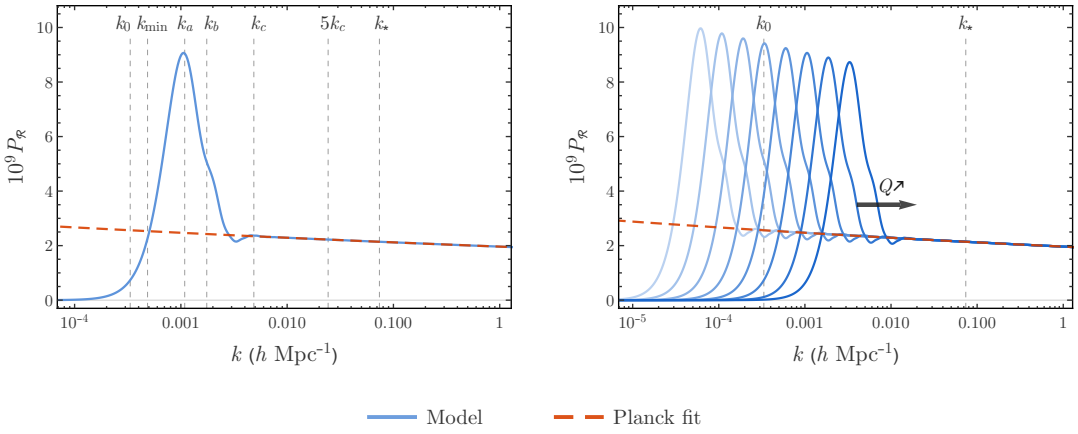

Figure 5.9.: (Left panel) The characteristic shape of the primordial power spectrum obtained for the model considered in Eq. (5.110) with $\beta = 6$ (blue) compared with the observational fit (red dashed). The imprints of the model on $\mathcal{P}_{\mathcal{R}}$ can be related to the characteristic scales $k_{\rm min}$, $k_{\rm a}$, $k_{\rm b}$ and $k_{\rm c}$. (Right panel) As the value of the free parameter Q_i increases (cf. Eq. (5.141)), the imprints on the primordial power spectrum are blue-shifted to higher wavenumbers. Lighter blue curves correspond to smaller values of Q. For all numerical runs, the theoretical prediction is indistinguishable from the observational fit well before the pivot scale is reached.

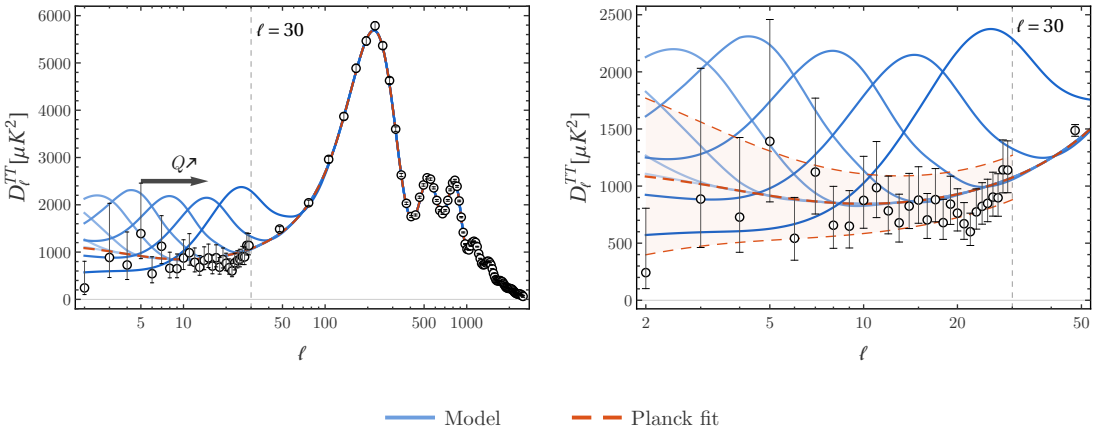

Figure 5.10.: (Left panel) The characteristic shape of the angular power spectra D_ℓ^{TT} obtained for the model considered in Eq. (5.110) with $\beta = 6$ (blue) compared with the observational fit (red dashed) and observational data points. The high peak on the primordial power spectrum leads to an extra peak in D_ℓ^{TT} for intermediate ℓ, while in the very low multipole range D_ℓ^{TT} becomes suppressed. As the value of the free parameter Q becomes higher, the imprints of the model start to affect higher multipoles. (Right panel) Zoom of the angular power spectra in the range $\ell < 50$. The shaded region, delimited by thin dashed lines, indicates the regions where deviations from the observational fit can be explained by the cosmic variance, as given by Eq. (2.62).

values of ℓ, while on the large multipole range all curves have a very good agreement with the observational data. As the value of the free parameter increases, the imprints on D_ℓ^{TT} are shifted to the right, with the two runs with higher values of the free parameter, Q_7 and Q_8, affecting the good agreement to the data points above the $\ell = 30$ mark. If we impose that the Planck fit is recovered for $\ell > 30$, then we arrive at the upper bound for Q:

$$Q \lesssim k_0^3 \,. \tag{5.142}$$

Unfortunately, the high amplitude of the extra peak in the intermediate multipole region–as can be seen on the r.h.s. of Fig. 5.10, the peaks are well above the curve of the observational fit and are even above the interval defined by the cosmic variance–means that there is a very poor agreement with the data unless Q is so small that all imprints are red-shifted away. We will show in the remainder of this section that a much better fitting to the data is obtained in the cases of $\beta = 4$ and $\beta = 3$.

Case 2: $\beta = 4$ (radiation)

In Fig. 5.11, we present the theoretical predictions for the primordial power spectra obtained from the different numerical runs for $\beta = 4$ and compare them with the observational fit. On the l.h.s. panel, where we present the spectrum obtained for a single run, Q_6, we can see how the shape of $\mathcal{P}_\mathcal{R}$ can be related to the characteristic scales $k_{\rm min}$, $k_{\rm a}$, $k_{\rm b}$ and $k_{\rm c}$ defined in the previous section from analysing k_H^2 and z''/z:

- For $k \lesssim k_{\rm min}$, the primordial power spectrum is highly suppressed. The suppression seems to be stronger than in the previous case, as we find that the predicted $\mathcal{P}_\mathcal{R}$ at $k = k_{\rm min}$ is still well below the observational fit: $\mathcal{P}_\mathcal{R}(k_{\rm min}) \approx 0.2\mathcal{P}_\mathcal{R}^{(\rm fit)}(k_{\rm min})$;
- For $k \approx k_{\rm a}$, we observe the presence of a faint knee in the primordial power spectrum. However, in this region $\mathcal{P}_\mathcal{R}$ is still suppressed when compared with the Planck fit: $\mathcal{P}_\mathcal{R}(k_{\rm a}) \approx 0.7\mathcal{P}_\mathcal{R}^{(\rm fit)}(k_{\rm a})$;
- For $k \approx k_{\rm b}$, we observe a small peak with amplitude $\mathcal{P}_\mathcal{R}(k_{\rm b}) \approx 1.2\mathcal{P}_\mathcal{R}^{(\rm fit)}(k_{\rm b})$;
- For $k \lesssim k_{\rm c}$, the primordial power spectrum predicted by the model starts to converge to the observational fit;
- For $k_{\rm c} < k$, no distinction exists between the predictions of the model and the observational fit.

Once more, no special features appear around the threshold $k = 5k_{\rm c}$, validating the strategy employed to define the initial conditions for the numerical integrations. On the r.h.s. panel we present the results for all eight runs, with lighter coloured curves corresponding to smaller value of Q. All the spectra obtained follow the observational fit well before the pivot scale is reached.

In Fig. 5.12, we present the normalised angular power spectra D_ℓ^{TT} obtained from the numerical results for $\mathcal{P}_\mathcal{R}$ (blue) and compare it with the theoretical prediction from the best-fit (red dashed) and with the observational (binned) data points from the Planck mission and their respective error bars. In both panels, lighter blue curves correspond to smaller values of the free parameter Q_i (cf. Eq. (5.141)). As in the previous case, the imprints of the model on D_ℓ^{TT} reflect the shape of the primordial power spectrum: on the lowest multipoles we find a strong suppression of the angular power spectra, followed by a faint peak on intermediate values of ℓ. On the large multipole range all curves are in very good agreement with the observational data. As the value of the free parameter increases,

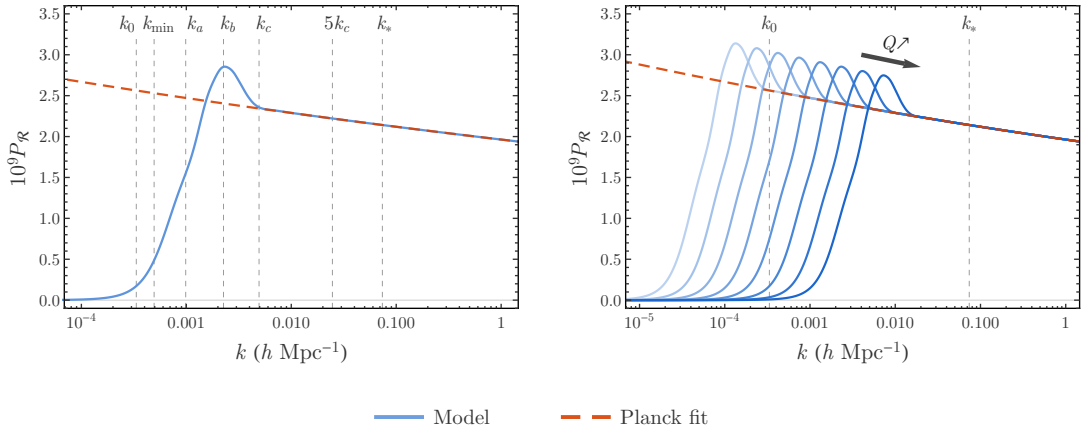

Figure 5.11.: (Left panel) The characteristic shape of the power spectrum obtained for the model considered in Eq. (5.110) with $\beta = 4$ (blue) compared with the observational fit (red dashed). The imprints of the model on $\mathcal{P}_\mathcal{R}$ can be related to the characteristic scales $k_{\rm min}$, $k_{\rm a}$, $k_{\rm b}$ and $k_{\rm c}$. (Right panel) As the value of the free parameter Q_i increases (cf. Eq. (5.141)), the imprints on the primordial power spectrum are blue-shifted to higher wavenumbers. Lighter blue curves correspond to smaller values of Q. For all numerical runs, the theoretical prediction is indistinguishable from the observational fit well before the pivot scale is reached.

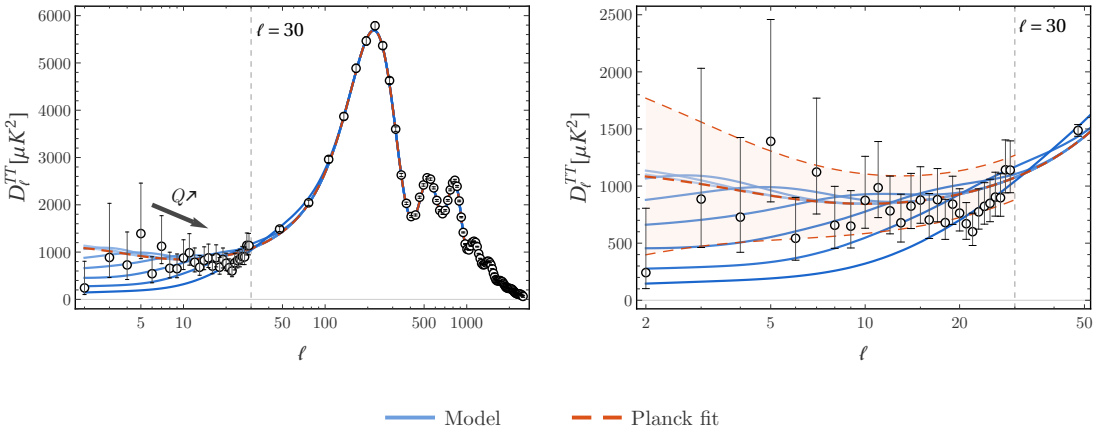

Figure 5.12.: (Left panel) The characteristic shape of the angular power spectra D_ℓ^{TT} obtained for the model considered in Eq. (5.110) with $\beta = 4$ (blue) compared with the observational fit (red dashed) and observational data points. The peak on the primordial power spectrum leads to an extra small peak in D_ℓ^{TT} for intermediate ℓ, while in the very low multipole range D_ℓ^{TT} becomes strongly suppressed. As the value of the free parameter Q becomes higher, the imprints of the model start to affect higher multipoles. (Right panel) Zoom of the angular power spectra in the range $\ell < 50$. The shaded region, delimited by thin dashed lines, indicates the regions where deviations from the observational fit can be explained by the cosmic variance, as given by Eq. (2.62).

the imprints on D_ℓ^{TT} are shifted to the right, with the last two runs, Q_7 and Q_8, affecting the good agreement with the data points above the $\ell = 30$ mark. If we impose that the Planck fit is recovered for $\ell > 30$, then we arrive at the upper bound for Q:

$$Q \lesssim k_0^2 \,. \tag{5.143}$$

Contrary to the previous case, the small amplitude of the extra peak that appears for $\ell < 30$ make this model compatible with the data. This leads to the possibility of suppressing the angular power spectrum for the very low multipoles $\ell \lesssim 5$. For example, for the run Q_5 the peak that appears for $\ell \approx 11$ is well within the error bars of the data points in that range and a suppression of D_ℓ^{TT} is observed for $\ell < 7$. Notice, however, that only the runs Q_7 and Q_8 are capable of achieving a suppression at large scales that goes beyond the interval defined by the cosmic variance, as given by Eq. (2.62).

Case 3: $\beta = 3$ (dust)

In Fig. 5.13, we present the theoretical predictions for the primordial power spectra obtained from the different numerical runs for $\beta = 3$ and compare them with the observational fit. On the l.h.s. panel, where we present the spectrum obtained for a single run, Q_6, we can see how the shape of $\mathcal{P}_\mathcal{R}$ can be related to the characteristic scales $k_{\rm min}$ and $k_{\rm c}$ defined in the previous section:

- For $k \lesssim k_{\rm min}$, the primordial power spectrum shows the highest suppression of the three cases considered. At $k = k_{\rm min}$ we find $\mathcal{P}_\mathcal{R} \approx 0.06 \mathcal{P}_\mathcal{R}^{(\rm fit)}$;
- The suppression of $\mathcal{P}_\mathcal{R}$ ends near the scale $k_{\rm c}$;
- For $k \approx k_{\rm c}$, we observe an almost indistinguishable peak in $\mathcal{P}_\mathcal{R}$;
- For $k_{\rm c} < k$, no distinction exists between the predictions of the model and the observational fit.

Once more, no special features appear around the threshold $k = 5k_{\rm c}$, validating the strategy employed to define the initial conditions for the numerical integrations. On the r.h.s. panel, we present the results for all eight runs, with lighter coloured curves corresponding to smaller value of Q. All the spectra obtained follow the observational fit well before the pivot scale is reached.

In Fig. 5.14, we present the normalised angular power spectra D_ℓ^{TT} obtained from the numerical results for $\mathcal{P}_\mathcal{R}$ (blue) and compare it with the theoretical prediction from the best-fit (red dashed) and with their observational (binned) data points from the Planck mission and respective error bars. In both panels, lighter blue curves correspond to smaller values of the free parameter Q_i (cf. Eq. (5.141)). In contrast with the previous cases of $\beta = 6$ and $\beta = 4$, the lack of discernible peaks in the primordial power spectrum means that no extra bumps appear on the theoretical predictions for D_ℓ^{TT}; we just observe a strong suppression of the angular power spectrum on the low multipole end of the spectrum after which all curves track the line for the best-fit of Planck, recovering a very good agreement with the observational data. As before, the imprints on D_ℓ^{TT} are shifted to the right as the value of the free parameter increases, with the last two runs, Q_7 and Q_8, affecting multipoles above the $\ell = 30$ mark. If we impose that the Planck fit is recovered for $\ell > 30$, then we arrive at the upper bound for Q:

$$Q \lesssim k_0^{3/2} \,. \tag{5.144}$$

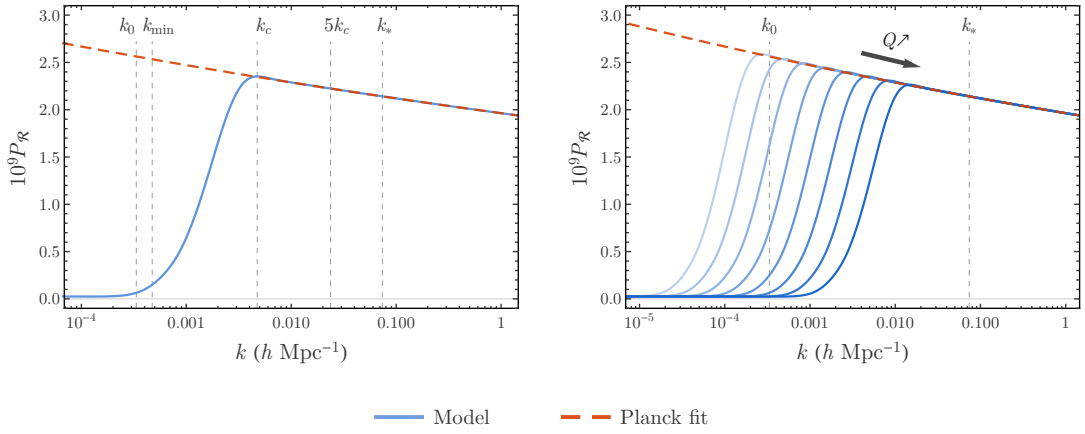

Figure 5.13.: (Left panel) The characteristic shape of the power spectrum obtained for the model considered in Eq. (5.110) with $\beta = 3$ (blue) compared with the observational fit (red dashed). The imprints of the model on $\mathcal{P}_\mathcal{R}$ can be related to the characteristic scales $k_{\rm min}$, $k_{\rm a}$, $k_{\rm b}$ and $k_{\rm c}$. (Right panel) As the value of the free parameter Q_i increases (cf. Eq. (5.141)), the imprints on the primordial power spectrum are blue-shifted to higher wavenumbers. Lighter blue curves correspond to smaller values of Q. For all numerical runs, the theoretical prediction is indistinguishable from the observational fit well before the pivot scale is reached.

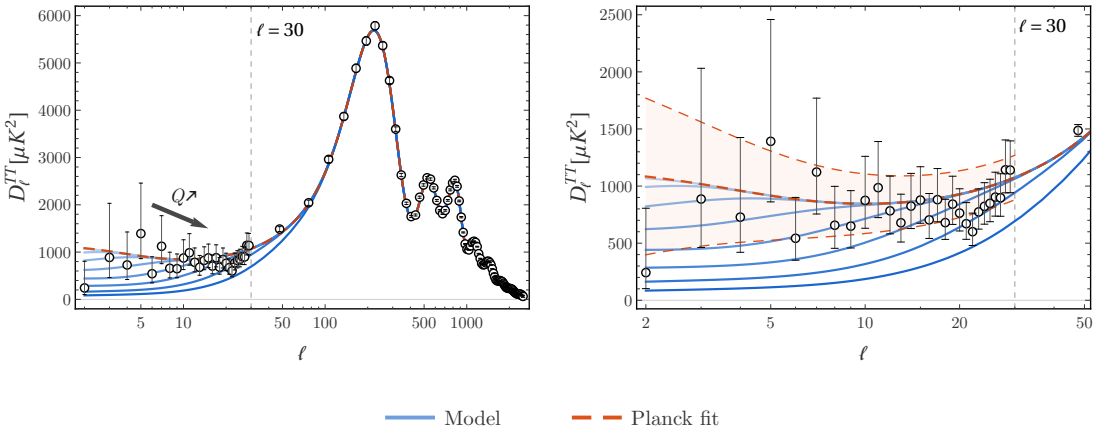

Figure 5.14.: (Left panel) The characteristic shape of the angular power spectra D_ℓ^{TT} obtained for the model considered in Eq. (5.110) with $\beta = 6$ (blue) compared with the observational fit (red dashed) and observational data points. The angular power spectrum becomes suppressed in the low multipole range. Contrary to the previous cases, no extra peak appears at intermediate multipoles, reflecting the absence of peaks in the primordial power spectrum. As the value of the free parameter Q becomes higher, the imprints of the model start to affect higher multipoles. (Right panel) Zoom of the angular power spectra in the range $\ell < 50$. The shaded region, delimited by thin dashed lines, indicates the regions where deviations from the observational fit can be explained by the cosmic variance, as given by Eq. (2.62).

Since no intermediate bumps appear in this case, it is possible to achieve a stronger suppression for multipoles closer to the $\ell = 30$ threshold. We note, for example that, the results for the runs Q_5 and Q_6, where the line for D_ℓ^{TT} is lowered with regards to the Planck fit for $\ell \lesssim 20$ without affecting the agreement with the data for larger multipoles. However, despite the fact that the suppression at large scales is larger than in the previous two cases, we find that only the runs Q_6, Q_7 and Q_8 are capable of achieving a suppression at large scales that goes beyond the error induced by the cosmic variance.

Implications for the multiverse

In this section, we have obtained upper limits for the free parameter Q computing the normalised angular power spectrum D_ℓ^{TT} of the CMB and imposing that no imprints appear for multipoles above the $\ell = 30$ threshold. By comparing Eqs. (5.68) and (5.103), we can relate Q with the interaction coupling λ_* and the l-number[19] that identifies the wave-function field Ψ_l of the universe as:

$$Q = k_*^{\frac{\beta}{2}-1}\frac{\lambda_*}{a_*}l\,, \tag{5.145}$$

which then leads to the constraint

$$\frac{\lambda_*}{a_*}l \lesssim k_*\left(\frac{k_0}{k_*}\right)^{\frac{\beta}{2}}\,. \tag{5.146}$$

The previous expression shows that the strength of the coupling must decrease with higher l-number in order for the observational constraints to be respected. In Ref. [302] it was argued that through a mechanism of vacuum decay, the most probable multiverse configurations correspond to those with small l. If we now take $l = 1$, then Eq. (5.146) becomes a constraint on λ_*, which in combination with Eq. (5.64) reads

$$\frac{\sqrt{C(a_*)}}{N_{\rm uni}} < \frac{a_*\sigma}{2\pi\hbar}k_*\left(\frac{k_0}{k_*}\right)^{\frac{\beta}{2}}\,. \tag{5.147}$$

Thus, in order for larger values of the universe-universe coupling $C(a)$ at a_* to be admissible, the total number of universe needs to grow quadratically with $C(a_*)$. On the other hand, if we increase the number of universes while maintaining the universe-universe coupling constant, its effect become too weak for any observational imprints to be observed. Assuming a very large number of universes, this suggests a very high quantum interaction between neighbouring universes or that the interaction model needs to be altered in order to accommodate a higher number of interactions per universe. Finally, we note that the constraint (5.147) has a dependence on the type of coupling chosen, i.e., on the behaviour of the universe before inflation sets in, which can change the upper limits on $C(a_*)/N_{\rm uni}^2$ by a few orders of magnitude.

[19] Not to be confused with the multipole number ℓ.

5.3.4. Discussion

In this section, we have studied the effects on the primordial power spectrum $\mathcal{P}_{\mathcal{R}}$ and the normalised angular power spectrum D_{ℓ}^{TT} originated from considering the existence of a pre-inflationary epoch described by the model (5.110), where the behaviour of the universe before inflation is determined by the parameter β. We have considered three cases in particular: $\beta = 6$ which leads to a stiff-matter-like behaviour; $\beta = 4$ that leads to a radiation-like behaviour; and $\beta = 3$ in which the initial epoch mimics a dust-filled universe. Based on the requirement that the shape of the observational fit for $\mathcal{P}_{\mathcal{R}}$ from the Planck mission is recovered near the pivot scale, we were able to fix three of the four parameters of the model and set upper bounds on the free parameter. A more strict bound was obtained by requiring that the agreement of D_{ℓ}^{TT} with the data for $\ell > 30$ is not affected. Using these constraints we were able to impose some bounds on the parameter space of the interacting model proposed in [28, 302].

We have shown that the range of wavenumbers where the imprints on the primordial power spectrum appear can be predicted by looking for characteristic features on the squared comoving Hubble horizon, k_H^2, the potential z''/z, and their ratio. While for all the three cases studied the primordial power spectrum is strongly suppressed on the large scale limit, for $\beta = 6$ and $\beta = 4$ we find an enhancement of $\mathcal{P}_{\mathcal{R}}$ on intermediate scales. This effect is stronger in the case of $\beta = 6$, milder in $\beta = 4$ and, in practice, absent for $\beta = 3$. In accordance, by looking at the value of $\mathcal{P}_{\mathcal{R}}$ at $k = k_{\min}$, we can be tempted to suggest that the suppression at the lower scales is stronger for $\beta = 3$ than for $\beta = 4$ and for $\beta = 4$ when compared to $\beta = 6$. This comparison, however, needs to be taken with some care as the value of the free parameter Q is not necessarily directly comparable between the three cases. This tendency for less prominent features to appear on the primordial power spectrum for lower values of β was also obtained in [83] for cases where $\beta \leq 2$ and in [118], where instantaneous transitions were considered.

The new features observed on the primordial power spectra carry themselves to the angular power spectra D_{ℓ}^{TT} calculated using the CLASS code. In particular, for the cases of $\beta = 6$ and $\beta = 4$, we find that the peaks on $\mathcal{P}_{\mathcal{R}}$ lead to the presence of an extra peak in D_{ℓ}^{TT} for intermediate multipole values. Nevertheless, in all the cases studied we observe a suppression of the angular power spectrum for the lowest multipoles. This effect, which is more noticeable for lower values of the parameter β, is in line with previous studies [83, 96, 114, 118, 122, 129, 292, 353] where a pre-inflationary epoch is considered in order to explain the quadropole anomaly of the CMB.

The study presented here works as a first approach to find imprints on the CMB from a multiverse picture based on the Third Quantisation interpretation of Canonical Quantum Gravity. Several levels of approximations were taken between the *more fundamental* description at the level of Quantum Cosmology and the phenomenological model used to compute the evolution of the scalar perturbation, namely: (I) assuming that the potential of the scalar field is (approximately) constant when solving the WDW equation that appears as the equation of motion for the wave-function field of the Third Quantisation; (II) applying a semi-classical approximation on the wave-function field which in the Third Quantisation can represent a multi-universe state; (III) treating the cosmological perturbations as quantum perturbations in a (semi) classical background, just as usually done in inflationary models, without considering possible quantum modifications to the Mukhanov-Sasaki equation; (IV) replacing the constant term in the Friedmann equation obtained from the Third Quantisation model by a power-law term that can give an appropriate shape of the primordial power spectrum around the pivot

scale.

The step that seems more simple to tackle in the immediate future and probably the one with a more direct impact on the predictions for the CMB is (III). In the treatment applied in this work, any effects coming from an interaction between different universes enter directly only at the background level. As such, the Mukhanov-Sasaki equation used to compute the evolution of the quantum perturbations is not modified with regards to the usual case. Finding the corrections to this equation coming from the universe-universe interaction in the Third Quantisation would go in the same direction of the results obtained for Canonical Quantum Cosmology [86, 87] and LQC [17, 97, 113].

Steps (I) and (IV) are intimately related, in the sense that considering more general scalar field potentials in the setting of quantum cosmology without imposing an extreme slow-roll approximation, would in principle lead to the appearance of non-constant terms in the effective Friedmann equation capable of driving primordial inflation. In such cases, step (IV) would no longer be necessary as inflation would no longer be purely de Sitter. However, when we consider non-constant potentials of the scalar field (or when we discard the extreme slow-roll approximation), the Fourier decomposition in Eqs. (5.39)–(5.42) which allows for a full description of the Hilbert space of the quantised wave-functions is no longer valid. In such cases, a more complex mode expansion procedure would have to be used, namely a Born-Oppenheimer approximation [209, 210] or a superadiabatic expansion [212, 214]. Following this route would rewards us with a richer description of the multiverse in the Third Quantisation upon which we could, in principle, derive a more fundamental description of quantum effects on the evolution of each universe.

Finally, a comment regarding step (II). The application of the semi-classical approximation to a third quantised state has been employed since the Third Quantisation started to be explored [306]. However, the validity of combining what are in essence two different interpretations of the WDW equation [221] has not been explored in detail in the literature. This possible conflict in interpretation seems particularly puzzling if we take into account that the third quantised wave-function can represent a multi-universe state where the number of quanta can vary during the evolution of the system, while in the semi-classical approximation we consider that we are dealing with *one* semi-classical universe. The difficulties in the physical interpretation of the Third Quantisation have been pointed out since the early 1990's by Christopher J. Isham [202] and Karel V. Kuchař [221]. In Ref. [221], it is stated that "*In third-quantized gravity, the many-particle states are replaced by many-geometry states. However, the analogy is not perfect. A three-geometry is not analogous to the position of a particle, because it contains also information about intrinsic time.*". In the present case, this question presents itself for example in the fact that the scale factor a is a coordinate of the minisuperspace and is also related to the intrinsic time of the individual universes in the semi-classical approximation. Unfortunately, at this point no conclusions on this topic can be offered, as it is connected with the very fundamental interpretation of the Third Quantisation picture, which is not the main focus of this work.

5.4. Cosmological Perturbations in a toy model II

In the previous section, we have studied the imprints on the primordial power spectrum, $\mathcal{P}_{\mathcal{R}}$, and on the normalised angular power spectrum, D_{ℓ}^{TT}, coming from a pre-inflationary epoch. Such an epoch resulted from the presence of the Q-dependent term in the effective Friedmann equation (5.110),

which dominates in the limit of small values of the scale factor, $a \ll a_*$. This term appeared due to considerations in a Third Quantisation picture of the multiverse and was obtained either by considering the contribution of the momentum of the scalar field φ, in the case of an initial stiff-matter-like epoch, or by introducing a universe-universe interaction with an appropriate coupling between different universes.

The fact that we considered a decelerated pre-inflationary epoch, led to the existence of a range of modes (with $k < k_{\rm min}$) that never enter the comoving Hubble horizon before inflation. For modes in this range, it was found that the primordial power spectrum is strongly suppressed, which then led to a suppression on the low multipole end of D_ℓ^{TT}. Such a suppression could in principle alleviate the issue of the quadropole anomaly of the CMB. However, on intermediate scales, we found a strong enhancement of $\mathcal{P}_\mathcal{R}$ which seemed to be associated to bumps on the potential z''/z during the transition from the initial decelerated epoch to inflation. This results suggests that the shape of $\mathcal{P}_\mathcal{R}$ at the end of inflation is strongly affected not only by the dynamics in the pre-inflationary epoch but also during this transition. In order to test how this transition affects the final results, in the next sections we calculate $\mathcal{P}_\mathcal{R}$ and D_ℓ^{TT} in an extension of the previous model (5.110), where a new parameter is introduced that controls how *fast* the transition from the initial to the final epoch occurs.

5.4.1. The Model

As a one-parameter extension of the previous model (5.110), we consider the effective Friedmann equation

$$H^2 = H_{\rm dS}^2 \left[\left(\frac{a_*}{a} \right)^{\alpha\lambda} + \left(\frac{Q^2}{(aH_{\rm dS})^\beta} \right)^\lambda \right]^{\frac{1}{\lambda}} , \tag{5.148}$$

where we recall that $H_{\rm dS}$ defines the energy scale of inflation which occurs when the first term inside the squared brackets dominates. Together with α and a_*, the value of $H_{\rm dS}$ will later be fixed using arguments from the observational data. Alternately, when the second term inside the squared brackets dominates, the Universe can undergo a different expansion epoch. The strength of this term is modulated by the parameter Q, while the behaviour of the Universe in this epoch is determined by the parameter[20] β. The new parameter λ has a double function. As will be made apparent below, its magnitude dictates whether the transition is sharper[21] ($|\lambda| \gg 1$) or takes longer to occur ($|\lambda| \ll 1$). On the other hand, the sign of λ defines whether at the transition the rate of acceleration of the universe increases ($\lambda > 0$) or decreases ($\lambda < 0$). In this work we are mainly concerned with a transition from a pre-inflationary epoch with a decelerated behaviour to a later period of power-law inflation and, as such, we will only consider values $\beta > 2$ and $\lambda > 0$.

The model in (5.148) can be seen as an extension of the modified Generalised Chaplygin Gas and was first considered in [83]. It can be shown that it leads to a transition in the total EoS parameter,

[20] We point out that, when the second term inside the squared brackets in Eq. (5.148) dominates, the effective total EoS parameter w can be written as $w \simeq -1 + \beta/3$. This situation corresponds to the limit $\tanh[(N - N_{\rm mid})/\Delta_\lambda] = -1$ in Eq. (5.149).

[21] In the limit of very large λ we obtain an instantaneous transition [36, 96, 110, 114, 122, 136, 176]. That case will be discussed in detail in Sect. 5.5.

$w := P/\rho$, modulated by a $\tanh$ function of the number of e-folds $N := \log(a/a_*)$:

$$w(N) = -1 - \frac{2}{3}\frac{\dot{H}}{H^2} = \left(\frac{\alpha+\beta}{6} - 1\right) + \frac{\alpha-\beta}{6}\tanh\left(\frac{N - N_{\rm mid}}{\Delta_\lambda}\right) . \tag{5.149}$$

Here, we introduce the reference value

$$N_{\rm mid} := \frac{1}{\beta-\alpha}\log\left[\frac{Q^2}{(a_* H_{\rm dS})^\beta}\right] , \tag{5.150}$$

which marks the moment when w reaches the mid point value between its asymptotic initial and final values, as well as the interval

$$\Delta_\lambda := \frac{2}{(\beta-\alpha)\,\lambda} , \tag{5.151}$$

that characterises the number of e-folds required for the transition in w to occur. Since $\Delta_\lambda \propto \lambda^{-1}$, we find that for smaller values of λ the transition takes longer to complete, while for large values of λ it happens more abruptly, becoming instantaneous in the limit of $\lambda \to \infty$. Given the exponential decay of the $\tanh$, for small values of α the EoS parameter w in defined Eq. (5.149) reaches $\sim 99.99\%$ of its asymptotic value when $|N - \tilde{N}| = 5\Delta_\lambda$. This can be seen on the top row of Fig. 5.15 where the interval $N_{\rm mid} \pm 5\Delta_\lambda$ is indicated by the shaded region and we choose the values $\beta = 6$ and $\alpha = 0.03275$ as a reference.

The comoving wavenumber of the Hubble horizon, k_H, can be expressed as well as a function of N:

$$k_H(N) = k_{\rm trans}\, \mathrm{e}^{\left(1-\frac{\alpha+\beta}{4}\right)(N-N_{\rm trans})}\left(\frac{\cosh\left(\frac{N-N_{\rm mid}}{\Delta_\lambda}\right)}{\cosh\left(\frac{N_{\rm trans}-N_{\rm mid}}{\Delta_\lambda}\right)}\right)^{\frac{1}{2\lambda}} , \tag{5.152}$$

where $N_{\rm trans}$ is given by

$$N_{\rm trans} := \frac{1}{\beta-\alpha}\left(\frac{1}{\lambda}\log\left|\frac{\beta-2}{2-\alpha}\right| + \log\left[\frac{Q^2}{(a_* H_{\rm dS})^\beta}\right]\right) , \tag{5.153}$$

and defines the moment of transition between the initial epoch and the final power-law inflationary era. The characteristic wavenumber during the transition, $k_{\rm trans} := k_H(N_{\rm trans})$, can be written as

$$k_{\rm trans} = a_* H_{\rm dS}\left(\frac{|\beta-2| + |2-\alpha|}{|2-\alpha|}\left|\frac{2-\alpha}{\beta-2}\right|^{\frac{\beta-2}{\beta-\alpha}}\right)^{\frac{1}{2\lambda}}\left[\frac{Q^2}{(a_* H_{\rm dS})^\beta}\right]^{\frac{1}{2}\frac{2-\alpha}{\beta-\alpha}} . \tag{5.154}$$

For $\beta > 2$ (and $\alpha < 2$) the comoving Hubble wavenumber reaches a minimum at $N_{\rm trans}$ which corresponds to the moment when the Universe transits from a decelerated to an accelerated expansion, i.e., $\ddot{a}(N_{\rm trans}) = 0$. We thus see that Eqs. (5.153) and (5.154) are, respectively, the generalisation of the definitions (5.112) and (5.111). For this reason, in the remainder of this section, we will use the notation of the previous section, $k_{\rm min}$, when referring to $k_{\rm trans}$. As we will discuss later, for physically reasonable values of α and β and as long as λ is not too small, the condition $Q \ll (a_* H_{\rm dS})^{\beta/2}$

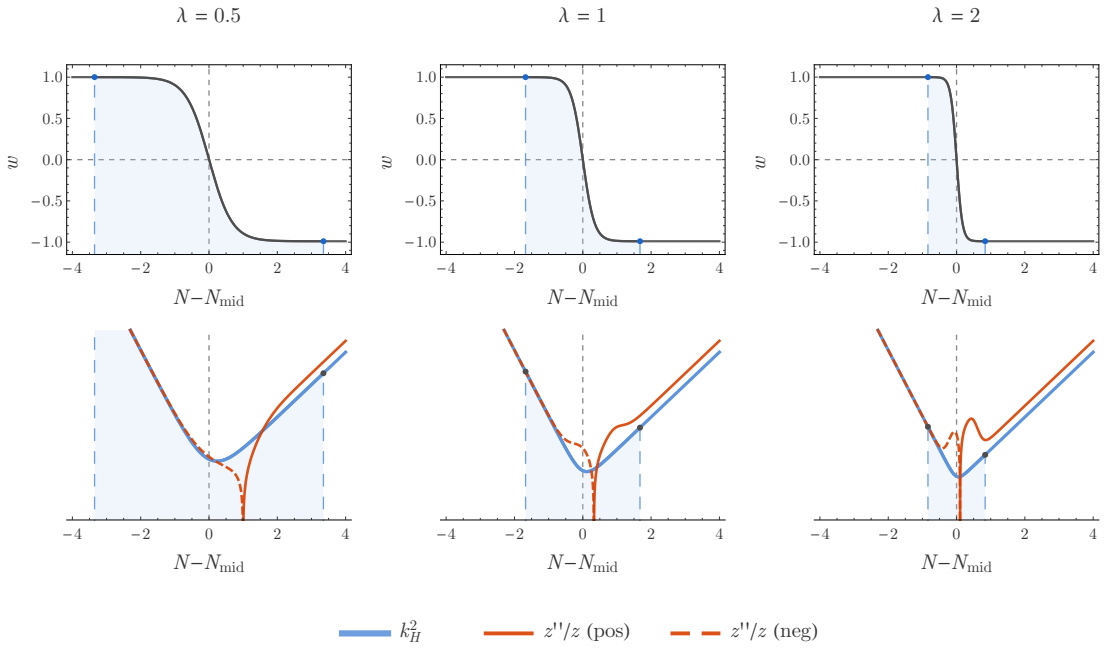

Figure 5.15.: (Top panels) As the value of the parameter λ increases, the EoS parameter, defined in Eq. (5.149), takes less number of e-folds to go from its initial to its final value. The shaded region indicates the interval where w is between 99.99% of its initial value and 99.99% of its final value. (Bottom panels) As the value of the parameter λ increases, the curve related to the comoving wavenumber of the Hubble horizon, k_H^2, becomes sharper around the position of its minimum at $N_{\rm trans}$, while the potential z''/z starts to present increasingly more prominent bumps. Notice that while $N_{\rm mid}$, defined in Eq. (5.150), and $N_{\rm trans}$, see Eq. (5.153), have similar values, they only coincide in the limit $\lambda \to +\infty$.

ensures that both $a_{\rm trans} \ll a_*$ and $k_{\rm trans} \ll a_* H_{\rm dS}$, so that when the mode $k = a_* H_{\rm dS}$ crosses, the horizon the universe is already well inside the inflationary epoch. Later on, we will use this to fix a_* through the equality $a_* H_{\rm dS} = k_*$, where k_* is the pivot scale from the Planck mission.

In the model at hand, the potential z''/z can be written as

$$\frac{z''}{z} = k_H^2(N)\left[2 - \epsilon(N) + \frac{C_{(\alpha,\beta,\lambda)}(N)}{\Delta_\lambda} + \frac{D_{(\alpha,\beta,\lambda)}(N)}{\Delta_\lambda^2}\right]. \tag{5.155}$$

where the slow-roll parameter ϵ reads

$$\epsilon(N) = -\frac{1}{2}\frac{(H^2)_N}{H^2} = \frac{\alpha+p}{4} + \frac{\alpha-\beta}{4}\tanh\left(\frac{N-N_{\rm mid}}{\Delta_\lambda}\right). \tag{5.156}$$

and the functions $C_{(\alpha,\beta,\lambda)}(N)$ and $D_{(\alpha,\beta,\lambda)}(N)$ are defined as

$$C_{(\alpha,\beta,\lambda)}(N) = \frac{\beta-\alpha}{8}\mathrm{sech}^2\left(\frac{N-N_{\rm mid}}{\Delta_\lambda}\right) + \frac{3}{2}\frac{\mathrm{sech}^2\left(\frac{N-N_{\rm mid}}{\Delta_\lambda}\right)}{\tanh\left(\frac{N-N_{\rm mid}}{\Delta_\lambda}\right) - \coth\left(\frac{N_1}{\Delta_\lambda}\right)}, \tag{5.157}$$

and

$$D_{(\alpha,\beta,\lambda)}(N) = \sinh\left(\frac{N_1}{\Delta_\lambda}\right) \frac{\sinh\left(\frac{N_1}{\Delta_\lambda}\right) + 2\sinh\left(\frac{2N-2N_{\rm mid}-N_1}{\Delta_\lambda}\right)}{\left[\cosh\left(\frac{N_1}{\Delta_\lambda}\right) + \cosh\left(\frac{2N-2N_{\rm mid}-N_1}{\Delta_\lambda}\right)\right]^2} \,. \tag{5.158}$$

For convenience, in Eqs. (5.157) and (5.158) we have introduced as well $N_1 := \Delta_\lambda \log(\sqrt{\beta/\alpha})$.

The first two terms inside the brackets on the r.h.s. of Eq. (5.155), which correspond to the potential a''/a that drives the evolution of the gravitational waves, define the shape of z''/z away from $N_{\rm mid}$. On the other hand, the terms in $C_{(\alpha,\beta,\lambda)}$ and $D_{(\alpha,\beta,\lambda)}$, which vanish asymptotically for $N \to \pm\infty$, encode the information regarding the evolution of the background around the value $N_{\rm trans}$ that marks the transition from the initial to the final epoch. On the bottom row of Fig. 5.15, it can be seen that as the transition from the initial to final epoch becomes more sudden (increasing values of λ), the potential z''/z starts to show the presence of peaks around $N_{\rm trans}$, which corresponds to the position of the minimum of k_H^2. Notice that while $N_{\rm mid}$, defined in Eq. (5.150), and $N_{\rm trans}$, see Eq. (5.153), have similar values, they only coincide in the limit $\lambda \to +\infty$, i.e., when the transition becomes instantaneous. In the last section, these peaks led to an undesired enhancement of the primordial power spectrum at the corresponding scales which, despite the desired suppression at the larger scales, could spoil the agreement with the CMB data at intermediate multipoles ℓ. Next, we consider the possibility of countering this enhancement by having a longer transitional period, i.e., lowering the value of the parameter β. In particular, we compute $\mathcal{P}_\mathcal{R}$ and D_ℓ^{TT} for $\lambda < 1$ in the cases $\beta = 6$ and $\beta = 4$.

5.4.2. Parameters of the model

In Sect. 5.3.2, we discussed how, for the toy model defined in Eq. (5.110), the assumption that $Q \ll (a_* H_{\rm dS})^{\beta/2}$ is a sufficient condition to assure that the system is well within the late power-law inflationary epoch for $a \gtrsim a_*$. This condition, together with the assumption that the modes that exit the Hubble horizon at $a \gtrsim a_*$ spend enough e-folds inside the horizon so as to reach a BD vacuum state, guaranteed that the shape of the $\mathcal{P}_\mathcal{R}$ predicted by power-law inflation was recovered for $k \gtrsim a_* H_{\rm dS}$. In turn, this allowed us to fix the value of three of the four parameters of the model in terms of the best-fit values of the cosmological observations, cf. Eqs. (5.123)–(5.126). We now extend that analysis to the case of the model (5.148) and see how we can go from a five dimensional parameter space $\{H_{\rm dS},\, a_*,\, \alpha,\, Q,\, \lambda\}$ to a two dimensional one $\{Q, \lambda\}$ by comparing the predictions of the model with the best-fit values of observational data.

If we assume that the first term on the r.h.s. of Eq. (5.148) dominates, then we can expand H^2 as

$$H^2 \approx H_{\rm dS}^2 \left(\frac{a_*}{a}\right)^\alpha \left[1 + \frac{1}{\lambda}\left(\frac{Q^2}{(a_* H_{\rm dS})^\beta}\right)^\lambda \left(\frac{a_*}{a}\right)^{\lambda(\beta-\alpha)} + \dots\right] . \tag{5.159}$$

We thus find that in order for power-law behaviour to be recovered around a_*, we must replace the

condition $Q \ll (a_* H_{\rm dS})^{\beta/2}$ by[22]

$$\frac{Q^2}{(a_* H_{\rm dS})^{\beta}} \ll \lambda^{\frac{1}{\lambda}} \,. \tag{5.160}$$

If this condition holds, we can once again use the argumentation of Sect. 5.3.2 to consider that the prediction for the primordial power spectrum (5.121) is recovered for $k \gtrsim a_* H_{\rm dS}$. Then, by a direct comparison with the fit to $\mathcal{P}_{\mathcal{R}}$ around the pivot scale and using the ansatz $k_* = a_* H_{\rm dS}$ to fix a_* we recover Eqs. (5.123)–(5.125). Then, using the best-fit values of the 2015 Planck mission in combination with lensing effects and external data (BAO+JLA+H0) [16], we can once again fix the values of $\{\alpha,\, H_{\rm dS},\, a_*\}$ as

$$\alpha \simeq 0.03275\,, \qquad H_{\rm dS} \simeq 1.055 \times 10^{-5}\,(M_{\rm P}/\hbar)\,, \qquad a_* \simeq 2.099 \times 10^{7}\,(\hbar/M_{\rm P})\,, \tag{5.161}$$

where the present day values for the Hubble rate and scale factor are $H_0 \approx 1.184 \times 10^{-61}\,(M_{\rm P}/\hbar)$ and $a_0 = H_0^{-1} \approx 8.449 \times 10^{60}\,(\hbar/M_{\rm P})$. As before, the corresponding wavenumbers are $k_0 = 1$ and $k_* \approx 221.3$.

Of the original five parameters, we are now left only with Q, which controls the amplitude of the second term on the r.h.s. of Eq. (5.110) and therefore the behaviour during the pre-inflationary phase, and with λ, which controls how many e-folds are necessary for the Universe to transit from the initial pre-inflationary epoch to the later power-law inflation. Next, we will impose lower and upper bounds on these parameters for the cases of $\beta = 6$ and $\beta = 4$. We remind that in these cases the pre-inflationary era mimics, respectively, a stiff-matter and a radiation dominated universe. The case of $\beta = 3$, which gives a pre-inflationary era that mimics a dust dominated universe, is excluded from the analysis since in the previous section we found no peaks in the primordial power spectrum when $\lambda = 1$.

Case 1: $\beta = 6$ (stiff matter)

In order to see if a smoother transition can improve the results of Sec. 5.3.3 for the case of $\beta = 6$, we first analyse how the shape of the potential z''/z around the transition from the initial decelerated epoch to the subsequent inflation varies as we decrease the value of λ. In Fig. 5.16, we plot the squared comoving Hubble horizon, k_H^2, the potential z''/z and their ratio for $\lambda = 1$ (lighter curve), $\lambda = 0.75$ and $\lambda = 0.5$ (darker curve). As can be observed on the l.h.s. panel, when we decrease the value of λ while maintaining constant the parameter Q, the pre-inflationary behaviour is not affected but the minimum wavenumber $k_{\rm min} = k_{\rm trans}$ increases and modes with higher wavenumbers start to be affected. On the other hand, if we decrease λ while maintaining $k_{\rm min}$ constant (right panel) then the value of Q decreases. As a consequence, the term of the pre-inflationary epoch becomes weaker and inflation starts to dominate earlier.

Following the procedure presented in Sect. 5.3.2, we define three extra characteristic wavenumbers, $k_{\rm a}$, $k_{\rm b}$ and $k_{\rm c}$, based on the shape of z''/z around the transition:

a) We define $k_{\rm a}$ as the wavenumber of the mode that crosses the potential z''/z at the moment when $(z''/z)/k_H^2$ reaches its minimum before inflation. Through a numerical investigation we

[22] For $0 \leq \lambda \leq 1$, the r.h.s. of (5.160) defines a bijective monotonically increasing function of λ.

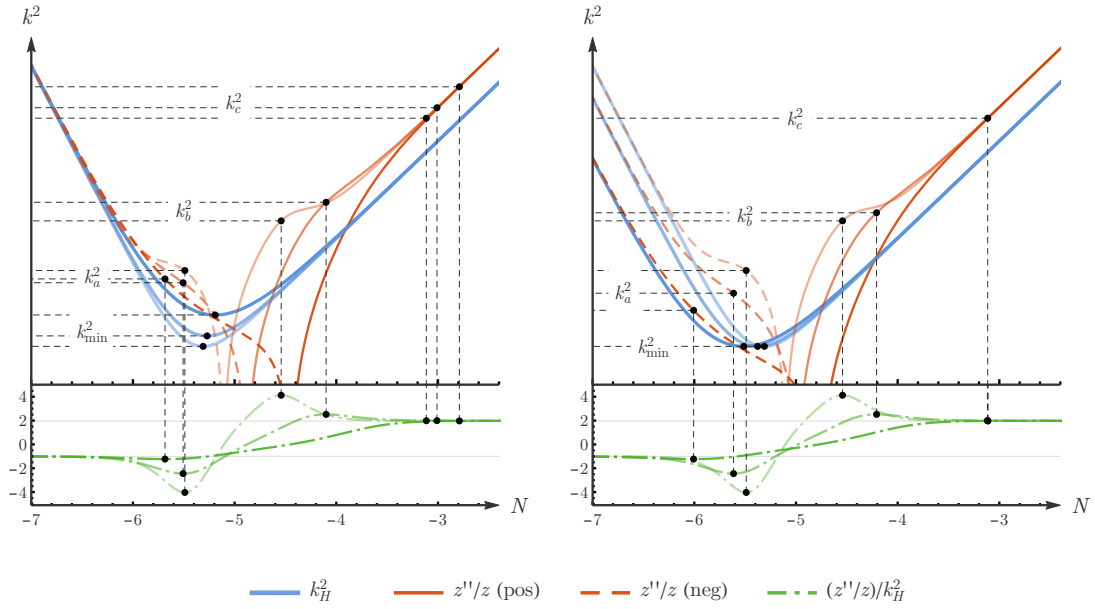

Figure 5.16.: Evolution of the squared comoving Hubble horizon, k_H^2, the potential z''/z and of the ratio $(z''/z)/k_H^2$ around the period of transition from the decelerated pre-inflationary epoch to the later power-law inflation for the model (5.148) with $\beta = 6$. (Left panel) Varying λ with Q constant does not affect the pre-inflationary behaviour but alters the minimum scale $k_{\rm min}$. (Right panel) Varying λ with $k_{\rm min}$ constant preserves the range $(k_{\rm min}, k_{\rm c})$ where the characteristic imprints of the model are expected on $\mathcal{P}_{\mathcal{R}}$ but affects the strength of the pre-inflationary epoch. (Bottom panels) As the value of λ becomes lower, the minimum and maximum on $(z''/z)/k_H^2$ become less prominent. On all panels: $\lambda = 1$ (lighter curve); $\lambda = 0.75$; $\lambda = 0.5$ (darker curve).

find

$$k_{\rm a} \simeq \begin{cases} 2.149 k_{\rm min}\,, & \text{for } \lambda = 1\,, \\ 1.710 k_{\rm min}\,, & \text{for } \lambda = 0.75\,, \\ 1.439 k_{\rm min}\,, & \text{for } \lambda = 0.5\,. \end{cases} \tag{5.162}$$

b) We define $k_{\rm b}$ as the wavenumber of the mode that crosses the potential z''/z at the moment when $(z''/z)/k_H^2$ reaches its maximum after the beginning of inflation. For $\lambda = 0.5$ the local maximum in $(z''/z)/k_H^2$ after the onset of inflation disappears; therefore no $k_{\rm b}$ is defined in this case. Through numerical investigation, we find

$$k_{\rm a} \simeq \begin{cases} 3.548 k_{\rm min}\,, & \text{for } \lambda = 1\,, \\ 3.851 k_{\rm min}\,, & \text{for } \lambda = 0.75\,. \end{cases} \tag{5.163}$$

c) When the mode with wavenumber $k_{\rm c} := 10 k_{\rm min}$ crosses the potential z''/z, the ratio $(z''/z)/k_H^2$

has already reached its asymptotic value. As such, we take $k_{\rm c}$ as a reference value of the maximum wavenumber for which we expect imprints of the model on the primordial power spectrum.

As a general effect, we find that as λ decreases, the extrema in $(z''/z)/k_H^2$ (and the associated bumps in z''/z) become less pronounced. In addition, they are shifted away from the moment of the transition from deceleration to inflation. This loss in amplitude suggests that the strong enhancement of $\mathcal{P}_\mathcal{R}$ at $k \approx k_{\rm a}$ and $k \approx k_{\rm b}$ in Fig. 5.9 may be softened by lowering λ. On the left panel in Fig. 5.17, we show the value of N at the maximum (top line) and at the minimum (bottom line) of $(z''/z)/k_H^2$ as a function of the parameter λ. For $\lambda = 0.5$, the maximum is effectively removed as it is shifted to very large values of N. For smaller values, we find that $(z''/z)/k_H^2$ no longer reaches its asymptotic value when $k_{\rm c} = 10 k_{\rm min}$ crosses the potential z''/z and, therefore, we cannot guarantee that the shape of $\mathcal{P}_\mathcal{R}$ for power-law inflation is recovered at $k \gtrsim k_{\rm c}$. In order to better control the results of the numerical integrations, we restrict our analysis to $\lambda \geq 0.5$.

In Sect. 5.3.3, we obtained the upper bound $Q \lesssim k_0^3$ by imposing that the angular power spectrum of the CMB is not affected for $\ell > 30$. When this bound is saturated, i.e., $Q = Q^+ := k_0^3$, Eq. (5.111) defines a maximum wavenumber $k_{\rm c}^+ = 10 k_{\rm min}(Q^+)$ given by:

$$k_{\rm c}^+ = 10 k_* \left(\frac{k_0}{k_*}\right)^{3\frac{2-\alpha}{6-\alpha}} \left[\frac{6-\alpha}{2-\alpha}\left(\frac{2-\alpha}{4}\right)^{\frac{4}{6-\alpha}}\right]^{\frac{1}{2}} \approx 1.457 \times 10^1 k_0 \,. \tag{5.164}$$

A minimum $k_{\rm c}^- = k_0$ can also be defined by imposing the requirement that the effects of the transition should appear on the observable range of the spectrum. By inverting Eq. (5.154), we obtain

$$Q(k_{\rm min}, \lambda) = k_*^{\beta/2} \left(\frac{k_{\rm min}}{k_*}\right)^{\frac{\beta-\alpha}{2-\alpha}} \left[\frac{|\beta-2|+|2-\alpha|}{|2-\alpha|}\left|\frac{2-\alpha}{\beta-2}\right|^{\frac{\beta-2}{\beta-\alpha}}\right]^{-\frac{1}{2\lambda}\frac{\beta-\alpha}{2-\alpha}} . \tag{5.165}$$

Consequently, we can define the following upper and lower bounds of Q:

$$Q^+(\lambda) := Q\left(\frac{k_{\rm c}^+}{10}, \lambda\right) \approx {\rm e}^{0.9615\frac{\lambda-1}{\lambda}} k_0^3 \,, \tag{5.166}$$

$$Q^-(\lambda) := Q\left(\frac{k_{\rm c}^-}{10}, \lambda\right) \approx 2.958 \times 10^{-4}\, {\rm e}^{0.9615\frac{\lambda-1}{\lambda}} k_0^3 \,. \tag{5.167}$$

These bounds are shown on the r.h.s. panel of Fig. 5.17.

Case 2: $\beta = 4$ (radiation)

We next check if a smoother transition can improve the results of Sec. 5.3.3 for the case of $\beta = 4$. In Fig. 5.16, we plot the squared comoving Hubble horizon, k_H^2, the potential z''/z and their ratio for $\lambda = 1$ (lighter curve), $\lambda = 0.75$ and $\lambda = 0.5$ (darker curve). As we decrease the value of λ while maintaining constant the parameter Q (left panel) the pre-inflationary behaviour is not affected but the minimum wavenumber $k_{\rm min} = k_{\rm trans}$ increases and modes with higher wavenumbers can become affected. On the other hand, if we decrease λ while maintaining $k_{\rm min}$ constant (right panel) the value of Q becomes lower and inflation starts to dominate earlier on.

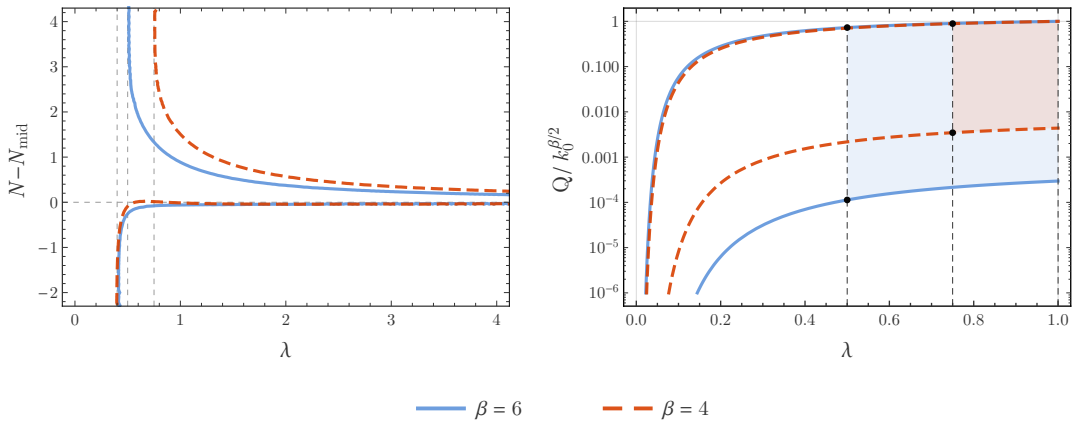

Figure 5.17.: (Left panel) Parametric plot in the $\{\lambda,\, N - N_{\rm mid}\}$ plane which shows the location of the local extrema of the ratio $(z''/z)/k_H^2$ for $\beta = 6$ (blue solid curve) and $\beta = 4$ (red dashed curve). The top curves indicate the location of the maximum and the bottom curves indicate the location of the minimum. For $\beta = 6$, the local maximum after the onset of inflation disappears for $\lambda \leq 0.5$. For $\beta = 4$, the local maximum after the onset of inflation disappears for $\lambda \leq 0.75$. For both cases, the local minimum before $N_{\rm mid}$ disappears for $\lambda \leq 0.4$. As λ increases to very large values, the positions of the minimum and the maximum converge to $N = N_{\rm mid}$. (Right panel) Upper and lower bounds of $Q/k_0^{\beta/2}$, as a function of the parameter λ as defined by Eqs. (5.166) and (5.167) for $\beta = 6$ and by Eqs. (5.171) and (5.172) for $\beta = 4$. In the intervals $\lambda \in [0.5,\, 1]$, for $\beta = 6$, and $\lambda \in [0.75,\, 1]$, for $\beta = 4$, the peaks in the power spectrum are softened and the value of maximum k affected by the pre-inflationary epoch can be predicted from the shape of z''/z near the moment of the transition to inflation. Shaded regions indicate the subsets of the parameter space delimited by these intervals and by the bounds imposed on $Q/k_0^{\beta/2}$.

As in the previous case, we define three extra characteristic wavenumbers, $k_{\rm a}$, $k_{\rm b}$ and $k_{\rm c}$, as:

a) We define $k_{\rm a}$ as the wavenumber of the mode that crosses the potential z''/z at the moment when $(z''/z)/k_H^2$ reaches its minimum before inflation. Through numerical investigation we find

$$k_{\rm a} \simeq \begin{cases} 1.381 k_{\rm min}\,, & \text{for } \lambda = 1\,, \\ 1.990 k_{\rm min}\,, & \text{for } \lambda = 0.875\,, \\ 1.001 k_{\rm min}\,, & \text{for } \lambda = 0.75\,. \end{cases} \tag{5.168}$$

b) We define $k_{\rm b}$ as the wavenumber of the mode that crosses the potential z''/z at the moment when $(z''/z)/k_H^2$ reaches its maximum after the beginning of inflation. For $\beta = 0.55$ the local maximum in $(z''/z)/k_H^2$ after the onset of inflation disappears; therefore no $k_{\rm b}$ is defined in this case. Through numerical investigation we find

$$k_{\rm a} \simeq \begin{cases} 4.626 k_{\rm min}\,, & \text{for } \beta = 1\,, \\ 6.364 k_{\rm min}\,, & \text{for } \beta = 0.875\,. \end{cases} \tag{5.169}$$

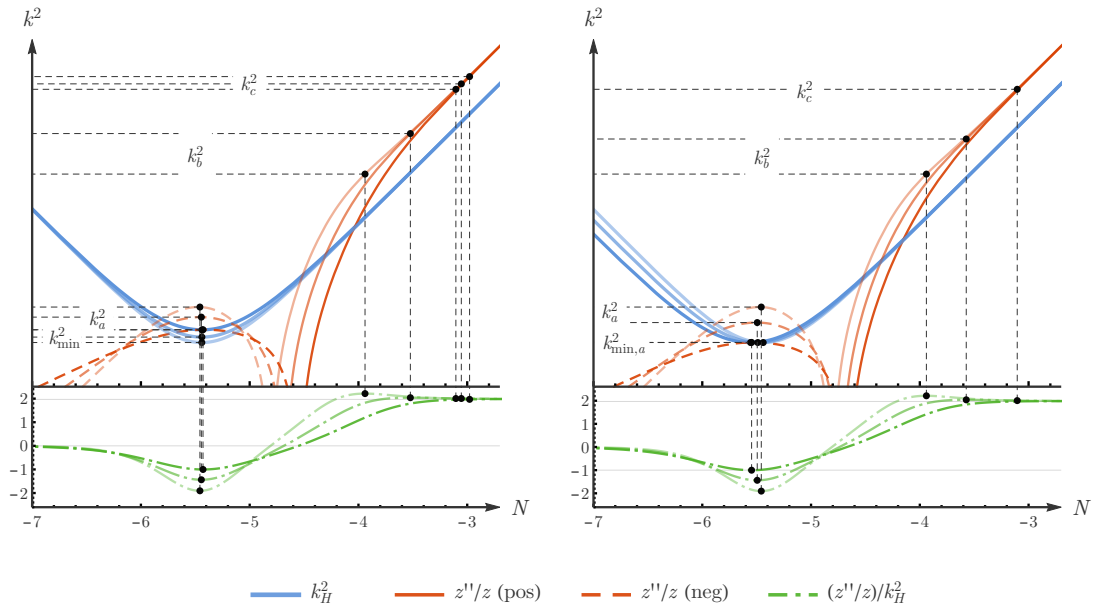

Figure 5.18.: Evolution of the squared comoving Hubble horizon, k_H^2, the potential z''/z and of the ratio $(z''/z)/k_H^2$ around the period of transition from the decelerated pre-inflationary epoch to the later power-law inflation for the model (5.148) with $\beta = 4$. (Left panel) Varying λ with Q constant does not affect the pre-inflationary behaviour but alters the minimum scale $k_{\rm min}$. (Right panel) Varying λ with $k_{\rm min}$ constant preserves the range $(k_{\rm min}, k_{\rm c})$ where characteristic imprints of the model are expected on $\mathcal{P}_\mathcal{R}$ but affects the strength of the pre-inflationary epoch. (Bottom panels) As the value of λ becomes lower, the minimum and maximum on $(z''/z)/k_H^2$ become less prominent. On all panels: $\lambda = 1$ (lighter curve); $\lambda = 0.875$; $\lambda = 0.75$ (darker curve).

c) When the mode with wavenumber $k_{\rm c} := 10 k_{\rm min}$ crosses the potential z''/z, the ratio $(z''/z)/k_H^2$ has already reached its asymptotic value. We take this value as a reference value of the maximum wavenumber for which we expect imprints of the model on the primordial power spectrum.

As in the case of $\beta = 6$, we find that as λ decreases, the extrema in $(z''/z)/k_H^2$ (and the associated bumps in z''/z) become less pronounced and are shifted away from the moment of transition to inflation, as seen on the left panel of Fig. 5.17. For $\lambda = 0.75$, the maximum is effectively removed as it is shifted to very large values of N. For smaller values of λ, we find that $(z''/z)/k_H^2$ no longer reaches its asymptotic value when $k_{\rm c} = 10 k_{\rm min}$ crosses the potential z''/z and, therefore, we cannot guarantee that the power-law inflation predictions for $\mathcal{P}_\mathcal{R}$ are recovered for $k \gtrsim k_{\rm c}$. As such, we restrict our analysis to $\lambda \geq 0.75$.

In Sect. 5.3.3, we obtained the upper bound $Q \lesssim k_0^2$ by imposing that the angular power spectrum of the CMB is not affected for $\ell > 30$. When this bound is saturated, i.e., $Q = Q^+ := k_0^2$, Eq. (5.111) defines a maximum wavenumber $k_{\rm c}^+ = 10 k_{\rm min}(Q^+)$:

$$k_{\rm c}^+ = 10 k_* \left(\frac{k_0}{k_*}\right)^{2\frac{2-\alpha}{4-\alpha}} \left[\frac{4-\alpha}{2-\alpha}\left(\frac{2-\alpha}{2}\right)^{\frac{2}{4-\alpha}}\right]^{\frac{1}{2}} \approx 1.479 \times 10^1 k_0 \,. \tag{5.170}$$

$\mathbf{i}$	$\lambda_{\mathbf{i}}\,(\beta=6)$	$\mathbf{Q_i}\,(\beta=6)$	$\lambda_{\mathbf{i}}\,(\beta=4)$	$\mathbf{Q_i}\,(\beta=4)$
1	0.5	$3.823\times10^{-1}k_0^3$	0.75	$7.922\times10^{-1}k_0^2$
2	0.6	$5.268\times10^{-1}k_0^3$	0.80	$8.397\times10^{-1}k_0^2$
3	0.7	$6.623\times10^{-1}k_0^3$	0.85	$8.840\times10^{-1}k_0^2$
4	0.8	$7.863\times10^{-1}k_0^3$	0.90	$9.253\times10^{-1}k_0^2$
5	0.9	$8.987\times10^{-1}k_0^3$	0.95	$9.639\times10^{-1}k_0^2$
6	1.0	$1.000\times10^{0}\ \ k_0^3$	1.00	$1.000\times10^{0}\ \ k_0^2$
$\mathbf{k_c^+}$	$1.457\times10^{1}k_0$		$1.479\times10^{1}k_0$	

Table 5.2.: The values of the free parameters $\{Q_i,\,\lambda_i\}$ for each of the six numerical runs, as defined in Eq. (5.173), with $Q_i = Q^+(\lambda_i)$. For completeness, we present for each case the value of $k_{\rm c}^+$ used in defining $Q^+(\lambda)$.

A minimum $k_{\rm c}^- = k_0$ can also be defined by imposing the requirement that the effects of the transition should appear on the observable range of the spectrum. Inserting $k_{\rm c}^-$ and $k_{\rm c}^+$ in Eq. (5.165) leads to the upper and lower bounds:

$$Q^+(\lambda) := Q\left(\frac{k_{\rm c}^+}{10},\,\lambda\right) \approx \mathrm{e}^{0.70\,\frac{\lambda-1}{\lambda}}k_0^2\,, \tag{5.171}$$

$$Q^-(\lambda) := Q\left(\frac{k_{\rm c}^-}{10},\,\lambda\right) \approx 4.37\times10^{-3}\,\mathrm{e}^{0.70\,\frac{\lambda-1}{\lambda}}k_0^2\,. \tag{5.172}$$

The bounds Q^+ and Q^- are shown on the r.h.s. panel of Fig. 5.17.

5.4.3. Numerical Results

By applying once again the method discussed in Sect. 5.3.3, we have integrated numerically the system of evolution equations (5.139). The evolution of the scalar perturbations v_k was computed till just after the Hubble horizon crossing during inflation. For each value of the parameter β discussed above, i.e., for $\beta = 6, 4$, we have performed six numerical runs where the values of the free parameters $\{Q\,,\lambda\}$ were fixed by setting Q to the maximum value $Q^+(\lambda)$ and changing the value of λ according to the rule

$$\lambda_i = 1 - \frac{\beta-2}{8}\frac{6-i}{5}\,, \tag{5.173}$$

with $i = 1, 2, \ldots, 6$. In Tab. 5.2, we present the numerical values of $\{Q_i,\,\lambda_i\}$ used for each run.

Using the results of the numerical integrations, we have computed the primordial power spectrum $\mathcal{P}_{\mathcal{R}}$ at the end of inflation and the normalised angular power spectrum D_ℓ^{TT} of the CMB for each numerical run. As in the previous section, the angular power spectrum was obtained by using the CLASS code [63, 227] and assuming the baseline 6-parameters ΛCDM model with the best-fit values for the late-time cosmology as given in [16].

Case 1: $\beta = 6$ (stiff matter)

In Fig. 5.19, we present the primordial power spectra obtained from the six numerical runs with $\beta = 6$ (cf. Tab. 5.2). From top-left to bottom-right, the first five panels present the characteristic shape of $\mathcal{P}_\mathcal{R}$ for $\lambda_{i=1,\dots,5}$ with the position of the characteristic scales $k_{\rm min}$, $k_{\rm a}$, $k_{\rm b}$ and $k_{\rm c}$, while in the last panel we show a superposition of all the six spectra obtained[23].

As in the previous section, the power spectrum is highly suppressed for large scales, $k < k_{\rm min}$, and follows the Planck best-fit for small scales, $k_{\rm c} < k$, while the characteristic imprints of the transition appear in the intermediate range $k_{\rm min} < k < k_{\rm c}$. Here, we find that the strong peaks that appeared around $k \approx k_{\rm a}$ and $k \approx k_{\rm b}$ in Sect. 5.3.3 start to become less pronounced as lower values of the parameter β are considered. In particular, for $\beta < 0.8 \sim 0.9$ the peak at $k \approx k_{\rm a}$ becomes sub-dominant with regards to the peak at $k \approx k_{\rm b}$. This effect seems to be related to the fact that, as λ decreases, the mode $k_{\rm a}$ if affected by the decrease of the two bumps of z''/z while $k_{\rm b}$ is affected only by the decrease of the second bump – we recall that the growth of the scalar perturbations occurs when k is below z''/z in Fig. 5.16. For the critical value $\lambda_1 = 0.5$, which corresponds to the case where the local maximum in $(z''/z)/k_H^2$ is no longer present, both peaks have disappeared and the primordial power spectrum shows a transition between the small/large scale behaviours with no distinct imprints apart from small oscillations in the intermediate range. This resembles the case in Sect. 5.3.3 where the pre-inflationary epoch mimics a dust-dominated universe ($\beta = 3$) and where no local maximum $(z''/z)/k_H^2$ existed.

The angular power spectra D_ℓ^{TT} obtained for each numerical run are presented in Fig. 5.20, where darker blue curves correspond to lower values of the parameter β. The theoretical predictions of the model are compared with the spectrum obtained from the Planck best-fit (red dashed) and the observational data points with their respective error bars. As the value of the parameter β is lowered, we find that the amplitude of the extra peak in D_ℓ^{TT} for intermediate multipoles decreases and the suppression for the low ℓ becomes stronger and affects an increasingly high range of multipoles. This effect mimics the one observed in the primordial power spectrum, cf. Fig. 5.19. In addition, we find that the two runs with lower value of λ are able to achieve a suppression at large scales that cannot be accommodated by the cosmic variance interval, as can be seen on the r.h.s. panel of Fig. 5.20. We single out the case of $\lambda_2 = 0.6$ for which D_ℓ^{TT} does not deviate significantly from the Planck best-fit for $\ell \gtrsim 20$ but becomes suppressed below that threshold, thus showing a good agreement with most data points in the low multipole range. On the other hand, the case of $\lambda_1 = 0.5$ fits very well the data in the $20 \lesssim \ell \lesssim 30$ range but the suppression becomes too strong in order for the theoretical curve to be within the error bars of most points in the $\ell \lesssim 15$ range.

Case 2: $\beta = 4$

In Fig. 5.21 we present the primordial power spectra obtained from the six numerical runs with $\beta = 4$ (cf. Tab. 5.2). From top-left to bottom-right, the first five panels present the characteristic shape of $\mathcal{P}_\mathcal{R}$ for $\lambda_{i=1,\dots,5}$, with the position of the characteristic scales $k_{\rm min}$, $k_{\rm a}$, $k_{\rm b}$ and $k_{\rm c}$, while in the last panel we show a superposition of all the six spectra obtained[24].

[23] For the case of $\lambda_6 = 1$, a discussion of the shape of $\mathcal{P}_\mathcal{R}$ at the end of inflation can be found in Sect. 5.3.3.
[24] For the case of $\lambda_6 = 1$, a discussion of the shape of $\mathcal{P}_\mathcal{R}$ at the end of inflation can be found in Sect. 5.3.3.

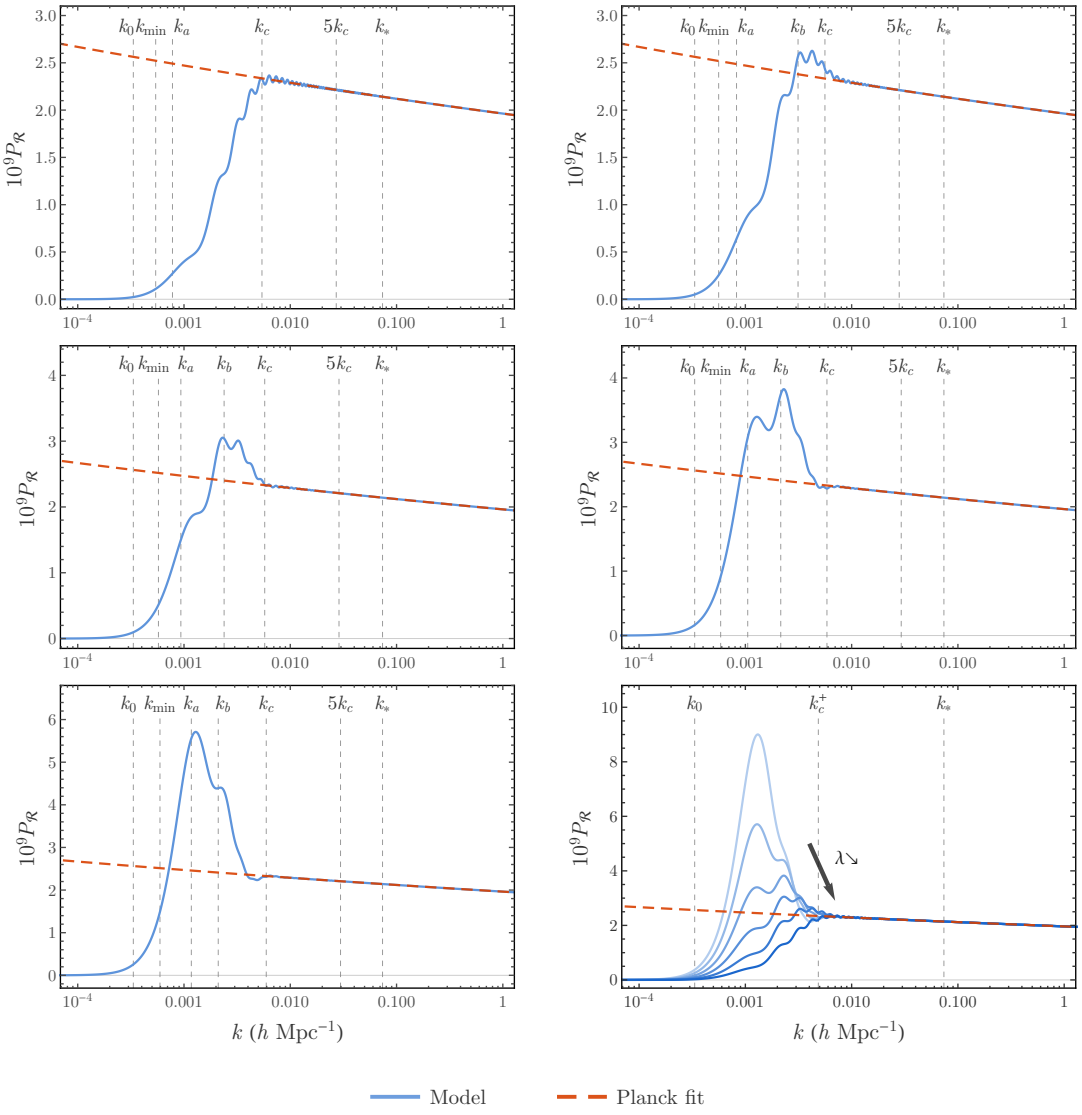

Figure 5.19.: The characteristic shape of the power spectrum obtained for the model considered in Eq. (5.110) with $\beta = 6$ (blue) compared with the observational fit (red dashed). Different values of the free parameter λ are considered (cf. Eq. (5.173)) while $k_{\rm min}$ is maintained constant: $\lambda_1 = 0.5$ (top-left); $\lambda_2 = 0.6$ (top-right); $\lambda_3 = 0.7$ (centre-left); $\lambda_4 = 0.8$ (centre-right); $\lambda_5 = 0.9$ (bottom-left). On the bottom-right panel, we present a superposition of all $\mathcal{P}_\mathcal{R}$ for $\lambda_{i=1,\ldots,6}$, where lighter blue curves correspond to higher values of the parameter λ. For all values of β, we find that $\mathcal{P}_\mathcal{R}$ is highly suppressed at large scales, $k \ll k_{\rm min}$, and indistinguishable from the observational fit at small scales, $k_{\rm c} \ll k$. On intermediate scales, the primordial power spectrum presents imprints from the transition to inflation which can be related to the characteristic scales $k_{\rm min}$, $k_{\rm a}$, $k_{\rm b}$ and $k_{\rm c}$. As the value of λ decreases, the peaks observed in $\mathcal{P}_\mathcal{R}$ between $k_{\rm min}$ and $k_{\rm c}$ become less pronounced, essentially vanishing in the case of λ_1 (top-left). For all the cases presented, the primordial power spectrum obtained reproduces the Planck best-fit for $k \gtrsim k_*$.

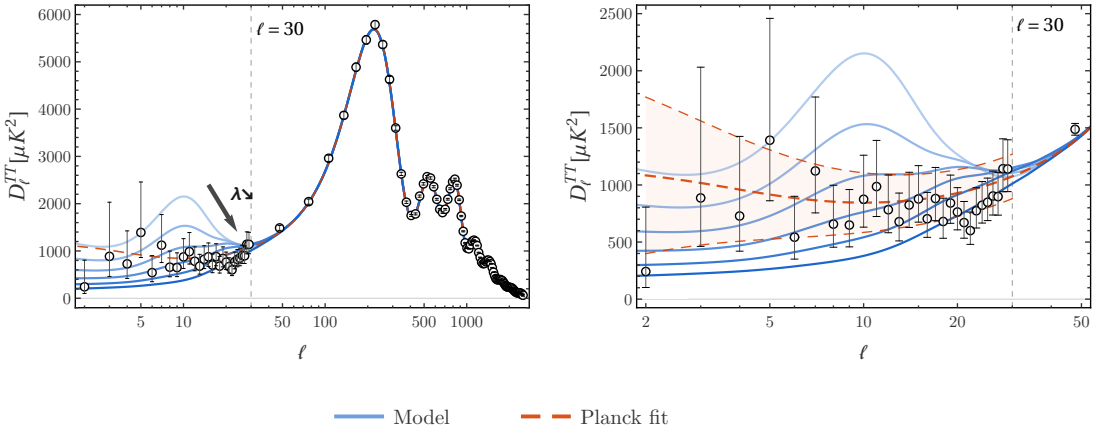

Figure 5.20.: (Left panel) The characteristic shape of the angular power spectra D_ℓ^{TT} obtained for the model considered in Eq. (5.148) with $\beta = 6$ (blue) compared with the observational fit (red dashed) and observational data points. The high peak on the intermediate multipoles observed for $\lambda_6 = 1$ becomes softer as the value of the free parameter λ is lowered. At the same time, the suppression of the spectrum for low ℓ becomes stronger and affects a wider range of multipoles. (Right panel) Zoom of the angular power spectra in the range $\ell < 50$. The shaded region, delimited by thin dashed lines, indicates the regions where deviations from the observational fit can be explained by the cosmic variance, as given by Eq. (2.62).

Once more, the power spectrum is highly suppressed for large scales, $k < k_{\rm min}$, and follows Planck best-fit for small scales, $k_{\rm c} < k$, while the characteristic imprints of the transition appear in the intermediate range $k_{\rm min} < k < k_{\rm c}$. In this case, we find that the main peak at $k \approx k_{\rm b}$ becomes less pronounced as lower values of the parameter β are considered. For the critical value $\lambda_1 = 0.75$, when the local maximum in $(z''/z)/k_H^2$ is no longer present, this peak has effectively disappeared. As a consequence, no noticeable characteristic imprints are found on the primordial power spectrum at intermediate scales, much like in the case of a dust pre-inflationary epoch discussed in Sect. 5.3.3. Notice that contrary to the previous case, no oscillations are found in the intermediate range.

The angular power spectra D_ℓ^{TT} obtained for each numerical run are presented in Fig. 5.22, where lighter blue curves correspond to lower values of the parameter β. The theoretical predictions of the model are compared with the spectrum obtained from the Planck best-fit (red dashed) and the observational data points and respective error bars. As the value of the parameter β is lowered we find that the small extra peak in D_ℓ^{TT} for intermediate multipoles starts to disappear and the suppression for the low ℓ becomes stronger and affects an increasingly high range of multipoles, an effect which mimic the one observed in the primordial power spectrum, cf. Fig. 5.21. While curves with higher β seem to fit better the data points in the range $6 \lesssim \ell \lesssim 15$, curves with lower values are almost superimposed with the data points in the $20 \lesssim \ell \lesssim 30$ range which present a lower amplitude. As can be seen on the r.h.s. panel of Fig. 5.22, all runs with $\lambda < 1$ are able to achieve a suppression at large or intermediate scales that cannot be explained by the cosmic variance. This effect clearly differentiates the model from the usual case of single inflation with BD initial conditions.

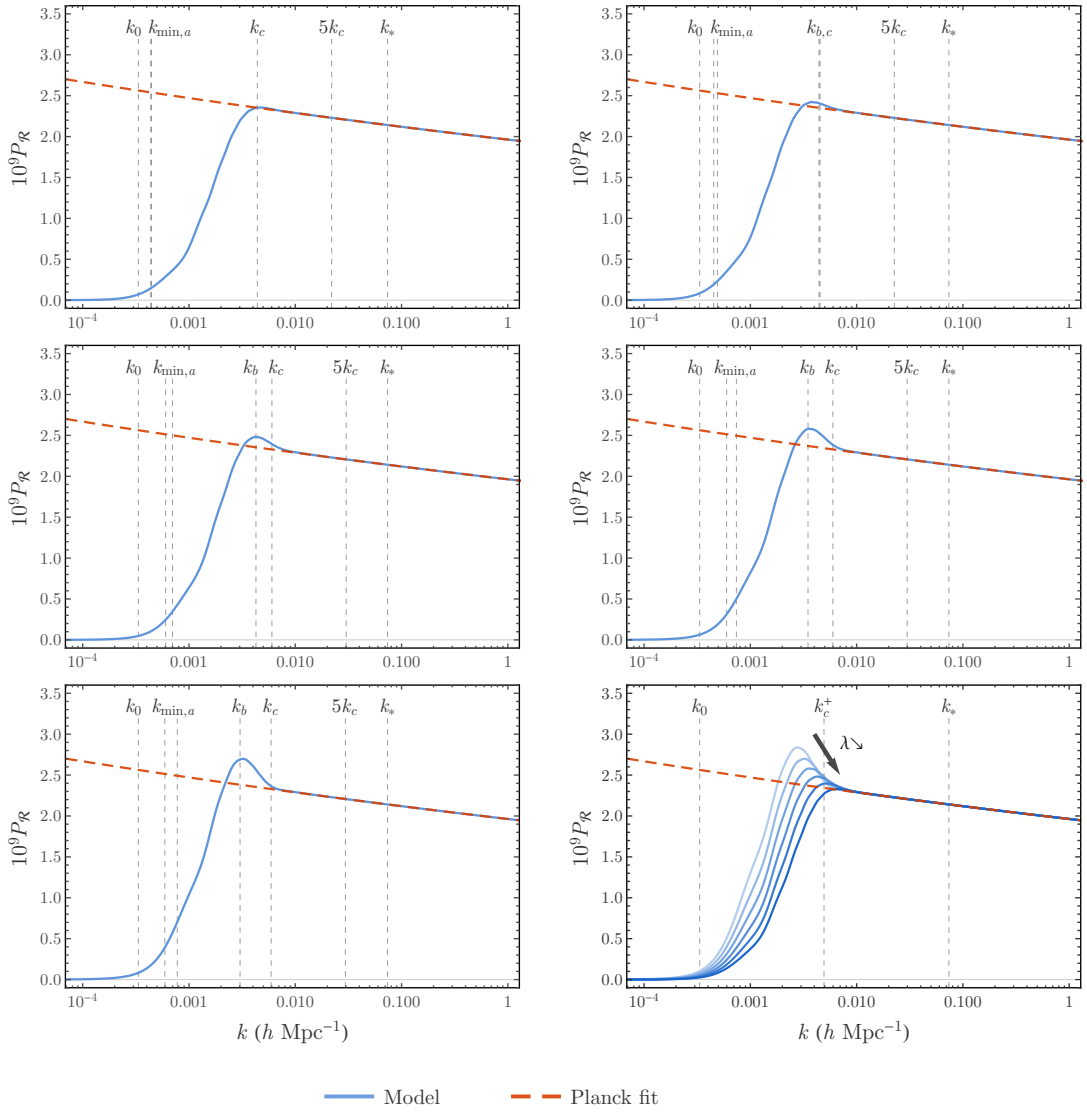

Figure 5.21.: The characteristic shape of the power spectrum obtained for the model considered in Eq. (5.110) with $\beta = 4$ (blue) compared with the observational fit (red dashed). Different values of the free parameter λ are considered (cf. Eq. (5.173)) while k_{min} is maintained constant: $\lambda_1 = 0.75$ (top-left); $\lambda_2 = 0.80$ (top-right); $\lambda_3 = 0.85$ (centre-left); $\lambda_4 = 0.90$ (centre-right); $\lambda_5 = 0.95$ (bottom-left). On the bottom-right panel, we present a superposition of all $\mathcal{P}_\mathcal{R}$ for $\lambda_{i=1,\ldots,6}$, where lighter blue curves correspond to higher values of the parameter β. For all values of λ, we find that $\mathcal{P}_\mathcal{R}$ is highly suppressed at large scales, $k < k_{\mathrm{min}}$, and indistinguishable from the observational fit at small scales, $k_{\mathrm{c}} < k$. On intermediate scales, the primordial power spectrum presents imprints from the transition to inflation which can be related to the characteristic scales k_{min}, k_{a}, k_{b} and k_{c}. A label $k_{x,y}$ indicates near superimposing lines corresponding, in order from left to right, to k_x and k_y. As the value of λ decreases, the peak observed in $\mathcal{P}_\mathcal{R}$ for $k \approx k_{\mathrm{b}}$ becomes less pronounced, essentially vanishing in the case of λ_1 (top-left).

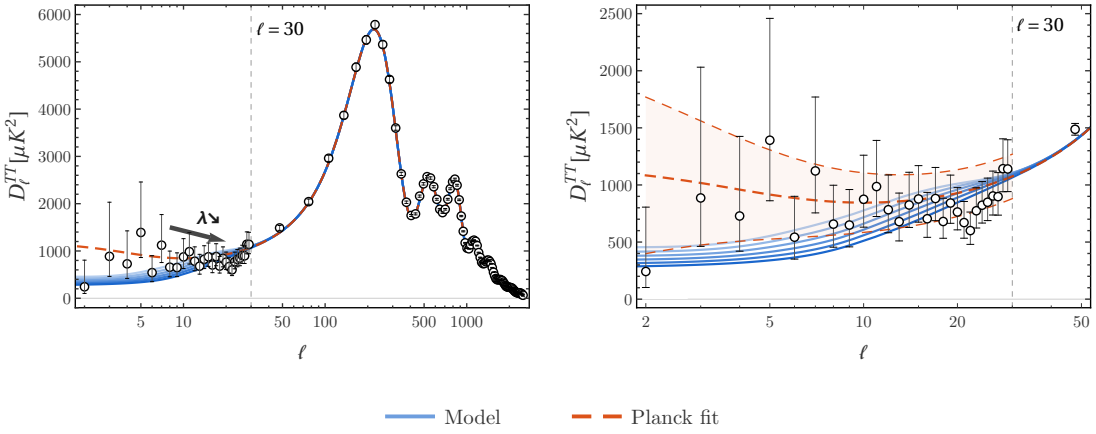

Figure 5.22.: (Left panel) The characteristic shape of the angular power spectra D_ℓ^{TT} obtained for the model considered in Eq. (5.148) with $\beta = 4$ (blue) compared with the observational fit (red dashed) and observational data points. The small peak on the intermediate multipoles observed for $\lambda_6 = 1$ starts to disappear as the free parameter β is lowered. At the same time, the suppression of the spectrum for low ℓ becomes stronger and affects a wider range of multipoles as the value of β is lowered. (Right panel) Zoom of the angular power spectra in the range $\ell < 50$. The shaded region, delimited by thin dashed lines, indicates the regions where deviations from the observational fit can be explained by the cosmic variance, as given by Eq. (2.62).

5.4.4. Discussion

In this section, we have considered the effects of the existence of a pre-inflationary decelerated epoch on the primordial power spectrum, $\mathcal{P}_\mathcal{R}$, and on the TT-component of the angular power spectrum of the CMB, D_ℓ^{TT}. This initial epoch, and its transition to a subsequent power-law inflationary era, were implemented using Eq. (5.148), which can be seen as a one-parameter extension of the model (5.110) considered in Sect. 5.3. The newly introduced parameter λ allowed us not only to control the number of e-folds necessary for the transition to occur–higher $|\lambda|$ leads to a quicker transition–but also to define whether the universe accelerates ($\lambda > 0$) or decelerates ($\lambda < 0$) in the transition. Such a model was also considered in Ref. [74, 75, 83] as a one-parameter extension of the modified Generalised Chaplygin Gas.

We have computed the explicit form of the potential z''/z that drives the evolution of the scalar perturbations and have shown how changing the value of the parameter λ can modify considerably the shape of z''/z around the moment of the transition to inflation. For the particular cases where the pre-inflationary epoch mimics a stiff-matter-dominated ($\beta = 6$) or a radiation-dominated epoch ($\beta = 4$), we found that the smaller is the value of λ, the lower are the bumps in the potential z''/z. This in turn led to the softening of the peaks on the $\mathcal{P}_\mathcal{R}$ for intermediate wavenumbers and of the extra peak on D_ℓ^{TT} for intermediate multipoles. At the same time, the suppression of $\mathcal{P}_\mathcal{R}$ and D_ℓ^{TT} at large scales became stronger. However, if the value of the parameter λ is set too low, i.e., if the time for the transition to happen is too long, the suppression at large-scales starts to affect intermediate scales, compromising the agreement with the observational data. By imposing that the imprints of the model are visible for modes currently inside the Hubble horizon without violating the constraints

on $\mathcal{P}_{\mathcal{R}}$ around the pivot scale, or compromising the agreement of D_ℓ^{TT} with the data for $\ell > 30$, we were able to define upper and lower bounds on the two parameters $\{Q,\, \lambda\}$ (cf. Fig. 5.17) not directly fixed by the Planck best-fit to the cosmological parameters. Notice that the predictions for $\mathcal{P}_{\mathcal{R}}$ and D_ℓ^{TT} were obtained using the maximum bounds Q^+, defined in Eqs. (5.166) and (5.171), so as to better visualise the full effects of the pre-inflationary phase and the transition to inflation. A complete scan of this reduced parameter space for the best fit to the observational data remains to be done.

One of the hypothesis of this section was that the shapes of the comoving Hubble wavelength $k_H^2 := (aH)^2$ and of the potential z''/z around the moment of the transition from the initial decelerated epoch to the subsequent inflationary era are imprinted on the primordial power spectrum. As a consequence, any deviation on $\mathcal{P}_{\mathcal{R}}$ and D_ℓ^{TT} from the predictions of the best-fit of Planck mission could in principle provide us with information regarding not only a potential pre-inflationary epoch but also about the transition itself. In order to test this hypothesis, for the two cases $\beta = 6$ and $\beta = 4$, we have defined four characteristic wavenumbers based on the shape of k_H^2 and z''/z around the transition: $k_{\rm min}$, $k_{\rm a}$, $k_{\rm b}$ and $k_{\rm c}$; and compared them with the regions of $\mathcal{P}_{\mathcal{R}}$ where imprints from the model appear. As a general rule, we found that $\mathcal{P}_{\mathcal{R}}$ is suppressed until $k \lesssim k_{\rm min}$ and tracks the prediction of the best-fit of Planck mission for $k_{\rm c} < k$. In addition, $k_{\rm a}$ and $k_{\rm b}$ are associated to the bumps observed in the intermediate range $k_{\rm min} < k < k_{\rm c}$, whose amplitude can be directly related to the amplitude of the features in z''/z that led to the definition of $k_{\rm a}$ and $k_{\rm b}$. We can thus conclude that the imprints of the model on $k_H^2 := (aH)^2$ and z''/z can serve as indicators for the features in the primordial power spectrum.

5.5. Revisiting Instantaneous Transitions

In the previous Sects. 5.3 and 5.4, we have seen how the existence of a pre-inflationary epoch of decelerated expansion can leave strong imprints on the predicted primordial power spectrum at the end of inflation and on the angular power spectrum of the CMB. The nature of these imprints, i.e., whether $\mathcal{P}_{\mathcal{R}}$ is enhanced or suppress with regards to the scenario with no pre-inflationary epoch, and the scales at which they appear depend not only on the type of evolution during the pre-inflationary epoch but also on how the transition to inflation occurs. In Sect. 5.4, we considered the phenomenological model (5.148) where the parameter λ controls the number of e-folds necessary for the universe to go from the initial decelerated epoch to the final power-law inflationary stage. By considering low values of this parameter, i.e., for $\lambda < 1$, we were able to soften the high amplitude peaks that appeared in the cases of a pre-inflationary epoch that mimics a stiff-matter-dominated universe or a radiation-dominated universe, as seen in Figs 5.19 and 5.21.

Alternatively, one could consider the opposite situation of very fast transitions and study the effects of taking very large values of λ on the scalar perturbations. Of particular interest is the limit of $\lambda \to +\infty$, which corresponds to an instantaneous transition, a situation that is often considered in the literature [12, 35, 36, 50, 96, 110, 114, 118, 122, 136, 157, 176, 200, 224, 252, 326]. In that limit, the asymptotic solutions (5.114) and (5.118) for the pre-inflationary epoch and the later inflationary epoch are valid until the moment of the transition. An explicit relation between the linear coefficients in the two epochs can then be deduced by fixing the boundary conditions for the linear perturbations at that moment. Unfortunately, there seems to be some confusion over the appropriate matching conditions, as different authors have used different strategies with significant implications on the final

primordial power spectra obtained. Among the various choices present in the literature we find:

i) Continuous v_k and v_k' at the moment of the transition – [96, 118, 122];

ii) Continuous v_k but discontinuous v_k' at the moment of the transition – [176];

iii) Continuous $\mathcal{R}_k$ and $\mathcal{R}_k'$ at the moment of the transition – [114];

iv) Continuous $\mathcal{R}_k$ and Φ_k at the moment of the transition – [35, 36, 50, 110, 157].

v) Continuous v_k and Φ_k at the moment of the transition in perfect fluids – [200].

Of course, not all of these strategies are equivalent and the discussion on the proper derivation of the matching conditions led to a series of contentious papers being published in the mid 90's [100, 136, 175–178, 252]. As pointed out in Ref. [252], this divergence in the results seems to arise form a difficulty in defining the proper physical hypersurface associated to the transition, with [175–178] using the conformal time η and [100, 136, 252] using an intrinsic variable of the matter fluid, such as the energy density or the value of the scalar field. More recently, another choice of matching conditions has been considered, derived from imposing the continuity of v_k and v_k' [96, 118, 122] or $\mathcal{R}_k$ and $\mathcal{R}_k'$ [114]. While the former comes from considering (incorrectly, as will be shown below) that the approximation $z''/z \approx a''/a$ holds at the moment of the transition, the latter seems to be derived from the convenience of imposing continuity of the perturbed variables rather than from physical considerations.

In Refs. [136, 252], the general matching conditions for scalar perturbations are deduced by imposing that on the hypersurface that defines the transition, the induced spatial metric h_{ij} and the extrinsic curvature Σ_{ij} are continuous[25]. By considering that the perturbed hypersurface is defined by the condition $q = q_0 + \delta q = 0$, where q is a 4-scalar, the following gauge-invariant matching conditions are obtained for the scalar perturbations[26] [136, 252]

$$\left[\psi + \mathcal{H}\frac{\delta q}{q_0'}\right]_{\pm} = 0\,, \tag{5.174}$$

$$[E]_{\pm} = 0\,, \tag{5.175}$$

$$\left[\psi' + \mathcal{H}A + \left(\mathcal{H}' - \mathcal{H}^2\right)\frac{\delta q}{q_0'}\right]_{\pm} = 0\,, \tag{5.176}$$

$$\left[B - E' + \frac{\delta q}{q_0'}\right]_{\pm} = 0\,. \tag{5.177}$$

In scalar field models where a jump in the EoS parameter is caused by a step-like feature of the potential $V(\varphi)$ at $\varphi_{\rm hyp}$ [224, 326], it is natural to define the hypersurface by the condition $\varphi = \varphi_0 + \delta\varphi = \varphi_{\rm hyp}$.

[25] At the background level, these same conditions imply the continuity of the scale factor a and the Hubble rate H.

[26] The quantities A , B and φ in Eqs. (5.174)–(5.177) are the scalar potentials that parameterise the perturbed FLRW line element, cf. Eq. (A.9).

The identifications $\delta q = \delta\varphi$ and $q_0' = \varphi_0'$ follow and the previous matching conditions become

$$[\mathcal{R}]_\pm = 0\,, \tag{5.178}$$

$$[E]_\pm = 0\,, \tag{5.179}$$

$$\left[\Psi' + \mathcal{H}\Phi - \frac{\kappa^2 a^2}{2}\varphi_0'\delta\varphi\right]_\pm = 0\,, \tag{5.180}$$

$$\left[\frac{\mathcal{R}-\Psi}{\mathcal{H}}\right]_\pm = 0\,, \tag{5.181}$$

where we recall that Φ and Ψ are the gauge-invariant Bardeen potentials [46] and $\mathcal{R}$ is the comoving curvature perturbation [49]. The second condition (5.179) does not carry relevant physical information as it can always be satisfied by means of a gauge transformation [136] and in models with a minimally coupled scalar field, the third condition (5.180) is automatically verified due to the $(i-0)$ component of the perturbed Einstein equations. Then, using the equality of the two Bardeen potentials in scalar field models, we arrive at the matching conditions used in [35, 36, 50, 110, 157]:

$$[\mathcal{R}]_\pm = 0\,, \qquad\qquad [\Phi]_\pm = 0\,. \tag{5.182}$$

5.5.1. A divergence in z''/z

The main focus of this section is to consider the limit $\lambda \to +\infty$ in the toy model presented in Sect. 5.4. In this limit the interval Δ_λ, Eq. (5.151), that determines how many e-folds are necessary for the transition to occur vanishes, thus, the transition occurs instantaneously at $N = N_{\rm mid}$[27]. This instantaneous change in behaviour can be seen in the Friedmann equation (5.148) which now reads

$$H^2(N) \overset{\lambda\to\pm\infty}{=} H_{\rm dS}^2\left[\frac{Q^2}{(a_* H_{\rm dS})^\beta}\right]^{1-\Theta_{(\alpha,\beta,\lambda)}(N-N_{\rm mid})} \mathrm{e}^{-\left[\beta+(\alpha-\beta)\,\Theta_{(\alpha,\beta,\lambda)}(N-N_{\rm mid})\right]N}\,, \tag{5.183}$$

where

$$\begin{aligned}\Theta_{(\alpha,\beta,\lambda)}(N-N_{\rm mid}) &= \Theta\Big(\mathrm{sign}\left[\lambda(\beta-\alpha)\right](N-N_{\rm mid})\Big) \\ &= \begin{cases}\Theta\left(N-N_{\rm mid}\right)\,, & \text{for } \mathrm{sign}\left[\lambda(\beta-\alpha)\right]>0\,,\\ 1-\Theta\left(N-N_{\rm mid}\right)\,, & \text{for } \mathrm{sign}\left[\lambda(\beta-\alpha)\right]<0\,,\end{cases}\end{aligned} \tag{5.184}$$

and $\Theta(x)$ is the Heaviside step function. We note that the first line on the last equality of Eq. (5.184) corresponds to cases where the rate of acceleration of the Universe increases at the transition, e.g., by going from a decelerated pre-inflationary epoch to inflation, while the second line corresponds to cases where the rate of acceleration decreases.

At the level of the EoS parameter w, given by Eq. (5.149), and of the slow-roll parameter ϵ, given

[27] Notice that $N_{\rm trans}$, defined in Eq. (5.153), which marks the moment at which the point of no acceleration in the transition between the initial decelerated and the later power-law inflation is reached, converges to $N_{\rm mid}$ as $\lambda \to +\infty$.

by Eq. (5.156), we observe a step-like discontinuity at $N = N_{\rm mid}$:

$$w(N) \overset{\lambda\to\pm\infty}{=} \frac{\beta-3}{3} + \frac{\alpha-\beta}{3}\Theta_{(\alpha,\beta,\lambda)}(N-N_{\rm mid})\,, \tag{5.185}$$

$$\epsilon(N) \overset{\lambda\to\pm\infty}{=} \frac{\beta}{2} + \frac{\alpha-\beta}{2}\Theta_{(\alpha,\beta,\lambda)}(N-N_{\rm mid})\,. \tag{5.186}$$

In the rest of this section we will use Eq. (5.186) to re-parameterise the model in terms of the value of the slow roll parameter before and after the transition $\epsilon^+ := \epsilon(N_{\rm mid} < N)$ and $\epsilon^- := \epsilon(N < N_{\rm mid})$. This allows us to generalise our results for arbitrary $\epsilon^\pm \in (0,\,1)\cup(1,\,3]$ while at the same time simplifying the notation, meaning that we can easily accommodate any pair of initial/final epochs with decelerated or accelerated expansion with the exclusion of epochs with pure de Sitter expansion or with zero acceleration.

The continuity of the scale factor and of the Hubble parameter in (5.183) leads to the continuity of the comoving Hubble horizon, Eq. (5.152), which now reads

$$\begin{aligned} k_H(N) &\overset{\lambda\to\pm\infty}{=} k^\infty_{\rm trans}\,{\rm e}^{\left[1-\epsilon^- -(\epsilon^+-\epsilon^-)\Theta(N-N_{\rm mid})\right](N-N_{\rm mid})} \\ &= \begin{cases} k^\infty_{\rm trans}\,{\rm e}^{(1-\epsilon^-)(N-N_{\rm mid})} & N < N_{\rm mid}\,, \\ k^\infty_{\rm trans}\,{\rm e}^{(1-\epsilon^+)(N-N_{\rm mid})} & N_{\rm mid} < N\,, \end{cases} \end{aligned} \tag{5.187}$$

where the value at the moment of the transition is given by

$$k^\infty_{\rm trans} := \lim_{\lambda\to\pm\infty} k_{\rm trans} = a_* H_{\rm dS}\left[\frac{Q}{(a_* H_{\rm dS})^{\epsilon^-}}\right]^{\frac{1-\epsilon^+}{\epsilon^- - \epsilon^+}}\,. \tag{5.188}$$

In contrast, in the potential z''/z, which depends on the slow-roll parameter ϵ and its derivatives, we find that discontinuous and divergent terms appear as λ is taken to infinity. We note that some care needs to be taken when deriving the asymptotic shape of z''/z as a direct substitution of the $\tanh$ and sech functions in the expressions (5.157) and (5.158) leads to non-linear combinations of the Θ function and the Dirac delta function that are not well defined from a mathematical point of view. Instead, a proper computation of the limit of Eq. (5.157) and (5.158) for very large λ leads to[28]

$$\begin{aligned} \frac{z''}{z} = k_H^2(N)\Bigg\{ 2-\epsilon(N) + \left[\frac{\epsilon^- - \epsilon^+}{2} - \frac{3}{2}\log\left(\frac{\epsilon^-}{\epsilon^+}\right)\right]\delta(N-N_{\rm mid}) \\ - \log\left(\frac{\epsilon^-}{\epsilon^+}\right)\delta_N(N-N_{\rm mid})\Bigg\}\,. \end{aligned} \tag{5.189}$$

While for $N \neq N_{\rm mid}$ the potential z''/z reduces to $a''/a = k_H^2(2-\epsilon)$, which is the potential that drives the production of tensorial perturbations, at $N = N_{\rm mid}$ we must take into account the presence of terms with a Dirac delta function and its derivative. As we will show below, these divergent terms lead to a discontinuity at the level of v_k and v_k' at the moment of transition and are crucial in the validity of the long-wavelength approximation ($k^2 \ll z''/z$) for scales way above the value of a''/a around the transition [224, 326].

[28] The derivation of Eq. (5.189) is presented in the Appendix (D.5). We are grateful to José M. M. Senovilla and Mikel A. Urkiola for useful suggestions and comments regarding this issue.

5.5.2. Matching conditions for $\mathcal{R}_k$ and v_k

In order to calculate the jump in v_k and its derivative at $N = N_{\rm mid}$, it is easier to change to the comoving curvature perturbation $\mathcal{R}_k = v_k/z$, whose evolution equation obtained from (5.105) reads

$$\frac{\mathrm{d}^2\mathcal{R}_k}{\mathrm{d}N^2} + \left(3 - \epsilon + \frac{\epsilon_N}{\epsilon}\right)\frac{\mathrm{d}\mathcal{R}_k}{\mathrm{d}N} + \left(\frac{k}{k_H}\right)^2 \mathcal{R}_k = 0\,. \tag{5.190}$$

In the limit of $\lambda \to +\infty$, we find that the previous equation can be written as

$$\frac{\mathrm{d}^2\mathcal{R}_k}{\mathrm{d}N^2} + \left[3 - \epsilon^- - (\epsilon^+ - \epsilon^-)\Theta(N - N_{\rm mid}) - \log\left(\frac{\epsilon^-}{\epsilon^+}\right)\delta(N - N_{\rm mid})\right]\frac{\mathrm{d}\mathcal{R}_k}{\mathrm{d}N} + \frac{k^2}{k_H^2}\mathcal{R}_k = 0\,. \tag{5.191}$$

As deduced in the Appendix D.6, the presence of a δ function in the friction term leads to a jump in the derivative $\mathrm{d}\mathcal{R}_k/\mathrm{d}N$ at $N = N_{\rm mid}$:

$$\frac{\mathrm{d}\mathcal{R}_k}{\mathrm{d}N}(N_{\rm mid}^+) = \frac{\epsilon^-}{\epsilon^+}\frac{\mathrm{d}\mathcal{R}_k}{\mathrm{d}N}(N_{\rm mid}^-)\,, \tag{5.192}$$

while at the same time $\mathcal{R}_k$ remains continuous[29]. The same boundary conditions were deduced in Ref. [36] based on the results of [110, 136]. From Eq. (5.192) and the continuity of $\mathcal{R}_k$, we find that the correct boundary conditions lead to a discontinuous jump of v_k and its N-derivative during the transition:

$$v_k(N_{\rm mid}^+) = \sqrt{\frac{\epsilon^+}{\epsilon^-}}\,v_k(N_{\rm mid}^-)\,, \tag{5.193}$$

$$\frac{\mathrm{d}v_k}{\mathrm{d}N}(N_{\rm mid}^+) = \left(\sqrt{\frac{\epsilon^+}{\epsilon^-}} - \sqrt{\frac{\epsilon^-}{\epsilon^+}}\right)v_k(N_{\rm mid}^-) + \sqrt{\frac{\epsilon^-}{\epsilon^+}}\frac{\mathrm{d}v_k}{\mathrm{d}N}(N_{\rm mid}^-)\,. \tag{5.194}$$

Equation (5.193) can be translated to the following matching condition for v_k':

$$v_k'(N_{\rm mid}^+) = k_{\rm trans}^{\infty}\left(\sqrt{\frac{\epsilon^+}{\epsilon^-}} - \sqrt{\frac{\epsilon^-}{\epsilon^+}}\right)v_k(N_{\rm mid}^-) + \sqrt{\frac{\epsilon^-}{\epsilon^+}}\,v_k'(N_{\rm mid}^-)\,. \tag{5.195}$$

Interestingly, the same boundary conditions (5.193) and (5.194) can be obtained by considering the long-wavelength approximation ($k^2 \ll z''/z$) [224, 326] even for the modes that are inside the comoving Hubble horizon and verify $a''/a \ll k^2$ at the moment of transition[30]. This apparently contradictory result[31] can be understood by the fact that, while for $N \neq N_{\rm mid}$ the evolution of the scalar perturbations is dictated by a''/a whose value can be below or above k^2 for a given mode, at the moment of the transition the potential z''/z has an infinite value due to the presence of terms with a Dirac delta function and its derivative. Therefore, the condition $k \ll z''/z$ becomes valid for

[29] Due to the continuity of the comoving Hubble horizon, the derivative $\mathcal{R}_k'$ satisfies the same boundary condition (5.192) as $\mathrm{d}\mathcal{R}_k/\mathrm{d}N$.

[30] A derivation of this result can be found in the Appendix D.7.

[31] The good agreement of the long wavelength approximation with the numerical results for all scales in a scalar field model with a jump in the potential is mentioned as a source of surprise by the authors of [224]. Here, we see that the long wavelength approximation leads precisely to the exact correct matching conditions for all k.

all k in an infinitesimal neighbourhood of $N = N_{\rm mid}$.

In the limit of instantaneous transitions ($\lambda \to +\infty$) discussed in this section, the asymptotic solutions (5.114) and (5.118) (cf. Appendix D.3 for a derivation of these solutions) can be extended up to the moment of the transition at $N = N_{\rm mid}$. By integrating (5.187), we obtain the conformal time η as a function of N:

$$\begin{aligned}\eta - \eta(N_{\rm mid}) &= \frac{1}{k^{\infty}_{\rm trans}}\frac{{\rm e}^{[\epsilon(N)-1](N-N_{\rm mid})}-1}{\epsilon(N)-1} \\ &= \begin{cases} \dfrac{1}{k^{\infty}_{\rm trans}}\dfrac{{\rm e}^{(\epsilon^{-}-1)(N-N_{\rm mid})}-1}{\epsilon^{-}-1} & N < N_{\rm mid}\,, \\ \dfrac{1}{k^{\infty}_{\rm trans}}\dfrac{{\rm e}^{(\epsilon^{+}-1)(N-N_{\rm mid})}-1}{\epsilon^{+}-1} & N_{\rm mid} < N\,. \end{cases}\end{aligned} \tag{5.196}$$

Furthermore, by setting $\eta(N_{\rm mid}) = 0$, we can write v_k during the whole evolution of the system as

$$\begin{aligned} v_k(N < N_{\rm mid}) = {} & \sqrt{\frac{\hbar}{2k}}\sqrt{\frac{\pi}{2}}\sqrt{\frac{q}{|\epsilon^{-}-1|}}\exp\left[\frac{\epsilon^{-}-1}{2}(N-N_{\rm mid})\right] \\ & \times\left[C^{-}_{1,k}\,H^{(1)}_{\nu^{-}}\left(\frac{q}{|\epsilon^{-}-1|}\exp\left[(\epsilon^{-}-1)(N-N_{\rm mid})\right]\right)\right. \\ & \left. + C^{-}_{2,k}\,H^{(2)}_{\nu^{-}}\left(\frac{q}{|\epsilon^{-}-1|}\exp\left[(\epsilon^{-}-1)(N-N_{\rm mid})\right]\right)\right]\,, \end{aligned} \tag{5.197}$$

$$\begin{aligned} v_k(N_{\rm mid} < N) = {} & \sqrt{\frac{\hbar}{2k}}\sqrt{\frac{\pi}{2}}\sqrt{\frac{q}{|\epsilon^{+}-1|}}\exp\left[\frac{\epsilon^{+}-1}{2}(N-N_{\rm mid})\right] \\ & \times\left[C^{+}_{1,k}\,H^{(1)}_{\nu^{+}}\left(\frac{q}{|\epsilon^{+}-1|}\exp\left[(\epsilon^{+}-1)(N-N_{\rm mid})\right]\right)\right. \\ & \left. + C^{+}_{2,k}\,H^{(2)}_{\nu^{+}}\left(\frac{q}{|\epsilon^{+}-1|}\exp\left[(\epsilon^{+}-1)(N-N_{\rm mid})\right]\right)\right]\,. \end{aligned} \tag{5.198}$$

To simplify the notation, here we have introduce the re-scaled wavenumber $q := k/k^{\infty}_{\rm trans}$. We recall that the order of the Hankel functions can be written in terms of the value of the slow-roll parameter ϵ before and after the transition, $\epsilon^{\pm}$, as

$$\nu^{\pm} = \frac{1}{2}\left|\frac{3-\epsilon^{\pm}}{\epsilon^{\pm}-1}\right|\,. \tag{5.199}$$

In addition, the linear coefficients $C^{\pm}_{1,k}$ and $C^{\pm}_{2,k}$ satisfy the constraint

$$\left|C^{\pm}_{1,k}\right|^2 - \left|C^{\pm}_{2,k}\right|^2 = {\rm sign}(1-\epsilon^{\pm})\,. \tag{5.200}$$

Using the matching conditions (5.193) and (5.195) we are able to relate the two pairs of coefficients

$\{C^-_{1,k}, C^-_{2,k}\}$ and $\{C^+_{1,k}, C^+_{2,k}\}$ through the linear transformation

$$\begin{pmatrix} C^+_{1,k} \\ C^+_{2,k} \end{pmatrix} = \mathrm{sign}(1-\epsilon^+) \begin{pmatrix} P_k & Q_k \\ Q^*_k & P^*_k \end{pmatrix} \cdot \begin{pmatrix} C^-_{1,k} \\ C^-_{2,k} \end{pmatrix} , \tag{5.201}$$

and its inverse

$$\begin{pmatrix} C^-_{1,k} \\ C^-_{2,k} \end{pmatrix} = \mathrm{sign}(1-\epsilon^-) \begin{pmatrix} P^*_k & -Q_k \\ -Q^*_k & P_k \end{pmatrix} \cdot \begin{pmatrix} C^+_{1,k} \\ C^+_{2,k} \end{pmatrix} . \tag{5.202}$$

It follows from the normalisation condition (5.200) that P_k and Q_k must satisfy the constraint $|P_k|^2 - |Q_k|^2 = \mathrm{sign}(1-\epsilon^+)\,\mathrm{sign}(1-\epsilon^-)$. The full expressions of P_k and Q_k for $\epsilon^\pm \in (0,\,1)\cup(1,\,3]$ can be found in the Appendix D.8. It can be checked that in the limit of no transition, i.e., if $\epsilon^+ = \epsilon^-$, the transformations (5.201) and (5.202) reduce to the identity transformation.

The transformation (5.201) allows us to fully describe the evolution of the mode functions during the late power-law inflation in terms of the evolution during the initial pre-inflationary epoch, which is encoded in the linear coefficients $C^-_{1,k}$ and $C^-_{2,k}$. Next, we will show how this allows us to derive, analytically, the theoretical prediction for the primordial power spectrum for a model with arbitrary initial conditions for the scalar perturbations where an epoch of power-law inflation is preceded by a pre-inflationary epoch with an abrupt transition.

5.5.3. The imprints on $\mathcal{P}_\mathcal{R}$

Let us go back to considering the case of power-law inflation. If we impose arbitrary initial conditions for the mode functions v_k, encoded in the linear coefficients $C^+_{1,k}$ and $C^+_{2,k}$, the prediction for the primordial power spectrum at the end of inflation reads

$$\begin{aligned} \mathcal{P}_\mathcal{R}(k) = {} & \frac{\hbar\, k^2}{8\pi} \frac{|\eta_\mathrm{end} - \eta_\mathrm{c}|}{z^2_\mathrm{end}} \left| H^{(1)}_\nu(k|\eta_\mathrm{end} - \eta_\mathrm{c}|) \right|^2 \\ & \times \left(|C^+_{1,k}|^2 + |C^+_{2,k}|^2 + 2\,\mathrm{Re}\left[C^+_{1,k}\,(C^+_{2,k})^*\,\mathrm{e}^{2\mathrm{i}\theta^+_k} \right] \right) . \end{aligned} \tag{5.203}$$

Here, η_c is an integration constant and θ^+_k is the phase of the $H^{(1)}_{\nu^+}$ function at η_end. For comparison, we note that in a scenario of power-law inflation with BD-like initial conditions, the prediction for the primordial power spectrum at the end of inflation is

$$\mathcal{P}^\mathrm{BD}_\mathcal{R}(k) = \frac{\hbar\, k^2}{8\pi} \frac{|\eta_\mathrm{end} - \eta_\mathrm{c}|}{z^2_\mathrm{end}} \left| H^{(1)}_\nu(k|\eta_\mathrm{end} - \eta_\mathrm{c}|) \right|^2 . \tag{5.204}$$

We thus find that the ratio between $\mathcal{P}_\mathcal{R}(k)$ with arbitrary initial conditions and $\mathcal{P}^\mathrm{BD}_\mathcal{R}$ is encoded almost entirely in the coefficients $C^+_{1,k}$ and $C^+_{2,k}$:

$$\frac{\mathcal{P}_\mathcal{R}(k)}{\mathcal{P}^\mathrm{BD}_\mathcal{R}(k)} = |C^+_{1,k}|^2 + |C^+_{2,k}|^2 + 2\,\mathrm{Re}\left[C^+_{1,k}\,(C^+_{2,k})^*\,\mathrm{e}^{2\mathrm{i}\theta^+_k} \right] . \tag{5.205}$$

In particular, for modes that are well outside the Hubble horizon at the end of inflation, the phase $\theta_k^+ \approx -\pi/2$ due to the asymptotic behaviour of the Hankel functions for very small argument [7, 283] and the ratio (5.205) reduces to

$$\frac{\mathcal{P}_{\mathcal{R}}(k)}{\mathcal{P}_{\mathcal{R}}^{\rm BD}(k)} = |C_{1,k}^+ - C_{2,k}^+|^2 \,. \tag{5.206}$$

The linear transformation (5.201) relates the solution for v_k during power-law inflation with the solution for v_k during a pre-inflationary epoch that ends abruptly at some $N_{\rm mid}$ e-folds before the pivot scale crosses the horizon. Therefore, inserting Eq. (5.201) in Eq. (5.206) allows us to compute the imprints on the primordial power spectrum due to the presence of a pre-inflationary epoch whose initial conditions are encoded in the linear coefficients $C_{1,k}^-$ and $C_{2,k}^-$:

$$\frac{\mathcal{P}_{\mathcal{R}}^{\rm PI}(k)}{\mathcal{P}_{\mathcal{R}}^{\rm BD}(k)} = |P_k - Q_k^*|^2 \left(|C_{1,k}^-|^2 + |C_{2,k}^-|^2\right) - 2{\rm Re}\left[C_{1,k}^-(C_{2,k}^-)^*(P_k - Q_k^*)^2\right] \,. \tag{5.207}$$

As discussed in Sect. 5.3.1, during epochs of decelerated (accelerated) expansion with constant $1 < \epsilon^-$ ($\epsilon^- < 1$), the BD vacuum solution (5.107) is recovered for modes well inside the Hubble horizon, i.e., when $k_H \ll k$, if the linear coefficients satisfy $C_{1,k} = 0$ and $|C_{2,k}| = 1$ ($|C_{1,k}| = 1$ and $C_{2,k} = 0$). By imposing any of these two conditions in Eq. (5.207), we obtain the following simplified expression:

$$\frac{\mathcal{P}_{\mathcal{R}}^{\rm PI}(k)}{\mathcal{P}_{\mathcal{R}}^{\rm BD}(k)} = |P_k - Q_k^*|^2 = \frac{\pi^2}{4}\frac{\Delta_0 + \Delta_1 q + \Delta_2 q^2}{|1-\epsilon^+||1-\epsilon^-|} \,, \tag{5.208}$$

where the factors Δ_i, with $i = 0, 1, 2$, are defined as

$$\Delta_0 := \left[\left(\frac{\epsilon^+}{\epsilon^-}\right)^{\frac{1}{2}}(3-\epsilon^+)\Theta(1-\epsilon^+) - \left(\frac{\epsilon^+}{\epsilon^-}\right)^{-\frac{1}{2}}(3-\epsilon^-)\Theta(1-\epsilon^-)\right]^2 (J_{\nu^+}^q)^2 |H_{\nu^-}^q|^2 \,, \tag{5.209}$$

$$\begin{aligned}\Delta_1 :=& -2\left[\left(\frac{\epsilon^+}{\epsilon^-}\right)^{\frac{1}{2}}(3-\epsilon^+)\Theta(1-\epsilon^+) - \left(\frac{\epsilon^+}{\epsilon^-}\right)^{-\frac{1}{2}}(3-\epsilon^-)\Theta(1-\epsilon^-)\right] \\ &\times\left[\left(\frac{\epsilon^+}{\epsilon^-}\right)^{\frac{1}{2}}{\rm sign}(1-\epsilon^+) J_{\nu^+}^q J_{1+\nu^+}^q |H_{\nu^-}^q|^2 \right. \\ &\left. - \left(\frac{\epsilon^+}{\epsilon^-}\right)^{-\frac{1}{2}}{\rm sign}(1-\epsilon^-)(J_{\nu^+}^q)^2 {\rm Re}[H_{\nu^-}^q (H_{1+\nu^-}^q)^*]\right] \,,\end{aligned} \tag{5.210}$$

$$\Delta_2 := \left|\left(\frac{\epsilon^+}{\epsilon^-}\right)^{\frac{1}{2}}{\rm sign}(1-\epsilon^+) J_{1+\nu^+}^q H_{\nu^-}^q - \left(\frac{\epsilon^+}{\epsilon^-}\right)^{-\frac{1}{2}}{\rm sign}(1-\epsilon^-) J_{\nu^+}^q H_{1+\nu^-}^q\right|^2 \,. \tag{5.211}$$

For shortness, here and throughout the rest of this section, we adopt the following notation:

$$\begin{aligned} H_{\nu^-}^q &:= H_{\nu^-}^{(1)}\left(\frac{q}{|1-\epsilon^-|}\right) \,, & H_{1+\nu^-}^q &:= H_{1+\nu^-}^{(1)}\left(\frac{q}{|1-\epsilon^-|}\right) \,, \\ J_{\nu^+}^q &:= J_{\nu^+}\left(\frac{q}{|1-\epsilon^+|}\right) \,, & J_{1+\nu^+}^q &:= J_{1+\nu^+}\left(\frac{q}{|1-\epsilon^+|}\right) \,. \end{aligned} \tag{5.212}$$

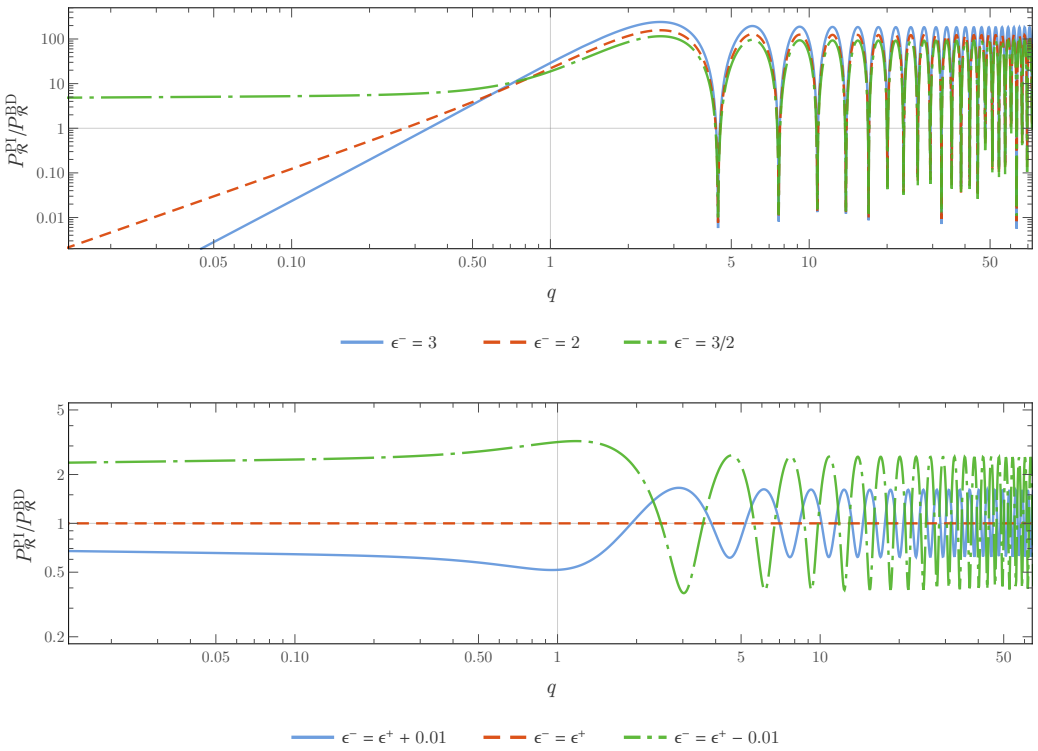

Figure 5.23.: The ratio $\mathcal{P}_{\mathcal{R}}^{\rm PI}/\mathcal{P}_{\mathcal{R}}^{\rm BD}$, given in Eq. (5.208), as a function of the normalised wavenumber $q := k/k_{\rm trans}^{\infty}$ for an inflationary final epoch with $\epsilon^+ = \alpha/2 \simeq 0.01638$ and different values of ϵ^-. (Top panel) blue solid curve – pre-inflationary epoch mimicking stiff-matter; red dashed curve – pre-inflationary epoch mimicking radiation; green dot-dashed curve – pre-inflationary epoch mimicking dust. (Bottom panel) blue solid curve – accelerated pre-inflationary epoch with $\epsilon^- = \epsilon^+ + 0.01$; red dashed curve – no transition ($\epsilon^- = \epsilon^+$); green dot-dashed curve – accelerated pre-inflationary epoch with $\epsilon^- = \epsilon^+ - 0.01$.

In Fig. 5.23, we plot the ratio $\mathcal{P}_{\mathcal{R}}^{\rm PI}/\mathcal{P}_{\mathcal{R}}^{\rm BD}$ as a function of the normalised wavenumber q for $\epsilon^+ = 0.01638$ and for different values of ϵ^-. Notice that in the limit of $\epsilon^+ = \epsilon^-$, i.e., when there is no transition, the r.h.s. of Eq. (5.208) reduces to unity (cf. r.h.s. panel of Fig. 5.23) as Δ_0 and Δ_1 vanish identically and, making use of the Wronskian identities for the Bessel and the Hankel functions (cf. Eq. (10.5.4) of Ref. [283]), it is possible to write $\Delta_2 = (4/\pi^2)|1-\epsilon^+||1-\epsilon^-|q^{-2}$.

At this point, we note that in deriving the expression (5.208), we have only assumed that $0 < \epsilon^{\pm} \leq 3$ and $\epsilon^{\pm} \neq 1$. Therefore, this expression remains valid for any combination of accelerated/decelerated initial and final epochs, as long as the considered modes are well outside the Hubble horizon at $\eta_{\rm end}$. In fact, while the initial motivation for this section is to find the imprints on the primordial power spectrum after the end of a power-law inflation, Eqs. (5.203)–(5.205) are valid as well for epochs where $1 < \epsilon^+$, as are Eqs. (5.206)–(5.208) as long as $k \ll k_H$ at $\eta_{\rm end}$. ,

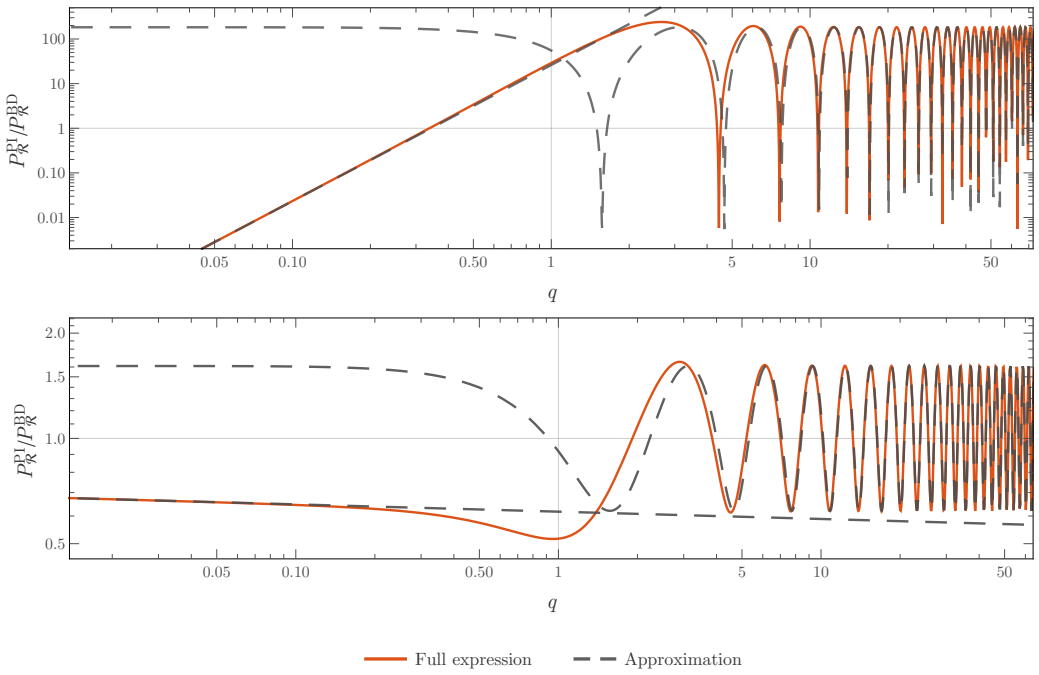

Figure 5.24.: Comparison of the asymptotic formulas (5.216) for short wavelengths, and (5.213) and (5.214) for long wavelengths (dashed curves) with the full expression (5.208) (red solid curve) for $\mathcal{P}_{\mathcal{R}}^{\rm PI}/\mathcal{P}_{\mathcal{R}}^{\rm BD}$. We recall that the re-scaled wavenumber is defined as $q = k/k_{\rm trans}^{\infty}$, where $k_{\rm trans}^{\infty}$ is given by Eq. (5.188). (Top panel) Results for an initial epoch that mimics a stiff-matter-dominated universe ($\epsilon^- = 3$) and a final power-law inflation epoch ($\epsilon^+ = 0.01638$). (Bottom panel) Results for initial and final inflating epochs where the rate of acceleration decreases at the transition ($\epsilon^- = \epsilon^+ + 0.01$ and $\epsilon^+ = 0.01638$).

Long wavelength limit

We now analyse the long wavelength behaviour, $q \ll |\epsilon^+ - 1|$and $q \ll |\epsilon^- - 1|$, of Eq. (5.208). Using the asymptotic behaviour of the Bessel and Hankel functions for small argument [7, 283], we find that if neither the initial or final epochs mimic a universe dominated by stiff-matter, $\epsilon^{\pm} \neq 3$, to leading order in q, the r.h.s. of Eq. (5.208) reduces to

$$\frac{\mathcal{P}_{\mathcal{R}}^{\rm PI}(k)}{\mathcal{P}_{\mathcal{R}}^{\rm BD}(k)}(q \ll |1-\epsilon^{\pm}|) = \frac{1}{4}\left[\left(\frac{\epsilon^+}{\epsilon^-}\right)^{\frac{1}{2}}(3-\epsilon^+)\Theta(1-\epsilon^+) - \left(\frac{\epsilon^+}{\epsilon^-}\right)^{-\frac{1}{2}}(3-\epsilon^-)\Theta(\epsilon^- - 1)\right]^2 \times \frac{\Gamma^2(\lambda^-)}{\Gamma^2(1+\lambda^+)}\frac{|1-\epsilon^-|^{2\lambda^- - 1}}{|1-\epsilon^+|^{2\lambda^+ + 1}}\left(\frac{q}{2}\right)^{2(\lambda^+ - \lambda^-)}. \tag{5.213}$$

On the other hand, if the initial epoch has $\epsilon^- = 3$ this expression should be replaced by[32]

$$\frac{\mathcal{P}_{\mathcal{R}}^{\rm PI}(k)}{\mathcal{P}_{\mathcal{R}}^{\rm BD}(k)}(q \ll |1-\epsilon^{\pm}|) = \frac{1}{6}\left[(\epsilon^+)^{\frac{1}{2}}(3-\epsilon^+)\Theta(1-\epsilon^+)\log\left(\frac{q}{2}\right) + 2\,(\epsilon^+)^{-\frac{1}{2}}\right]^2 \times \frac{1}{\Gamma^2(1+\lambda^+)}\frac{1}{|1-\epsilon^+|^{2\lambda^+ +1}}\left(\frac{q}{2}\right)^{2\lambda^+}. \tag{5.214}$$

From Eqs. (5.213) and (5.214), we find that for long wavelengths the ratio $\mathcal{P}_{\mathcal{R}}^{\rm PI}/\mathcal{P}_{\mathcal{R}}^{\rm BD}$ evolves as a power of the re-scaled wavenumber q, whose exponent depends on the orders λ^+ and λ^-. More precisely, we find that $\mathcal{P}_{\mathcal{R}}^{\rm PI}/\mathcal{P}_{\mathcal{R}}^{\rm BD}$ converges to 0 if $\lambda^- < \lambda^+$, and diverges for $\lambda^+ < \lambda^-$. This behaviour is evident in both panels of Fig. 5.23 for $q \ll 1$.

In Fig. 5.24 we compare the asymptotic formula (5.213) (dashed curve) with the full expression (5.208) (red solid curve) for the cases of $\epsilon^- = 3$ (top panel) and $\epsilon^- = \epsilon^+ + 0.01$ (bottom panel). We note that for a decelerated pre-inflationary epoch followed by a power-law inflationary period, a suppression at large scales is obtained for most of the cases of interest, including the ones studied in previous sections where we considered initial stiff-matter-, radiation- and dust-like behaviours. However, if ϵ^- becomes too close to 1 the primordial power spectrum might become enhanced instead.

Alternatively, if we consider two successive epochs of power-law inflation, the behaviour at very long wavelengths depends critically on whether the rate of acceleration increases or decreases at the transition. If it increases ($\epsilon^+ < \epsilon^-$), the exponent of q is negative and the ratio (5.213) diverges as we consider larger and larger scales. Notice, however, that for $q \approx 1$ there might exist an intermediate region where $\mathcal{P}_{\mathcal{R}}^{\rm PI}$ is actually suppressed with regards to $\mathcal{P}_{\mathcal{R}}^{\rm BD}$, as can be seen on the top panels of Figs. 5.23 and 5.24. On the other hand, if the rate of acceleration decreases at the time of the transition ($\epsilon^- < \epsilon^+$), the ratio (5.213) vanishes as $q \to 0$, meaning that we recover a suppression of the primordial power spectrum at large scales. Nevertheless, if the values of ϵ^- and ϵ^+ are very close, the exponent $2(\lambda^+ - \lambda^-)$ might become so small that any suppression/enhancement would only be significant at scales larger than the Hubble horizon today, i.e., for modes that are outside the observable range at the present time.

Finally, we point out that when the final epoch represents a period of power-law inflation with $\epsilon^+ \ll 1$, which is the case of interest in this work, and we take into account that $\mathcal{P}_{\mathcal{R}}^{\rm BD} \sim k^{n_s-1}$, then at very large scales $\mathcal{P}_{\mathcal{R}}^{\rm PI}$ behaves as

$$\mathcal{P}_{\mathcal{R}}^{\rm PI}(q \ll |1-\epsilon^{\pm}|) \sim \begin{cases} k^{3-\frac{3-\epsilon^-}{|1-\epsilon^-|}}\,, & \text{for } \epsilon^- \neq 3\,, \\ k^3\log^2(k)\,, & \text{for } \epsilon^- = 3\,. \end{cases} \tag{5.215}$$

This is precisely the shape of $\mathcal{P}_{\mathcal{R}}$ during the pre-inflationary epoch for modes outside the Hubble horizon. For $0 < \epsilon^- < 3/2$, the exponent on the first line of the r.h.s. of the previous equation is negative, meaning that $\mathcal{P}_{\mathcal{R}}^{\rm PI}$ diverges for small k, while for $3/2 < \epsilon^- \leq 3$ it vanishes as $k \to 0$. In the limiting case of $\epsilon^- = 3/2$, which corresponds to a pre-inflationary epoch that mimics a dust-dominated universe, the primordial power spectrum converges to a non-vanishing constant at very large scales.

[32] A derivation Eqs. (5.213) and (5.214) can be found in the Appendix D.9.

Short wavelength limit

We now look at the short wavelength limit, $|\epsilon^+ - 1| \ll q$ and $|\epsilon^- - 1| \ll q$, of Eq. (5.208). Using the asymptotic behaviour of the Bessel and Hankel functions for large argument [7, 283] we find that, to leading order in q^{-1}, the ratio (5.208) is given by[33]

$$\frac{\mathcal{P}_{\mathcal{R}}^{\rm PI}(k)}{\mathcal{P}_{\mathcal{R}}^{\rm BD}(k)}(|1-\epsilon^{\pm}| \ll q) \approx \cosh\left[\log\left(\frac{\epsilon^+}{\epsilon^-}\right)\right] - \sinh\left[\log\left(\frac{\epsilon^+}{\epsilon^-}\right)\right]\sin\left(\frac{2q}{1-\epsilon^+} - \pi\lambda^+\right) . \quad (5.216)$$

This shows that in a scenario where a pre-inflationary epoch transitions instantaneously to an ensuing power-law inflation, the primordial power spectrum at the end of inflation will present an oscillatory behaviour at small scales, with an amplified mean value $\langle \mathcal{P}_{\mathcal{R}}^{\rm PI}/\mathcal{P}_{\mathcal{R}}^{\rm BD}\rangle$ and standard deviation $\sigma_{\mathcal{P}_{\mathcal{R}}^{\rm PI}/\mathcal{P}_{\mathcal{R}}^{\rm BD}} := \sqrt{\langle(\mathcal{P}_{\mathcal{R}}^{\rm PI}/\mathcal{P}_{\mathcal{R}}^{\rm BD})^2\rangle - \langle \mathcal{P}_{\mathcal{R}}^{\rm PI}/\mathcal{P}_{\mathcal{R}}^{\rm BD}\rangle^2}$ given by:

$$\langle \mathcal{P}_{\mathcal{R}}^{\rm PI}/\mathcal{P}_{\mathcal{R}}^{\rm BD}\rangle = \cosh\left[\log\left(\frac{\epsilon^+}{\epsilon^-}\right)\right] , \qquad \sigma_{\mathcal{P}_{\mathcal{R}}^{\rm PI}/\mathcal{P}_{\mathcal{R}}^{\rm BD}} = \frac{1}{\sqrt{2}}\sinh\left[\left|\log\left(\frac{\epsilon^+}{\epsilon^-}\right)\right|\right] . \quad (5.217)$$

Such an oscillatory behaviour is evident in both panels of Fig. 5.23 for $1 \ll q$. In Fig. 5.24, we compare the asymptotic formula (5.216) (dashed curve) with the full expression (5.208) (solid red curve) for the cases of $\epsilon^- = 3$ (top panel) and $\epsilon^- = \epsilon^+ + 0.01$ (bottom panel). Notice that the agreement between the two formulas becomes increasingly better for $1 \ll q$.

If we assume that (5.216) is valid for $k \gtrsim k_*$, and impose that the mean value of $\mathcal{P}_{\mathcal{R}}^{\rm PI}(k_*)$ is within the 1-σ interval of A_s as measured by the Planck mission [16]: $A_s = (2.142 \pm 0.049)\times 10^{-9}$; then we can derive the constraint $0.81 < \epsilon^-/\epsilon^+ < 1.24$. Taking into account the observation-motivated value $\alpha = 2\epsilon^+ = 0.03275$, cf. Eq. (5.126), this constraint translates into

$$0.013 < \epsilon^- < 0.020\,, \qquad \Leftrightarrow \qquad 0.027 < \beta < 0.041\,, \quad (5.218)$$

where we recall β is the original parameter that defines the behaviour during the pre-inflationary epoch, cf. Eq. (5.183). Alternatively, a more strict constraint can be obtained by imposing that the mean value plus the standard deviation are within the aforementioned 1-σ interval of A_s. In this case, we obtain $0.97 < \epsilon^-/\epsilon^+ < 1.03$, which after fixing $\alpha = 2\epsilon^+ = 0.03275$ leads to

$$0.016 < \epsilon^- < 0.017\,, \qquad \Leftrightarrow \qquad 0.032 < \beta < 0.034\,. \quad (5.219)$$

Note that these results clearly exclude the possibility of a decelerated pre-inflationary epoch with an instantaneous transition. We note that the constraints (5.218) and (5.219) are in agreement with the constraints presented in Tables IV and V of Ref. [36] for $\ell > 30$.

5.5.4. Comparison with numerical Results

Finally, we compare the analytical expression (5.208) for the case of an instantaneous transition to inflation, $\lambda \to +\infty$, with the numerical results obtained from numerically integrating the system (5.139) for the model (5.148) with increasingly higher λ, i.e., in cases where the characteristic interval

[33] A derivation of this result is presented in the Appendix D.10.

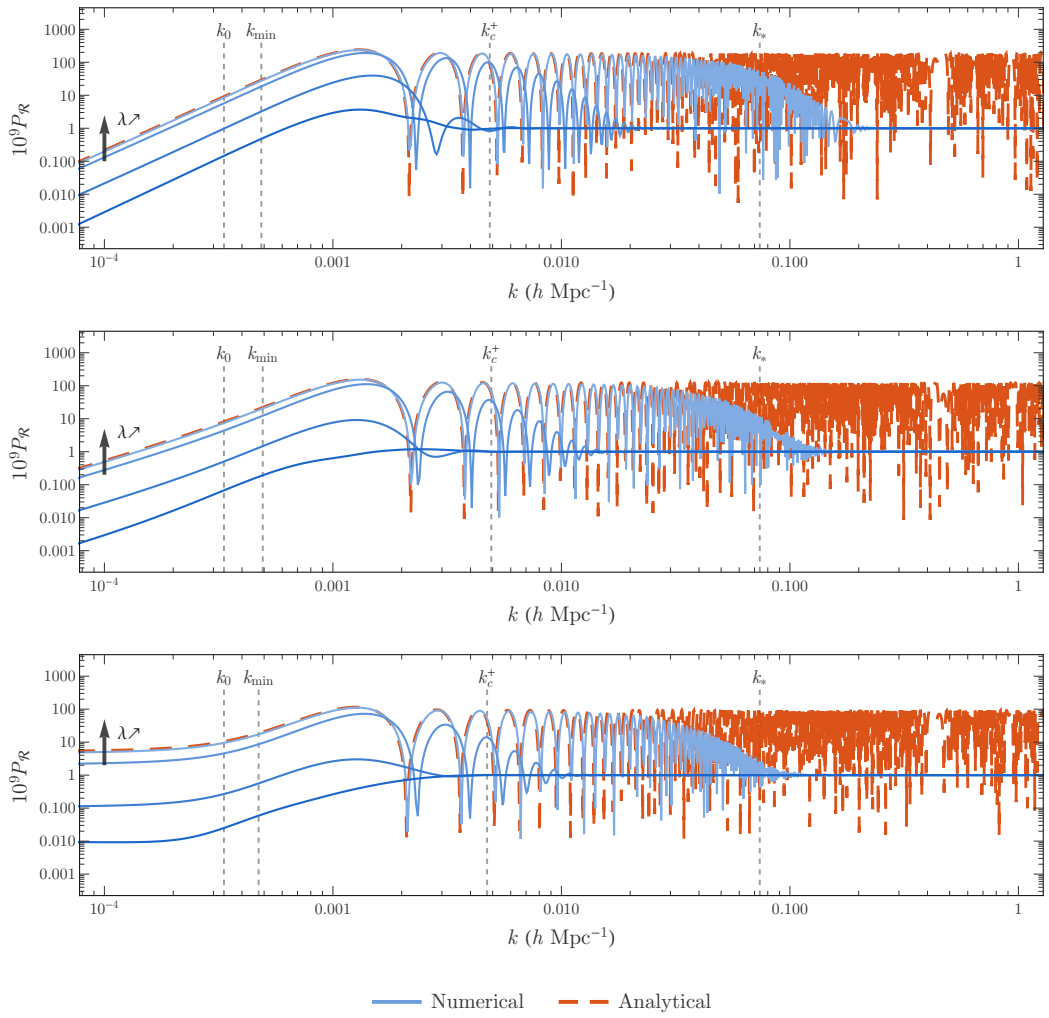

Figure 5.25.: Comparison of the primordial power spectrum (red dashed curve) obtained from the analytical formula (5.208) with the numerical results obtained for the model (5.148) with increasingly faster transitions: $\lambda = 1$ (darker blue curve); $\lambda = 2$; $\lambda = 10$; and $\lambda = 100$ (lighter blue curve). As the value of λ increases, the numerical results tend towards the shape of the analytical prediction for increasingly higher wavenumbers. For large wavelengths (low k), the analytical prediction for instantaneous transitions captures the correct tilt of $\mathcal{P}_\mathcal{R}$ but not the correct amplitude. (Top panel) Results for a pre-inflationary epoch mimicking stiff-matter ($\beta = 6$). (Middle panel) Results for a pre-inflationary epoch mimicking radiation ($\beta = 4$). (Bottom panel) Results for a pre-inflationary epoch mimicking dust ($\beta = 3$).

for the transition, Δ_λ, is gradually shortened, cf. Eq. (5.151).

In Fig. 5.25, we present the results obtained for the cases where the pre-inflationary epoch mimics (top panel) a stiff-matter-dominated universe with- $\epsilon^- = 3$, (middle panel) a radiation-dominated universe with $\epsilon^- = 2$, and (bottom panel) a dust-dominated universe with $\epsilon^- = 3/2$. For all the cases, we compute numerically the primordial power spectrum for four different values of λ: 1, 2, 10 and

100; and fix ϵ^+ to the observationally motivated value $\alpha/2 \simeq 0.01638$, cf. Eq. (5.126). Independently of the pre-inflationary behaviour, we find that, as the value of λ increases and the period of transition becomes smaller, the ratio $\mathcal{P}_{\mathcal{R}}^{\rm PI}/\mathcal{P}_{\mathcal{R}}^{\rm BD}$ tends to converge to the shape defined by Eq. (5.208).

At large scales, i.e., for $k < k_{\rm min}$, we find that the asymptotic expressions (5.213) and (5.214) correctly predict the power-law, or power-law and $\log$, dependence of the spectrum but not the amplitude. For lower values of λ, the numerical results show that a correction factor needs to be applied to these formulas in order to recover the correct behaviour.

On the other hand, for $k_{\rm min} < k$ we find that, as λ increases, the peaks observed in the previous sections start to transform into the oscillatory behaviour predicted by the short wavelength approximation (5.216). In addition, the value of the highest wavenumber affected by the oscillation grows with λ. This was to be expected, as the bumps in the potential z''/z around the transition increase and start to affect modes with higher wavenumbers as the interval of transition becomes shorter. Nevertheless, for each value λ there is a wavenumber above which the usual prediction of power-law inflation is recovered. This corresponds to the modes whose wavenumber is much larger than the bumps of z''/z around the transition. A similar picture is obtained in Figs. 4 and 5 of Ref. [36]. Notice, however, that in [36] only the range $1 < q$ is plotted, meaning that the behaviour observed for the largest scales is not captured.

5.5.5. Discussion

In this section, we have revisited the topic of instantaneous transitions in the pre-inflationary universe and its implications in the primordial power spectrum at the end of inflation. Over the past three decades, various works can be found in the literature with often contradictory results regarding the matching conditions for the perturbation variables at the moment of the transition between different epochs[34]. Following the seminal work of Deruelle and Mukhanov [136], we reviewed the correct matching conditions in a scenario of an instantaneous transition resulting from a discontinuity in the potential of a minimally coupled scalar field, which imply the continuity of the Bardeen potentials Φ and Ψ and of the comoving curvature perturbation $\mathcal{R}$ at all scales.

After identifying the model introduced in Sect. 5.4 as a phenomenological mapping of a scalar field model, we considered the limit of $\lambda \to \pm\infty$ which leads the characteristic interval of the transition to shrink to zero, i.e., corresponds to an instantaneous transition. We showed how, in this limit, the EoS parameter $w = P/\rho$ and the slow-roll parameter ϵ present a step-like discontinuity at the moment of the transition, while the potential z''/z, which controls the evolution of the scalar perturbations, diverges at the moment of the transition due to the presence of terms with a Dirac delta function and its derivative. This contrasts with the behaviour of the potential a''/a which remains finite, despite having a discontinuity at the transition. As such, we have shown explicitly that the approximation $z''/z = a''/a$, often encountered in the literature [96, 118, 122], is not valid at the moment of the transition. We hope that these results can help to the discussion on the proper matching conditions for scalar perturbations in the case of instantaneous changes of EoS in the pre-inflationary universe.

Using the continuity of the comoving curvature perturbation $\mathcal{R}_k$, we showed that the divergence in the potential z''/z at the moment of the transition leads to a discontinuity in $\mathcal{R}_k'$, as derived in

[34] See, for example, Ref. [252] for a discussion regarding this issue.

Ref. [36], and then calculated the boundary conditions for the Mukhanov-Sasaki variable v_k and its derivative. By combining this result with the known general solutions for v_k in terms of Hankel functions, we were able to explicitly define a transformation that relates the linear coefficients of those solutions before and after the transition, thus allowing us to predict the shape of the primordial power spectrum at the end of inflation based on the initial conditions set in the pre–inflationary epoch. Notice that similar transformations were defined in Refs. [118] and [96], albeit in those works the continuity of v_k and v'_k or of $\mathcal{R}_k$ and $\mathcal{R}'_k$ was considered. A further interesting result found in our analysis is that the same matching conditions for v_k and v'_k can be obtained by using the long wavelength approximation ($k^2 \ll z''/z$) at the moment of the transition, even for the modes that are well inside the comoving Hubble horizon ($k_H^2 \ll k^2$) and that satisfy the condition $a''/a \ll k^2$. That such an approximation works at all scales can be justified by the fact that z''/z diverges, i.e., has infinite values, at the particular moment of the transition.

Given that he main focus of this chapter was to study the effects of pre-inflationary epochs on the primordial power spectrum (and on the CMB), we then explicitly calculated the ratio $\mathcal{P}_{\mathcal{R}}^{\rm PI}/\mathcal{P}_{\mathcal{R}}^{BD}$ between the primordial power spectrum at the end of inflation in a scenario with a pre-inflationary epoch with arbitrary initial conditions, $\mathcal{P}_{\mathcal{R}}^{\rm PI}$, and the primordial power spectrum predicted by a standard inflationary scenario with Bunch-Davies (BD) initial conditions, $\mathcal{P}_{\mathcal{R}}^{BD}$. In particular, we considered the case where a BD vacuum state is recovered during the initial epoch when the condition $z''/z \ll k^2$ is met and analysed the shape of $\mathcal{P}_{\mathcal{R}}^{\rm PI}/\mathcal{P}_{\mathcal{R}}^{BD}$ for physically relevant modes which are well outside the Hubble horizon at the end of inflation. The asymptotic expressions for the behaviour at large and small scales were then obtained. We found that for $k < k_{\rm min}$, where $k_{\rm min}$ is the value of the Hubble horizon at the moment of the transition to inflation, the shape of $\mathcal{P}_{\mathcal{R}}$ during the pre-inflationary epoch is preserved at later times. On the other hand, for $k_{\rm min} < k$ the primordial power spectrum becomes amplified and develops an oscillatory behaviour.

By assuming that the pivot scale $k_* = 0.05$ Mpc^{-1} falls within this oscillatory regime, we were able to impose lower and upper bounds on the initial value of the slow-roll parameter $\epsilon = -\dot{H}/H^2$, so that the prediction for the primordial power spectrum is compatible with the observational constraints. These bounds, which allow for a minimal change of up to 3% in the value of ϵ at the moment of the transition, are compatible with the results of previous studies [36] and clearly exclude the possibility of a decelerated pre-inflationary epoch (with an instantaneous transition to inflation). Notice, however, that these constraints were obtained assuming that the instantaneous change in the EoS parameter and in the slow-roll parameter are introduced by a discontinuity of the potential of the scalar field at the value $\varphi_{\rm hyp}$. Such a condition uniquely defines the hypersurface of the transition at the perturbative level and, consequently, imposes the appropriate boundary conditions for the perturbation variables. However, if the condition that defines the discontinuity of the EoS parameter and the slow-roll parameter is changed, see for example Ref. [136] where a transition of the EoS parameter is imposed at a fixed $\rho_{\rm hyp}$, the boundary conditions for the perturbation variables may differ from the ones obtained here, possibly leading to different imprints on the primordial power spectrum.

Finally, we have compared the analytical predictions for the case of the instantaneous transition with the numerical results obtained for the toy model II introduced in Eq. (5.148). As shown in Fig. 5.25, the analytical and the numerical results for the primordial power spectrum coincide up to a maximum wavenumber when the parameter λ is fixed at large values, i.e, for very fast transitions. This result corroborates the analysis presented above, showing that the analytical expressions obtained capture

the correct limiting behaviour of the model for very fast transitions between the initial and the final epochs. Furthermore, the disagreement, at very low scales $k_{\rm min} \ll k$, between the numerical results and the analytical expressions can be explained by the fact that, for finite λ, the bumps in z''/z near the transition to inflation are very large but have a finite maximum value. Therefore, modes with k^2 above this maximum will be in a BD-like vacuum at the onset of inflation and the usual prediction of power-law inflation is recovered.

PART IV

Final Comments

6 General Conclusions

In this thesis, we have presented the results obtained during the last four years of research regarding three different scenarios that explore possible extensions of the Standard Model of Cosmology: modified theories of gravity in the late-time Universe (cf. Chapter 3), dynamical dark energy (DE) described by a 3-form field (cf. Chapter 4) and effects of quantum cosmology in the primordial Universe (cf. Chapter 5). For each case, we have explored different methodologies that allow us to better understand the dynamics of the model at hand. Likewise, we have computed the theoretical predictions for different cosmological observables and compared them with the available data from the observations, in order to decide on the physical viability of the model and define constraints on its parameters.

In Chapter 3, we have studied the effects that a modified theory of gravity, namely metric $f(R)$-gravity, can have on the evolution of the Universe and on the cosmological observables, in particular at late-time. Following the line of reconstruction efforts in $f(R)$ gravity, also known as *designer* $f(R)$ approach [103, 106, 133, 143], we have presented in Sect. 3.2 a novel method to $f(R)$ actions compatible with the evolution of a universe that is characterised by a given barotropic equation of state. This new strategy is based on mapping the modifications of gravity to an effective fluid and can be used to find appropriate solutions for $f(R)$. Using our reconstruction method, we have been able to obtain, for the first time, a complete analytical mapping of the modified generalised Chaplygin gas (mGCG) in $f(R)$-gravity in the absence of other types of matter. We recall that this type of fluid generalises the original Chaplygin gas model [57, 60, 205] and has found applications in several areas of Cosmology, from describing a pre-inflationary evolution, to providing a unified description of the dark sector of the Universe. Given the complexity of the solutions found–a common drawback in reconstruction methods–and the number of free parameters of the model, we then focused our attention in the case where the mGCG interpolates between the behaviour of a radiation fluid and of a cosmological constant. This case was found to be particularly interesting since it can also be applied to model the transition from inflation to the Hot Big Bang cosmology (see for example [74]) and to unify DE with another (hypothetical) dark component–dark radiation (DR). Furthermore, it was found that the complexity of the analytical solutions is greatly reduced in this specific case, which allowed us to have a better control of the solutions obtained and to perform a more detailed analysis of their physical viability. In particular, we were able to define the intervals in the 1-dimensional parameter space where solutions can be obtained that satisfy the conditions of $f(R)$-gravity for physical viability and stability.

In the subsequent Sect. 3.3, we have considered the possibility of explaining DE and DR in terms

of modifications of gravity introduced by an $f(R)$ theory. In particular, we have used the mGCG model to describe an effective $f(R)$ fluid that mimics radiation in the distant past and a cosmological constant around the present time. Even though the vacuum solutions obtained with the aforementioned reconstruction method could not be employed in this case–we were also considering the presence of radiation, CMB photons and relativistic neutrinos, and of pressureless matter, DM and non-relativistic baryons–we obtained a numerical solution compatible with the model that satisfied all the requirements for being physically acceptable. In addition, we were able to derive a full analytical solution in the asymptotic past, when the mGCG behaves like radiation and the modifications to gravity become stronger. Using this asymptotic behaviour, we were able to show that the $R^{4/3}$ dependence of the numerical solution at large R was a generic feature of the model and not an artifice of the initial conditions. By employing a cosmographic approach we were able to constrain the model at the level of the FLRW background, guaranteeing that it mimics almost exactly the evolution of ΛCDM with a radiation component and that we recover GR with a cosmological constant since the matter era till the present time.

In order to break this degeneracy at the background level, we then proceeded to study the evolution of the linear cosmological perturbations, since well inside the early radiation dominated epoch till the present time. We found that, as long as the initial conditions imposed were analogous to the ones derived from single field inflation in GR, no significant imprints from the modifications of gravity are obtained at the level of the linear perturbations for large and intermediate scales, i.e., for wave-numbers $k \lesssim k_{\rm eq} \approx 0.01$ Mpc^{-1} where $k_{\rm eq}$ is the wave-number of the mode corresponding to the moment of radiation-matter equality. However, for $k_{\rm eq} \lesssim k$, we found that the evolution of the matter perturbations started to deviate from the predictions of the ΛCDM model; in particular, for these scales we observed a higher growth rate of matter and a change in the amplitude and in the slope of the matter power spectrum. These results were found to be in perfect agreement with the predictions of metric $f(R)$-gravity [134]. Furthermore, we have shown that, for $k_{\rm eq} \lesssim k$, the gravitational potentials do not remain constant and instead grow with time. This result corroborates other works found in the literature that criticise the use of the quasi-static approximation in $f(R)$ gravity [55, 134]. In order to make the model compatible with the observational constraints of the matter power spectrum at small scales, i.e., for large k, one possibility is to reduce the amount of DR considered. This would reduce the strength of the effects of modifications to gravity during the whole evolution of the model which could, in principle, blue-shift the imprints of the model to larger k (smaller scales) and therefore avoid the tight constraints on the matter power spectrum in the range $2 \times 10^{-2} h$ Mpc$^{-1} \lesssim k \lesssim 2 \times 10^{-1}$ h Mpc^{-1} [19]. We note the final results of the Planck mission [19] have brought further down the value of the number of effective degrees of freedom, reducing the deviation from the prediction of the Standard Model of particles, $N_{\rm eff} = 3.046$ [249], and favouring a very small contribution from DR. However, given that in this work the fraction of relativistic content corresponding to DR was $\lesssim 1.4\%$, as derived from the best-fit values of Planck 2015 [16] and used in our published work [264], it is not clear whether the agreement with the observations at the level of the matter power spectrum can be achieved, while at the same time maintaining a sufficiently significant contribution of DR to $N_{\rm eff}$ that cannot be explained by a statistical fluctuation of the data. An alternative approach that could alter the predictions of the model at the perturbative level is related to the initial conditions for the linear perturbations that are imposed during the radiation dominated epoch. Since the deviations from GR were dominant in this initial epoch, we lacked a mechanism to unequivocally define the initial conditions for the numerical perturbations. In order to overcome this difficulty, we took advantage of

the linearity of the evolution equations for the perturbations to obtain four solutions with different initial conditions and then look for the combination that better fitted the results from GR. In addition, we assumed that the initial conditions satisfied a power-law dependence on the wave-number k, as predicted by single field inflation; the validity of this assumption requires a more detailed investigation. In the future it might be of interest to explore whether general and consistent initial conditions can be obtained for the perturbations when the dominant term in the $f(R)$ action is $R^{4/3}$ or, more generally, R^n.

In Chapter 4, we have explored the possibility of explaining the late-time acceleration of the Universe, not through a modification of the laws of gravitation, but by considering a new dynamical field, in particular a massive 3-form field, that can play the role of DE. In the last decade, p-forms have drawn attention in the literature as alternatives to the minimally coupled scalar field [166, 216, 217, 219]. The 3-form was found to be well suited for applications in FLRW cosmology, as it can be naturally mapped to perfect fluid without the need for imposing any additional constraints or special multi-field configurations. In fact, a 3-form field was originally introduced to describe an effective cosmological constant [142], a behaviour which is recovered for constant potentials. In order to better understand the dynamics of models with this kind of field, in Sect. 4.2, we investigated the use of a dynamical system analysis in models with 3-forms and DM, a method which can be extremely useful in understanding cosmological models with extra dynamical degrees of freedom [44]. Due to the particular constraints in the evolution of the 3-form, we found that the asymptotic past of the system should correspond to states with infinite amplitude of the 3-form field, independently of the shape of the potential. As such, we stressed the importance of obtaining a global picture of the dynamics of the model which includes the behaviour at infinity. To this end, a novel dynamical system description was presented, in which an intuitive interpretation of the dynamical variables is forfeited in exchange for a better control of the behaviour at infinity. As an example, we applied this new representation to the case of the Gaussian potential $V \propto \mathrm{e}^{-\alpha\chi^2}$, where α is a constant that controls the flatness of the potential around the origin, and showed that the new representation allows us to lift some ambiguities that were previously found in the study of the stability of the fixed points at infinity. We note that while this new description is not suitable to all kinds of potentials, e.g., it presents problems for potentials with zeroes at finite values of the 3-form field, it can serve as a guideline for future applications.

In Sect. 4.3, we analysed the occurrence of a Little Sibling of the Big Rip (LSBR) event in models with 3-form fields [77]. This type of cosmic event, which is not ruled out by the current observations, occurs due to a phantom-like behaviour of DE that leads, in resemblance to the Big Rip singularity and the Little Rip cosmic events, to a divergence of the Hubble H rate in the distant future and to the eventual destruction of the structure observed in the Universe. The LSBR is characterised by the fact that the first derivative of the Hubble rate remains finite and positive during the whole future evolution, meaning that the blow-up of H and the dissociation of structure take a longer time to occur than in the Little Rip or the Big Rip [77]. Within the context of 3-form cosmology, the LSBR can appear even in the cases where the field has a canonical kinetic term and a positive-valued potential, in contrast with scalar field models where a phantom kinetic term or a negative valued potential are necessary for such a cosmic event to occur. In particular, we found that a LSBR can occur whenever the 3-form potential $V(\chi)$ satisfies the conditions $V > 0$ and $\mathrm{d}V/\mathrm{d}\chi^2 < 0$ at the critical points $\chi = \pm\chi_\mathrm{c} = \pm\sqrt{2/(3\kappa^2)}$ and that the existence of other types of non-interacting matter that verify the null energy condition does not prevent this catastrophic fate of the Universe. However, the LSBR can in principle be avoided if an appropriate interaction is considered between DM and DE,

that prevents the energy density of DM from decaying completely and, consequently, shifts the field χ away from the critical points that correspond to a LSBR.

In order to test this hypothesis, we have studied a model with interacting DM and DE, in which DE is described by a 3-form field with a Gaussian potential. Taking a phenomenological approach, we have considered a class of quadratic interactions that can accommodate several of the phenomenological interactions considered in the literature. Through a comprehensive study of the system based on a dynamical system approach, we have been able to show that the LSBR can indeed be avoided if and only if the interaction term is not proportional to the energy density of DM or to its square. We point out that, while these results have been obtained for a 3-form field with a Gaussian potential, they can be generalised for any potential that leads to a LSBR in the absence of interactions. We used the statefinder hierarchy, a diagnostic tool based on a cosmographic approach, and the composite null diagnosis, which complements the statefinders with information regarding the growth of matter perturbations, to characterise the non-interaction model and two interacting cases where the LSBR is removed as the end state of the Universe: $Q_{\rm IV} \propto \alpha_\chi H \rho_\chi$ and $Q_{\rm V} \propto \alpha_{\chi\chi} H \rho_\chi^2/(\rho_{\rm m} + \rho_\chi)$. In order to facilitate the comparison of the results obtained, we imposed the same value for the coupling constants $\alpha_\chi = \alpha_{\chi\chi} = -0.03$. This value ensured that the energy transfer was from DE to DM, as required to prevent the complete decay of DM, and satisfied the observational constraints derived for the wCDM model [125], which were used as guidelines in our work. For each case, we selected the trajectories whose evolution closely mimics the ΛCDM model till the present time and confirmed that the statefinder hierarchy and the composite null diagnosis are able to positively distinguish between the three cases at hand and between the ΛCDM model. In particular, we have found that the mapping $\{S_3^{(1)}, S_4^{(1)}\}$ is preferable to identify the characteristic imprints of the model close to the present time, while $\{S_3^{(1)}, S_3^{(2)}\}$ is particularly efficient in detecting deviations of DE from the behaviour of a cosmological constant during the past matter dominated era. In order to check the compatibility of the results with the observational data, we compared the predicted values for the growth rate f with the measurements of SDSS III BOSS DR12 [312]: $f(z_{\rm eff} = 0.38) = 0.638 \pm 0.080$, $f(z_{\rm eff} = 0.51) = 0.715 \pm 0.090$, and $f(z_{\rm eff} = 0.61) = 0.753 \pm 0.088$. In addition, we have computed the evolution of $f\sigma_8$ in all the three models and compared the results with the predictions of ΛCDM and with the available data points and respective error bars. Despite an increase in the growth rate of matter fluctuations, which becomes more noticeable near the present time when the interactions becomes stronger, we have found that all the models are compatible with the observations.

Finally, in Chapter 5, we have analysed the possibility of finding imprints from a pre-inflationary era in models inspired by the Third Quantisation [45, 255, 306, 330]. This formalism is based on an alternative interpretation of the Wheeler–DeWitt equation of Canonical Quantum Gravity that draws parallels with the Klein–Gordon equation and with the quantum field description of a minimally coupled scalar field. Within the context of cosmology, the Third Quantisation leads, in a natural way, to the concept of the multiverse–the quanta of the theory are individual universes–and provides a formalism to study possible universe-universe interactions. In a first instance, we have considered in Sect. 5.2 a toy model of a multiverse filled by a massive scalar field minimally coupled to gravity. When a closed spatial section of the FLRW is considered ($\mathcal{K} = -1$), a finite potential barrier emerges in the minisuperspace which, for low values of the kinetic term of the scalar field, divides the space-time in two classical regions where the semi-classical, I and III, separated by a classically forbidden region II (cf. Fig. 5.1). Using a semi-classical approximation, we have computed the analytical solutions for the scale factor in the two classical regions–in the region I the solutions obtained represent small recollapsing *baby*

universes and in the region III the semi-classical solutions represent initially contracting universes that start to inflate after reaching a minimum size–and inside the region II, where the solutions represent Euclidean wormholes that connect the two classical regions. Using Vilenkin's proposal for the probability to tunnel through a potential barrier [341, 342], we have computed the probability for a small *baby* universe to traverse the Euclidean wormhole and emerge as an inflating universe. We have found that the probability of tunnelling is exponentially suppressed for physically acceptable values of the scale of inflation, in conformity with the case of *creation from nothing* [341]. However, for the cases where the kinetic energy density of the scalar field is sufficiently close to the maximum of the potential barrier, the probability that the *baby* universe traverses the wormhole approaches unity. This provides a mechanism to make more likely the appearance of an initially inflating universe like our own.

In Sect. 5.3, we have considered a similar model (model I) of a multiverse filled by a massive scalar field and where universe-universe interactions where introduced, inspired by effects of quantum entanglement [28, 302]. By using a discrete Fourier transform, it is possible to obtain a new non-interacting representation of the model where the effects of the quantum entanglement appear instead as a new term in the effective Friedmann equation of each individual universe. This term leads to the existence of a pre-inflationary era, in which different types of behaviour can be obtained by considering different couplings between universes. Using, as a first approach, the techniques employed in the study of quantum cosmological perturbations during inflation, we have calculated the imprints of the model in the primordial power spectrum, $\mathcal{P}_{\mathcal{R}}$, and in the angular spectrum of the CMB, C_{ℓ}^{TT}. We have found that the existence of a pre-inflationary epoch can lead to a suppression of $\mathcal{P}_{\mathcal{R}}$ and C_{ℓ}^{TT} at large scales (low k and ℓ), in accordance with previous studies where similar models where considered [83, 122, 292]. This effect can in principle alleviate some of the anomalies of the CMB first detected by WMAP and confirmed by Planck [19], like the low quadropole anomaly (the lack of power measured for $\ell = 2$) and the dip in the angular power spectrum in the range $20 \lesssim \ell \lesssim 30$. However, it was found that the pre-inflationary era also leads to the appearance of high amplitude peaks in $\mathcal{P}_{\mathcal{R}}$ and C_{ℓ}^{TT} at intermediate scales, and effect which partially spoils the agreement with the data. This effect was found to be more intense in the case of a pre-inflationary epoch that mimics a universe dominated by stiff-matter than in the cases where the initial epoch mimics a radiation dominated or a dust dominated universe. By comparing the results obtained with the observational constraints from the CMB observations [18], we were able to impose constraints on the parameters of the model and discuss its implications for the interaction couplings between the different universes in the original representation. In particular, we have imposed upper bounds on the ratio $C(a_*)/N_{\rm uni}^2$, where $C(a_*)$ defines the strength of the interaction at the reference scale a_* and $N_{\rm uni}$ is the number of universes in the model. While in the present work we were not able to impose individual constraints on $C(a_*)$ or $N_{\rm uni}$, a future more detailed exploration of the implications of the Third Quantisation on the primordial Universe might provide us with a mechanism to improve the bounds on these parameters.

We have found that the general features of the imprints of the model in $\mathcal{P}_{\mathcal{R}}$ can be predicted from the shape of z''/z, the potential that drives the evolution of the scalar perturbations, around the onset of inflation. In particular, the amplitude and position of the new peaks in the primordial power spectrum can be related to the two bumps that appear in z''/z around the moment when inflation begins, suggesting that the period of the transition to inflation also leaves imprints in $\mathcal{P}_{\mathcal{R}}$. This relation was confirmed in Sect. 5.4, where we considered a 1-parameter extension (model II) of the model I, with the extra parameter λ controlling how abrupt is the transition to inflation, i.e.,

how many e-folds does it take for the Universe to go from the initial pre-inflationary epoch to the final asymptotic power-law inflation. We found that by increasing the period of the transition, i.e., by lowering the value of λ, the amplitude of the two bumps in z''/z was decreased, thus softening the peaks in the primordial power spectrum and, consequently, in the angular power spectrum of the CMB. In this way, we were able to improve the agreement of the model with the observational data. In order to derive constraints for the parameters of the model, we imposed that no imprints of the pre-inflationary era should appear near the pivot scale of Planck mission $k_* = 0.05$ Mpc^{-1} [18] or on multipoles above $\ell = 30$. We point out that the extension introduced in the model II was purely phenomenological and was inspired from the previous model. It is possible that a further exploration of the Third Quantisation might be able to embed such a behaviour within that formalism.

In Sect. 5.5, we have analysed the effects of an instantaneous transition from a pre-inflationary epoch to inflation. Using the model II in the limit of very large values of the parameter λ, we have derived the matching conditions for the Mukhanov–Sasaki variable at the moment of the transition and showed that they correspond to the matching conditions obtained by following the reasoning of Deruelle and Mukhanov [136] in a scalar field model where the transition is provoked by a discontinuity in the potential (see also Refs. [36, 110]). In this case, the Mukhanov–Sasaki variable and its derivative become discontinuous at the moment of the transition. In addition, we found that due to the appearance of divergent terms in the potential z''/z at the moment of the transition, the long wavelength approximation of the Mukhanov–Sasaki equation, $k^2 \ll z''/z$, predicts the correct behaviour of the linear perturbations during the transition for all scales, even for modes inside the comoving Hubble horizon, $(aH)^2 \ll k^2$. We studied the imprints left by the transition in the primordial power spectrum at the end of inflation and showed that an oscillatory regime is obtained for the modes that verify $(aH)^2 \ll k^2$ at the moment of the transition to inflation. By comparing the predictions of the model with the constraints on $\mathcal{P}_\mathcal{R}$ around the pivot scale $k_* = 0.05$ Mpc^{-1}, we have excluded sudden transitions in the primordial Universe, except for the cases there the slow-roll parameter $\epsilon = -\dot{H}/H^2$ varies by less than 3% during the transition, in agreement with previous studies [36]. In order to corroborate our results, we performed a comparison with the numerical integrations obtained from considering increasingly large values of the parameter λ. For $\lambda \gg 1$, we found that the numerical results for $\mathcal{P}_\mathcal{R}$ are well approximated by the analytical formulas in the case of an instantaneous transition. We stress that the results obtained are specific to scalar field models where the instantaneous transition is obtained from a discontinuity in the scalar field potential at $\varphi_{\rm hyp}$. As such, the matching conditions for the Mukhanov–Sasaki variables and the imprints in the cosmological observables may change in a model where a sudden transition is defined by a different condition.

As a final comment, we point out that the three main themes explored in this thesis ($f(R)$-gravity, 3-form DE, pre-inflation in the Third Quantisation) are only a small number of possibilities within the plethora of models and theories that have been proposed over the last few decades in order to explain several phenomena of our Universe. The existence of such an amount of concurrent proposals in Theoretical Cosmology can sometimes give the impression that we are lacking a guiding light, possibly from a lack of sufficient observational data, that is capable of discerning which model or theory is best suited to understand the laws of physics at high energies or at large scales. At the same time, it is worth reminding that we are currently living in a golden age of precision cosmology, where cosmological parameters are calculated with percent precision, and it is expected that we will soon enter the next stage of *accuracy Cosmology* [285, 339], which will focus on bringing equally under

control the systematic errors of observational missions. During this period, several state of the art observational missions have allowed us to map the cosmos with an unprecedented resolution, both at low redshift and at the time of the last scattering surface. In addition, we are watching the first steps of the field of gravitational wave astronomy [2, 3], which has opened to us a completely new way of probing the cosmos and has already allowed us to impose severe constraints on possible modifications to GR [126, 147]. Together with the numerous efforts to search for DM, advances in lensing astronomy and the maturing of the numerical codes that will allow us to understand better complex processes of non-linear collapse and galaxy formation, the next few decades have the potential to become exquisite times for Cosmology and Astronomy where answers might start to appear for fundamental questions such as *What is the nature of dark matter (DM) and dark energy (DE), which combined account for roughly* 95% *of all the content of the Universe? Is General Relativity (GR) the correct theory of gravitation at the classical level or does it need to be modified in order to explain phenomena at astronomical and cosmological scales? What is the road to a full quantum description of gravity?* If so, we might soon witness a revolution of Physics akin to the advent of General Relativity and Quantum Mechanics in the beginning of the twentieth century. Hopefully, as the poet says, *the times they are a-changin'*.

PART V

Appendix

A Linear perturbations around a FLRW background

In this appendix we review some key aspect of the Theory of Linear Cosmological Perturbations. Linear perturbations around a FLRW background were first considered by Lifshitz [234] and were extensively studied in subsequent decades, including seminal works by Hideo Kodama and Misao Sasaki [215] and Viatcheslav F. Mukhanov, H. A. Feldman and Robert H. Brandenberger [270], a thorough study of cosmological perturbations in extended theories of gravity by Jai-chan Hwang [196, 197] and J.-c. Hwang and Hye-rim Noh [198, 199], as well as more recent contributions by David Wands and Karim A. Malik [246–248] among others.

From a formal point of view, linear perturbations around a background metric can be introduced by considering a one-parameter family of space-times $(\mathcal{M}_\epsilon, \hat{g}_\epsilon)$, $\epsilon \in \mathbb{R}$, of 4-dimensional manifolds manifold $\mathcal{M}_\epsilon$ and Lorentzian metrics $\hat{g}_\epsilon$, in which we single out one element $(\mathcal{M}_0, \hat{g}_0)$ that will represent the background geometry [251, 294]. By requiring that all $\mathcal{M}_\epsilon$ can be mapped onto $\mathcal{M}_0$ through a diffeomorphism f_ϵ [251, 294]

$$f_\epsilon : \mathcal{M}_0 \times \mathbb{R} \longrightarrow \mathcal{M}_\epsilon \,, \tag{A.1}$$

we can relate tensors in $\mathcal{M}_\epsilon$ with tensors in $\mathcal{M}_0$ via pullback, f_ϵ^*, and pushforward, df_ϵ^{-1}, operations. In this way, we can construct a one-parameter family of metrics g_ϵ on $\mathcal{M}_0$, each of which is related to the metric $\hat{g}_\epsilon$ on $\mathcal{M}_\epsilon$ through $g_\epsilon := f_\epsilon^* \, \hat{g}_\epsilon$, as well as a new tensor δg_ϵ defined as the difference between the two metrics g_ϵ and g_0 [251, 294]:

$$[\delta g_\epsilon]_{\mu\nu} := [g_\epsilon]_{\mu\nu} - [g_0]_{\mu\nu} \,. \tag{A.2}$$

The tensor $[\delta g_\epsilon]_{\mu\nu}$ defined in (A.2) fully encodes the deformation of the geometry described by $[g_\epsilon]_{\mu\nu}$ with regards to the geometry imposed by $[g_0]_{\mu\nu}$. In a cosmological setting we can identify $(\mathcal{M}_0, \hat{g}_0)$ with the highly symmetrical cosmological background and $(\mathcal{M}_\epsilon, \hat{g}_\epsilon)$ with a more realistic description of our Universe where (small) departures from homogeneity and isotropy are considered. In general, however, working with the full perturbation tensor proves too difficult for any sensible computation. Instead, we can point to the smallness of such inhomogeneities and anisotropies, as suggested by the observations [16], and employ a perturbative approach.

If we assume that the mapping (A.1) is differentiable up to order N, we can approximate δg_ϵ using

a Taylor expansion of the metric g_ϵ around the nominal value $\epsilon = 0$:

$$[\delta g_\epsilon]_{\mu\nu} = [g_\epsilon]_{\mu\nu} - [g_0]_{\mu\nu} \approx \sum_{n=1}^{N} \frac{\epsilon^n}{n!} [\,\delta^{(n)} g_\epsilon]_{\mu\nu}\,, \tag{A.3}$$

where $\delta^{(n)} g_\epsilon := (\mathrm{d}^n g_\epsilon / \mathrm{d}\epsilon^n)_{\epsilon=0}$. In a similar manner, we can expand the *perturbation* δX_ϵ for any tensor X_ϵ as

$$\delta X_\epsilon = X_\epsilon - X_0 \approx \sum_{n=1}^{N} \frac{\epsilon^n}{n!}\, \delta^{(n)} X_\epsilon\,. \tag{A.4}$$

where $\delta^{(n)} X := (\mathrm{d}^n X_\epsilon / \mathrm{d}\epsilon^n)_{\epsilon=0}$. Since in this thesis we are interested in studying the evolution of small linear perturbations around a FLRW background, we disregard terms of order $\mathcal{O}(\epsilon^2)$ in the expansions (A.3) and (A.4). As long as these linear perturbations remain small, their evolution can be fully obtained in a consistent way by perturbing the action up to second order in ϵ, or by perturbing the field equations up to first order in ϵ. In order to simplify the notation, we identify *unperturbed* tensors by an overbar, $X_0 = \bar{X}$, and the linear perturbations $\delta^{(1)} X_\epsilon$ will be referred to simply as δX. In addition, we drop the ϵ subscript from *perturbed* tensors, i.e., $X_\epsilon = X = \bar{X} + \delta X$.

A.1. Gauge transformations

As we expand the geometry of the Universe beyond the FLRW background, we are confronted with the issue of dealing with the appearance of gauge degrees of freedom. Although these are spurious in nature, the general covariance of GR implies that selecting a particular gauge corresponds to specifying a particular way of mapping the perturbed universe to the background geometry. Thus, a gauge transformation generated by an infinitesimal vector ξ^μ is associated to an infinitesimal coordinate change [46, 198, 270]

$$x^\mu \to \widetilde{x}^\mu + \xi^\mu\,. \tag{A.5}$$

In the remainder of this section we adopt the notation $\xi^0 = \delta t$ and $\xi^i = \mathrm{D}^i \xi$. Since there is no *a priori* physical argument to choose a particular gauge fixing, we are faced with ambiguities in how to relate the perturbation variables with physical observable quantities. This gauge issue was tackled by James M. Bardeen by pointing out that "only gauge-invariant quantities have any inherent physical meaning" [46] and therefore re-writing the theory of cosmological perturbations in terms of gauge-invariant (GI) variables was necessary.

In order to define such variables, we require a rule that dictates how a given tensorial quantity $X^{\alpha_1\ldots\alpha_p}_{\beta_1\ldots\beta_q}$ changes under a gauge transformation generated by an infinitesimal vector[1] $-\xi^\mu$ [248]:

$$X^{\alpha_1\ldots\alpha_p}_{\beta_1\ldots\beta_q} \to \widetilde{X}^{\alpha_1\ldots\alpha_p}_{\beta_1\ldots\beta_q} = \mathrm{e}^{-\mathcal{L}_\xi} X^{\alpha_1\ldots\alpha_p}_{\beta_1\ldots\beta_q}\,, \tag{A.6}$$

[1] In another example of lack of uniformity of notation in the literature, here we reverse the sign of the transformation generator with regards to [248] so that we have the same sign in the coordinate transformation rule as Refs. [46, 198, 270].

where $\mathcal{L}_\xi$ is the Lie derivative with respect to the vector ξ^μ [347]

$$\mathcal{L}_\xi X^{\alpha_1\ldots\alpha_p}_{\beta_1\ldots\beta_q} = \xi^\mu \partial_\mu X^{\alpha_1\ldots\alpha_p}_{\beta_1\ldots\beta_q} - X^{\alpha_1\ldots\mu\ldots\alpha_p}_{\beta_1\ldots\beta_q}\partial_\mu \xi^{\alpha_i} + X^{\alpha_1\ldots\alpha_p}_{\beta_1\ldots\mu\ldots\beta_q}\partial_{\beta_i}\xi^\mu \,. \tag{A.7}$$

If we now consider a gauge transformation generated by an infinitesimal vector that vanishes in the background, i.e., $\xi^\mu = \delta^{(1)}\xi^\mu$, then the background value of any quantity $X^{\alpha_1\ldots\alpha_p}_{\beta_1\ldots\beta_q}$ is left unaffected while its first order perturbation $\delta X^{\alpha_1\ldots\alpha_p}_{\beta_1\ldots\beta_q}$ changes according to the rule

$$\delta^{(1)} X^{\alpha_1\ldots\alpha_p}_{\beta_1\ldots\beta_q} \to \delta^{(1)} X^{\alpha_1\ldots\alpha_p}_{\beta_1\ldots\beta_q} - \mathcal{L}_\xi \bar{X}^{\alpha_1\ldots\alpha_p}_{\beta_1\ldots\beta_q} \,. \tag{A.8}$$

Eq. (A.8) allows us to calculate the gauge transformation of any cosmological perturbation and look for appropriate GI quantities that can represent physical quantities.

A.2. The perturbed metric

The FLRW line element up to linear perturbations in the scalar sector can be written as [49, 198, 246]

$$\mathrm{d}s^2 = -N^2\,(1+2A)\,\mathrm{d}t^2 + 2Na\,\mathrm{D}_i B\,\mathrm{d}t\mathrm{d}x^i + a^2\left[(1-2\psi)\gamma_{ij} + 2\mathrm{D}_{(i}\partial_{j)}E\right]\mathrm{d}x^i\mathrm{d}x^j \,, \tag{A.9}$$

where the four degrees of freedom in the scalar sector are encoded in the four potentials $A = A(t,\,\vec{x})$, $B = B(t,\,\vec{x})$, $\psi = \psi(t,\,\vec{x})$ and $E = E(t,\,\vec{x})$. In Eq. (A.9), D_i is the covariant derivative constructed from the 3-metric $\gamma_{ij} = \gamma_{ij}(\vec{x})$ and in this section we use γ_{ij} to raise and lower purely spatial indices. From the perturbed line element (A.9) we can write the perturbation of the metric $g_{\mu\nu}$ and of its inverse[2] $g^{\mu\nu}$ as

$$\delta g_{\mu\nu} = \begin{pmatrix} -2N^2 A & N\,a\,\mathrm{D}_j B \\ N\,a\,\mathrm{D}_i B & -2a^2\left(\psi\gamma_{ij} - \mathrm{D}_i\mathrm{D}_j E\right) \end{pmatrix} , \tag{A.10}$$

$$\delta[g^{-1}]^{\mu\nu} = \begin{pmatrix} 2N^{-2} A & N^{-1}\,a^{-1}\,\mathrm{D}^j B \\ N^{-1}\,a^{-1}\,\mathrm{D}^i B & 2a^{-2}\left(\psi\gamma^{ij} - \mathrm{D}^i\mathrm{D}^j E\right) \end{pmatrix} . \tag{A.11}$$

To first order in perturbations, the unit 4-vector normal to the spatial hypersurfaces n^μ reads [246]

$$n_\mu = -N\left(1+A,\,\vec{0}\right) , \qquad n^\mu = \left(\frac{1-A}{N},\,-\frac{\partial^i B}{a}\right) , \tag{A.12}$$

which shows that the scalar potential A can be seen as the relative perturbation of the lapse function $\delta N/N$. From Eq. (A.12), we can compute the perturbed expansion scalar θ, the shear tensor σ_{ij} and

[2] Here, we use the notation $\delta[g^{-1}]^{\mu\nu}$ to refer to the linear perturbation of the inverse metric $g^{\mu\nu}$, which at first order in perturbations differs from the perturbation of the metric with raised indices by a difference of sign: $\delta[g^{-1}]^{\mu\nu} = -\bar{g}^{\mu\rho}\bar{g}^{\nu\sigma}\delta g_{\rho\sigma} = -\delta g^{\mu\nu}$.

the acceleration vector a_μ in a perturbed FLRW universe as [246]

$$\theta := \frac{3}{N}\frac{\dot{a}}{a} - \frac{3}{N}\left(\dot{\psi} + \frac{\dot{a}}{a}A\right) + \frac{1}{a^2}\nabla^2\sigma\,, \tag{A.13}$$

$$\sigma_{ij} := 0 + \left(\mathrm{D}_i\mathrm{D}_j - \frac{\gamma_{ij}}{3}\nabla^2\right)\sigma\,, \tag{A.14}$$

$$a_i := 0 + \partial_i A\,, \tag{A.15}$$

where $\nabla^2 := \mathrm{D}^i\mathrm{D}_i$ is the Laplacian operator for the metric γ_{ij}. In Eq. (A.14) we have introduced as well the scalar shear potential[3]

$$\sigma := a\left(\frac{a}{N}\dot{E} - B\right)\,. \tag{A.16}$$

Since we are dealing only with scalar perturbations, there is no contribution to the vorticity tensor $\omega_{\mu\nu}$, which also vanishes in a FLRW background. From Eq. (A.13) we can identify the perturbation of the Hubble rate as[4]

$$\delta H = -\frac{1}{N}\left(\dot{\psi} + \frac{\dot{a}}{a}A\right) + \frac{1}{3a^2}\nabla^2\sigma\,. \tag{A.17}$$

The perturbation of the intrinsic curvature is given by

$$\delta^{(3)}R = \frac{4}{a^2}\left(\nabla^2 + 3\mathcal{K}\right)\psi\,, \tag{A.18}$$

and, therefore, the potential ψ is often called the curvature perturbation.

The four scalar potentials that encode the perturbations of the metric $g_{\mu\nu}$ in the scalar sector change under a gauge transformation as

$$A \to A - \frac{\dot{N}}{N}\delta t - \dot{\delta t}\,, \qquad B \to B + \frac{N}{a}\delta t - \frac{a}{N}\dot{\xi}\,, \qquad \psi \to \psi + \frac{\dot{a}}{a}\delta t\,, \qquad E \to E - \xi\,. \tag{A.19}$$

Notice that both A and ψ are gauge independent with regards to purely spatial gauge transformations, as is the scalar shear potential defined in (A.16)

$$\sigma \to \sigma - N\delta t\,. \tag{A.20}$$

Using only geometrical quantities, there are only two GI potentials that can be constructed:

$$\Phi := A - \frac{\dot{\sigma}}{N}\,, \qquad\qquad \Psi := \psi + \frac{\dot{a}}{a}\frac{\sigma}{N}\,. \tag{A.21}$$

These potentials were first identified by Bardeen [46] and they coincide with the scalar potentials A and ψ in the Newtonian gauge defined by $B = E = 0$ (which implies $\sigma = 0$).

[3] The quantity defined in (A.16) corresponds to $\tilde{\sigma}$ in Ref. [246] and to χ in Ref. [198].
[4] The perturbation δH as given in (A.17), is defined as $-\kappa/3$ in the notation of Ref. [198].

A.3. Christoffel symbols

The Christoffel symbols that define the connection are given in term of the metric $g_{\mu\nu}$ by [347]

$$\Gamma^{\rho}{}_{\mu\nu} := \frac{1}{2} g^{\rho\sigma} \left(\partial_\mu g_{\sigma\nu} + \partial_\nu g_{\mu\sigma} - \partial_\sigma g_{\mu\nu} \right) . \tag{A.22}$$

Inserting (A.9) in Eq. (A.22), we find that the components with at least one temporal index read [198, 248]:

$$\Gamma^{0}{}_{00} = \frac{\dot{N}}{N} + \dot{A} \,, \tag{A.23}$$

$$\Gamma^{0}{}_{0i} = 0 + \mathrm{D}_i \left(A + \frac{\dot{a}}{N} B \right) , \tag{A.24}$$

$$\Gamma^{0}{}_{ij} = \frac{a\dot{a}}{N^2} \gamma_{ij} - \frac{a^2}{N^2} \left[\dot{\psi} + 2 \frac{\dot{a}}{a} \left(\psi + A \right) \right] \gamma_{ij} + \mathrm{D}_i \mathrm{D}_j \left[- \frac{a}{N} B + \frac{a^2}{N^2} \left(\dot{E} + 2 \frac{\dot{a}}{a} E \right) \right] , \tag{A.25}$$

$$\Gamma^{i}{}_{00} = 0 + \frac{N^2}{a^2} \mathrm{D}^i \left[A + \frac{a}{N} \left(\dot{B} + \frac{\dot{a}}{a} B \right) \right] , \tag{A.26}$$

$$\Gamma^{i}{}_{0j} = \frac{\dot{a}}{a} \delta^i_j - \dot{\psi} \delta^i_j + \mathrm{D}^i \mathrm{D}_j \dot{E} \,, \tag{A.27}$$

while for the purely spatial components we find [198, 248]:

$$\Gamma^{i}{}_{ij} = \frac{1}{2} \partial^i \gamma_{ij} - \frac{\dot{a}}{N} \mathrm{D}_j B - 3 \mathrm{D}_j \psi + \mathrm{D}_j \nabla^2 E \,, \tag{A.28}$$

$$\begin{aligned} \Gamma^{i}{}_{jk} = {} & \frac{1}{2} \left(2 \gamma^{il} \partial_{(j} \gamma_{k)l} - \mathrm{D}^i \gamma_{jk} \right) - \frac{\dot{a}}{N} \gamma_{jk} \mathrm{D}^i B - \left(2 \delta^i_{(j} \mathrm{D}_{k)} - \gamma_{jk} \mathrm{D}^i \right) \psi \\ & + \left(\mathrm{D}_j \mathrm{D}_k \mathrm{D}^i + \mathrm{D}_k \mathrm{D}^i \mathrm{D}_j - \mathrm{D}^i \mathrm{D}_j \mathrm{D}_k \right) E \,. \end{aligned} \tag{A.29}$$

A.4. The Ricci and Einstein tensors

The Ricci tensor can be calculated in terms of the Christoffel symbols as [347]

$$R_{\mu\nu} = \partial_\rho \Gamma^{\rho}{}_{\mu\nu} - \partial_\nu \Gamma^{\rho}{}_{\mu\rho} + \Gamma^{\sigma}{}_{\mu\nu} \Gamma^{\rho}{}_{\sigma\rho} - \Gamma^{\sigma}{}_{\mu\rho} \Gamma^{\rho}{}_{\sigma\nu} \,. \tag{A.30}$$

Using the previous results, we can obtain the individual elements of the perturbed Ricci tensor [198]

$$R_{00} = -3\left(\frac{\ddot{a}}{a} - \frac{\dot{N}}{N}\frac{\dot{a}}{a}\right) + 3\left[\ddot{\psi} + \left(2\frac{\dot{a}}{a} - \frac{\dot{N}}{N}\right)\dot{\psi} + \frac{\dot{a}}{a}\dot{A}\right] + \frac{N^2}{a^2}\nabla^2\left(A - \frac{\dot{\sigma}}{N}\right), \tag{A.31}$$

$$R_{0i} = 0 + 2\partial_i\left(\dot{\psi} + \frac{\dot{a}}{a}A\right) + \left[\frac{\ddot{a}}{a} + 2\left(\frac{\dot{a}}{a}\right)^2 - \frac{\dot{N}}{N}\frac{\dot{a}}{a} + 2\frac{N^2}{a^2}\mathcal{K}\right]\frac{a}{N}\mathrm{D}_i B + 2\left(\frac{N^2}{a^2}\mathcal{K}\right)\partial_i\frac{\sigma}{N}, \tag{A.32}$$

$$\begin{aligned} R_{ij} = {} & \frac{a^2}{N^2}\left[\frac{\ddot{a}}{a} + 2\left(\frac{\dot{a}}{a}\right)^2 - \frac{\dot{N}}{N}\frac{\dot{a}}{a} + 2\frac{N^2}{a^2}\mathcal{K}\right]\gamma_{ij} + \gamma_{ij}\nabla^2\left(\psi + \frac{\dot{a}}{a}\frac{\sigma}{N}\right) \\ & - \frac{a^2}{N^2}\left[\ddot{\psi} + \left(6\frac{\dot{a}}{a} - \frac{\dot{N}}{N}\right)\dot{\psi} + \frac{\dot{a}}{a}\dot{A} + 2\left(\frac{\ddot{a}}{a} + 2\left(\frac{\dot{a}}{a}\right)^2 - \frac{\dot{N}}{N}\frac{\dot{a}}{a}\right)(\psi + A)\right]\gamma_{ij} \\ & + \mathrm{D}_i\mathrm{D}_j\left[\psi - A + \frac{\dot{\sigma}}{N} + \frac{\dot{a}}{a}\frac{\sigma}{N} + 2\frac{a^2}{N^2}\left(\frac{\ddot{a}}{a} + 2\left(\frac{\dot{a}}{a}\right)^2 - \frac{\dot{N}}{N}\frac{\dot{a}}{a} + 2\frac{N^2}{a^2}\mathcal{K}\right)E\right]. \end{aligned} \tag{A.33}$$

while the perturbed Ricci scalar reads [198]

$$\begin{aligned} R = {} & \frac{6}{N^2}\left[\frac{\ddot{a}}{a} + \left(\frac{\dot{a}}{a}\right)^2 - \frac{\dot{N}}{N}\frac{\dot{a}}{a} + \frac{N^2}{a^2}\mathcal{K}\right] \\ & - \frac{6}{N^2}\left[\ddot{\psi} + \left(4\frac{\dot{a}}{a} - \frac{\dot{N}}{N}\right)\dot{\psi} + \frac{\dot{a}}{a}\dot{A} + 2\left(\frac{\ddot{a}}{a} + \left(\frac{\dot{a}}{a}\right)^2 - \frac{\dot{N}}{N}\frac{\dot{a}}{a}\right)A - 2\frac{N^2}{a^2}\mathcal{K}\psi\right] \\ & + \frac{2}{a^2}\nabla^2\left[2\psi - A + \frac{\dot{\sigma}}{N} + 2\frac{\dot{a}}{a}\frac{\sigma}{N}\right]. \end{aligned} \tag{A.34}$$

Finally, the individual components of the perturbed Einstein tensor $G^{\mu}{}_{\nu} := R^{\mu}{}_{\nu} - \frac{1}{2}R\,\delta^{\mu}_{\nu}$ read [198]

$$G^0{}_0 = -\frac{3}{N^2}\left[\left(\frac{\dot{a}}{a}\right)^2 + \frac{N^2}{a^2}\mathcal{K}\right] + \frac{6}{N^2}\left[\frac{\dot{a}}{a}\dot{\psi} + \left(\frac{\dot{a}}{a}\right)^2 A - \frac{N^2}{a^2}\mathcal{K}\psi\right] - \frac{2}{a^2}\nabla^2\left(\psi + \frac{\dot{a}}{a}\frac{\sigma}{N}\right), \tag{A.35}$$

$$G^0{}_i = 0 - \frac{2}{N^2}\partial_i\left[\dot{\psi} + \frac{\dot{a}}{a}A + \left(\frac{N^2}{a^2}\mathcal{K}\right)\frac{\sigma}{N}\right], \tag{A.36}$$

$$G^i{}_0 = 0 + \frac{2}{a^2}\partial^i\left[\dot{\psi} + \frac{\dot{a}}{a}A - \frac{a}{N}\left(\frac{\ddot{a}}{a} - \left(\frac{\dot{a}}{a}\right)^2 - \frac{\dot{N}}{N}\frac{\dot{a}}{a} - \frac{N^2}{a^2}\mathcal{K}\right)B + \left(\frac{N^2}{a^2}\mathcal{K}\right)\frac{\sigma}{N}\right], \tag{A.37}$$

$$\begin{aligned} G^i{}_j = {} & -\frac{1}{N^2}\left[2\frac{\ddot{a}}{a} + \left(\frac{\dot{a}}{a}\right)^2 - 2\frac{\dot{N}}{N}\frac{\dot{a}}{a} + \frac{N^2}{a^2}\mathcal{K}\right]\delta^i_j \\ & + \frac{2}{N^2}\left[\ddot{\psi} + \left(3\frac{\dot{a}}{a} - \frac{\dot{N}}{N}\right)\dot{\psi} + \frac{\dot{a}}{a}\dot{A} + \left(2\frac{\ddot{a}}{a} + \left(\frac{\dot{a}}{a}\right)^2 - 2\frac{\dot{N}}{N}\frac{\dot{a}}{a}\right)A - \frac{N^2}{a^2}\mathcal{K}\psi\right]\delta^i_j \\ & - \frac{2}{3a^2}\delta^i_j\nabla^2\left(\psi - A + \frac{\dot{\sigma}}{N} + \frac{\dot{a}}{a}\frac{\sigma}{N}\right) + \frac{1}{a^2}\left(\mathrm{D}^i\mathrm{D}_j - \frac{1}{3}\delta^i_j\nabla^2\right)\left[\psi - A + \frac{\dot{\sigma}}{N} + \frac{\dot{a}}{a}\frac{\sigma}{N}\right]. \end{aligned} \tag{A.38}$$

A.5. Fluid variables

While in the FLRW background the fluid elements are at rest with the comoving frame, i.e., the fluid 4-velocity u^μ coincides with the unit normal n^μ [246, 248], this is no longer necessarily true in the perturbed universe where a fluid element can move with respect to the comoving frame with a peculiar velocity $\partial^i v = a\delta u^i$, where v is the scalar velocity potential. Imposing the constraint $u^\mu u_\mu = -1$ at first order in the perturbations we find that $\delta u^0 = -A/N$, which then allows us to write [198, 248]

$$u_0 = -N(1+A)\,, \qquad u_i = a\,\partial_i(v+B)\,, \tag{A.39}$$

$$u^0 = \frac{1}{N}(1-A)\,, \qquad u^i = \frac{1}{a}\partial^i v\,. \tag{A.40}$$

Notice that we can choose the comoving frame simply by setting $v + B = 0$ in which case we promptly recover $\delta u_\mu = \delta n_\mu$ (cf. Eq. (A.12)).

The perturbed stress-energy-momentum tensor $T_{\mu\nu}$, cf. Eq. (1.12), reads

$$\begin{aligned} T_{\mu\nu} = {} & (\rho + P)\,\bar{u}_\mu\bar{u}_\nu + P\bar{g}_{\mu\nu} + 2\bar{u}_{(\mu}\bar{q}_{\nu)} + \bar{\pi}_{\mu\nu} \\ & + (\delta\rho + \delta P)\,\bar{u}_\mu\bar{u}_\nu + \delta P\bar{g}_{\mu\nu} + 2(\rho+P)\,\bar{u}_{(\mu}\delta u_{\nu)} + P\delta g_{\mu\nu} \\ & + 2\left(\delta u_{(\mu}\bar{q}_{\nu)} + \bar{u}_{(\mu}\delta q_{\nu)}\right) + \delta\pi_{\mu\nu}\,, \end{aligned} \tag{A.41}$$

where $\delta\rho$ and δP are, respectively, the perturbations of the energy density and of the isotropic pressure. While in a FLRW background level the energy flux $\bar{q}_\mu$ and the anisotropic stress $\bar{\pi}_{\mu\nu}$ vanish, the same does not apply necessarily to the perturbations δq_μ and $\delta\pi_{\mu\nu}$. In fact, the orthogonality conditions $u^\mu q_\mu = 0$ and $u^\mu\pi_{\mu\nu} = 0$ imply only that the non-zero components of the δq_μ and $\delta\pi_{\mu\nu}$ are purely spatial. In addition, since we are only interested in perturbations within the scalar sector, we can decompose the perturbations δq_i and $\delta\pi_{ij}$ in terms of scalar potentials q and Π as

$$\delta q_i = \frac{1}{a}\partial_i q\,, \qquad \delta\pi_{ij} = \left(\mathrm{D}_i\mathrm{D}_j - \frac{1}{3}\gamma_{ij}\nabla^2\right)\Pi\,. \tag{A.42}$$

Using Eqs. (A.39)–(A.42), we can write the individual components of the perturbed stress-energy momentum tensor $T^\mu{}_\nu$ as[5]

$$T^0{}_0 = -\rho - \delta\rho\,, \tag{A.43}$$

$$T^0{}_i = 0 + \frac{a}{N}\mathrm{D}_i\left[\left(\bar{\rho}+\bar{P}\right)(v+B) + q\right]\,, \tag{A.44}$$

$$T^i{}_0 = 0 - \frac{N}{a}\mathrm{D}^i\left[\left(\bar{\rho}+\bar{P}\right)v + q\right]\,, \tag{A.45}$$

$$T^i{}_j = \bar{P}\delta^i_j + \delta P\delta^i_j + \frac{1}{a^2}\left(\mathrm{D}^i\mathrm{D}_j - \frac{1}{3}\delta^i_j\nabla^2\right)\Pi\,. \tag{A.46}$$

[5] As pointed out in [197], most works on cosmological perturbations found in the literature use the energy frame defined by the condition $q_\mu = 0$. As such, the off-diagonal elements $\delta T^0{}_i$ and $\delta T^i{}_0$ usually are written in terms of the peculiar velocity potential v and the metric potential B. In the general case, however, the perturbation q also contributes to the off-diagonal terms of the stress-energy-momentum tensor, as seen in Eqs. (A.44) and (A.45). A frame invariant 4-velocity can then be defined by $u^\mu + q^\mu/(\rho+P)$.

The energy density perturbation is often written in terms of the fractional energy density perturbation δ, also called density contrast,

$$\delta := \frac{\delta\rho}{\bar{\rho}}\,. \tag{A.47}$$

In addition, the isotropic pressure perturbation δP can be decomposed into its adiabatic and non-adiabatic part as [248, 337]

$$\delta P = \delta P^{(\mathrm{ad})} + \delta P^{(\mathrm{nad})} = c_a^2\,\delta\rho + \delta P^{(\mathrm{nad})}\,, \tag{A.48}$$

where $c_a^2 := \dot{\bar{P}}/\dot{\bar{\rho}}$ is dubbed the adiabatic squared speed of sound. Following the literature, we expand $\delta P^{(\mathrm{nad})}$ as [54, 337]

$$\delta P^{(\mathrm{nad})} = \left(c_s^2 - c_a^2\right)\left[\delta\rho + \dot{\bar{\rho}}\frac{a}{N}\left(v+B\right)\right]\,, \tag{A.49}$$

where c_s^2 corresponds to the squared speed of sound in the rest frame of the fluid defined by $v+B=0$:

$$c_s^2 := \left.\frac{\delta P}{\delta\rho}\right|_{\mathrm{r.f.}}\,. \tag{A.50}$$

Inserting (A.49) in Eq. (A.48) and making use of the background continuity equation we finally obtain[6] [22, 54, 337]

$$\delta P = \bar{\rho}\left[c_s^2\delta - 3\frac{\dot{a}}{a}\left(c_s^2 - c_a^2\right)\left(1+\bar{w}\right)\frac{a}{N}\left(v+B\right)\right]\,. \tag{A.51}$$

The energy density and pressure perturbations transform as true scalars under a gauge transformation

$$\delta\rho \to \delta\rho - \dot{\bar{\rho}}\,\delta t\,, \qquad\qquad \delta P \to \delta P - \dot{\bar{P}}\,\delta t\,, \tag{A.52}$$

while the velocity potential v transforms as

$$v \to v + \frac{a}{N}\dot{\xi}\,. \tag{A.53}$$

Using the metric perturbations, we can construct GI quantities that reduce to $\delta\rho$, δP and v in the Newtonian gauge as [46]

$$\delta\rho^{(N)} := \delta\rho - \dot{\bar{\rho}}\frac{\sigma}{N}\,, \qquad \delta P^{(N)} := \delta P - \dot{\bar{P}}\frac{\sigma}{N}\,, \qquad v^{(N)} := v + B + \frac{a}{N}\dot{E}\,. \tag{A.54}$$

Similarly to the comoving shear potential, the combination $v+B$ is invariant with regards to purely spatial gauge transformations

$$v + B \to v + B + \frac{N}{a}\delta t\,. \tag{A.55}$$

[6] Please note that here we are assuming non-interacting fluids, in which case the continuity equation reads $\dot{\bar{\rho}} = -3(\dot{a}/a)(\bar{\rho}+\bar{P})$. In the case of interacting fluids, the changes to the continuity equation will be reflected in Eq. (A.51).

We can therefore construct alternative GI invariant quantities for the energy density and pressure perturbations which reduce to $\delta\rho$ and δP in the comoving gauge $(v + B = 0)$ as

$$\delta\rho^{(C)} := \delta\rho + \frac{a}{N}\dot{\bar{\rho}}(v + B) = \delta\rho^{(N)} + \frac{a}{N}\dot{\bar{\rho}}v^{(N)}\,, \tag{A.56}$$

$$\delta P^{(C)} := \delta P + \frac{a}{N}\dot{\bar{P}}(v + B) = \delta P^{(N)} + \frac{a}{N}\dot{\bar{P}}v^{(N)}\,. \tag{A.57}$$

These quantities are of particular importance when discussing the matter power spectrum. Notice that GI quantities related to the density contrast δ can be constructed by using Eq. (A.47), e.g., $\delta^{(N)} := \delta\rho^{(N)}/\bar{\rho}$.

Another GI quantity of interest is the GI comoving curvature perturbation $\mathcal{R}$, defined as [49]

$$\mathcal{R} := \psi - \frac{a}{N}\frac{\dot{a}}{a}(v + B) = \Psi - \frac{a}{N}\frac{\dot{a}}{a}v^{(N)}\,. \tag{A.58}$$

This variable gains special relevance in the context of inflation and reheating as it becomes constant at large scales during a period of adiabatic evolution, for example in the case of single field inflation driven by a minimally coupled scalar field. From Eqs. (A.48) and (A.52), we find that $\delta P^{(\mathrm{nad})}$ is GI, as are the energy flux potential q and the anisotropic stress perturbation Π due to the fact that their background quantities vanish.

A.6. Multiple fluids

Let us now consider a setting of multiple, possibly interacting, fluids j, each with its own stress-energy-momentum tensor $[T_{(\mathrm{j})}]_{\mu\nu}$ such that

$$T_{\mu\nu} = \sum_{(\mathrm{j})}[T_{(\mathrm{j})}]_{\mu\nu}\,. \tag{A.59}$$

If for each fluid we define a 4-velocity vector $[u_{(\mathrm{j})}]^{\mu}$, given by (A.39) and (A.40), with a velocity potential $v_{(\mathrm{j})}$, then we can decompose $[T_{(\mathrm{j})}]_{\mu\nu}$ as in Eq. (A.41). This allows us to define the energy density $\rho_{(\mathrm{j})} = \bar{\rho}_{(\mathrm{j})} + \delta\rho_{(\mathrm{j})}$, the isotropic pressure $P_{(\mathrm{j})} = \bar{P}_{(\mathrm{j})} + \delta P_{(\mathrm{j})}$ and the energy flux $q_{(\mathrm{j})}$ and anisotropic stress $\Pi_{(\mathrm{j})}$ potentials that contribute to $[T_{(\mathrm{j})}]_{\mu\nu}$ through spatial tensors defined by Eq. (A.42). The individual components of the perturbed $[T_{(\mathrm{j})}]_{\mu\nu}$ can then be written in terms of these quantities by an adequate substitution in Eqs. (A.43)–(A.46). In addition, from the condition (A.59) we can also derive the relations between the individual and total quantities as

$$\delta\rho = \sum_{(\mathrm{j})}\delta\rho_{(\mathrm{j})}\,, \qquad \delta P = \sum_{(\mathrm{j})}\delta P_{(\mathrm{j})}\,, \tag{A.60}$$

$$\delta = \sum_{(\mathrm{j})}\frac{\bar{\rho}_{(\mathrm{j})}}{\bar{\rho}}\delta_{(\mathrm{j})}\,, \qquad v = \sum_{(\mathrm{j})}\frac{\bar{\rho}_{(\mathrm{j})} + \bar{P}_{(\mathrm{j})}}{\bar{\rho} + \bar{P}}v_{(\mathrm{j})}\,, \tag{A.61}$$

$$q = \sum_{(\mathrm{j})}q_{(\mathrm{j})}\,, \qquad \Pi = \sum_{(\mathrm{j})}\Pi_{(\mathrm{j})}\,. \tag{A.62}$$

As in the case of the total pressure perturbation, each $\delta P_{(\mathrm{j})}$ can be decomposed into its adiabatic and non-adiabatic component

$$\delta P_{(\mathrm{j})} = \delta P^{(\mathrm{ad})}_{(\mathrm{j})} + \delta P^{(\mathrm{nad})}_{(\mathrm{j})} = c^2_{a,(\mathrm{j})}\,\delta\rho_{(\mathrm{j})} + \delta P^{(\mathrm{nad})}_{(\mathrm{j})}\,, \tag{A.63}$$

where now $c^2_{a,(\mathrm{j})} := \dot{\bar{P}}_{(\mathrm{j})}/\dot{\bar{\rho}}_{(\mathrm{j})}$ is the adiabatic squared speed of sound of the fluid j. The individual non-adiabatic parts can be decomposed as in (A.49). However, if we take into account the possible existence of interactions between the different fluids, then Eq. (A.51) must be replaced by [337]

$$\delta P_{(\mathrm{j})} = c^2_{s,(\mathrm{j})}\delta\rho_{(\mathrm{j})} - \left(c^2_{s,(\mathrm{j})} - c^2_{a,(\mathrm{j})}\right)\left[3\frac{\dot{a}}{a}\left(\bar{\rho}_{(\mathrm{j})} + \bar{P}_{(\mathrm{j})}\right) - N\,Q_{(\mathrm{j})}\right]\frac{a}{N}\left(v_{(\mathrm{j})} + B\right)\,. \tag{A.64}$$

Due to the additive property of the total pressure perturbation, we find that apart from the intrinsic non-adiabatic term $\delta P^{(\mathrm{nad})}_{(\mathrm{j})}$, each fluid contributes to the total non-adiabaticity by a relative term proportional to the difference $c^2_{a,(\mathrm{j})} - c^2_a$ [248]:

$$\begin{aligned}\delta P &= \sum_{(\mathrm{j})}\left(\delta P^{(\mathrm{ad})}_{(\mathrm{j})} + \delta P^{(\mathrm{nad})}_{(\mathrm{j})}\right)\\ &= \sum_{(\mathrm{j})} c^2_a\delta\rho_{(\mathrm{j})} + \sum_{(\mathrm{j})}\left(c^2_{a,(\mathrm{j})} - c^2_a\right)\delta\rho_{(\mathrm{j})} + \sum_{(\mathrm{j})}\delta P^{(\mathrm{nad})}_{(\mathrm{j})}\\ &= \delta P^{(\mathrm{ad})} + \delta P^{(\mathrm{rel})} + \delta P^{(\mathrm{int})}\,.\end{aligned} \tag{A.65}$$

The relative non-adiabatic term can also be expressed as

$$\delta P^{(\mathrm{rel})} = \frac{1}{6\dot{\rho}}\frac{a}{\dot{a}}\sum_{(\mathrm{j}),(\mathrm{l})}\dot{\rho}_{(\mathrm{j})}\dot{\rho}_{(\mathrm{k})}\left(c^2_{a(\mathrm{j})} - c^2_{a(\mathrm{k})}\right)\mathcal{S}_{\mathrm{jk}}\,, \tag{A.66}$$

where $\mathcal{S}_{\mathrm{jk}}$ is the relative entropy perturbation[7] between the fluids j and k [247, 248]

$$\mathcal{S}_{\mathrm{jm}} := -3\frac{\dot{a}}{a}\left(\frac{\delta\rho_{(\mathrm{j})}}{\dot{\rho}_{(\mathrm{j})}} - \frac{\delta\rho_{(\mathrm{k})}}{\dot{\rho}_{(\mathrm{k})}}\right)\,. \tag{A.67}$$

Thus, a condition for adiabaticity in a multi-fluid scenario with vanishing $\delta P^{(\mathrm{nad})}_{(\mathrm{j})}$ is

$$\frac{\delta\rho_{(\mathrm{j})}}{\dot{\rho}_{(\mathrm{j})}} - \frac{\delta\rho_{(\mathrm{k})}}{\dot{\rho}_{(\mathrm{k})}} = 0\,, \tag{A.68}$$

which for non-interacting fluids becomes

$$\frac{\delta\rho_{(\mathrm{j})}}{\rho_{(\mathrm{j})} + P_{(\mathrm{j})}} - \frac{\delta\rho_{(\mathrm{k})}}{\rho_{(\mathrm{k})} + P_{(\mathrm{k})}} = 0\,. \tag{A.69}$$

Finally, we note that all the individual fluid quantities transform under a gauge transformation as the respective total matter quantities, cf. Eqs. (A.52) and (A.53), and that analogous gauge invariant

[7] A slightly different definition of the relative entropy perturbation, which coincides with (A.67) in the case of non-interacting fluids, is given in Ref. [215].

quantities can be constructed using the rules (A.54), (A.56) and (A.57). Notice that by construction $\mathcal{S}_{\rm jl}$ is gauge invariant.

A.7. Einstein field equations

At a classical level, the evolution of the linear perturbations of the metric around a fixed background is dictated by the first order perturbation of Einstein field equations

$$\delta G^{\mu}{}_{\nu} = \kappa^2 \delta[T^{(\rm m)}]^{\mu}{}_{\nu}\,, \tag{A.70}$$

For simplicity, from this point onward we choose to work in the Newtonian gauge $(B = E = 0)$ where the perturbed line element (A.9) is reduced to the particular simple form[8] [49, 198, 246]

$$\mathrm{d}s^2 = -N^2\,(1+2\Phi)\,\mathrm{d}t^2 + a^2(1-2\Psi)\gamma_{ij}\mathrm{d}x^i\mathrm{d}x^j\,. \tag{A.71}$$

In addition, we will disregard the spatial curvature of the Universe ($\mathcal{K} = 0$). With these considerations, the $(0-0)$, $(0-i)$, $(i-i)$ and $(i-j)$, with $i \neq j$, components of Eq. (A.70) read

$$\frac{\dot{a}}{a}\dot{\Psi} + \left(\frac{\dot{a}}{a}\right)^2\Phi - \frac{N^2}{3a^2}\nabla^2\Psi = -\frac{\kappa^2 N^2}{6}\bar{\rho}\,\delta^{(N)}\,, \tag{A.72}$$

$$\partial_i\left(\dot{\Psi} + \frac{\dot{a}}{a}\Phi\right) = -\frac{\kappa^2 a N}{2}\partial_i\left[\left(\bar{\rho}+\bar{P}\right)v^{(N)} + q\right]\,, \tag{A.73}$$

$$\ddot{\Psi} + \left(3\frac{\dot{a}}{a} - \frac{\dot{N}}{N}\right)\dot{\Psi} + \frac{\dot{a}}{a}\dot{\Phi} + \left[2\frac{\ddot{a}}{a} + \left(\frac{\dot{a}}{a}\right)^2 - 2\frac{\dot{N}}{N}\frac{\dot{a}}{a}\right]\Phi$$
$$-\frac{1}{3}\frac{N^2}{a^2}\nabla^2\left(\Psi-\Phi\right) = \frac{\kappa^2 N^2}{2}\delta P^{(N)}\,, \tag{A.74}$$

$$\mathrm{D}^i\mathrm{D}_j\left(\Psi-\Phi\right) = \kappa^2\mathrm{D}^i\mathrm{D}_j\Pi\,. \tag{A.75}$$

In order to take full advantage of the linearity of the equations, we apply a Fourier decomposition of the perturbations

$$X(t,\,\vec{x}) = \int\frac{\mathrm{d}^3\vec{k}}{(2\pi)^{3/2}}X_{\vec{k}}(t)\,\mathrm{e}^{\mathrm{i}\vec{k}\cdot\vec{x}}\,, \qquad X_{\vec{k}}(t) = \int\frac{\mathrm{d}^3\vec{k}}{(2\pi)^{3/2}}X(t,\,\vec{x})\,\mathrm{e}^{\mathrm{i}\vec{k}\cdot\vec{x}}\,, \tag{A.76}$$

which allows us to re-arrange Eqs. (A.72)–(A.75) as two constraints

$$\frac{k^2}{a^2}\Psi_{\vec{k}} = -\frac{\kappa^2}{2}\bar{\rho}\,\delta^{(C)}_{\vec{k}}\,, \tag{A.77}$$

$$\Psi_{\vec{k}} - \Phi_{\vec{k}} = \kappa^2\Pi_{\vec{k}}\,, \tag{A.78}$$

[8] More precisely, we work with the GI variables defined above, Φ, Ψ, $\delta\rho^{(N)}$, $\delta P^{(N)}$ and $v^{(N)}$, that in the Newtonian gauge coincide with the perturbations A, ψ, $\delta\rho$, δP and v.

and two evolution equations for the Bardeen potentials

$$\dot{\Psi}_{\vec{k}} + \frac{\dot{a}}{a}\Phi_{\vec{k}} = -\frac{\kappa^2 a N}{2}\left[\left(\bar{\rho}+\bar{P}\right)v_{\vec{k}}^{(N)} + q\right], \tag{A.79}$$

$$\ddot{\Psi}_{\vec{k}} + \left[3(1+c_a^2)\frac{\dot{a}}{a} - \frac{\dot{N}}{N}\right]\dot{\Psi}_{\vec{k}} + \frac{\dot{a}}{a}\dot{\Phi}_{\vec{k}} + \left[2\frac{\ddot{a}}{a} + (1+3c_a^2)\left(\frac{\dot{a}}{a}\right)^2 - 2\frac{\dot{N}}{N}\frac{\dot{a}}{a}\right]\Phi_{\vec{k}} + c_a^2 N^2\frac{k^2}{a^2}\Psi_{\vec{k}} = \frac{\kappa^2 N^2}{2}\delta P_{\vec{k}}^{(\mathrm{nad},N)} - \frac{\kappa^2 N^2}{3}\frac{k^2}{a^2}\Pi_{\vec{k}}\,. \tag{A.80}$$

The first of the constraint equations, Eq. (A.77), is nothing more than the Poisson equation which relates the gravitational potential with the matter distribution and which reduces to Newton's law of gravitation in the Minkowskian limit. The second equation, Eq. (A.78), leads to the well known result in GR of the equality of the Bardeen potentials in the absence of anisotropies and Eq. (A.79) relates the GI perturbation of the Hubble rate, cf. Eq. (A.17), with the total momentum as

$$\delta H_{\vec{k}}^{(N)} = -\frac{\kappa^2 a}{2}\left[\left(\bar{\rho}+\bar{P}\right)v_{\vec{k}}^{(N)} + q\right]. \tag{A.81}$$

Finally, for an adiabatic evolution and in the absence of anisotropies, Eq. (A.80) provides a closed equation for the gravitational potential Ψ. In particular, for an EoS with constant $w = c_a^2$ we obtain

$$\frac{\mathrm{d}^2\Psi_{\vec{k}}}{\mathrm{d}\,x^2} + \frac{5+3w}{2}\frac{\mathrm{d}\Psi_{\vec{k}}}{\mathrm{d}\,x} + w\frac{k^2}{a^2H^2}\Psi_{\vec{k}} = 0\,. \tag{A.82}$$

In the long wavelength limit ($k^2 \ll a^2H^2$), the last term on the l.h.s. of this equation can be disregarded which allows us to find the explicit general solution

$$\Psi_{\vec{k}}(x) = C_1 + C_2\,\mathrm{e}^{-\frac{5+3w}{2}x}\,. \tag{A.83}$$

In a matter-dominated universe where $w = 0$, this solution is valid even for modes well inside the Hubble horizon which do not satisfy the long wavelength limit.

A.8. Conservation Equations

While the metric perturbations are governed by the perturbed Einstein equations, the evolution of the matter variables for each fluid j is dictated by the first order perturbation of the conservation equation

$$\nabla_\mu \delta[T_{(\mathrm{j})}]^\mu{}_\nu + \delta\Gamma^\mu_{\mu\rho}[\bar{T}_{(\mathrm{j})}]^\rho{}_\nu - \delta\Gamma^\rho_{\mu\nu}[\bar{T}_{(\mathrm{j})}]^\mu{}_\rho = [\delta Q_{(\mathrm{j})}]_\nu\,, \tag{A.84}$$

where $[\delta Q_{(\mathrm{j})}]_\nu$ is the first order perturbation of the energy-momentum transfer 4-vector. Following [247, 337], we decompose $[\delta Q_{(\mathrm{j})}]_\nu$ as

$$[\delta Q_{(\mathrm{j})}]_0 = -N\left(\bar{Q}_{(\mathrm{j})}A + \delta Q_{(\mathrm{j})}\right), \qquad [\delta Q_{(\mathrm{j})}]_i = \partial_i\left[f_{(\mathrm{j})} + a\,\bar{Q}_{(\mathrm{j})}\,(v+B)\right]. \tag{A.85}$$

Here, we point out that v is the total peculiar velocity potential. The two new scalar quantities $\delta Q_{(\mathrm{j})}$ and $f_{(\mathrm{j})}$ are GI by construction and satisfy the constraints

$$\sum_{\mathrm{j}} \delta Q_{(\mathrm{j})} = 0\,, \qquad\qquad \sum_{\mathrm{j}} f_{(\mathrm{j})} = 0\,. \tag{A.86}$$

In the Newtonian gauge and in Fourier space[9], the temporal and spatial components, respectively, of Eq. (A.84) read [247, 337]

$$\begin{aligned}\dot{\delta\rho}^{(N)}_{(\mathrm{j})} + 3\frac{\dot{a}}{a}\left(\delta\rho^{(N)}_{(\mathrm{j})} + \delta P^{(N)}_{(\mathrm{j})}\right) \; - \frac{N}{a}k^2\left[\left(\bar{\rho}_{(\mathrm{j})} + \bar{P}_{(\mathrm{j})}\right) v^{(N)}_{(\mathrm{j})} + q_{(\mathrm{j})}\right] \\ = 3\left(\bar{\rho}_{(\mathrm{j})} + \bar{P}_{(\mathrm{j})}\right)\dot{\Psi} - N\left(\Phi\bar{Q}_{(\mathrm{j})} + \delta Q_{(\mathrm{j})}\right)\,,\end{aligned} \tag{A.87}$$

$$\begin{aligned}\partial_0\left[\left(\bar{\rho}_{(\mathrm{j})} + \bar{P}_{(\mathrm{j})}\right) v^{(N)}_{(\mathrm{j})} + q_{(\mathrm{j})}\right] + 4\frac{\dot{a}}{a}\left[\left(\bar{\rho}_{(\mathrm{j})} + \bar{P}_{(\mathrm{j})}\right) v^{(N)}_{(\mathrm{j})} + q_{(\mathrm{j})}\right] + \frac{N}{a}\left(\delta P^{(N)}_{(\mathrm{j})} - \frac{2}{3}\frac{k^2}{a^2}\Pi_{(\mathrm{j})}\right) \\ = \frac{N}{a}\left[-\left(\bar{\rho}_{(\mathrm{j})} + \bar{P}_{(\mathrm{j})}\right)\Phi + f_{(\mathrm{j})} + a\,\bar{Q}_{(\mathrm{j})}v^{(N)}\right]\,.\end{aligned} \tag{A.88}$$

If we decompose the isotropic pressure perturbation into its adiabatic and non-adiabatic components, according to Eq. (A.64), and then replace the energy density perturbation $\delta\rho^{(N)}_{(\mathrm{j})}$ by the density contrast $\delta^{(N)}_{(\mathrm{j})}$, the previous equations can be re-written as [247, 337]

$$\begin{aligned}\dot{\delta}^{(N)}_{(\mathrm{j})} \; + 3\frac{\dot{a}}{a}\left(c^2_{s,(\mathrm{j})} - \bar{w}_{(\mathrm{j})}\right)\delta^{(N)}_{(\mathrm{j})} - \left(1+\bar{w}_{(\mathrm{j})}\right)\left[9\left(\frac{\dot{a}}{a}\right)^2\left(c^2_{s,(\mathrm{j})} - c^2_{a,(\mathrm{j})}\right) + \frac{N^2}{a^2}k^2\right]\frac{a}{N}v^{(N)}_{(\mathrm{j})} - \frac{N}{a}k^2\frac{q_{(\mathrm{j})}}{\bar{\rho}_{(\mathrm{j})}} \\ = 3\left(1+\bar{w}_{(\mathrm{j})}\right)\dot{\Psi} - N\frac{\bar{Q}_{(\mathrm{j})}}{\bar{\rho}_{(\mathrm{j})}}\left[\Phi - 3\frac{\dot{a}}{a}\left(c^2_{s,(\mathrm{j})} - c^2_{a,(\mathrm{j})}\right)\frac{a}{N}v^{(N)}_{(\mathrm{j})}\right] - N\frac{\delta Q_{(\mathrm{j})}}{\bar{\rho}_{(\mathrm{j})}}\,,\end{aligned} \tag{A.89}$$

$$\begin{aligned}\dot{v}^{(N)}_{(\mathrm{j})} \; + \frac{\dot{a}}{a}\left(1 - 3c^2_{s,(\mathrm{j})}\right)v^{(N)}_{(\mathrm{j})} + \frac{N}{a}\left(\frac{c^2_{s,(\mathrm{j})}}{1+\bar{w}_{(\mathrm{j})}}\delta^{(N)}_{(\mathrm{j})} - \frac{2}{3}\frac{k^2}{a^2}\frac{\Pi_{(\mathrm{j})}}{\bar{\rho}_{(\mathrm{j})} + \bar{P}_{(\mathrm{j})}}\right) + \frac{1}{\bar{\rho}_{(\mathrm{j})} + \bar{P}_{(\mathrm{j})}}\left(\dot{q}_{(\mathrm{j})} + 4\frac{\dot{a}}{a}q_{(\mathrm{j})}\right) \\ = \frac{N}{a}\left\{-\Phi + \frac{f_{(\mathrm{j})}}{\bar{\rho}_{(\mathrm{j})} + \bar{P}_{(\mathrm{j})}} + \frac{a\,\bar{Q}_{(\mathrm{j})}}{\bar{\rho}_{(\mathrm{j})} + \bar{P}_{(\mathrm{j})}}\left[v^{(N)} - \left(1 + c^2_{s,(\mathrm{j})}\right)v^{(N)}_{(\mathrm{j})}\right]\right\}\,.\end{aligned} \tag{A.90}$$

In the case of non-interacting fluids and in the energy-frame where $q_{(\mathrm{j})} \equiv 0$, these equations reduce to

$$\begin{aligned}\dot{\delta}^{(N)}_{(\mathrm{j})} \; + 3\frac{\dot{a}}{a}\left(c^2_{s,(\mathrm{j})} - \bar{w}_{(\mathrm{j})}\right)\delta^{(N)}_{(\mathrm{j})} - \left(1+\bar{w}_{(\mathrm{j})}\right)\left[9\left(\frac{\dot{a}}{a}\right)^2\left(c^2_{s,(\mathrm{j})} - c^2_{a,(\mathrm{j})}\right) + \frac{N^2}{a^2}k^2\right]\frac{a}{N}v^{(N)}_{(\mathrm{j})} \\ = 3\left(1+\bar{w}_{(\mathrm{j})}\right)\dot{\Psi}\,,\end{aligned} \tag{A.91}$$

$$\dot{v}^{(N)}_{(\mathrm{j})} \; + \frac{\dot{a}}{a}\left(1 - 3c^2_{s,(\mathrm{j})}\right)v^{(N)}_{(\mathrm{j})} + \frac{N}{a}\left(\frac{c^2_{s,(\mathrm{j})}}{1+\bar{w}_{(\mathrm{j})}}\delta^{(N)}_{(\mathrm{j})} - \frac{2}{3}\frac{k^2}{a^2}\frac{\Pi_{(\mathrm{j})}}{\bar{\rho}_{(\mathrm{j})} + \bar{P}_{(\mathrm{j})}}\right) = -\frac{N}{a}\Phi\,. \tag{A.92}$$

[9] In the remainder of this section, we omit the subscript $\vec{k}$ in order to simplify the notation. Nevertheless, in the equations that follow, all the perturbation variables should be interpreted as representing the Fourier mode obtained from the expansion (A.76).

B $f(R)$-gravity

B.1. Cosmography in metric $f(R)$-gravity

The coefficients $\mathcal{A}_i$, $\mathcal{B}_i$ and $\mathcal{D}$ introduced in Eqs. (3.76)–(3.79) are defined as

$$
\begin{aligned}
\mathcal{A}_0 = & \left[j_0 - q_0 - 2\left(1+\Omega_{\mathcal{K},0}\right)\right] l_0 \\
& - \left[3s_0 + \left(7+9w_0\right) j_0 + 6q_0^2 + \left(41 - 9w_0 + 12\Omega_{\mathcal{K},0}\right) q_0 + 2\left(11 - 9w_0\right)\left(1+\Omega_{\mathcal{K},0}\right)\right] s_0 \\
& - \Big\{\left[3q_0 + 16 + 6w_0 + 4\Omega_{\mathcal{K},0} + 9\left(1+w_0\right) c_{a,0}^2\right] j_0 - \left(20+9w_0\right) q_0^2 \\
& \quad + 2\left(32 + 30w_0 - 9\left(1+w_0\right) c_{a,0}^2 + \left(8+9w_0\right)\Omega_{\mathcal{K},0}\right) q_0 \\
& \quad + 6\left(1+\Omega_{\mathcal{K},0}\right)\left(2 + 5w_0 - 6\left(1+w_0\right) c_{a,0}^2 - 2\Omega_{\mathcal{K},0}\right)\Big\} j_0 \\
& - 3q_0^4 - \left(25 - 9w + 12\Omega_{\mathcal{K},0}\right) q_0^3 \\
& - 3\left[4\left(8-7w\right) + 3\left(1+w_0\right) c_{a,0}^2 + 4\left(5-3w\right)\Omega_{\mathcal{K},0} + 4\Omega_{\mathcal{K},0}^2\right] q_0^2 \\
& - 6\left[\left(12-29w\right) + 6\left(1+w_0\right)\left(1+\Omega_{\mathcal{K},0}\right) c_{a,0}^2 + \left(16 - 35w_0\right)\Omega_{\mathcal{K},0} + \left(4-6w_0\right)\Omega_{\mathcal{K},0}^2\right] q_0 \\
& - 4\left(1+\Omega_{\mathcal{K},0}\right)^2\left[5 - 21w_0 + 9\left(1+w_0\right) c_{a,0}^2 + 2\Omega_{\mathcal{K},0}\right] , \qquad \text{(B.1)} \\
\mathcal{B}_0 = & - \left[j_0 - q_0 - 2\left(1+\Omega_{\mathcal{K},0}\right)\right] q_0 l_0 \\
& + \Big[3q_0 s_0 + \left(4q_0 + 6 + 6\Omega_{\mathcal{K},0}\right) j_0 \\
& \quad + 6q_0^3 + 4\left(11 + 3\Omega_{\mathcal{K},0}\right) q_0^2 + 22\left(1+\Omega_{\mathcal{K},0}\right) q_0 - 12\left(1+\Omega_{\mathcal{K},0}\right)^2\Big] s_0 \\
& + \Big\{2j_0^2 + \left[3q_0^2 + \left(10 + 4\Omega_{\mathcal{K},0}\right) q_0 - 6\left(1+\Omega_{\mathcal{K},0}\right)\right] j_0 \\
& \quad + 17q_0^3 + 4\left(13 + 2\Omega_{\mathcal{K},0}\right) q_0^2 + 54\left(1+\Omega_{\mathcal{K},0}\right) q_0 + 36\left(1+\Omega_{\mathcal{K},0}\right)^2\Big\} j_0 \\
& + 3q_0^5 + 4\left(7 + 3\Omega_{\mathcal{K},0}\right) q_0^4 + 2\left(59 + 33\Omega_{\mathcal{K},0} + 6\Omega_{\mathcal{K},0}^2\right) q_0^3 + 12\left(6 + 7\Omega_{\mathcal{K},0} + \Omega_{\mathcal{K},0}^2\right) q_0^2 \\
& - 4\left(1+\Omega_{\mathcal{K},0}\right)^2\left(19 + 4\Omega_{\mathcal{K},0}\right) q_0 - 64\left(1+\Omega_{\mathcal{K},0}\right)^3 , \qquad \text{(B.2)} \\
\mathcal{A}_2 = & \, 9\left(1+w_0\right) s_0 + 3\left(2 + 3c_{a,0}^2\right)\left(1+w_0\right) j_0 + 9\left(1+w_0\right) q_0^2 \\
& + 3\left(1+w_0\right)\left(22 - 3c_{a,0}^2 + 6\Omega_{\mathcal{K},0}\right) q_0 + 6\left(1+\Omega_{\mathcal{K},0}\right)\left(1+w_0\right)\left(7 - 3c_{a,0}^2\right) , \qquad \text{(B.3)} \\
\mathcal{B}_2 = & - 6\left(q_0 + 1 + \Omega_{\mathcal{K},0}\right) s_0 - 2\left[j_0 + q_0 - \left(1+\Omega_{\mathcal{K},0}\right)\right] j_0 - 6q_0^3 - 2\left(25 + 9\Omega_{\mathcal{K},0}\right) q_0^2 \\
& - 2\left(37 + 43\Omega_{\mathcal{K},0} + 6\Omega_{\mathcal{K},0}^2\right) q_0 \qquad \text{(B.4)}
\end{aligned}
$$

$$\begin{aligned}
\mathcal{A}_3 = & -3\left(1+w_0\right) l_0 - 3\left(1+w_0\right)\left(1+3c_{a,0}^2\right) s_0 + 3\left(1+w_0\right)\left(3q_0+12+3c_{a,0}^2+4\Omega_{\mathcal{K},0}\right) j_0 \\
& + 9\left(1+w_0\right)\left(5-c_{a,0}^2\right) q_0^2 + 3\left(1+w_0\right)\left[26-27c_{a,0}^2+2\left(5-3c_{a,0}^2\right)\Omega_{\mathcal{K},0}\right] q_0 \\
& + 12\left(1+\Omega_{\mathcal{K},0}\right)\left(1+w_0\right)\left(1-6c_{a,0}^2\right) , \qquad \text{(B.5)} \\
\mathcal{B}_3 = & -6\left(q_0+1+\Omega_{\mathcal{K},0}\right) s_0 - 2\left[j_0+q_0-\left(1+\Omega_{\mathcal{K},0}\right)\right] j_0 - 6q_0^3 - 2\left(25+9\Omega_{\mathcal{K},0}\right) q_0^2 \\
& - 2\left(37+43\Omega_{\mathcal{K},0}+6\Omega_{\mathcal{K},0}^2\right) q_0 \qquad \text{(B.6)} \\
\mathcal{D}_0 = & -\left[j_0-q_0-2-2\Omega_{\mathcal{K},0}\right] l_0 \\
& + \left[3s_0-2j_0+6q_0^2+2\left(25+6\Omega_{\mathcal{K},0}\right) q_0+40+40\Omega_{\mathcal{K}}\right] s_0 \\
& + \left[\left(10+3q_0+4\Omega_{\mathcal{K},0}\right) j_0+11q_0^2+2\left(2-\Omega_{\mathcal{K},0}\right) q_0-6\left(3+5\Omega_{\mathcal{K},0}+2\Omega_{\mathcal{K},0}^2\right)\right] j_0 \\
& + \left[3q_0^3+2\left(17+\Omega_{\mathcal{K},0}\right) q_0^2+12\left(15+8\Omega_{\mathcal{K},0}+\Omega_{\mathcal{K},0}^2\right) q_0+6\left(41+61\Omega_{\mathcal{K},0}+10\Omega_{\mathcal{K},0}^2\right)\right] q_0 \\
& + 8\left(1+\Omega_{\mathcal{K},0}\right)^2\left(13+\Omega_{\mathcal{K},0}\right) , \qquad \text{(B.7)}
\end{aligned}$$

In the presence of J fluids with fractional energy density $\Omega_{(\mathrm{j})}$, $\mathrm{j}=1,\ldots,\mathrm{J}$, we can make use of the relations

$$\Omega^{(\mathrm{m})} = \sum_{\mathrm{j}=1}^{\mathrm{J}} \Omega_{(\mathrm{j})} , \qquad \text{(B.8)}$$

$$w\,\Omega^{(\mathrm{m})} = \sum_{\mathrm{j}=1}^{\mathrm{J}} w_{(\mathrm{j})}\Omega_{(\mathrm{j})} , \qquad \text{(B.9)}$$

$$c_a^2\left(1+w\right)\Omega^{(\mathrm{m})} = \sum_{\mathrm{j}=1}^{\mathrm{J}} c_{a,(\mathrm{j})}^2\left(1+w_{(\mathrm{j})}\right)\Omega_{(\mathrm{j})} , \qquad \text{(B.10)}$$

to expand $\mathcal{A}_i\Omega_0^{(\mathrm{m})}$ as

$$\mathcal{A}_i\Omega_0^{(\mathrm{m})} = \sum_{n=1}^{N} \mathcal{A}_{i,(\mathrm{j})}\Omega_{(\mathrm{j}),0} , \qquad \text{(B.11)}$$

where $\mathcal{A}_{i,(\mathrm{j})}$, $i=0,2,3$ are defined by Eqs. (B.1)–(B.5) in which w_0 and $c_{a,0}^2$ are replaced by the present day values of the EoS parameter, $w_{(\mathrm{j})}$, and of the adiabatic squared speed of sound, $c_{a,(\mathrm{j})}^2$, of the fluid j.

B.2. The extra degree of freedom δF

In metric $f(R)$-gravity, the variable $\delta F := \delta^{(1)} f_R$ represents a new scalar degree of freedom at the level of first order perturbations. Being a scalar quantity, δF transforms under a gauge transformation as

$$\delta F \to \delta F - \dot{f}_R \delta t . \qquad \text{(B.12)}$$

As such, we can construct two GI quantities that reduce to δF in the Newtonian and comoving gauges as

$$\delta F^{(N)} := \delta F - \dot{f}_R \frac{\sigma}{N}\,, \qquad\qquad \delta F^{(C)} := \delta F + \dot{f}_R \frac{a}{N}\left(v + B\right)\,. \tag{B.13}$$

Using the relation $\delta F = f_{RR}\delta R$ we can write the new scalar degree of freedom δF in terms of the metric potentials as

$$\begin{aligned}\delta F = & -\frac{6}{N^2} f_{RR}\left[\ddot{\psi} + \left(4\frac{\dot{a}}{a} - \frac{\dot{N}}{N}\right)\dot{\psi} + \frac{\dot{a}}{a}\dot{A} + \partial_0\left(\frac{1}{N}\frac{\dot{a}}{a}\right)A - 2\frac{N^2}{a^2}\mathcal{K}\psi\right] \\ & + \frac{2}{a^2} f_{RR}\nabla^2\left[2\psi - A + \frac{\dot{\sigma}}{N} + 2\frac{\dot{a}}{a}\frac{\sigma}{N}\right]\,.\end{aligned} \tag{B.14}$$

This equation has no analogue in GR, as both δF on the l.h.s. and f_{RR} on the r.h.s. vanish in the limit of vanishing f_R.

B.3. The modified Einstein equations

The first order perturbation of the modified Einstein field equations is given by Eq. (3.34)

$$(1+f_R)\delta G^{\mu}{}_{\nu} + \left(\bar{R}^{\mu}{}_{\nu} + \delta^{\mu}_{\nu}\Box - \nabla^{\mu}\nabla_{\nu}\right)\delta f_R \; - \delta^{(1)}\left(\nabla^{\mu}\nabla_{\nu} - \delta^{\mu}_{\nu}\Box\right) f_R = \kappa^2[\delta T^{(\mathrm{m})}]^{\mu}{}_{\nu}\,. \tag{B.15}$$

The first and third terms on the l.h.s. of the previous equation can be expanded in terms of the perturbations of the metric as

$$\begin{aligned}(1+f_R)\delta G^{\mu}{}_{\nu} = & (1+f_R)\left[\delta^{\mu}_{\sigma}\bar{R}_{\rho\nu} + \frac{1}{2}\delta^{\mu}_{\nu}\bar{R}_{\rho\sigma} - \delta^{\mu}_{\nu}\bar{\nabla}_{(\rho}\bar{\nabla}_{\sigma)} + \frac{1}{2}\left(\bar{g}^{\mu\lambda}\bar{g}_{\nu\sigma} + \delta^{\mu}_{\sigma}\delta^{\lambda}_{\nu}\right)\bar{\nabla}_{\rho}\bar{\nabla}_{\lambda}\right]\delta g^{\rho\sigma} \\ & - (1+f_R)\left(\bar{R} + \frac{1}{2}\bar{\Box}\right)\delta g^{\mu}_{\nu} + (1+f_R)\frac{1}{2}\left(\delta^{\mu}_{\nu}\bar{\Box} - \bar{\nabla}^{\mu}\bar{\nabla}_{\nu}\right)\delta g^{\rho}_{\rho}\,,\end{aligned} \tag{B.16}$$

$$\begin{aligned}\delta^{(1)}\left(\nabla^{\mu}\nabla_{\nu} - \delta^{\mu}_{\nu}\Box\right) f_R = & -\left(\bar{\nabla}_{\rho}\bar{\nabla}_{\nu}f_R\right)\delta g^{\mu\rho} + \delta^{\mu}_{\nu}\left(\bar{\nabla}_{\sigma}\bar{\nabla}_{\rho}f_R\right)\delta g^{\rho\sigma} \\ & + \frac{1}{2}\bar{\nabla}_{\rho}f_R\left[2\delta^{\mu}_{\nu}\bar{\nabla}^{\lambda}\delta g^{\rho}_{\lambda} + \bar{\nabla}^{\rho}\left(\delta g^{\mu}_{\nu} - \delta^{\mu}_{\nu}\delta g^{\sigma}_{\sigma}\right) - \bar{\nabla}^{\mu}\delta g^{\rho}_{\nu} - \bar{\nabla}_{\nu}\delta g^{\rho\mu}\right]\,.\end{aligned} \tag{B.17}$$

This allows us to calculate the first order perturbation of $(0-0)$, $(0-i)$, $(i-i)$ and $(i-j)$, with $i \neq j$, components of the modified Einstein equations (3.34) in the so called gauge-ready form as:

$$\begin{aligned}(1+f_R)\left[\frac{\dot{a}}{a}\dot{\psi} + \left(\frac{\dot{a}}{a}\right)^2 A - \frac{N^2}{a^2}\mathcal{K}\psi - \frac{N^2}{3a^2}\nabla^2\left(\psi + \frac{\dot{a}}{a}\frac{\sigma}{N}\right)\right] - \frac{1}{2}\dot{f}_R\left[\dot{\psi} + 2\frac{\dot{a}}{a}A\right] \\ - \frac{1}{2}\left[\frac{\dot{a}}{a}\delta\dot{F} - \left(\frac{\ddot{a}}{a} - \frac{\dot{N}}{N}\frac{\dot{a}}{a}\right)\delta F\right] + \frac{1}{6}\frac{N^2}{a^2}\nabla^2\left(\delta F - \dot{f}_R\frac{\sigma}{N}\right) = -\frac{\kappa^2 N^2}{6}\delta\rho\,,\end{aligned} \tag{B.18}$$

$$\mathrm{D}_i\left\{(1+f_R)\left[\dot{\psi}+\frac{\dot{a}}{a}A+\left(\frac{N^2}{a^2}\mathcal{K}\right)\frac{\sigma}{N}\right]+\frac{1}{2}\frac{\dot{a}}{a}\delta F-\frac{1}{2}\dot{f}_R A\right\}$$
$$=-\frac{\kappa^2 N a}{2}\mathrm{D}_i\left[\left(\bar{\rho}+\bar{P}\right)(v+B)+q\right], \tag{B.19}$$

$$(1+f_R)\left[\ddot{\psi}+\left(3\frac{\dot{a}}{a}-\frac{\dot{N}}{N}\right)\dot{\psi}+\frac{\dot{a}}{a}A+\left(\frac{\ddot{a}}{a}-\left(\frac{\dot{a}}{a}\right)^2-\frac{\dot{N}}{N}\frac{\dot{a}}{a}\right)A-\frac{N^2}{a^2}\mathcal{K}\psi\right]$$
$$-\frac{N^2}{3a^2}(1+f_R)\nabla^2\left(\psi-A+\frac{\dot{\sigma}}{N}+\frac{\dot{a}}{a}\frac{\sigma}{N}\right)+\frac{1}{2}\left[\dot{f}_R\left(\dot{A}+2\dot{\psi}\right)+2\left(\ddot{f}_R-\frac{\dot{N}}{N}\dot{f}_R\right)A\right]$$
$$-\frac{1}{2}\left[\delta\ddot{F}+\left(2\frac{\dot{a}}{a}+\frac{\dot{N}}{N}\right)\delta\dot{F}\right]+\frac{1}{2}\left[\frac{\ddot{a}}{a}+2\left(\frac{\dot{a}}{a}\right)^2-\frac{\dot{N}}{N}\frac{\dot{a}}{a}+2\frac{N^2}{a^2}\mathcal{K}\right]\delta F$$
$$+\frac{N^2}{3a^2}\nabla^2\left(\delta F-\dot{f}_R\frac{\sigma}{N}\right)=\frac{\kappa^2N^2}{2}\delta P, \tag{B.20}$$

$$\left(\mathrm{D}^i\mathrm{D}_j-\frac{1}{3}\delta^i_j\nabla^2\right)\left\{(1+f_R)\left[\psi-A+\frac{\dot{\sigma}}{N}+\frac{\dot{a}}{a}\frac{\sigma}{N}\right]-\left(\delta F-\dot{f}_R\frac{\sigma}{N}\right)\right\}$$
$$=\kappa^2\left(\mathrm{D}^i\mathrm{D}_j-\frac{1}{3}\delta^i_j\nabla^2\right)\Pi. \tag{B.21}$$

We now consider the particular case of spatially flat geometry in the Newtonian gauge and with $q=0$. In Fourier space, we can write these equations in terms of gauge invariant quantities as

$$(1+f_R)\left[\frac{\dot{a}}{a}\dot{\Psi}_{\vec{k}}+\left(\frac{\dot{a}}{a}\right)^2\Phi_{\vec{k}}+\frac{1}{3}\frac{N^2}{a^2}k^2\Psi_{\vec{k}}\right]-\frac{1}{2}\dot{f}_R\left[\dot{\Psi}_{\vec{k}}+2\frac{\dot{a}}{a}\Phi_{\vec{k}}\right]$$
$$-\frac{1}{2}\left[\frac{\dot{a}}{a}\delta\dot{F}^{(N)}-\left(\frac{\ddot{a}}{a}-\frac{\dot{N}}{N}\frac{\dot{a}}{a}\right)\delta F^{(N)}_{\vec{k}}\right]-\frac{1}{6}\frac{N^2}{a^2}k^2\delta F^{(N)}_{\vec{k}}=-\frac{\kappa^2N^2}{6}\delta\rho^{(N)}_{\vec{k}}, \tag{B.22}$$

$$(1+f_R)\left(\dot{\Psi}_{\vec{k}}+\frac{\dot{a}}{a}\Phi_{\vec{k}}\right)+\frac{1}{2}\frac{\dot{a}}{a}\delta F^{(N)}_{\vec{k}}-\frac{1}{2}\dot{f}_R\Phi_{\vec{k}}=-\frac{\kappa^2Na}{2}\left(\bar{\rho}+\bar{P}\right)v^{(N)}_{\vec{k}}, \tag{B.23}$$

$$(1+f_R)\left[\ddot{\Psi}_{\vec{k}}+\left(3\frac{\dot{a}}{a}-\frac{\dot{N}}{N}\right)\dot{\Psi}_{\vec{k}}+\frac{\dot{a}}{a}\Phi_{\vec{k}}+\left(\frac{\ddot{a}}{a}-\left(\frac{\dot{a}}{a}\right)^2-\frac{\dot{N}}{N}\frac{\dot{a}}{a}\right)\Phi_{\vec{k}}\right]$$
$$+\frac{1}{3}(1+f_R)\frac{N^2}{a^2}k^2\left(\Psi_{\vec{k}}-\Phi_{\vec{k}}\right)+\frac{1}{2}\left[\dot{f}_R\left(\dot{\Phi}_{\vec{k}}+2\dot{\Psi}_{\vec{k}}\right)+2\left(\ddot{f}_R-\frac{\dot{N}}{N}\dot{f}_R\right)\Phi_{\vec{k}}\right]$$
$$-\frac{1}{2}\left[\delta\ddot{F}^{(N)}_{\vec{k}}+\left(2\frac{\dot{a}}{a}+\frac{\dot{N}}{N}\right)\delta\dot{F}^{(N)}_{\vec{k}}\right]+\frac{1}{2}\left[\frac{\ddot{a}}{a}+2\left(\frac{\dot{a}}{a}\right)^2-\frac{\dot{N}}{N}\frac{\dot{a}}{a}\right]\delta F^{(N)}_{\vec{k}}-\frac{1}{3}\frac{N^2}{a^2}k^2\delta F^{(N)}_{\vec{k}}$$
$$=\frac{\kappa^2N^2}{2}\delta P^{(N)}_{\vec{k}}, \tag{B.24}$$

$$(1+f_R)\left(\Psi_{\vec{k}}-\Phi_{\vec{k}}\right)-\delta F^{(N)}_{\vec{k}}=\kappa^2\Pi_{\vec{k}}. \tag{B.25}$$

B.4. $f(R)$ mapping of the mGCG for $\beta = 1/3$

In this section, we show how the solutions (3.113)–(3.116), obtained for the $f(R)$ mapping of the mGCG with $\beta = 1/3$, can also be derived from the general solution (3.109). We begin by setting

$\beta = 1/3$ in Eqs. (3.110) and (3.111), which allows us to write the solution $g_+(y)$ in Eq. (3.109) as

$$g_+(y) = \left(1+\frac{1}{2}\frac{1}{1+\alpha}\right)\frac{1}{1+\alpha}(y-1)\,y\,F\left[1+\frac{1}{1+\alpha},2+\frac{1}{2}\frac{1}{1+\alpha};2+\frac{5}{4}\frac{1}{1+\alpha};y\right] + \frac{3}{2}\frac{1}{1+\alpha}\left(1+\frac{5}{4}\frac{1}{1+\alpha}\right)\left(y-\frac{5}{6}\right)F\left[\frac{1}{1+\alpha},1+\frac{1}{2}\frac{1}{1+\alpha};1+\frac{5}{4}\frac{1}{1+\alpha};y\right]. \quad \text{(B.26)}$$

Then, by using the contiguous relation (15.5.19) of Ref. [283] with $a = b_1^+ - 1$, $b = b_2^+ - 1$ and $c = b_3^+ - 2$, we can write Eq. (B.26) in a simplified form as

$$g_+(y) = \frac{5}{4}\frac{1}{1+\alpha}\left(1+\frac{5}{4}\frac{1}{1+\alpha}\right)F\left[-1+\frac{1}{1+\alpha},\frac{1}{2}\frac{1}{1+\alpha};\frac{5}{4}\frac{1}{1+\alpha};y\right], \quad \text{(B.27)}$$

which is proportional to $g_1(y)$ in Eq. (3.113).

At the same time, the solution $g_-(y)$ in Eq. (3.109) becomes

$$g_-(y) = \frac{1}{4}\frac{1}{1+\alpha}y^{-\frac{5}{4}\frac{1}{1+\alpha}}\left\{\left(1-\frac{5}{4}\frac{1}{1+\alpha}\right)y\,F\left[-\frac{1}{4}\frac{1}{1+\alpha},1-\frac{3}{4}\frac{1}{1+\alpha};1-\frac{5}{4}\frac{1}{1+\alpha};y\right] - \left(1-\frac{3}{4}\frac{1}{1+\alpha}\right)(y-1)\,y\,F\left[1-\frac{1}{4}\frac{1}{1+\alpha},2-\frac{3}{4}\frac{1}{1+\alpha};2-\frac{5}{4}\frac{1}{1+\alpha};y\right]\right\}. \quad \text{(B.28)}$$

In order to simplify this expression, we point out that the relations (15.5.13) and (15.5.15) of Ref. [283] can be combined to give

$$F[a,b,c-1,y] = \frac{(c-a-1)(c-b-1)}{(c-1)(c-a-b-1)}F[a,b,c,y] - \frac{ab}{(c-1)(c-a-b-1)}(1-y)\,F[a+1,b+1,c,y]. \quad \text{(B.29)}$$

By setting $a = b_1^-$, $b = b_2^-$ and $c = b_3^-$ in the previous equation, we obtain

$$F\left[-\frac{1}{4}\frac{1}{1+\alpha},1-\frac{3}{4}\frac{1}{1+\alpha},1-\frac{5}{4}\frac{1}{1+\alpha},y\right] = 2\frac{1-\frac{1}{1+\alpha}}{1-\frac{5}{4}\frac{1}{1+\alpha}}F\left[-\frac{1}{4}\frac{1}{1+\alpha},1-\frac{3}{4}\frac{1}{1+\alpha},2-\frac{5}{4}\frac{1}{1+\alpha},y\right] - \frac{1-\frac{3}{4}\frac{1}{1+\alpha}}{1-\frac{5}{4}\frac{1}{1+\alpha}}(1-y)\,F\left[1-\frac{1}{4}\frac{1}{1+\alpha},2-\frac{3}{4}\frac{1}{1+\alpha},2-\frac{5}{4}\frac{1}{1+\alpha},y\right], \quad \text{(B.30)}$$

which, after substitution in Eq. (B.28) leads to the reduced expression

$$g_-(y) = \frac{1}{2}\frac{\alpha}{(1+\alpha)^2}y^{1-\frac{5}{4}\frac{1}{1+\alpha}}F\left[-\frac{1}{4}\frac{1}{1+\alpha},1-\frac{3}{4}\frac{1}{1+\alpha},2-\frac{5}{4}\frac{1}{1+\alpha},y\right]. \quad \text{(B.31)}$$

Notice that $g_-(y)$ In Eq. (B.31) is proportional to the solution $g_2(y)$ in Eq. (3.114). Finally, by applying the linear transformation (15.8.4) of Ref. [283] to the solutions (B.27) and (B.31), we can obtain $g_3(y)$ and $g_4(y)$.

C 3-form field

C.1. Hurwitz criterion for cubic Polynomials

Let $\mathcal{P}_3(z)$ be a polynomial of degree 3 on z with real coefficients a_i $(i = 0, 1, \ldots, 3)$ and $a_3 \neq 0$:

$$\mathcal{P}_3(z) = a_0 + a_1 z + a_2 z^2 + a_3 z^3 \,. \tag{C.1}$$

According to Hurwitz criterion [283], all roots of $\mathcal{P}_3(z)$ have negative real parts if and only if for

$$D_1 = a_1 \,, \qquad D_2 = \begin{vmatrix} a_1 & a_3 \\ a_0 & a_2 \end{vmatrix} \,, \qquad D_3 = \begin{vmatrix} a_1 & a_3 & 0 \\ a_0 & a_2 & 0 \\ 0 & a_1 & a_3 \end{vmatrix} \,, \tag{C.2}$$

we have $a_0 \neq 0$, $D_2 > 0$ and $\operatorname{sign} D_1 = \operatorname{sign} D_3 = \operatorname{sign} a_0$.

Let us now consider an autonomous dynamical system

$$\vec{\mathbf{x}}' = \vec{\mathbf{f}}\,(\vec{\mathbf{z}}) \,, \tag{C.3}$$

with at least a fixed point at $\vec{\mathbf{x}} = \vec{\mathbf{x}}_{fp}$. Let $J \equiv \nabla \cdot \vec{\mathbf{f}}$ be the Jacobian of the system and evaluated at the fixed point $\vec{\mathbf{x}}_{fp}$. The characteristic polynomial of J, $p_J(\gamma)$, is defined by

$$p_J(\gamma) = \det\left(J - \gamma \mathbb{I}_3\right) = a_0 + a_1 \gamma + a_2 \gamma^2 - \gamma^3 \,, \tag{C.4}$$

where $\mathbb{I}_3$ is the 3×3 identity matrix. Following Hurwitz's criterion, we find that p_J is stable if

$$a_0 \neq 0 \,, \qquad \operatorname{sign} a_1 = \operatorname{sign} a_0 \,, \qquad a_1 a_2 + a_0 > 0 \,. \tag{C.5}$$

D Third Quantisation

D.1. Conserved Noether current of the wave-function field

The Lagrangian density of the wave-function field Ψ in the Third Quantisation scheme is (cf. Eq. (5.22))

$$\mathcal{L}^{\Psi} = \sqrt{-\tilde{G}}\left(\tilde{G}^{AB}\partial_A\Psi^*\partial_B\Psi + \frac{2\mathrm{Vol}^2}{\hbar}\mathcal{V}(q^A)\Psi^*\Psi\right) . \tag{D.1}$$

Under an infinitesimal transformation $\Psi \to \Psi + \delta\Psi$ this Lagrangian density transforms as

$$\begin{aligned}\delta\mathcal{L}^{\Psi} &= \sqrt{-\tilde{G}}\left[\tilde{G}^{AB}\left(\partial_A\delta\Psi^*\partial_B\Psi + \partial_A\Psi^*\partial_B\delta\Psi\right) + \frac{2\mathrm{Vol}^2}{\hbar}\mathcal{V}(q^A)\left(\delta\Psi^*\Psi + \Psi^*\delta\Psi\right)\right] \\ &= \partial_A\left[\sqrt{-\tilde{G}}\left(\delta\Psi^*\partial^A\Psi + \delta\Psi\,\partial^A\Psi^*\right)\right] \\ &\quad + \left[-\partial_A\left(\sqrt{-\tilde{G}}\tilde{G}^{AB}\partial_B\Psi\right) + \frac{2\mathrm{Vol}}{\hbar}\mathcal{V}(q^A)\Psi\right]\delta\Psi^* \\ &\quad + \left[-\partial_A\left(\sqrt{-\tilde{G}}\tilde{G}^{AB}\partial_B\Psi^*\right) + \frac{2\mathrm{Vol}}{\hbar}\mathcal{V}(q^A)\Psi^*\right]\delta\Psi\,.\end{aligned} \tag{D.2}$$

Notice that the last two lines of this equation vanish if the equations of motion of Ψ and Ψ^* hold. Under an infinitesimal transformation of $\Psi \to \mathrm{e}^{-\mathrm{i}\theta}\Psi$ the variation $\delta\Psi$ is given by $-\mathrm{i}\theta\Psi$ and we can identify the Noether conserved current of Ψ (cf. Eq. (5.23)) j^A as

$$j^A = \mathrm{i}\sqrt{-\tilde{G}}\left(\Psi^*\partial^A\Psi - \Psi\,\partial^A\Psi^*\right) . \tag{D.3}$$

D.2. Interacting Hamiltonian

In Sect. 5.1.4, a system of N interacting wave-function fields Ψ_n with an interaction term (5.59)

$$H^{(\mathrm{int})} = \int \mathrm{d}\varphi \sum_{n=1}^{N} C(\alpha)\left|\Psi_n - \Psi_{n+1}\right|^2 , \tag{D.4}$$

was considered. We now show how, by means of a discrete Fourier transformation (5.60) and (5.61), such a Hamiltonian can be re-written as the sum of N non-interacting Hamiltonians. Using the inverse Fourier transformations

$$\Psi_n = \frac{1}{\sqrt{N}} \sum_{n=1}^{n} \mathrm{e}^{2\pi \mathrm{i}\, ln/N} \Psi_l \,, \qquad \Psi_n^* = \frac{1}{\sqrt{N}} \sum_{n=1}^{N} \mathrm{e}^{-2\pi \mathrm{i}\, ln/N} \Psi_l^* \,, \tag{D.5}$$

$$\pi_n = \frac{1}{\sqrt{N}} \sum_{n=1}^{N} \mathrm{e}^{2\pi \mathrm{i}\, ln/N} \pi_l \,, \qquad \pi_n^* = \frac{1}{\sqrt{N}} \sum_{n=1}^{N} \mathrm{e}^{-2\pi \mathrm{i}\, ln/N} \pi_l^* \,, \tag{D.6}$$

we can expand the interaction Hamiltonian as

$$\begin{aligned}
H^{(\mathrm{int})} &= \frac{1}{N} \int \mathrm{d}\varphi \sum_{n=1}^{N} C(\alpha) \sum_{l=1}^{N} \mathrm{e}^{-2\pi \mathrm{i}\, ln/N} \Psi_l^* \left(1 - \mathrm{e}^{-2\pi \mathrm{i}\, l/N}\right) \sum_{l'=1}^{N} \mathrm{e}^{2\pi \mathrm{i}\, l' n/N} \Psi_{l'} \left(1 - \mathrm{e}^{2\pi \mathrm{i}\, l'/N}\right) \\
&= \frac{1}{N} \int \mathrm{d}\varphi \sum_{n,l,l'=1}^{N} C(\alpha)\, \mathrm{e}^{-2\pi \mathrm{i}\, (l-l')n/N} \Psi_l^* \Psi_{l'} \left(1 - \mathrm{e}^{-2\pi \mathrm{i}\, l/N}\right) \left(1 - \mathrm{e}^{2\pi \mathrm{i}\, l'/N}\right) \\
&= \int \mathrm{d}\varphi \sum_{l,l'=1}^{N} C(\alpha)\, \delta_{ll'} \Psi_l^* \Psi_{l'} \left(1 - \mathrm{e}^{-2\pi \mathrm{i}\, l/N}\right) \left(1 - \mathrm{e}^{2\pi \mathrm{i}\, l'/N}\right) \\
&= 2 \int \mathrm{d}\varphi \sum_{l=1}^{N} C(\alpha)\, \Psi_l^* \Psi_l \left[1 - \cosh\left(\frac{2\pi l}{N}\right)\right] \\
&= 4 \int \mathrm{d}\varphi \sum_{l=1}^{N} C(\alpha)\, \Psi_l^* \Psi_l \cosh^2\left(\frac{\pi l}{N}\right) .
\end{aligned} \tag{D.7}$$

Thus, in the new l-representation, $H^{(\mathrm{int})}$ contributes only to the self-interaction term of the wave-function fields Ψ_l, leading to the appearance of the additional l-dependent term in Eq. (5.63). Since the terms in $\pi_n^* \pi_n$ and $\Psi_n^* \Psi_n$ lead to the appearance of terms in $\pi_l^* \pi_l$ and $\Psi_l^* \Psi_l$, respectively, the total Hamiltonian in the new representation does not have interaction terms.

D.3. Single field inflation

In the context of single field inflation, where the primordial acceleration is driven by a single canonical scalar field minimally coupled to gravity – the inflaton, the scalar sector has one dynamical degree of freedom which, at the linear level of cosmological perturbations, can be identified with the GI Mukhanov-Sasaki variable [215, 269, 270, 311]

$$v := a \left(\delta\varphi + \frac{\bar{\varphi}'}{\mathcal{H}} \psi\right) . \tag{D.8}$$

The evolution equation for v is obtained from the second order action [53, 267]

$$\delta_2 \mathcal{S} = \frac{1}{2} \int \mathrm{d}\eta\, \mathrm{d}^3\vec{x} \left[(v')^2 - \mathrm{D}^i v\, \mathrm{D}_i v + \frac{z''}{z} v^2\right] , \tag{D.9}$$

which is analogous to the action of a scalar field in a flat space-time and with an effective time-dependent mass z''/z. The variable z introduced in the last term of the action (D.9), defined as $z := a(\bar{\varphi}'/\mathcal{H})$, allows us to relate v with the comoving curvature perturbation $\mathcal{R} = v/z$. Minimisation of (D.9) with regards to variations δv then leads to the Mukhanov-Sasaki equation [53, 267]

$$v'' - \left(\nabla^2 + \frac{z''}{z}\right) v = 0\,. \tag{D.10}$$

Writing the canonical momentum density as $\pi_v = \partial\mathcal{L}/\partial v' = v'$, we arrive at the Hamiltonian

$$H = \int \mathrm{d}^3\vec{x}\,(\pi_v v' - \mathcal{L}) = \frac{1}{2}\int \mathrm{d}^3\vec{x}\left[\pi_v^2 + \mathrm{D}^i v\,\mathrm{D}_i v - \frac{z''}{z}v^2\right]. \tag{D.11}$$

We can now proceed with the canonical quantisation procedure by elevating v and π_v to quantum operators $\hat{v}$ and $\hat{\pi}_v$ which satisfy the usual equal-time commutation relations

$$[\hat{v}(\eta,\vec{x}_1),\,\hat{\pi}_v(\eta,\vec{x}_2)] = \mathrm{i}\hbar\delta^3(\vec{x}_1 - \vec{x}_2)\,, \tag{D.12}$$

$$[\hat{v}(\eta,\vec{x}_1),\,\hat{v}(\eta,\vec{x}_2)] = [\hat{\pi}_v(\eta,\vec{x}_1),\,\hat{\pi}_v(\eta,\vec{x}_2)] = 0\,. \tag{D.13}$$

These operators can then be decomposed in Fourier space via the expansion[1] [53, 268]

$$\hat{v}(\eta,\,\vec{x}) = \int \frac{\mathrm{d}^3\vec{k}}{(2\pi)^{3/2}}\left[v_{\vec{k}}(\eta)\,\mathrm{e}^{\mathrm{i}\vec{k}\cdot\vec{x}}\hat{a}^-_{\vec{k}} + v^*_{\vec{k}}(\eta)\,\mathrm{e}^{-\mathrm{i}\vec{k}\cdot\vec{x}}\hat{a}^+_{\vec{k}}\right], \tag{D.14}$$

$$\hat{\pi}_v(\eta,\,\vec{x}) = \int \frac{\mathrm{d}^3\vec{k}}{(2\pi)^{3/2}}\left[v'_{\vec{k}}(\eta)\,\mathrm{e}^{\mathrm{i}\vec{k}\cdot\vec{x}}\hat{a}^-_{\vec{k}} + v^{*\prime}_{\vec{k}}(\eta)\,\mathrm{e}^{-\mathrm{i}\vec{k}\cdot\vec{x}}\hat{a}^+_{\vec{k}}\right], \tag{D.15}$$

where $\hat{a}^-_{\vec{k}}$ and $\hat{a}^+_{\vec{k}}$ are, respectively, the annihilation and creation operators of quanta of the field $\hat{v}$ and satisfy the standard commutation relations

$$\left[\hat{a}^-_{\vec{k}_1},\,\hat{a}^+_{\vec{k}_2}\right] = \delta^3(\vec{k}_1 - \vec{k}_2)\,, \tag{D.16}$$

$$\left[\hat{a}^-_{\vec{k}_1},\,\hat{a}^-_{\vec{k}_2}\right] = \left[\hat{a}^+_{\vec{k}_1},\,\hat{a}^+_{\vec{k}_2}\right] = 0\,. \tag{D.17}$$

The mode functions $v_{\vec{k}}(\eta)$ in Eq. (D.14) satisfy the evolution equation [53, 268]

$$v''_{\vec{k}} + \left(k^2 - \frac{z''}{z}\right) v_{\vec{k}} = 0\,, \qquad\qquad k^2 := \vec{k}\cdot\vec{k}\,. \tag{D.18}$$

In addition, by imposing the consistency between the commutation relations (D.12), (D.13), (D.16)

[1] From this point onward, we will follow the convention adopted in [53] for the mode expansion of the quantum field $\hat{v}$, while at the same time maintaining the use of the angular unitary Fourier transformation used in [267–270]. For this reason, some normalisation factors and signs in the mode functions might differ from the ones found in [267–270] while the powers of $(2\pi)^{1/2}$ in Fourier space will differ from the ones found in [53].

and (D.17), we obtain the normalisation condition for the mode functions [53, 268]

$$v_{\vec{k}} v_{\vec{k}}^{*\prime} - v_{\vec{k}}^{\prime} v_{\vec{k}}^{*} = \mathrm{i}\hbar \,. \tag{D.19}$$

Using the mode decomposition (D.14) and (D.15), we can write the quantum operator for the Hamiltonian as [268, 333]

$$\hat{H}^{v}(\eta) = \frac{1}{2} \int \mathrm{d}^3\vec{k} \left[\hat{a}_{\vec{k}}^{-} \hat{a}_{-\vec{k}}^{-} F_{\vec{k}}(\eta) + \hat{a}_{\vec{k}}^{+} \hat{a}_{-\vec{k}}^{+} F_{\vec{k}}^{*}(\eta) + \left(2\hat{a}_{\vec{k}}^{+} \hat{a}_{\vec{k}}^{-} + \delta^3(0) \right) E_{\vec{k}}(\eta) \right] , \tag{D.20}$$

where

$$E_{\vec{k}}(\eta) := |v_{\vec{k}}^{\prime}|^2 + \left(k^2 - \frac{z^{\prime\prime}}{z} \right) |v_{\vec{k}}|^2 \,, \qquad F_{\vec{k}}(\eta) := v_{\vec{k}}^{\prime\,2} + \left(k^2 - \frac{z^{\prime\prime}}{z} \right) v_{\vec{k}}^{2} \,. \tag{D.21}$$

If we define an instantaneous vacuum state $|0\rangle$ in the usual way by the relation $\hat{a}_{\vec{k}}^{-}|0\rangle = 0$, then the vacuum expectation value of the Hamiltonian (D.20) at a time η_0 is

$$\langle 0|\hat{H}^{v}(\eta_0)|0\rangle = \frac{\delta^3(0)}{2} \int \mathrm{d}^3\vec{k}\, E_{\vec{k}}(\eta_0) \,. \tag{D.22}$$

In order to find the vacuum state with lowest energy expectation value, we must minimise each $E_{\vec{k}}(\eta_0)$ separately. In the case of $k^2 \gg z^{\prime\prime}/z$, the normalisation (D.19) lead us to the conclusion that the lowest energy vacuum state corresponds to the Bunch-Davies vacuum [94, 115, 313]:

$$v_{\vec{k}} = \sqrt{\frac{\hbar}{2k}}\, \mathrm{e}^{-\mathrm{i}k(\eta-\eta_0)} \,. \tag{D.23}$$

Mode functions for $P/\rho = const.$

While in general the mode equation (D.18) can only be solved numerically, for particular cases we are able to find analytical solutions for $v_{\vec{k}}$. Here, we present a re-derivation of the general solution for the mode functions when the EoS parameter $w := P/\rho$ is constant[2]. In such a case, the proportionality factor between the variable z and the scale factor a becomes constant:

$$\frac{z}{a} = \frac{\varphi^{\prime}}{\mathcal{H}} = \sqrt{-2\frac{\dot{H}}{H^2}} = \sqrt{3(1+w)} \,, \tag{D.24}$$

and, consequently, the mode equation (D.18) reduces to

$$v_{\vec{k}}^{\prime\prime} + \left(k^2 - \frac{a^{\prime\prime}}{a} \right) v_{\vec{k}} = 0 \,. \tag{D.25}$$

To find the explicit form of $a^{\prime\prime}/a$ as a function of the conformal time η, we begin by writing the

[2] In the context of models with one minimally coupled scalar field, this behaviour appears as an attractor solution for exponential potentials [124, 231, 363].

Friedmann equation as

$$\left(\frac{a'}{a}\right)^2 = a_1^2 H_1^2 \left(\frac{a_1}{a}\right)^{1+3w} , \tag{D.26}$$

where a_1 is an arbitrary constant and H_1 is the value of the Hubble rate at $a = a_1$. By integrating the previous equation and setting $\eta(a_1) = \eta_1$, we obtain

$$a_1 H_1 (\eta - \eta_1) = \begin{cases} \dfrac{2}{1+3w}\left[\left(\dfrac{a}{a_1}\right)^{\frac{1+3w}{2}} - 1\right] , & \text{for } w \neq -\frac{1}{3} , \\ \log\left(\dfrac{a}{a_1}\right) , & \text{for } w = -\frac{1}{3} . \end{cases} \tag{D.27}$$

For $w > -1/3$, the conformal time in (D.27) is defined in the interval $(\eta_c, +\infty)$, where we introduce the critical value $\eta_c := \eta_1 - 2/(1+3w)(a_1 H_1)^{-1}$, while for $w < -1/3$ we find that $\eta \in (-\infty, \eta_c)$. In the boundary case of $w = -1/3$, the conformal time is defined in the entire real axis.

By inverting (D.27) and differentiating twice with regards to the conformal time, we are able to find the explicit expressions for the potential a''/a when the parameter of EoS is constant:

$$\frac{a''}{a} = \frac{1-3w}{2} \frac{(a_1 H_1)^2}{\left[1 + \frac{1+3w}{2} a_1 H_1 (\eta - \eta_1)\right]^2} = \frac{1-3w}{2} a^2 H^2 . \tag{D.28}$$

This expression is valid for all values of w. In the special case of $w = -1/3$, the r.h.s. of Eq. (D.28) reduces to the constant $a_1^2 H_1^2$. Substitution in the mode equation (D.25) then leads to the trivial general solution [83]

$$v_{\vec{k}} = A_- \sqrt{\frac{\hbar}{2\tilde{k}}}\, \mathrm{e}^{-\mathrm{i}\tilde{k}\eta} + A_+ \sqrt{\frac{\hbar}{2\tilde{k}}}\, \mathrm{e}^{+\mathrm{i}\tilde{k}\eta} , \tag{D.29}$$

where $\tilde{k} := \sqrt{k^2 + a_1^2 H_1^2}$. The solution (D.29) resembles the solutions for a Minkowski space-time with a modified wave-number. In addition, the normalisation condition (D.19) imposes the relation between the linear coefficients

$$|A_-|^2 - |A_+|^2 = 1 . \tag{D.30}$$

In the general case $w \neq -173$, the solution (D.29) is no longer valid. Nevertheless, by means of the substitutions $\eta \to \tilde{\eta} := |\eta - \eta_c|$ and $v_{\vec{k}} \to u_{\vec{k}} := v_{\vec{k}}/\sqrt{\tilde{\eta}}$, we can express (D.25) as a Bessel differential equation [7, 283]:

$$(k\tilde{\eta})^2 \frac{\mathrm{d}^2 u_{\vec{k}}}{\mathrm{d}(k\tilde{\eta})^2} + (k\tilde{\eta}) \frac{\mathrm{d}u_{\vec{k}}}{\mathrm{d}\, k\tilde{\eta}} + \left[(k\tilde{\eta})^2 - \lambda^2\right] u_{\vec{k}} = 0 , \qquad \nu := \frac{3}{2}\left|\frac{1-w}{1+3w}\right| . \tag{D.31}$$

The solutions of this equation can be written as a linear combination of the Hankel function $H_\nu^{(1)}$ and

$H_{\lambda}^{(2)}$ [7, 283]:

$$v_{\vec{k}} = \frac{\sqrt{\pi\hbar\,\tilde{\eta}}}{2}\left[B_1\, H_{\nu}^{(1)}(k\tilde{\eta}) + B_2\, H_{\lambda}^{(2)}(k\tilde{\eta})\right], \tag{D.32}$$

where B_1 and B_2 are arbitrary constants. Due to the normalisation condition (D.19), the linear coefficients B_1 and B_2 satisfy

$$|B_1|^2 - |B_2|^2 = \mp 1\,. \tag{D.33}$$

On the r.h.s. of the previous equation, the upper negative sign corresponds to $w > -1/3$, while the lower positive sign corresponds to $w < -1/3$.

In the short-wave limit, $k\tilde{\eta} \gg 1$, the Hankel functions behave as

$$H_{\nu}^{(1)}(x) \sim \sqrt{\frac{2}{\pi x}}\,\mathrm{e}^{\mathrm{i}\left(x-\frac{\lambda}{2}\pi-\frac{1}{4}\pi\right)}, \qquad H_{\lambda}^{(2)}(x) \sim \sqrt{\frac{2}{\pi x}}\,\mathrm{e}^{-\mathrm{i}\left(x-\frac{\lambda}{2}\pi-\frac{1}{4}\pi\right)}. \tag{D.34}$$

Comparing Eq. (D.34) with the BD vacuum in Eq. (D.23), we find that the solution (D.32) reduces to the Bunch-Davies vacuum for $k\tilde{\eta} \gg 1$ if we impose (i) $B_1 = 0$ and $|B_2| = 1$ for $w > -1/3$ and (ii) $|B_1| = 1$ and $B_2 = 0$ for $w < -1/3$. Notice that in the case of pure de Sitter inflation, the order parameter is half-integer and therefore we can use the relations between the spherical Bessel functions of the third kind with the Hankel functions to write (D.32) as

$$v_{\vec{k}} = -B_1\sqrt{\frac{\hbar}{2k}}\left(1+\frac{\mathrm{i}}{k(\eta-\eta_c)}\right)\mathrm{e}^{-\mathrm{i}k(\eta-\eta_c)} - B_2\sqrt{\frac{\hbar}{2k}}\left(1-\frac{\mathrm{i}}{k(\eta-\eta_c)}\right)\mathrm{e}^{\mathrm{i}k(\eta-\eta_c)}. \tag{D.35}$$

D.4. Background quantities in the Model II

In this section, we compute the explicit dependence of the background quantities of the toy model presented in Sect. 5.4 with regards to the number of e-folds, $N = \log(a/a_*)$, where a_* is a reference scale. We begin by re-writing (5.148) as

$$H^2(N) = 2^{\frac{1}{\lambda}} H_{\mathrm{dS}}^2 \exp\left[\frac{\beta-\alpha}{2}N_{\mathrm{mid}} - \frac{\alpha+\beta}{2}N\right]\cosh^{\frac{1}{\lambda}}\left[\frac{N-N_{\mathrm{mid}}}{\Delta_\lambda}\right], \tag{D.36}$$

where we recall that per Eqs. (5.150) and (5.151) we have

$$N_{\mathrm{mid}} := \frac{1}{\beta-\alpha}\log\left[\frac{Q^2}{(a_* H_{\mathrm{dS}})^{\beta}}\right], \qquad \Delta_\lambda := \frac{2}{(\beta-\alpha)\,\lambda}. \tag{D.37}$$

From the expression (D.36) for the Hubble rate, we can obtain the comoving Hubble horizon:

$$k_H(N) = a_* H_{\mathrm{dS}} \exp\left[\frac{\beta-\alpha}{4}N_{\mathrm{mid}} + \left(1-\frac{\alpha+\beta}{4}\right)N\right]\left[\frac{\cosh\left(\frac{N-N_{\mathrm{mid}}}{\Delta_\lambda}\right)}{2}\right]^{\frac{1}{2\lambda}}. \tag{D.38}$$

By differentiating this expression once with regards to N and equating it to zero, we find that k_H has an extremum whenever the condition

$$\frac{2-\alpha}{2-\beta} = -\frac{1-\tanh\left[\frac{N-N_{\rm mid}}{\Delta_\lambda}\right]}{1+\tanh\left[\frac{N-N_{\rm mid}}{\Delta_\lambda}\right]} \,. \tag{D.39}$$

holds for some $N = N_{\rm trans}$. Inverting this relation, we can define $N_{\rm trans}$ corresponding to the extremum of k_H as

$$N_{\rm trans} := N_{\rm mid} + \frac{\Delta_\lambda}{2}\log\left|\frac{\beta-2}{2-\alpha}\right| = \frac{1}{\beta-\alpha}\log\left(\left|\frac{\beta-2}{2-\alpha}\right|^{\frac{1}{\lambda}}\frac{Q^2}{(a_* H_{\rm dS})^\beta}\right) \,. \tag{D.40}$$

We note that the comoving Hubble horizon has a minimum if $\beta > 2$ and $\alpha < 2$ and a maximum if $\beta < 2$ and $\alpha > 2$. Notice that since $\ddot{a} = (1/a)(a'/a)' = (1/a)k_H'$, an extremum of the comoving Hubble horizon corresponds to a moment of no acceleration, i.e., $\ddot{a} = 0$. By setting N to $N_{\rm trans}$ in Eq. (D.38), we can calculate the value of k_H at the extremum:

$$k_{\rm trans} := k_H(N_{\rm trans}) = a_* H_{\rm dS}\left(\frac{|\beta-2|+|2-\alpha|}{|2-\alpha|}\left|\frac{2-\alpha}{\beta-2}\right|^{\frac{\beta-2}{\beta-\alpha}}\right)^{\frac{1}{2\lambda}}\left[\frac{Q^2}{(a_* H_{\rm dS})^\beta}\right]^{\frac{1}{2}\frac{2-\alpha}{\beta-\alpha}} \,. \tag{D.41}$$

We note that $k_{\rm trans}$ defined in Eq. (D.41) is the generalisation of $k_{\rm min}$ in Eq. (5.111), while Eq. (D.40) corresponds to the generalisation of Eq. (5.112). By inserting Eqs. (D.40) and (D.41) in Eq. (D.38) we can re-write the comoving Hubble horizon in a simplified form as

$$k_H(N) = k_{\rm trans}\, \mathrm{e}^{\left(1-\frac{\alpha+\beta}{4}\right)(N-N_{\rm trans})}\left(\frac{\cosh\left(\frac{N-N_{\rm mid}}{\Delta_\lambda}\right)}{\cosh\left(\frac{N_{\rm trans}-N_{\rm mid}}{\Delta_\lambda}\right)}\right)^{\frac{1}{2\lambda}} \,. \tag{D.42}$$

The EoS parameter w, defined in Eq. (5.149), and the first slow-roll parameter, ϵ, of the model can be obtained by differentiating Eq. (D.36) once with regards to N and dividing the result by $2H^2$. This leads to

$$w(N) = -1 - \frac{1}{6}\frac{(H^2)_N}{H^2} = \left(\frac{\alpha+\beta}{6}-1\right) + \frac{\alpha-\beta}{6}\tanh\left(\frac{N-N_{\rm mid}}{\Delta_\lambda}\right) \,, \tag{D.43}$$

$$\epsilon(N) = -\frac{1}{2}\frac{(H^2)_N}{H^2} = \frac{\alpha+\beta}{4} + \frac{\alpha-\beta}{4}\tanh\left(\frac{N-N_{\rm mid}}{\Delta_\lambda}\right) \,. \tag{D.44}$$

Then, by using the definition of the variable $z := a\dot{\varphi}/H = a\sqrt{2\epsilon}$ in conjunction with the chain rule $\partial_\eta(\cdot) = aH\,\partial_N(\cdot)$, we obtain the expression for the potential z''/z:

$$\frac{z''}{z} = k_H^2\left[2-\epsilon(N) + \frac{C_{(\alpha,\beta,\lambda)}(N)}{\Delta_\lambda} + \frac{D_{(\alpha,\beta,\lambda)}(N)}{\Delta_\lambda^2}\right] \,, \tag{D.45}$$

where the functions $C_{(\alpha,\beta,\lambda)}(N)$ and $D_{(\alpha,\beta,\lambda)}(N)$ are defined as

$$\begin{aligned} C_{(\alpha,\beta,\lambda)}(N) &:= \frac{3-\epsilon}{2\epsilon}\epsilon_N \\ &= \frac{\beta-\alpha}{8}\mathrm{sech}^2\left(\frac{N-N_{\rm mid}}{\Delta_\lambda}\right) + \frac{3}{2}\frac{\mathrm{sech}^2\left(\frac{N-N_{\rm mid}}{\Delta_\lambda}\right)}{\tanh\left(\frac{N-N_{\rm mid}}{\Delta_\lambda}\right) - \coth\left(\frac{N_1}{\Delta_\lambda}\right)}\,, \end{aligned} \tag{D.46}$$

$$\begin{aligned} D_{(\alpha,\beta,\lambda)}(N) &:= \frac{1}{2}\left(\frac{\epsilon_{NN}}{\epsilon} - \frac{1}{2}\frac{(\epsilon_N)^2}{\epsilon^2}\right) \\ &= \sinh\left(\frac{N_1}{\Delta_\lambda}\right)\frac{\sinh\left(\frac{N_1}{\Delta_\lambda}\right) + 2\sinh\left(\frac{2N-2N_{\rm mid}-N_1}{\Delta_\lambda}\right)}{\left[\cosh\left(\frac{N_1}{\Delta_\lambda}\right) + \cosh\left(\frac{2N-2N_{\rm mid}-N_1}{\Delta_\lambda}\right)\right]^2}\,, \end{aligned} \tag{D.47}$$

$$\frac{N_1}{\Delta_\lambda} := \log\left(\sqrt{\frac{\beta}{\alpha}}\right)\,. \tag{D.48}$$

Notice that while the first equality in each of the definitions (D.46) and (D.47) is valid for any model of single field inflation, in writing the second equality we have imposed the model dependent expression (D.44). As discussed in Sect. 5.4.1, the terms of the potential z''/z that depend on $C_{(\alpha,\beta,\lambda)}$ and $D_{(\alpha,\beta,\lambda)}$ define the shape of the potential around the transition from the initial epoch to the later power-law inflation. On the other hand, it can be checked that the the r.h.s. of Eqs. (D.46) and (D.47) vanishes asymptotically for very large (positive and negative) values of N, i.e., $C_{(\alpha,\beta,\lambda)}$ and $D_{(\alpha,\beta,\lambda)}$ do not contribute to the shape of the potential z''/z in the asymptotic initial and final epochs where the EoS parameter is constant.

D.5. The limit of z''/z for large λ

In this section, we present the derivation of the shape of the potential z''/z in the case of instantaneous transitions. This requires the calculation of the limiting expression, for very large λ, of the terms $\Delta_\lambda^{-1}C_{(\alpha,\beta,\lambda)}(N)$ and $\Delta_\lambda^{-2}D_{(\alpha,\beta,\lambda)}(N)$ that appear in the expansion (5.155). In order to better understand how to take such limits, we work in Fourier space using the following convention for the Fourier transform $\mathcal{F}$ and its inverse $\mathcal{F}^{-1}$:

$$\mathcal{F}_\omega[f(N)] := \int_{-\infty}^{+\infty}\frac{\mathrm{d}N}{\sqrt{2\pi}}f(N)e^{-i\omega N} = f(\omega)\,, \tag{D.49}$$

$$\mathcal{F}_N^{-1}[f(\omega)] := \int_{-\infty}^{+\infty}\frac{\mathrm{d}\omega}{\sqrt{2\pi}}f(\omega)e^{i\omega N} = f(N)\,. \tag{D.50}$$

Applying a Fourier transform to $\Delta_\lambda^{-1} C_{(\alpha,\beta,\lambda)}(N)$, we find

$$\begin{aligned}\frac{C_{(\alpha,\beta,\lambda)}(\omega)}{\Delta_\lambda} &= \frac{1}{\Delta_\lambda}\left\{\frac{\beta-\alpha}{8}\mathcal{F}_\omega\left[\operatorname{sech}^2\left(\frac{N-N_{\mathrm{mid}}}{\Delta_\lambda}\right)\right] + \frac{3}{2}\mathcal{F}_\omega\left[\frac{\operatorname{sech}^2\left(\frac{N-N_{\mathrm{mid}}}{\Delta_\lambda}\right)}{\tanh\left(\frac{N-N_{\mathrm{mid}}}{\Delta_\lambda}\right) - \coth\left(\frac{N_1}{\Delta_\lambda}\right)}\right]\right\} \\ &= \mathrm{e}^{-\mathrm{i}\omega N_{\mathrm{mid}}}\left\{\frac{\beta-\alpha}{8}\mathcal{F}_{\omega\Delta_\lambda}\left[\operatorname{sech}^2(\tilde{N})\right] + \frac{3}{2}\mathcal{F}_{\omega\Delta_\lambda}\left[\frac{\operatorname{sech}^2(\tilde{N})}{\tanh(\tilde{N}) - \coth\left(\frac{N_1}{\Delta_\lambda}\right)}\right]\right\}, \quad \text{(D.51)}\end{aligned}$$

where $\tilde{N} := \Delta_\lambda^{-1}(N - N_{\mathrm{mid}})$. We now note that taking the limit $\lambda \to +\infty$ in the previous expression corresponds to selecting the 0-mode of the Fourier transform. As such, we can write

$$\frac{C_{(\alpha,\beta,\lambda)}(\omega)}{\Delta_\lambda} \overset{\lambda\to+\infty}{=} \frac{1}{\sqrt{2\pi}}\left[\frac{\beta-\alpha}{4} - \frac{3}{2}\log\left(\frac{\beta}{\alpha}\right)\right], \quad \text{(D.52)}$$

and by applying the inverse transform, we obtain

$$\frac{C_{(\alpha,\beta,\lambda)}(N)}{\Delta_\lambda} \overset{\lambda\to+\infty}{=} \left[\frac{\beta-\alpha}{4} - \frac{3}{2}\log\left(\frac{\beta}{\alpha}\right)\right]\delta(N - N_{\mathrm{mid}})\,. \quad \text{(D.53)}$$

The Fourier transform of $\Delta_\lambda^{-2} D_{(\alpha,\beta,\lambda)}(N)$ can be decomposed as

$$\begin{aligned}\frac{D_{(\alpha,\beta,\lambda)}(\omega)}{\Delta_\lambda^2} &\overset{\lambda\to+\infty}{=} \frac{\sinh\left(\frac{N_1}{\Delta_\lambda}\right)}{\Delta_\lambda^2}\mathcal{F}_\omega\left[\frac{\sinh\left(\frac{N_1}{\Delta_\lambda}\right) + 2\sinh\left(\frac{2N-2N_{\mathrm{mid}}-N_1}{\Delta_\lambda}\right)}{\left[\cosh\left(\frac{N_1}{\Delta_\lambda}\right) + \cosh\left(\frac{2N-2N_{\mathrm{mid}}-N_1}{\Delta_\lambda}\right)\right]^2}\right] \\ &= \omega\sinh\left(\frac{N_1}{\Delta_\lambda}\right)\mathrm{e}^{-\mathrm{i}\omega\left(N_{\mathrm{mid}}+\frac{N_1}{2}\right)}\left\{-\mathrm{i}\,\mathcal{F}_{\omega\Delta_\lambda}\left[\left(\cosh\left(\frac{N_1}{\Delta_\lambda}\right) + \cosh(2\mathcal{N})\right)^{-1}\right]\right. \\ &\qquad \left. + \frac{\sinh\left(\frac{N_1}{\Delta_\lambda}\right)}{\omega\Delta_\lambda}\mathcal{F}_{\omega\Delta_\lambda}\left[\left(\cosh\left(\frac{N_1}{\Delta_\lambda}\right) + \cosh(2\mathcal{N})\right)^{-2}\right]\right\}, \quad \text{(D.54)}\end{aligned}$$

where $\mathcal{N} := \Delta_\lambda^{-1}(N - N_{\mathrm{mid}} - \frac{1}{2}N_1)$ and on the first term of the second equality, we have performed an integration by parts. In order to eliminate the Δ_λ^{-1} factor on the last line of Eq. (D.54), we rewrite $(\omega\Delta_\lambda)^{-1}$ in terms of the Fourier transform of the sign function:

$$\begin{aligned}\frac{D_{(\alpha,\beta,\lambda)}(\omega)}{\Delta_\lambda^2} &= -\mathrm{i}\omega\sinh\left(\frac{N_1}{\Delta_\lambda}\right)\mathrm{e}^{-\mathrm{i}\omega\left(N_{\mathrm{mid}}+\frac{N_1}{2}\right)}\left\{\mathcal{F}_{\omega\Delta_\lambda}\left[\left(\cosh\left(\frac{N_1}{\Delta_\lambda}\right) + \cosh(2\mathcal{N})\right)^{-1}\right]\right. \\ &\qquad \left. + \sqrt{\frac{\pi}{2}}\sinh\left(\frac{N_1}{\Delta_\lambda}\right)\mathcal{F}_{\omega\Delta_\lambda}\left[\operatorname{sign}(\mathcal{N})\right]\mathcal{F}_{\omega\Delta_\lambda}\left[\left(\cosh\left(\frac{N_1}{\Delta_\lambda}\right) + \cosh(2\mathcal{N})\right)^{-2}\right]\right\}. \quad \text{(D.55)}\end{aligned}$$

Once more, taking the limit $\lambda \to +\infty$ corresponds to selecting the 0-mode of the Fourier transforms

in the previous expression, resulting in

$$\frac{D_{(\alpha,\beta,\lambda)}(\omega)}{\Delta^2_\lambda} \overset{\lambda\to+\infty}{=} -\frac{1}{\sqrt{2\pi}}\log\left(\frac{\beta}{\alpha}\right)\mathrm{i}\,\omega\,. \tag{D.56}$$

By applying an inverse Fourier transform to the previous equation, we obtain

$$\frac{D_{(\alpha,\beta,\lambda)}(N)}{\Delta^2_\lambda} \overset{\lambda\to+\infty}{=} -\log\left(\frac{\beta}{\alpha}\right)\delta_N(N-N_{\rm mid})\,. \tag{D.57}$$

Finally, by inserting Eqs. (D.53) and (D.57) in Eq. (5.155), we obtain the expression in Eq. (5.189), i.e.,

$$\begin{aligned}\frac{z''}{z} = k_H^2(N)\Bigg\{2-\epsilon(N)+\left[\frac{\beta-\alpha}{4}-\frac{3}{2}\log\left(\frac{\beta}{\alpha}\right)\right]\delta(N-N_{\rm mid})\\ -\log\left(\frac{\beta}{\alpha}\right)\delta_N(N-N_{\rm mid})\Bigg\}\,.\end{aligned} \tag{D.58}$$

D.6. A jump in $\mathrm{d}\mathcal{R}_{\vec{k}}/\mathrm{d}N$ for large λ

The evolution equation for the comoving perturbation $R_{\vec{k}}$ is (cf. (5.190))

$$\frac{\mathrm{d}^2\mathcal{R}_{\vec{k}}}{\mathrm{d}N^2}+\left(3-\epsilon+\frac{\epsilon_N}{\epsilon}\right)\frac{\mathrm{d}\mathcal{R}_{\vec{k}}}{\mathrm{d}N}+\left(\frac{k}{k_H}\right)^2\mathcal{R}_{\vec{k}}=0\,. \tag{D.59}$$

In the limit of very large λ, we find that the slow-roll parameter ϵ has a discontinuity given by a Θ function, as seen in Eq. (5.186) and, therefore, its derivative ϵ_N gives rise to a Dirac delta function. In order to obtain the proper limit of the quotient ϵ_N/ϵ in the second term of Eq. (D.59), we follow the same method applied in Sect. D.5 and find

$$\frac{\epsilon_N}{\epsilon} \overset{\beta\to+\infty}{=} -\log\left(\frac{\beta}{\alpha}\right)\delta(N-N_{\rm mid})\,. \tag{D.60}$$

By inserting this result, as well as Eq. (5.186), in Eq. (D.59), we obtain

$$\frac{\mathrm{d}^2\mathcal{R}_{\vec{k}}}{\mathrm{d}N^2}+\left[\frac{6-\beta}{2}-\frac{\alpha-\beta}{2}\Theta(N-N_{\rm mid})-\log\left(\frac{\beta}{\alpha}\right)\delta(N-N_{\rm mid})\right]\frac{\mathrm{d}\mathcal{R}_{\vec{k}}}{\mathrm{d}N}+\frac{k^2}{k_H^2}\mathcal{R}_{\vec{k}}=0\,. \tag{D.61}$$

If we compare Eq. (D.61) with the Mukhanov-Sasaki equation with the potential given in eq. (D.58), we find that the divergent terms that appear on the potential z''/z are replaced by a single divergent term, a Dirac delta function, in the coefficient of $\mathrm{d}\mathcal{R}_{\vec{k}}/\mathrm{d}N$ in Eq. (D.61). The presence of this terms suggests that the derivative $\mathrm{d}\mathcal{R}_{\vec{k}}/\mathrm{d}N$ has a discontinuity at $N=N_{\rm mid}$. However, since this means that $\delta(N)$ is multiplied by a discontinuous function, a direct integration of (D.61) to find the jump in the derivative of the comoving curvature perturbation can be tricky [102, 174]. Instead, we choose

the ansatz

$$\frac{\mathrm{d}\mathcal{R}_{\vec{k}}}{\mathrm{d}N} = \mathrm{e}^{\log\left(\frac{\beta}{\alpha}\right)\Theta(N-N_{\mathrm{mid}})} f_{\vec{k}}(N)\,, \tag{D.62}$$

where $f_{\vec{k}}(N)$ is by hypothesis a continuous function at $N = N_{\mathrm{mid}}$. Then, inserting Eq. (D.62) in Eq. (D.61), leads to

$$\frac{\mathrm{d}f_{\vec{k}}}{\mathrm{d}N} + \left[\frac{6-\beta}{2} - \frac{\alpha-\beta}{2}\Theta(N-N_{\mathrm{mid}})\right] f_{\vec{k}} + \mathrm{e}^{-\log\left(\frac{\beta}{\alpha}\right)\Theta(N-N_{\mathrm{mid}})}\frac{k^2}{k_H^2}\mathcal{R}_{\vec{k}} = 0\,. \tag{D.63}$$

For $\mathcal{R}_k$ continuous at $N = N_{\mathrm{mid}}$, this equation is compatible with the continuity of $f_{\vec{k}}$, confirming that the exponential in (D.62) carries the discontinuity of the derivative of the comoving curvature perturbation. Therefore, we obtain following the boundary condition (5.192):

$$\frac{\mathrm{d}\mathcal{R}_{\vec{k}}}{\mathrm{d}N}(N^+_{\mathrm{mid}}) = \frac{\beta}{\alpha}\frac{\mathrm{d}\mathcal{R}_{\vec{k}}}{\mathrm{d}N}(N^-_{\mathrm{mid}})\,. \tag{D.64}$$

D.7. Matching conditions in the long-wavelength approximation

In the long-wavelength regime $k^2 \ll z''/z$, the general solution of the mode evolution equation (5.105) reads:

$$v_{\vec{k}} = z(\eta)\left(C_{1\vec{k}} + C_{2\vec{k}}\int_{\eta_{\mathrm{ini}}}^{\eta}\frac{\mathrm{d}\tau}{z^2(\tau)}\right) = z(N)\left(C_{1\vec{k}} + C_{2\vec{k}}\int_{N_{\mathrm{ini}}}^{N}\frac{\mathrm{d}\tilde{N}}{z^2(\tilde{N})k_H(\tilde{N})}\right)\,, \tag{D.65}$$

where we recall that $z = a\sqrt{2\epsilon(N)}$. Since both ϵ and k_H are finite at $N = N_{\mathrm{mid}}$, the integral on the r.h.s. of the previous equation does not contribute to the jump of $v_{\vec{k}}$ in the transition to inflation. Thus, by evaluating Eq. (D.65) at $N = N^+_{\mathrm{mid}}$ and $N = N^-_{\mathrm{mid}}$, we obtain

$$\frac{v_{\vec{k}}(N^+_{\mathrm{mid}})}{v_{\vec{k}}(N^-_{\mathrm{mid}})} = \frac{a_{\mathrm{trans}}\sqrt{2\epsilon^+}}{a_{\mathrm{trans}}\sqrt{2\epsilon^-}} = \sqrt{\frac{\epsilon^+}{\epsilon^-}}\,, \tag{D.66}$$

which is equivalent to the first matching condition (5.193).

On the other hand, after differentiating (D.65) with regards to the number of e-folds, we find that

$$\begin{aligned}\frac{\mathrm{d}v_{\vec{k}}}{\mathrm{d}N} &= z_N(N)\left(C_{1\vec{k}} + C_{2\vec{k}}\int_{N_{\mathrm{ini}}}^{N}\frac{\mathrm{d}\tilde{N}}{z^2(\tilde{N})k_H(\tilde{N})}\right) + \frac{C_{2\vec{k}}}{z(N)k_H(N)} \\ &= \left(1 + \frac{1}{2}\frac{\epsilon_N}{\epsilon}\right)v_{\vec{k}}(N) + \frac{C_{2\vec{k}}}{z(N)k_H(N)}\,.\end{aligned} \tag{D.67}$$

The discontinuity, at the time of the transition, on the second term on the r.h.s. of the last equality in Eq. (D.67) can be washed away by multiplying both sides by $\sqrt{\epsilon}$. Then, by evaluating $\sqrt{\epsilon}(\mathrm{d}v_{\vec{k}}/\mathrm{d}N)$

at $N = N^{+}_{\rm mid}$ and $N = N^{-}_{\rm mid}$, we obtain

$$\sqrt{\epsilon^{+}}\frac{{\rm d}v_{\vec{k}}}{{\rm d}N}(N^{+}_{\rm mid}) - \sqrt{\epsilon^{-}}\frac{{\rm d}v_{\vec{k}}}{{\rm d}N}(N^{-}_{\rm mid}) = \sqrt{\epsilon^{+}}v_{\vec{k}}(N^{+}_{\rm mid}) - \sqrt{\epsilon^{-}}v_{\vec{k}}(N^{-}_{\rm mid})\,. \tag{D.68}$$

Finally, by using Eq. (D.66) to eliminate $v_{\vec{k}}(N^{+}_{\rm mid})$ in Eq. (D.68), we obtain the second matching condition (5.194).

D.8. The coefficients $P_{\vec{k}}$ and $Q_{\vec{k}}$

The coefficients $P_{\vec{k}}$ and $Q_{\vec{k}}$ introduced in Sect. 5.5.3, which constitute the matrix of the linear transformation (5.201), are defined, for $\epsilon^{\pm} \in]0,\,3] \setminus \{1\}$, as

$$\begin{aligned}\mathcal{P}_{\vec{k}} \;&= {\rm i}\frac{\pi}{4}\frac{1}{\sqrt{|\epsilon^{-}-1||\epsilon^{+}-1|}} \\ &\times\Bigg\{\left[\left(\frac{\epsilon^{+}}{\epsilon^{-}}\right)^{\frac{1}{2}}(3-\epsilon^{+})\Theta(1-\epsilon^{+}) - \left(\frac{\epsilon^{+}}{\epsilon^{-}}\right)^{-\frac{1}{2}}(3-\epsilon^{-})\Theta(1-\epsilon^{-})\right]H^{q}_{\gamma^{-}}(H^{q}_{\gamma^{+}})^{*} \\ &- q\left[\left(\frac{\epsilon^{+}}{\epsilon^{-}}\right)^{\frac{1}{2}}{\rm sign}(1-\epsilon^{+})H^{q}_{\gamma^{-}}(H^{q}_{1+\gamma^{+}})^{*} - \left(\frac{\epsilon^{+}}{\epsilon^{-}}\right)^{-\frac{1}{2}}{\rm sign}(1-\epsilon^{-})H^{q}_{1+\gamma^{-}}(H^{q}_{\gamma^{+}})^{*}\right]\Bigg\}, \end{aligned}\tag{D.69}$$

and

$$\begin{aligned}Q_{\vec{k}} \;&= {\rm i}\frac{\pi}{4}\frac{1}{\sqrt{|\epsilon^{-}-1||\epsilon^{+}-1|}} \\ &\times\Bigg\{\left[\left(\frac{\epsilon^{+}}{\epsilon^{-}}\right)^{\frac{1}{2}}(3-\epsilon^{+})\Theta(1-\epsilon^{+}) - \left(\frac{\epsilon^{+}}{\epsilon^{-}}\right)^{-\frac{1}{2}}(3-\epsilon^{-})\Theta(1-\epsilon^{-})\right](H^{q}_{\gamma^{-}})^{*}(H^{q}_{\gamma^{+}})^{*} \\ &- q\left[\left(\frac{\epsilon^{+}}{\epsilon^{-}}\right)^{\frac{1}{2}}{\rm sign}(1-\epsilon^{+})(H^{q}_{\gamma^{-}})^{*}(H^{q}_{1+\gamma^{+}})^{*} - \left(\frac{\epsilon^{+}}{\epsilon^{-}}\right)^{-\frac{1}{2}}{\rm sign}(1-\epsilon^{-})(H^{q}_{1+\gamma^{-}})^{*}(H^{q}_{\gamma^{+}})^{*}\right]\Bigg\}. \end{aligned}\tag{D.70}$$

Here, $\gamma^{\pm} = (1/2)|3-\epsilon^{\pm}|/|1-\epsilon^{\pm}|$, cf. Eq. (5.199), and $q := k/k^{\infty}_{\rm trans}$ is a renormalised wave-number, where $k^{\infty}_{\rm trans}$ is the value of the comoving Hubble horizon at the moment of the transition, as defined in Eq. (5.188). In addition, we use the notation

$$H^{q}_{\gamma^{\pm}} := H^{(1)}_{\gamma^{\pm}}\left(\frac{q}{|1-\epsilon^{\pm}|}\right), \qquad\qquad H^{q}_{1+\gamma^{\pm}} := H^{(1)}_{1+\gamma^{\pm}}\left(\frac{q}{|1-\epsilon^{\pm}|}\right). \tag{D.71}$$

For $\epsilon^{+} = \epsilon^{-}$, one can easily check that the terms inside the curly brackets on the r.h.s. of Eq. (D.70) cancel each other, leading to $Q_{\vec{k}} = 0$. At the same time, we find that if we impose $\epsilon^{+} = \epsilon^{-}$ in Eq. (D.69), the first term inside the curly brackets vanishes and, using the Wronskian equalities for the Hankel functions [7, 283], we find that the second term inside the curly brackets leads to $P_{\vec{k}} = 1$.

D.9. Long-wavelength limit of $\mathcal{P}_{\mathcal{R}}^{\rm PI}/\mathcal{P}_{\mathcal{R}}^{\rm BD}$

In this section, we compute the long-wavelength approximation, $q \ll |\epsilon^+ - 1|$and $q \ll |\epsilon^- - 1|$, of Eq. (5.208). Using the asymptotic behaviour of the Bessel and the Hankel functions for small argument and non-zero order [7, 283], i.e., for $\gamma^{\pm} \neq 0$ which corresponds to $\epsilon^{\pm} \neq 3$, we find that to leading order in q, the terms Δ_0, $\Delta_1 q$ and $\Delta_2 q^2$ in Eq. (5.208) read

$$\Delta_0 \approx \frac{1}{\pi^2}\left[\left(\frac{\epsilon^+}{\epsilon^-}\right)^{\frac{1}{2}}(3-\epsilon^+)\Theta(1-\epsilon^+) - \left(\frac{\epsilon^+}{\epsilon^-}\right)^{-\frac{1}{2}}(3-\epsilon^-)\Theta(1-\epsilon^-)\right]^2 \times \frac{\Gamma^2(\gamma^-)}{\Gamma^2(1+\gamma^+)}\frac{|1-\epsilon^-|^{2\gamma^-}}{|1-\epsilon^+|^{2\gamma^+}}\left(\frac{q}{2}\right)^{2(\gamma^+-\gamma^-)}, \tag{D.72}$$

$$\Delta_1 q \approx \frac{2}{\pi^2}\left[\left(\frac{\epsilon^+}{\epsilon^-}\right)^{\frac{1}{2}}(3-\epsilon^+)\Theta(1-\epsilon^+) - \left(\frac{\epsilon^+}{\epsilon^-}\right)^{-\frac{1}{2}}(3-\epsilon^-)\Theta(1-\epsilon^-)\right] \times \left[\left(\frac{\epsilon^+}{\epsilon^-}\right)^{-\frac{1}{2}}(3-\epsilon^-)\,\mathrm{sign}(1-\epsilon^-)\right]\frac{\Gamma^2(\gamma^-)}{\Gamma^2(1+\gamma^+)}\frac{|1-\epsilon^-|^{2\gamma^-}}{|1-\epsilon^+|^{2\gamma^+}}\left(\frac{q}{2}\right)^{2(\gamma^+-\gamma^-)}, \tag{D.73}$$

$$\Delta_2 q^2 \approx \frac{1}{\pi^2}\left[\left(\frac{\epsilon^+}{\epsilon^-}\right)^{-\frac{1}{2}}(3-\epsilon^-)\,\mathrm{sign}(1-\epsilon^-)\right]^2\frac{\Gamma^2(\gamma^-)}{\Gamma^2(1+\gamma^+)}\frac{|1-\epsilon^-|^{2\gamma^-}}{|1-\epsilon^+|^{2\gamma^+}}\left(\frac{q}{2}\right)^{2(\gamma^+-\gamma^-)}. \tag{D.74}$$

Notice that on the second lines of Eqs. (D.73) and (D.74), we have used the equality $\Gamma(1+z) = z\Gamma(z)$ and the definition of $\gamma^{\pm}$ to eliminate $\Gamma(1+\gamma^-)$. Adding Eqs. (D.72), (D.73) and (D.74), we obtain

$$\Delta_0 + \Delta_1 q + \Delta_2 q^2 \approx \frac{1}{\pi^2}\left[\left(\frac{\epsilon^+}{\epsilon^-}\right)^{\frac{1}{2}}(3-\epsilon^+)\Theta(1-\epsilon^+) + \left(\frac{\epsilon^+}{\epsilon^-}\right)^{-\frac{1}{2}}(3-\epsilon^-)\Theta(\epsilon^- - 1)\right]^2 \times \frac{\Gamma^2(\gamma^-)}{\Gamma^2(1+\gamma^+)}\frac{|1-\epsilon^-|^{2\gamma^-}}{|1-\epsilon^+|^{2\gamma^+}}\left(\frac{q}{2}\right)^{2(\gamma^+-\gamma^-)}. \tag{D.75}$$

Here, we note that in the case of a transition from an accelerated epoch with $\epsilon^- < 1$ to a decelerated epoch with $1 < \epsilon^+$ the previous expression vanishes, indicating that beyond-leading-order terms need to be considered in Eqs. (D.72), (D.73) and (D.74). However, since we are interested mainly on the case where the universe is inflating for $N_{\rm mid} < N$ (i.e., $\epsilon^+ < 1$), we will not explore such cases. Finally, substitution in (5.208) leads to (5.213).

In the case that the initial epoch mimics a universe dominated by stiff matter ($\epsilon^- = 3$ and $\gamma^- = 0$), the asymptotic expressions (D.72), (D.73) and (D.74) are no longer valid since the Hankel functions of zero order behave instead as a logarithm for small argument [7, 283]. In this case the asymptotic

behaviour of Δ_0, $\Delta_1 q$ and $\Delta_2 q^2$ is given by

$$\Delta_0 \approx \frac{4}{\pi^2}\left(\frac{\epsilon^+}{3}\right)\left[(3-\epsilon^+)\Theta(1-\epsilon^+)\right]^2 \frac{1}{\Gamma^2(1+\gamma^+)}\frac{1}{|1-\epsilon^+|^{2\gamma^+}}\left(\frac{q}{2}\right)^{2\gamma^+}\log^2\left(\frac{q}{2}\right), \tag{D.76}$$

$$\Delta_1 q \approx \frac{8}{\pi^2}(3-\epsilon^+)\Theta(1-\epsilon^+)\frac{1}{\Gamma^2(1+\gamma^+)}\frac{1}{|1-\epsilon^+|^{2\gamma^+}}\left(\frac{q}{2}\right)^{2\gamma^+}\log\left(\frac{q}{4}\right), \tag{D.77}$$

$$\Delta_2 q^2 \approx \frac{4}{\pi^2}\left(\frac{\epsilon^+}{3}\right)^{-1}\frac{1}{\Gamma^2(1+\gamma^+)}\frac{1}{|1-\epsilon^+|^{2\gamma^+}}\left(\frac{q}{2}\right)^{2\gamma^+}. \tag{D.78}$$

By adding Eqs. (D.76), (D.77) and (D.78), we obtain

$$\begin{aligned}\Delta_0+\Delta_1 q+\Delta_2 q^2 = \frac{4}{\pi^2}&\left[\left(\frac{\epsilon^+}{3}\right)^{\frac{1}{2}}(3-\epsilon^+)\Theta(1-\epsilon^+)\log\left(\frac{q}{2}\right)+2\left(\frac{\epsilon^+}{3}\right)^{-\frac{1}{2}}\right]^2\\ &\times\frac{1}{\Gamma^2(1+\gamma^+)}\frac{1}{|1-\epsilon^+|^{2\gamma^+}}\left(\frac{q}{2}\right)^{2\gamma^+}.\end{aligned} \tag{D.79}$$

Finally, a substitution of the previous result in Eq. (5.208) leads to Eq. (5.214).

D.10. Short wavelength limit of $\mathcal{P}_{\mathcal{R}}^{\mathrm{PI}}/\mathcal{P}_{\mathcal{R}}^{\mathrm{BD}}$

In this section, we compute the short wavelength approximation, $|\epsilon^+ - 1| \ll q$ and $|\epsilon^- - 1| \ll q$, of Eq. (5.208). We recall that this expression relates the primordial power spectrum at the end of power-law inflation in a scenario with a pre-inflationary epoch with constant EoS parameter, $\mathcal{P}_{\mathcal{R}}^{\mathrm{PI}}$, with the primordial power spectrum obtained in power-law inflation with BD-like initial conditions. Using the asymptotic behaviour of the Bessel and the Hankel functions for large argument [7, 283], we find that in Eq. (5.208) the leading term for large q is given by $\Delta_2 q^2$. In the short wavelength approximation this term reads, cf. Eq. (5.211),

$$\begin{aligned}\Delta_2 q^2 \approx{}& \frac{4|1-\epsilon^+||1-\epsilon^-|}{\pi^2}\\ &\times\left[\cosh\left(\log\left(\frac{\epsilon^+}{\epsilon^-}\right)\right)-\sinh\left(\log\left(\frac{\epsilon^+}{\epsilon^-}\right)\right)\sin^2\left(\frac{2q}{|1-\epsilon^+|}-\pi\gamma^+\right)\right].\end{aligned} \tag{D.80}$$

A substitution the previous result in Eq. (5.208) leads to the asymptotic formula (5.216).

Bibliography

[1] K. N. Abazajian et al., *"Light Sterile Neutrinos: A White Paper"*, [arXiv:1204.5379].

[2] B. P. Abbott et al., *"Observation of Gravitational Waves from a Binary Black Hole Merger"*, Physical Review Letters **116**, 061102 (2016), [arXiv:1602.03837].

[3] B. P. Abbott et al., *"Multi-messenger Observations of a Binary Neutron Star Merger"*, The Astrophysical Journal Letters **848**, L12 (2017), [arXiv:1710.05833].

[4] B. P. Abbott et al., *"Gravitational Waves and Gamma-rays from a Binary Neutron Star Merger: GW170817 and GRB 170817A"*, The Astrophysical Journal Letters **848**, L13 (2017), [arXiv:1710.05834].

[5] B. P. Abbott et al., *"GW170817: Observation of Gravitational Waves from a Binary Neutron Star Inspiral"*, Physical Review Letters **119**, 161101 (2017), [arXiv:1710.05832].

[6] T. M. C. Abbott et al., *"Dark Energy Survey Year 1 Results: Cosmological Constraints from Galaxy Clustering and Weak Lensing"*, Physical Review D **98**, 043526 (2018), [arXiv:1708.01530].

[7] M. Abramowitz and I. A. Stegun. *Handbook of Mathematical Functions with Formulas, Graphs, and Mathematical Tables*. Dover Publications, (1964).

[8] R. Abuter et al., *"Detection of the gravitational redshift in the orbit of the star S2 near the Galactic centre massive black hole"*, Astronomy & Astrophysics **615**, L15 (2018), [arXiv:1807.09409].

[9] L. Ackerman, M. R. Buckley, S. M. Carroll, and M. Kamionkowski, *"Dark Matter and Dark Radiation"*, Physical Review D **79**, 023519 (2009), [arXiv:0810.5126].

[10] M. Ackermann et al., *"Searching for Dark Matter Annihilation from Milky Way Dwarf Spheroidal Galaxies with Six Years of Fermi Large Area Telescope Data"*, Physical Review Letters **115**, 231301 (2015), [arXiv:1503.02641].

[11] R. Adam et al., *"Planck 2015 results. I. Overview of products and scientific results"*, Astronomy & Astrophysics **594**, A1 (2016), [arXiv:1502.01582].

[12] J. A. Adams, B. Cresswell, and R. Easther, *"Inflationary perturbations from a potential with a step"*, Physical Review D **64**, 123514 (2001), [arXiv:astro-ph/0102236].

[13] P. A. R. Ade et al., *"Planck 2013 results. XXII. Constraints on inflation"*, Astronomy & Astrophysics **571**, A22 (2014), [arXiv:1303.5082].

[14] P. A. R. Ade et al., *"Joint Analysis of BICEP/Keck Array and Planck Data"*, Physical Review Letters **114**, 101301 (2015), [arXiv:1502.00612].

[15] P. A. R. Ade et al., *"Planck 2015 results. XX. Constraints on inflation"*, Astronomy & Astrophysics **594**, A20 (2016), [arXiv:1502.02114].

[16] P. A. R. Ade et al., *"Planck 2015 results. XIII. Cosmological parameters"*, Astronomy & Astrophysics **594**, A13 (2016), [arXiv:1502.01589].

[17] I. Agullo, A. Ashtekar, and W. Nelson, *"The pre-inflationary dynamics of loop quantum cosmology: Confronting quantum gravity with observations"*, Classical and Quantum Gravity **30**, 085014 (2013), [arXiv:1302.0254].

[18] Y. Akrami et al., *"Planck 2018 results. X. Constraints on inflation"*, [arXiv:1807.06211].

[19] Y. Akrami et al., *"Planck 2018 results. I. Overview and the cosmological legacy of Planck"*, [arXiv:1807.06205].

[20] S. Alam et al., *"The clustering of galaxies in the completed SDSS-III Baryon Oscillation Spectroscopic Survey: cosmological analysis of the DR12 galaxy sample"*, Monthly Notices of the Royal Astronomical Society **470**, 2617-2652 (2017), [arXiv:1607.03155].

[21] U. Alam, V. Sahni, T. D. Saini, and A. A. Starobinsky, *"Exploring the expanding universe and dark energy using the Statefinder diagnostic"*, Monthly Notices of the Royal Astronomical Society **344**, 1057 (2003), [arXiv:astro-ph/0303009].

[22] I. Albarran, M. Bouhmadi-López, and J. Morais, *"Cosmological perturbations in an effective and genuinely phantom dark energy Universe"*, Physics of the Dark Universe **16**, 94-108 (2017), [arXiv:1611.00392].

[23] I. Albarran, M. Bouhmadi-López, F. Cabral, and P. Martín-Moruno, *"The Avoidance of the Little Sibling of the Big Rip Abrupt Event by a Quantum Approach"*, Galaxies **6**, 21 (2018).

[24] I. Albarran, M. Bouhmadi-López, and J. Morais, *"What if gravity becomes really repulsive in the future?"*, The European Physical Journal C **78**, 260 (2018), [arXiv:1706.01484].

[25] A. Albrecht and P. J. Steinhardt, *"Cosmology for Grand Unified Theories with Radiatively Induced Symmetry Breaking"*, Physical Review Letters **48**, 1220-1223 (1982).

[26] A. Alho and C. Uggla, *"Inflationary α-attractor cosmology: A global dynamical systems perspective"*, Physical Review D **95**, 083517 (2017), [arXiv:1702.00306].

[27] A. Alho, J. Hell, and C. Uggla, *"Global dynamics and asymptotics for monomial scalar field potentials and perfect fluids"*, Classical and Quantum Gravity **32**, 145005 (2015), [arXiv:1503.06994].

[28] A. Alonso-Serrano, C. Bastos, O. Bertolami, and S. Robles-Pérez, *"Interacting universes and the cosmological constant"*, Physics Letters B **719**, 200-205 (2013), [arXiv:1207.6852].

[29] A. Alonso-Serrano, M. Bouhmadi-López, and P. Martín-Moruno, *"$f(R)$ quantum cosmology: avoiding the Big Rip"*, [arXiv:1802.03290].

[30] R. A. Alpher and R. C. Herman, *"Remarks on the Evolution of the Expanding Universe"*, Physical Review **75**, 1089–1095 (1949).

[31] R. A. Alpher, H. Bethe, and G. Gamow, *"The origin of chemical elements"*, Physical Review **73**, 803-804 (1948).

[32] L. Amendola, *"Coupled quintessence"*, Physical Review D **62**, 043511 (2000), [arXiv:astro-ph/9908023].

[33] N. Andersson and G. L. Comer, *"Relativistic fluid dynamics: Physics for many different scales"*, Living Reviews in Relativity **10**, 1 (2007), [arXiv:gr-qc/0605010].

[34] M. Arabsalmani and V. Sahni, *"The Statefinder hierarchy: An extended null diagnostic for concordance cosmology"*, Physical Review D **83**, 043501 (2011), [arXiv:1101.3436].

[35] A. Aravind, D. Lorshbough, and S. Paban, *"Non-Gaussianity from Excited Initial Inflationary States"*, Journal of High Energy Physics **07**, 076 (2013), [arXiv:1303.1440].

[36] A. Aravind, D. Lorshbough, and S. Paban, *"Primordial equation of state transitions"*, Physical Review D **93**, 123519 (2016), [arXiv:1604.03516].

[37] M. Archidiacono, E. Calabrese, and A. Melchiorri, *"The Case for Dark Radiation"*, Physical Review D **84**, 123008 (2011), [arXiv:1109.2767].

[38] F. Arevalo, A. P. R. Bacalhau, and W. Zimdahl, *"Cosmological dynamics with non-linear interactions"*, Classical and Quantum Gravity **29**, 235001 (2012), [arXiv:1112.5095].

[39] R. L. Arnowitt, S. Deser, and C. W. Misner. *"The Dynamics of general relativity"*. In L. Witten, editor, *Gravitation: an introduction to current research*, chapter 7, page 227–265. John Wiley & Sons Inc, New York, (1962). Republication in General Relativity and Gravitation **40**, 1997-2027 (2008).

[40] K. Arun, S. B. Gudennavar, and C. Sivaram, *"Dark matter, dark energy, and alternate models: A review"*, Advances in Space Research **60**, 166-186 (2017), [arXiv:1704.06155].

[41] B. Aulbach. *Continuous and Discrete Dynamics near Manifolds of Equilibria*, volume 1058 of *Lecture Notes in Mathematics*. Springer-Verlag Berlin Heidelberg, Germany, (1984).

[42] A. Aviles, L. Bonanno, O. Luongo, and H. Quevedo, *"Holographic dark matter and dark energy with second order invariants"*, Physical Review D **84**, 103520 (2011), [arXiv:1109.3177].

[43] A. Aviles, A. Bravetti, S. Capozziello, and O. Luongo, *"Updated constraints on f(R) gravity from cosmography"*, Physical Review D **87**, 044012 (2013), [arXiv:1210.5149].

[44] S. Bahamonde, C. G. Böhmer, S. Carloni, E. J. Copeland, W. Fang, and N. Tamanini, *"Dynamical systems applied to cosmology: dark energy and modified gravity"*, [arXiv:1712.03107].

[45] T. Banks, *"Prolegomena to a Theory of Bifurcating Universes: A Nonlocal Solution to the Cosmological Constant Problem Or Little Lambda Goes Back to the Future"*, Nuclear Physics B **309**, 493-512 (1988).

[46] J. M. Bardeen, *"Gauge Invariant Cosmological Perturbations"*, Physical Review D **22**, 1882-1905 (1980).

[47] B. J. Barros and N. J. Nunes, *"Three-form inflation in type II Randall-Sundrum"*, Physical Review D **93**, 043512 (2016), [arXiv:1511.07856].

[48] N. Bartolo et al., *"Science with the space-based interferometer LISA. IV: Probing inflation with gravitational waves"*, Journal of Cosmology and Astroparticle Physics **1612**, 026 (2016), [arXiv:1610.06481].

[49] B. A. Bassett, S. Tsujikawa, and D. Wands, *"Inflation dynamics and reheating"*, Reviews of Modern Physics **78**, 537-589 (2006), [arXiv:astro-ph/0507632].

[50] T. Battefeld and R. C. Freitas, *"A Universal Bound on Excitations of Heavy Fields during Inflation"*, Journal of Cosmology and Astroparticle Physics **1409**, 029 (2014), [arXiv:1405.7969].

[51] R. A. Battye, B. Bolliet, and J. A. Pearson, *"$f(R)$ gravity as a dark energy fluid"*, Physical Review D **93**, 044026 (2016), [arXiv:1508.04569].

[52] R. A. Battye, B. Bolliet, and F. Pace, *"Do cosmological data rule out $f(\mathcal{R})$ with $w \neq -1$?"*, Physical Review D **97**, 104070 (2018), [arXiv:1712.05976].

[53] D. Baumann. *"Inflation"*. In *Physics of the large and the small, TASI 09, proceedings of the Theoretical Advanced Study Institute in Elementary Particle Physics, Boulder, Colorado, USA, 1-26 June 2009*, pages 523–686, (2011), [arXiv:0907.5424].

[54] R. Bean and O. Dore, *"Probing dark energy perturbations: The Dark energy equation of state and speed of sound as measured by WMAP"*, Physical Review D **69**, 083503 (2004), [arXiv:astro-ph/0307100].

[55] R. Bean, D. Bernat, L. Pogosian, A. Silvestri, and M. Trodden, *"Dynamics of Linear Perturbations in f(R) Gravity"*, Physical Review D **75**, 064020 (2007), [arXiv:astro-ph/0611321].

[56] C. L. Bennett et al., *"First year Wilkinson Microwave Anisotropy Probe (WMAP) observations: Preliminary maps and basic results"*, The Astrophysical Journal Supplement Series **148**, 1-27 (2003), [arXiv:astro-ph/0302207].

[57] M. C. Bento, O. Bertolami, and A. A. Sen, *"Generalized Chaplygin gas, accelerated expansion and dark energy matter unification"*, Physical Review D **66**, 043507 (2002), [arXiv:gr-qc/0202064].

[58] D. Bettoni, S. Liberati, and L. Sindoni, *"Extended LCDM: generalized non-minimal coupling for dark matter fluids"*, Journal of Cosmology and Astroparticle Physics **1111**, 007 (2011), [arXiv:1108.1728].

[59] F. Beutler, C. Blake, M. Colless, D. H. Jones, L. Staveley-Smith, G. B. Poole, L. Campbell, Q. Parker, W. Saunders, and F. Watson, *"The 6dF Galaxy Survey: $z \approx 0$ measurement of the growth rate and $sigma_8$"*, Monthly Notices of the Royal Astronomical Society **423**, 3430-3444 (2012), [arXiv:1204.4725].

[60] N. Bilic, G. B. Tupper, and R. D. Viollier, *"Unification of dark matter and dark energy: The Inhomogeneous Chaplygin gas"*, Physics Letters B **535**, 17-21 (2002), [arXiv:astro-ph/0111325].

[61] C. Blake et al., *"The WiggleZ Dark Energy Survey: Joint measurements of the expansion and growth history at z ¡ 1"*, Monthly Notices of the Royal Astronomical Society **425**, 405-414 (2012), [arXiv:1204.3674].

[62] C. Blake et al., *"Galaxy And Mass Assembly (GAMA): improved cosmic growth measurements using multiple tracers of large-scale structure"*, Monthly Notices of the Royal Astronomical Society **436**, 3089 (2013), [arXiv:1309.5556].

[63] D. Blas, J. Lesgourgues, and T. Tram, *"The Cosmic Linear Anisotropy Solving System (CLASS) II: Approximation schemes"*, Journal of Cosmology and Astroparticle Physics **1107**, 034 (2011), [arXiv:1104.2933].

[64] C. G. Boehmer, G. Caldera-Cabral, R. Lazkoz, and R. Maartens, *"Dynamics of dark energy with a coupling to dark matter"*, Physical Review D **78**, 023505 (2008), [arXiv:0801.1565].

[65] C. G. Boehmer, N. Chan, and R. Lazkoz, *"Dynamics of dark energy models and centre manifolds"*, Physics Letters B **714**, 11-17 (2012), [arXiv:1111.6247].

[66] C. G. Boehmer, N. Tamanini, and M. Wright, *"Interacting quintessence from a variational approach Part I: algebraic couplings"*, Physical Review D **91**, 123002 (2015), [arXiv:1501.06540].

[67] C. G. Boehmer, N. Tamanini, and M. Wright, *"Interacting quintessence from a variational approach Part II: derivative couplings"*, Physical Review D **91**, 123003 (2015), [arXiv:1502.04030].

[68] Yu. L. Bolotin, A. Kostenko, O. A. Lemets, and D. A. Yerokhin, *"Cosmological Evolution With Interaction Between Dark Energy And Dark Matter"*, International Journal of Modern Physics D **24**, 1530007 (2014), [arXiv:1310.0085].

[69] Yu. L. Bolotin, V. A. Cherkaskiy, and O. A. Lemets, *"New Cosmographic Constraints on the Dark Energy and Dark Matter Coupling"*, International Journal of Modern Physics D **25**, 1650056 (2016), [arXiv:1503.04056].

[70] M. Bouhmadi-López and J. A. Jiménez Madrid, *"Escaping the big rip?"*, Journal of Cosmology and Astroparticle Physics **0505**, 005 (2005), [arXiv:astro-ph/0404540].

[71] M. Bouhmadi-López, L. J. Garay, and P. F. González-Díaz, *"Quantum behavior of FRW radiation filled universes"*, Physical Review D **66**, 083504 (2002), [arXiv:gr-qc/0204072].

[72] M. Bouhmadi-López, P. F. González-Díaz, and P. Martín-Moruno, *"On the generalised Chaplygin gas: Worse than a big rip or quieter than a sudden singularity?"*, International Journal of Modern Physics D **17**, 2269-2290 (2008), [arXiv:0707.2390].

[73] M. Bouhmadi-López, S. Capozziello, and V. F. Cardone, *"Cosmography of f(R) - brane cosmology"*, Physical Review D **82**, 103526 (2010), [arXiv:1010.1547].

[74] M. Bouhmadi-López, P. Frazão, and A. B. Henriques, *"Stochastic gravitational waves from a new type of modified Chaplygin gas"*, Physical Review D **81**, 063504 (2010), [arXiv:0910.5134].

[75] M. Bouhmadi-López, P. Chen, and Y.-W. Liu, *"Cosmological Imprints of a Generalized Chaplygin Gas Model for the Early Universe"*, Physical Review D **84**, 023505 (2011), [arXiv:1104.0676].

[76] M. Bouhmadi-López, J. Morais, and A. B. Henriques, *"Smoking guns of a bounce in modified theories of gravity through the spectrum of gravitational waves"*, Physical Review D **87**, 103528 (2013), [arXiv:1210.1761].

[77] M. Bouhmadi-Lopez, A. Errahmani, P. Martin-Moruno, T. Ouali, and Y. Tavakoli, *"The little sibling of the big rip singularity"*, International Journal of Modern Physics D **24**, 1550078 (2015), [arXiv:1407.2446].

[78] M. Bouhmadi-López, J. Morais, and A. Zhuk, *"The late Universe with non-linear interaction in the dark sector: the coincidence problem"*, Physics of the Dark Universe **14**, 11-20 (2016), [arXiv:1603.06983].

[79] M. Bouhmadi-López, M. Krämer, J. Morais, and S. Robles-Pérez, *"What if? Exploring the Multiverse through Euclidean wormholes"*, The European Physical Journal C **77**, 718 (2017), [arXiv:1708.00025].

[80] M. Bouhmadi-López, J. Marto, J. Morais, and C. M. Silva, *"Cosmic infinity: A dynamical system approach"*, Journal of Cosmology and Astroparticle Physics **1703**, 042 (2017), [arXiv:1611.03100].

[81] M. Bouhmadi-López, D. Brizuela, and I. Garay, *"Quantum behavior of the "Little Sibling" of the Big Rip induced by a three-form field"*, [arXiv:1802.05164].

[82] M. Bouhmadi-López, M. Krämer, J. Morais, and S. Robles-Pérez, *"The interacting multiverse and its effect on the cosmic microwave background"*.

[83] M. Bouhmadi-López, P. Chen, Y.-C. Huang, and Y.-H. Lin, *"Slow-roll inflation preceded by a topological defect phase à la Chaplygin gas"*, Physical Review D **87**, 103513 (2013), [arXiv:1212.2641].

[84] M. Bouhmadi-López, M. Brilenkov, R. Brilenkov, J. Morais, and A. Zhuk, *"Scalar perturbations in the late Universe: viability of the Chaplygin gas models"*, Journal of Cosmology and Astroparticle Physics **1512**, 037 (2015), [arXiv:1509.06963].

[85] C. Brans and R. H. Dicke, *"Mach's principle and a relativistic theory of gravitation"*, Physical Review **124**, 925-935 (1961).

[86] D. Brizuela, C. Kiefer, and M. Krämer, *"Quantum-gravitational effects on gauge-invariant scalar and tensor perturbations during inflation: The de Sitter case"*, Physical Review D **93**, 104035 (2016), [arXiv:1511.05545].

[87] D. Brizuela, C. Kiefer, and M. Krämer, *"Quantum-gravitational effects on gauge-invariant scalar and tensor perturbations during inflation: The slow-roll approximation"*, Physical Review D **94**, 123527 (2016), [arXiv:1611.02932].

[88] M. Bronstein, *"Republication of: Quantum theory of weak gravitational fields"*, General Relativity and Gravitation **44**, 267–283 (2012).

[89] J. D. Brown, *"Action functionals for relativistic perfect fluids"*, Classical and Quantum Gravity **10**, 1579-1606 (1993), [arXiv:gr-qc/9304026].

[90] M. Bruni, R. Crittenden, K. Koyama, R. Maartens, C. Pitrou, and D. Wands, *"Disentangling non-Gaussianity, bias and GR effects in the galaxy distribution"*, Physical Review D **85**, 041301 (2012), [arXiv:1106.3999].

[91] H. A. Buchdahl, *"Non-linear Lagrangians and cosmological theory"*, Monthly Notices of the Royal Astronomical Society **150**, 1-8 (1970).

[92] E. Bulbul, M. Markevitch, A. Foster, R. K. Smith, M. Loewenstein, and S. W. Randall, *"Detection of An Unidentified Emission Line in the Stacked X-ray spectrum of Galaxy Clusters"*, The Astrophysical Journal **789**, 13 (2014), [arXiv:1402.2301].

[93] P. Bull et al., *"Beyond ΛCDM: Problems, solutions, and the road ahead"*, Physics of the Dark Universe **12**, 56-99 (2016), [arXiv:1512.05356].

[94] T. S. Bunch and P. C. W. Davies, *"Quantum Field Theory in de Sitter Space: Renormalization by Point Splitting"*, Proceedings of the Royal Society of London A: Mathematical, Physical and Engineering Sciences **360**, 117–134 (1978).

[95] V. C. Busti, Á. de la Cruz-Dombriz, P. K. S. Dunsby, and D. Sáez-Gómez, *"Is cosmography a useful tool for testing cosmology?"*, Physical Review D **92**, 123512 (2015), [arXiv:1505.05503].

[96] Y. Cai, Y.-T. Wang, and Y.-S. Piao, *"Preinflationary primordial perturbations"*, Physical Review D **92**, 023518 (2015), [arXiv:1501.01730].

[97] T. Cailleteau, A. Barrau, J. Grain, and F. Vidotto, *"Consistency of holonomy-corrected scalar, vector and tensor perturbations in Loop Quantum Cosmology"*, Physical Review D **86**, 087301 (2012), [arXiv:1206.6736].

[98] G. Caldera-Cabral, R. Maartens, and B. M. Schaefer, *"The Growth of Structure in Interacting Dark Energy Models"*, Journal of Cosmology and Astroparticle Physics **0907**, 027 (2009), [arXiv:0905.0492].

[99] G. Caldera-Cabral, R. Maartens, and L. A. Urena-Lopez, *"Dynamics of interacting dark energy"*, Physical Review D **79**, 063518 (2009), [arXiv:0812.1827].

[100] R. R. Caldwell, *"On the evolution of scalar metric perturbations in an inflationary cosmology"*, Classical and Quantum Gravity **13**, 2437-2448 (1996), [arXiv:gr-qc/9509027].

[101] R. R. Caldwell, R. Dave, and P. J. Steinhardt, *"Cosmological imprint of an energy component with general equation of state"*, Physical Review Letters **80**, 1582-1585 (1998), [arXiv:astro-ph/9708069].

[102] M. G. Calkin, D. Kiang, and Y. Nogami, *"Proper treatment of the delta function potential in the one-dimensional Dirac equation"*, American Journal of Physics **55**, 737-739 (1987).

[103] S. Capozziello, *"Curvature quintessence"*, International Journal of Modern Physics D **11**, 483-492 (2002), [arXiv:gr-qc/0201033].

[104] S. Capozziello and M. De Laurentis, *"Extended Theories of Gravity"*, Physics Reports **509**, 167-321 (2011), [arXiv:1108.6266].

[105] S. Capozziello and M. Francaviglia, *"Extended Theories of Gravity and their Cosmological and Astrophysical Applications"*, General Relativity and Gravitation **40**, 357-420 (2008), [arXiv:0706.1146].

[106] S. Capozziello, V. F. Cardone, and A. Troisi, *"Reconciling dark energy models with f(R) theories"*, Physical Review D **71**, 043503 (2005), [arXiv:astro-ph/0501426].

[107] S. Capozziello, V. F. Cardone, and V. Salzano, *"Cosmography of f(R) gravity"*, Physical Review D **78**, 063504 (2008), [arXiv:0802.1583].

[108] S. Capozziello, R. Lazkoz, and V. Salzano, *"Comprehensive cosmographic analysis by Markov Chain Method"*, Physical Review D **84**, 124061 (2011), [arXiv:1104.3096].

[109] S. Carloni, R. Goswami, and P. K. S. Dunsby, *"A new approach to reconstruction methods in $f(R)$ gravity"*, Classical and Quantum Gravity **29**, 135012 (2012), [arXiv:1005.1840].

[110] D. Carney, W. Fischler, S. Paban, and N. Sivanandam, *"The Inflationary Wavefunction and its Initial Conditions"*, Journal of Cosmology and Astroparticle Physics **1212**, 012 (2012), [arXiv:1109.6566].

[111] J. Carr. *Applications of Center Manifold Theorem*. Springer-Verlag, (1981).

[112] S. M. Carroll, I. Sawicki, A. Silvestri, and M. Trodden, *"Modified-Source Gravity and Cosmological Structure Formation"*, New Journal of Physics **8**, 323 (2006), [arXiv:astro-ph/0607458].

[113] L. Castelló Gomar, G. A. Mena Marugán, D. Martín De Blas, and J. Olmedo, *"Hybrid loop quantum cosmology and predictions for the cosmic microwave background"*, Physical Review D **96**, 103528 (2017), [arXiv:1702.06036].

[114] P. Chen and Y.-H. Lin, *"What initial condition of inflation would suppress the large-scale CMB spectrum?"*, Physical Review D **93**, 023503 (2016), [arXiv:1505.05980].

[115] N. A. Chernikov and E. A. Tagirov, *"Quantum theory of scalar fields in de Sitter space-time"*, Annales de l'Institut Henri Poincaré A, Physique Théorique **9**, 109 (1968).

[116] M. Chevallier and D. Polarski, *"Accelerating universes with scaling dark matter"*, International Journal of Modern Physics D **10**, 213-224 (2001), [arXiv:gr-qc/0009008].

[117] L. P. Chimento, A. S. Jakubi, D. Pavon, and W. Zimdahl, *"Interacting quintessence solution to the coincidence problem"*, Physical Review D **67**, 083513 (2003), [arXiv:astro-ph/0303145].

[118] M. Cicoli, S. Downes, B. Dutta, F. G. Pedro, and A. Westphal, *"Just enough inflation: power spectrum modifications at large scales"*, Journal of Cosmology and Astroparticle Physics **1412**, 030 (2014), [arXiv:1407.1048].

[119] R. G. Clowes, K. A. Harris, S. Raghunathan, L. E. Campusano, I. K. Soechting, and M. J. Graham, *"A structure in the early universe at $z \sim 1.3$ that exceeds the homogeneity scale of the R-W concordance cosmology"*, Monthly Notices of the Royal Astronomical Society **429**, 2910-2916 (2013), [arXiv:1211.6256].

[120] S. R. Coleman and F. De Luccia, *"Gravitational Effects on and of Vacuum Decay"*, Physical Review D **21**, 3305 (1980).

[121] A. A. Coley. *Dynamical Systems and Cosmology*, volume 291 of *Astrophysics and Space Science Library*. Springer Netherlands, Dordrecht, (2003).

[122] C. R. Contaldi, M. Peloso, L. Kofman, and A. D. Linde, *"Suppressing the lower multipoles in the CMB anisotropies"*, Journal of Cosmology and Astroparticle Physics **0307**, 002 (2003), [arXiv:astro-ph/0303636].

[123] E. J. Copeland, A. Lahiri, and D. Wands, *"String cosmology with a time dependent antisymmetric tensor potential"*, Physical Review D **51**, 1569-1576 (1995), [arXiv:hep-th/9410136].

[124] E. J. Copeland, A. R. Liddle, and D. Wands, *"Exponential potentials and cosmological scaling solutions"*, Physical Review D **57**, 4686-4690 (1998), [arXiv:gr-qc/9711068].

[125] A. A. Costa, X.-D. Xu, B. Wang, and E. Abdalla, *"Constraints on interacting dark energy models from Planck 2015 and redshift-space distortion data"*, Journal of Cosmology and Astroparticle Physics **1701**, 028 (2017), [arXiv:1605.04138].

[126] P. Creminelli and F. Vernizzi, *"Dark Energy after GW170817 and GRB170817A"*, Physical Review Letters **119**, 251302 (2017), [arXiv:1710.05877].

[127] J.-L. Cui, L. Yin, L.-F. Wang, Y.-H. Li, and X. Zhang, *"A closer look at interacting dark energy with statefinder hierarchy and growth rate of structure"*, Journal of Cosmology and Astroparticle Physics **1509**, 024 (2015), [arXiv:1503.08948].

[128] P. Cushman et al. *"Working Group Report: WIMP Dark Matter Direct Detection"*. In *Proceedings, 2013 Community Summer Study on the Future of U.S. Particle Physics: Snowmass on the Mississippi (CSS2013): Minneapolis, MN, USA, July 29-August 6, 2013*, (2013), [arXiv:1310.8327].

[129] S. Das, G. Goswami, J. Prasad, and R. Rangarajan, *"Revisiting a pre-inflationary radiation era and its effect on the CMB power spectrum"*, Journal of Cosmology and Astroparticle Physics **1506**, 001 (2015), [arXiv:1412.7093].

[130] A. De Felice and S. Tsujikawa, *"f(R) theories"*, Living Reviews in Relativity **13**, 3 (2010), [arXiv:1002.4928].

[131] A. De Felice, K. Karwan, and P. Wongjun, *"Stability of the 3-form field during inflation"*, Physical Review D **85**, 123545 (2012), [arXiv:1202.0896].

[132] A. De Felice, K. Karwan, and P. Wongjun, *"Reheating in 3-form inflation"*, Physical Review D **86**, 103526 (2012), [arXiv:1209.5156].

[133] Á. de la Cruz-Dombriz and A. Dobado, *"A f(R) gravity without cosmological constant"*, Physical Review D **74**, 087501 (2006), [arXiv:gr-qc/0607118].

[134] Á. de la Cruz-Dombriz, A. Dobado, and A. L. Maroto, *"On the evolution of density perturbations in f(R) theories of gravity"*, Physical Review D **77**, 123515 (2008), [arXiv:0802.2999].

[135] P. F. de Salas and S. Pastor, *"Relic neutrino decoupling with flavour oscillations revisited"*, Journal of Cosmology and Astroparticle Physics **1607**, 051 (2016), [arXiv:1606.06986].

[136] N. Deruelle and V. F. Mukhanov, *"On matching conditions for cosmological perturbations"*, Physical Review D **52**, 5549-5555 (1995), [arXiv:gr-qc/9503050].

[137] B. S. DeWitt, *"Quantum Theory of Gravity. I. The Canonical Theory"*, Physical Review **160**, 1113-1148 (1967).

[138] P. A. M. Dirac, *"Generalized Hamiltonian dynamics"*, Canadian Journal of Mathematics **2**, 129-148 (1950).

[139] P. A. M. Dirac, *"Generalized Hamiltonian dynamics"*, Proceedings of the Royal Society of London A: Mathematical, Physical and Engineering Sciences **246**, 326-332 (1958).

[140] S. Dodelson. *Modern Cosmology*. Academic Press, Amsterdam, (2003).

[141] A. D. Dolgov and M. Kawasaki, *"Can modified gravity explain accelerated cosmic expansion?"*, Physics Letters B **573**, 1-4 (2003), [arXiv:astro-ph/0307285].

[142] M. J. Duff and P. van Nieuwenhuizen, *"Quantum Inequivalence of Different Field Representations"*, Physics Letters B **94**, 179-182 (1980).

[143] P. K. S. Dunsby, E. Elizalde, R. Goswami, S. Odintsov, and D. S. Gomez, *"On the LCDM Universe in f(R) gravity"*, Physical Review D **82**, 023519 (2010), [arXiv:1005.2205].

[144] J. Ehlers, *"Contributions to the relativistic mechanics of continuous media"*, General Relativity and Gravitation **25**, 1225-1266 (1993). [Abh. Akad. Wiss. Lit. Mainz. Nat. Kl.11,793(1961)].

[145] A. Einstein, *"Feldgleichungen der Gravitation (The Field Equations of Gravitation)"*, Sitzungsber. Preuss. Akad. Wiss. Berlin (Math. Phys.) **1915**, 844-847 (1915). English translation in Kox, A. J., Klein, Martin J., and Schulmann, Robert, *The Collected Papers of Albert Einstein, Volume 6: The Berlin Years: Writings, 1914-1917*, Princeton University Press, Princeton, New Jersey, (1996).

[146] U. Elias and H. Gingold, *"Critical points at infinity and blow up of solutions of autonomous polynomial differential systems via compactification"*, Journal of Mathematical Analysis and Applications **318**, 305–322 (2006).

[147] J. M. Ezquiaga and M. Zumalacárregui, *"Dark Energy After GW170817: Dead Ends and the Road Ahead"*, Physical Review Letters **119**, 251304 (2017), [arXiv:1710.05901].

[148] V. Faraoni. *Cosmology in Scalar-Tensor Gravity*. Fundamental Theories of Physics. Springer Netherlands, (2004).

[149] V. Faraoni, *"Modified gravity and the stability of de Sitter space"*, Physical Review D **72**, 061501 (2005), [arXiv:gr-qc/0509008].

[150] V. Faraoni, *"Solar System experiments do not yet veto modified gravity models"*, Physical Review D **74**, 023529 (2006), [arXiv:gr-qc/0607016].

[151] V. Faraoni, *"Matter instability in modified gravity"*, Physical Review D **74**, 104017 (2006), [arXiv:astro-ph/0610734].

[152] V. Faraoni and S. Capozziello. *Beyond Einstein Gravity*, volume 170. Springer, Dordrecht, (2011).

[153] V. Faraoni, J. B. Dent, and E. N. Saridakis, *"Covariantizing the interaction between dark energy and dark matter"*, Physical Review D **90**, 063510 (2014), [arXiv:1405.7288].

[154] C. Feng, B. Wang, E. Abdalla, and R.-K. Su, *"Observational constraints on the dark energy and dark matter mutual coupling"*, Physics Letters B **665**, 111-119 (2008), [arXiv:0804.0110].

[155] E. G. M. Ferreira, J. Quintin, A. A. Costa, E. Abdalla, and B. Wang, *"Evidence for interacting dark energy from BOSS"*, Physical Review D **95**, 043520 (2017), [arXiv:1412.2777].

[156] F. Finelli and R. Brandenberger, *"On the generation of a scale invariant spectrum of adiabatic fluctuations in cosmological models with a contracting phase"*, Physical Review D **65**, 103522 (2002), [arXiv:hep-th/0112249].

[157] H. Firouzjahi and M. H. Namjoo, *"Jump in fluid properties of inflationary universe to reconcile scalar and tensor spectra"*, Physical Review D **90**, 063525 (2014), [arXiv:1404.2589].

[158] D. J. Fixsen, *"The Temperature of the Cosmic Microwave Background"*, The Astrophysical Journal **707**, 916-920 (2009), [arXiv:0911.1955].

[159] A. Friedman, *"Über die Krümmung des Raumes (On the curvature of space)"*, Zeitschrift für Physik **10**, 377–386 (1922). English translation in Lang, K. and Gingerich, O., *A Source Book in Astronomy and Astrophysics, 1900–1975*, Harvard University Press, (1979).

[160] A. Friedmann, *"Über die Möglichkeit einer Welt mit konstanter negativer Krümmung des Raumes (On the possibility of a universe with a constant negative curvature of space)"*, Zeitschrift für Physik **21**, 326–332 (1924). English translation in General Relativity and Gravitation **31**, 2001-2008 (1999).

[161] G. Gamow, *"Expanding universe and the origin of elements"*, Physical Review **70**, 572-573 (1946).

[162] I. Garay and S. Robles-Pérez, *"Effects of a scalar field on the thermodynamics of interuniversal entanglement"*, International Journal of Modern Physics D **23**, 1450043 (2014), [arXiv:1311.1387].

[163] J. Garcia-Bellido, A. D. Linde, and D. Wands, *"Density perturbations and black hole formation in hybrid inflation"*, Physical Review D **54**, 6040-6058 (1996), [arXiv:astro-ph/9605094].

[164] M. Gasperini and G. Veneziano, *"Constraints on pre - big bang models for seeding large scale anisotropy by massive Kalb-Ramond axions"*, Physical Review D **59**, 043503 (1999), [arXiv:hep-ph/9806327].

[165] M. J. Geller and J. P. Huchra, *"Mapping the universe"*, Science **246**, 897-903 (1989).

[166] C. Germani and A. Kehagias, *"P-inflation: generating cosmic Inflation with p-forms"*, Journal of Cosmology and Astroparticle Physics **0903**, 028 (2009), [arXiv:0902.3667].

[167] S. B. Giddings and A. Strominger, *"Axion Induced Topology Change in Quantum Gravity and String Theory"*, Nuclear Physics B **306**, 890-907 (1988).

[168] S. B. Giddings and A. Strominger, *"Baby Universes, Third Quantization and the Cosmological Constant"*, Nuclear Physics B **321**, 481-508 (1989).

[169] H. Gingold, *"Approximation of unbounded functions via compactification"*, Journal of Approximation Theory **131**, 284–305 (2004).

[170] H. Gingold and D. Solomon, *"More Compactification for Differential Systems"*, Advances in Pure Mathematics **03**, 190–203 (2013).

[171] J. R. Gott, III, M. Juric, D. Schlegel, F. Hoyle, M. Vogeley, M. Tegmark, N. A. Bahcall, and J. Brinkmann, *"A map of the universe"*, The Astrophysical Journal **624**, 463 (2005), [arXiv:astro-ph/0310571].

[172] P. W. Graham and S. Rajendran, *"New Observables for Direct Detection of Axion Dark Matter"*, Physical Review D **88**, 035023 (2013), [arXiv:1306.6088].

[173] J. A. Grayson et al., *"BICEP3 performance overview and planned Keck Array upgrade"*, Proceedings of SPIE **9914**, 99140S (2016), [arXiv:1607.04668].

[174] D. Griffiths and S. Walborn, *"Dirac deltas and discontinuous functions"*, American Journal of Physics **67**, 446-447 (1999).

[175] L. P. Grishchuk. *"Cosmological perturbations of quantum mechanical origin and anisotropy of the microwave background radiation"*. In *Current topics in astrofundamental physics: The Early universe. Proceedings, NATO Advanced Study Institute, Erice, Italy, September 4-16, 1994*, pages 205–254, (1994), [arXiv:gr-qc/9410025].

[176] L. P. Grishchuk, *"Density perturbations of quantum mechanical origin and anisotropy of the microwave background"*, Physical Review D **50**, 7154-7172 (1994), [arXiv:gr-qc/9405059].

[177] L. P. Grishchuk. *"Statistics of the microwave background anisotropies caused by cosmological perturbations of quantum mechanical origin"*. (1995), [arXiv:gr-qc/9511074].

[178] L. P. Grishchuk, *"Comment on the paper of Leonard Parker and Yang Zhang 'Cosmological perturbations of a relativistic condensate'"*, [arXiv:gr-qc/9506010].

[179] A. H. Guth, *"The Inflationary Universe: A Possible Solution to the Horizon and Flatness Problems"*, Physical Review D **23**, 347-356 (1981).

[180] J. B. Hartle and S. W. Hawking, *"Wave Function of the Universe"*, Physical Review D **28**, 2960-2975 (1983).

[181] J. Hasenkamp and J. Kersten, *"Dark radiation from particle decay: cosmological constraints and opportunities"*, Journal of Cosmology and Astroparticle Physics **1308**, 024 (2013), [arXiv:1212.4160].

[182] J.-h. He and B. Wang, *"Revisiting $f(R)$ gravity models that reproduce ΛCDM expansion"*, Physical Review D **87**, 023508 (2013), [arXiv:1208.1388].

[183] A. B. Henriques, *"Graviton creation in an inflationary universe"*, Physical Review D **49**, 1771-1776 (1994).

[184] D. Hilbert, *"Die Grundlagen der Physik. 1."*, Gott. Nachr. **27**, 395-407 (1915).

[185] E. Hille. *Ordinary Differential Equations in the Complex Domain*. Dover books on mathematics. Dover Publications, (1997).

[186] H. Hoekstra, M. Bartelmann, H. Dahle, H. Israel, M. Limousin, and M. Meneghetti, *"Masses of galaxy clusters from gravitational lensing"*, Space Science Reviews **177**, 75-118 (2013), [arXiv:1303.3274].

[187] G. W. Horndeski, *"Second-order scalar-tensor field equations in a four-dimensional space"*, International Journal of Theoretical Physics **10**, 363-384 (1974).

[188] I. Horvath, J. Hakkila, and Z. Bagoly, *"Possible structure in the GRB sky distribution at redshift two"*, Astronomy & Astrophysics **561**, L12 (2014), [arXiv:1401.0533].

[189] A. Hosoya and M. Morikawa, *"Quantum Field Theory of Universe"*, Physical Review D **39**, 1123 (1989).

[190] C. Howlett, A. Ross, L. Samushia, W. Percival, and M. Manera, *"The clustering of the SDSS main galaxy sample – II. Mock galaxy catalogues and a measurement of the growth of structure from redshift space distortions at $z = 0.15$"*, Monthly Notices of the Royal Astronomical Society **449**, 848-866 (2015), [arXiv:1409.3238].

[191] B. Hu, M. Raveri, N. Frusciante, and A. Silvestri, *"Effective Field Theory of Cosmic Acceleration: an implementation in CAMB"*, Physical Review D **89**, 103530 (2014), [arXiv:1312.5742].

[192] W. Hu and I. Sawicki, *"Models of f(R) Cosmic Acceleration that Evade Solar-System Tests"*, Physical Review D **76**, 064004 (2007), [arXiv:0705.1158].

[193] E. Hubble, *"A relation between distance and radial velocity among extra-galactic nebulae"*, Proceedings of the National Academy of Sciences **15**, 168-173 (1929).

[194] D. Huterer and D. L. Shafer, *"Dark energy two decades after: Observables, probes, consistency tests"*, Reports on Progress in Physics **81**, 016901 (2018), [arXiv:1709.01091].

[195] D. Huterer, D. Shafer, D. Scolnic, and F. Schmidt, *"Testing ΛCDM at the lowest redshifts with SN Ia and galaxy velocities"*, Journal of Cosmology and Astroparticle Physics **1705**, 015 (2017), [arXiv:1611.09862].

[196] J.-c. Hwang, *"Cosmological perturbations in generalised gravity theories: formulation"*, Classical and Quantum Gravity **7**, 1613 (1990).

[197] J.-c. Hwang, *"Perturbations of the Robertson-Walker space - Multicomponent sources and generalized gravity"*, The Astrophysical Journal **375**, 443-462 (1991).

[198] J.-c. Hwang and H.-r. Noh, *"Cosmological perturbations in generalized gravity theories"*, Physical Review D **54**, 1460-1473 (1996).

[199] J.-c. Hwang and H.-r. Noh, *"Gauge ready formulation of the cosmological kinetic theory in generalized gravity theories"*, Physical Review D **65**, 023512 (2002), [arXiv:astro-ph/0102005].

[200] J.-c. Hwang and E. T. Vishniac, *"Gauge-invariant joining conditions for cosmological perturbations"*, The Astrophysical Journal **382**, 363-368 (1991).

[201] D. Iakubovskyi, *"Observation of the new emission line at ~ 3.5 keV in X-ray spectra of galaxies and galaxy clusters"*, Advances in Astronomy and Space Physics **6**, 3-15 (2016), [arXiv:1510.00358].

[202] C. J. Isham. *"Canonical quantum gravity and the problem of time"*. In *19th International Colloquium on Group Theoretical Methods in Physics (GROUP 19) Salamanca, Spain, June 29-July 5, 1992*, pages 157–288, (1992), [arXiv:gr-qc/9210011].

[203] P. Ivanov and S. V. Chernov, *"Stochastic quasiclassical wave function of the Universe from the third quantization procedure"*, Physical Review D **92**, 063507 (2015), [arXiv:1507.06507].

[204] D. W. Jordan and P. Smith. *Nonlinear ordinary differential equations: an introduction for scientists and engineers*. Oxford University Press, (2007).

[205] A. Yu. Kamenshchik, U. Moschella, and V. Pasquier, *"An Alternative to quintessence"*, Physics Letters B **511**, 265-268 (2001), [arXiv:gr-qc/0103004].

[206] D. Kazanas, *"Dynamics of the Universe and Spontaneous Symmetry Breaking"*, The Astrophysical Journal **241**, L59-L63 (1980).

[207] W. O. Kermack and W. H. McCrea, *"On Milne's theory of world structure"*, Monthly Notices of the Royal Astronomical Society **93**, 519-529 (1933).

[208] J. Khoury, B. A. Ovrut, P. J. Steinhardt, and N. Turok, *"The Ekpyrotic universe: Colliding branes and the origin of the hot big bang"*, Physical Review D **64**, 123522 (2001), [arXiv:hep-th/0103239].

[209] C. Kiefer, *"Continuous Measurement of Minisuperspace Variables by Higher Multipoles"*, Classical and Quantum Gravity **4**, 1369 (1987).

[210] C. Kiefer, *"Wave Packets in Minisuperspace"*, Physical Review D **38**, 1761-1772 (1988).

[211] C. Kiefer. *Quantum Gravity*. Oxford University Press, New York, (2007).

[212] S. P. Kim, *"Quantum mechanics of conformally and minimally coupled Friedmann-Robertson-Walker cosmology"*, Physical Review D **46**, 3403-3434 (1992).

[213] S. P. Kim, *"Third Quantization and Quantum Universes"*, Nuclear Physics B - Proceedings Supplements **246-247**, 68-75 (2014), [arXiv:1212.5355].

[214] S. P. Kim, J. Kim, and K. S. Soh, *"Quantized fields of the universe in superspace. 1: The Single universe"*, Nuclear Physics B **406**, 481-498 (1993).

[215] H. Kodama and M. Sasaki, *"Cosmological Perturbation Theory"*, Progress of Theoretical Physics Supplement **78**, 1-166 (1984).

[216] T. S. Koivisto and N. J. Nunes, *"Inflation and dark energy from three-forms"*, Physical Review D **80**, 103509 (2009), [arXiv:0908.0920].

[217] T. S. Koivisto and N. J. Nunes, *"Three-form cosmology"*, Physics Letters B **685**, 105-109 (2010), [arXiv:0907.3883].

[218] T. S. Koivisto and N. J. Nunes, *"Coupled three-form dark energy"*, Physical Review D **88**, 123512 (2013), [arXiv:1212.2541].

[219] T. S. Koivisto, D. F. Mota, and C. Pitrou, *"Inflation from N-Forms and its stability"*, Journal of High Energy Physics **09**, 092 (2009), [arXiv:0903.4158].

[220] T. S. Koivisto, E. N. Saridakis, and N. Tamanini, *"Scalar-Fluid theories: cosmological perturbations and large-scale structure"*, Journal of Cosmology and Astroparticle Physics **1509**, 047 (2015), [arXiv:1505.07556].

[221] K. V. Kuchař, *"Time and interpretations of quantum gravity"*, International Journal of Modern Physics D **20**, 3-86 (2011).

[222] K. S. Kumar, J. Marto, N. J. Nunes, and P. V. Moniz, *"Inflation in a two 3-form fields scenario"*, Journal of Cosmology and Astroparticle Physics **1406**, 064 (2014), [arXiv:1404.0211].

[223] D. Langlois, R. Saito, D. Yamauchi, and K. Noui, *"Scalar-tensor theories and modified gravity in the wake of GW170817"*, Physical Review D **97**, 061501 (2018), [arXiv:1711.07403].

[224] S. M. Leach, M. Sasaki, D. Wands, and A. R. Liddle, *"Enhancement of superhorizon scale inflationary curvature perturbations"*, Physical Review D **64**, 023512 (2001), [arXiv:astro-ph/0101406].

[225] A. G. Lemaître, *"Un Univers homogène de masse constante et de rayon croissant rendant compte de la vitesse radiale des nébuleuses extra-galactiques (A homogeneous universe of constant mass and increasing radius accounting for the radial velocity of extra-galactic nebulae)"*, Annales de la Société Scientifique de Bruxelles **47**, 49-59 (1927). English translation in Monthly Notices of the Royal Astronomical Society **91**, 483-490 (1931).

[226] A. G. Lemaître, *"Contributions to a British Association Discussion on the Evolution of the Universe."*, Nature **128**, 704-706 (1931).

[227] J. Lesgourgues, *"The Cosmic Linear Anisotropy Solving System (CLASS) I: Overview"*, [arXiv:1104.2932].

[228] H. R. Lewis, *"Class of exact invariants for classical and quantum time-dependent harmonic oscillators"*, Journal of Mathematical Physics **9**, 1976-1986 (1968).

[229] H. R. Lewis and W. B. Riesenfeld, *"An Exact quantum theory of the time dependent harmonic oscillator and of a charged particle time dependent electromagnetic field"*, Journal of Mathematical Physics **10**, 1458-1473 (1969).

[230] Z.-L. Liang and Y.-L. Wu, *"Direct detection and solar capture of spin-dependent dark matter"*, Physical Review D **89**, 013010 (2014), [arXiv:1308.5897].

[231] A. R. Liddle, *"Power Law Inflation With Exponential Potentials"*, Physics Letters B **220**, 502-508 (1989).

[232] A. R. Liddle. *"An Introduction to cosmological inflation"*. In *Proceedings, Summer School in High-energy physics and cosmology: Trieste, Italy, June 29-July 17, 1998*, pages 260–295, (1999), [arXiv:astro-ph/9901124].

[233] A. R. Liddle and D. H. Lyth, *"The Cold dark matter density perturbation"*, Physics Reports **231**, 1-105 (1993), [arXiv:astro-ph/9303019].

[234] E. Lifshitz, *"On the gravitational stability of the expanding universe"*, Zhurnal Eksperimentalnoi i Teoreticheskoi Fiziki **16**, 587-602 (1946). [Republication of english version in General Relativity and Gravitation **49**, 2 (2017)].

[235] A. D. Linde, *"A New Inflationary Universe Scenario: A Possible Solution of the Horizon, Flatness, Homogeneity, Isotropy and Primordial Monopole Problems"*, Physics Letters B **108**, 389-393 (1982).

[236] A. D. Linde, *"Chaotic Inflation"*, Physics Letters B **129**, 177-181 (1983).

[237] E. V. Linder, *"Exploring the expansion history of the universe"*, Physical Review Letters **90**, 091301 (2003), [arXiv:astro-ph/0208512].

[238] E. V. Linder, *"Cosmic growth history and expansion history"*, Physical Review D **72**, 043529 (2005), [arXiv:astro-ph/0507263].

[239] E. V. Linder and R. N. Cahn, *"Parameterized Beyond-Einstein Growth"*, Astroparticle Physics **28**, 481-488 (2007), [arXiv:astro-ph/0701317].

[240] E. V. Linder and A. Jenkins, *"Cosmic structure and dark energy"*, Monthly Notices of the Royal Astronomical Society **346**, 573 (2003), [arXiv:astro-ph/0305286].

[241] F. Lucchin and S. Matarrese, *"Power Law Inflation"*, Physical Review D **32**, 1316 (1985).

[242] F. Lucchin, S. Matarrese, and N. Vittorio, *"Primordial spectrum and density parameter-problem in a power-law inflation"*, Astronomy & Astrophysics **162**, 13-15 (1986).

[243] A. Lukas, B. A. Ovrut, and D. Waldram, *"String and M theory cosmological solutions with Ramond forms"*, Nuclear Physics B **495**, 365-399 (1997), [arXiv:hep-th/9610238].

[244] C.-P. Ma and E. Bertschinger, *"Cosmological perturbation theory in the synchronous and conformal Newtonian gauges"*, The Astrophysical Journal **455**, 7-25 (1995), [arXiv:astro-ph/9506072].

[245] E. Macaulay, I. K. Wehus, and H. K. Eriksen, *"Lower Growth Rate from Recent Redshift Space Distortion Measurements than Expected from Planck"*, Physical Review Letters **111**, 161301 (2013), [arXiv:1303.6583].

[246] K. A. Malik. *Cosmological perturbations in an inflationary universe*. PhD thesis, Portsmouth U., (2001), [arXiv:astro-ph/0101563].

[247] K. A. Malik and D. Wands, *"Adiabatic and entropy perturbations with interacting fluids and fields"*, Journal of Cosmology and Astroparticle Physics **0502**, 007 (2005), [arXiv:astro-ph/0411703].

[248] K. A. Malik and D. Wands, *"Cosmological perturbations"*, Physics Reports **475**, 1-51 (2009), [arXiv:0809.4944].

[249] G. Mangano, G. Miele, S. Pastor, T. Pinto, O. Pisanti, and P. D. Serpico, *"Relic neutrino decoupling including flavor oscillations"*, Nuclear Physics B **729**, 221-234 (2005), [arXiv:hep-ph/0506164].

[250] M. Markevitch, A. H. Gonzalez, D. Clowe, A. Vikhlinin, L. David, W. Forman, C. Jones, S. Murray, and W. Tucker, *"Direct constraints on the dark matter self-interaction cross-section from the merging galaxy cluster 1E0657-56"*, apj **606**, 819-824 (2004), [arXiv:astro-ph/0309303].

[251] M. Mars, *"First and second order perturbations of hypersurfaces"*, Classical and Quantum Gravity **22**, 3325-3348 (2005), [arXiv:gr-qc/0507005].

[252] J. Martin and D. J. Schwarz, *"The Influence of cosmological transitions on the evolution of density perturbations"*, Physical Review D **57**, 3302-3316 (1998), [arXiv:gr-qc/9704049].

[253] J. Mathews and R. Walker. *Mathematical Methods of Physics*. Addison-Wesley World Student Series. W. A. Benjamin, (1970).

[254] W. H. McCrea and E. A. Milne, *"Newtonian Universes and the curvature of space"*, The Quarterly Journal of Mathematics **5**, (1934).

[255] M. McGuigan, *"Third Quantization and the Wheeler-dewitt Equation"*, Physical Review D **38**, 3031-3051 (1988).

[256] M. McGuigan, *"Universe Creation From the Third Quantized Vacuum"*, Physical Review D **39**, 2229 (1989).

[257] M. McGuigan, *"Third quantization and black holes"*, [arXiv:hep-th/9212044].

[258] L. E. Mendes, A. B. Henriques, and R. G. Moorhouse, *"An Exact calculation of the energy density of cosmological gravitational waves"*, Physical Review D **52**, 2083-2088 (1995), [arXiv:gr-qc/9410033].

[259] J. L. Menestrina and R. J. Scherrer, *"Dark Radiation from Particle Decays during Big Bang Nucleosynthesis"*, Physical Review D **85**, 047301 (2012), [arXiv:1111.0605].

[260] J. Mielczarek and T. Trześniewski, *"Towards the map of quantum gravity"*, General Relativity and Gravitation **50**, 68 (2018), [arXiv:1708.07445].

[261] E. A. Milne, *"World-Structure and the Expansion of the Universe. Mit 6 Abbildungen."*, Zeitschrift für Astrophysik **6**, 1 (1933).

[262] C. W. Misner, K. S. Thorne, and J. A. Wheeler. *Gravitation*. W. H. Freeman, San Francisco, (1973).

[263] R. G. Moorhouse, A. B. Henriques, and L. E. Mendes, *"Graviton creation in an expanding universe"*, Physical Review D **50**, 2600-2604 (1994).

[264] J. Morais, M. Bouhmadi-López, and S. Capozziello, *"Can $f(R)$ gravity contribute to (dark) radiation?"*, Journal of Cosmology and Astroparticle Physics **1509**, 041 (2015), [arXiv:1507.02623].

[265] J. Morais, M. Bouhmadi-López, K. Sravan Kumar, J. Marto, and Y. Tavakoli, *"Interacting 3-form dark energy models: distinguishing interactions and avoiding the Little Sibling of the Big Rip"*, Physics of the Dark Universe **15**, 7-30 (2017), [arXiv:1608.01679].

[266] J. Morais, M. Bouhmadi-López, M. Krämer, and S. Robles-Pérez, *"Pre-inflation from the multiverse: Can it solve the quadrupole problem in the cosmic microwave background?"*, The European Physical Journal C **78**, 240 (2018), [arXiv:1711.05138].

[267] V. Mukhanov. *Physical Foundations of Cosmology*. Cambridge University Press, Oxford, (2005).

[268] V. Mukhanov and S. Winitzki. *Introduction to quantum effects in gravity*. Cambridge University Press, (2007).

[269] V. F. Mukhanov, *"Quantum Theory of Gauge Invariant Cosmological Perturbations"*, Soviet Physics - Journal of Experimental and Theoretical Physics **67**, 1297-1302 (1988). [Zh. Eksp. Teor. Fiz. 94N7, 1 (1988)].

[270] V. F. Mukhanov, H. A. Feldman, and R. H. Brandenberger, *"Theory of cosmological perturbations. Part 1. Classical perturbations. Part 2. Quantum theory of perturbations. Part 3. Extensions"*, Physics Reports **215**, 203-333 (1992).

[271] D. J. Mulryne, J. Noller, and N. J. Nunes, *"Three-form inflation and non-Gaussianity"*, Journal of Cosmology and Astroparticle Physics **1212**, 016 (2012), [arXiv:1209.2156].

[272] S. Nadathur, *"Seeing patterns in noise: Gigaparsec-scale 'structures' that do not violate homogeneity"*, Monthly Notices of the Royal Astronomical Society **434**, 398-406 (2013), [arXiv:1306.1700].

[273] A. Neronov and D. Malyshev, *"Toward a full test of the νMSM sterile neutrino dark matter model with Athena"*, Physical Review D **93**, 063518 (2016), [arXiv:1509.02758].

[274] T. Ngampitipan and P. Wongjun, *"Dynamics of three-form dark energy with dark matter couplings"*, Journal of Cosmology and Astroparticle Physics **1111**, 036 (2011), [arXiv:1108.0140].

[275] S. Nojiri and S. D. Odintsov, *"Modified gravity and its reconstruction from the universe expansion history"*, Journal of Physics: Conference Series **66**, 012005 (2007), [arXiv:hep-th/0611071].

[276] S. Nojiri and S. D. Odintsov, *"Unified cosmic history in modified gravity: from F(R) theory to Lorentz non-invariant models"*, Physics Reports **505**, 59-144 (2011), [arXiv:1011.0544].

[277] R. C. Nunes, S. Pan, and E. N. Saridakis, *"New constraints on interacting dark energy from cosmic chronometers"*, Physical Review D **94**, 023508 (2016), [arXiv:1605.01712].

[278] J. O'Hanlon, *"Intermediate-range gravity - a generally covariant model"*, Physical Review Letters **29**, 137-138 (1972).

[279] Y. Ohkuwa, M. Faizal, and Y. Ezawa, *"Virtual Black Holes in a Third Quantized Formalism"*, Annals of Physics **384**, 105-115 (2017), [arXiv:1707.06405].

[280] A. Oka, S. Saito, T. Nishimichi, A. Taruya, and K. Yamamoto, *"Simultaneous constraints on the growth of structure and cosmic expansion from the multipole power spectra of the SDSS DR7 LRG sample"*, Monthly Notices of the Royal Astronomical Society **439**, 2515-2530 (2014), [arXiv:1310.2820].

[281] T. Okumura et al., *"The Subaru FMOS galaxy redshift survey (FastSound). IV. New constraint on gravity theory from redshift space distortions at $z \sim 1.4$"*, Publications of the Astronomical Society of Japan **68**, 38 (2016), [arXiv:1511.08083].

[282] G. J. Olmo, *"Limit to general relativity in f(R) theories of gravity"*, Physical Review D **75**, 023511 (2007), [arXiv:gr-qc/0612047].

[283] F. W. J. Olver, D. W. Lozier, R. F. Boisvert, and C. W. Clark. *NIST Handbook of Mathematical Functions*. Cambridge University Press, (2010).

[284] P. J. E. Peebles, *"Tests of Cosmological Models Constrained by Inflation"*, The Astrophysical Journal **284**, 439-444 (1984).

[285] P. J. E. Peebles. *"From Precision Cosmology to Accurate Cosmology"*. In *Proceedings, 37th Rencontres de Moriond, The cosmological Model: Les Arcs, Savoie, France, Mar 16-23, 2002*, pages 3–12, (2003). URL `http://moriond.in2p3.fr/J02/Talks2002/J.Peebles/peebles.ps`, [arXiv:astro-ph/0208037].

[286] A. A. Penzias and R. W. Wilson, *"A Measurement of excess antenna temperature at 4080-Mc/s"*, The Astrophysical Journal **142**, 419-421 (1965).

[287] S. Perlmutter et al., *"Measurements of Omega and Lambda from 42 high redshift supernovae"*, The Astrophysical Journal **517**, 565-586 (1999), [arXiv:astro-ph/9812133].

[288] A. Pezzotta et al., *"The VIMOS Public Extragalactic Redshift Survey (VIPERS): The growth of structure at 0.5 ¡ z ¡ 1.2 from redshift-space distortions in the clustering of the PDR-2 final sample"*, Astronomy & Astrophysics **604**, A33 (2017), [arXiv:1612.05645].

[289] L. O. Pimentel, *"Energy Momentum Tensor in the General Scalar - Tensor Theory"*, Classical and Quantum Gravity **6**, L263-L265 (1989).

[290] L. Pogosian and A. Silvestri, *"The pattern of growth in viable f(R) cosmologies"*, Physical Review D **77**, 023503 (2008), [arXiv:0709.0296]. [Erratum: Physical Review **D81**, 049901 (2010)].

[291] A. Pourtsidou, C. Skordis, and E. J. Copeland, *"Models of dark matter coupled to dark energy"*, Physical Review D **88**, 083505 (2013), [arXiv:1307.0458].

[292] B. A. Powell and W. H. Kinney, *"The pre-inflationary vacuum in the cosmic microwave background"*, Physical Review D **76**, 063512 (2007), [arXiv:astro-ph/0612006].

[293] B. Ratra and P. J. E. Peebles, *"Cosmological Consequences of a Rolling Homogeneous Scalar Field"*, Physical Review D **37**, 3406 (1988).

[294] B. Reina. *Matching of spacetimes theory applied to rotating stars and quadratic gravity*. PhD thesis, Universidad del País Vasco - Euskal Herriko Unibertsitatea, Leioa, Spain, (2016).

[295] A. D. Rendall, *"Cosmological models and center manifold theory"*, General Relativity and Gravitation **34**, 1277-1294 (2002), [arXiv:gr-qc/0112040].

[296] A. G. Riess et al., *"Observational evidence from supernovae for an accelerating universe and a cosmological constant"*, The Astronomical Journal **116**, 1009-1038 (1998), [arXiv:astro-ph/9805201].

[297] H. P. Robertson, *"Kinematics and World-Structure"*, The Astronomical Journal **82**, 284 (1935).

[298] H. P. Robertson, *"Kinematics and World-Structure II."*, The Astronomical Journal **83**, 187 (1936).

[299] H. P. Robertson, *"Kinematics and World-Structure III."*, The Astronomical Journal **83**, 257 (1936).

[300] S. Robles-Pérez and P. F. González-Díaz, *"Quantum state of the multiverse"*, Physical Review D **81**, 083529 (2010), [arXiv:1005.2147].

[301] S. Robles-Pérez and P. F. González-Díaz, *"Quantum entanglement in the multiverse"*, Journal of High Energy Physics **118**, 34-53 (2014), [arXiv:1111.4128].

[302] S. Robles-Pérez, A. Alonso-Serrano, C. Bastos, and O. Bertolami, *"Vacuum decay in an interacting multiverse"*, Physics Letters B **759**, 328-335 (2016), [arXiv:1512.04073].

[303] S. Robles-Pérez, A. Balcerzak, M. P. Dabrowski, and M. Krämer, *"Interuniversal entanglement in a cyclic multiverse"*, Physical Review D **95**, 083505 (2017), [arXiv:1701.04773].

[304] L. Roszkowski, E. M. Sessolo, and S. Trojanowski, *"WIMP dark matter candidates and searches–current status and future prospects"*, Reports on Progress in Physics **81**, 066201 (2018), [arXiv:1707.06277].

[305] C. Rovelli. *"Notes for a brief history of quantum gravity"*. In *Recent developments in theoretical and experimental general relativity, gravitation and relativistic field theories. Proceedings, 9th Marcel Grossmann Meeting, MG'9, Rome, Italy, July 2-8, 2000. Pts. A-C*, pages 742–768, (2000), [arXiv:gr-qc/0006061].

[306] V. A. Rubakov, *"On the Third Quantization and the Cosmological Constant"*, Physics Letters B **214**, 503-507 (1988).

[307] V. C. Rubin and W. K. Ford, Jr., *"Rotation of the Andromeda Nebula from a Spectroscopic Survey of Emission Regions"*, The Astrophysical Journal **159**, 379-403 (1970).

[308] V. Sahni, T. D. Saini, A. A. Starobinsky, and U. Alam, *"Statefinder: A New geometrical diagnostic of dark energy"*, Journal of High Energy Physics **77**, 201-206 (2003), [arXiv:astro-ph/0201498]. [Pisma Zh. Eksp. Teor. Fiz.77,249(2003)].

[309] V. Salvatelli, N. Said, M. Bruni, A. Melchiorri, and D. Wands, *"Indications of a late-time interaction in the dark sector"*, Physical Review Letters **113**, 181301 (2014), [arXiv:1406.7297].

[310] S. Sarkar, *"Big bang nucleosynthesis and physics beyond the standard model"*, Reports on Progress in Physics **59**, 1493-1610 (1996), [arXiv:hep-ph/9602260].

[311] M. Sasaki, *"Gauge Invariant Scalar Perturbations in the New Inflationary Universe"*, Progress of Theoretical Physics **70**, 394 (1983).

[312] S. Satpathy et al., *"The clustering of galaxies in the completed SDSS-III Baryon Oscillation Spectroscopic Survey: On the measurement of growth rate using galaxy correlation functions"*, Monthly Notices of the Royal Astronomical Society **469**, 1369-1382 (2017), [arXiv:1607.03148].

[313] C. Schomblond and P. Spindel, *"Conditions d'unicité pour le propagateur $\Delta^1(x,y)$ du champ scalaire dans l'univers de de Sitter"*, Annales de l'I.H.P. Physique théorique **25**, 67-78 (1976).

[314] B. F. Schutz, *"Perfect Fluids in General Relativity: Velocity Potentials and a Variational Principle"*, Physical Review D **2**, 2762-2773 (1970).

[315] B. F. Schutz, *"Hamiltonian Theory of a Relativistic Perfect Fluid"*, Physical Review D **4**, 3559-3566 (1971).

[316] B. F. Schutz and R. Sorkin, *"Variational aspects of relativistic field theories, with application to perfect fluids"*, Annals of Physics **107**, 1-43 (1977).

[317] P. Scott, J. Conrad, J. Edsjo, L. Bergstrom, C. Farnier, and Y. Akrami, *"Direct Constraints on Minimal Supersymmetry from Fermi-LAT Observations of the Dwarf Galaxy Segue 1"*, Journal of Cosmology and Astroparticle Physics **1001**, 031 (2010), [arXiv:0909.3300].

[318] J. Solà Peracaula, J. de Cruz Pérez, and A. Gómez-Valent, *"Dynamical dark energy vs. Λ = const in light of observations"*, Europhysics Letters **121**, 39001 (2018), [arXiv:1606.00450].

[319] Y.-S. Song and W. J. Percival, *"Reconstructing the history of structure formation using Redshift Distortions"*, Journal of Cosmology and Astroparticle Physics **0910**, 004 (2009), [arXiv:0807.0810].

[320] Y.-S. Song, W. Hu, and I. Sawicki, *"The Large Scale Structure of f(R) Gravity"*, Physical Review D **75**, 044004 (2007), [arXiv:astro-ph/0610532].

[321] T. P. Sotiriou. *Modified Actions for Gravity: Theory and Phenomenology*. PhD thesis, SISSA, Trieste, (2007), [arXiv:0710.4438].

[322] T. P. Sotiriou and V. Faraoni, *"f(R) Theories Of Gravity"*, Reviews of Modern Physics **82**, 451-497 (2010), [arXiv:0805.1726].

[323] K. Sravan Kumar, D. J. Mulryne, N. J. Nunes, J. Marto, and P. Vargas Moniz, *"Non-Gaussianity in multiple three-form field inflation"*, Physical Review D **94**, 103504 (2016), [arXiv:1606.07114].

[324] A. A. Starobinsky, *"Spectrum of relict gravitational radiation and the early state of the universe"*, Soviet Journal of Experimental and Theoretical Physics Letters **30**, 682-685 (1979).

[325] A. A. Starobinsky, *"A New Type of Isotropic Cosmological Models Without Singularity"*, Physics Letters B **91**, 99-102 (1980).

[326] A. A. Starobinsky, *"Spectrum of adiabatic perturbations in the universe when there are singularities in the inflation potential"*, Journal of Experimental and Theoretical Physics Letters **55**, 489-494 (1992). [Pisma Zh. Eksp. Teor. Fiz.55,477(1992)].

[327] A. A. Starobinsky, *"Disappearing cosmological constant in $f(R)$ gravity"*, Journal of Experimental and Theoretical Physics Letters **86**, 157-163 (2007), [arXiv:0706.2041].

[328] K. S. Stelle, *"Renormalization of Higher Derivative Quantum Gravity"*, Physical Review D **16**, 953-969 (1977).

[329] K. S. Stelle, *"Classical Gravity with Higher Derivatives"*, General Relativity and Gravitation **9**, 353-371 (1978).

[330] A. Strominger. *"Baby Universes"*. In *Theoretical Advanced Study Institute in Elementary Particle Physics: Particles, Strings and Supernovae (TASI 88) Providence, Rhode Island, June 5-July 1, 1988*, pages 315–391, (1988).

[331] A. H. Taub, *"General Relativistic Variational Principle for Perfect Fluids"*, Physical Review **94**, 1468-1470 (1954).

[332] P. Teyssandier and P. Tourrenc, *"The Cauchy problem for the $R+R^2$ theories of gravity without torsion"*, Journal of Mathematical Physics **24**, 2793 (1983).

[333] D. Tong. *Quantum Field Theory: University of Cambridge Part III Mathematical Tripos*. (2006).

[334] D. F. Torres, *"Quintessence, superquintessence and observable quantities in Brans-Dicke and nonminimally coupled theories"*, Physical Review D **66**, 043522 (2002), [arXiv:astro-ph/0204504].

[335] M. A. Troxel et al., *"Dark Energy Survey Year 1 Results: Cosmological Constraints from Cosmic Shear"*, Physical Review D **98**, 043528 (2018), [arXiv:1708.01538].

[336] S. Tsujikawa, *"Matter density perturbations and effective gravitational constant in modified gravity models of dark energy"*, Physical Review D **76**, 023514 (2007), [arXiv:0705.1032].

[337] J. Valiviita, E. Majerotto, and R. Maartens, *"Instability in interacting dark energy and dark matter fluids"*, Journal of Cosmology and Astroparticle Physics **0807**, 020 (2008), [arXiv:0804.0232].

[338] L. Verde, *"A practical guide to Basic Statistical Techniques for Data Analysis in Cosmology"*, [arXiv:0712.3028].

[339] L. Verde, *"Precision cosmology, Accuracy cosmology and Statistical cosmology"*, Proceedings of the International Astronomical Union **10**, 223–234 (2014).

[340] A. Vilenkin, *"Creation of Universes from Nothing"*, Physics Letters B **117**, 25-28 (1982).

[341] A. Vilenkin, *"Quantum Creation of Universes"*, Physical Review D **30**, 509-511 (1984).

[342] A. Vilenkin, *"The Quantum cosmology debate"*, AIP Conference Proceedings **478**, 23-29 (1999), [arXiv:gr-qc/9812027].

[343] M. Visser, *"Jerk and the cosmological equation of state"*, Classical and Quantum Gravity **21**, 2603-2616 (2004), [arXiv:gr-qc/0309109].

[344] M. Visser, *"Cosmography: Cosmology without the Einstein equations"*, General Relativity and Gravitation **37**, 1541-1548 (2005), [arXiv:gr-qc/0411131].

[345] J. Väliviita and E. Palmgren, *"Distinguishing interacting dark energy from wCDM with CMB, lensing, and baryon acoustic oscillation data"*, Journal of Cosmology and Astroparticle Physics **1507**, 015 (2015), [arXiv:1504.02464].

[346] J. Wainwright and G. Ellis. *Dynamical Systems in Cosmology*. Cambridge University Press, (2005).

[347] R. M. Wald. *General Relativity*. University of Chicago Press, (1984).

[348] A. G. Walker, *"On Milne's Theory of World-Structure"*, Proceedings of the London Mathematical Society **42**, 90-127 (1937).

[349] A. G. Walker and E. A. Milne, *"On the Formal Comparison of Milne's Kinematical System with the Systems of General Relativity"*, Monthly Notices of the Royal Astronomical Society **95**, 263-269 (1935).

[350] D. Wands and A. Slosar, *"Scale-dependent bias from primordial non-Gaussianity in general relativity"*, Physical Review D **79**, 123507 (2009), [arXiv:0902.1084].

[351] D. Wands, J. De-Santiago, and Y. Wang, *"Inhomogeneous vacuum energy"*, Classical and Quantum Gravity **29**, 145017 (2012), [arXiv:1203.6776].

[352] D. Wands, O. F. Piattella, and L. Casarini, *"Physics of the Cosmic Microwave Background Radiation"*, Astrophysics and Space Science Proceedings **45**, 3-39 (2016), [arXiv:1504.06335].

[353] I.-C. Wang and K.-W. Ng, *"Effects of a pre-inflation radiation-dominated epoch to CMB anisotropy"*, Physical Review D **77**, 083501 (2008), [arXiv:0704.2095].

[354] L.-M. Wang and P. J. Steinhardt, *"Cluster abundance constraints on quintessence models"*, The Astrophysical Journal **508**, 483-490 (1998), [arXiv:astro-ph/9804015].

[355] S. Wang, M. Li, and Y. Hu, *"Cosmological implications of different baryon acoustic oscillation data"*, Science China Physics, Mechanics & Astronomy **60**, 040411 (2017), [arXiv:1506.08274].

[356] Y. Wang et al., *"Designing a space-based galaxy redshift survey to probe dark energy"*, Monthly Notices of the Royal Astronomical Society **409**, 737 (2010), [arXiv:1006.3517].

[357] S. Weinberg. *Gravitation and Cosmology*. John Wiley and Sons, New York, (1972).

[358] S. Weinberg, *"The Cosmological Constant Problem"*, Reviews of Modern Physics **61**, 1-23 (1989).

[359] J. A. Wheeler. *"Superspace and the Nature of Quantum Geometrodynamics"*. In *Topics in Nonlinear Physics*, pages 615–724. Springer Berlin Heidelberg, Berlin, Heidelberg, (1968).

[360] C. M. Will, *"The Confrontation between General Relativity and Experiment"*, Living Reviews in Relativity **17**, 4 (2014), [arXiv:1403.7377].

[361] P. Wongjun, *"Perfect fluid in Lagrangian formulation due to generalized three-form field"*, Physical Review D **96**, 023516 (2017), [arXiv:1602.00682].

[362] J. K. Yadav, J. S. Bagla, and N. Khandai, *"Fractal Dimension as a measure of the scale of Homogeneity"*, Monthly Notices of the Royal Astronomical Society **405**, 2009 (2010), [arXiv:1001.0617].

[363] J. Yokoyama and K.-i. Maeda, *"On the Dynamics of the Power Law Inflation Due to an Exponential Potential"*, Physics Letters B **207**, 31-35 (1988).

[364] P. Zarrouk et al., *"The clustering of the SDSS-IV extended Baryon Oscillation Spectroscopic Survey DR14 quasar sample: measurement of the growth rate of structure from the anisotropic correlation function between redshift 0.8 and 2.2"*, Monthly Notices of the Royal Astronomical Society **477**, 1639-1663 (2018), [arXiv:1801.03062].

[365] P. Zhang, *"Testing $f(R)$ gravity against the large scale structure of the universe."*, Physical Review D **73**, 123504 (2006), [arXiv:astro-ph/0511218].

[366] Z.-f. Zhang, T.-R. Ding, W.-z. Huang, and Z.-x. Dong. *Qualitative theory of differential equations*. Collæge Press, University of Beijing, (1998).

[367] G.-B. Zhao et al., *"Dynamical dark energy in light of the latest observations"*, Nature Astronomy **1**, 627-632 (2017), [arXiv:1701.08165].